A new function for the *Arabidopsis thaliana* SNARE SYP121

Annegret Honsbein

December 2010

Thesis submitted for the degree of Doctor of Philosophy

College of Medical, Veterinary and Life Sciences
Institute of Molecular, Cell and Systems Biology

University of Glasgow

Abstract

Eukaryotic cells maintain a compartmental cellular organization of membrane-enclosed organelles that communicate with each other through the exchange of trafficking vesicles. Members of a superfamily of membrane proteins, the so-called SNAREs, are essential for the necessary fusion of vesicle membranes to the membrane of target organelles. SNAREs are needed to overcome the energy barrier that prevents spontaneous membrane fusion events. A number of studies from the past decade indicated that SNARE proteins might fulfill a function beyond merging membranes. The mammalian plasma membrane SNARE Syntaxin1A was shown to directly interact with and through this interaction modify the activity of, for example, a calcium ion channel and a potassium ion channel. In its classical function as SNARE protein, Syntaxin1A mediates specialized vesicle fusion events such as synaptic transmission in neurons or secretion of insulin from pancreatic cells. These specialized vesicle fusion events require precise timing that is controlled by intracellular signaling events. These intracellular signaling events involve the coordinated action of members from different families of ion channels. Current models suggest that the dual functions of a SNARE protein in ion channel regulation and membrane fusion serve to fine-tune highly regulated vesicle fusion events. This thesis provides evidence for the first direct interaction between a SNARE protein and an ion channel from plants and suggests a function for this interaction in *Arabidopsis* potassium nutrition. Three different protein-protein interaction assays for full-length membrane proteins that comprised a yeast mating based split-ubiquitin assay, co-immunoprecipitation after expression in insect cells and bi-molecular fluorescence complementation after transient *Arabidopsis* root transformation, confirm that the *Arabidopsis* plasma membrane SNARE SYP121 interacts *in vitro* and *in vivo* with the Shaker ion channel subunit KC1. Furthermore, the interaction between KC1 and SYP121 is specific over the closest homologue of Syp121, namely SYP122. Shaker channels are plasma membrane proteins with four subunits that transport the essential macronutrient potassium in response to changes in membrane voltage. The KC1 subunit is unique among the Shaker channels. It can only act as a regulatory subunit that modifies channel properties when forming heterotetramers with other Shaker subunits such as AKT1, not as functional homotetramer. AKT1 is expressed predominantly in the root epidermis, i.e. root hairs, where it overlaps with the more broadly expressed KC1 and SYP121. Previous publications showed that a low external potassium concentration combined with high levels of ammonium that is used to block all root potassium uptake systems apart from AKT1, causes *akt1* null mutants to display strongly reduced main root length as well as whole plant potassium content compared to wild type plants. It is shown here that the phenotype of both *syp121* and *kc1* null mutants is identical to the *akt1* mutant under these growth conditions. The design of new antibodies against native AKT1 and KC1 and an optimized protocol for root plasma membrane protein enrichment and solubilisation allowed for the first time visualization of native *Arabidopsis* AKT1 protein. This technical advance made it possible to confirm that both Shaker channel subunits are present in equal amounts in the plasma membrane of roots cells from *syp121* mutant and wild type plants. It is concluded that the potassium uptake phenotype of the *syp121* mutant is not caused by the absence of channel proteins

from the plasma membrane due to a disruption of the vesicle trafficking function of the SNARE SYP121. An alternative function for SYP121 in potassium nutrition that involves direct interaction with AKT1-KC1 heterotetrameric channels is supported by electrophysiological measurements after heterologous expression in *Xenopus leavis* oocytes. SYP121 modifies the voltage-dependent potassium uptake characteristics of AKT1-KC1 heterotetramers in a way most easily understood in context of a conformational change within the voltage sensing protein parts of the Shaker channel that are caused by the direct interaction with the SNARE protein. It is concluded that the identical potassium uptake phenotype of the *akt1*, *kc1* and *syp121* mutants is caused by the inability to form a functional tripartite complexes. As KC1 is able to form heterotetrameric channels with several different Shaker channel subunits, for example KAT1 that is highly expressed in guard cells, it is likely that this novel interaction between KC1 and SYP121 might modulate channel activities in different tripartite complexes to affect various cellular functions.

Table of Contents

List of Tables

List of Figures

List of Accompanying Material

List of Abbreviations

2P	Two-Phase (partioning)
aa	amino acid (s)
ABA	abscisic acid
Ade; a	adenine
ATP	adenosine triphosphate
BiFC	bimolecular fluorescent complementation
CCV	Clathrin-coated vesicles
CDS	coding sequence
CMC	critical micelle concentration
Co-IP	co-immunoprecipitation
cRNA	complementary RNA
Cub	C-terminal half of ubiquitin
DEPC	diethyl pyrocarbonate
DEPC	Diethyl pyrocarbonate
DMSO	dimethyl sulfoxide
DNA	deoxyribonucleic acid
DTT	dithiothreitol
EDTA	ethylenediaminetetraacetic acid
EE	early endosome
eFP	electronic fluorescent pictograph
EM	endomembranes
ER	endoplasmic reticulum
ERAD	ER-associated degradation
ET	ethylene
EtBr	ethidium bromide
EtOH	ethanol
FP	fluorescent protein
FRET	fluorescence resonance energy transfer
GFP	green fluorescent protein
GUS	β-glucuronidase
HA tag	hemagglutinin epitope tag
HEK	human embryonic kidney
His; h	histidine
JA	jasmonic acid
kDa	kilo Dalton
LB	Luria-Bertani medium
Leu; l	leucine
LPC	L-α-lysophosphatidylcholine
M&M	material and methods
mbSUS	mating based split ubiquitin system
MCS	multiple cloning site
mRNA	messenger RNA (ribonucleic acid)
MS	Murashige and Skoog salts
MVB	multi vesicular body
NSDB	non-detergent sulfobetaines
OGP	octyl-β-glucopyranoside
PAGE	polyacrylamide gel electrophoresis
PBS-T	phosphate based saline, Tween20
PM	plasma membrane
PMSF	phenylmethanesulfonyl fluoride
RE	recycling endosome
ROS	reactive oxygen species
RT	room temperature
RT-PCR	reverse transcription-PCR
SA	salicylic acid
SA-I	type I signal anchor
SA-II	type II signal anchor
SC	synthetic complete
PAGE	polyacrylamide gel electrophoresis
PBS-T	phosphate based saline, Tween20
SDS	sodium dodecyl sulphate
SN	supernatant
SNARE	soluble NSF attachment protein receptor
SP	signal peptide
SRP	signal recognition particle
sSN	solubilised supernatant
St	stop-transfer
SVC	secretory vesicle cluster
SDS	sodium dodecyl sulphate
SN	supernatant
TA	tail-anchored
TAE	tris acetate EDTA
TCA	tri chloroacetic acid
TEVC	two-electron-voltage clamp
TGN	trans Golgi network
UBS	ubiquitin specific proteases
UPR	unfolded protein response
UTR	untranslated region
UV	ultraviolet
UPR	unfolded protein response
UTR	untranslated region
UV	ultraviolet
VAMP	vesicle-associated membrane protein
WB	Western Blot analysis
wt	wild type
UPR	unfolded protein response
MS	Murashige and Skoog basal medium
MVB	multi vesicular body
NSDB	non-detergent sulfobetaines
X-GAL	5-bromo-4-chloro-3-indolyl-β-D-galactopyranoside
YNB	yeast nitrogen base
β-gal	β-galactosidase enzyme

Acknowledgement

I am very grateful that my supervisor, Prof. M. Blatt, gave me the opportunity to join his group for this project. I feel I have learned many interesting and useful things not only of a scientific nature. I would like to thank him for his continuing support and his willingness to help with every problem, as soon as it appears. I especially appreciate his composure and the tolerance that he shows to all persons.

My special thanks are also to Bernadette Gehl, who has made Glasgow and the lab a place where I liked to stay from the beginning. I greatly miss her humour and her warm friendship since she left at the end of her Ph.D.

I would also like to thank Maria Papanatsiou, Christopher Grefen, Cornelia Eisenach, Mary Williams and especially Anna Amtmann for very helpful discussions, moral encouragement and proof-reading of the manuscript during the writing process.

I am grateful to all past and present members of the Blatt/Amtmann labs for their help and friendship over the past years, especially to Naomi Donald whom I have never seen in a bad mood and Cornelia Eisenach who comes to check up on me when I'm ill.

My family, especially my parents and my three great-aunts Magarete, Eva und Elsa Raabe are my greatest support. Their acceptance and interest in my life, their kindness and humor always give me perspective.

Author's Declaration

I hereby declare that all the work presented as part of this thesis is my own, except where explicitly stated otherwise.

Annegret Honsbein

22nd December 2010

Part of this work has been published (see Appendix II, p. 281)

General Introduction

Plant ion channels

Three types of membrane transport proteins mediate solute transport across biological membranes: channels, carriers and pumps (see Fig. 1).

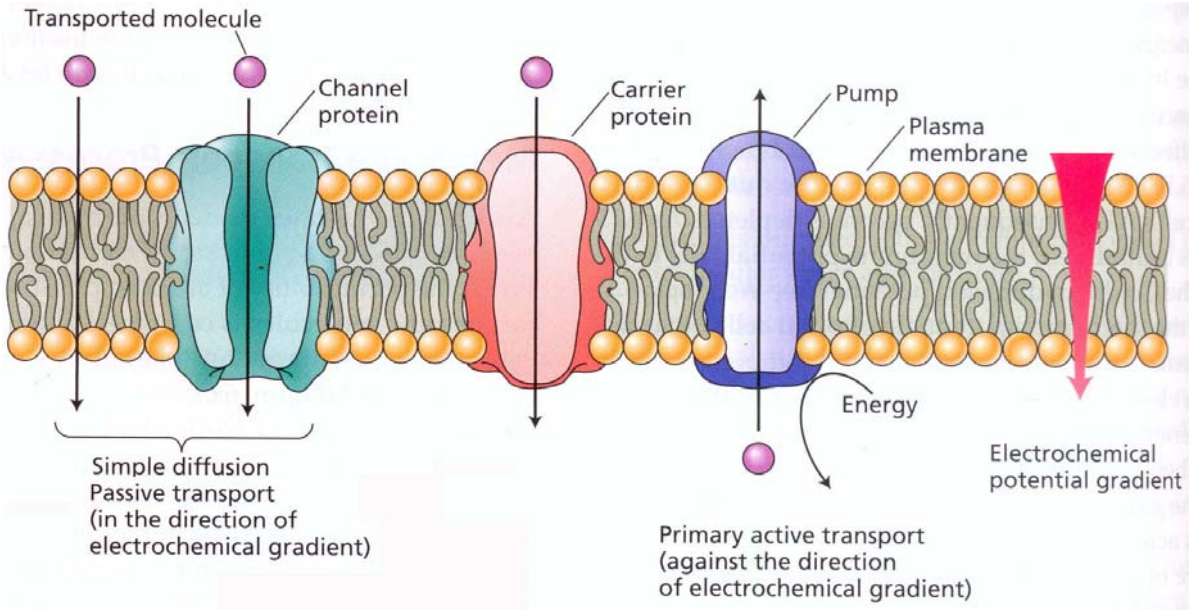

Fig. 1 Three classes of membrane transport proteins

In plant membranes, three different types of membrane transport proteins can be found: pumps, channels and carriers. Pumps transport solutes against the gradient of their electrochemical potential for which energy, usually from ATP hydrolysis, is needed. Hence, these processes are called primary active transport. In contrast, channels are transmembrane proteins that transport solutes by simple diffusion that follows the direction of the electrochemical gradient. This process is also called passive transport and takes places through a pore that spans the membrane. This pore is open and closed in response to specific signals. Carrier proteins bind the transported molecule on one side of the membrane and then undergo a conformational change that releases it on the other side. Transport through carriers can be either passive or secondary active, i.e. directly coupled to primary active transport.
The image was adapted from a previous publication (Taiz & Zeiger, 1998).

The most important pumps in plant plasma membranes (PM) are those who transport protons (H^+) and calcium (Ca^{2+}). The plasma membrane H^+-ATPase, for example, is a pump that drives H^+ from the cytosol to the external medium, creating a pH gradient. This pH gradient is also called the electrochemical potential gradient for H^+ (see Fig. 1), as it represents a simultaneous separation of electrical charge (more positive ions on the outside) and a chemical difference in the concentration of H^+ (more H^+ outside) across the cell membrane. However, H^+ diffuse passively back into the cell following the chemical concentration gradient (less H^+ inside) and the greater negative charge of the cytoplasm. Therefore, to uphold the pH gradient, protons must be transported against this electrochemical potential gradient, which requires energy. Pumps obtain the required energy from the hydrolysis of ATP, which is why these transport processes are called primary active transport. The gradient of electrochemical potential for H^+, also called the proton

motive force, represents stored free energy that can be used in secondary active transport to drive the transport of many other substrates against their gradients of electrochemical potentials (Taiz & Zeiger, 1998).

Whenever an ion moves in or out of a cell without being balanced by countermovement of an ion of opposite charge, a voltage is created across the membrane, i.e. a membrane potential. Typical membrane potentials across plant cell membranes range from between -60 to -240 mV. The electrical charge separation that is intrinsic to the pH gradient created by the H^+-ATPase in the PM contributes significantly to the membrane potential in plants. However, the asymmetric distribution of other ions, i.e. their electrochemical potential gradients, contributes to the membrane potential as well. In addition, membranes show differential permeability to different ions. In most plant cells, potassium (K^+) and anions (ions with negative charge) have both the greatest internal concentration and highest membrane permeability and together with the pump-mediated H^+ extrusion make the membrane potential negative. In conclusion, every ion that moves across a membrane is subjected to gradients of both ion concentration and electrical potential that are linked to the membrane potential. A change in the membrane potential caused by H^+-ATPase pumps will change the driving forces for diffusion of all ions across the membrane. In this way, for example, the outward transport of H^+ can create a driving force for the passive diffusion of K^+ into the cell. Passive diffusion, i.e. passive transport, in contrast to active transport, follows the electrochemical gradient and takes places spontaneously (Taiz & Zeiger, 1998).

Channels (see Fig. 1) are the proteins that mediate passive transport of e.g. ions such as K^+, by simple diffusion. Channels, such as the Shaker channels, are transmembrane proteins that act as selective pores in the membrane, through which molecules or ions can diffuse. The size of a pore and the density and nature of surface charges on its interior lining determine its ion specificity. As long as the channel pore is open, solutes that can penetrate the pore diffuse through it very rapidly, about 10^8 ions per second through each channel protein (Taiz & Zeiger, 1998). However, channels are not continuously open. They open and close their pores in a so-called gating process that is triggered by external signals. Ion channels can be classified according to which chemical or physical modulator controls their gating activity. For example, in plants, voltage-gated channels respond to a change in membrane potential, mechanosensitive channels respond to osmotic pressure or membrane curvature and second messenger gated channels respond to nucleotides.

In contrast to channels, carrier proteins (see Fig. 1) do not have pores that extend completely across the membrane. Instead, the substance being transported, e.g. K^+ is initially bound to a specific site on the carrier protein. Binding causes a conformational change in the protein, which exposes the substance to the solution on the other side of the membrane. Transport is complete when the substance dissociates from the carrier's binding site. Carrier-mediated transport, unlike transport through channels, can be either passive or secondary active (see above). There are two types of secondary active transport. Symport, mediated by carriers called Symporters, is achieved when the co-transported solute moves in the same direction of the transported solute (e.g. H^+ from primary active transport). Antiport, mediated by carriers called Antiporters, refers to a coupled transport where both solutes move in opposite directions (Taiz & Zeiger, 1998). Fig. 2

shows an overview of the various transport processes mediated by pumps, channels and carriers on the PM and the vacuolar membrane of plants cells.

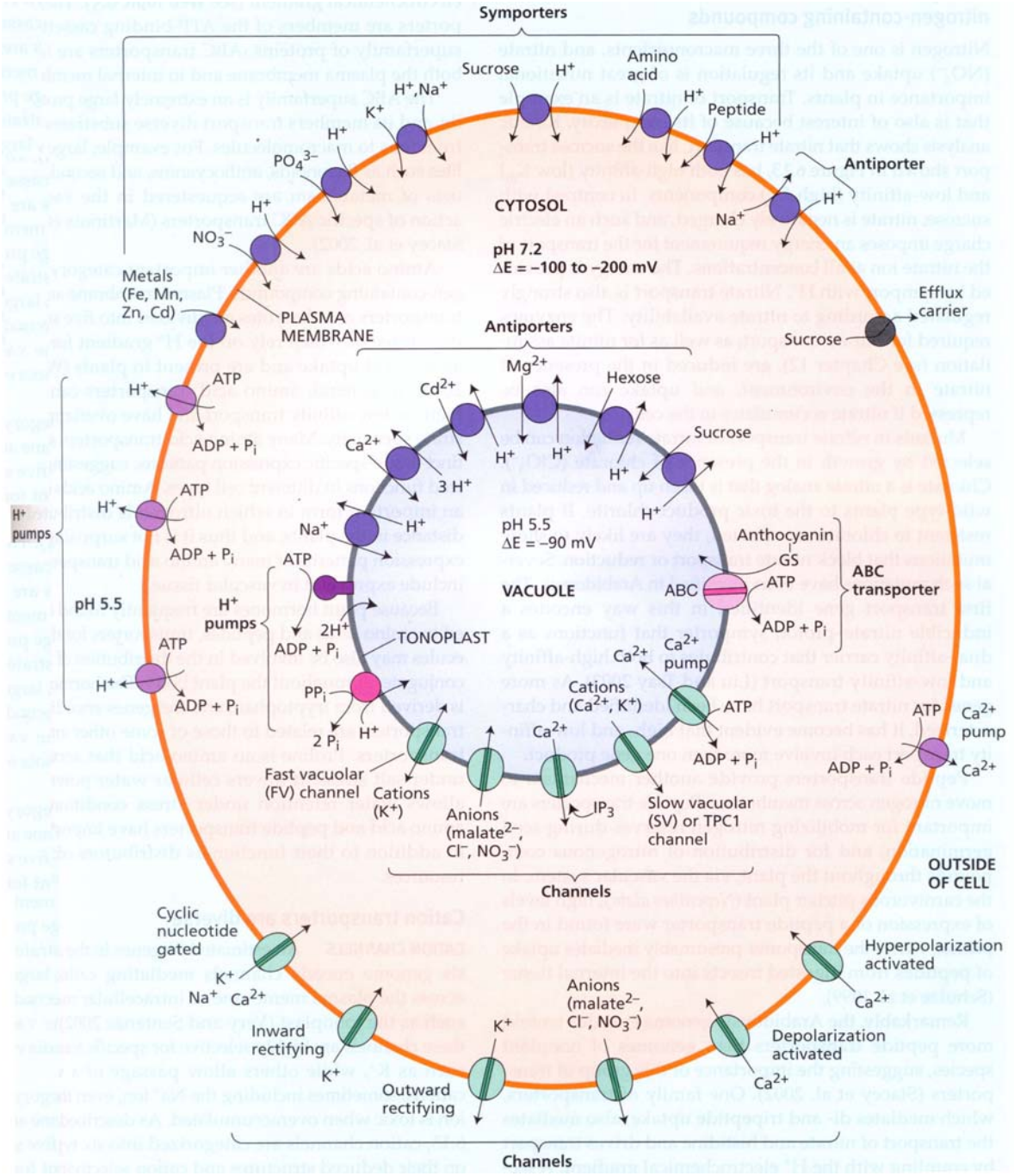

Fig. 2 Transport processes in plant cells

This image shows an overview of the various transport processes mediated by pumps, channels and carriers on the PM and the tonoplast of plants cells. Channels are marked in green, carriers in dark purple and pumps in light purple. The molecular identities of the majority of the proteins mediating the pictured channel activities still need to be identified.
The image was taken from a previous publication (Taiz & Zeiger, 1998).

Ion channels in plant cells play crucial functions not only in the uptake of nutrients from the soil. Modulation of ion channel activity provides a means for rapid signal generation that allows plants to adapt to and overcome abiotic and biotic stresses such as drought, salinity, nutrient deficiency, detoxification of heavy metals and interactions with pathogens and symbiotic organisms. In

general, Ca^{2+}-permeable channels are associated with signal transduction. Cytosolic Ca^{2+} concentrations are tightly controlled in a submicromolar range. Increases in cytosolic Ca^{2+} concentrations transduce environmental stimuli into Ca^{2+}-encoded messages, which in turn modulate K^+- and anion channel activities and/or may alter developmental gene expression. K^+- and anion channel activities in turn effect adjustment of cellular physiology and plant development by participating in the control of membrane voltage and facilitating generation of cell turgor that is important for e.g. tropisms, cell elongation and stomatal aperture control (Uozumi & Schroeder, 2010).

It appears that plant cells use discrete assemblies of co-localised Ca^{2+}/ K^+/ anion channels in a similar way to achieve different goals in different cell types, e.g. cell elongation in growing root hairs or pollen tubes or stomatal aperture control in guard cells. Although most of the available information about these intracellular networks of ion channels is in fact derived from these three model cell types, it appears that related ion channels are found in most other cell types (Ward *et al.*, 2009; Uozumi & Schroeder, 2010).

Stomatal closure, for example, which is achieved by osmotically driven reversible cellular movements of guard cells and serves to regulate the exchange of CO_2 and water with the atmosphere and thereby plant carbon fixation and water status, depends on these networks of ion channel activity in the following way. A rise in the cytoplasmic Ca^{2+} concentration occurs through the activation of PM Ca^{2+} influx channels by upstream signalling events. Increased cytosolic Ca^{2+} in turn signals for and/ or directly effects the activation of anion efflux channels on the PM and K^+ efflux channels on the tonoplast. Anion efflux changes the membrane potential in a way that activates K^+ efflux channels on the PM. This net cellular efflux of K^+ and anions such as Cl^-, and malate causes water efflux and contributes to turgor and volume loss in guard cells that effects stomatal closure (Ward *et al.*, 2009).

It is important to realise that many of the ion channels involved the networks as described for the guard cells are so far only characterized by electrophysiological measurements. Their molecular identities, in particularly those of anion and Ca^{2+} channels, still need to be identified (Ward *et al.*, 2009; Uozumi & Schroeder, 2010).

Plant calcium channels

Electrophysiological analysis of the *Arabidopsis* root hair apical PM has revealed the co-existence of two Ca^{2+} channels that are differentially regulated by changes in the membrane potential (Miedema *et al.*, 2008). Changes in membrane potential that render it more negative are called hyperpolarisation, while changes that render it more positive are called depolarisation. Miedema *et al.*, (2008) discovered in root hair cells hyperpolarisation-activated Ca^{2+}-permeable cation channels (HACCs) and depolarisation-activated Ca^{2+} channels (DACCs) (compare also Fig. 2). HACCs were also characterised via electrophysiological measurements in the PM of stomatal guard cells (Hamilton *et al.*, 2000). The molecular identities of HACCs and DACCs remain unknown so far, probably due to the presence of large gene families with overlapping functions. Candidate genes in

Arabidopsis may be found in a family of 20 cyclic nucleotide–gated (CNG) channel homologs (Kaplan *et al.*, 2007) and/or in a family of 20 genes encoding homologs to animal glutamate receptor channels (Lacombe *et al.*, 2001). Ionotropic glutamate receptors form Ca^{2+}-permeable cation channels in animals and are essential for central nervous system function. So far, *Arabidopsis* GLR1.1, 1.4, 3.4, and 3.7 appear able to translocate Ca^{2+}. Cyclic nucleotide-gated channels (CNGCs) also form Ca^{2+}-permeable cation channels in animals. Studies that analyzed *Arabidopsis* CNGC functions after heterologous expression in yeast indicated that they may encode Ca^{2+}-permeable channels, although this may not apply to all members of the CNGC family (Leng *et al.*, 1999).

Plants also have stretch-activated Ca^{2+} channels, for which the genes and functional mechanisms are barely studied to date. For example, mechanical stimulation of *Arabidopsis* roots causes a rapid rise in the cytoplasmic Ca^{2+} concentration. A recent study identified *Arabidopsis* Mca1, as potential component for a PM mechanosensitive Ca^{2+} channel (Nakagawa *et al.*, 2007). AtMCA1 is thought to have a role in root mechanosensing and growth as a loss-of-function mutant cannot penetrate hard agar (Nakagawa *et al.*, 2007).

In addition to these Ca^{2+} channel activities all found on the PM, land plants also encode one type of voltage-dependent, non-selective cation channel in the vacuolar membrane that can transport Ca^{2+} as well as K^+. This channel has been well characterized and is named TPC1 (Peiter *et al.*, 2005) (see below).

Plant anion/chloride channels

On the PM of plant cells two types of depolarisation activated anion channel conductance co-exist: slow/sustained (S-type) currents and rapid (R-type) currents. R-type anion channels are characterized as rapidly activating with kinetics that are time- and voltage-dependent and that show inactivation. The S-type anion channels exhibit extremely slow voltage-dependent activation and deactivation properties (Uozumi & Schroeder, 2010). Both the S-type and the R-type anion channels allow Cl^- and malate efflux from guard cells (Ward *et al.*, 2009). In addition, many responses in plants, including plant pathogen responses, involve membrane potential depolarization that is caused by anion efflux (Jabs *et al.*, 1997). Recently, a gene named SLAC1 (Slow Anion Channel-Associated 1) was isolated that encodes a PM protein in guard cells (Vahisalu *et al.*, 2008; Negi *et al.*, 2008). Electrophysiological analysis of two *slac1* mutant alleles showed that slow/sustained (S-type) anion channel currents were greatly impaired, whereas the rapid (R-type) anion channels were intact in guard cells. SLAC1 is part of a novel, plant specific anion/Cl^- channel family with five members in *Arabidopsis*. Candidate genes for the R-type anion channels are plant homologs of an animal Cl^- channel family called CLC. Seven homologs of CLC are present in the *Arabidopsis* genome. Research so far indicates that only three *Arabidopsis* CLCs may encode anion channels, whereas most plant CLC transporters may encode H^+/anion carriers (Ward *et al.*, 2009). Other anion channels activities were also identified in guard cells that are permeable to Cl^-, nitrate, sulphate, and malate (Schmidt & Schroeder, 1994). Again, the encoding

genes for these channels activities remain mostly unidentified so far. Electrophysiological analysis of intact vacuoles identified a malate uptake channel activity (see Fig. 2, p. 15). Recently, a knockout mutant plant in a so-called ALMT9 gene was discovered, where this vacuolar malate current is absent (Kovermann *et al.*, 2007). ALMTs are members of a family with 13 members in *Arabidopsis* that are known to function as malate transporters when activated by aluminium ions.

Plant potassium channels

In contrast to Ca^{2+} and anion/ Cl^- channel activities, far more of the proteins that mediate K^+ channel activities are known. According to sequence homologies with animal channels, 57 of the ~70 genes for ion channels identified in the *Arabidopsis* genome potentially encode highly selective K^+ or poorly discriminating cation-selective channels (Very & Sentenac, 2002). The previously mentioned CNG channels that have a C-terminal cyclic nucleotide (cNMP) binding domain and are allosterically activated by cyclic nucleotides, belong to the poorly selective cation channels and are therefore expected to transport K^+ as well as Ca^{2+} (Ward *et al.*, 2009).

Electrophysiological measurements on vacuoles have identified three classes of K^+ transporting cation channel activities that were named SV (Slow Vacuolar), VK (Vacuolar K^+), and FV (Fast Vacuolar) (see also Fig. 2, p. 15). The fast vacuolar (FV) channel is a voltage dependent, low conductance, non-selective cation channel that is inhibited by elevated cytosolic Ca^{2+} concentrations. FV channels were suggested to function as a pathway for K^+ efflux from the vacuole into the cytoplasm during proposed Ca^{2+}-independent stomatal closing. The genes encoding FV channels have not been identified yet (Ward *et al.*, 2009).

SV channels are voltage-dependant, non-selective cation channel as well. In contrast to the FV channel, however, the SV channel is activated by Ca^{2+} and permits large-conductance (Uozumi & Schroeder, 2010). In guard cell vacuoles, SV channels were found to be Ca^{2+}-permeable as well as K^+ permeable, which led to the hypothesis that SV channels participate in Ca^{2+} signalling by releasing Ca^{2+} from the vacuole (Ward *et al.*, 2009). A reverse genetic approach led to the identification of the gene encoding the SV channel in *Arabidopsis*, namely TPC1 (Peiter *et al.*, 2005) (see above). TPC1 is a unique gene in plants, the only homolog of voltage-dependent Ca^{2+} channels in the *Arabidopsis* genome. TPC1 is highly expressed in all tissues. An *Arabidopsis tpc1* knockout mutant was defective in the inhibition of stomatal opening by external Ca^{2+}. This finding is consistent with a function for SV channels in guard cell Ca^{2+} signalling.

In contrast to FV and SV, the Ca^{2+}-activated VK channels are highly K^+ selective channels (Gobert *et al.*, 2007). VK channels were suggested to function as a pathway for vacuolar K^+ release into the cytosol in response to elevated cytosolic Ca^{2+} concentrations during stomatal closure (see above). The protein that mediates VK channel activity was indentified as well. When expressed in yeast, *Arabidopsis* TPK1 (formerly KCO1) mediated vacuolar channel activity consistent with hallmark properties of VK channels (Bihler *et al.*, 2005). *Arabidopsis* mutants disrupted in TPK1 lacked detectable VK channel activity and exhibited slower stomatal closing in response to the phytohormon ABA. TPK1 is a member of the two-pore-domain K^+ channel superfamily with five

members in *Arabidopsis*. Two EF-hand Ca^{2+} binding domains in the C-terminus of TPK1 indicate that Ca^{2+} binds and activates the channel directly (Gobert *et al.*, 2007).

The *Arabidopsis* genome further encodes one homolog of a superfamily of KcsA-type channels, which are the most rudimentary of the highly selective K^+ channels and consist of just two transmembrane domains and one pore per subunit. The function of this homolog, named Kir1 (formerly KCO3), in *Arabidopsis* remains to be investigated (Ward *et al.*, 2009).

The third of the superfamilies of highly selective K^+ channels that have homologs in *Arabidopsis* are the Shaker channels, so named after the first member of this family cloned in *Drosophila.*

The family of *Arabidopsis* Shaker channels

As mentioned earlier, all ion channels provide an ion-conducting pore in the hydrophobic environment of the lipid bilayer. In the fully assembled channel complex, the pore is shielded from the lipid bilayer by the surrounding protein. TPK, Kir- and Shaker channels share a highly conserved K^+ selectivity filter in form of the hallmark motif TxGYGD. This motif is part of the ion-conducting pore (P). The pore region in Shaker channels is present between the 5^{th} and 6^{th} transmembrane spanning domain (TMD), designated S1-S6 (Fig. 3A). In this pore region a short α-helical stretch (the pore helix) is followed by the selectivity filter for K^+. The picture in Fig. 3A shows a typical Shaker channel α-subunit with six TMDs, cytoplasmic N- and C-terminus and P region.

Shakers channels are multimeric proteins that reside in the plasma membrane (PM) (Very & Sentenac, 2002). In a functional Shaker channel, the K^+ conducting pathway across the lipid bilayer is formed from the assembled P regions of four α-subunits. Fig. 3B shows the crystal structure of the mammalian Shaker channel Kv1.2 (top view) with the four α-subunits in different colours (Long *et al.*, 2005). The S1-S4 domains of each α-subunit are positioned adjacent to the S5 and S6 of the neighbouring subunit. The black dot in the middle represents a K ion in the pore. Although no crystal structure has been obtained for a plant Shaker channel yet, it is assumed based on sequence homology and biochemical investigations that in plants four α-subunits also form a functional channel (Dreyer *et al.*, 1997; Urbach *et al.*, 2000).

In *Arabidopsis*, nine different Shaker channel α-subunits are present: KC1, AKT1, AKT2, AKT5, AKT6, KAT1, KAT2, GORK and SKOR (Fig. 3C). Most of the α-subunits form channels that are strongly voltage sensitive, i.e. their K^+ conducting properties change in response to changes in membrane potential (relative conductance). Membrane potential is the difference in voltage between the interior and exterior of a cell. It is the result of asymmetric ion distribution between the inside and the outside of the PM. Within each subunit, S1-S4 form a voltage sensor complex that is offset roughly 90° radially around the tetrameric channel complex. The S4 TMD of each α-subunit contains conserved basic amino acid residues (arginine or lysine) which allow it to act as a sensor for the membrane voltage (Fig. 3A). The movement of these four voltage sensor complex in

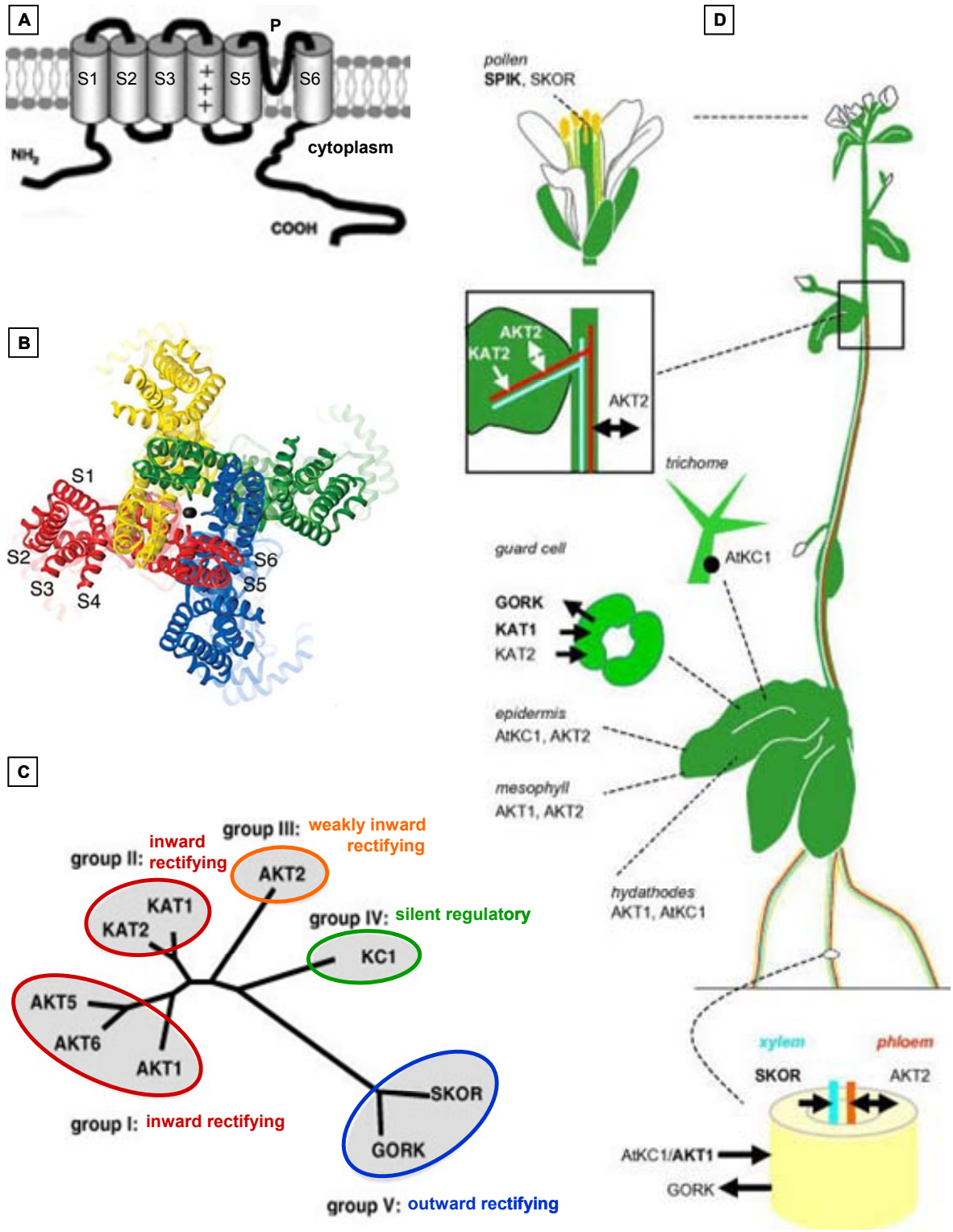

Fig. 3 The family of *Arabidopsis* Shaker channels

(A) A Shaker channel α-subunit with six transmembrane domains (S1-S6), cytoplasmic N- and C-terminus, voltage sensor in S4 and pore domain (P).
(B) Crystal structure (top view) of the mammalian Shaker channel Kv1.2 with the four α-subunits in different colours.
(C) Phylogenetic tree of *Arabidopsis* Shaker channel α-subunits distinguishes five groups: Group I and group II form inward rectifying channels, group III contains one channel with weak inward rectifying properties, group IV contains one regulatory subunit and group V members form outward rectifying channels.
(D) Expression patterns of the nine *Arabidopsis* Shaker channel α-subunits.
Images were adapted from previous publications (Very & Sentenac, 2002) (A), (Long *et al.*, 2005) (B), (Lebaudy *et al.*, 2008) (C, D).

response to changes in membrane potential are thought to result in conformational changes in the assembled channel protein, leading to either opening or closing of the aqueous K^+ conducting pore.

Electrophysiological measurements revealed that in most plant tissues and cell types (e.g. root cortex, root hairs, xylem parenchyma, guard cells, mesophyll cells) a voltage-gated highly selective K^+ conductance dominates the PM permeability to K^+ upon membrane hyperpolarisation or depolarization at millimolar external K^+ concentrations (Roberts & Tester, 1995; Lebaudy *et al.*, 2007). Membrane hyperpolarisation that renders the membrane potential more negative, activates inward K^+ conductance, i.e. the influx of K^+ (inward rectifier). In contrast, outward rectifying K^+ currents, i.e. K^+ efflux, are activated by membrane depolarization that shifts the membrane potential to more positive values. In addition, voltage-insensitive or weakly sensitive background conductance has been shown to be active at the PM in some cell types, i.e. mesophyll cells and is thought to contribute along with the inward and outward-rectifying K^+ conductance to the overall membrane permeability to K^+ (Very & Sentenac, 2002). It is assumed that in most tissues, the inward and outward-rectifying K^+ conductance are carried by Shaker channels (Very & Sentenac, 2003). When individually expressed in heterologous systems, five of the nine *Arabidopsis* Shaker family members are involved in the formation of hyperpolarisation activated channels, i.e. mediate K^+ influx: AKT1, AKT5, AKT6, KAT1, KAT2 (Very & Sentenac, 2002). Based on the analysis of amino acid (aa) sequence similarities, these five inward rectifying K^+ channels fall into two separate phylogenetic groups; group I and II (Fig. 3C). Group III contains only AKT2 that gives rise to weakly inwardly-rectifying currents (Lacombe *et al.*, 2000). Subunits that form depolarization activated channels i.e. mediate K^+ efflux belong to group V: SKOR, GORK. A special case is the so-called regulatory subunit of inward K^+ channels (KC1) found in group IV. KC1 does not form functional channels on its own but is thought to be involved in the formation of heteromeric channels with the other inward but not outward rectifying Shaker α-subunits (Dreyer *et al.*, 1997).

The assembly of heteromeric channels was initially observed after expression in heterologous systems. New types of conductance, displaying unique features, not yet associated to any α-subunit when individually expressed, were observed upon co-expression of different α-subunits in *Xenopus* oocytes (Dreyer *et al.*, 1997; Cherel, 2004). In general, heteromerisation is thought to give rise to increased diversity in channel functional properties and regulation processes.

Fig. 3D shows the expression patterns of the nine *Arabidopsis* Shaker channel α-subunits, taken from a review by Lebaudy *et al.* (2008). The outward rectifying channel SKOR, which is expressed in pericycle and xylem parenchyma, was shown to contribute to about 50 % of K^+ secretion into the xylem sap for translocation to the shoot (Gaymard *et al.*, 1998). With regard to phloem K^+ transport, *GUS* reporter gene analyses showed *AKT2* expression in the phloem vasculature of both leaves and roots. The current hypothesis states that AKT2 plays a role in both K^+ loading in source leaves and K^+ unloading in sink organs such as roots. AKT2 thus controls the phloem membrane potential in a way that favours sugar loading in source leaves.

KAT2 is expressed in the phloem vasculature of the leaf specifically (Pilot *et al.*, 2001). When expressed alone, KAT2 α-subunits form inwardly-rectifying channels, suggesting a role in

K^+ loading in source leaves. However, recent heterologous expression experiments indicated that AKT2 and KAT2 subunits preferentially form heteromeric channels with weak inward rectification properties, a feature inherited from the AKT2 subunit. SPIK has been shown to mediate growth sustaining K^+ influx into the growing pollen tube (Mouline *et al.*, 2002). Also in guard cells, Shaker K^+ channels dominate the PM conductance. GORK mediates most of the K^+ efflux during stomatal closure as shown by the impaired response to darkness or ABA after disruption of the GORK gene (Hosy *et al.*, 2003). With regard to the inward K^+ conductance that plays a role during stomatal opening, quantitative RT-PCR experiments indicated that *Arabidopsis* guard cells express at least five genes coding for Shaker α-subunits (*KAT1*, *KAT2*, *AKT1*, *AKT2* and *KC1*), of which *KAT1* transcripts levels were by far the most abundant (Szyroki *et al.*, 2001).

Early attempts to determine the electrophysiological activity of KC1 Shaker channels in *Xenopus oocytes* had failed, leading to the hypothesis that KC1 is a silent α-subunit, unable to form functional homotetrameric channels (Dreyer *et al.*, 1997). When other plant α-subunit of the inward rectifying type (Group I and II, see above, Fig. 3D) with known functional characteristics (e.g. KAT1) were co-expressed with KC1 in animal expression systems, their activity appeared to be altered, suggesting that they interacted with KC1 and formed heterotetrameric channels endowed with novel properties (Dreyer *et al.*, 1997). KC1 is expressed in root peripheral tissues including root hairs, along with the inward rectifying Shaker AKT1 (Lagarde *et al.*, 1996; Reintanz *et al.*, 2002). Electrophysiological experiments on *Arabidopsis* root hairs provided further support to the hypothesis that KC1 forms heteromeric channels (Reintanz *et al.*, 2002). Comparison of inward voltage-dependent current recorded in root hair protoplasts of wild type (wt), *kc1*- and *akt1*- knock-out plants suggested that KC1 contributed to K^+ influx in the wt plants, probably in association with AKT1 within heteromeric channels (Reintanz *et al.*, 2002). Heteromerization between KC1 and AKT was also observed when those α-subunit were heterologously expressed in a plant expression system (tobacco protoplasts) (Duby *et al.*, 2008). Here, the heteromeric channels displayed displaying unique features, in particular a channel activation at more negative membrane potential (about −50 mV) when compared with AKT1 homomeric channels (Duby *et al.*, 2008; Geiger *et al.*, 2009). It was speculate that this shift in activation threshold towards more negative values prevents AKT1 from mediating K^+ efflux at low external K^+ concentrations (Geiger *et al.*, 2009). Duby *et al.* (2008) further suggested that KC1 α-subunits are unable to leave the ER unless co-assembled with an inward rectifying α-subunit. Finally, KC1 was not regulated on the transcript level by K^+ starvation or phytohormones but showed a strong increase in gene expression in leaf peripheral tissues upon salt stress (Pilot *et al.*, 2003a).

Shaker channels in K^+ uptake from the soil

K^+ is an essential macronutrient for all living organisms, including plants, to complete their life cycles. It is the most abundant cation in the cytosol and can comprise up to 10 % of the total plant dry weight (Marschner, 1995). K^+ is involved in a number of vital functions in metabolism, growth and stress adaptation. These functions can be classified into those that rely on high and relatively

stable concentrations of K^+ and those that rely on K^+ movement (Amtmann *et al.*, 2006).

Stable K^+ concentrations of about 100- 200 mM represent the optimal range for activation of the large number of K^+ dependent enzyme in metabolically active compartments such as cytoplasm, nucleus, stroma of chloroplasts and matrix of mitochondria (Gobert *et al.*, 2006). In addition, K^+ stabilises the pH between 7 and 8 in cytosol and chloroplast, which is the optimum for most enzyme reactions (Marschner, 1995). Due to its high concentration in the cytosol and chloroplast K^+ also neutralizes negative charges on proteins and other soluble (e.g. organic acid anions) and insoluble macromolecular anions.

K^+ movement over membranes (uptake or efflux) is the usual way through which cells control their membrane potential and osmotic potential. The uptake of K^+ by plant cells, and its accumulation in vacuoles, drives their osmotic expansion. Rapid cell expansion relies on high mobility of the active osmoticum and, for this reason, only a few other inorganic ions can replace K^+ in this role (Amtmann *et al.*, 2006). Thus, in addition to the functions in pollen tube growth and stomatal opening mentioned above, the accumulation of K^+ is essential for the growth of the root system, both for cell expansion in the elongation zone and for the elongation of root hair cells.

Potassium uptake by roots and accumulation by plants are determined by the K^+ uptake capacity of the roots and the K^+ concentration gradient between the rhizosphere and the soil solution. Other factors influencing K^+ acquisition include the release of non-exchangeable K^+ by root exudates, which increases K^+ concentration and availability in the soil solution and the transpiration rate of the plant, which drives mass flow of the soil solution to the root (Rengel & Damon, 2008).

In *Arabidopsis* roots, two major groups of K^+ uptake systems exist: carriers (see above, Fig. 1, p. 13) and channels. The main K^+ channel involved in K^+ nutrition of *Arabidopsis* is AKT1 (Hirsch *et al.*, 1998; Spalding *et al.*, 1999; Rubio *et al.*, 2010). As mentioned above, KC1 is thought to be a regulatory subunit for AKT1 in root hairs (Reintanz *et al.*, 2002; Pilot *et al.*, 2003a; Duby *et al.*, 2008; Geiger *et al.*, 2009). HAK5, a carrier (transporter) from the KT/KUP/HAK family is highly expressed in the root epidermal cells (including root hairs) as well (Gierth *et al.*, 2005; Qi *et al.*, 2008; Rubio *et al.*, 2008). The KUP/HAK/KT family comprises 13 members in *Arabidopsis*. Many of these proteins have been shown to mediate K^+ transport or to be involved in K^+-dependent growth processes and at least four members are expressed in roots (Rigas *et al.*, 2001). In principle, root K^+ influx can also be mediated by less selective cation/H^+ symporters (CHXs), e.g. *At*CHX13 (Zhao *et al.*, 2008) or other K^+ transporters such as TRH1/AtKT3 (Rigas *et al.*, 2001; Desbrosses *et al.*, 2003). The variability of K^+ concentrations in the soil solutions in time and space induce in plant roots K^+ uptake systems with different capacities to secure K^+ acquisition. Classical studies on barley roots had described two major uptake components operating primarily at low (<1 mM) or high (>1 mM) external K^+ concentrations, termed mechanism I (high-affinity transport system) and mechanism II (low-affinity transport system) (Epstein *et al.*, 1963). However, it is not the “affinity” for K^+ that differentiates K^+ transport mechanisms in the root PM, but their coupling to pH and voltage gradients (Karley & White, 2009). Electrophysiological studies indicate that K^+ influx across the PM of root cells occurs against its electrochemical gradient at rhizosphere

concentrations less than about 1 mM K^+ (Walker *et al.*, 1996). This can be catalysed by H^+/K^+ symporters such as HAK5 and is energized by the pH and voltage gradients generated by the PM H^+-ATPase, which are capable of accumulating K^+ from rhizosphere solutions containing less than 0.1 mM K^+. The solution K^+ concentration (i.e. freely available K^+) in most soils lies between 0.1 and 1 mM (Rengel & Damon, 2008).

At rhizosphere K^+ concentrations above 1 mM, which are common in well-fertilised agricultural soils, K^+ influx to root cells can be energised by the voltage gradient alone and facilitated by K^+ channels such as AKT1. Thus, it was initially proposed that 'high-affinity' K^+ uptake is mediated by transporters (e.g. HAK5) and 'low-affinity' K^+ uptake is mediated by channels (e.g. AKT1) (Maathuis & Sanders, 1992).

However, studies with single and double T-DNA insertion lines showed that in *Arabidopsis* both systems, HAK5 and AKT1, participate in the high-affinity range of concentrations and AKT1 together with unknown systems participate in the low-affinity range (Hirsch *et al.*, 1998; Spalding *et al.*, 1999; Gierth *et al.*, 2005; Rodriguez-Navarro & Rubio, 2006; Gierth & Maser, 2007; Nieves-Cordones *et al.*, 2007; Rubio *et al.*, 2008; Nieves-Cordones *et al.*, 2010; Pyo *et al.*, 2010; Rubio *et al.*, 2010). Rubio *et al.* (2010) summarised the current knowledge about the contributions of the three systems to K^+ uptake at a range of K^+ concentrations in the scheme pictured below in Fig. 4.

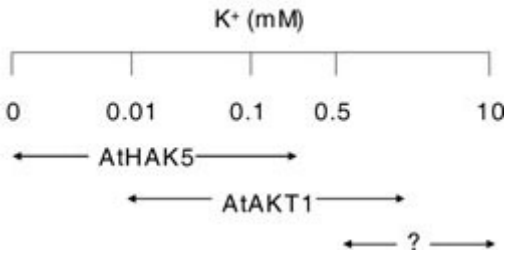

Fig. 4 Potassium uptake systems in *Arabidopsis* roots

This model shows the contributions of different root K^+ uptake systems to K^+ nutrition at varying external K^+ concentrations. The image was taken from a previous publication (Rubio *et al.*, 2010).

HAK5 is the only system mediating K+ uptake at concentrations below 0.01 mM. In the range between 0.01 and 0.05 mM K^+ HAK5 and AKT1 are the only contributors to K^+ acquisition. At higher K^+ concentrations, unknown systems come into operation and participate together with AKT1 in low-affinity K^+ uptake. Thus, AKT1 can adjust its apparent affinity for K^+ from the low-affinity to the high-affinity range. HAK5 and the unknown system can supply sufficient K^+ to promote plant growth even in the absence of AKT1 or in the presence of 10 mM K^+ where AKT1 is not essential. Candidates for these unknown systems are members of the cyclic nucleotide-gated channels (Kaplan *et al.*, 2007; Chin *et al.*, 2009).

When plants are exposed to low K^+ conditions, a number of physiological adaptations are necessary, because K^+ has so many vital functions (see above). Adaptations to low K^+ supply include the replacement of vacuolar K^+ with alternative osmotica, redistribution of K^+ from mature to developing tissues, and reducing plant growth to maintain appropriate tissue K^+ concentrations

for cell function. However, in contrast to nitrogen and phosphate deficiencies, K^+ deprivation does not generally result in greater biomass partitioning to roots or major alterations to root architecture (exceptions are root hairs, see below) (Hermans *et al.*, 2006). In consequence, plants experiencing severe K^+ deficiency exhibit slow growth, poorly-developed root systems, decreased turgor, impaired stomatal regulation and reduced transpiration, decreased water content, impaired phloem transport (particularly of sucrose) and a reduction in chlorophyll concentrations (Amtmann *et al.*, 2008).

It was suggested that K^+ channels such as AKT1 are the immediate targets for regulating K^+ fluxes, e.g. in response to fluctuations in apoplastic K^+ concentration and the membrane potential of root cells. Transporters such as HAK5 contribute to an increase in K^+ uptake by roots over a period of hours to days (Amtmann *et al.*, 2006). This is supported by the observation that AKT1 is regulated on the post-translational level (see below) by K^+ deprivation, but not on the transcript level (Lagarde *et al.*, 1996). In contrast, K^+ deprivation is a common inductor in the gene expression of the high-affinity H^+/K^+ symporters, such as HAK5 (Qi *et al.*, 2008). Also *CHX13* gene expression was up-regulated in roots in response to K^+ deprivation (Zhao *et al.*, 2008).

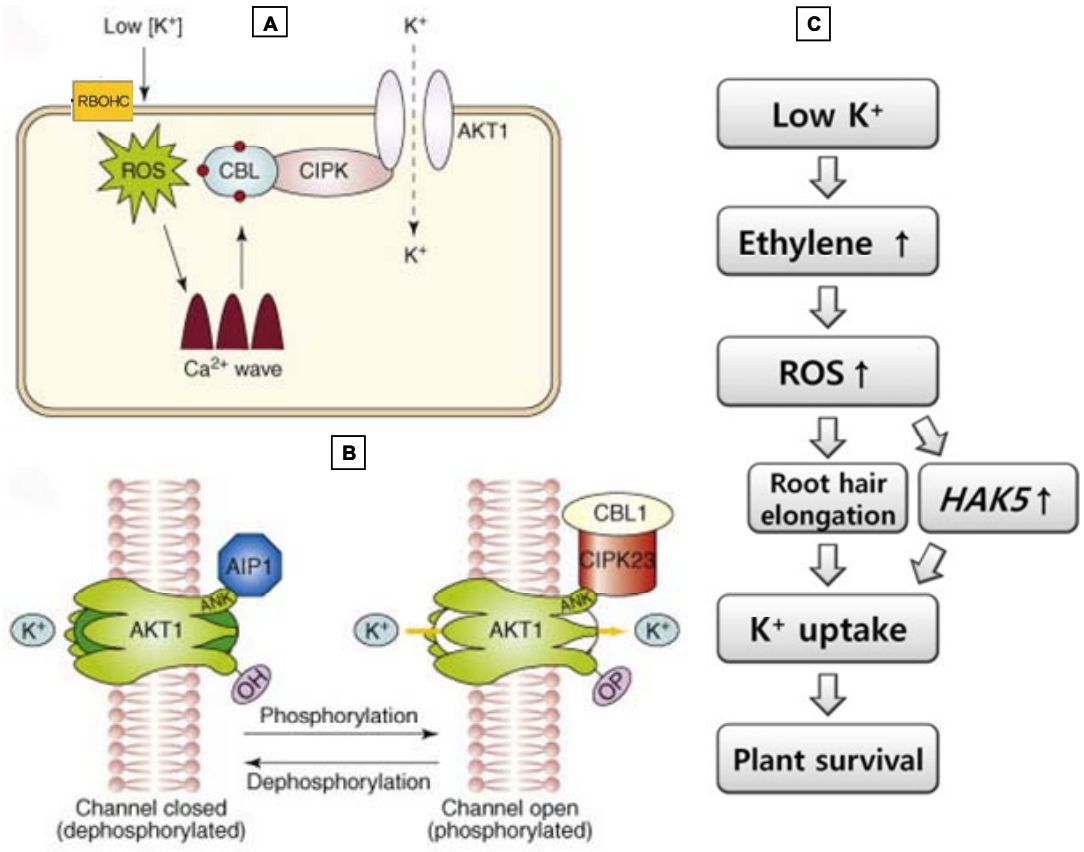

Fig. 5 A model for intracellular signalling during *Arabidopsis* low K^+ response

(A, B) Low K^+ growth conditions trigger increased levels of reactive oxygen species (ROS), which induces cytoplasmic Ca^{2+} fluctuations. Ca^{2+} binding to CBL activates this Ca^{2+} sensor and leads to CBL–CIPK complex formation and targeting of the complex to the PM. The CIPK23 kinase domain physically interacts with the C-terminus of AKT1, phosphorylates it and activates the channel, resulting in K^+ uptake into the cell. Inactivation of AKT1 by dephosphorylation might be achieved with the PP2C-type phosphatase AIP1.
(C) The activation of ethylene signalling by K^+ deprivation positively regulates ROS production in roots. ROS stimulates root hair elongation and *HAK5* expression.
Images were adapted from previous publications (Luan, 2009) (A, B) and (Jung *et al.*, 2009) (C).

How plants sense and transduce the stress signals initiated by K^+ deprivation is poorly understood. It was known for a long time that culturing plants under conditions of low rhizosphere K^+ concentrations enhances the K^+ uptake capacity of roots (Ashley *et al.*, 2006). Two different groups simultaneously discovered a dependence of AKT1 activity on Ca^{2+} mediated phosphorylation (Li *et al.*, 2006; Xu *et al.*, 2006). From their results, a model for intracellular signalling events was developed that connects for the first time a 'low K^+ condition' signal (for which the receptor is still unknown) with the observed enhanced K^+ uptake. It is thought that in *Arabidopsis* low external K^+ causes PM hyperpolarisation (shift to more negative membrane potential) and initiates the production of reactive oxygen species (ROS) through the activity of the NADPH oxidase, RBOHC (Fig. 5A). These events increase Ca^{2+} influx through hyperpolarisation-activated Ca^{2+} channels in the PM. The rise in the cytoplasmic Ca^{2+} concentration causes the Ca^{2+}-sensor protein calcineurin B-like (CBL) protein CBL1 (and/or CBL9) to bind Ca^{2+} (Fig. 5A). The activated CBL1 then activates in turn the CBL-interacting protein kinase CIPK23 and recruits it to the PM via complex formation (Fig. 5A) (Xu *et al.*, 2006; Cheong *et al.*, 2007). CBLs have conserved myristoylation and palmytoylation sites. The CIPK23 kinase domain is thought to physically interact with an ankyrin domain in the C-terminus of AKT1 (Fig. 5B). Subsequent phosphorylation of AKT1 at its C-terminus activates the channel and results in K^+ uptake into the cell (Li *et al.*, 2006; Xu *et al.*, 2006; Lee *et al.*, 2007). CIPK23 exclusively interacts with AKT1 but not KC1 or other K^+ transporters from *Arabidopsis* (Lee *et al.*, 2007). Dependence of AKT1 activation on phosphorylation via the CBL1/CIPK23 complex was demonstrated through heterologous expression in *Xenopus leavis* oocytes, where AKT1 channel is electrically silent when expressed alone. Co-expression with CBL1 (or CBL9) and CIPK23 allowed the recording of typical Shaker inward-rectifying currents under voltage clamp (Li *et al.*, 2006; Xu *et al.*, 2006). *In planta* evidence was obtained from patch-clamp studies of *cipk23* mutant and *cbl1/cbl9* double mutant root hairs that showed significant reduction of AKT1 dominated inward currents (Cheong *et al.*, 2007; Lee *et al.*, 2007). In agreement with this observation, CIPK23 had been identified from a genetic screen for mutants sensitive to low K^+ conditions (Li *et al.*, 2006; Xu *et al.*, 2006). While *cbl1* and *cbl9* single mutants did not display a deficiency phenotype under low K^+ conditions, cbl1/cbl9 double mutants were as sensitive as *akt1* and *cipk23* mutants, indicating a co-operative function of CBL1 and CBL9 in AKT1 activation *in planta* (Xu *et al.*, 2006; Cheong *et al.*, 2007).

In addition, the PP2C-type phosphatase AIP1 has been shown to specifically bind to AKT1 and inhibit K^+ transport in oocytes by dephosphorylation of the channel. Thus, K^+ uptake via AKT1 is potentially regulated by alternating changes in the AKT1 phosphorylation status (Fig. 5B) (Lee *et al.*, 2007).

In addition to these immediate effects of hyperpolarisation on AKT1 in response to low rhizosphere K^+ concentrations, transcriptional responses to K^+ deprivation (e.g. up-regulation of HAK5) are initiated by the prolonged hyperpolarisation of root cells as well (Nieves-Cordones *et al.*, 2008).

Recently another component was added to the 'low K^+' signalling cascade that addresses the more long-term changes in response to K^+ deprivation (Jung *et al.*, 2009). They were able to

show that ethylene acts upstream of ROS in response to low K^+, i.e. stimulated production of ROS (Fig. 5C). Both ethylene production and the transcription of genes involved in ethylene biosynthesis increased when plants were deprived of K^+. ROS in turn stimulated root hair elongation and HAK5 expression (Fig. 5C).

Other genes regulated in response to K^+ deprivation in *Arabidopsis* are the outward rectifier SKOR, which is thought to load K^+ into the xylem (see above), and AKT2, an inward rectifier responsible for the recirculation of K^+ from the shoot to the root (see above). Both genes were down-regulated by low K^+ availability (Schachtman & Shin, 2007a). These measures are thought to maintain the cytoplasmic K^+ concentration of root cells and to restrict long-distance K^+ transport. The magnitude of the K^+ flux re-circulated from the shoots to the roots might act as a signal of plant K^+ status and thus also regulate root K^+ uptake (Lebaudy *et al.*, 2007). Other K^+ deficiency symptoms (see above) appear to arise as secondary consequences of impaired energy metabolism, redistribution of solutes within the plant and/or reduced growth.

Intracellular trafficking of Shaker channels

Co-translational insertion into the ER

KC1, KAT1 and AKT1 are PM proteins and as such are thought to follow the traditional secretory pathway to reach their target membrane (Bassham *et al.*, 2008). The secretory pathway (Fig. 6A) begins with the co-translational translocation of proteins into the endoplasmic reticulum (ER) (Fig. 6B) (Cross *et al.*, 2009). This process, that couples protein synthesis to membrane translocation, is enabled by the so-called signal recognition particle (SRP). This chaperone recognizes and binds signal sequences that lack a precise sequence arrangement but are hydrophobic in nature (see below) on the N-terminus of the nascent polypeptide as soon as it emerges from the ribosome. During the binding event, SRP undergoes substantial structural rearrangements that allow its GTPase domain to be loaded with GTP. Translation stops until the entire ribosome–nascent chain–SRP targeting complex is recruited to the ER membrane by interaction with a dedicated SRP receptor (SR). SR is in a similar GTP-bound state and reciprocal GTP hydrolysis between the GTPase domains in both proteins triggers conformational rearrangements in the complex. As a result, the ribosome with the nascent chain docks onto the ER protein translocation channel, the so-called translocon, in a transfer step. The signal sequence is released from SRP and inserted into the translocon. In mammalians the signal sequence interacts with the Sec61α-subunit of the core translocon that is comprised of a heterotrimeric αβγ Sec61 complex. Subsequently, protein synthesis resumes. The targeting complex is disassembled to free SRP and its receptor for another round of delivery.

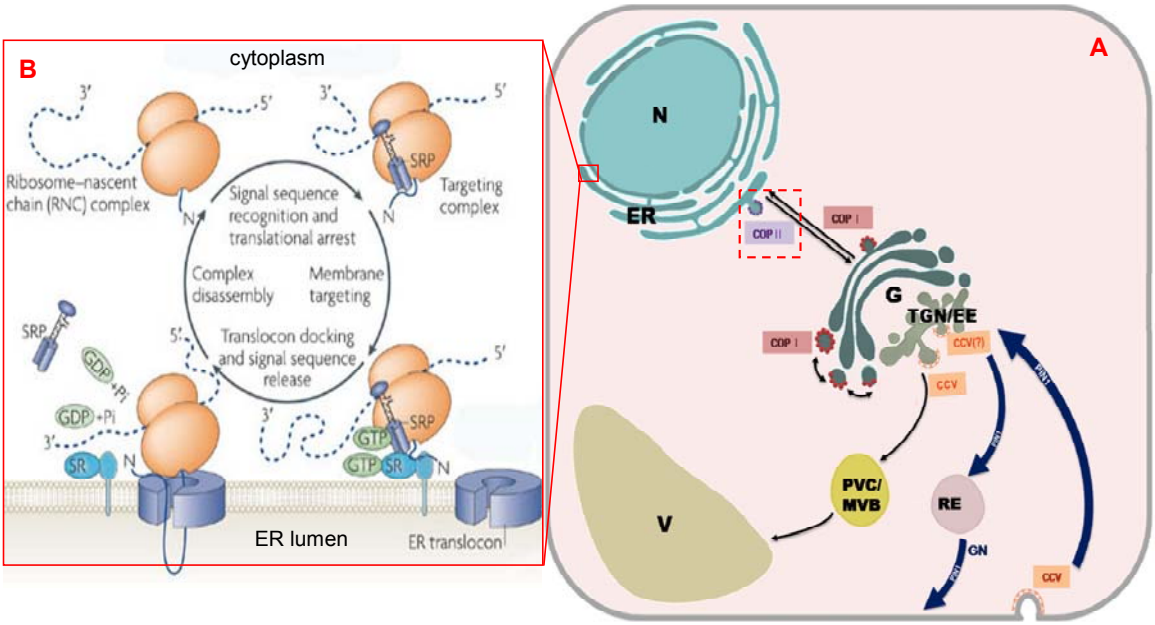

Fig. 6 The secretory pathway and co-translational insertion into the ER

(A): Anterograde trafficking pathway for secretory proteins in plant cells. N, nucleus; ER, endoplasmatic reticulum; G, Golgi apparatus; TGN/EE, trans-Golgi network/ early endosome; V, vacuole; PVC/MVB, prevacuolar compartment/ multivesicular body; RE, recycling endosome; CCV, clathrin-coated vesicles, COPII, coat protein complex II vesicles; COPI, coat protein complex I vesicles; GN, GNOM
(B): Co-translational protein insertion into the ER; explanations see text.
Images were adapted from previous publications (Cross *et al.*, 2009; Hwang & Robinson, 2009).

Based on hydropathy plots the members of the plant Shaker channel family were predicted to be polytopic membrane proteins with 6 TMDs and cytoplasmic N-and C-termini (Anderson *et al.*, 1992), consistent with the model for their animal counterparts (Shih & Goldin, 1997). For KAT1, *in vitro* studies that investigated the translocation mechanism confirmed this topology in ER membranes (Sato *et al.*, 2002; Sato *et al.*, 2003). Sato *et al.* (2002; 2003) analyzed individual and combined KAT1 TMDs for their preference of orientation and coordinated membrane insertion. The authors made use of peptides that were obtained by *in vitro* translation in the presence of mammalian ER preparations. These peptides were designed to be either unmodified or a fusion to an N-glycosylation acceptor sequence. Membrane orientation was determined by glycosylation indicating presence in the lumen of such ER membrane vesicles or digest with proteinase K that could reach only domains facing the external medium, i.e. the equivalent to the cytoplasm in a cellular environment. As seen in C, the first TMD (S1) was found to possess a type II signal-anchor sequence (SA-II). Signal-anchor sequences (type I or type II, i.e. SA-I and SA-II, respectively) are one type of ER targeting signals that are recognized by the SRP as soon as they emerge from the ribosome during co-translational translocation (see above). They differ from signal peptides (SP), the other type of ER targeting signals, in several features. While SPs are N-terminal extensions that are cleaved off the translocated preprotein (membrane and soluble proteins) by membrane-bound enzymes called signal peptidases during maturation in the ER, the SA sequences are internally positioned and remain uncleaved (Kida *et al.*, 2005). SP are made of 7-14 predominantly apolar residues, while SA sequences consist of three distinct regions: a central hydrophobic region (H-

region) that is flanked by a N-terminal hydrophilic region and a C-terminal polar region (Kida *et al.*, 2000). The H-region is with 17–27 apolar amino acid (aa) residues longer than the SP, since it will form the later transmembrane α-helix. However, initially, both SP and the H-region of SA-II fulfil the same function of anchoring the nascent polypeptide chain in the translocon with the N-terminus of the nascent polypeptide facing the cytoplasmic side (Fig. 7).

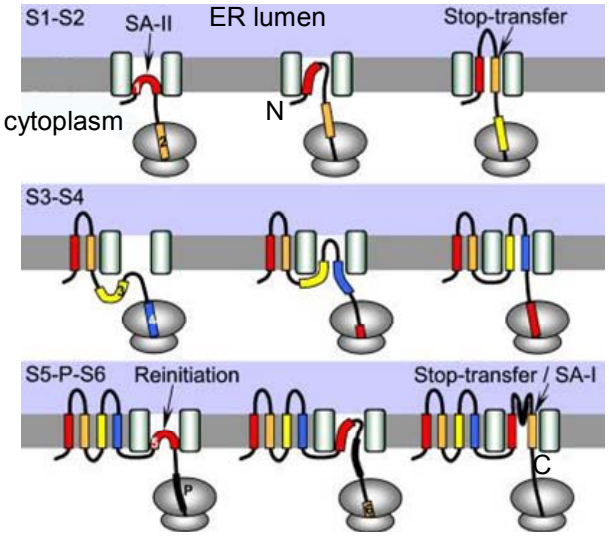

Fig. 7 Co-translational insertion of KAT1 into the ER membrane

Co-translational insertion of KAT1 into the ER membrane is determined by signal-anchor (SA) sequences and stop-transfer signals; S, transmembrane domain; P, pore domain; N, hydrophilic N-terminus of KAT1; C, hydrophilic C-terminus of KAT1; explanations see text.
The image was adapted from a previous publication (Sato *et al.*, 2002).

Signal-anchor sequences (type I or type II, i.e. SA-I and SA-II, respectively) are one type of ER targeting signals that are recognized by the SRP as soon as they emerge from the ribosome. Translation resumes and the ongoing protein elongation is thought to push the polypeptide portion downstream (C-terminal) of the SA-II sequence through the translocon tunnel into the ER lumen (Kida *et al.*, 2005). Thus, the resulting topology is $N_{cytosol}$-$C_{ER\text{-}luminal}$ with the hydrophilic N-terminus in the cytoplasm and the hydrophilic C-terminus in the ER lumen. Single-spanning as well as multi-spanning membrane proteins, where the first TMD adopts this orientation are called Type II membrane proteins. The converse membrane topology ($N_{ER\text{-}luminal}$-$C_{cytosol}$) is derived from SA-I sequences in the first TMD that engage with the translocon in the opposite orientation and lead to Type III membrane proteins.

The nascent polypeptide chain of KAT1 is translocated into the ER lumen until a hydrophobic signal sequence encoded in the future second TMD (S2) emerges from the ribosome. This category of topogenic signal sequences is termed stop-transfer (St) sequence. It comprises only a H-region and functions in preventing further extrusion of the nascent chain into the ER lumen, so that the C-terminus of the preprotein remains in the cytoplasm (Sato *et al.*, 2002; Sato *et al.*, 2003). Thus, after synthesis of S1 and S2, both ends of the nascent chain are in the cytosol and a loop faces the ER lumen. Owing to their hydrophobic properties, the two TMDs of this α-helical hairpin then passively partition in a lateral move through the proteins that line the side of the

translocon into the ER bilayer, where they anchor the nascent polypeptide chain while it's C-terminus continues to grow in the cytosol (Fig. 7).

Sato *et al.* (2002; 2003) observed that, in contrast to the classical 'linear insertion' model for polytopic membrane proteins (Goder & Spiess, 2001), S3 and S4 failed to integrate sequentially into the membrane. According to this model, the most N-terminal signal sequence defines its own orientation as well as the orientations of all subsequent transmembrane segments that should act alternately as internal SA sequence for reinsertion (odd numbered TMDs, e.g. S3) or as stop-transfer sequences (even numbered TMDs, e.g. S4). However, in case of KAT1, neither S3 nor S4 possessed any topogenic functions. Translocation for these two TMDs was only successful as a hairpin unit in a posttranslational fashion. Sato *et al.* (2002; 2003) suggested that conserved charged residues of the Shaker family, namely the negatively charged aspartic acid residue located in the middle of S3 and several positively charged arginine residues of S4 which serve as a voltage sensor (see above, p. 13) prevented translocation, since conversion of the aspartic acid to an uncharged valine conferred membrane integration for S3 expressed on its own (Sato *et al.*, 2002; Sato *et al.*, 2003). Thus, specific interactions between S3 and S4, established prior to translocation, serve to mask both charges. Similarly, Sato *et al.* (2002; 2003) suggested that intramolecular interactions between positive arginine residues in S4 and negative aspartic acids in S2 may contribute to the retention of S4 in the membrane despite its lack of St function. KAT1 S5 had the expected ability of translocation reinitiation, and S6 exhibited a strong SA-I sequence combined with a St function resulting in a cytoplasmic localisation for the C-terminus of KAT1 (see Fig. 7). The pore region between S5 and S6 was found to reside in the ER lumen (Sato *et al.*, 2002).

In contrast to an SA-II sequence, a SA-I sequence mediates the translocation of its preceding region through the ER membrane. Thus, translocation cannot be driven by polypeptide chain elongation. It was recently suggested that instead, the SA sequence itself initially provides the motive force for N-terminal domain translocation when the H-region strokes into the translocon (Kida *et al.*, 2009). According to their hypothesis, the motive force is likely dependent on the free energy of the hydrogen bonds formed during TMD α-helix establishment from the H-region and its hydrophobic interactions with the lipid environment of the translocon. Thereafter, movement might be driven by a ratchet function of ER lumenal chaperones such as the mammalian hsp70 homolog BiP that bind and retain the polypeptide chain emerging from the translocon channel under ATP consumption (Kida *et al.*, 2009).

Similarly, it is not well understood how the SA-I and SA-II sequences confer opposite membrane topology. Several parameters are likely to contribute to the process (High & Dobberstein, 1992; Kida *et al.*, 2000; Goder & Spiess, 2001; Kida *et al.*, 2006). The signal core, the H-region, is thought to encode topogenic effects in its hydrophobicity, length and helix propensity. Goder *et al.* (2001) observed a correlation between signal orientation and a hydropathy gradient along the sequence of hydrophobic aa of the H-region: the more hydrophobic end was more efficiently translocated across the membrane. These authors propose that the effect of a hydrophobicity gradient in the signal could be explained by a similar gradient in the signal binding site of the translocon. Another important feature in the topogenesis of membrane proteins on the

ER membrane are the hydrophilic residues that flank the H-region of SA sequences (Kida *et al.*, 2006). A general rule, derived from statistical analysis, states that the charge difference between the 15 residues flanking both sides of a signal's hydrophobic core correlates with transmembrane orientation: the flanking segment that carries the greatest net positive charge remains on the cytosolic face of the membrane ('positive inside rule') (Goder & Spiess, 2001). It is speculated that positive N-terminal flanking sequence will interact with negative charges at the cytosolic surface of the translocon, either on proteins or on lipids (Goder & Spiess, 2001). Another topologically important feature of polytopic membrane proteins is the folding state of the extramembrane hydrophilic domains. A long folded N-terminal extension, will favour $N_{cytosol}$-$C_{ER\text{-}luminal}$ orientation, since polypeptide chains need to be unfolded for translocation (High & Dobberstein, 1992). The opposite orientation, $N_{ER\text{-}luminal}$-$C_{cytosol}$, tends to be favoured by glycosylation on an ER luminal position (High & Dobberstein, 1992). Sato *et al.* (2002; 2003) found that the 'positive inside rule' applied to the SA-II of the first TMD.

It is generally accepted that the topology of most polytopic membrane proteins, once established co-translationally during membrane insertion at the ER, is maintained during subsequent steps of biogenesis, cellular trafficking, and function (Dowhan & Bogdanov, 2009). This was confirmed for KAT1 by showing that the topology for this plant Shaker channel is identical in the final target membrane (PM) and thus most likely maintained during the secretory pathway (Mura *et al.*, 2004). With the help of various tags inserted at predicted cytoplasmic or extracellular hydrophilic protein parts and the corresponding ABs, it was possible to determine the topology of KAT1 expressed in both mammalian culture cells and *Xenopus laevis* oocytes. All tagged KAT1 proteins formed functional channels with electrophysiological properties similar to those of the wt protein, strongly indicating that the epitope insertion did not lead to changes in the overall membrane topology or channel function. Although no published data exist for the related Shaker channels KC1 or AKT1, it is very likely that their identical topology predictions are established *in vivo* following the model of KAT1 (Sato *et al.*, 2003).

Channel assembly in the ER

Global folding of polypeptides entering the endoplasmic reticulum (ER) starts as soon as they emerge from the narrow Sec61 translocon (Dowhan & Bogdanov, 2009). The environment of the ER has a high concentration of molecular chaperones and enzymes that support this folding process (Green & Millar, 1995). Dowhan *et al.* (2009) stated that although the translocon in coordination with SA and St sequences imparts initial TMD orientation, the final compact native structure of a multi-spanning membrane protein is also governed by short-range and long-range intra-protein interactions within TMDs and associated extramembrane domains as well as interactions between the protein and the lipid environment that occur mostly after exit from the translocon and follow thermodynamically driven routes (Dowhan & Bogdanov, 2009).

For KAT1, as well as all other animal and plant Shaker channels alike, the situation is even more complex. These voltage-gated ion channels are oligomeric proteins derived from the

association of four subunits such as the one pictured in Fig. 3A (p. 20). The ER has been recognized as the site where most secretory and membrane proteins oligomerize (Green & Millar, 1995). Evidence to that effect has been obtained both for mammalian brain Shaker channels and KAT1 from plants. However, the ER assembly pathways followed by these proteins remain largely elusive (Schwappach, 2008).

Green *et al.* (1995) stated in their review about ion channel assembly, that during synthesis, proteins rapidly achieve an intermediate state in their folding, the so called 'molten globule' state. In this state, much of the final secondary structure is formed, but the tertiary structure is not yet well defined. Until attainment of the native structure, that can take from several minutes to hours, depending on the gene product, non-native folding intermediates must be protected from ER resident chaperones involved in quality control mechanisms. Those chaperones recognize the presence of exposed hydrophobic aa residues in misfolded proteins and unassembled complexes and could prematurely interrupt folding programs by re-directing folding intermediates to disposal-specific dislocons within the ER membrane where they are transferred to the cytoplasm for proteasome-mediated degradation (Hebert *et al.*, 2010). Green *et al.* (1995) suggested that, in case of tetrameric ion channels, for this reason, the much slower transition from the molten globule state to the subunit's native tertiary structure is likely to occur after the rapid formation of specific subunit associations and that these subunit associations are required before the completion of subunit folding. They based this suggestion on a previous publication (Deal *et al.*, 1994) that had shown that interactions between the mammalian voltage-gated Shaker channel subunits Kv1.1 and Kv1.4, expressed by *in vitro* translation, occurred as fast as subunit synthesis.

However, Green *et al.* (1995) proposed that it would be unlikely that two partially synthesized subunits associate with each other because the space between the ribosomes in an ER membrane bound polysome is 500 Å and thereby should prevent associations between subunits during synthesis. Thus, these authors concluded that during synthesis, a subunit is likely to interact only with other completed subunits or chaperones. They further proposed a model that envisions the rapid subunit associations as a way to stabilize regions of unfolded or partially folded subunits through domain-specific (extracellular, membrane or cytoplasmic) interactions that would otherwise lead to subunit misfolding and rapid intracellular degradation as well as aggregation of subunits (Green & Millar, 1995). Furthermore, this assembly of subunits is supposedly a very dynamic process in the sense that subunits change conformation during assembly with other subunits, resulting in new subunit-recognition sites. Thus, while certain subunits form partially assembled intermediate complexes soon after or during synthesis, the integration of other subunits is dependent upon the prior formation of these partial subunit complexes. Green *et al.* (1995) suggested that this ordered acquisition of new subunit recognition sites might provide a mechanism for ensuring accurate and ordered subunit assembly that is encoded in the subunit themselves.

In accordance with this model, another group (Tu & Deutsch, 1999) later proposed for the assembly of the mammalian voltage-gated K^+ channel Kv1.3 a sequential pathway involving a dimerization of dimers to obtain the final tetrameric structure. They based this model on the electrophysiological analysis of the specific ion conducting features elicited by a variety of wild-

type and mutant Kv1.3 subunits, expressed singly, in combination and as tandem constructs (Tu & Deutsch, 1999). Further biochemical evidence was found in non-denaturating gel electrophoresis of *in vitro* translated Kv1.3, where only tetramers and dimers could be detected (Tu & Deutsch, 1999). Data obtained by another group (Urbach *et al.*, 2000) supported the same hypothesis for plant Shaker channels. These authors expressed KAT1 in *Sf9* insect cells and analyzed protein extracts by size exclusion chromatography. The chromatogram displayed two major peaks, corresponding to the molecular weight of tetramers or dimers, respectively. No peaks likely to correspond to monomers or trimers were detected. Similar results were obtained for AKT1 (Urbach *et al.*, 2000).

Export from the ER

The ER is the first compartment of the secretory pathway where protein synthesis, folding, quality control and generally assembly into protein complexes take place. For further movement along the secretory pathway proteins exit the ER either by unspecific bulk flow or by selective recruitment into vesicles that bud from the ER depending on the secretory cargo; e.g. export of soluble proteins in the secretory pathway occurs mostly via bulk-flow and no export signals are required (Pimpl *et al.*, 2006; Dancourt & Barlowe, 2010). Experiments on trafficking of the membrane protein KAT1 demonstrated that a diacidic motif (DxE), consisting of the acidic aa aspartate (D) and glutamate (E), functions as an ER export signal (Mikosch *et al.*, 2006). A later study revealed that third acidic residue (D) ahead of the diacidic motif is part of the motif and necessary for efficient ER export (Mikosch *et al.*, 2009). This triacidic motif (DxDxE) is located in the cytoplasmic C-terminus of KAT1 (aa 392–396: DIDAE) (Mikosch *et al.*, 2009). Single, double and triple aa exchanges of the three acidic residues to alanine caused a gradual reduction of channel trafficking to the PM in both *Vicia faba* guard cell protoplasts and human embryonic kidney (HEK293) cells (Mikosch *et al.*, 2009). While wt KAT1 was located in the PM and some endosomal compartments of HEK293 cells, localisation of the ER export mutants was restricted to a small perinuclear ring that was identified as part of the ER (Mikosch *et al.*, 2009). Increasing accumulation in the ER was dependent on the number, but not the position of the mutated acidic residues within the ER export motif (Mikosch *et al.*, 2009).

In HEK239 cells, surface expression of ER export mutants of KAT1 could be rescued through co-expression with wt KAT1, as was demonstrated by the use of different fluorescent tags and confocal analysis (Reuff *et al.*, 2010). Both fusion constructs completely co-localized at the PM. Mikosch *et al.* (2009) concluded that via heterotetramerisation in the ER, the export signal of one channel subunit can affect trafficking of other channels subunits lacking a functional signal. Similar observations were made for different subunits of the Kir family of mammalian voltage-gated Shaker channels. Those K^+ channels function in neuronal signalling both as homotetramers or heterotetramer and tetrameric assembly occurs in the ER (Ma & Jan, 2002). Ma *et al.* (2002) demonstrated that heterotetramers containing Kir subunits with and without diacidic ER export signals are localised to the PM. In contrast, homotetramers of subunits that do not contain an ER

export signal accumulated in the ER. They suggested that this phenomenon represents a regulatory mechanisms that, at the level of ER export, affects ion channel density in the PM as well as the subunit composition of tetramers to create channels with specific ion conducting features (Ma & Jan, 2002).

Diacidic ER export motifs have been identified in a number of mammalian membrane proteins beside Kir with channels and transporters accounting for the largest part (Ma & Jan, 2002; Hanton *et al.*, 2005; Zuzarte *et al.*, 2007; Mikosch *et al.*, 2009). In plants, also e.g. the tandem-pore K^+ vacuolar channel AtTPK1 and ZmPIP2.4 depend on this ER export signal (Mikosch *et al.*, 2009). In mammalians, it has been shown that the function of this diacidic motif is the interaction with proteins that mediate the budding of vesicles from the ER (coat protein II, COPII), so that their respective membrane proteins are incorporated into these vesicles as cargo (Dancourt & Barlowe, 2010). To initiate coat protein assembly at specific ER exit sites (ERES), the soluble GDP-bound Sar1 GTPase is recruited to the membrane by the GTP-exchange factor Sec12 (see Fig. 8B). The activated Sar1, then in its GTP-bound form and inserted into the ER membrane, recruits the Sec23-Sec24 complex. The Sec24 subunit in turn recognizes and binds to specific aa motifs signaling ER export (e.g. the diacidic motif) that are displayed by membrane protein cargo on a cytoplasmic domain. The outer layer, the Sec13-Sec31 dimer, assembles around this ternary pre-budding complex of Sec23-Sec24, Sar1p-GTP and membrane protein cargo. Thus a caged structure is formed that induces outwardly directed curvature of the ER membrane bilayer and buds the COPII vesicles (Dancourt & Barlowe, 2010).

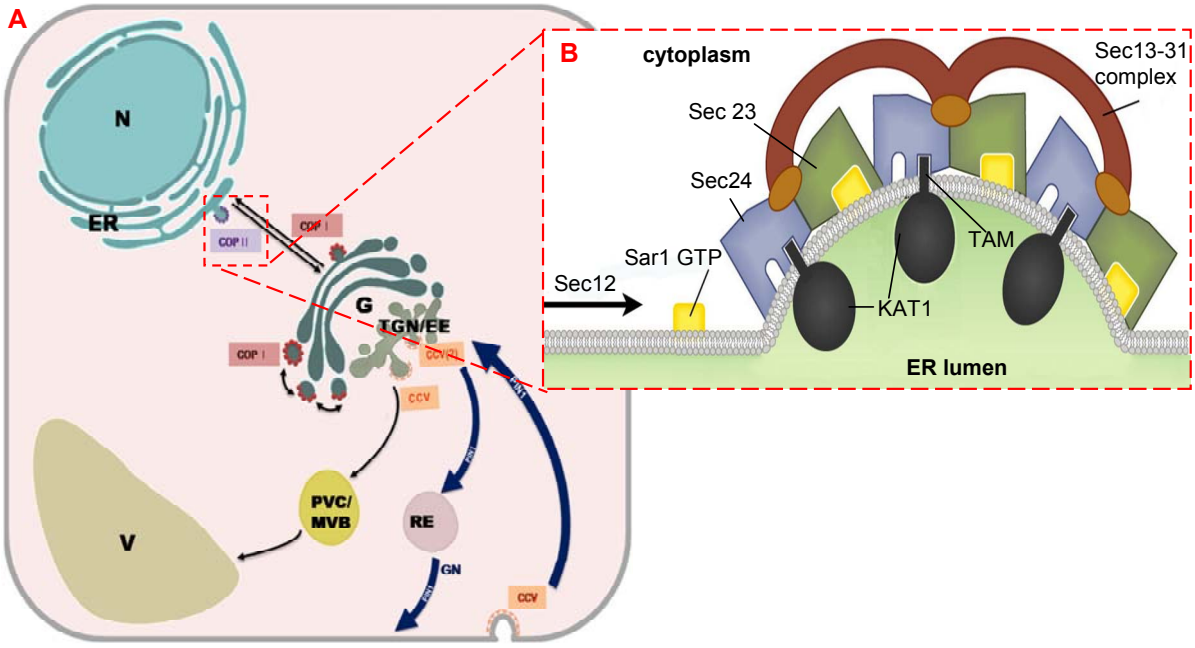

Fig. 8 COPII- dependent ER export

Shown is a model for coat protein complex II (COPII)-dependent ER export of KAT1, i.e. Sec24 mediated cargo selection and COPII vesicle formation; TAM, triacidic motif; explanations see text. Images were adapted from previous publications (Hwang & Robinson, 2009; Dancourt & Barlowe, 2010).

Only very little information is known about COPII- dependent ER export in plants (Bassham *et al.*, 2008). Although the plant genome revealed homologues to all identified proteins that contribute in animals, in many cases with an even greater number of isoforms, functional studies for most of the plant COPII proteins are still missing. Indirect evidence was obtained by interference with the pathway, e.g. through dominant-negative mutants of Sar1 (Bassham *et al.*, 2008). Mikosch *et al.* (2009) pointed out, that mutation of the acidic ER export motif of KAT1 not only affected trafficking of this channel in plant cells but also in human cells, suggesting that the ER export mechanism is highly conserved. Additional insights into COPII-mediated trafficking in plants were derived from a different study (Sieben *et al.*, 2008). Fluorescence resonance energy transfer (FRET) measurements of *Vicia faba* guard cells transfected via particle bombardment to co-express fusions of KAT1 to cerulean fluorescent protein (CFP) and Sec24 to yellow fluorescent protein (YFP) demonstrated that KAT1 interacts directly with Sec24. This interaction was observed only at distinct sites in the perinuclear region of the ER, interpreted as ERES, and found strictly dependent on the acidic ER export motif of KAT1: channels with a mutated ER export motif can not be recognized by Sec24 and in turn are not included into COPII vesicles but remain in the ER (Sieben *et al.*, 2008).

Anterogade traffic to the plasma membrane

COPII vesicles fuse with the Golgi apparatus to deliver their cargo (Bassham *et al.*, 2008). Prior to fusion, the COPII coat removal is triggered by the GTPase activation function of SEC23, which triggers the intrinsic GTPase activity of SAR1. The cotamers are released back to the cytoplasm for future coating steps.

In contrast to mammalian cells, the plant Golgi apparatus is made of hundreds of individual stacks of flattened cisternae that remain intact during cell division (Hwang & Robinson, 2009). Furthermore, Golgi stacks are mobile and movement has been shown to depend on actin integrity with a possible involvement of myosin and microtubules. It is thought that in plant cells where the vacuole occupies 95 % of the total volume, mobile Golgi may facilitate a global communication with proximal and distal secretory compartments such as vacuoles, chloroplasts, and the plasma membrane (Faso *et al.*, 2009). However, it is currently unclear, how a continuous flow of proteins from the ER to mobile Golgi stacks is maintained, i.e. whether COPII vesicles or tubules, physical connections that link the ER and the Golgi, are involved (Hwang & Robinson, 2009). The latter were discovered in highly vacuolated tobacco leaf epidermal cells, where Golgi stacks are physically attached to ER tubules and lateral movements of individual Golgi stacks results in the rapid elongation of an attached ER tubule (Sparkes *et al.*, 2009). These authors further showed that a Golgi stack collects cargo from this mobile ERES while it is moving (Sparkes *et al.*, 2009). In contrast, in electron microscopy images of root columella cells, 87% of Golgi stacks were seen separated from the ER. It was concluded that differences in the ER and Golgi organization may exist depending on cell types (Faso *et al.*, 2009).

After passing through the Golgi, cargo proteins reach the trans-Golgi network (TGN)

responsible for intracellular sorting (see Fig. 8A). In contrast to animals, the vesiculate TGN is often closely associated with the trans-face of the Golgi stack (Richter *et al.*, 2009). Like their animal and yeast counterparts, plant TGNs are involved in anterograde traffic to the PM. However, the secretory route to the PM in plants has not been mapped out in detail. It is thus unknown whether secretory carriers move from the TGN to the PM directly or/and indirectly via other endosomal compartments. Furthermore, although it is assumed that clathrin-coated vesicles (CCV) are the secretory carriers, those have not been structurally identified in plants and the machinery involved is largely unknown (Richter *et al.*, 2009). Also from the TGN, vacuolar traffic passes through multiple multivesicular bodies (MVBs) en route to the lytic vacuole (equivalent of the lysosome in animal cells). MVB serve as prevacuolar compartments (PVCs) and thus correspond to late endosomes (LE) of animal cells (Richter *et al.*, 2009). In animal cells, the LE and the EE are two separate entities involved in CCV dependent anterograde traffic of lysosome-destined cargo as well as CCV dependent recycling of PM proteins. In contrast, plant TGNs also serve as early endosomes (EE) as demonstrated by the very rapid labelling with the endocytic tracer FM4-64 (Richter *et al.*, 2009). Although sometimes controversially discussed, the more hydrophobic of the styryl dys, such as FM4-64, are considered to be almost completely membrane non-permeable (Betz *et al.*, 1996; Meckel *et al.*, 2004). Therefore, in general, all fluorescent label, which accumulates inside a cell during incubation with this marker, is interpreted to be a result of endocytosis (Betz *et al.*, 1996). Thus, in plants secretory and endocytic traffic meet at the TGN. Plant cells may have additional endosomal compartments that are structurally difficult to identify. For example a study that investigated the role of GNOM, a GDP/GTP exchange factor for ARF GTPases, in the BFA-sensitive recycling of endocytosed AtPIN1 to the plasma membrane, suggested the presence of a functionally distinct 'recycling endosome' (RE) (Geldner *et al.*, 2003) (see Fig. 8A). Since vesicle budding profiles and tubular protrusions are absent from the PVC it is likely that it is not involved in PM protein recycling events (Faso *et al.*, 2009).

A similar lack of knowledge exists for trafficking events of KAT1 until it reaches the PM. However, there is evidence, that KAT1 at least, like PIN1 and other plant PM proteins (e.g. *Arabidopsis* boron exporter BOR1, brassinosteroid receptor BRI1) cycles constitutively between the PM and some endosomal compartment labelled by the endocytosis marker FM4-64 (Meckel *et al.*, 2004; Hurst *et al.*, 2004; Mikosch *et al.*, 2009). The nature of the endosomal compartment that is involved in KAT1 turnover is unclear. Meckel *et al.* (2004) who investigated endocytosis of KAT1 in guard cells using confocal fluorescence microscopy stated that it could correspond either to PVC or a RE.

Even less details than for KAT1 are known about the trafficking of the other Shaker channel subunits of *Arabidopsis*. Still, it was observed that KC1, when over-expressed as fusion to green fluorescent protein (GFP) in tobacco mesophyll protoplasts, was retained in the ER, whereas in parallel experiments an AKT1-GFP fusion was targeted to the PM (Duby *et al.*, 2008). Duby *et al.* (2008) were able to demonstrate that co-expression of KC1 with AKT1 (or KAT1) in this system, redirected KC1 to the PM. At the same time, patch-clamp analysis showed that protoplasts co-expressing KC1 and AKT1 (or KC1 and KAT1) displayed K^+ uptake currents different from

those expressing either AKT1 (or KAT1) on their own (Duby *et al.*, 2008). It was concluded that the formation of heterotetrameric channels with AKT1 (or KAT1), as indicated by the changing electrophysiological properties compared to homomeric AKT1 (or KAT1) channels, allowed KC1 to escape the ER (Duby *et al.*, 2008). The mechanism responsible for this conditional targeting is not yet known. In both tobacco protoplast (Duby *et al.*, 2008) and *Xenopus leavis* oocytes (Dreyer *et al.*, 1997) expression of KC1 alone failed to yield exogenous current, hence it was termed 'silent'. It was suggested that KC1 is not able to form homotetramers, which is supported by yeast-two hybrid (Pilot *et al.*, 2003a) and split-ubiquitin (Obrdlik *et al.*, 2004) assays that showed an inability of KC1 to interact with itself, whereas interaction with both AKT1 and KC1 was confirmed. Hence, Duby *et al.* (2008) proposed that as KC1 is unable to form homotetramers it might be retained in the ER as monomer by a putative ER retention signal. This signal would be 'overwritten' by ER export signals in AKT1 (or KAT1) when heterotetramers are formed in the ER. An alignment of the identified triacidic ER export motif of KAT1 with other Shaker channel subunits from *Arabidopsis* revealed that only KAT2 contains the triacidic motif (Reuff *et al.*, 2010). In all other Shaker channels only the final 'E' is conserved. However, lack of the acidic motif does not seem to negatively affect ER export of subunits such as AKT1 (see above).

SNAREs for vesicle fusion to target membranes

The structure of SNARE proteins

As described for anterograde traffic of KAT1, membrane (protein) traffic consists of the following sequence of steps. Transport vesicles (e.g. COPII) are generated by budding from a precursor compartment, transported to the appropriate subcellular destination, and finally fused with the membrane of the target compartment to deliver their cargo. Membranes in themselves are designed not to fuse spontaneously so that membrane bound subcellular compartments can remain distinct from each other in a cell. To overcome the forces that keep membranes apart and thus achieve vesicle fusion target membranes, SNARE proteins are needed (Jahn & Scheller, 2006).

SNAREs comprise an evolutionarily conserved superfamily of small transmembrane or membrane-anchored proteins (Jahn & Scheller, 2006; Lang & Jahn, 2008; Sudhof & Rothman, 2009). They vary in structure and size, but share a conserved stretch of 60– 70 aa with eight heptad repeats, which was termed the SNARE motif (Fig. 9, left side, red, green and blue bars) (Brunger, 2005). Each fusion step requires a specific set of four different SNARE motifs (Qa, Qb, Qc and R) that are contributed by three or four different SNAREs (Qb and Qc might be on one or separate proteins). Also, each of the membranes destined to fuse, must contain at least one SNARE with a TMD. In most cases, the two (or three) Q-SNAREs are anchored in the target membrane, while the R-SNARE is found on the vesicle membrane.

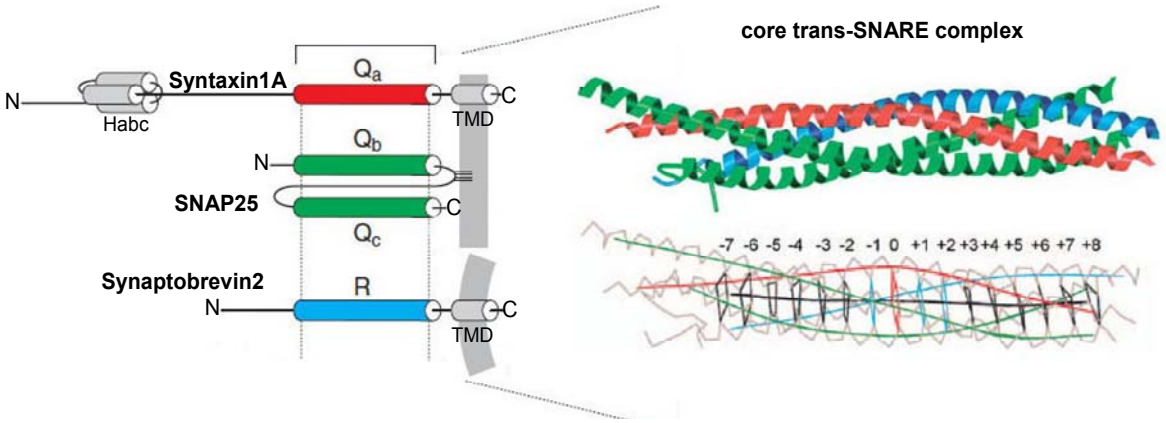

Fig. 9 Four different SNARE motifs form a SNARE complex

Shown on the right is the Qa-, QbQc- and R-SNARE protein structure, here by the example of SNAREs that assemble in a trans-SNARE complex to mediate vesicle fusion during neurotransmitter release in mammalian presynapses. X-ray crystallography of the core of this trans-SNARE complex that is formed by layers of interaction between the α-helices of the four SNARE motifs is shown on the left.
Images were adapted from previous publications (Jahn & Scheller, 2006; Lang & Jahn, 2008).

With the exception of the Qb-Qc-SNAREs, most SNARE proteins contain a C-terminal TMD and a single SNARE motif. In Qa-SNAREs (also called syntaxins), such as the mammalian Syntaxin1A, the SNARE motif (Fig. 9, left side, red bar: Qa) is surrounded by an independently folded N-terminal domain and the TMD at the C-terminus. This TMD is connected to the SNARE motif by a short linker. In contrast, a long flexible linker region connects the SNARE motif to the N-terminal domain. This N-terminal domain is composed of an antiparallel three-helix bundle, the so-called Habc domain and has a small N-terminal extension. Syntaxins are able to form intramolecular interactions by folding back the Habc domain onto the SNARE motif, resulting in the auto-inhibitory so-called closed conformation (Fernandez *et al.*, 1998; Dulubova *et al.*, 1999; Lerman *et al.*, 2000; Munson *et al.*, 2000).

R-SNAREs, such as Synaptobrevin2, resemble Qa-SNAREs. However, instead of the independently folded N-terminal domain, they contain a short N-terminal proline-rich extension (Fig. 9, left hand side, blue bar). Qb-Qc SNAREs, such as SNAP25 contain two SNARE motifs, joined by a flexible linker region. They lack a TMD, but become anchored to the membrane by palmitoylation of a cluster of four cysteine residues that reside in the linker region. The SNAP-class of SNAREs specialize in exocytosis, other membrane fusion steps might involve different single SNARE motif proteins that provide either the Qb or the Qc- motif. These Qb- and Qc-SNAREs resemble R-SNAREs with a C-terminal TMD followed by the SNARE motif and an N-terminal extension (Jahn & Scheller, 2006; Lang & Jahn, 2008; Sudhof & Rothman, 2009).

SNARE complex formation catalyses membrane fusion

SNAREs are both necessary and sufficient for membrane fusion. Mammalian cultured cells expressing SNARE proteins in an inverted position, i.e. on the cell surface, were found to fuse

spontaneously (Hu *et al.*, 2003). Further experiments confirmed that compatible individual SNARE proteins spontaneously assemble into a stable four-helix bundle that forms between opposing membranes as a 'trans-SNARE' complex. Complex formation is mediated by the SNARE motifs. It is associated with conformational and free-energy changes that result in a core complex of extraordinary stability (Sudhof & Rothman, 2009). When SNAREs are monomer, their SNARE motifs are unstructured. In contrast, in the core trans-SNARE complex, all four SNARE motifs adopt an α-helical structure and are aligned in parallel, forming a twisted coiled-coil (Fig. 9, right hand) (Sutton *et al.*, 1998).

This observation was first made by Sutton *et al.* (1998) who obtained the crystal structure of the core trans-SNARE complex involved in mammalian synaptic vesicle fusion, i.e. the assembled SNARE motifs of Syntaxin1A and SNAP25 from the presynaptic PM and Synaptobrevin2 from a synaptic vesicle membrane (see Fig. 9, right hand) (Sutton *et al.*, 1998). Sutton *et al.* (1998) further suggested that stability of the complex is mediated by 16 stacked layers of interacting side chains that can be found along the longitudinal axis in the centre of the four helix bundle (Fig. 9, right hand, lower part). Each layer is formed by four aa that are contributed by one of the four different SNARE motifs. The layers (-7 to +8) are largely hydrophobic, with the exception of one ionic central layer that contains three glutamines (Q) and one arginine (R), all highly conserved in SNARE proteins (Fasshauer *et al.*, 1998). The central layer is used as reference for the remaining layers and called '0-layer'. The Q-/R SNARE classification refers to the conserved aa present in this 0-layer (Sutton *et al.*, 1998). Further classification into Qa-, Qb-, and Qc-SNAREs was derived from the observation that the individual position of each SNARE motif is conserved in all investigated core complexes. Thus, all functional SNARE complexes assigned to trafficking steps in yeast and mammals were discovered to have a conserved final QaQbQcR-composition (Jahn & Scheller, 2006; Kloepper *et al.*, 2007).

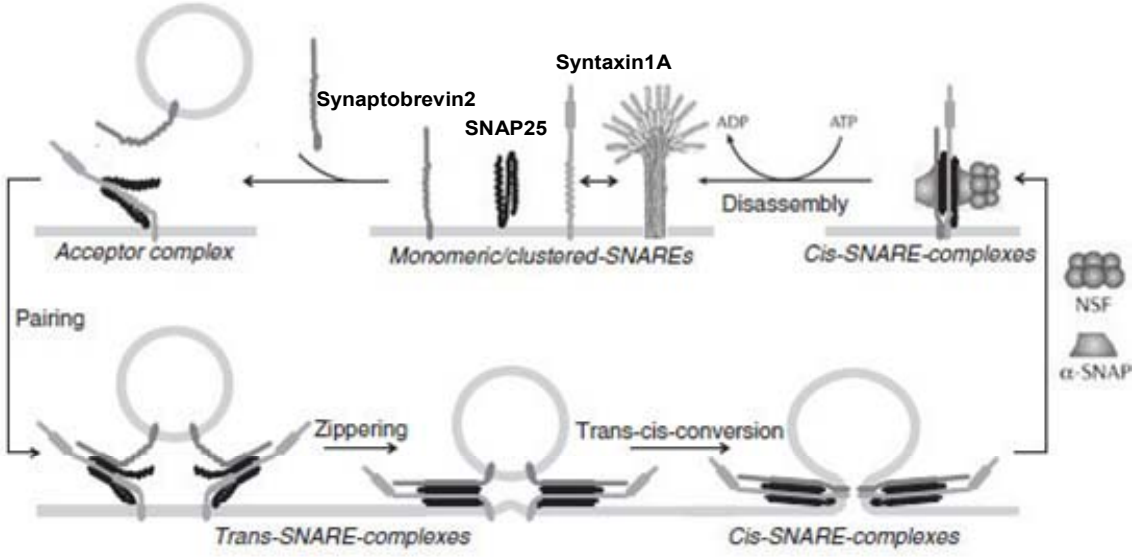

Fig. 10 The conformational SNARE cycle that mediates membrane fusion

To mediate membrane fusion events, SNARE proteins cycle between a free (or clustered) state and the fully assembled cis-SNARE complex, where the membranes are fused with the intermediate trans-SNARE complex state, where zippering is initiated. Disassembly of the cis-SNARE complexes is mediated by the ATPase NSF and its co-factor α-SNAP (for more details see text). The image was adapted from previous publications (White, 2007; Lang & Jahn, 2008).

In vitro studies of neuronal SNARE complexes showed that assembly of the QaQbQcR-composition proceeds through a defined and partially helical QaQbQc intermediate (Brunger, 2005; Lang & Jahn, 2008; Sudhof & Rothman, 2009). This intermediate of target membrane SNAREs (here Syntaxin1A and SNAP25) is called acceptor complex (see Fig. 10, upper left side). It is not yet known whether other SNAREs form such intermediate acceptor complexes. However, Lang *et al.* (Lang & Jahn, 2008) stated that very likely SNARE assembly in general is an ordered, sequential reaction via such intermediates rather than a random collision of four different SNARE motifs. SNAREs function as fusion catalysts. Current models postulate that as unfolded SNARE proteins fold into a four helix bundle, the free energy released is used to merge bilayers. Evidence was obtained that proved an active role in membrane fusion for the SNARE complex that exceeds simply pinning two bilayers together (Mcnew *et al.*, 2000b). These authors found that the TMDs of Qa- and R-SNAREs (anchored in target and vesicle membrane respectively) as well as the precise distance between their SNARE motifs and TMDs were critical for fusion (Mcnew *et al.*, 2000b). For example, increasing the length of the linker region between SNARE motifs and TMD prevented fusion, but the trans-SNARE complex still assembled (Mcnew *et al.*, 2000b).

Based on these results, the current model for the catalytic function of the trans-SNARE complex during membrane fusion is that the four SNARE motifs resemble a molecular zipper. The above mentioned layers of interaction between the four SNARE motif helices are thought to form sequentially one after another (-7 to +8 layer) in analogy to a closing zipper. Thus, assembly of SNARE motifs from their N-terminal toward their C-terminal regions actively pulls the opposing membranes stepwise together (Fig. 10, lower part). During formation of the last layers, membranes are close enough to fuse (Skarp *et al.*, 2008; Lang & Jahn, 2008; Sudhof & Rothman, 2009).

The shortness of the linkers between SNARE motifs and TMDs is thought to render them inflexible enough to function as critical force transducer that translate the energy released upon trans-SNARE complex zippering into the catalytic force that fuses the apposing bilayers. Or in other words, during zippering the trans-SNARE complex proceeds from a loose to tight state. Tightening exerts a mechanical force on the stiff linkers that in turn pull at the membrane anchors. Thus, straining the linkers transmits energy onto membranes, bending them and/or disturbing the hydrophilic–hydrophobic boundary for fusion (Mcnew *et al.*, 2000b).

Complete zippering is sterically prevented until fusion occurs, so that fusion and the completion of zippering are thermodynamically coupled. Therefore, when fusion has occurred, the force vanishes and all SNAREs are present in the low-energy, relaxed cis-SNARE complex (Weber *et al.*, 1998; Lang & Jahn, 2008; Sudhof & Rothman, 2009) (Fig. 10, right side). In this cis-complex, the assembled SNARE motifs are aligned in parallel and the TMDs of the Qa-SNARE and the R-SNARE are close to each other and now in the same membrane, the target membrane.

Until very recently, the minimal number of SNARE complexes needed to overcome the energy barrier in membrane fusion was not known. Indirect approaches by *in vivo* titration of inhibitors while measuring fusion kinetics, estimated between 3 and 15 SNARE complexes per fusion event (Tse *et al.*, 1993). More recently, other authors were able to show directly with the help of a special assay involving fluorescence resonance energy transfer (FRET) that liposomes

bearing only a single SNARE molecule are capable of fusion with liposomes carrying their cognate partner SNAREs (van den Bogaart *et al.*, 2010). They concluded that, at least *in vitro*, one SNARE complex is sufficient for membrane fusion. This challenges the current model where the fusion pore (i.e. the place where the vesicle opens during fusion, Fig. 10, lower right side, p. 39) is thought to be surrounded by a ring-shaped arrangements of multiple SNARE complexes, i.e. their TMDs (Han *et al.*, 2004; Montecucco *et al.*, 2005).

As mentioned above, bilayer fusion is thermodynamically coupled to exergonic folding of SNARE proteins, i.e. a major release of energy (Jahn & Scheller, 2006; Lang & Jahn, 2008; Sudhof & Rothman, 2009). In contrast, in the post-fusion state the fully zippered cis-SNARE complex is in a highly stable low-energy state that can not disassemble spontaneously (Jahn & Scheller, 2006; Lang & Jahn, 2008; Sudhof & Rothman, 2009) (Fig. 10, right side, p. 39). Therefore, the process of reactivating individual SNAREs to their initial free state for another round of fusion is endergonic. It requires the action of a specialised hexameric adenosine triphosphatase (ATPase) that presumably uses three to six ATPs to disrupt one SNARE complex (Jahn & Scheller, 2006). The ATPase, called NSF, cannot act alone. It requires a cofactor, the adapter protein α-SNAP (not related to the 'SNAP'-type Q-SNAREs described above). SNAPs bind to the cis-SNARE complex first (at the '0' layer) and in turn recruit NSF, followed by stimulation of its ATPase activity (Fig. 10, upper right side, p. 39). The hydrolysis of ATP induces major conformational changes resulting in the disassembly of the entire complex into its free and 'refueled' constituents (Jahn & Scheller, 2006; Lang & Jahn, 2008; Sudhof & Rothman, 2009).

NSF (*N*-ethylmaleimide–sensitive factor) and SNAP (soluble NSF attachment protein) were purified on the basis of their essential requirement for vesicle fusion in a cell-free system (Clary *et al.*, 1990). As described, SNARE proteins act as 'receptors' for SNAP and NSF, hence the name SNARE (soluble NSF attachment protein receptor) (Sollner *et al.*, 1993). The R-SNAREs are then separated from the target membrane for example, by endocytosis to eventually reside on a vesicle membrane again (Fig. 10, p. 39). In summary, in order to catalyse membrane fusion, SNAREs undergo a conformational cycle that is driven by ATP–dependent dissociation of the cis-complex (Jahn & Scheller, 2006; Lang & Jahn, 2008; Sudhof & Rothman, 2009) (Fig. 10, p. 39).

Regulation of membrane fusion

SNARE clustering

The above described SNARE cycle (Fig. 10, p. 39) is controlled by an array of regulatory factors that even in the far more investigated animal systems are only partially understood (Lang & Jahn, 2008). Such regulatory factors are needed on a very basic level to prevent rampant fusion events. As mentioned above, trans-SNARE complex formation is driven by a thermodynamically spontaneous process of protein folding. In addition to clamping fusion until it is desired (temporal control), regulation of fusion is needed to match vesicles to their appropriate target compartments (spatial control). Accuracy in the delivery of specific cargo to programmed locations is vital for the

establishment and maintenance of eukaryotic cell compartmentalization as well as growth and division of cells.

The SNARE proteins themselves are thought to impart a layer of compartmental specificity in membrane trafficking. It was found after *in vitro* testing hundreds of combinations of yeast SNAREs that only about a dozen of them were fusogenic (Mcnew *et al.*, 2000a). In addition to this specificity confered by inherent physico-chemical properties, specific SNAREs are intrinsic to different intracellular compartments. However, the examples of some particular SNAREs made it clear that these features can not encode sufficient information to ensure the fidelity of intracellular transport pathways (Jahn & Scheller, 2006). The yeast Qa-SNARE Sed5 showed multiple specificity, i.e. formed cognate SNARE complexes on the Golgi with two sets of partners. Another yeast SNARE, the Qb-SNARE Vti1 was detected on multiple compartments (e.g. vacuole and Golgi), and mediated fusion steps for each with different specific SNARE partners (Jahn & Scheller, 2006). Thus, it was suggested that SNAREs provide the core, evolutionarily conserved and usually static code for fusion to individual membrane compartments (Mcnew *et al.*, 2000a). Other regulatory factors, as detailed below, would then be responsible for spatial and temporal fine-tuning of the fusion reaction.

With the conclusion that regulatory factors must exist to prevent spontaneous trans-SNARE complex assembly, it is assumed that in turn free SNARE molecules *in vivo* are short-lived (Lang & Jahn, 2008). One possible mechanism that might control free SNARE molecules *in vivo* is clustering. It was discovered, that some Qa-SNAREs (e.g. Syntaxin1A) are not uniformly distributed in the membrane, but cluster into nanodomains of about 60 nm in diameter (Sieber *et al.*, 2007). On average, these oligomeric syntaxin clusters contained 75 densely crowded molecules. The current model suggests that cluster formation depends on weak homophilic attraction between the SNARE motifs of monomers and possibly interaction of their TMDs (Sieber *et al.*, 2007). As a consequence, most syntaxins are thought to be present in a tightly packed open confirmation within these clusters (as opposed to the closed confirmation, see p. 37). Towards the rim of the cluster, molecules would be less conformationally constrained so that the bulky N-termini would cause syntaxins to adopt a half-closed conformation. The result would be an anemone-like structure for the syntaxin clusters (White, 2007) (indicated Fig. 10, p. 39).

Secretory vesicles were shown to selectively dock and fuse at such clusters. It is envisioned that only the outer arms of the anemone-like structure function in vesicle capture (Low *et al.*, 2006). According to the so-called 'Icebreaker' model, acidic lipids would then 'break off' syntaxins with docked vesicles from the larger clusters by binding a polybasic domain of the syntaxin that lies close to its TMD (Murray & Tamm, 2009). These freed trans-SNARE complexes would then undergo the actual membrane fusion step. This model invokes clusters of syntaxin as well as individual syntaxins as important contributors to the overall fusion reaction and shows how free Qa-SNAREs might be controlled e.g. in presynaptic membranes (Murray & Tamm, 2009).

Vesicle capturing is likely more efficient at the sites of high local Qa-SNARE concentrations that these clusters provide than it would be for freely diffusing individual syntaxins. In consequence, clustering was suggested to enhance the rate of vesicle fusion during e.g.

exocytosis of neurotransmitters (Sieber *et al.*, 2007). In addition, Low *et al.* (2006) had observed that different syntaxin family members segregated into different clusters in the same membrane. Capturing vesicles on these individual clusters would enhance the sorting of different fusogenic vesicles to their cognate fusion sites. It is still unclear, whether cluster formation is a hallmark of all SNAREs or occurs only with Qa-SNAREs.

SM proteins

Free SNAREs that could undergo uncontrolled fusion might also be avoided by binding to special SNARE-interacting proteins. The so-called SM proteins (Sec1/ Munc18-like), for example, are small cytosolic proteins with a highly conserved structure in from of an arch-shaped 'clasp'.

Several different modes of SNARE binding by this clasp have been suggested (see Fig. 11). The crystal structure of the mammalian Munc18-1/Syntaxin1A complex indicated that the SM protein Munc18-1 is able to bind to the so-called closed conformation (see p. 37) of the Qa-SNARE Syntaxin1A (Misura *et al.*, 2000) (Fig. 11-1). Here, the SM protein is thought to clamp the

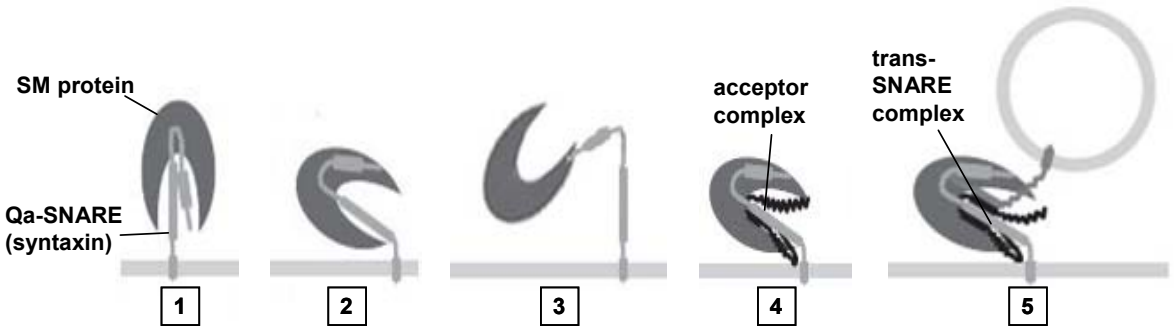

Fig. 11 SM protein interaction with SNAREs

Different modes for SNARE binding by SM proteins were proposed. SM proteins might clasp the closed confirmation of Qa-SNAREs (1), their half-open (2) or open form (3). In addition, interaction between SM protein and SNARE acceptor complexes (4) or fully assembled trans-SNARE complexes have been observed. It was further suggested that each of the observed binding modes might represent an intermediate on a SM protein controlled molecular pathway of specific SNARE complex assembly.
The images were adapted from previous publications (Lang & Jahn, 2008; Sudhof & Rothman, 2009)

N-terminal Habc domain of the syntaxin onto its SNARE motif, mimicking the parallel four-α-helix bundle of the SNARE complex. This arrangement effectively prevents the syntaxin from assembling into fusogenic trans-complexes with cognate SNARE partners.

In contrast, other authors provided evidence that *in vivo* Munc18-1 stabilizes a half-closed conformation of Syntaxin1A (Zilly *et al.*, 2006) (Fig. 11-2). In this mode the syntaxin would still be capable of engaging in trans-SNARE complex assembly (see above described situation in SNARE clusters). Zilly *et al.* (2006) further reported Munc18-1 binding to an acceptor complex formed by syntaxin and QbQc-SNARE on the target membrane (Fig. 11-4).

A mode of binding that was observed in the majority of all investigated yeast and mammalian SM proteins so far, is SM binding to syntaxin in its 'open' conformation (Fig. 11-3) (Rizo & Sudhof, 2002; Lang & Jahn, 2008). Here, only the short N-terminal peptide that precedes the syntaxin's Habc domain is thought to bind in a small groove on the surface of the SM protein, with no involvement of the central cleft (Dulubova *et al.*, 2002; Yamaguchi *et al.*, 2002). This is believed to be the universal state in which Qa-SNAREs are open, i.e., reactive (Lang & Jahn, 2008; Rizo & Rosenmund, 2008). As in this mode, i.e. open with a bound SM protein, the Qa-SNARE is able to form complete trans-SNARE complexes with cognate SNARE partners, the last of the observed SM modes was suggested to be a subsequent step (Sudhof & Rothman, 2009) (Fig. 11-5). Here, the SM protein uses its free arch-shaped body to fold back on the assembled trans-SNARE complex. Thus, the SM protein clasps again a four-helix bundle similar to the situation in binding the closed Syntaxin1A (Shen *et al.*, 2007; Dulubova *et al.*, 2007). Also this mode was observed for several SM proteins, including Munc18-1 (Dulubova *et al.*, 2007).

Similar to the envisioned transition in SM binding modes, i.e. SM binding of an open syntaxin to binding of the subsequently formed trans-complex, Lang *et al.* (2008) speculated that each of the observed binding modes might represent an intermediate on a SM protein controlled molecular pathway of specific SNARE complex assembly (i.e. closed, half-open, open, acceptor-complex, trans-complex; see Fig. 11).

In *in vitro* fusion assays the need for an SM protein can be bypassed with a higher than physiological concentrations of SNAREs (Tareste *et al.*, 2008). In contrast, all investigated genetic deletions of an SM protein led to a block of the corresponding fusion reaction *in vivo* (Lang & Jahn, 2008; Sudhof & Rothman, 2009). These results indicated that SM proteins are as essential for membrane fusion events as SNAREs. However, the observed multiple distinct binding modes between these two partners suggested that SM proteins may not share a common mode of action (Lang & Jahn, 2008; Sudhof & Rothman, 2009; Furgason *et al.*, 2009). It is envisioned, for example, that SM proteins may assist in the formation of acceptor complexes needed for trans-SNARE interaction in a manner of catalysts. In doing so they may also be involved in proofreading, i.e. differentiating between cognate and non-cognate SNAREs and thus promoting compartmental specificity. The observed modes of binding would allow also for an action in regulating the speed of fusion by clamping trans-complexes until fusion is triggered by a specific signal (Lang & Jahn, 2008; Sudhof & Rothman, 2009). In all modes, however, SM proteins potentially can prevent uncontrolled fusion by free Qa-SNAREs.

Currently debated is also the Munc18-1 binding to the closed confirmation of Syntaxin1A. This particular mode of SM binding, i.e. negative regulation by interfering with the formation of SNARE complexes, appears so far to be unique to this specific SM protein. In addition, as mentioned above, all of the other suggested binding modes for Munc18-1 are thought to act in promoting fusion. Promoting fusion is in agreement with an observed block in synaptic exocytosis after genetic deletion of Munc18-1 (Shen *et al.*, 2007; Lang & Jahn, 2008; Sudhof & Rothman, 2009). Thus, the proposed negative regulation by binding the closed formation of Syntaxin1A was surprising. It has been suggested that this situation might represent a non-physiological extreme

situation that does not occur in intact cells (Lang & Jahn, 2008; Sudhof & Rothman, 2009). In conclusion, it is not yet known how exactly SM proteins cooperate with SNAREs to regulate fusion (Sudhof & Rothman, 2009).

SM proteins comprise a small family with only seven members in mammals and four in yeast. The *Arabidopsis* genome encodes six SM proteins including KEULE (Lipka *et al.*, 2007). *In vitro*, KEULE was shown to bind directly to the Qa-SNARE SYP111 (see below, p. 54) (Assaad *et al.*, 2001). Both *keule* and *syp111* mutant plants are cytokinesis-defective which supported the hypothesis that their interaction is as essential as the individual proteins for vesicle fusion to the cell plate during cell division (Lauber *et al.*, 1997; Waizenegger *et al.*, 2000; Assaad *et al.*, 2001). A double mutant between *keule* and *syp111* is embryo lethal (Waizenegger *et al.*, 2000). With such small numbers of SM proteins it has to be expected that some of them operate in more than one fusion reaction. In agreement with this assumption, the *keule* mutant exhibited aberrant root hair morphogenesis that was not observed in the *syp111* mutant (Sollner *et al.*, 2002). In addition, the KEULE gene is expressed in both proliferating and non-proliferating cells , while SYP111 is only found in proliferating cells (see below) (Waizenegger *et al.*, 2000; Assaad *et al.*, 2001).Thus, also SM proteins only add another layer to specificity of intracellular membrane trafficking events.

GTPases and tethering factor complexes

According to current concepts, individual fusion reactions are executed by distinct combinations of SNARE and SM proteins to ensure specificity. The SM-SNARE fusion machinery is controlled by additional upstream regulators that embed it into a physiological context. Regulatory factors of the trafficking machinery include the large conserved protein families of Rab GTPases, tethering factors, and phosphoinositides.

As mentioned briefly for anterogate traffic of KAT1 (p. 33), cargo-laden vesicles are created when they are sculpted out of the membrane of one compartment by the assembly of coat proteins. To deliver their cargoes, the vesicles must traffic to their destinations. Vesicle transport through the cytoplasm is thought to dependent on either actin-dependent motors (myosins) or microtubule-dependent motors (kinesins or dyneins). In the vicinity of their subcellular target, vesicles must lose their coats, and fuse with the target compartment's membrane. Tethering factors take their name from the idea that they act as the initial connection, or tether, between an intracellular trafficking vesicle and its target membrane (Yu & Hughson, 2010). There are two classes of tethering factors. The first class consists of long coiled-coil proteins (e.g. p115) and the Golgins. The second class is represented by large multi-subunit complexes. Seven multisubunit tethering complexes have been conserved among all eukaryotes including the e.g. the exocyst, the TRAPP complexes and HOPS (Yu & Hughson, 2010). Each of these tethering factor complexes resides on a specific cellular compartment and mediates vesicle fusion to it (see Fig. 12A for a mammalian cell) (Yu & Hughson, 2010). For example, the exocyst tethers secretory vesicles to the PM for the process of exocytosis.

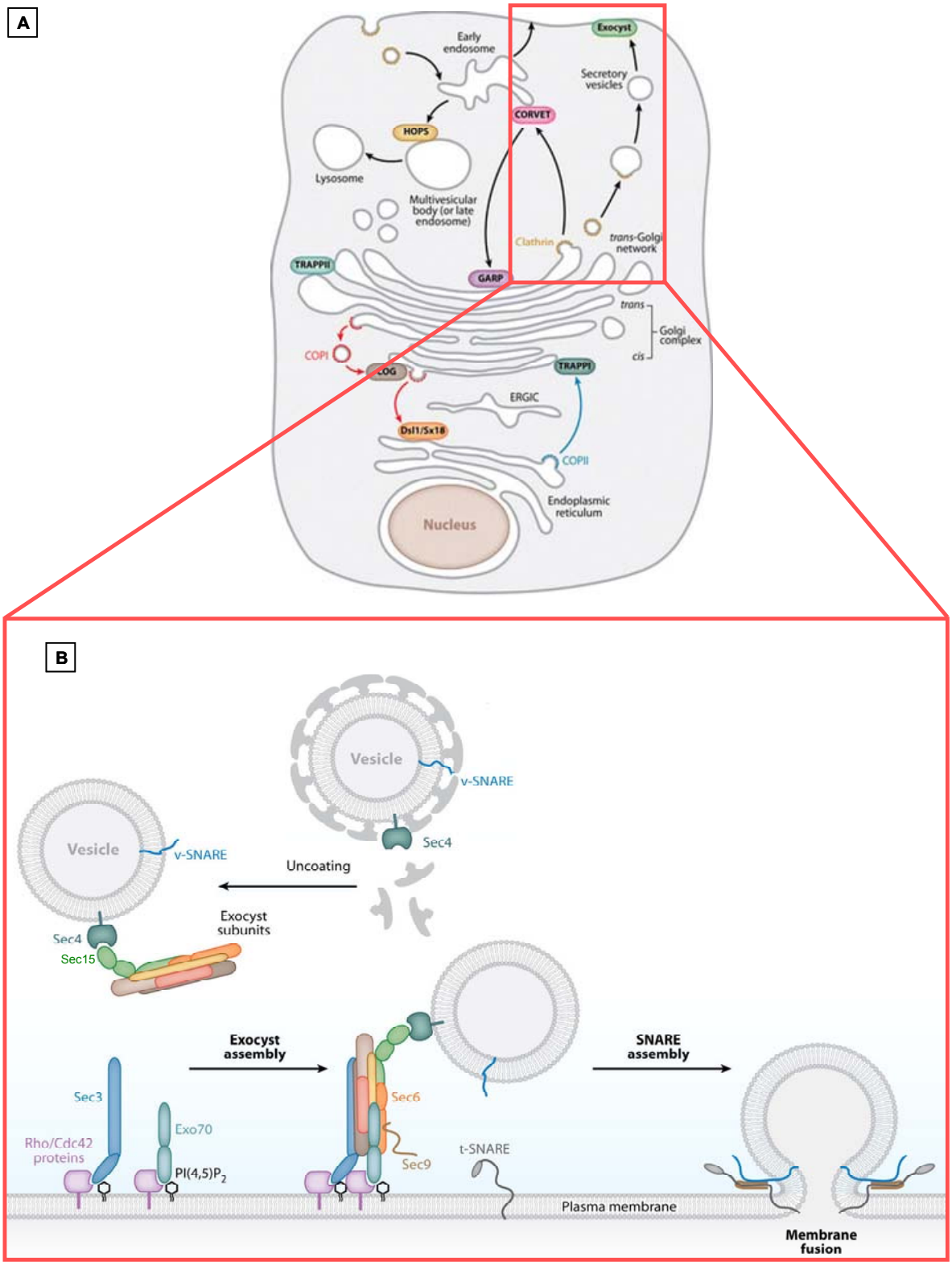

Fig. 12 Regulation of membrane fusion by GTPases and tethering factors

For more details see text. The images were adapted from a previous publication (Yu & Hughson, 2010).

Exocytosis is a fundamental process in all eukaryotic cells, vital e.g. for cell growth. In most cell types, exocytosis was found to be localized, i.e. it occurs preferentially at specific locations rather than equally all over the cell surface. In plants, polarized exocytosis has been implicated in the

positioning of PIN proteins to certain sides of the PM, which plays an important role in controlling the direction in which the plant growth regulator auxin leaves the cell (Vanneste & Friml, 2009). Also, tip growth of root hairs and pollen tubes are examples of polarized exocytosis in plants (Zhang *et al.*, 2010). The plant exocyst complex responsible for this has not been studied in great detail yet (Elias *et al.*, 2003). It is known that homologues of all the eight subunits that make up the yeast and mammalian exocyst exist in the genome of *Arabidopsis* (Elias *et al.*, 2003). T-DNA insertions that disrupt expression of specific *Arabidopsis* exocyst subunits (SEC6 or SEC8) are pollen lethal mutants, which was suggested to be due to defects in pollen tube germination and/or growth because of the missing exocyst (Hala *et al.*, 2008).

The mammalian exocyst that is responsible e.g. for vesicle tethering during neurotransmission in synapses, comprises an octamer of the individual subunits SEC3, SEC5, SEC6 SEC8, SEC10, SEC15, EXO70, and EXO84 (Fig. 12B) (Yu & Hughson, 2010). To allow this octameric exocyst complex to function as tether that mediates initial contact between vesicle and target membrane, some subunits need to be attached to the incoming clathrin-coated vesicle and some to the PM.

A sub-complex containing six of the eight exocyst subunits, including SEC15, is believed to function as the vesicle membrane located tether half. This sub-complex is present in the cytoplasm and becomes attached to the vesicle membrane only after the clathrin coat has been shed (Fig. 12B) (Yu & Hughson, 2010). Recruitment of tethering factors to vesicles in general, i.e. also for other tethering complexes, such as HOPS is mediated by a member of the family of Rab GTPases. In some cases, other small GTPases, lipids or SNARE proteins themselves were found to have this function as well (Yu & Hughson, 2010). For the exocyst, interaction between the Rab protein SEC4 and the sub-complex member SEC15 is essential for recruitment to the vesicle membrane (Fig. 12B) (Yu & Hughson, 2010).

Rab GTPases function as molecular switches that cycle between an active, membrane-bound and an inactive, cytosolic state (Yu & Hughson, 2010). This cycle is linked to the binding and hydrolysis of GTP. The membrane-bound state of Rab proteins is achieved by reversible attachment of a prenyl anchor. While membrane-bound, Rabs become activated through the action of guanine nucleotide exchange factors (GEFs), which catalyze the release of GDP and thereby the binding of GTP. Only in their membrane attached, active, GTP-bound state can Rab proteins recruit other so-called effector proteins such as the above described exocyst sub-complex. Following tethering, when exocytosis by trans-SNARE complexes assembly is triggered, Rab-bound GTP is hydrolyzed to GDP, and the resulting Rab-GDP forms a complex with GDI (guanine dissociation inhibitor). Formation of this GDI-Rab-GDP complex leads to its dissociation from the vesicle membrane.

Due to this ability to capture tethers, Rab proteins function as evolutionary conserved master regulators of membrane docking and fusion. The *Arabidopsis* genome encodes 57 Rab GTPases, and among these the RabA family is the most expanded with 26 members (Zhang *et al.*, 2010). It is known that RabA4b localizes to the tips of growing root hairs and RabA4d to the tips of growing pollen tubes, where it has a clear role in pollen tube growth. However, in plants, direct

interactions between exocyst subunits and small GTPases have not been reported yet (Zhang *et al.*, 2010).

The second half of the exocyst tethering complex, i.e. the remaining two of the eight subunits, Sec3 and Exo70, are thought to be stably associated with the PM (Fig. 12B). In yeast, Sec3 and Exo70 bind to the inner leaflet of the PM through direct interactions with both phosphatidylinositol 4,5-bisphosphate ($PI(4,5)P_2$) and Rho family GTPases such as Rho1, Rho3, Cdc42 (Fig. 12B). As $PI(4,5)P_2$ is present throughout the PM, it is thought that the positional information for polar localization of exocytosis is provided by these Rho family GTPases (Yu & Hughson, 2010). Different Rho GTPases may contribute to tethering different populations of secretory vesicles to defined PM subdomains, i.e. mediate exocytosis of different vesicle cargos such as cell wall components or defense substances against fungal attack (see below). Recruitment of SEC3 and Exo70 by Rho GTPases follows a similar process as described above for Rab GTPases. In plants, PM exocyst subunits binding by $PI(4,5)P_2$ and Rho binding has not yet been studied (Zhang *et al.*, 2010).

Beyond encoding spatial information and in general accelerating the rate-limiting step of vesicle capture, Rabs, Rhos and tethering factors are thought to contribute to temporal regulation of exocytotic events as well as trans-SNARE complex assembly itself (Yu & Hughson, 2010). For example, a loss-of-function mutation in Rho3 specifically blocked exocytosis without affecting exocyst localisation at the PM (Yu & Hughson, 2010). Other exocyst subunit mutants are known to cause defects in SNARE assembly and the PM SNARE SEC9 and the exocyst subunit SEC6 interact (Fig. 12B). There is also evidence that the exocyst acts in conjunction with SM proteins to control the speed and timing of SNARE complex formation. The HOPS and CORVET tethering complexes even contain a built-in SM protein (Fig. 12A) (Yu & Hughson, 2010). However, even in yeast and mammalian cells, these processes are still poorly understood. Similarly, it is largely unknown what factors regulate the selective activation and localisation of Rab and Rho GTPases themselves (He & Guo, 2009).

The situation is even more complex in specialised forms of exocytosis found in mammalian cells, e.g. secretion of hormones and neurotransmitter release at the synapse. Here, additional regulatory proteins such as complexin and synaptotagmin contribute to precise timing and regulation of vesicle fusion to the PM (Rizo & Rosenmund, 2008). It is thought that newly assembled trans-SNARE complexes are prevented from zippering by the binding of complexin. Zippering, i.e. fusion is eventually triggered by a specific signal, a rise in the intracellular Ca^{2+} concentration. Ca^{2+} binds to synaptotagmin, which reverses the action of complexin and allows fusion to be completed (Rizo & Rosenmund, 2008).

Arabidopsis SNARE proteins

Plants show a considerably expanded repertoire of SNAREs compared to yeast and mammals. While in the latter 25 and 36 different SNARE proteins are present respectively, the genome of the

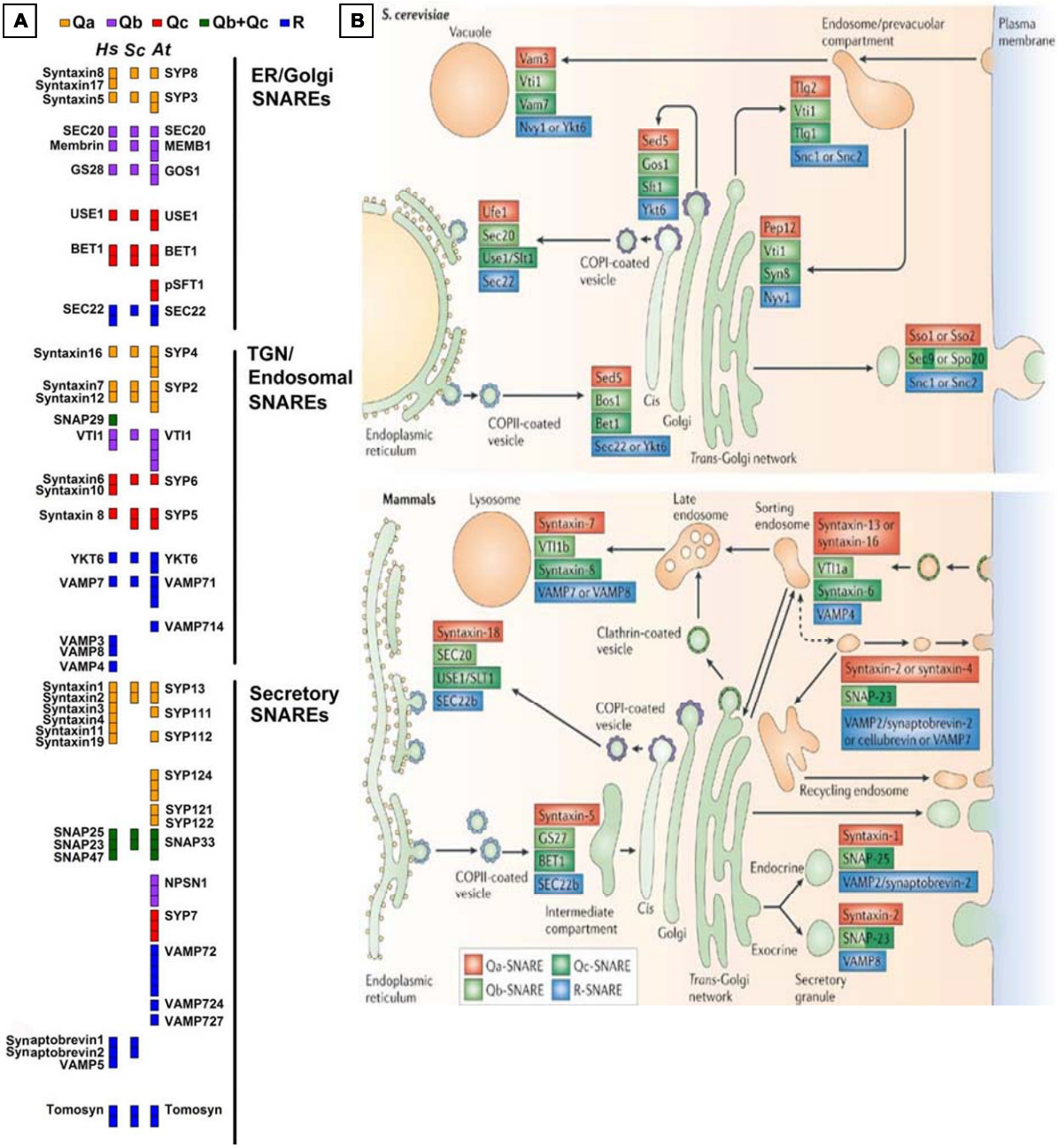

Fig. 13 SNARE proteins from mammalians, yeast and *Arabidopsis*

(A) Comparison of SNARE gene families in *Homo sapiens* (*Hs*), *Saccharomyces cerevisiae* (*Sc*), and *Arabidopsis thaliana* (*At*). SNAREs are divided into three basic modules based upon the site of action: ER/Golgi, TGN/endosomal (including vacuole), and secretory/PM. SNARE genes are indicated by individual boxes with the type of SNARE labelled with a colour (Qa, orange; Qb, purple; Qb + Qc, violet; Qc, red; R, blue). Each box indicates a single genomic locus and linked boxes represent a phylogenetic subfamily.
(B) An overview of the cognate SNARE complexes of *Saccharomyces cerevisiae* (top) and mammalian (bottom) Qa-, Qb-, Qc- and R-SNAREs (see colour-code) and their assignment to the fusion events at the different subcellular organelles of the secretory pathway.
Images adapted from previous publications (Jahn & Scheller, 2006; Sanderfoot, 2007).

dicotyledonous *Arabidopsis thaliana* encodes for 60 and the genome of the monocotyledonous rice for 57 different SNAREs (Pratelli *et al.*, 2004; Jahn & Scheller, 2006; Sutter *et al.*, 2006a). Sequence comparisons revealed that the higher number of SNAREs in plant species is for the most part not due to the evolution of novel SNARE isoforms (Sanderfoot *et al.*, 2000; Sanderfoot, 2007). Instead, it appeared that the number of paralogous SNAREs in some conserved subfamilies

was expanded by gene duplications (Sanderfoot *et al.*, 2000; Sanderfoot, 2007). This is indicated in Fig. 13A, taken from Sanderfoot *et al.* (2007). Here, the Qa-, Qb, Qc- and R-SNAREs of *A. thaliana*, *S. cerevisiae* and *Homo sapiens* were divided into three basic modules based upon the site of their membrane fusion action: ER/Golgi, TGN/endosomal (including vacuole), and secretory (PM). It is thought that the greater diversification of SNARE isoforms supports plant-specific biological processes such as for example the plant-specific type of cytokinesis, gravitropic responses, and the transport of phytohormones such as auxin in a manner that establishes polarity at the subcellular level (Pratelli *et al.*, 2004; Surpin & Raikhel, 2004). Similarly, an increase in the number of endosomal SNAREs might be associated with the development of the typical large central vacuole of plant compared to animal and yeast cells (Sanderfoot, 2007). Only two entirely novel subfamilies were discovered in plants: the NPSN (novel plant-specific SNARE) Qb-SNAREs and the SYP7 Qc-SNAREs (Sanderfoot *et al.*, 2000). Their functions remain mostly elusive so far. The *Arabidopsis* NPSN11 protein, for example, was co-localised with SYP111 to the cell plate in dividing cells and immuno-precipitated from total *Arabidopsis* membrane proteins by SYP111. Both proteins are thought to play a critical role in membrane fusion during cell plate formation (see below, p. 54) (Lauber *et al.*, 1997; Zheng *et al.*, 2002; Surpin & Raikhel, 2004). However, *npsn11* knockout mutants did not show any obvious phenotype, suggesting that other members of the NPSN family can functionally substitute for NPSN11 (Zheng *et al.*, 2002).

There were indications that SYP71 in turn might interact with SYP111, which would place this Qc-SNARE in a cognate SNARE complex with NPSN11 (Qb) and SYP111 (Qa) for cytokinesis (Sanderfoot, 2007). This hypothesis was supported by the observations of two other groups (Uemura *et al.*, 2004; Suwastika *et al.*, 2008) who localised SYP71 to the ER in the dividing cells of various types of tissues. In fact, this particular SNARE showed a dual localisation pattern both to the ER and the PM at the dividing cells stage and the PM in all other vegetative tissues (Alexandersson *et al.*, 2004; Marmagne *et al.*, 2004; Suwastika *et al.*, 2008). These results suggested that SYP71 may be involved in multiple membrane fusion steps.

In comparisons to animals and yeast, plants further lack a particular R-SNARE subfamily called brevins. R-SNAREs (p. 37) can have either a short or long N-terminal region, further subdividing them into brevins (e.g. Synaptobrevin2) and longins (Uemura *et al.*, 2005). *Arabidopsis* longins are for the most part VAMPs (vesicle-associated membrane proteins). The *Arabidopsis* genome harbours 12 VAMP encoding genes, which fall into two subfamilies, VAMP71 and VAMP72 (see Fig. 13A).The VAMP72 subfamily appears to be specific to green plants (Sanderfoot, 2007). In general, very little is known about the biological roles of plant R-SNAREs. An *Arabidopsis* antisense line, where the entire VAMP71 subfamily was suppressed, suggested at least partial redundancy for these R-SNAREs (Leshem *et al.*, 2006; Leshem *et al.*, 2010). The antisense plants exhibited both increased salt tolerance and decreased stomatal closure during drought or after treatment with ABA. Impaired stomatal closure was associated with increased vacuole number and size in line with the disruption of vacuolar fusion events by missing VAMP71 R-SNAREs (Leshem *et al.*, 2006; Leshem *et al.*, 2010).

With regard to QbQc-SNAREs, *Arabidopsis* harbours a total of three proteins: SNAP29,

SNAP30 and SNAP33. In contrast to mammalian SNAP25 that is attached to the PM by palmitoylation of conserved cysteines, *Arabidopsis* SNAPs have no conserved cysteine residues and SNAP33 localise to the PM by an unknown posttranslational modification (Heese *et al.*, 2001). SNAP30 appears to be expressed exclusively in pollen (Lipka *et al.*, 2007). In contrast, SNAP29 and SNAP33 are both expressed in a variety of different tissues. SNAP33, however, has significantly higher expression levels than SNAP29 (Wick *et al.*, 2003; Lipka *et al.*, 2007).

The subcellular localisation of most *Arabidopsis* SNAREs is known, although for the most part determined only by transient (over-)expression of fluorophore-labelled proteins (Uemura *et al.*, 2004; Enami *et al.*, 2009). Much less is known about which of the Qa-, Qb-, Qc- and R-SNAREs localised to the various compartments form cognate SNARE-complexes to drive vesicle fusion. Analysis of knock-out plants are often complicated by redundancy between the above mentioned presence of large numbers of paralogous SNAREs in some subfamilies. Apart from a larger scale interaction study based on co-immunoprecipitation (Sanderfoot *et al.*, 2001), only very recently, a systematic investigation of SNARE-SNARE interactions was attempted by (Kato *et al.*, 2010). A split luciferase complementation assay was developed to detect binary protein–protein interactions in *Arabidopsis* leaf protoplasts in a 96-well plate format (Kato *et al.*, 2010). However, the interpretation of both studies was hampered by the promiscuous interaction of non-cognate SNAREs that do not drive vesicle fusion but simply co-localise in the same membranes. In addition, due to the detection of strictly binary interactions, conclusions about individual assembled SNARE complexes that contain three or four proteins were only indirectly possible.

So far only one functional cognate *Arabidopsis* SNARE complex was identified that involves the Qa-SNARE SYP121 (see below, p. 55). In contrast, for mammalian and yeast cells it is already known, which of the Qa-, Qb-, Qc- and R-SNAREs form cognate SNARE complexes for specific fusion events in the secretory pathway (Fig. 13B). Comparisons of the available data from yeast and mammals revealed that in most cases orthologous proteins formed cognate SNARE complexes for identical subcellular fusion events (Jahn & Scheller, 2006). For example, in yeast cells, the SNARE complex that mediates anterograde traffic from the ER to the Golgi consists of Sed5 (Qa), Bos1 (Qb), Bet1 (Qc) and Sec22 (R) (Fig. 13B) (Jahn & Scheller, 2006). In mammals the orthologues Syntaxin5 (Qa), Gs27 (Qb), BET1 (Qc) and SEC22 (R) fulfil the same function (Fig. 13B) (Jahn & Scheller, 2006). *Arabidopsis* has proteins that are orthologous to each of these SNAREs: SYP31 (Qa), MEMB1 (Qb), BET1 (Qc), and SEC22 (R). It is assumed that these *Arabidopsis* orthologous SNAREs will operate as cognate SNARE complex for the fusion of ER-derived vesicles to the Golgi as well (Sanderfoot, 2007). Investigations into a few of these genes have indicated that this is indeed the case (Chatre *et al.*, 2005; Chatre *et al.*, 2008). A similar situation is likely true for cognate SNARE complexes operating on the other subcellular locations of the secretory pathway (Sanderfoot, 2007).

The SYP1 subfamily of *Arabidopsis* SNAREs

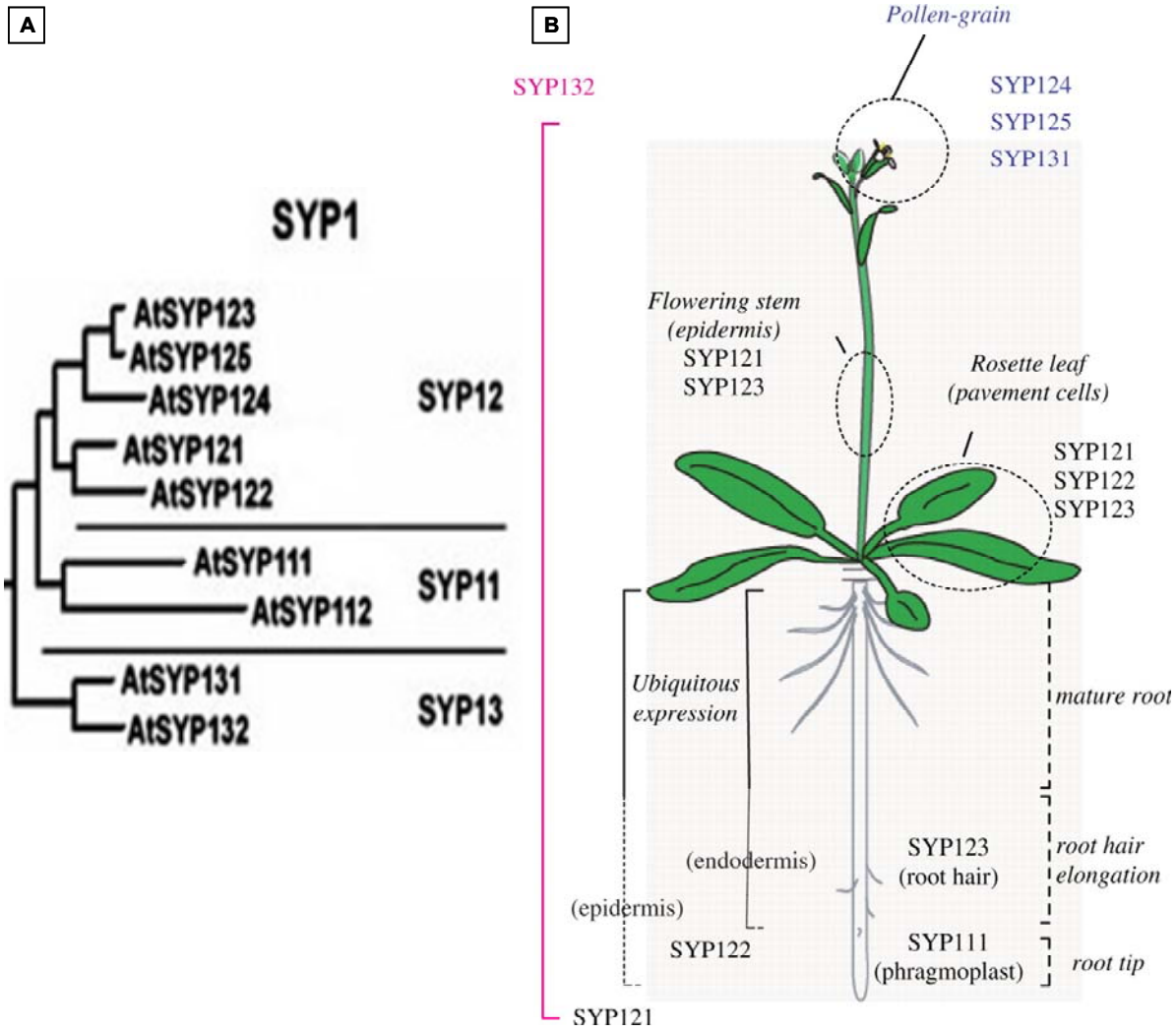

Fig. 14 The *Arabidopsis* SYP1 subfamily of plasma membrane Qa-SNAREs

(A) A phylogenetic tree of the SYP1 subfamily of *Arabidopsis* PM SNAREs shows three further subgroups: SYP11, SYP12 and SYP13.
(B) A schematic illustration of the expression profiles of all members of the *Arabidopsis* SYP1 subfamily. Stable transformants of promoter-*SYP1-GFP* were analyzed.
Images were adapted from previous publications (Sanderfoot *et al.*, 2000; Enami *et al.*, 2009).

Among mammalians, many distinct types of Qa-SNAREs (syntaxins) reside on the PM (syntaxins 1, 2, 3, 4, 11, and 19, see Fig. 13A) (Jahn & Scheller, 2006). They were shown to have diverse and specialized functions in delivery of vesicles to various domains of the PM, i.e. in polarised exocytosis in the context of the exocyst as described above (p. 45ff.). Yeast has only one paralogous pair of PM-type syntaxins (Jahn & Scheller, 2006). All *Arabidopsis* Qa-SNAREs localised to the PM belong to the SYP1 subfamily (Fig. 13A) (Pratelli *et al.*, 2004). SYP stands for syntaxin of plants (Sanderfoot *et al.*, 2000). Based on phylogenic analysis, Sanderfoot *et al.* (2000) categorized the *Arabidopsis* PM-resident SYP1 subfamily into three subgroups, SYP11, SYP12 and SYP13 (Fig. 14A). The same authors suggested that the presence of these three subgroups reflects a complexity and specialization of roles associated with the rise of land plants

and their multicellularity (Sanderfoot, 2007).

According to their hypothesis, the SYP13 subgroup represents the basal PM syntaxin inherited from the chlorophyte ancestors, and would be involved in general housekeeping roles (e.g. constitutive secretion). The SYP12 subgroup would arise in the mosses to support more specialized roles of secretion (e.g. defence related). Finally, specialized syntaxins of the SYP11 subgroup would evolve to operate in essential processes in seed plants (e.g. cytokinesis).

The only *Arabidopsis* SYP1 SNAREs for which functional studies have been published are SYP121, SYP122 and SYP111. What is known of their roles in vesicle trafficking processes so far, coincides well with the hypothesis of Sanderfoot *et al.* (2007). The putative functions of the remaining SYP1 subfamily members are at this point speculations based upon their expression data. In particular a study published by Enami *et al.* (2009) is worth mentioning.

These authors generated transgenic *Arabidopsis* lines stably expressing GFP-fused SYP1 SNAREs under the control of their native promoters. Their analysis of the spatio-temporal expression profiles of all nine SYP1s allowed Enami *et al.* (2009) to compile the overview pictured in Fig. 14B. Enami *et al.* (2009) found that SYP132 was the only SYP1 family member to be expressed ubiquitously in all investigated tissues of root and shoot and throughout plant development (Fig. 14B). This result supported the suggestion by Sanderfoot *et al.* (2007) that SYP13 subgroup members might function in housekeeping, i.e. constitutive membrane trafficking to the PM.

In contrast, the expression patterns of the other SYP1s were tissue specific, and all different from one another although sometimes with partial overlap (Fig. 14B). Enami *et al.* (2009) interpreted this result as an indication that, in analogy to the situation in animal cells, multiple membrane trafficking pathways to particular domains of the PM might exist and serve specialised diverse functions. Redundancy in the same cell would allow, for example, the transport of various functional molecules in a polarized or non-polarized manner.

In contrast to SYP132, SYP131 was pollen-specific and localised uniformly to the PM of pollen tubes and pollen grains. In these tissues the GFP-SYP132 signal was lower compared to SYP131. Another very specifically localised SYP1 SNARE was SYP123. SYP123 was predominantly expressed in growing root hair cells during root development. SYP124 and SYP125 were pollen-specific. Their fluorescent signal was found in the tip region of pollen tubes during pollen tube elongation. More specifically, GFP–SYP125 localized to the apical region of the pollen tube, while GFP–SYP124 localized to the subapical region of the tip.

Enami *et al.* (2009) detected no expression of GFP–SYP112 in any of the examined tissues. SYP112 is the closest paralog of SYP111. It has been reported that SYP112 can completely complement the phenotype of a *syp111* loss-of-function mutant (see below) (Muller *et al.*, 2003). However, Enami *et al.* (2009) stated that a microarray database quarry had indicated very low native expression levels under normal growth conditions.

SYP111

Loss-of-function mutants of the SYP1 Qa-SNARE SYP111 ('KNOLLE') are seedling-lethal (Lukowitz *et al.*, 1996). Embryos of the *syp111* mutant revealed incomplete cell divisions that resulted in multinucleate and enlarged cells (Lauber *et al.*, 1997). Membrane vesicles accumulated at the equator of dividing cells but did not fuse normally (Lauber *et al.*, 1997). Cytokinesis represents the final stage of eukaryotic cell division that occurs after nuclear division (Jurgens, 2005). During cytokinesis the cytoplasm becomes partitioned between daughter cells by a nascent cross cell wall that is deposited from the middle out. From early telophase onward, the phragmoplast, a microtubule and actin-filament-based structure directs vesicle accumulation to the mid-plane of the cell. There, vesicles undergo homotypic fusion events to form a transient membrane-bounded compartment, the cell plate. Cell-plate formation progresses centrifugally until fusion with the lateral cell sites. This stage represents a new cell wall with two flanking plasma membranes (Jurgens, 2005).

Consistent with a role as Qa-SNARE specifically promoting vesicle fusion during cytokinesis, *SYP111* mRNA and protein expression was detected only in proliferating cells. *SYP111* mRNA accumulated strongly but transiently during the cell cycle in actively dividing tissues of developing flowers and siliques, in the shoot apex and the root tip (Lukowitz *et al.*, 1996; Lauber *et al.*, 1997; Volker *et al.*, 2001). GFP–SYP111 was also found to specifically localise to the developing cell plates in dividing guard cells (Enami *et al.*, 2009). In such proliferating tissues SYP111-positive vesicles appeared at the onset of the cell cycle (during M phase of mitosis). Detection with anti-SYP111 antibody revealed that SYP111 protein relocated to the cell plate plane during telophase, and disappeared at the end of cytokinesis (Lukowitz *et al.*, 1996; Lauber *et al.*, 1997; Assaad *et al.*, 2001).

The membrane vesicles that deliver cell wall building and membrane material to form the cell plate were initially believed to originate from Golgi stacks only. Subsequent work provided evidence that endocytic delivery of cell surface material through sorting and recycling endosomes significantly contributes to speedy cell plate initiation and expansion (redirected through the sorting platform of the TGN, see p. 35) (Volker *et al.*, 2001; Dhonukshe *et al.*, 2006; Reichardt *et al.*, 2007). Volker *et al.* (2001) and Dhonukshe *et al.* (2006) showed that SYP111 accumulated at the PM before cell plate initiation. During cytokinesis, part of the above described SYP111-positive vesicles co-localised with endosomal markers (Volker *et al.*, 2001; Dhonukshe *et al.*, 2006). In addition, SYP111 co-fractionated with endosomal but not Golgi markers on sucrose gradients. SYP111 was further suggested to contribute to homotypic fusion events between endosomes (as well as between golgi-derived vesicles) before their fusion to the cell plate (Dhonukshe *et al.*, 2006).

Vesicle fusion during cell plate formation likely involves homologues of all the proteins generally needed to promote and regulate trans-SNARE complex assembly. As mentioned earlier, the Qb-SNARE NPSN11 and the Qc-SNARE SYP71 were implicated to form a cognate SNARE complex with the Qa-SNARE SYP111 (Sanderfoot, 2007). Immunofluorescence microscopy had

shown that SYP111 and NPSN11 co-localise at the cell plate and in punctuate subcellular organelles, which did not correspond to Golgi stacks. In addition, yeast two-hybrid experiments indicated interaction between SYP111 and the QbQc-SNARE SNAP33 which similarly co-localised with SYP111 at the cell plate (Heese *et al.*, 2001). Consistent with a role in cell plate vesicle fusion processes, *snap33* mutants showed among other defects incomplete cell walls implicating disturbed cytokinesis (see below) (Heese *et al.*, 2001).

The R-SNAREs contributing the fourth SNARE motif for both putative SYP111 involving cognate SNARE complexes are still unknown. Two types of cognate SNARE complexes are in agreement with two types of fusion events for Golgi- and endosome-derived compartments during cytokinesis. There is evidence that SYP111 assembles into a complex with the cis-SNARE complex disassociating proteins Sec18 (NSF) and an α-SNAP (Rancour *et al.*, 2002). As mentioned earlier, KEULE, which was the mutated gene in another cytokinesis-defective *Arabidopsis* line is thought to be an SM protein for a cognate SNARE complex involving SYP111 (p. 45) (Assaad *et al.*, 2001). Very recently, it was reported that the *AtTRS120* locus of the TRAPPII tethering complex (see Fig. 12, p. 46) is required for cell plate formation during cytokinesis (Thellmann *et al.*, 2010). Finally, it is worth mentioning that SYP111 has no close counterpart among yeast or animal syntaxins (Lukowitz *et al.*, 1996; Sanderfoot *et al.*, 2000). This is believed to be related to the unique mechanism of cell division in plants that needs to create a cell wall. In animal cells, a contractile phragmoblast-like ring simply pinches a dividing cell in two (Jurgens, 2005).

SYP121 and SYP122

As indicated by the phylogenetic tree published by Sanderfoot *et al.* (2000), SYP121 and SYP122 are the closest paralogs among the *Arabidopsis* SYP1 Qa-SNAREs (see Fig. 14A). Their PM localisation was confirmed by several approaches. Fusions of both syntaxins to fluorophores (expressed either from their own or the strong constitutive 35S promoter) were localised to the PM in all tissues investigated in either transient or stable transformation experiments (Collins *et al.*, 2003; Assaad *et al.*, 2004; Uemura *et al.*, 2004; Foresti *et al.*, 2006; Pajonk *et al.*, 2008; Kwon *et al.*, 2008; Enami *et al.*, 2009). Furthermore, proteomic approaches identified SYP121 and SYP122 in the PM enriched fractions of *Arabidopsis* suspension-cultured cells and shoot tissue respectively (Nuhse *et al.*, 2003; Alexandersson *et al.*, 2004; Marmagne *et al.*, 2004).

Alexandersson *et al.* (2004) also identified the Qa-SNARE SYP132 and Marmagne *et al.* (2004) found the Qb-SNARE NPSN13 and the R-SNARE VAMP722. Thus, in addition to the SYP1 subgroup of Qa-SNAREs and the Qc-SNAREs of the SYP7 subgroup, 5 VAMPs (R-SNARE), 3 Qb-SNAREs (NPSN11, NPSN12 and NPSN13) and the three QbQc-SNAREs (SNAP29, SNAP30 and SNAP33) showed PM localisation (Alexandersson *et al.*, 2004; Marmagne *et al.*, 2004; Uemura *et al.*, 2004). It was suggested that from among these SNAREs, similar to the situation at the cell plate during cytokinesis, two types of SNARE complexes might formed to mediate exocyst depending secretion events at the PM: The SYP1 Qa-SNAREs and vesicle-bound R-SNAREs of the VAMP72 subgroup might form cognate SNARE complexes with Qb-SNAREs

from the NPSN1 subgroup and Qc-SNAREs from the SYP7 subgroup. Alternatively, a QbQc-SNARE of the SNAP subgroup might be involved (Sanderfoot, 2007).

The first cognate SNARE complex of plants, only recently discovered, proved to be of the latter type. The PM Qa-SNARE SYP121 interacted with SNAP33 and VAMP722 (or VAMP721) to form functional SNARE complexes involved in defence against pathogenic fungi *in planta* (Kwon *et al.*, 2008).

A role for SYP121 ('PEN1') in *Arabidopsis* non-host resistance against barley powdery mildew fungus *Blumeria graminis* f. sp. *hordei* had originally been described by different authors (Collins *et al.*, 2003). A genetic screen for mutations that resulted in increased cell wall penetration by this fungus (pen mutants) identified PEN1. The *pen1-1* mutation, in the following referred to as *syp121* mutant, resulted in a stop codon early in the open reading frame and complete loss SYP121 protein, i.e. function (Collins *et al.*, 2003).

Collins *et al.* (2003) had already proposed an involvement of exocytosis via a SYP121 depending SNARE-complex in immunity against this ascomycet. GFP-SYP121 accumulated in the PM below the sites of fungal attack (Assaad *et al.*, 2004). With regard to the missing SNARE complex partners, it had been discovered early on that *in vitro Arabidopsis* SNAP33 interacts with the tobacco homolog of SYP121 (NtSYR1) (Kargul *et al.*, 2001). Kwon *et al.* (2008) confirmed that upon challenge with powdery mildew, indeed both SNAP33 transcript and protein increased in abundance. YFP-SNAP33 and GFP–VAMP722 co-localised with CFP-SYP121 in the focal accumulation sites directly beneath *B.graminis* appressoria (fungus hyphae specialized to breach the cell wall) (Kwon *et al.*, 2008). Homozygous T-DNA insertion lines for all 6 VAMP72 subfamily members showed wt-like entry rates of *B.graminis* into leaf epidermal cells indicating genetic redundancy. VAMP722 is most closely sequence-related to VAMP721 and homozygous double knock-outs for these two genes were lethal. However, transgenic *Arabidopsis* lines for conditional VAMP722/ VAMP721 co-silencing phenocopied the *syp121* mutant after challenge with *B. graminis*.

These experiments provided evidence for the dependence of the wt defence against *B. graminis* on a functional cognate SNARE complex involving SYP121, SNAP33 and the two functionally redundant VAMP72 subfamily members, VAMP722 and VAMP721. Direct *in vitro* and *in planta* evidence for the formation of a cognate trans-SNARE complex between these SNAREs was obtained by Kwon *et al.* (2008). Co-precipitation of tagged purified proteins showed that, in the presence of SYP121, SNAP33 was able to form complexes with VAMP722 and to a lesser extent with VAMP721.

The specificity of SNARE complex formation between these three proteins could be shown with the help of the *pen1-3* allele. This allele shows a point mutation that does not result in the loss of SYP121 protein but rather in the exchange of a glycine residue to glutamate. This aa exchange is located in a residue that is conserved in the SNARE motif of all SYP12 subgroup members. In *vitro*, SNAP33 and VAMP722 were unable to form SNARE complexes with this mutated SYP121 protein and *pen1-3* were moderately defence-compromised upon exposure to *B. graminis* (Collins *et al.*, 2003; Kwon *et al.*, 2008). It was concluded that the aa substitution destabilized an interaction

needed to correctly 'zipper' the layers between the helices of the four SNARE motifs in a cognate trans-SNARE complex. Indeed, Kwon *et al.* (2008) could not co-precipitate *in planta* existing SNARE-complexes when a tagged PEN1-3 protein was stably expressed under the control of the *SYP121* promoter in a *syp121* mutant. In contrast, exchanging PEN1-3 with a GFP-SYP121 fusion, led to co-precipitation of a protein complex from leaf protein extracts that contained both native SNAP33 and VAMP722 (or VAMP721). Together these experiments provided direct evidence for *in planta* SYP121–SNAP33-VAMP722/VAMP721 cognate trans-SNARE complexes.

The cargo that is transported by vesicle fusion through this SNARE complex is still unknown. Wt *Arabidopsis* is immune to non-adapted powdery mildew fungi such as *B. graminis* which in nature colonize grasses. This immunity is mediated by pre-invasive defence mechanism, one of which is the formation of the so-called papillae. Papillae are dome-shaped cell-wall appositions in the paramural space (inner side of cell walls) that form directly beneath invading fungal appressoria (specialised hyphae) to prevent a breach in the plant cell wall. They are agglomerations of a variety of plant cell-derived components including cellulose, callose, pectins, phenolics such as lignin, hydroxyproline-rich glycoproteins, and antimicrobial polypeptides such as thionins. An additional pre-invasive defence mechanism is the timely production and localised discharge of toxic compounds at sites of fungal attack.

During challenge with *B. graminis* GFP-SYP121 accumulated in the PM at the periphery of forming papillae. A second GFP-SYP121 signal had been observed in intracellular compartments that accumulated in the vicinity of papillae (Collins *et al.*, 2003; Assaad *et al.*, 2004). With roughly 1 μm in diameter, these compartments were unusually large, i.e. visible by light microscopy, compared to most exocytotic vesicles described in animals and plants (Collins *et al.*, 2003). Collins *et al.* (2003) suggested an involvement of SYP121 in homotypic vesicle fusion events to create these large vesicles. The large vesicles stained positive for H_2O_2, a plant defence compound that can perform e.g. antimicrobial and cell-wall cross-linking functions (Thordal-Christensen, 2003). Thus, it was suggested that the SYP121 SNARE complex directs reactive oxygen species toward infection sites. In addition, SYP121 mediated vesicle fusion could deliver building material to forming papillae via SNARE-complex-mediated exocytosis. However, SYP121 is clearly not the only PM SNARE involved in delivering cell wall components for papillae formation as in the *syp121* mutant papillae formation is not abolished, only delayed by about 2 h (Collins *et al.*, 2003; Assaad *et al.*, 2004; Meyer *et al.*, 2009). The *syp121* papillae were morphologically indistinguishable from wt papillae (Assaad *et al.*, 2004). Assaad *et al.* (2004) speculated that in the race between the fungus and the plant, the timing of papilla formation might be critical and thus delay in papillae formation is the primary defect in *syp121* mutants and correlates with impaired pre-invasion resistance. Similarly, papillae formation was only delayed in the inducible co-silencing lines for VAMP721/VAMP722 (see above) (Kwon *et al.*, 2008). In conclusion, SYP121 has a very definite but not essential role in pre-invasive defence against powdery mildew attack that involves exocytosis of an unknown cargo.

SYP122 was initially identified as a likely candidate to share redundancy with SYP121 in the task of delivering cell wall components to forming papillae (Nuhse *et al.*, 2003; Assaad *et al.*,

2004). The *syp122-1* mutation, in the following referred to as *syp122*, was originally characterised by Nuhse *et al.* (2003) and identified as a true null allele lacking SYP122 protein. These authors had observed that SYP122 was phosphorylated in response to a microbial elicitor of defence (flagellin) in suspension-cultured *Arabidopsis* cells. Flagellin in general stimulates callose deposition in plants. In accordance, *Arabidopsis syp122* mutant plants showed pronounced primary cell wall defects. In contrast, only subtle cell wall defects were found in the *syp121* mutant (Assaad *et al.*, 2004). Furthermore, transcript levels of *SYP122* were strongly up-regulated in response to a broad range of bacterial, viral, and fungal pathogens (up to 59-fold), as detected by real-time PCR. In contrast, the *SYP121* gene showed a relatively weak up-regulation (up to 5-fold) in response to the same tested pathogens (including *B. graminis*) (Assaad *et al.*, 2004). Despite cell wall defects and the lack of otherwise up-regulated SYP122 protein, Assaad *et al.* (2004) failed to uncover a defence-related phenotype in *syp122* mutant plants. For example, the *syp122* mutant retained wt levels of pre-invasion resistance against the non-host powdery mildew in suspension-cultured *Arabidopsis* cells. After exposure to this pathogen, a CFP-SYP122 fusion accumulated in the PM below attempted fungus entry sites (Assaad *et al.*, 2004). However, the local intensity of CFP-SYP122 at the attack site was only about 2-fold higher than at the PM in general, whereas the GFP-SYP121 had shown a 6-fold higher recruitment to the site of attempted penetration. Furthermore, a *syp121*/*syp122* double mutant did not differ from the *syp121* mutant with respect to the rate of successful cell wall breaches by *B. graminis* (Assaad *et al.*, 2004).

Assaad *et al.* (2004) concluded that SYP122 has a general function in secretion, including a role in cell wall deposition that is up-regulated during general pathogen attack. By contrast, SYP121 mediates a specialised defence-related function in response to powdery mildew fungi, being required for the polarized secretion events that give rise to papilla formation. Thus, with respect to pre-invasion defence against *B. graminis*, SYP121 and SYP122 were not redundant.

In contrast, the phenotype of the *syp121/syp122* double mutant suggested that both SNAREs share a function distinct from that of SYP121 in penetration resistance. Although the SYP121 and SYP122 single mutants have no visible phenotypes, the *syp121/syp122* double mutant becomes dwarfed and develops severe necrosis after a period of 2– 3 weeks of normal growth (Zhang *et al.*, 2007). Zhang *et al.* (2007) discovered that the level of salicylic acid (SA) in the syntaxin double mutant was dramatically elevated compared to wt plants and the single mutants.

SA is involved in post-invasive pathogen defence. Post-invasion resistance is a secondary line of defence that is triggered when a fungus such as *B. graminis* has overcome pre-invasive defences at the plant cell wall. Post-invasion resistance is based on suicide of cells surrounding the infection site (hypersensitive response) (Thordal-Christensen, 2003).

The presence of elevated levels of SA indicated the up-regulation of the SA defence signalling pathway that in turn was partially responsible for the necrosis and dwarfism phenotype. Silencing of the SA pathway by using mutations in genes for SA signal components, partially rescued the double mutant phenotype. In addition to the SA signaling pathway, a pathway that potentiates a programmed cell death response was up-regulated in *syp121/syp122* plants. The programmed cell death response is similar to the hypersensitive response, i.e. contributed in part to

the necrosis phenotype as well (Zhang *et al.*, 2007). Finally, also jasmonic acid (JA) and ethylene (ET) defense signaling pathways were up-regulated in the double mutant.

Zhang *et al.* (2007) concluded that SYP121 and SYP122 partially complement each other in a function as negative regulators of programmed cell death, SA, JA and ET pathways in post-invasive defence. The loss of both SNAREs in the *syp121/syp122* mutant then causes specifically defense-like gene expression changes resulting in dwarfism and necrosis. It is currently not clear how SYP121 and SYP122 inhibit the defence signaling pathways.

Intracellular trafficking of Syntaxins

Post-translational insertion into the ER

Most SNAREs, including the syntaxins of the SYP1 subfamily of *Arabidopsis*, are Type IV membrane proteins also called 'tail-anchored' (TA) proteins (Borgese *et al.*, 2003). TA proteins are sorted posttranslational to various organelles. They constitute a large and heterogeneous group in animals, yeast and plants alike. Although the SNAREs involved in membrane trafficking represent the largest functional class of TA proteins, other non-SNARE TA proteins are responsible for a variety of equally important cellular processes, including redox reactions, apoptosis and protein translocation (Dhanoa *et al.*, 2010).

The earlier described protein structure of SNAREs such as Syntaxin1A and SYP121 (Fig. 9, p. 38) is characteristic for TA proteins: a functional N-terminal region located in the cytosol is anchored to the lipid bilayer by a transmembrane domain (TMD) very close to the C-terminus, followed by a short luminal polar sequence (Rabu *et al.*, 2009). The C-terminal membrane anchor generally represents the sole membrane-targeting signal for delivery to the correct subcellular compartment, no N-terminal hydrophobic signal sequences as described for KAT1 are present (Kutay *et al.*, 1993; Borgese *et al.*, 2007). Due to its proximity to the C-terminus (less than 30 residues in general), the TMD it is still contained within the ribosomal exit tunnel during chain termination (Borgese *et al.*, 2007): a typical TMD contains 20 residues and the ribosomal exit tunnel holds a chain of about 30 residues (Jarvis *et al.*, 1998). Thus, as the C-terminal TMD emerges from the ribosome only after release of the finished TA polypeptide from the ribosome, it will also remain hidden from cytosolic targeting factors until then (Kriechbaumer *et al.*, 2009). Therefore, TA proteins do not have a chance to interact with the SRP and the usual way of co-translational membrane insertion, coupled to ongoing protein synthesis, is prohibited (see p. 27). Instead, these proteins are obliged to target and insert into their destined membranes by post-translational mechanisms (Borgese *et al.*, 2007). Most of the information about this post-translational ER insertion mechanism is so far derived from studies of animal and yeast proteins and even there it is still very incomplete.

After release from the ribosome in the cytosol, TA proteins can be inserted into a number of target membranes. As other, non-TA proteins, they can insert directly into the outer mitochondrial membrane (MOM), the Chloroplast Outer Envelope (COE), or the peroxisomal

membrane. However, the ER represents the major destination for post-translational TA protein insertion. Membranes of the secretory pathway downstream of the ER (e.g. Golgi, TGN, endosome and PM) are non-permissive for direct TA protein insertion (Kalbfleisch *et al.*, 2007). As for co-translational translocated proteins (e.g. the Shaker channels), localization to these compartments is only attained by vesicular transport downstream from the ER (Rabu *et al.*, 2009; Kriechbaumer *et al.*, 2009; Borgese & Fasana, 2011). In contrast to co-translational translocated proteins, insertion of TA proteins into the ER has been shown to be independent of the heterotrimeric Sec61 translocon complex (Borgese *et al.*, 2007). *In vivo* studies, with yeast mutants defective in components of the ER translocation machinery, demonstrated that efficient transmembrane integration of the representative TA protein cytochrome b5 occured in the absence of known functions of the translocon and its accessory proteins (Kalbfleisch *et al.*, 2007). Further *in vitro* studies revealed the existence of an unassisted pathway by which some TA proteins spontaneously translocate their C-terminus across the membrane of pure lipid vesicles confirming that no ER protein or other membrane or cytosolic factors play a facilitating role in the translocation (Brambillasca *et al.*, 2005). However, lipid composition of the vesicles markedly affected insertion. Even low concentrations of cholesterol, incorporated into vesicles at levels only slightly higher than those found in native ER membranes, completely abolished cytochrome b5's transmembrane integration (Brambillasca *et al.*, 2005; Kemper *et al.*, 2008). The inhibitory effect was attributed to an increase in bilayer order imparted by the sterol and may explain the incapability of TA proteins to directly insert into the cholesterol-enriched membranes of the exocytotic and endocytotic pathways downstream of the ER (see above). However, other investigated TA proteins, for example the R-SNARE Synaptobrevin2, were incapable of unassisted insertion into membranes, which implied a need for ER membrane proteins and energy (Kutay *et al.*, 1993). TMD swapping experiments led to the conclusion that TMD hydrophobicity is the main determinant for access to, or exclusion from, the unassisted pathway (Brambillasca *et al.*, 2006). Only TA proteins with moderately hydrophobic TMDs seemed to have the ability for unassisted insertion into pure lipid bilayers. It is likely, that TA proteins with more hydrophobic TMDs will be prevented from spontaneous insertion because of the increasing difficulty for a hydrophobic sequence to cross the barrier of phospholipid polar headgroups at the interface between the bilayer and the surrounding aqueous phase. In addition, while moderately hydrophobic TMDs confer a certain degree of water solubility, TA proteins with more hydrophobic TMDs are very likely to rapidly form insoluble aggregates in the cytoplasm, unless assisted by a chaperone. Indeed, it has been shown, that most ER-targeted TA substrates seem to reach their destination by chaperone-mediated, energy-requiring pathways, that keeps these proteins in an insertion-competent form (see Fig. 15) (Borgese *et al.*, 2007; Borgese & Fasana, 2011).

Three chaperone systems have been described so far (Fig. 15) (Rabu *et al.*, 2009; Borgese & Fasana, 2011). The first features the SRP in an unusual post-translational mode but still using GTP as energy source (Cross *et al.*, 2009). Instead, the heat shock protein Hsc70/Hsp40 chaperone system is ATP-dependent, as Hsc70 is a cytosolic ATPase. The third system relies on a novel

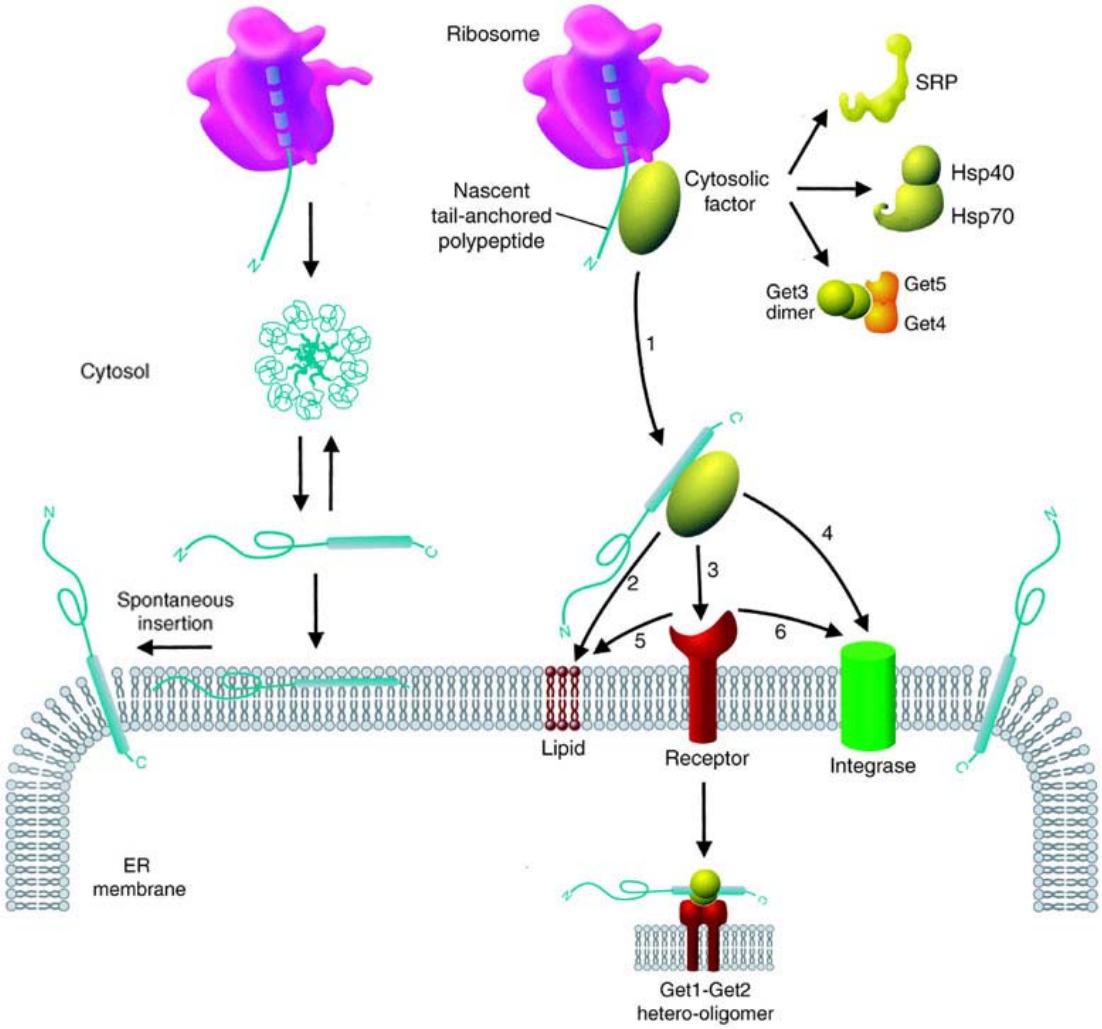

Fig. 15 Model for post-translational ER insertion of TA proteins

(left hand part) TA proteins (turquoise) with moderately hydrophobic TMDs are endowed with a certain degree of water solubility. After contacting the bilayer without assistance from chaperones, they insert spontaneously into the ER. (right hand part) TA proteins with more hydrophobic TMDs tend to form aggregates that are incompetent for insertion. A chaperone (green) is required to keep these proteins in an insertion-competent form. Three different chaperone systems might be involved in assisting different TA proteins (SRP, Hsp40/70, Get3/4/5 complex). The TA protein precursor is recognised by cytosolic factors as the TMD folds inside the ribosome (purple), or just after it emerges from the exit tunnel, thus forming a TMD recognition complex (1). At the ER membrane, this complex either directly supports unassisted partitioning into the membrane (2), docks with a receptor (3) as for example the Get1-Get2 hetero-oligomer, or hands the substrate to a dedicated integrase (4). Alternatively, after docking with the receptor (3), the TA protein might then either undergo unassisted partitioning into the bilayer (5) or be passed on to the integrase (6). Figure was adapted from pictures published by different groups (Borgese *et al.*, 2007; Rabu *et al.*, 2009).

cytosolic ATPase named TRC40 in mammals and GET3 in yeast, respectively (Rabu *et al.*, 2009). The observation that deletion of TRC40 is embryo lethal (Mukhopadhyay *et al.*, 2006), in contrast to inhibition of either the SRP or the Hsp40/Hsc70 system, was interpreted to indicate that the GET mediated pathway is the most important one for targeting TA proteins to the ER (Borgese & Fasana, 2011). GET3 (as a dimer and in a complex with two other co-chaperones named GET4 and GET5) is proposed to specifically recognize ribosomes that carry a TMD within the tunnel and thus capture TA proteins immediately upon their release (Rabu *et al.*, 2009). Once a TA protein has

been delivered to the ER membrane, either unassisted or aided by either of the three chaperone systems, the final insertion step may occur spontaneously in both cases depending on the hydrophobicity of the TMD (Fig. 15, 2). Alternatively, the chaperone-TA complex might dock to a cognate receptor in the ER membrane, in analogy to co-translational translocation (SRP receptor, see above (Fig. 15, 3). For the GET pathway, this receptor has already been identified. A hetero-oligomer of the ER integral membrane proteins Get1 and Get2 binds to Get3 that chaperones a TA protein (Rabu *et al.*, 2009). After binding to its cognate receptor, the chaperone releases its substrate to the bilayer, where the final insertion step occurs again either spontaneously (Fig. 15, 5) or via an integrase that could help TA proteins with very hydrophobic TMDs to cross the membrane (Fig. 15, 6). It might also be possible for the chaperone to pass the TA protein directly to an integrase without the help of a receptor (Fig. 15, 4).

Many aspects of the mechanisms by which TA proteins translocate their C-terminus across phospholipid bilayers are still unknown. Similarly, understanding of the step before insertion, the sorting of TA proteins to their correct subcellular destinations, is still rudimentary, especially in plants (Dhanoa *et al.*, 2010). For TA proteins that interact with a chaperone system that is recognized by a receptor in a specific target membrane, such as Get1/2 in the ER, the chaperone aids in the targeting as well as membrane insertion. However, upon release from the ribosome, TA proteins presumably encounter a number of potential chaperones. Also, newly synthesized TA proteins capable of spontaneous transmembrane must discriminate between ER, the MOM, POM and peroxisomes to avoid opportunistic insertion into any available bilayer. Only some of the intrinsic molecular targeting signals that allow specific targeting for these unassisted TA proteins and the binding of specific chaperones for assisted ones, have been revealed yet. It was concluded that targeting signals in the tail region are from their organization similar to SA (Signal-Anchor, see p. 29) sequences: Rather than primary sequence motifs, they are made from distinct physico-chemical properties, such as the overall hydrophobicity and length of the TMD and the net charge of immediately flanking residues (Brambillasca *et al.*, 2005; Borgese *et al.*, 2007).

However, no simple correlations between targeting and tail anchor features were discovered. A net positive charge in the tail region generally conveys sorting to mitochondria and a net negative or null charge conveys sorting to the ER (Borgese *et al.*, 2007). It has also been observed that in general, the hydropathy of the TMD is lower in mitochondrial TA proteins compared with Plastid and ER TA proteins (Kriechbaumer *et al.*, 2009). With regard to the chaperone systems, tail anchors that are more hydrophobic appear to be targeted by SRP or GET complex, while Hsc70/Hsp40 seems more important for TA proteins with TMDs of a lower net hydrophobicity. One of the first studies made recently on plant TA protein targeting revealed that the overall three-dimensional configuration of the tail region appears to play an important additional role in targeting specificity to the chloroplast outer envelope. (Dhanoa *et al.*, 2010) For TA proteins with moderately hydrophobic TMDs that in vitro showed the ability for unassisted insertion into membranes, the lipids of e.g. ER membranes and MOM should be equally permissive so that they could potentially integrate into both organelles.

A model was suggested in which competition between chaperones, possibly in conjunction

with differences in target bilayer lipid composition, kinetically favours the final translocation step of selected TA proteins, underlies the complexities of TA protein targeting (Borgese & Fasana, 2011). Thus most rapidly and stably binding chaperone will determine the TA substrate's destination, while preventing inappropriate insertion into otherwise permissive bilayers. Therefore, even TA proteins with moderately hydrophobic TMDs may require *in vivo* chaperones for faithful targeting (Borgese & Fasana, 2011). In conclusion, for the TA proteins of the SYP1 subfamily of *Arabidopsis* SNAREs, with special regard to SYP121, currently no information is available about their post-translational membrane insertion process or membrane targeting features.

ER export and anterograde trafficking to the plasma membrane

As mentioned above, all TA proteins that follow the secretory pathway, i.e. SNAREs, must insert posttranslational into the ER first. Similar to the situation in plant Shaker channels almost no information is available about the ER export of SNARE proteins. Only recently, a diacidic motif (EXXD) was identified that facilitated ER export of *Arabidopsis* SYP31 (Chatre *et al.*, 2008). SYP31 is required for anterograde trafficking between the ER and the Golgi and is localized in the Golgi (Bubeck *et al.*, 2008). Deletion mutants revealed that ER export is blocked to a great extent, if not entirely, when a region between the helices Hb and Hc of the Habc domain (p. 37) is deleted, whereas deletion of the SNARE domain did not result in ER retention. Interestingly, deletion of the entire N-terminal cytosolic section up to the SNARE domain did not lead to a total retention/block of SYP31 in the ER suggesting that, although the diacidic motif can clearly contribute to the export of SYP31 out of the ER to the Golgi, other attributes may influence protein targeting. It was suggested that SYP31 may make similar use of the COPII machinery for ER export via interaction of its diacidic motif with Sec24 as was described earlier for KAT1 (p. 33) (Chatre *et al.*, 2008). Also, diacidic motifs were shown to be functional in type I, type II, and multispanning membrane proteins (Hanton *et al.*, 2005).

After ER export, the various SNARE proteins need to be sorted to their specific subcellular localisations to ensure that each intracellular membrane is equipped with the appropriate set of SNARE proteins to mediate fusion events with incoming cargo vesicles. In addition, after completing fusion, vesicle associated SNAREs need to be returned to their correct donor compartment for another round of vesicle budding. These sorting mechanisms are even in the animal field mostly undiscovered (Jahn & Scheller, 2006). Although the cytoplasmic (N-terminal) domains of SNAREs are essential for their correct sorting, no defined sorting signals have been identified yet (Jahn & Scheller, 2006). In addition, many SNARE mutations that cause miss-sorting were found in aa side chains of the central layers of the SNARE motif that are needed to form a stable trans-SNARE complex (Fig. 9, p. 38). Thus, Jahn *et al.* (2006) suggested sorting might also depend on SNARE conformation, i.e. whether it syntaxins are open or closed or already present as part of an acceptor complex (see Fig. 10, p. 39). Other SNARE binding proteins with regulatory function of fusion events might be involved in SNARE sorting and recycling by associating with SNAREs during transport. For example, when *Arabidopsis* SYP121 or SYP122 were expressed as

GFP-fusions in tomato protoplasts in co-transformation with a dominant-negative mutant of tomato Rab11a, SYP122 but not SYP121 was blocked in internal compartments, including the ER, indicating that the secretory pathway that delivers SYP122 to the PM depended on this Rab protein (Rehman *et al.*, 2008). Just very recently, it was discovered that sterol-dependent, clathrin and dynamin-mediated endocytosis maintains specificity of SYP111 localisation in the plane of cell division during late cytokinesis (Boutte *et al.*, 2010). On interference with endocytosis by treatment with energy inhibitors, SYP111 miss- localized to lateral PMs causing transport vesicles to deliver components for the new cell wall to the wrong target membrane.

Mechanisms of ion channel regulation

Regulatory mechanisms of Arabidopsis Shaker channels

Regulation of Shaker channels can take place in all the different stages of a proteins lifecycle from regulation of transcription to degradation. The specific regulatory mechanism, the sensitivity to stimuli as well as the kind of response differ from one channel to another.

Starting with transcription, it has been observed that only few *Arabidopsis* Shaker channels are regulated on this level. As mentioned before, *AKT1*, for example, did not show change at a transcriptional level in response to low K^+ stress (Pilot *et al.*, 2003a). However, it appears that transcription of *KC1* is induced in *Arabidopsis* roots under K^+ starvation (Shin & Schachtman, 2004). Pilot *et al.* (2003) further observed that K^+ starvation decreased the levels of *SKOR* and *AKT2* transcripts, which might reduce K^+ secretion into the xylem sap and K^+ transport via the phloem sap, respectively, to keep the roots provided with for growth. Salt stress led to a strong increase in expression of *KC1* in leaves, possibly to mediate the process of guttation in trichomes, while *AKT1*, *AKT2* and *SKOR* were not affected (Pilot *et al.*, 2003a). ABA, a hormone that is involved in drought stress adaption, reduced the mRNA levels of *SKOR* in roots while the mRNA level of *AKT2* in shoots was increased, which could result in increased accumulation in the apical region, favouring root growth under reduced soil water content K^+ (Pilot *et al.*, 2003a). It was further observed that expression levels of *AKT2* fluctuate in response to light and sugars, indicating a coupling between phloem K^+ transport with sugar production and allocation. *AKT2* transcripts reached a peak around noon, decayed to almost 50 % in the afternoon and reached a low background level in the following dark period (Deeken *et al.*, 2000).

The mode of assembly of Shaker channel α-subunits constitutes another level of regulation for Shaker derived K^+ currents. Assembly of tetrameric channels is thought to take place in the ER (see above). Therefore, ER retention or export may serve as a mechanism to control the number of channels at the cell surface and thus current amplitudes. In addition, the combination of different α-subunits into heteromeric instead homomeric channels, is thought to lead to an increased diversity in functional properties, i.e. new electrical properties with unique features that are not displayed by any homomeric channel. Considering the importance of K^+ in determining the overall membrane potential (see above), cell surface density of Shaker channels as well as hetero- and

homotetramerisation can have a large impact on membrane voltage and thus alter the response of cells to the environment. In mammalian voltage-gated Shaker K^+ channels (Kv), a domain located in the N-terminal region, the so-called T1 domain, contributes to discriminating compatible and incompatible channel α-subunits in the ER (Xu *et al.*, 1995). Xu *et al.* (1995) discovered that heterotetramerization between mammalian Kv channels is only possible within each of the 12 subfamilies (Kv1–Kv12) that were identified based on relative sequence homology. In contrast, it appears that in plant Shaker channels such discrimination involves the cytoplasmic C-terminus, although the exact molecular determinants of subunit compatibility have not yet been identified (Daram *et al.*, 1997; Ehrhardt *et al.*, 1997; Urbach *et al.*, 2000; Dreyer *et al.*, 2004).

Data obtained after co-expression experiments in heterologous expression systems, such as *Xenopus* oocytes, yeast cells or in plant expression systems have provided evidence that heteromerization is possible among different *Arabidopsis* inward rectifying Shaker channel α-subunits (e.g., KAT1 and KAT2 or AKT1 and KAT1) (Dreyer *et al.*, 1997; Urbach *et al.*, 2000; Pilot *et al.*, 2001) (see Fig. 3). For example, co-expression of the electrically silent AKT1 with a Ca^{2+}-sensitive KAT1 mutant in *Xenopus* oocytes resulted in a change in the Ca^{2+} sensitivity of the K^+ current (Dreyer *et al*., 1997) . Heteromerization was also detected between different outward rectifying K^+ channel α-subunits (e.g., GORK and SKOR) (Dreyer *et al*., 2004). However, in this case, it was suggested that this interaction might not have physiological meaning, as the temporal and special expression patterns of GORK and SKOR do not seem to overlap *in planta* (Jeanguenin *et al*., 2008). No heterotetramerisation was observed so far between outward-and inward rectifying *Arabidopsis* Shaker channel α-subunits (e.g., SKOR and KAT1) (Dreyer *et al*., 2004).

Functional heteromeric channels were also reported for combinations of different inward rectifying Shaker α-subunits and the weakly inward rectifying subunit AKT2 (see Fig. 3) (Baizabal-Aguirre *et al*., 1999; Xicluna *et al*., 2007) and between different inward rectifying Shaker α-subunits and the silent regulatory subunit KC1 (Dreyer *et al*., 1997; Duby *et al*., 2008). Mammalians have a much greater number of silent α-subunits, the Kv5, Kv6 and Kv8-12 subfamilies, that are not able to form functional homomeric channels (Kerschensteiner *et al*., 2005). Just as in the case of KC1 and AKT1 co-expression (see above), the co-expression of these α-subunits, together with those capable of forming functional potassium channels, produced heteromeric channels with new electrical properties. Similar to the situation with AKT1 and KC1, subcellular localization studies with mammalian silent α-subunits showed that in several cases these regulatory subunits exhibit conditional PM targeting that depended on the presence of other functional α-subunits were present (Kerschensteiner *et al.*, 2005).

Only very recently, evidence could be obtained that heteromeric channels involving *Arabidopsis* KAT1 actually exist and have a function *in planta* (Lebaudy *et al.*, 2008). Furthermore, evidence was provide that, in heterologous expression systems as well as *in vivo*, assembly of heteromeric *Arabidopsis* KAT1-KAT2 channels is favoured above that of homomeric KAT1 or KAT2 channels (Lebaudy *et al*., 2010). As these two Shaker channel subunits are the most highly expressed ones in *Arabidopsis* guard cells, Lebaudy *et al.* (2010) concluded that the native inward K^+ conductance in these cells relies mainly on channels made of two KAT1 and two

KAT2 subunits.

Once the α-subunits are assembled and trafficked to the PM, the resulting channels can be targets for post-translational regulation. Channel activity in the PM can be controlled by intracellular factors such as H^+, Ca^{2+} and cyclic nucleotides (Hoshi, 1995; Gaymard *et al.*, 1996; Very & Sentenac, 2003) or protein-protein interactions. In contrast to mammalian shaker channels, not a lot is known about regulation of channel activity by interactions with protein partners in plant cells (Cherel, 2004). However, conserved actors in the plant and animal regulatory networks are β-subunits (Tang *et al.*, 1996), actin skeleton proteins (Hwang *et al.*, 1997), G proteins (Li & Assmann, 1993), 14.3.3 proteins (Sottocornola *et al.*, 2008), kinases and phosphatases (Mori *et al.*, 2000; Berkowitz *et al.*, 2000). Evidence for direct interactions with the target channel has been obtained in four cases: for 14.3.3 proteins with KAT1 (Sottocornola *et al.*, 2006; Sottocornola *et al.*, 2008), for β-subunits (Tang *et al.*, 1996) and the phosphatase PP2CA with AKT2 (Vranova *et al.*, 2001), and CIPK23 with AKT1 (Xu *et al.*, 2006) as described above.

14-3-3 proteins are known in general for their involvement in the control of ion transport across plasma and vacuolar membrane through interaction with H^+-ATPase and V-ATPase. When recombinant plant 14-3-3 protein was injected into oocytes expressing *Arabidopsis* KAT1, the KAT1 mediated currents increased in amplitude more than 100 %. It was concluded that the 14-3-3 protein increased the number of active KAT1 channels in the oocyte PM by an unknown mechanism (Sottocornola *et al.*, 2006; Sottocornola *et al.*, 2008). It is known that in mammalians 14-3-3 proteins interact with e.g. the ATP-sensitive K^+ channel Kir6.2. This interaction masks an ER retention signal in this channel and thereby increases its rate of ER export, i.e. the number of channels at the PM. It was suggested that plant 14-3-3 might work in a similar mechanism to promote anterograde trafficking of KAT1 in oocytes. A second effect of 14-3-3 proteins on KAT1 was observed, where the activation threshold, i.e. the membrane voltage which the channel senses to open its gates, was shifted to more positive values (11 mV) (Sottocornola *et al.*, 2006; Sottocornola *et al.*, 2008). These second effect supported the idea of a direct interaction between the 14-3-3 protein and KAT1.

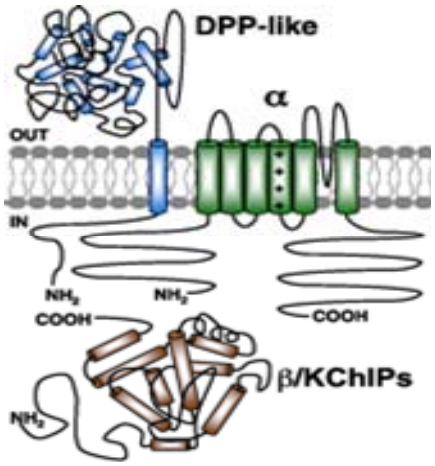

Fig. 16 Auxiliary subunits of mammalian Shaker channels

Shown are the structures of the three types of auxiliary subunits that form regulatory complexes with mammalian voltage gated Shaker channel α-subunits. The image was adapted from a previous publication (Vacher *et al.*, 2008).

In mammalians, the α-subunits of Kv Shaker channels are typically associated with smaller auxiliary subunits (Vacher *et al.*, 2008). These complexes are formed in the ER. Three types of auxiliary subunits exist: Kvβ, KChlP1-4 and DPP-like (see Fig. 16). The best characterized of these auxiliary subunits are the cytoplasmic Kvβ subunits that associate with the subfamily of Kv1 channels. Four Kvβ subunit genes exist in the human genome, and alternative splicing can generate a number of functionally distinct isoforms. In general, Kvβ subunits exhibit weak overall sequence but strong structural similarity to aldo-keto reductase enzymes and enzymatic activity against artificial substrates could be demonstrated. Inclusion of the Kvβ1.1 subunit in Kv channel complexes containing Kv1.1 or Kv1.2 strongly alters the channel gating properties, i.e. their response to changes in membrane voltage. Moreover, the specific α- and β-subunit composition of native complexes can impact both the expression level and the localization of Kv1 channels (Vacher *et al.*, 2008). For example, Kv1.2 α-subunits that are over-expressed in cultured hippocampal neurons exhibit a somatodendritic localization, whereas co-transfection of the Kvβ2 subunit, which in itself is preferentially localized to axons, yields a pronounced axonal localization of Kv1.2 (Gu *et al.*, 2003). A second type of auxiliary subunits belong to family of cytoplasmic calcium binding proteins, called KChIPs, that are members of the neuronal calcium sensor gene family. KChIP isoforms associate with the subfamily of Kv4 channels to increase their surface density and speed the kinetics of recovery after inactivation (Vacher *et al*., 2008). The third type of auxiliary subunits comprise membrane proteins with one TMD, the dipeptidyl-peptidase-like (DPP-like) protein (Nadal *et al*., 2006). They were reported to associate with Kv4 channel complexes as well and affect their trafficking to the cell surface in addition to modulation of the Kv4 channel electrical properties (Nadal *et al*., 2006).

Some homologues of mammalian auxiliary Kv subunits have been identified in plants and shown to actually interact with plant Shaker channels. For example, co-expression of the *Arabidopsis* KAB1 β-subunit with KAT1 in *Xenopus* oocytes resulted in increased current levels with no change in gating properties (Zhang *et al.*, 1999), suggesting that the interaction would stabilize the channel in the PM.

Finally, the number of channels present at the PM might be regulated by endocytosis or endocytotic cycling between the PM and an endosomal body. Evidence to this effect was obtained for *Arabidopsis* KAT1 and implicated in the regulation of guard cell turgor during stomatal opening and closing (see below) (Meckel *et al.*, 2004; Hurst *et al.*, 2004; Homann *et al.*, 2007; Reuff *et al.*, 2010).

SYP121 in ion channel regulation

The tobacco homologue of *At*SYP121, *Nt*SYP121 ('SYR1') was first identified by Prof. Blatt's group through experiments designed to identify an ABA receptor (Leyman *et al.*, 1999). Among other functions, the phytohormone ABA is the central regulator of a complex network that enables abiotic stress response to e.g. drought or high salinity in plants. One important function of ABA under drought stress conditions is the initiation of stomatal closure to reduce water loss.

ABA inhibits stomatal opening and causes stomatal closure through complex signalling pathways that are mediated by kinases/ phosphatases (e.g. families of SnRK2s/ PP2Cs), secondary messengers (e.g. ROS), and Ca^{2+}-elevation dependent and Ca^{2+}-elevation independent inactivation of K^+ influx channels (e.g. KAT1) and H^+ pumps (Li *et al.*, 2006). More specifically, when guard cells perceive increased ABA levels Ca^{2+}-influx channels are activated on the PM. As mentioned earlier (see p. 16), the rising cytosolic Ca^{2+}-concentration in turn stimulates anion efflux channels on the PM (e.g. SLAC1) and K^+ efflux channels on the vacuolar membrane (e.g. TPC1, TPK1). Predominantly Cl^- but also malate efflux through the PM anion channels drives membrane depolarization that in turn activates the outward-rectifying K^+ Shaker channel GORK. This net cellular efflux of solutes causes water efflux and the resulting decrease in guard cell turgor and volume causes closing of the stomatal pore.

Stomatal opening is initiated by hyperpolarisation of the guard cell PM, which is caused by H^+ efflux pumps (e.g. AHA1/OST2). Membrane hyperpolarisation in turn activates inward-rectifying PM Shaker K^+ channels (e.g. KAT1) and induces K^+ influx followed by water uptake into guard cells. At the vacuolar membrane, proton pumps acidify the vacuole lumen and thus effect sequestration of the incoming K^+ into the vacuole. Also, production of maltase from osmotically inactive starch and the uptake of anions such Cl^- into the vacuole helps to decrease water potential and leads to subsequent water uptake. Turgor elevation from water uptake increases guard cell volume, which widens stomatal apertures because of the asymmetric positioning of microfibrils in the guard cell wall of *Arabidopsis*.

In order to discover a receptor for ABA, Leyman *et al.* (1999) screened a cDNA library created from leaves of drought-stressed *Nicotiana tabacum* for sensitivity to ABA using *Xenopus laevis* oocytes. This strategy allowed for a cross-coupling between plant-derived ABA-sensitive elements and the endogenous signalling pathways of the oocyte. Injected oocytes that reacted to the application of exogenous ABA specifically with an otherwise only Ca^{2+}-induced Cl^- current allowed identification of *Nt*SYP121. Disrupting *Nt*SYP121 function by competition with a soluble truncated version of the protein suppressed ABA-dependent regulation of the K^+ and Cl^- channel currents in tobacco guard cells in an unknown mechanism (Leyman *et al.*, 1999).

Direct binding of ABA in a receptor-like manner could not be shown for *Nt*SYP121 (Prof. Blatt, unpublished results). However, these observations placed *Nt*SYP121 function in the ABA signalling cascade that depends on ion channel regulation. Subsequent work showed that transient over-expression of the cytosolic domain of *Nt*SYP121 caused retention of *At*KAT1-GFP in the ER (Sutter *et al.*, 2006b). In addition, expression of this soluble SNARE fragment negatively affected

the normal cluster-like organization of the KAT1 in the PM which resulted in a uniform distribution instead. These results would allow for a SYP121 function in ion channel regulation via the control of surface expression of KAT1. In addition, it was found that expression of the same soluble *Nt*SYP121 fragment blocked ABA-evoked stomatal closure (Sokolovski *et al.*, 2008). In addition, Ca^{2+} channel gating at the PM was altered by the *in vivo* expression of the SNARE fragment in a manner that led to a pronounced suppression of evoked cytoplasmic Ca^{2+} transients. These observations indicated a functional coupling of SYP121 with Ca^{2+} channels at the PM and thus might affect stomatal closure via the Ca^{2+} dependent control of K^+ and Cl^- channel currents (Sokolovski *et al.*, 2008). In summary, it is not yet fully understood how exactly SYP121 contributes to ion channel regulation in guard cells.

A model for Syntaxin1A function in ion channel regulation

Kv1.1, a mammalian Shaker expressed in neurons, was the first voltage-gated K^+ channel for which interaction with a SNARE, namely Syntaxin1A, had been reported (Fili *et al.*, 2001). Syntaxin1A is the mammalian syntaxin that showed the highest degree of aa sequence identity to *Arabidopsis* SYP121 (23 %) (Sanderfoot *et al.*, 2000). Direct physical interaction between Syntaxin1A and Kv1.1 was found in reciprocal co-immunoprecipitation experiments using rat brain tissue. Syntaxin1A binding to the N-terminus of Kv1.1 decreased the amplitude of the K^+ currents flowing through this channel (Michaelevski *et al.*, 2002). In pancreatic islet ß-cells, the Shaker channel Kv2.1 is the predominant voltage gated K^+ channel. Syntaxin1A and SNAP25 were shown to co-localize with Kv2.1 and the voltage-gated Ca^{2+} channel Cav1.2 in PM lipid raft microdomains of these pancreatic ß-cells (Xia *et al.*, 2004). Direct interaction between Syntaxin1A and Kv2.1 was reported to reduce Kv2.1 current amplitude, but also changed its gating behaviour, i.e. its response to changes in the membrane potential (Leung *et al.*, 2003). Specifically, co-expression of Syntaxin1A with Kv2.1 in HEK cells (human embryonic kidney cell line) increased the voltage sensitivity of the inactivation of Kv2.1, suggesting that Syntaxin1A decreased channel availability upon depolarization (shifting membrane potential to more negative voltages).

In contrast to the Syntaxin1A binding to the N-terminus of Kv1.1 (Michaelevski *et al.*, 2002), the interaction between this SNARE and Kv2.1 is mediated by two neighbouring domains in the cytoplasmic C-terminus of the Kv2.1 Shaker channel (Leung *et al.*, 2003). The interacting domain on Syntaxin1A was identified as the SNARE motif, which is thought to exert the inhibitory effect on Kv2.1 (Leung *et al.*, 2003). As mentioned earlier (p. 37), syntaxins, including Syntaxin1A are thought to exist in an open and closed form. In the closed form, the N-terminal Habc domain is thought to fold back to form an auto-inhibitory four helix bundle with the SNARE motif. The introduction of two aa exchanges in the linker region between Habc and SNARE motif domain (L165A, E166A), created a constitutively open mutated Syntaxin1A form (Dulubova *et al.*, 1999; Richmond *et al.*, 2001). Single-molecule FRET measurement demonstrated that in solution

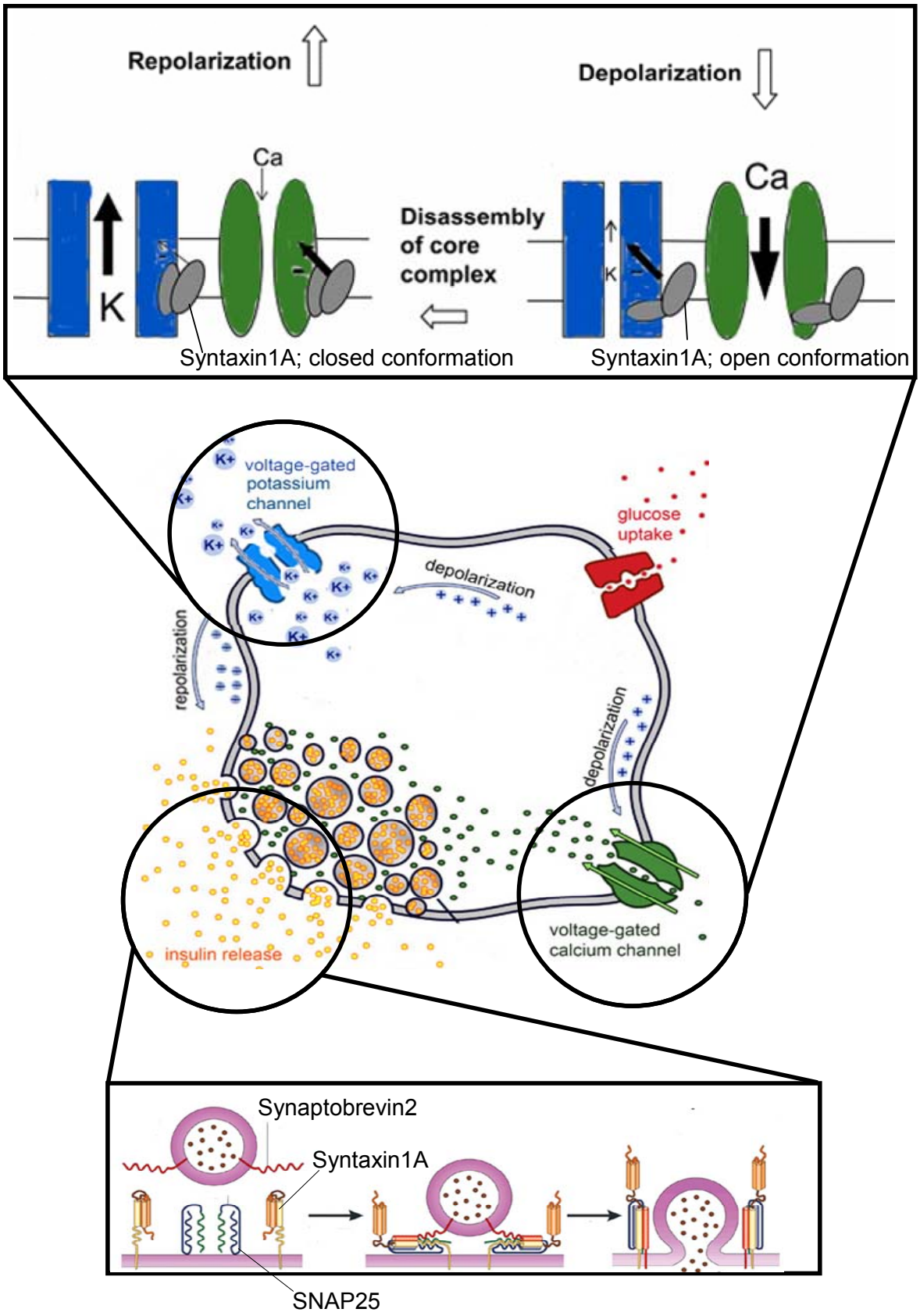

Fig. 17 A model for Syntaxin1A function in ion channel regulation during exocytosis

Shown is a mammalian pancreatic islet ß-cell that secretes the hormone insulin in response to signalling events that are triggered by high glucose in the bloodstream. Exocytosis of insulin depends on a trans-SNARE complex involving Syntaxin1A (lower box). This model further suggests that Syntaxin1A simultaneously acts to fine-tune the voltage gated K^+ and Ca^{2+} channels that are involved in the signalling events by interacting directly with them (upper box). For more details see text.

Syntaxin1A exhibited a rapid dynamic equilibrium between the closed and open forms (Margittai *et al.*, 2003). Dialysis of recombinant proteins of mutated open form or wt Syntaxin1A into Kv2.1-expressing HEK cells showed that the mutated open form of Syntaxin1A was more potent than wt Syntaxin1A in mediating the observed effects of reducing Kv2.1 current amplitude and decreasing channel availability upon depolarization (Leung *et al.*, 2005). In extension of these experiments it was suggested that the closed form of wt Syntaxin1A inhibits Kv2.1 less than the native open form of wt Syntaxin1A (Margittai *et al.*, 2003).

In mammalian cells it was further observed that Syntaxin1A interacts directly with and modulates the electrophysiological properties of members of the superfamily of voltage-gated Ca^{2+} channels. In all observed cases, Syntaxin1A interacted with a conserved cytoplasmic domain of the respective voltage-gated Ca^{2+} channel that links the second and third S1-S6 repeat and was termed the synprint site (Catterall, 1999; Bezprozvanny *et al.*, 2000).

In secretory cells such as neurons and pancreatic ß-cells, Ca^{2+} influx through opening of voltage-gated Ca^{2+} channels triggers the fusion of vesicle to the PM and thereby the release of neurotransmitters or the hormone insulin, respectively. It was demonstrated that in contrast to the stronger inhibition of Kv2.1 by the mutated open form of Syntaxin1A, the availability of a pancreatic voltage-gated Ca^{2+} channel was decreased only by interaction with wt Syntaxin1A. The mutated open form of Syntaxin1A did not show this effect on Kv2.1 (Leung *et al.*, 2005).

The cognate trans-SNARE complex that mediates fusion of insulin transporting vesicles to the PM of pancreatic ß-cells includes the same three SNARE proteins that operate in the PM of presynaptic membranes to mediate neurotransmitter release (see p. 38ff.): Syntaxin1A, SNAP25 and Synaptobrevin2 (Fig. 17, lower box). For these specialised forms of mammalian polarised exocytosis, it is thought that a process termed “priming” precedes formation of the trans-SNARE complex. Before priming, Syntaxin1A exists in the closed conformation that blocks the SNARE motif from interacting with SNAP25 and Synaptobrevin2. Activation of Syntaxin1A from the closed conformation to the open form, i.e. priming, is therefore a key event required to enable SNARE complex assembly. As mentioned earlier (p. 43), SM proteins such as Munc18 have been implicated to control and mediate the Syntaxin1A conformation changes.

The signal that triggers insulin secretion from pancreatic ß-cells is a high level of glucose in the bloodstream. Glucose uptake via the glucose transporter GLUT2 initiates a signalling cascade that eventually leads to membrane depolarization (Fig. 17, middle). Membrane depolarisation in turn activates voltage gated Ca^{2+} channel to allow Ca^{2+} influx that triggers vesicle fusion for insulin secretion. As a result of membrane depolarization, voltage gated K^+ channels (mostly Kv2.1) become activated as well. They provide the K^+ efflux necessary to repolarise i.e. hyperpolarise, the membrane potential to the resting state. Repolarisation closes the voltage gated Ca^{2+} channels, which terminates Ca^{2+} influx and hence exocytosis (MacDonald *et al.*, 2001).

Leung *et al.* (2007) have proposed a model that integrates the conformational changes of Syntaxin-1A between open and closed form during priming for vesicle fusion with the observed reciprocal functional modulations that the two forms impose on voltage gated Ca^{2+} and K^+ channels of pancreatic ß-cells. It is their opinion that the dual functions of Syntaxin1A in vesicle fusion and

ion channel regulation serve to fine-tune cell excitability and insulin secretion.

In the resting state, the insulin filled vesicles are docked onto the PM and Syntaxin1A assumes its closed form. The process of priming in exocytosis leads to a conformational change of Syntaxin1A to its open form. At this primed state, both voltage gated K^+ and Ca^{2+} channels are still closed so that neither of the interacting forms of Syntaxin1A will have a measurable effect. Depolarization of the pancreatic ß-cell then activates both voltage gated K^+ and Ca^{2+} channels that are now in a stage of interaction with the open form of Syntaxin1A (Fig. 17, upper box, right part). Because the open form of Syntaxin1A does not reduce availability of voltage gated Ca^{2+} channels, it allows maximal Ca^{2+} influx. At the same time, the open form of Syntaxin1A strongly inhibits Kv2.1 to limit K^+ efflux, thus slowing down repolarisation and consequently enhancing Ca^{2+} influx during exocytosis. The cis-SNARE complex disassembles after exocytosis (see p.40) And Syntaxin1A resumes its closed form (Fig. 17, upper box, left part). The closed form of Syntaxin1A now reduces availability of voltage gated Ca^{2+} channels. As a consequence, Ca^{2+} influx is substantially reduced. Meanwhile, the closed form Syntaxin1A inhibits Kv2.1 only weakly, permitting more K^+ efflux and therefore speeding up repolarisation. Eventually, both the voltage gated K^+ and Ca^{2+} channels close, because the pancreatic ß-cell repolarises to its resting membrane potential.

In summary, in this model Syntaxin1A not only participates in vesicle fusion, but also physically and functionally interacts with voltage gated K^+ and Ca^{2+} channels to form a so-called excitosome that precisely regulates Ca^{2+} entry at the site of exocytosis. An excitosome is thought to ensure a rapid release response of insulin because the interaction of Syntaxin1A with voltage gated Ca^{2+} channels exposes the secretory machinery immediately to the high local Ca^{2+} concentration permeating through the open Ca^{2+} channels (Catterall, 1999; Bezprozvanny *et al.*, 2000). In addition, Syntaxin1A provides a feedback loop via its conformational stage that depends on the status of the exocytotic cycle to control the rate and amount of Ca^{2+} influx. A similar model was proposed to operate in neurotransmitter exocytosis in neurons (Atlas, 2001).

Methods for the detection of protein-protein interactions

In the cell, proteins participate in extensive networks of protein-protein interactions that are intrinsic to virtually every cellular process. These interactions can be stable or transient. Stable protein-protein interactions are irreversible and therefore associated with proteins that can be purified as multi-subunit complexes, e.g. most of the cellular cytoskeleton or transport proteins such as e.g. Shaker channel heterotetramers (Phizicky & Fields, 1995). Such stable interactions feature a low dissociation constant (in the nM range), i.e. the protein complex does not disassemble over time (Perkins *et al.*, 2010). Transient interactions typically require a specific set of conditions that promote the interaction, e.g. post-translational modification in the form of phosphorylation. While in contact with their binding partners, transiently interacting proteins are expected to be involved in a whole range of cellular processes including protein modification, protein folding by chaperones, metabolic pathways and signal transduction. Many transient protein interactions are of an enzymatic nature. Transiently interacting protein complexes can be further subdivided into weak and strong. Proteins interacting in a weakly transient manner show a fast bound-unbound equilibrium with dissociation constant values typically in the mM range and thus lifetimes of seconds. The strong transient protein interactions are triggered/stabilized by an effector molecule or conformational change. They last longer and have a lower dissociation constant in the nM range. An example are the Ras proteins, which form tight complexes with their partners when GTP-bound and only weak complexes when GDP-bound (Perkins *et al.*, 2010).

Usually a combination of techniques is necessary to validate a protein interaction. This approach significantly reduces the risk of characterising an artefact that might arise from the experimental conditions of any particular technique. A common method to investigate a newly proposed interaction between two proteins with relatively little effort or to screen for novel protein interaction partners is the yeast-two-hybrid system (Phizicky & Fields, 1995). This method is based on the ability of an interacting protein pair to reconstitute *in vivo* an active transcription factor that was split into its DNA-binding and activation domain which triggers expression of the linked reporter genes.

To confirm a physical interaction between proteins indicated by an initial yeast two-hybrid strategy, *in vitro* affinity-based methods are often employed. Such a technique is, for example, co-immunoprecipitation (Co-IP). Co-IP is mediated by the affinity of an antibody against a target antigen on the protein of interest that in turn precipitates an interacting protein. Pull-down assays are very similar to immunoprecipitation except that a tagged protein of interest is used instead of an antibody. Alternatively, Far-Western analysis can be employed. Far-Western is different from a typical Western blot only in the method of detection that substitutes an antibody with an appropriately labelled bait protein as the probe. Surface Plasmon Resonance can confirm the interaction between two proteins by monitoring changes in the resonance angle of light impinging on a gold surface, to which a protein of interest has been attached. Protein partners that interact with the immobilized protein are retained on the gold surface, which alters the resonance angle of

impinging light as a result of the change in refractive index brought about by increased amounts of protein near the surface (Berggard *et al.*, 2007). This technique is furthermore able to determine the binding constant between two proteins as the changes are proportional to the extent of protein binding. Two other advanced *in vitro* methods not only prove interaction between proteins but are usually used to characterise an interaction in more detail: NMR (Nuclear Magnetic Resonance) is mainly used to structurally characterize interactions between soluble protein domains and small peptides, as this technique is constrained in the size of the complexes it can deal with (Vaynberg & Qin, 2006). Domain-peptide interactions are typical for transient protein-protein interactions. X-ray crystallography allows definition of the three-dimensional structure formed by a protein-protein interaction interface.

Ultimately, an interaction detected by an *in vitro* technique such as e.g. Co-IP must be evaluated with an experiment that proves its occurrence *in vivo*, i.e. in the organism from which the proteins originate. This also helps to investigate the significance this particular interaction has at the cellular level. For this type of experiments, techniques such as fluorescence resonance energy transfer (FRET) are often used (Sekar & Periasamy, 2003). FRET is based on the transfer of excitation energy without emission of a photon between two fluorophores (FP), the so-called donor and acceptor. Energy transfer can take place when both FP are brought into close spatial proximity via the interaction of two protein complex partners to which they are fused. Following excitation, changes in the second FP's emission intensity can be monitored and attributed to protein-protein interaction. FRET also has the advantage that stable and transient interactions can be detected equally well. Thus, FRET might be able to detect a transient and weak interaction that was hard to verify with an *in vitro* method.

Many of the above mentioned techniques will be useful only with soluble proteins or soluble domains of membrane proteins. The work presented in this thesis is concerned only with membrane proteins, i.e. the Shaker channel subunits KC1, AKT1 and KAT1 and the SNAREs SYP121, SYP122 and SYP111. As a putative interaction between KC1 and SYP121 was to be explored, it was decided from the start that techniques would be used that allowed the use of full-length membrane proteins instead of their soluble domains. Although the soluble domains of membrane proteins are most likely to mediate an interaction, it is easily conceivable that an interaction interface might be created by intra-protein interactions that involve the TMDs, i.e. depend on the three-dimensional structure of the native full-length protein.

For this reason, a former member of Prof. Blatt's group, Dr. Pratelli (Stanford University, USA) screened an *Arabidopsis thaliana* membrane protein library for putative interaction partners of SYP121, which yielded KC1. The technique that allowed screening for full-length membrane protein interactions in yeast is called mating-based split ubiquitin system (mbSUS). It was developed as an alternative to the classical yeast two-hybrid system (Johnsson & Varshavsky, 1994a; Stagljar *et al.*, 1998; Stagljar & Fields, 2002; Obrdlik *et al.*, 2004; Grefen *et al.*, 2007; Grefen *et al.*, 2009). As mentioned above, protein–protein interaction in the yeast two-hybrid system leads to the reconstitution of an active transcription factor. As this must occur on the promoter of the reporter gene, the interacting proteins have to be located in the nucleus to detect the

interaction. Therefore, transmembrane proteins, which tend to be insoluble and form aggregates if not present within membranes, are poor candidates for this assay. Only their soluble parts are usable and these need to be re-localized to the nucleus. In comparison, mbSUS not only allows the use of full-length membrane proteins instead of their soluble domains, but also abolishes the need for artificial nuclear re-localization and allows instead detection of interactions at their natural subcellular sites.

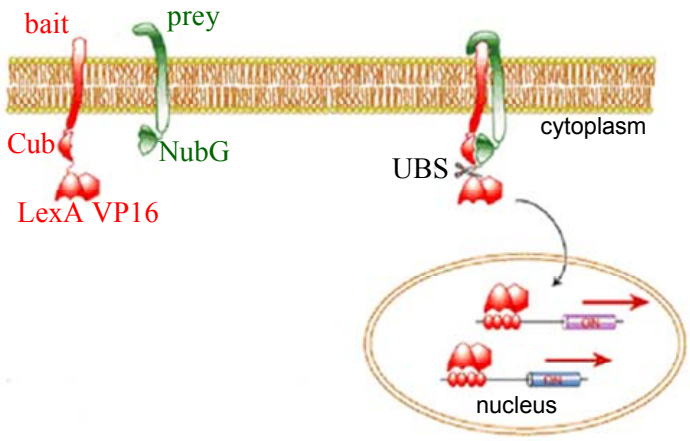

Fig. 18 Principle of the yeast mating-based split ubiquitin system (mbSUS)

The bait (red) is expressed as a fusion to the C-terminal half of ubiquitin (Cub) and an artificial transcription factor (LexA-VP16). The prey (green) is fused to the mutated N-terminal half of ubiquitin (NubG). Interaction between bait and prey brings Cub and NubG into close proximity and results in the reconstitution of quasi-native ubiquitin. Re-assembled ubiquitin can be recognized by yeast Ubiquitin-specific proteases (UBS) which then cleave the polypeptide chain between Cub and LexA-VP16. The released transcription factor diffuses to the nucleus where it activates the reporter genes. The image was adapted from http://www.dualsystems.com.

This is achieved by fusing two putatively interacting proteins each to one half of the yeast ubiquitin protein (see Fig. 18). Ubiquitin is a small, highly conserved protein of 76 amino acids, which is usually attached to the N-terminal lysine residues of other proteins. Ubiquitin-tagged proteins are recognized by Ubiquitin-specific proteases that cleave after the C-terminal residue (Gly76) of Ubiquitin and the first residue of the target protein to release it for degradation by the 26S proteasome. This highly specific cleavage presumably depends upon the folded structure of Ubiquitin. Native Ubiquitin can be split into an N-terminal half (Nub: amino acids 1–34) and a C-terminal half (Cub: amino acids 35–76) (Johnsson & Varshavsky, 1994b). The two halves retain a basic affinity for each other and reassemble spontaneously to form quasi-native Ubiquitin. If a reporter protein is fused to the C-terminus of Cub, it will be cleaved off by the Ubiquitin-specific proteases (UBS) of the yeast's own ubiquitin-degradation pathway upon assembly of the Nub and Cub moieties. A point mutation in the N-terminal domain of Ubiquitin that replaces the wild-type isoleucine residue at position 13 (NubI) with that of glycine (NubG) abolishes the affinity of the two halves for each other by decreasing the conformational stability of the N-terminal domain. Therefore, NubG and Cub fail to refold into Ubiquitin when co-expressed in yeast. However, if the two Ubiquitin halves are fused to interacting proteins, i.e. bait and prey, this interaction brings the NubG and Cub moieties close enough together to reconstitute quasi-native Ubiquitin. This results in the release of a reporter protein as described above. For this assay the reporter protein consists of

an artificial transcription factor made up from the entire bacterial DNA-binding LexA protein followed by the transcriptional activation domain of the *Herpes simplex* VP16 transactivator protein. After this artificial transcription factor is cleaved off, it diffuses to the nucleus where it activates a set of reporter genes. The reporter genes under the control of the targeted lexA promoter are *ADE*2, *HIS*3 and *lacZ* for adenine (Ade; A) and histidine (His; H) biosynthesis and β-galactidose (β-gal) activity respectively. The internal negative control of the mbSUS system that should not lead to activation of reporter genes is therefore the co-expression of the bait fused to the Cub-artificial transcription factor moiety with the empty prey vector expressing NubG. Conversely, the internal positive control is co-expression of the same bait fusion with the Nub-wild type (NubI) that should strongly activate reporter genes as NubI will associate with Cub independent of additional protein-protein contacts.

The nature of the detection system underlying mbSUS, meaning the reconstitution of quasi-native Ubiquitin as soon as its halves are in close enough proximity, makes it impossible to distinguish a close spatial co-localisation in a multiprotein complex and direct protein-protein interaction. Such was demonstrated for ER resident membrane proteins (Wittke *et al.*, 1999). It is, for example, potentially possible for a yeast protein to function as bridge between heterologous bait and prey protein and thus mediate an artificial, false positive interaction. For these reasons, it was decided to confirm a direct physical interaction of KC1 and SYP121 with a Co-IP experiment. Ideally, a Co-IP (or pull-down) should take place between native proteins, i.e. isolated from *Arabidopsis* in this case. However, this requires antibodies against both proteins that are highly specific and as such able to distinguish the target protein from closely related proteins. At the time this project was started, such an antibody was only available against SYP121 (Tyrrell *et al.*, 2007), not for KC1. The next best scenario, a Co-IP or pull-down between epitope-tagged proteins stably expressed in *Arabidopsis* under their own promoter or over-expressed under a 35S promoter was excluded on base of the very low expression levels that are generally observed for native ion channels, even when under control of a strong constitutive promoter such as the cauliflower mosaic virus 35S promoter (Wagner *et al.*, 2006; Sutter *et al.*, 2006b). For similar reasons, tandem affinity purification (TAP) was not considered at this point. For TAP, a tag with multiple epitope sequences is added to the target protein, which is then over-expressed, e.g. stable in *Arabidopsis*, to facilitate purification of protein complexes with gentle native conditions (Puig *et al.*, 2001; Collins & Choudhary, 2008).

Instead, insect cells were chosen as heterologous expression system to obtain full-length tagged versions of the two membranes proteins, KC1 and SYP121, for Co-IP. In addition to high expression levels, insect cells have proven very efficient for membrane protein production. Successful expression and purification of various plant (Zimmermann *et al.*, 1998; Hartje *et al.*, 2000) and animal ion channels, e.g. the Drosophila Shaker K1 (Klaiber *et al.*, 1990; Li *et al.*, 1994) has been reported. An important factor in this success is considered to be the fact that insect cells represent an eukaryotic expression system capable of performing most eukaryotic post-translational modifications such as signal peptide cleavage, phosphorylation and fatty acid acylation (Kost *et al.*, 2005). Taken together with generally observed proper protein folding and disulfide bond formation,

heterologous expression in insect cells resulted in most cases in membrane proteins, e.g. ion channels that were functionally active and structurally similar to their native counterparts (Kidd & Emery, 1993). The ability of the insect cells to perform the correct posttranslational modifications for plant membrane proteins was also the reason that this expression system was chosen over a bacterial expression system. Expression in *E.coli* is more straightforward than first creating a recombinant Baculovirus with the protein of interest that is then used to infect insect cells (see Chapter 2, p. 145). However, eukaryotic proteins expressed in bacteria are often without the proper posttranslational modifications (Wagner *et al.*, 2006). The absence of these posttranslational modifications, e.g. the failure to phosphorylate a protein, might prevent transient interactions from taking place in the first place and would thus lead to a false negative result in Co-IP experiments. Another advantage of the insect cell system is that several copies of the same Baculovirus promoter (polyhedrin or p10 promoter, see p. 145) can be used simultaneously within a single infected insect cell without competition (Kohno *et al.*, 2000). This feature permits the production of oligomeric proteins and reconstitution of other protein complexes (Roy *et al.*, 1997), which was of special interest for this work.

Finally, an interaction between KC1 and SYP121 was to be confirmed, as discussed above, with an *in planta* experimental technique as both the mbSUS and Co-IP studies rely on heterologous expression, a situation that might not accurately represent the native cellular environment of the two *Arabidopsis thaliana* proteins. Detection of false-positive protein interactions after expression in heterologous systems has been observed previously (Phizicky & Fields, 1995). Heterologously expressed proteins might interact with high specificity even though they would never encounter one another in the native cell environment.

The above mentioned FRET has been used successfully in plants (Zelazny *et al.*, 2007; Glick *et al.*, 2008). However, FRET is technically challenging, as it can be affected by various factors, including autofluorescence and irreversible photobleaching. Furthermore, it requires specialized equipment for fluorescence lifetime measurements of high quantitative accuracy as well as special algorithms for data analysis (Sekar & Periasamy, 2003; Bhat *et al.*, 2006).

In contrast, a technique called bimolecular fluorescent complex formation (BiFC) relies on the reconstruction and subsequent standard detection of a functional fluorescent protein from two non-fluorescent fragments. Two such fragments that fulfilled the prerequisite for use in the detection of protein interactions, i.e. fragments that were unable to associate with each other efficiently in the absence of a specific interaction between their fused protein partners, were identified from YFP (Hu *et al.*, 2002). Thus, the BiFC technique shares a common principle with mbSUS. To this date, BiFC has proven successful for the visualization of interactions between soluble as well as integral membrane proteins (de Virgilio *et al.*, 2004; Li *et al.*, 2005; Giese *et al.*, 2005) in all major subcellular compartments not only of mammalian cells (Nagai *et al.*, 2001; Hu & Kerppola, 2003; Fang & Kerppola, 2004; Nakahara *et al.*, 2006) but also of plant cells: in the ER (Zamyatnin *et al.*, 2006), in chloroplasts, e.g. for dimerisation of ChrD (Citovsky *et al.*, 2006), in the vacuole, e.g. for dimerisation of the vacuolar K+ channel TPK1 (Voelker *et al.*, 2006) and in the nucleus, e.g. for interactions between two ABA-induced WRKY transcription factors (Xie *et*

al., 2006). Studies were conducted in various tissues such as intact leaves (Lacroix *et al.*, 2005), seedlings (Stolpe *et al.*, 2005) or protoplasts (Jach *et al.*, 2006) and different plant species, e.g. tobacco (Zamyatnin *et al.*, 2006), *Arabidopsis* (Voelker *et al.*, 2006), parsley and mustard (Stolpe *et al.*, 2005).

At the time that BiFC was chosen here to verify the interaction between KC1 and SYP121, its first adaption for a plant expression system had just been published (Walter *et al.*, 2004) and no attempt at using it for membrane proteins had been made yet. Nevertheless, this novel technique was preferred over FRET for several reasons. BiFC enables direct visualization of protein interactions and their subcellular localization without depending on the detection of secondary effects. Furthermore, it can be used without prior knowledge of the location or the structural nature of the protein interaction interface. For FRET analysis, the maximum distance over which significant energy transfer between acceptor and donor can be detected requires the two FPs to be within 100 Å of each other and in an orientation that permits dipole coupling. Therefore, structural information, especially in the case of large proteins, is needed to place the FPs correctly and in close spatial proximity (Sekar & Periasamy, 2003). In contrast, for BiFC, fluorescence complementation can occur even when the YFP fragments are fused to positions that are separated by more 100 Å (Kerppola, 2009). Furthermore, it is not required that the interaction partners position the fragments in the correct relative orientation as long as there is sufficient freedom of motion to allow association. Therefore, with the use of flexible linkers, BiFC for the interacting mammalian proteins Jun and Fos was observed between Jun-YFP^N (N-terminal half of YFP at the C-terminus of Jun) and Fos-YFP^C (C-terminal half of YFP at the C-terminus of Fos) as well as Jun-YFP^N and YFP^C-Fos (C-terminal half of YFP at the N-terminus of Fos) (Hu *et al.*, 2002). Another useful characteristic of BiFC with regard to the unknown nature of the KC1-SYP121 interaction *in planta* was considered its ability to efficiently detect also transient and weak interactions. This feature is a consequence of irreversible complex formation between fusion proteins, which has been observed in all *in vitro* and the vast majority of *in vivo* BiFC studies (Kerppola, 2006b). Complex formation is thought to occur in steps. Initially, contact is established between the proteins fused to the YFP fragments. This step is readily reversible, and alternative interaction partners can compete for formation of the initial complex. Subsequently, the YFP fragments associate as well, and this part of the process is irreversible. The result is a stabilized complex resistant to competition by alternative interaction partners. Therefore, even an initial protein partner complex with a short half life can be detected as it gets trapped by the association of the fluorescent protein fragments (Kerppola, 2006a). One limitation of the BiFC approach is the delay between the interaction of fusion proteins and the appearance of fluorescence, which is due to the slow rate of chemical reactions that form the mature FP from its fragments (Hu *et al.*, 2002). Hence, the BiFC approach, in contrast to FRET, does not enable real-time detection of complex formation between two proteins. However, for the purpose of verifying an interaction, there was no immediate need for this feature here. The BiFC studies were also intended here to investigate the subcellular localisation of the membrane in which interaction between KC1 and SYP121 takes place *in planta*. The mbSUS technique and Co-IP can not answer this question with absolute certainty because they

represent heterologous over-expression systems. In addition, as mentioned above, the mbSUS assay allows the detection of membrane protein interactions at any membrane in living yeast, as long as Nub and Cub meet in the cytoplasm (Stagljar *et al.*, 1998; Grefen *et al.*, 2007; Grefen *et al.*, 2009). Thus, even though both KC1 and SYP121 were shown to be plasma membrane proteins, their interaction might take place already in the ER. Neither mbSUS nor Co-IP would distinguish these two possibilities. For all these reasons, the BiFC technique seemed ideal to verify the interaction of KC1 and SYP121 and its subcellular localisation *in planta*. In conclusion, the combination of mbSUS, Co-IP and BiFC was expected to provide a reliable answer to the question whether the two *Arabidopsis* membrane proteins KC1 and SYP121 interact.

Material and Methods

General Material and Methods

All chemicals were purchased from Sigma Aldrich (Poole, UK), VWR International (Poole, UK) or Fisher Scientific (Southampton, UK) unless otherwise stated. Enzymes for molecular biology procedures were either from Invitrogen (Paisley, UK), New England Biolabs (NEB, Hitchin, UK) or Promega (Madison, USA). Custom primers were purchased from Invitrogen.

PCR

All primers used for the experiments shown were given a number and are listed accordingly in the Appendix Table A 1 (p. 242). The term 'overhang' refers to an overhanging, i.e. non-homologous sequence in a primer that generally encodes for a restriction enzyme site to be attached to the PCR product. These overhangs were extended by a varying number of yet more bps that are designed to optimize the site for recognition by the respective restriction enzyme. The individual bps necessary were attached according to the data provided by the NEB catalogue (www.neb.com).

PCR reactions were prepared in 0.2 ml PCR standard thin-walled PCR tubes. As a general rule, the PCR reaction mix was kept on ice until the lid of the thermocycler (PTC-200, MJ Research) was preheated to 104 °C and the block preheated to the respective initial denaturation temperature. The program was then paused until insertion of the PCR reaction. This modified hot-start was applied to minimise template degradation by 3´-5´exonuclease activity of the polymerase and unspecific primer extension at lower temperatures. Primers were stored in a concentration of 100 µm; the working concentration was 50 µm. The dNTP mixture (10 µm of each NTP) was obtained by mixing 1M stock solutions for each nucleotide (NEB) in the appropriate dilution. Primer design and calculation of annealing temperature was performed with the Primer3 software (http://frodo.wi.mit.edu/primer3/input.htm).

PCR with Taq polymerase

Colony PCR or PCR on plasmid mini-preparations ('miniprep') to confirm a positive cloning event were carried out with Taq DNA polymerase (NEB) in a total volume of either 20 µl or 50 µl. For multiple samples a mastermix was pipetted in the order and with the components as indicated (see table below) that left out the yeast/*E.coli*/*Agrobacterium* cells or the DNA templates. Templates were added individually to each tube before the mastermix. The typical cycling conditions are given in the second table below.

component	µl added/ reaction
distilled water to	20 µl or 50
10x Reaction Buffer	2
dNTP (10 mM)	0.4
primers (50 µM)	0.8 forward and reverse
colony template or	in 5 µl distilled water or
plasmid template (50 ng μl^{-1})	0.5
Taq polymerase (5 U μl^{-1})	0.1

frequency	step	temperature [°C]	duration [min]
1x	initial denaturation	94	02:00
30-35 cycles	denaturation	94	01:00
	primer annealing	individual	0:30-1:00
	primer extension	72	1:00/ 1000 bp
1x	final extension	72	10:00
1x	final temperature	4	∞

PCR with proofreading polymerase

For the purpose of cloning PCR products into plasmids (in vivo or standard cloning), the amplification was carried out with the proofreading Phusion™ High fidelity DNA polymerase (Finnzymes; Espoo, Finland) as follows in the first table below. The typical cycling conditions are given in the second table below.

component	µl added/reaction
distilled water to	50
5x Reaction Buffer	5
dNTP mix (10 µM)	1
primers (50 µM)	0.5 forward and reverse
plasmid template (10 ng μl^{-1})	1
Phusion Taq (2 U μl^{-1})	0.5

frequency	step	temperature [°C]	duration [sec]
1x	initial denaturation	98	30
20-25 cycles	denaturation	98	7
	primer annealing	individual + 3	30
	primer extension	72	30 /1000 bp
1x	Final extension	72	600
1x	Final temperature	4	∞

Agarose gel electrophoresis and gel purification

PCR products or restriction enzyme digests were resolved by agarose gel electrophoresis after appropriate addition of 6x loading buffer (0.25 % bromophenol blue, 0.25 % xylene cyanol, 15% Ficoll) to achieve a final 1x dilution. In general, for expected fragments of 400- 3000 bp, a 1 %

agarose gel was used: 1 % agarose powder dissolved in 1 x TAE and 40 µl l^{-1} ethidium bromide solution (50x TAE stock solution: 2 M Tris, 5.7 % acetic acid, 50 mM EDTA). Separation of DNA bands was performed in 1x TAE buffer by application of 100- 150 V for approx. 15- 30 min. DNA bands were visualised under UV light on a GelDoc 2000 scanner (Bio-Rad). Where necessary, DNA bands were excised under UV light. DNA was extracted from the agarose with the QiaQuick Gel Extraction Kit spin columns and buffers (Qiagen) according to the manufacturer's instructions. Elution was always performed with distilled water.

DNA quantification and sequencing

DNA was quantified by measuring the absorbance (in optical density units) of a suitable dilution in distilled water at 260nm. A 1 ml quartz cuvette was used in combination with the Lambda35 UV spectrophotometer (Perkin Elmer). The absorbance value, corrected against a water blank, was multiplied with the dilution factor and the factor 50 (40) to obtain DNA (RNA) concentration in ng μl^{-1}. DNA sequencing was carried out by the University of Dundee sequencing service (Dundee, UK). Sequencing data were analysed with the SeqMan software (part of the DNASTAR package).

Restriction enzyme digests

PCR products and plasmids were digested with restriction enzymes that were obtained from NEB or Promega. Unless otherwise required by the individual enzyme, all digests were carried out in a volume of 20 µl at 37 °C or for 1- 2 hours or overnight. BSA and reaction buffer were added according to the manufacturer's instructions. In general, 1 µg plasmid DNA was digested by 5 U of enzyme. Following digest, the samples were generally separated on agarose gels, the desired DNA bands excised and eluted from the gel as described above. Alternatively, digested PCR products were transferred to a gel-extraction column directly for purification. A double digest was performed with two enzymes that were able to work efficiently in the same reaction buffer.

DNA ligation reactions

All ligation reactions of cohesive and blunt DNA ends were carried out with T4 DNA ligase (Invitrogen). Reactions were set up essentially as instructed by the manufacturer. The 5x Ligase buffer was stored in small aliquots to avoid degradation of its ATP content. Normally, an insert: vector ratio of 3:1 was used, but this was increased in certain reactions to 5:1 or even 10:1, especially for large inserts. For difficult ligations, incubation times were changed from 26 °C for two hours to o.n. at 4 °C. In general, the entire ligation reaction was used for *E.coli* XL1blue transformation (see below).

DNA dephosphorylation

Dephosphorylation of DNA ends was performed with Calf Intestine Alkaline Phosphatase according to the manufacturer's instructions (# 713 023, Roche, Mannheim, Germany). The reaction was purified with a gel-extraction Quiagen column before subsequent cloning steps.

Preparation of chemical-competent *E.coli*

medium	**composition in g l^{-1}**
Medium A	20 Bacto Tryptone, 5 Yeast Extract, 0.58 NaCl, 2 $MgCl_2x6H_2O$, 2.46 $MgSO_4$
TB	3 PIPES to pH 6.8 with 2 M KOH, 8.9 $MnCl_2x2H_2O$, 2.2 $CaCl_2x2H_2O$, 18.6 KCl
LB	10 NaCl, 10 Bacto Tryptone, 5 Yeast Extract

All media were used in sterile conditions after autoclaving. For plates, 15g l^{-1} Bacto Agar was added.

A 5 ml o.n. pre-culture of *E.coli* XL1blue MRF` in LB with tetracycline (12.5 µg ml^{-1}) was grown up at 37 °C o.n. This pre-culture was used to inoculate (1:1000) the main culture consisting of 250 ml Medium A in a 1000 ml Erlenmeyer Schikane-flask. This culture was incubated at RT (around 22 °C) while shaking until an OD (600 nm) of about 0.6 was reached. The unusual low incubation temperature is thought to improve transformation efficiency but the reason is still unknown. Before harvesting the cells at 2200x g (Multifuge 3 S-R, Heraeus), 10 min, 4 °C, they were incubated for 10 min on ice. All the following steps were performed on ice as well. Cells were washed two times by resuspension in 80 ml pre-cooled TB with a 20 ml sterile plastic pipette, followed by incubation on ice for 10 min and centrifugation as above. The final cell pellet was resuspended in 20 ml TB. 7 % (1.4 ml) DMSO was added drop by drop while slowly stirring on ice under the fume hood. After another 10 min of incubation on ice, the *E.coli* cells were aliquoted (200 µl) into Eppendorf cups by filling them quickly with a multipette. Aliquoting took place under a lamillar flow hood. Before filling, the Eppendorf cups were placed with open lids in a bath with liquid nitrogen to shock freeze the cells as fast as possible. The aliquots were stored at -80 °C.

Transformation of chemical-competent *E.coli*

Transformation of chemical-competent *E.coli* XL1blue was performed with the following heat shock procedure: An aliquot of the competent cells was thawed on ice and mixed with either a ligation reaction or 1- 10 ng of plasmid DNA. Following incubation on ice for 30 min, while carefully tapping the tubes occasionally, the transformation mixture was transferred to a 42 °C hot water bath for 60 sec. After immediate removal to ice for another 5 min, 900 µl of LB were added. The cells were incubated at 37 °C for 1 h with gentle shaking and in a flat position to increase the movement of air and liquid to provide oxygen for bacterial growth. Cells were then harvested by brief centrifugation for 2 min at 4000 rpm in a microcentrifuge (Eppendorf 5417R) and resuspended in 1 ml of fresh LB. 100 µl were spread on LB agar plates (1.2 % agar) under a

lamillar flow hood using a Drigalski spatula sterilised by ethanol flaming. The remaining cells were pelleted again by centrifugation as above and resuspended in 100 µl LB. These cells were similarly spread onto LB plates. The agar plates contained the appropriate antibiotics for selection of positive transformants (see table below). All plates were incubated for at least 16 h at 37 °C.

antibiotic	**final concentration [µg ml^{-1}]**
ampicillin	100
kanamycin	50
spectinomycin	100

Plasmid minipreps

Single colonies were picked with a sterile pipette tip and inoculated into 5 ml liquid sterile LB containing antibiotics as required. The cultures were grown on a shaker at 37 °C o.n. Cells were harvested by centrifugation at maximum speed in a microcentrifuge for three minutes. Plasmids destined for DNA sequencing were extracted with the QiaPrep Miniprep kit (Qiagen) on spin columns as instructed by the manufacturer. Alternatively, to obtain greater quantities, plasmid DNA from 50 ml cultures was extracted with the QiaPrep Midiprep kit (Qiagen) on spin columns as instructed by the manufacturer. Elution in both cases was performed with distilled water. When such superior purity (of contaminating e.g. salts, proteins) was not needed, as for example with plasmids destined for a restriction enzyme digest to confirm positive transformants, plasmids were extracted with the following alternative protocol.

buffer	**composition**
resuspension buffer	50 mM Tris-Cl pH 8.0, 10 mM EDTA, 100 µg/ml RNAse A
lysis buffer	200 mM NaOH, 1 % SDS
neutralisation buffer	3 M K acetate pH 5.5

The cell pellet was completely resuspended in 100 µl of resuspension buffer by vortexing and/or pipetting up and down. 200 µl of lysis buffer was added, the tube gently inverted three times and incubated on ice for 5 min. Subsequently, 200 µl of neutralisation buffer was added and the tube again inverted several times. The lysate was centrifuged at max. speed in a microcentrifuge for 10 min and the SN (SN) transferred to a fresh tube. One volume of isopropanol was added and mixed with the DNA by vortexing. The mixture was incubated at RT for 10 min to precipitate the plasmid DNA. Centrifugation at max. speed for 20 min at 4 °C collected the precipitated DNA in a pellet that was washed with 1 ml of 70 % ethanol. The pellet was then dried in the vacuum concentrator at 60 °C and resuspended in 50 µl of distilled water. For restriction digestions, five 5 µl of such miniprep DNA were normally added to the standard reaction setup (see above).

Glycerol stocks

To prepare glycerol stocks for storage of yeast, *E.coli* or *Agrobacterium* at -80 °C, a respective culture from the saturated growth phase was used. For yeast, the final concentration of glycerol was 20 % and for *E.coli* or *Agrobacterium* 25 %. A sterile 40 % glycerol stock solution was prepared and mixed with the respective culture under sterile conditions to obtain the final glycerol concentrations given above.

Preparation of electro-competent *Agrobacterium*

Electro-competent *Agrobacterium rhizogenes* MSU440 or *Agrobacterium tumefaciens* GV3101 cells were produced with the following materials and method:

medium	**Composition in g l^{-1}**
YEB	5 Beef Extract, 1 Yeast Extract, 5 Peptone, 5 Saccharose, 0.49 $MgSO_4x7H_2O$ (+ 15 Bacto Agar for solid medium)

A single colony of *Agrobacterium* was grown o.n. in a 5 ml liquid YEB pre-culture at 28 °C in a shaker. Cultures of *Agrobacterium tumefaciens* included the antibiotics gentamycin (25 µg ml^{-1}, Ti-plasmid resistance) and rifampicin (50 ug ml^{-1}, chromosomal resistances). This pre-culture was used to inoculate the main culture (1:1000) of a final volume of 250 ml. This culture was grown to an OD_{600} of about 0.8- 1 and harvested at 3000x g at 4 °C for 10 min. Afterwards 7 washing steps with one volume of ice-cold sterile distilled water followed before final resuspension in 1/20 volume of ice-cold sterile 10 % glycerol. Aliquots of 40 µl were made as described for chemical-competent cells and frozen at –80 °C.

Transformation of *Agrobacterium*

Transformation was performed by thawing an aliquot of electro-competent *Agrobacterium rhizogenes* MSU440 or *Agrobacterium tumefaciens* GV3101 cells on ice and mixing it with ~1 µg of plasmid DNA obtained by Quiagen Miniprep Kit (see above). After 1 min incubation on ice the mix was quickly transferred with a cold pipette tip (stored at -20 °C) into an ice-cold cuvette (Gen Pulser Cuvette, 0.2 cm gap, Bio-Rad) and an electric pulse of 1.8 kV for 5 msec was applied (Gene Pulser Xcell system, Bio-Rad). As fast as possible 1 ml of YEB without antibiotics was added to the cells and mixed carefully. After one hour incubation while shaking at 28 °C in an Eppendorf cup the cells were plated on YEB plates containing the appropriate antibiotic resistance to be conferred to a successfully transformed cell. These plates were incubated at 28 °C for about 2 d.

Colonies appearing on selective plates were picked and grown in sterile 5 ml liquid YEB medium as described above. 5 µl of each culture were used in a colony PCR reaction as described above and with appropriate primers for the desired target CDS. Cultures that yielded a positive

signal from PCR were used to inoculate a new 5 ml subculture and then harvested. Plasmid miniprep was performed essentially as described above with one additional step to help dissolve the *Agrobacterium* cell walls. After cell resuspension in resuspension buffer, 20 µl of a 20 µg/µl lysozyme solution was added. Following a thorough mixing by vortex, the cell suspension was incubated 15 min at 37 °C before proceeding with the miniprep as usual. 10 µl of the resulting plasmid miniprep were used for chemical transformation of *E.coli* (see above) because binary vectors are usually low-copy (7-8 copies per cell) and DNA needs to be amplified prior to subsequent procedures. After selection of positive *E.coli* transformants, plasmid DNA was in turn recovered from these cells and used for restriction enzyme digest and/ or sequencing to confirm the target CDS in the binary backbone. For plasmids that had proven positive during this procedure, the corresponding *Agrobacterium* sub-culture was used to prepare a glycerol stock (see above). This glycerol stock was used for all subsequent experiments involving the respective constructs.

Amidoblack assay

In general, protein concentrations were quantified with the Amidoblack assay. Amidoblack is an anionic dye that reacts with protein to yield a blue colour, the absorbance of which is measured at 615 nm. The Amidoblack assay is based on the co-precipitation of proteins with the Amidoblack dye dissolved in methanol/acetic acid followed by dissolution of the precipitate in NaOH and determination of absorbance (Schaffner & Weissman, 1973). This precipitation step makes the Amidoblack assay compatible with high concentrations of detergents as were used here for the isolation of membrane proteins. In contrast, detergent concentrations of more than 0.1 % SDS or Triton-X-100 interfere with the more common and technically easier to perform Bradford assay. The Bradford assay relies on the binding of a dye to proteins which results in a dye–protein complex with increased molar absorbance (Bradford, 1976). Interference with the absorbance values may be caused by detergent-protein and/or detergent-dye interactions.

For the Amidoblack assay 2- 10 µl of protein sample were made up to a volume of 40 µl with distilled water. To these samples 160 µl of colouring solution (10 % acetic acid, 90 % methanol, 0.05 % Amidoblack dye) were added followed by incubation at RT for 15 min. The samples were then centrifuged at max. speed in a microcentrifuge for 10 min and the SNs discarded. The dyed protein pellets were washed with 200 µl of decolouring solution (10 % acetic acid, 90 % methanol) and centrifuged again. The SN was taken off and the pellets resuspended in 800 µl of 0.2 N NaOH. The absorbance at $OD_{615\ nm}$ was measured against 0.1 N NaOH as a blank and the protein content calculated in µg $µl^{-1}$ based on a standard curve. For the standard curve, BSA protein samples were prepared with the following amounts: 0, 0.25, 0.5, 1, 2, 5, 10, 15 and 20 µg BSA in a volume of 40 µl with distilled water. These samples were treated as described and used to plot a standard curve.

SDS-PAGE

Protein samples were separated by SDS polyacrylamide gel electrophoresis using a mini gel format (Protean III, Bio-Rad) according to the Laemmli procedure (Laemmli, 1970). A 10 % separation gel with a 4 % stacking gel was used unless otherwise stated. The two SDS gel parts were prepared by mixing the compounds in the order as given in the table below:

component	amount for 10 % separation gel	amount for 4 % stacking gel
H_2O	2 ml	1.85 ml
4x Separation buffer	1.25 ml	
8x Stacking buffer		312 µl
30% Acrylamide	1.66 ml	416 µl
10 % Ammonium persulfate in H_2O	50 µl	25 µl
TEMED	5 µl	2.5 µl

The separation gel was poured first and covered with isopropanol during the polymerization time of ca. 40 min to prevent drying. After removing the isopropanol, the stacking gel with an appropriate comp was added. After another polymerisation time of about 20 min, the gel was loaded with the protein samples of interest. These samples were prepared before loading by adding one volume of 2x SDS Sample Loading buffer (see table below). Unless otherwise stated the protein samples were incubated at RT or 37 °C for about 15- 30 min before loading to avoid possible aggregation of membrane proteins. Remaining samples were stored at -20 °C. As molecular weight standard 10 µl of the NEB broad range prestained protein ladder was loaded in parallel. Typically, 5- 10 µg of proteins were separated per lane unless otherwise stated. Gels were run in 1x SDS Running Buffer at 100 V until the proteins were concentrated at the end of the stacking gel. Subsequently, 150- 170 V were applied.

buffer	composition in g l^{-1}
4x Separation buffer	17.4 Tris base, 0.4 SDS, pH 8.8
8x Stacking buffer	11.1 Tris base, 0.8 SDS, pH 6.8
2x SDS Sample loading buffer	in g per 100 ml: 1.52 Tris base, 20 Glycerol, 3 DTT, 4 SDS, 0.001 Bromophenol blue
8x Running buffer	24.2 Tris base, 115.2 Glycin, 8 SDS, pH 8.3

Western Blot analysis

The transfer membrane (PVDF, Millipore) was prepared according to the manufacturer's instructions. For the transfer of proteins from the gel to the membrane, a wet blot system (Mini-PROTEAN, Bio-Rad) was used. SDS gels were briefly rinsed in distilled water and then equilibrated in cold Transfer buffer (see table below) for about 10 min, together with two pieces of Whatman paper (9.5 x 7.5 cm) and the membrane (8.5 x 6 cm).

buffer	composition in g l^{-1}
Transfer buffer	3.03 Tris base, 14.4 Glycine, 200 ml methanol freshly prepared each time, pH 8.3 should be achieved without adjusting
PonceauS:	2 PonceauS in 5 % acetic acid
PBS-T	11.5 Na_2HPO_4, 2.96 NaH_2PO_4, 5.84 NaCl, 0.1 % Tween20, pH 7.5
Blocking solution	4 % milk powder (Marvel, Iceland, UK) in PBS-T, 0.02 % NaN_3
Antibody solution	antibody, PBS-T, 0.5 % milk powder, 0.02 % NaN_3
Stripping buffer	100 mM 2-Mercaptoethanol, 2 % SDS, 62.5 mM Tris-HCl pH 6.7

The sandwich between membrane and SDS gel was assembled between Whatman papers according to the manufacturer's instructions. The Blot was generally run at 4 °C with cold Transfer buffer and the provided cooling compartment. During the run, the buffer was stirred in the chamber by means of a small stirring bar and a magnetic stirrer. Unless stated otherwise, the blotting conditions were 100 V for 1 h. After blotting, the membrane was incubated in the water soluble dye PonceauS for 5 min at RT with gentle shaking to detect transferred proteins. Excess stain was washed off with distilled water, and the stained membrane was scanned. To avoid drying during the scan, the membrane was wrapped in a piece of SaranWrap. Destaining was performed in distilled water for 10 min at RT.

The membrane was then placed into Blocking solution (see table above) and incubated for 1 h at RT with slow movement on a horizontal shaker. After the blocking step, the membrane was directly transferred into Antibody solution (see table above) containing a suitable dilution of the respective primary antibody. For small Antibody solution volumes (3-5 ml), the membrane was sealed into SaranWrap for incubation steps. Incubation was either 1 h at RT or o.n. at 4 °C. Unbound antibody was removed in four wash steps, each performed with excess volumes of PBS-T for 15 min at RT with fast movement on a horizontal shaker. After subsequent incubation with a suitable dilution of the secondary antibody as described for the primary antibody, these wash steps were repeated. Incubation time for the secondary antibody was always 1 h (at RT). Unless stated otherwise, the secondary antibody was either an anti-rabbit HRP (horseradish peroxidase) conjugate (Sigma, # A6184) or an anti-mouse HRP conjugate (Sigma, # A9044) depending on the animal species the primary antibody was raised in. Anti-SYP121, anti-SYP122 and anti-SYP111 were published by Tyrell *et al.* (2007).

Detection was generally by a chemiluminescence signal derived from a suitable substrate for the HRP enzyme that was part of varying ECL kits (see individual chapter M&M). ECL detection was performed according to the manufacturer's instructions of the respective kit. In all cases, detection was performed under safe-light conditions in a darkroom. The chemiluminescent signal was caught on X-ray film (# 8143059, Kodak, Bagnolet, France). Films were developed using a Compact X4 Xograph (Imaging Systems, Tedbury, UK).

If membranes were to be re-probed, the original primary and secondary antibody were stripped off by incubating the membrane at 70 °C for 30 min in Stripping buffer (see table above) with gentle agitation. Stripping was followed by six washing steps with large PBS-T volumes for

30 min at RT each. Subsequently, the membrane was blocked and probed with antibodies as described above.

Confocal imaging

Confocal imaging was performed on a Carl Zeiss CLSM510 inverted confocal microscope. The images shown in Fig. 47 (p. 181) and Fig. 46e (p. 179) were taken with a Plan neofluar 20x/0.5 objective. BiFC-YFP was excited using an Argon laser with the 514 nm laser line and transmission set to 18 % output. Emitted fluorescence was passed through a first dichroic mirror (458/514 nm) and transmitted light was collected in the brightfield channel. An NFT545 dichroic mirror was used to further split the emitted fluorescent light and BiFC-YFP fluorescence was collected with a band pass 530-560 nm filter. All images were taken with standardized confocal settings: pinhole set to 1 airy unit, image size set to 512 x 512 pixels, line scan with average of 8, z-stack with 14-16 slices.

A 63x apochromat water immersion objective was used for Fig. 46f. All other confocal images shown were obtained with a 40x 1.2 apochromat water immersion objective. Pictures in Fig. 47 and Fig. 52A (p. 209) are three-dimensional projections from confocal fluorescence image z-stacks that were reconstructed with the Zeiss LSM software. The same software was used for quantification of three-dimensional projections in combination with SigmaBlot.

GFP (for AKT1-GFP fusion) was excited with an Argon laser run at 6.1 A using the 488 nm laser line and transmission set to 12 % output. Laser excitation and emission was passed through a first dichroic mirror (488/543/633 nm) and transmitted light was collected in the brightfield channel. An NFT545 dichroic filter was used to further split the emitted fluorescent light and GFP fluorescence was collected with a band pass 505-530 nm filter. YFP (for KC1-YFP fusion) was excited using an Argon laser as above with the 514 nm laser line and transmission set to 15 % output. Emitted fluorescence was passed through a first dichroic mirror (458/514 nm) and transmitted light was collected in the brightfield channel. An NFT545 dichroic mirror was used to further split the emitted fluorescent light and YFP fluorescence was collected with a band pass 530-560 nm filter.

Material and Methods for Chapter 1

Cloning of a novel Cub-X vector for mbSUS

The idea behind the design of the Cub-X vector (see next page, Fig. 19) was to allow fusions of the Cub moiety to the N-terminus of a protein of interest. The ability to attach the Cub moiety to the N-terminus of bait proteins is of particular interest for TA proteins, such as SNAREs, to ensure that the Cub moiety resides in the cytoplasm. So far, only Cub fusions to the C-terminus of a protein of interest had been possible with the pMetYCgate published by Orbdlik *et al.* (2004). Modification of the existing pMetYCgate vector rather than assembly of an entirely new plasmid was chosen for the purpose of convenience and to facilitate comparisons between Cub-X and X-Cub fusions of the

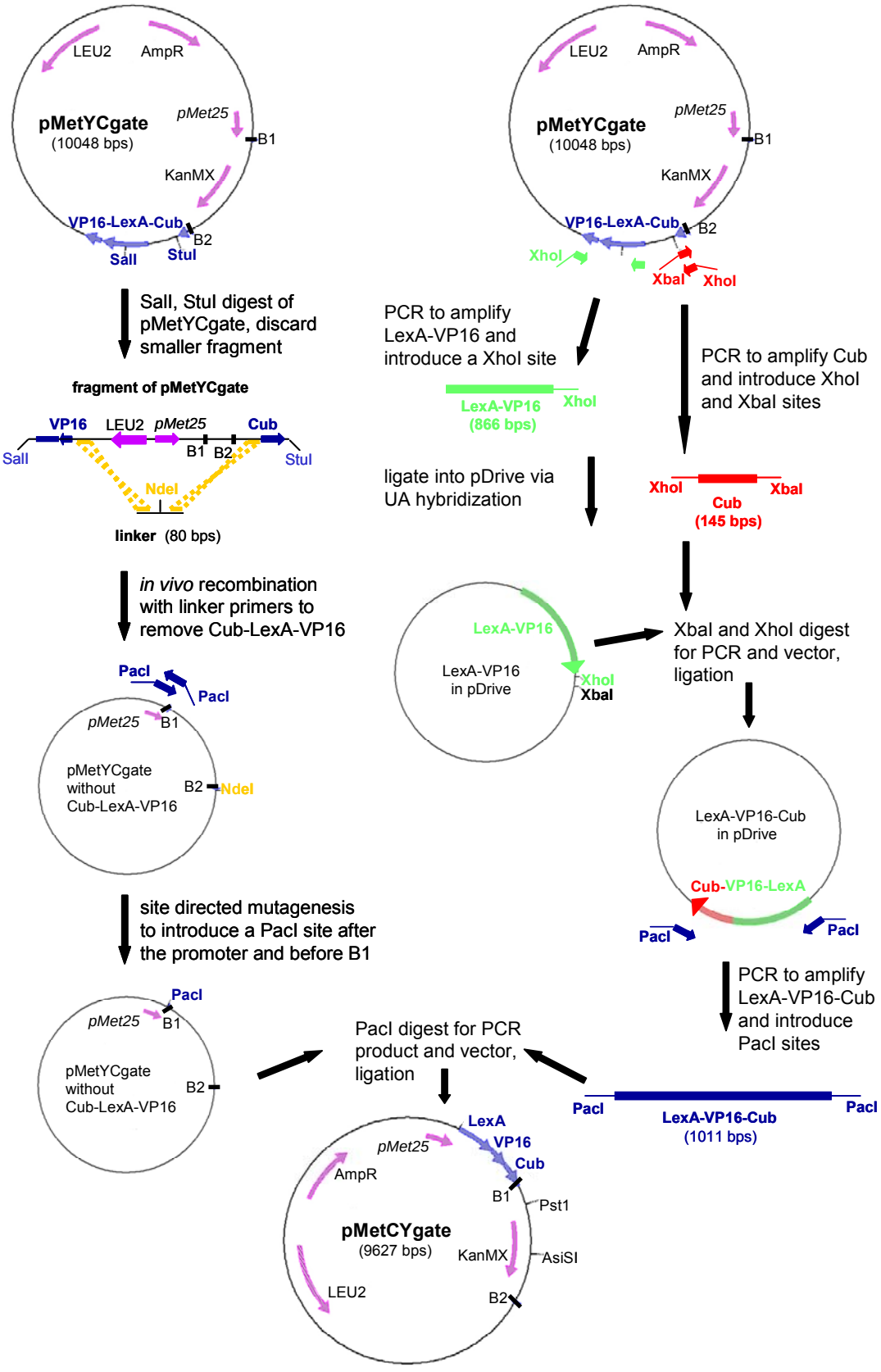

Fig. 19 Design of the Cub-X vector pMetCYgate

The original vector pMetYCgate (Obrdlik *et al.*, 2004) allows fusions of the Cub part to the C-terminus of a CDS of interest (X-Cub) by exchanging it for the KanMX cassette between the B1 and B2 recombination sites. The series of cloning steps pictured above modified pMetYCgate into pMetCYgate that now permits converse Cub-X fusions with the Cub located at the N-terminus of a protein of interest.

same bait protein based on an identical vector backbone and promoter. Two major modifications were necessary that are indicated in the two 'columns' in Fig. 19. On the left is shown the process of deleting the existing Cub-LexA-VP16 (Cub with artificial transcription factor) from pMetYCgate from its position behind the B2 recombination site. To reintroduce it before the B1 recombination site and thus directly behind the *Met24* promoter, a PacI restriction site was inserted into the vector backbone. The right hand side of Fig. 19 shows rearrangement of the Cub-LexA-VP16 part into a LexA-VP16-Cub part. This step was necessary to ensure that the ubiquitin-specific proteases that recognize quasi-native ubiquitin reformed from Nub-and Cub interaction still release the artificial transcription factor at the same time.

Starting on the left side again for a more detailed description of the cloning procedure, pMetYCgate was first linearized the two unique restriction enzyme sites SalI and StuI. This digest with two different enzymes removed a 686 bp fragment out of the Cub-LexA-VP16 part and was necessary to prevent re-ligation of the vector during the subsequent *in vivo* cloning procedure. The process of *in vivo* cloning in yeast combines the processes of cloning an insert into a vector backbone with the transformation of yeast. *In vivo* cloning relies on a recombination step between homologous sequences in insert and vector that is performed by yeast endogenous enzymes. Therefore, the yeast is transformed with the insert and the linearized vector backbone at the same time. This principle is used for the mbSUS vectors to insert the CDS of interest between the B1 and B2 recombination sites (see below). Here, a linker was designed which sequence was homologous to 37 bps in front of the Cub sequence and 37 bps behind the VP16 sequence of pMetYCgate. In addition, an NdeI was included site that is absent form this vector. A linker is basically an artificial piece of DNA, i.e. two primers were ordered (No. 1-for and 2-rev, see Appendix, p. 235) with complementary sequences, denaturated at 98 °C for 5 min to remove secondary structure and slowly cooled down to RT (30 min) to allow the two strands to anneal. This linker was used together with the SalI, StuI digested pMetYCgate for in vivo cloning as described below. Recovered plasmids were checked for the successful insertion of the linker, i.e. the complete absence of the Cub-LexA-VP16 part (sequence between the bps 2219- 3640 deleted), first by NdeI digest and subsequently by sequencing.

For the next step of introducing a PacI restriction enzyme site between Met25 promoter and B1 recombination, a modified site directed mutagenesis was used. A 5' phosphorylated primer pair was designed, of which forward (No. 3) and reverse (No. 4) primer were homologous to the same target sequence between promoter and recombination site. Each primer carried in addition the information for one half of the PacI site that was absent in pMetYCgate. Subsequently, a proofreading PCR with Phusion polymerase amplified the whole vector (no bps lost, 5 ng pMetYCgate as template). The PCR was incubated with 2 µl of DpnI restriction enzyme for 2 h at 37 °C before 10 µl of the reaction were used for *E.coli*XL1 blue transformation. DpnI is an enzyme that digests only methylated DNA as will be obtained from *E.coli* during plasmid Miniprep. Therefore, the original vector, i.e. the PCR template was digested but the PacI primer-amplificated sequence remained intact. Subsequently, a ligation was performed with the DpnI digested PCR product after gel-purification, followed by transformation of *E.coli*. Recovered plasmids were

tested for successful ligation, i.e. the creation of the PacI site from its two halves, by PacI digest and sequencing. This vector was then digested with PacI and dephosphorylated to prevent spontaneous re-ligation.

To assemble the LexA-VP16-Cub insert to clone into this PacI digested vector, two PCRs were performed with the original pMetYCgate as template. The first PCR amplified the LexA-VP16 part with a reverse primer (No. 6) that encoded an XhoI restriction site. The forward primer (No. 5) was unmodified. To the ends of this PCR product adenine residues were added by stopping the PCR program after the final elongation step, mixing 1µl Taq and 1.5 µl 10 mM ATP with the reaction and continuing the incubation at 72 °C for another 20 min. The 'A-tailed' PCR products (by means of the non-proofreading function of the Taq polymerase) were than cloned into the vector pDrive of the Quiagen PCR cloning kit (Quiagen, # 231122) according to the manufacturer's instructions. This strategy relies on uracil overhangs in the linearized vector that hybridize with high specificity to the A-overhangs.

The second PCR amplified the Cub moiety with the pMetYCgate as template and an XhoI restriction site overhang in the forward primer (No. 7) and an XbaI- overhang in the reverse primer (No. 8). Both this PCR product and the pDrive vector containing LexA-VP16 were double digested with XbaI and XhoI. These two enzymes are part of the MCS of the pDrive vector backbone. Subsequent ligation of Cub into LexA-VP16-pDrive, assembled the ubiquitin half and the artificial transcription factor in the desired orientation as directed by the two different restriction enzyme sites.

A final PCR was performed with the resulting plasmid as template. The forward (No. 9) and reverse (No. 10) primer contained each a PacI restriction site to amplify the LexA-VP16-Cub assembly. Subsequently, the PCR product PacI digested and ligated into the PacI digested and dephosphorylated vector backbone described above. After transformation the resulting clones were screened for events where LexA-VP16-Cub had inserted in the correct orientation with a directional digest. XhoI is present in the insert and a unique site in the vector backbone and a digest lead to fragments of different sizes corresponding to both orientations. After sequencing this new vector was named pMetCYgate.

Insert and vector preparation for *in vivo* cloning of mbSUS constructs

As mentioned above, the creation an insert of interest for *in vivo* cloning required only a PCR product that includes the B1 and B2 recombination sites, no restriction enzyme digest was needed. Attachment of the B1 site (5'-3': acaagtttgtacaaaaaagcaggctctccaaccacc) was mediated as overhanging sequence in the respective forward primer and attachment of the B2 site (5'-3': tccgccaccaccaaccactttgtacaagaaagctgggta) as an overhang in the respective reverse primer. Depending on the destination vector, a stop-codon was needed in the reverse primer or provided by the vector itself. The first table below indicates the primer combination used for proof-reading PCR to obtain mbSUS inserts for the listened CDSs. Template for these PCRs were various constructs that had been designed by other members of the group for different purposes.

CDS	No. forward primer	No. reverse primer w/o stop	No. reverse primer with stop
KC1	11 (29)*	17	23
KAT1	12	18	24
AKT1	13	19	25
SYP121	14 (30)*	20	26
SYP111	15 (31)*	21	27
SYP122	16	22	28

* These forward primers were needed to clone in frame within the Cub-X vector only.

The table below indicates the requirement of the different mbSUS vectors for an insert with or without stop-codon. In addition, the restriction enzymes sites for the digest necessary to linearize the mbSUS vectors before *in vivo* cloning are given. All these enzymes cut between the B1 and B2 restriction site, i.e. the sequence that will be replaced by the insert during successful recombination in yeast.

mbSUS vector	requires insert with stop-codon	requires insert without stop-codon	digested for *in vivo* cloning with
Nub-X	√		EcoRI/ SmaI
Cub-X	√		PstI/ AsiI*
X-Cub		√	PstI/ HindIII
X-Nub		√	EcoRI/ SmaI
X-Nub-HA		√	EcoRI/ SmaI
Nub-X-HA		√	EcoRI/ SmaI

* The cloning strategy for the design of pMetCYgate as described above introduced a HindIII site with the LexA-VP16-Cub part so that this enzyme was not unique anymore.

In vivo cloning and yeast transformation

Yeast transformation after the method developed by Gietz *et al.* (1995) requires that every time cells are made freshly competent. Two different yeast strains were used for mbSUS assays: THY.AP4 and THY.AP5 that were transformed with Cub- and Nub-containing vector backbones respectively (see p. 121).

buffer	composition in g l^{-1}
YPD	10 Yeast Extract, 20 Bacto Peptone, 20 glucose (+ 15 Bacto Agar for plates)
10x TE buffer	100 mM Tris-HCl pH 7.5, 10 mM EDTA
LiAc stock solution	1M LiAc pH 7.5 (with acetic acid), filter sterilized
PEG solution	50 % PEG 4000 in distilled water, filter sterilized
TE/LiAc buffer	1x TE, 0.1 M LiAc in distilled water, filter sterilized
PEG/LiAc buffer	1x TE, 0.1 M LiAc in PEG solution, filter sterilized
SC medium	1.7 YNB, 5 ammonium sulfate, 20 glucose, pH 6.3 with NaOH, drop-out-mix*, (+ 15 Oxoid agar** for plates)

All media were used in sterile conditions after autoclaving or filter sterilisation. * Individual drop-out-mixes were obtained from Bio 101 systems (www.qbiogene.com/products/bio101) and contained all amino acids apart from the desired selective one(s); they were used in the amounts stated by the manufacturer. ** Oxoid agar was obtained from Oxoid (Basingstoke, Hampshire, England, # LP0011).

A single yeast colony from an YPD plate was inoculated in 5 ml liquid YPD medium and grown o.n. at 28 °C. This pre-culture was used to inoculate 100 ml YPD in a way that two doubling times (~ 2 h doubling time for yeast in the logarithmic phase) would lead to an OD_{600} of 0.8- 1. A 500 ml Erlenmeyer Schikane-flask was used to incubate this culture in a shaker at 28 °C to increase oxygen supply to the cells. When the desired OD_{600} (0.8- 1) was reached the yeast was harvested in 50 ml Falcon tubes for 10 min at 1550xg and 4 °C. From this point on, the cells were kept strictly on ice and all work was performed under a lamillar flow hood. The SN was discarded and the cells were washed in 20 ml sterile ice-cold distilled water. Resuspension was done with a 20 ml sterile plastic pipette to minimize shear forces. After centrifugation as above, the cell pellet was washed with 20 ml of ice-cold TE/LiAc buffer and finally resuspended in 200 µl ice-cold TE/LiAc buffer. From this point on yeast cells were considered chemical-competent.

For each transformation 7 µl salmon sperm DNA (10 mg ml^{-1}) was denatured in an Eppendorf cup for 3 min at 95°C before being snap-cooled on ice. About 500- 800 ng of insert and 1000- 1500 ng of linearized vector were mixed with the salmon sperm DNA using a 1 ml pipette tip to avoid shearing it. The total added volume did not exceed 10 µl. Insert and linearized vector had been obtained from gel elution with the Quiagen kit as described after PCR and /or restriction enzyme digest.

To this DNA mixture, 50 µl competent yeast cells and 300 µL PEG/LiAc buffer were added by carefully pipetting up and down each time with a 1 ml pipette tip. This transformation reaction was incubated for 20 min at 28 °C in a flat position while shaking slowly (~ 50 rpm). Additionally, competent yeast were mixed with either the linearized vector and distilled water instead of insert or water only as described above. These mixes served as experimental controls for the amount of background transformation derived from e.g. incompletely linearized vector or spontaneous mutation. Following incubation at 28 °C, a heat shock was applied for 20 min in a water bath pre-heated to 42 °C. Subsequently, 800 µl of sterile distilled water were added and an even suspension was obtained by pipetting. An aliquot of 100 µl was spread onto appropriate SC plates that selected for the respective vector backbone, i.e. SC medium without leucine (SC_l) for Cub-X and X-Cub vectors or SC medium without tryptophan and uracil (SC_{tu}) for Nub-X and X-Nub vectors. Plates were incubated at 28 °C for about 2 d.

To select from the yeast colonies that were positive for the presence of a vector backbone the ones where the *in vivo* cloning procedure had been successful, colonies were picked from plates to grow in selective liquid SC medium with and without the antibiotic G418 (200 µg ml^{-1}). The KanMX cassette between the B1 and B2 recombination sites in the Cub- and Nub-containing vector backbones encodes for the neo gene product (see p. 90). This neomycin phosphotransferase prevents the lethal action of G418 that inhibits eukaryotic ribosomes. Through the process of successful *in vivo* cloning the KanMX cassette is replaced by the insert of interest. Thus, all yeast cells that do not grow on G418 are supposed to carry the insert of interest. The corresponding yeast culture without G418 was harvested and the plasmid DNA extracted to be sent out for sequencing.

Yeast DNA extraction

buffer	composition
lysis buffer	10 mM Tris base, 1 mM EDTA, 100 mM NaCl, 1 % SDS, 2 % TritonX-100, pH 8

Yeast culture (4 ml) was harvested by centrifugation at max. speed for 1 min in a microcentrifuge. A leftover of each culture was stored at 4 °C. To the cell pellet 0.2 g of acid washed glass beads (0.7- 1 mm), 0.2 ml lysis buffer and 0.2 ml of a 25:24:1 mix of phenol:chloroform:isoamylalkohol were added before vortexing for 2 min. Vortexing was repeated for a few seconds after adding an additional 0.2 ml of 1xTE buffer (see above). Following a centrifugation step at max. speed for 5 min, the aqueous (upper) phase was transferred to a fresh 1.5 ml Eppendorf cup and 2 volumes of 100% EtOH were mixed thoroughly with it. From this mixture the precipitating plasmid DNA was obtained as described for the plasmid miniprep procedure without the Quiagen kit (p. 84). The final pellet was resuspended 30 µl of distilled water and 5 µl were used to transform chemical-competent *E.coli* XL1blue as described above (p. 83). Plasmid DNA from positive transformants was obtained as described above and send for sequencing. For clones that contained an in frame and error free insert, the leftover of the original yeast culture was used to prepare a glycerol stock as described for *Agrobacterium* (p. 85). These glycerol stocks were subsequently used for mbSUS assays.

mbSUS assay

For this assay, all steps were performed under sterile conditions and with sterilized media. The first step of an mbSUS assay was mating haploid yeasts that carried the individual Nub-and Cub-constructs to obtain diploids with the desired combinations of constructs. For this purpose, 5 ml cultures were grown o.n. in selective SC medium using the glycerol stocks described above. Cells (1 ml) were harvested by centrifugation (5 min, 2500xg, RT) and resuspended in 200 µl YPD. In sterile conditions, 15 µl of the respective Cub-and Nub-carrying haploids were mixed by pipetting and 7 µl of this mix were dropped onto YPD plates. The plates were incubated at 28 °C for 6 h. A portion of each 'mating spot' was scraped of the YPD plate with a sterile pipette tip and streaked out onto a diploid-selective SC_{tlu} plate that was incubated for 2 d at 28 °C. Diploids from this plate were grown up in a 3 ml liquid SC_{tlu} pre-culture o.n. The next morning, the OD_{600} was determined, cells were diluted to OD_{600} 0.2 in the same medium and re-grown until OD_{600} 0.8- 1 was reached to obtain the same growth-phase stadium for all dipolids. In a 96 well plate, serial dilutions in distilled water were obtained for each diploid (OD_{600} of 0.1, 0.01 and 0.001 respectively). A 7 µl aliquot of each dilution was spotted for each diploid onto plates from the following SC media: SC_{tlu}, SC_{tluahm} (additionally: no adenine, histidine, methionine), SC_{tluahm} with reconstituted methionine in three different concentrations: 0.07 mM, 0.15 mM, 0.4 mM, SC_{tlum} and SC_{tlum} with 0.4 mM methionine. All plates were incubated at 28 °C for 6 d before imaging with the exception of the SC_{tlum} and

SC_{tlum} with 0.4 mM methionine plates. These two plates were used after 3 d of incubation for X-Gal overlay assays performed as follows:

buffer	composition g/l
Z-buffer	16.1 $Na_2HPO_4 \cdot 7\ H_2O$, 5.5 $NaH_2PO_4 \cdot H_2O$, 0.75 KCl, 0.246 $MgSO_4 \cdot 7H_2O$, pH 7.2

For two square plates, 0.25 g agarose was dissolved in 50 ml Z-buffer with moderate heating in a microwave oven. The agarose solution was cooled down to 50 °C in a 50 °C water bath before adding 1 ml of 10 % SDS and 1 ml of X-Gal solution (100 mg/ml in dimethylformamide). The mixture was quickly but gently layered over the plates and left until the agarose had solidified before incubation at 37 °C for approx. 1 h.

Quantitative liquid β-gal assay

An o.n. pre-culture (SC_{tlum}) of each diploid yeast was used to inoculate 3 ml liquid SC_{tlum} with an OD_{600} of 0.2. Cultures were grown at 28 °C until OD_{600} 1- 1.5 was reached to obtain a similar growth-phase stadium for all dipolids. The OD_{600} of all dipolids was adjusted to 1 with SC_{tlum}. Three replicas of 300 µl each per diploid culture were mixed with 75 µl of MUG (1 mg/ml in DMSO) and incubated in a 37 °C water bath for 30 min. The water bath was covered with aluminium foil to exclude light. The reaction was stopped by the addition of 90 µl 2 M Na_2CO_3 and immediately put on ice for 15 min. MUG releases 4-methylumbelliferone that emits fluorescence when exposed to UV light. Fluorescence was measured in a luminometer (Perkin Elmer, LS55) with a 360 nm excitation filter and a 460 nm emission filter and a quartz cuvette. Arbitrary units of β-gal activity dependent MUG hydrolysis, so called MUG units, were calculated from the measured amount of fluorescence that was divided by the reaction time and OD_{600} of the sample.

Yeast protein extraction for Western Blot analysis

For total protein extraction, 5 ml of a saturated yeast culture were harvested by centrifugation at max. speed for 1 min in a microcentrifuge. The cell pellet was washed once with 1 mM EDTA solution (EDTA in water) before adding 200 µl 2 M NaOH and incubation on ice for 10 min. To precipitate proteins, 200 µl of a 50 % TCA solution were added and after thorough mixing the solution was incubated on ice for 2 h. A centrifugation step at max. speed for 20 min at 4 °C in a microcentrifuge pelleted the precipitated proteins that were subsequently dissolved in 200 µl ice-cold acetone. After centrifugation as before 200 µl 5 % SDS were used to resuspend the pellet. An equal volume of 2x SDS Sample Loading Buffer (see p. 87) was added and samples were incubated at 37 °C for 15 min. After centrifugation at max. speed for 5 min samples were used either for SDS-PAGE and Western Blot directly and/or stored at -20 °C.

The primary antibody (anti-SYP111, anti-SYP121, anti-SYP122) dilution for the Western Blot pictured in Fig. 23 (p. 126) was 1:40,000. The secondary anti-rabbit-HRP antibody was used

1: 80,000. The detection kit was Amersham ECL (GE Healthcare, Piscataway, NJ, USA, #1990). For the Western Blot in Fig. 32 (p. 135) the primary antibodies (anti-SYP111, anti-SYP121, anti-VP16) were diluted 1:1000 and the secondary anti-rabbit-HRP was used 1:10,000. The detection kit was Amersham ECL Advance (GE Healthcare, #2002). Anti-VP16 was from Abcam (# ab4808-00).

Material and Methods for Chapter 2

Constructs for protein expression in *Sf9* insect cells

All constructs for the production of recombinant virus stocks had the Baculovirus Transfer Vector pVL1939 (BD Bioscience, New Jersey, USA, # 21486P) as backbone. This vector was digested either with EcoRI/PstI or BamHI/PstI to clone *AKT1* and KAT1 via the indicated restriction enzyme sites that had been included into PCR primer as overhangs (see table below). The VSVG and HA-HA tags were attached to the respective CDS as additional long overhangs in the reverse primer (see table below). As template for the *KAT1* construct served the *KAT1-HA$_{(external\ loop)}$-GFP* construct published by Sutter *et al.* (2006). Templates for *AKT1* and *KAT1* were sequenced mbSUS clones.

CDS	**C-terminal tag**	**external loop tag**	**N-terminal tag**	**No. of forward primer with restriction site overhang**	**No. of reverse primer with restriction site overhang**
AKT1	VSVG			(32) EcoRI	(33) PstI
KAT1	HA-HA			(34) BamHI	(35) PstI
KAT1		HA_{ext}		(34) BamHI	(36) PstI
SYP121			FLAG-HIS	Dr. Johansson, Dr. Sokolovski (Prof. Blatt's group)	
SYP122			FLAG-HIS		
SYP111			FLAG-HIS		
KC1	Myc-HIS				

Sf9 insect cell culture

Insect cultures were maintained in a 27 °C incubator. The *Sf9* cells were obtained from (Invitrogen, California, USA, # B825-01). The growth medium was Baculogold TNM-FH (BD Bioscience, # 554760) supplemented with Fetal bovine serum according to the manufacturer's instructions (Biosera, # S1810). Cell culture flasks (Corning) with vented lids in two different sizes were used: 25 cm^2 (# 430639) and 75 cm^2 (# 430641). All procedures took place in a special room only for insect cell culture and under sterile conditions in a laminar flow hood. Pre-sterilised 5 ml, 10 ml and 25 ml pipettes (Corning) and filter tips (Rainin) for normal pipettes were used. Generally, *Sf9* cells double every 18- 24 h. To maintain healthy cultures, cells were sub-cultured every Monday and Friday. Sub-culturing required a ratio of 1:3 cells: fresh medium. The culture was maintained

generally in 25 cm^2 flasks as a monolayer of ~1-1.5×10^6 cells (as counted by hemocytometer). Two new flasks per old culture were generally made, one as back-up in case of infection. This was up-scaled according to the amount of cells needed for infection with virus. The growth medium was pre-warmed to 27 °C in a water bath and 2 ml added to each new flask. Cells from the old culture where dislodged from the monolayer attached to the bottom of the flask with a gentle stream of medium from sterile a Pasteur pipette (with cotton wool filter in the neck). To each new flask 1 ml of washed down cells was added and mixed by gentle horizontal movement. The flasks were placed on a flat surface to ensure the development of homogenous cell density.

After 20- 30 min at RT, the adhesion of the seeded cells was checked under the microscope before proceeding to exchange the medium. To remove the old medium, the flask was tilted to onto one edge and the liquid removed with a 10 ml pipette. Immediately 3 ml fresh medium was gently added and the flask tilted back to cover the cells with medium. The cell density in the fresh flasks was then ~ 30%. The remainder of the original culture was stored at 4 °C as back-up.

Production of recombinant virus

To obtain cells for infection with virus, about 2×10^6 cells (~1.5 ml) were transferred from the old culture to the new flask (initial cell density of 50- 70 %). Cells were infected within the hour by simply adding virus stock with a filtertip to the growth medium and distributing it with gentle horizontal movements. Cells were then placed at 27 °C for the desired amount of time. Unless otherwise indicated, all infected cell cultures used for the experiments shown in Chapter 2 (p. 149ff.) had been incubated for 48 h after infection. All virus stocks that were used to infect those cultures were second generation recombinant viruses.

The preceding recombinant generation 'zero' virus stocks were created with 2×10^6 cells in a 25 cm^2 flasks using BaculoGold™ kit (BD Bioscience, # 554740) according to the manufacturer's instructions. The respective constructs with the Transfer Vector pVL1939 backbone (see above) needed for this purpose were purified with Quiagen Miniprep columns before use, as insects cells are sensitive to some contaminants found in crude plasmid preparations. The cells were incubated for 5 d at 27 °C, before the overlaying growth medium was collected as generation 'zero' stock. For the harvest, cells were washed down from the bottom of the flask as described for culture maintenance and transferred to a 15 ml Falcon tube. After centrifugation for 10 min at 2000xg and 4 °C, the cell pellet was discarded and the SN stored in the fridge.

This generation 'zero' virus stock was used to infect 5×10^6 cells in a 75 cm^2 flask. The growth medium was replaced with 1 ml of virus stock and incubated at 27 °C for 1 h with occasional gentle rocking to re-distribute the liquid. Subsequently, 8 ml fresh growth medium was added and the flask incubated at 27 °C for 4 d. As a control, a second flask was mock-infected with growth medium only and incubated in parallel. The successful infection with virus could be assessed by the visible slower growth of Baculovirus treated cells. The infected culture was harvested as described above as first generation virus stock and kept in the fridge as well. The second generation virus stock was obtained by infecting cells with the first generation stock exactly

as described above.

The standard for infection with second generation recombinant virus was 15 µl of SYP121, SYP111- or SYP122- stock and 25 µl of KC1 stock unless otherwise indicated. Second generation virus stocks for AKT1 and the two KAT1 constructs had been used with 25 µl as well to obtain the results in Fig. 37 (p. 151). Cells from one 25 cm^2 flask infected with the virus amounts per construct as indicated above, were harvested and solubilised for experiments shown in Fig. 36- Fig. 39. For all Co-IP experiments shown in Fig. 40- Fig. 44, 75 cm^2 flasks were infected with the appropriately up-scaled virus amounts. In general, one flask was used per sample.

Standard protocol for solubilisation

buffer	composition
Resuspension	10 mM HEPES pH 6, 130 mM NaCl
Solubilisation	x % of detergent, 10 mM HEPES pH 6, 130 mM NaCl, 10 mM NaF, 1 mM Na-orthovanadate, Pi, 1 mM PMSF, 0.02 % NaN_3

* Pi (Protease Inhibitor Cocktail Tablets, Roche, # 11836153001), used according to the manufacturer's instructions, **PMSF (phenylmethanesulfonylfluoride) from a 200 mM stock in EtOH

Infected insect cells were harvested as described above. After centrifugation for 10 min at 1000xg and 4 °C, the SN was discarded and the cell pellet washed with 10 ml of ice-cold Resuspension buffer. Resuspension was performed with a cut-off 1 ml pipette tip to avoid cell rupture at this stage. The pellet was washed again with 2 ml Resuspension buffer and transferred to a 2 ml Eppendorf cup. After centrifugation as before, the SN was discarded and the cell pellet underwent either a freeze/thaw cycle at -20 °C to support cell disruption or remained in the freezer for storage. Before thawing, 150 µl or 400 µl ice-cold Solubilisation buffer were added for cells harvested from 25 cm^2 or 75 cm^2 flasks respectively. Cells were disrupted by pipetting up and down with a 100 µl tip until a homogenous suspension had been obtained. This suspension was incubated with slow head-over-end rotation o.n. at 4 °C. Following centrifugation at 16000xg for 30 min and at 4 °C, the SN was removed to a fresh Eppendorf cup and termed solubilisation supernatant (sSN).

All following detergents for solubilisation had been obtained from Sigma (Poole, UK): TritonX-100 (#T 8532); Tween20 (# P 8942), CHAPS (# C 9426); CHAPSO (#C 9551); OGP (#O 8001); Digitonin (# D141); LPC (# L4129); NDSB-201 (# 82804). NP-40 was obtained from Pierce (Thermo Fisher Scientific, # 28324). It is indicated for each figure in Chapter 2 which detergent had been used as well the concentration for solubilisation.

Initially, sonication (3x 5 sec, on ice) of a syringe and 27G needle were tried as alternatives for cell disruption. However, insect cells are naturally quite fragile so that it was recognized over time that simply pipetting as described above was sufficient. Similarly, initially a membrane fraction was prepared before solubilisation, which was time consuming. As trial experiments with whole cell lysate let to successful Co-IP, this procedure was discontinued.

Optimized protocol for Co-IP

To prepare the solid support for Co-IP, 600 µl SepharoseG (Sigma, # P3296) was transferred into a 2 ml Eppendorf cup. Care was taken to homogenise the slurry of SepharoseG in 20 % EtOH that is provided by the supplier by pipetting before removal of the 600 µl aliquot (equal to ~ 400 µl bedvolume). The EtOH was removed by washing the slurry ten times with 2 ml Resuspension buffer, centrifugation steps were performed at 3 min, 5000xg and RT.

buffer	**composition**
Resuspension	10 mM HEPES pH 6, 130 mM NaCl
Block	1 % BSA, 0.1 % Tween20, 10 mM HEPES pH 6, 130 mM NaCl, 10 mM NaF, 1 mM Na-orthovanadate, Pi, 1 mM PMSF, 0.02 % NaN_3
Antibody	15 µl anti-FLAG *, 0.3 % BSA, 0.1 % Tween20,10 mM HEPES pH 6, 130 mM NaCl, 10 mM NaF, 1 mM Na-orthovanadate, Pi, 1 mM PMSF, 0.02 % NaN_3
Co-IP	10 mM HEPES pH 6, 0.15 % BSA, 130 mM NaCl, 10 mM NaF, 1 mM Na-orthovanadate, Pi, 1 mM PMSF
Wash	$1/10^{th}$ of x % detergent, 0.1 % BSA, 10 mM HEPES pH 6, 140 mM NaCl, 10 mM NaF, 1 mM Na-orthovanadate, Pi, 1 mM PMSF
Elution	$1/10^{th}$ of x % detergent, 0.1 M glycine HCl, pH 3.5

* Anti-FLAG antibody was obtained from Sigma (# F1804).

The SepharoseG was then transferred with 5 ml Block buffer for 1 h at RT with slow head-over-end rotation. After centrifugation as before, the SepharoseG was incubated with 5 ml Antibody buffer containing anti-FLAG o.n. with slow head-over-end rotation at 4 °C. After subsequent centrifugation as above, the SepharoseG was washed three times with 10 ml Block buffer to remove unbound antibody. Finally, 800 µl of Block buffer were added and this stock was stored at 4 °C.

For Co-IP, solubilisation SN as described above was diluted 1:10 with Co-IP buffer and 20 µl of the SepharoseG-anti-FLAG stock were added before incubation at RT for 1 h with slow head-over-end rotation. The SN after subsequent centrifugation as above was saved on ice as 'flow-through' fraction. The Sepharose was washed 6 times with 4 ml Wash buffer. The last wash fraction was saved on ice as well. Finally, the Sepharose was incubated with 20 µl Elution buffer and incubated 2 min with slow head-over-end rotation at RT. The SN obtained after centrifugation as above was transferred to a fresh tube containing 2 µl of 1 M Tris pH 8 for neutralisation. A total of five elution steps were performed in a similar manner before discarding the Sepharose. The flow-through, last wash fraction and the five combined elution factions were incubated with 5 µl StrataClean™ resin to concentrate proteins according to the manufacturer's instructions (Stratagene, Sydney, Australia, # 400714). This resin was used with an appropriate volume of 2x SDS Sample Loading Buffer, incubated for 30 min at 37 °C and either used for SDS-PAGE directly or stored at -20 °C.

Western Blot was performed as described earlier (p. 87). All primary antibodies were used in a standard 1:1000 dilution. Anti-Myc, anti-His, anti-HA and anti-FLAG were from Sigma (# M5546, # H1029, # H9658 and # F316 respectively). Anti-VSVG was from Bethyl (Universal

Biologicals Ltd, Cambridge, UK, # A190-131A). Secondary anti-rabbit HRP was used to detect anti-VSVG and secondary anti-mouse HRP was used for detection of all other primary antibodies. Both secondary antibodies were used in 1:10,000 dilution. The detection kit was ECL Advance.

The Co-IP procedure as described above was used for the experiments pictured in Fig. 41, Fig. 42, Fig. 43B. For all experiments, where the expression levels of KC1 and SNAREs had been verified before Co-IP (e.g. Fig. 41B or Fig. 44B, C), 10 µl of sSN were used for SDS-PAGE and Western Blot.

For the experiments shown in Fig. 40 and Fig. 41 different solid supports had been used. Anti-c-Myc agarose conjugate (Sigma, # A7470) and anti-FLAG M2 affinity gel (Sigma, # 2220) were prepared according to the manufacturer's instructions and 10 µl were used per sample. ProFound^{TM} Co-IP Kit (Pierce, now Thermo Fisher Scientific, # 23600) was used in combination with anti-FLAG (Sigma, # F7425) according to the manufacturer's instructions (data not shown). Sepharose A (Sigma, # P9424) was prepared and used as SepharoseG (data not shown).

For the experiment shown in Fig. 41A, the FLAG peptide (Sigma, # F3290) was prepared according to the manufacturer's instructions and used to block anti-FLAG binding sites in a final concentration of 100 µg ml^{-1}.

The wt Baculovirus provided with the BaculoGold™ kit used to create the recombinant virus was used in an aliquot of 5 µl per 75 cm^2 flask.

Material and Methods for Chapter 3

Design of BiFC vectors for N-terminal fusions and BiFC constructs

At the time, the available vectors for plant BiFC from the publication of Walter *et al.* (2004) allowed fusions of the YFP halves only to the C-terminus of a protein of interest. With regard to SNAREs as TA proteins, it was considered necessary to design additional vectors that would allow fusions of YFP-halves to the N-terminus of a protein of interest. To achieve this goal, the vectors pSPYCE-35S (containing the C-terminal half of YFP) and pSPYNE-35S (containing the N-terminal half of YFP) developed by Walter *et al.* (2004) were modified as follows (see next page, Fig. 20): In a first step, the YFP half was removed from the vector p-SPYNE-35S. For this purpose the vector was first digested SmaI, which was unique in its sequence. The digest was purified directly over a Quiagen Gel extraction column according to the manufacturer's instructions. The eluate was then digested with the unique enzyme Ecl136II. Both enzymes created blunt ends. Therefore, subsequent ligation to close the vector backbone, now missing the fluorophore half, was possible without further modifications. Colonies obtained after transformation into *E.coli* XL1 blue were checked for the absence of the fluorophore half by SmaI digest. Re-ligation of the blunt ends destroyed both SmaI and Ecl136II site and therefore, all undigested colonies were considered positive for the loss of N-terminal YFP.

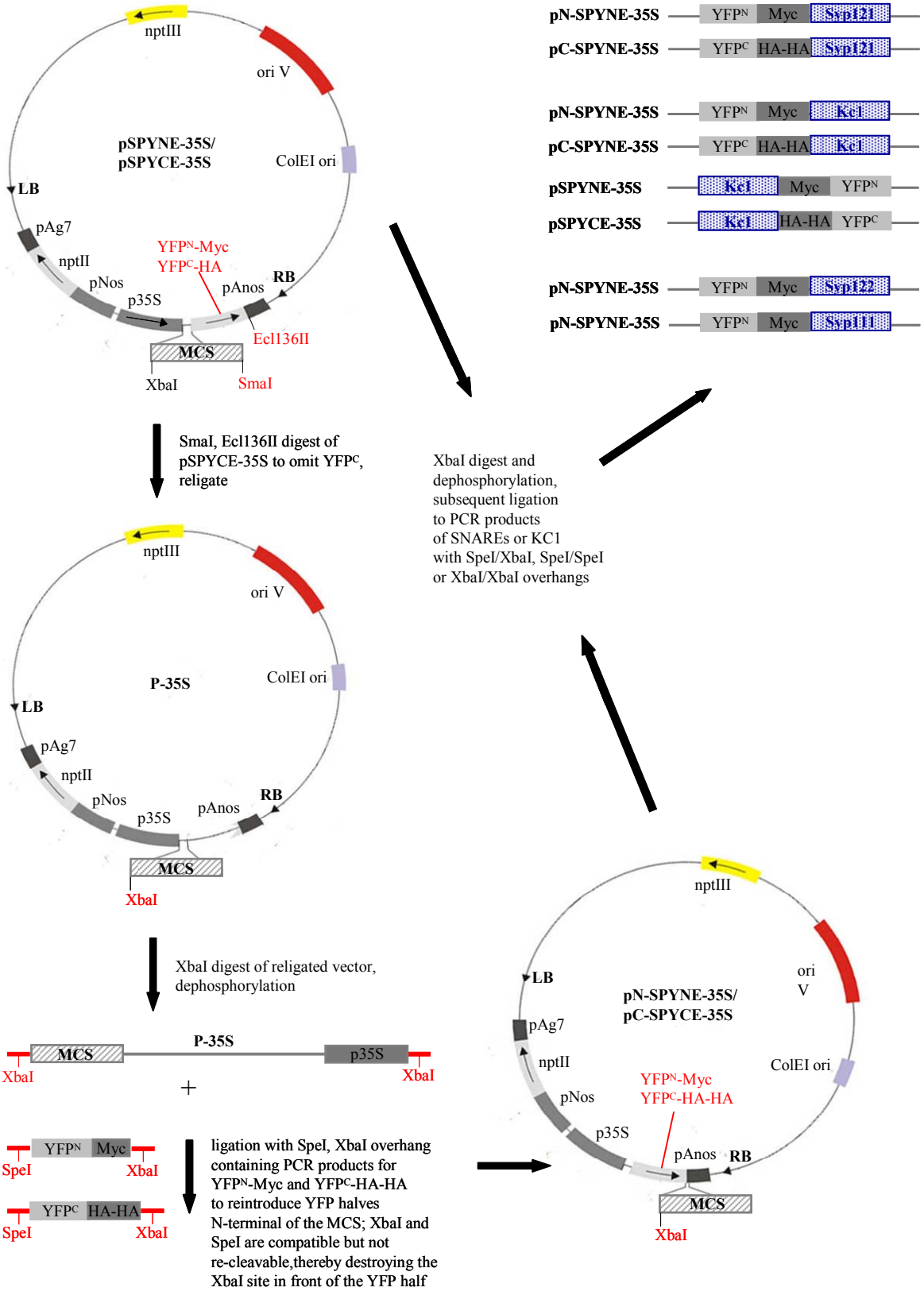

Fig. 20 Design of BiFC vectors and constructs

The existing plant BiFC vectors allowed fusions of the YFP halves to the C-terminus of a protein of interest only (p-SPYNE-35S and p-SPYCE-35S) (Walter *et al.*, 2004). To be able to attach the FP fragments to the N-terminus of a protein of interest instead, the existing vectors were modified in a series of steps as pictured above. In short, the FP fragment and epitope tag were first removed from p-SPYCE-35S and then reintroduced in front of the MCS. The new vectors were named pN-SPYNE-35S and pC-SPYCE-35S. Subsequently, the three SYP1 SNAREs and KC1 were cloned into these four vectors as indicated above.

In a next step, either the N-terminal or the C-terminal half of YFP (YFP^N or YFP^C) was reintroduced into this vector backbone in a way that the MCS was now behind instead before the fluorophore half. To achieve this, the re-ligated vector was digested with XbaI (first enzyme of the MCS) and dephosphorylated. Dephosphorylation was necessary to prevent spontaneous re-ligation without insert during the subsequent cloning steps.

The YFP^N and YFP^C inserts to be introduced into the linearized dephosphorylated vector were obtained by performing proof-reading PCR with p-SPYNE-35S and p-SPYCE-35S as template respectively (primers No. 37-for and 38-rev for YFP^N; primers No. 39-for and 40-rev for YFP^C). The forward primers for each PCR contained sequence overhangs that encoded a SpeI restriction enzyme site. The reverse primer for amplification of YFP^N contained a long overhang encoding a linker sequence, a Myc tag and an XbaI site in this order. The reverse primer for amplification of YFP^C had a similarly long overhang for a linker sequence, a double-HA tag and an XbaI site in this order.

Both PCR products were double digested with SpeI and XbaI. These inserts were ligated with the dephosphorylated vector in a molar ratio of 5:1. After transformation of *E.coli*, colonies appearing on selective medium were checked for the presence of the respective fluorophore half by a test digest with HindIII and XbaI. Ligation of SpeI to XbaI is possible but the resulting sequence is no longer recognized by either enzyme. HindIII was located in the original vector backbone immediately before the MCS (end of 35S promoter). During ligation, the inserts could have inserted either way, resulting in a correct and inverted orientation of the respective fluorophore half. Digest with HindIII and XbaI would have given a 890 bp fragment for the wrong orientation of both fluorophore halves and a 1300 bp and 1000 bp fragment respectively for the correct orientation of YFP^N and YFP^C respectively. Positive clones were sent to sequencing. The new vectors were named pN-SPYCE-35S (contains YFP^N) and pN-SPYNE-35S (contains $YFP^{C)}$.

Subsequently, constructs of C- and N-terminal fusions of SNAREs and KC1 were cloned as indicated in Fig. 20 (right hand side). As the XbaI site in front of the YFP half had been destroyed by ligation with SpeI when either fluorophore half had been inserted in the correct orientation, the re-build XbaI site at the reverse primer site could be used in both new vectors to open them for inserting the CDS of *SYP121*, *SYP111*, *SYP122* and *KC1*. As the same XbaI site was available in the original vectors p-SPYNE-35S and p-SPYCE-35S, all four vectors were digested with XbaI and dephosphorylated as described above. All four CDS were obtained for ligation into these vectors by proofreading PCR using the sequenced respective mbSUS Nub-X constructs as template. Primers for amplification of *SYP121* had a SpeI coding overhang in the forward primer (No. 41) and a stop codon as well as XbaI coding overhang in the reverse primer (No. 42). The forward and reverse primer used to amplify *SYP111* (No. 43 and 44) and *SYP122* (No. 45 and 46) all contained SpeI overhangs (and a stop codon in the reverse primer). PCR products for the three syntaxins were digested and purified as described above before ligation with linearized dephosphorylated pN-SPYNE-35S (and pC-SPYNE-35S for *SYP121* only*)* in a molar ratio of 10:1. Plasmid DNA of positive clones after *E.coli* transformation were checked for the correct orientation of the insert with a HindIII, XbaI digest for *SYP121* and an HpaI digest for *SYP111* and

SYP122 positive clones were send for sequencing.

The CDS of KC1 was amplified with XbaI overhangs in both forward (No. 47) and reverse primer. Two different reverse primers were used without (No. 48) and with stop codon (No. 49) to ligate the XbaI digested PCR products into p-SPYNE-35S/p-SPYCE-35S and pN-SPYCE-35S/pN-SPYNE-35S respectively and as described for the syntaxins. Sequenced plasmid DNA for all constructs was used to transform *Agrobacterium rhizogenes* or *A.tumefaciens* as needed.

Repeated attempts to clone KAT1 or AKT1 with C-terminal or N-terminal FP halves were unsuccessful.

KC1-YFP was cloned into the binary vector pPTbar (kindly provided by Karin Schumacher, ZMBP, Tuebingen). The CDS for *KC1-YFP* was obtained by proofreading PCR using a clone as template that a former post-doc of Prof. Blatt's lab, Dr. M. Paneque, had designed for a different purpose that did not need a binary vector backbone. As forward primer the above mentioned XbaI containing *KC1* primer (No. 49) was used. The reverse primer recognized the C-terminus of YFP and had an XhoI overhang (No. 50). PCR products were double digested with XhoI and XbaI and ligated into XbaI and SalI digested pPTbar in a molar ratio of 1:10 (vector: insert). XhoI and SalI create compatible ends for ligation but both sides are destroyed afterwards. Thus, this cloning strategy allowed for directional cloning and the absence of a SalI site was used to identify positive clones. The AKT1-GFP fusion (binary vector backbone pGWB5) was kindly provided by Dr. M. Paneque.

Onion epidermis particle bombardment

A mature white onion was purchased on the day of the experiment and after removing the brown outer layers and the outer scales the epidermis layer of inner scales (2- 3 cm slices) was peeled of and placed onto 0.5x MS-plates: 2.2 g l^{-1} MS (Sigma, # M5519) in distilled water, 1 % sucrose, pH 5.8 with 1 M KOH, 1 % Plant Cell agar from Sigma, # A-1296) slightly wetted with sterile water. The plates were sealed with parafilm until bombardment to prevent drying of the epidermis.

For the preparation of gold particles (1 µm, Bio-Rad, # 165-2263), 40 mg were mixed with 1 ml 100 % EtOH and sonicated for 2 min. The gold particles were pelleted with a 3 sec spin in a microcentrifuge and this washing step was repeated two times. After removing the final SN, 1 ml of sterile distilled water was added to the gold and the mix was again sonicated for 2 min. After centrifugation as above, the SN was replaced with a fresh 1 ml of sterile distilled water. Aliquots of 50 µl were stored at -20 °C.

One aliquot of gold particles was coated with DNA for 10 individual shots. The gold was first sonicated for 1 min, vortexed vigorously for 2 min and sonicated for another 1 min before adding 5 µg of plasmid DNA obtained from Quiagen Midiprep columns. When co-transformation was attempted, the final amount of DNA stayed 5 µg for the two or three different plasmids. The mix of gold and DNA was vortexed vigorously for 10 min, 50 µl of 2.5 M $CaCl_2$ and 20 µl of 0.1 M spermidine (in sterile distilled water) were added and after short vortex for 10 sec incubated at RT for 10 min. A short spin as above pellet the gold which was washed with 150 µl 100 % EtOH as

above and finally resuspended in 85 µl 100 % EtOH. The DNA-coated gold particles were kept on ice before an aliquot of 5 µl was placed onto the centre of a macrocarrier.

The macrocarrier was ready for bombardment when all ethanol had evaporated. Bombardment was performed with 1100 psi rupture discs in a Bio-Rad PDS-1000/He biolistic particle delivery system according to the manufacturer's instructions. A pressure of 200 psi was applied and the MS plates with the onion epidermis slices were placed in a distance of 2 cm below the gun. As a control DNA was omitted and onion bombarded with uncoated particles. The plates were sealed with parafilm and incubated at RT for 36 h before confocal imaging.

Arabidopsis suspension cell culture and protoplast transformation

medium	**composition in g l^{-1}**
NAA stock	0.05 first dissolved in a small amount of 1M NaOH, stored in aliquots at -20 °C
Kinetin stock	0.05 first dissolved in a small amount of 1M NaOH, stored in aliquots at -20 °C
culture medium	30 sucrose, 4.43 MSMO (Sigma, # M-6899), 10 ml NAA stock, 10 ml Kinetin stock, pH 5.8 with 1 M KOH

Miss Janet Laird (University of Glasgow) kindly provided an aliquot of her *Arabidopsis* suspension culture that was derived from shoot callus. The culture was dark adapted here over a period of two months by covering the culture flasks with aluminium foil. Sub-culturing was done every 7 d by transferring 20 ml to 180 ml of fresh culture medium in a 500 ml Erlmeyer Schikane-flask. All procedures were performed under sterile conditions and with sterilised materials. Cultures were grown with constant shaking at 150 rpm at 20 °C.

The protocol for the generation of protoplasts from *Arabidopsis* suspension culture cells and PEG-mediated transformation of these protoplasts was kindly provided by Miss Caterina Brancato (Transformation Unit, ZMBP, University of Tuebingen, Germany).

solution	**composition**
Wall digestion w/o enzymes	8 mM $CaCl_2$, 0.4 M mannitol, pH 5.5, filter sterilised
Wall digestion	1% cellulase, 0.25% macerozym, 8 mM $CaCl_2$, 0.4 M mannitol, pH 5.5, filter sterilised
W5	154 mM NaCl, 125 mM $CaCl_2$, 5 mM KCl, 5 mM glucose, pH 5.8– 6.0, autoclaved
MMM	15 mM $MgCl_2$, 0.1% MES, 0.5 M mannitol, pH 5.8, autoclaved
PEG	40% PEG 4000, 0.4 M mannitol, 0.1 M $Ca(NO_3)_2$, pH 8– 9 (the pH needs 1–2 h to stabilize), autoclaved
Macro stock (in g/ l)	1.5 $NaH_2PO_4 \cdot H_2O$, 9.0 $CaCl_2 \cdot 2H_2O$, 25 KNO_3, 2.5 NH_4NO_3, 1.34 $(NH_4)_2SO_4$, 2.5 $MgSO_4 \cdot 7H_2O$, autoclaved
Micro stock (in mg/100 ml)	75 KI, 300 H_3BO_3, 1000 $MnSO_4 \cdot 7H_2O$, 200 $ZnSO_4 \cdot 7H_2O$, 25 $Na_2MoO_4 \cdot 2H_2O$, 2.5 $CuSO_4 \cdot 5\ H_2O$, 2.5 $CoCl_2 \cdot 6H_2O$, filter sterilised and frozen
Vitamin stock (in mg/100 ml)	100 nicotinacid, 100 pyridoxin • HCl, 1000 thiamin • HCl, filter sterilised and frozen
EDTA stock (in g/ l)	7.46 EDTA dissolve in 300 ml H_2O and cook, 5.56 $Fe(II)SO_4\ 7H_2O$ dissolve in 300 ml H_2O and cook, autoclaved and kept in the dark

Ca-phosphate stock (per 200 ml)	1.26 g $CaHPO_4$ •$2H_2O$, pH 3 with 25% HCl, autoclaved and kept in the dark
K3 (per 100 ml)	10 ml macro stock, 0.1 ml micro stock, 0.1 ml vitamin stock, 0.5 ml EDTA stock, 1 ml Ca-phosphate stock, 10 mg myo-inositol, 25 mg D(+)-xylose, 13.7 g sucrose, pH 5.6, filter sterilised, frozen in 10 ml aliquots

Protoplasts were derived from 10 ml *Arabidopsis* suspension cells 3 d after sub-cultivation. All After centrifugation at 400x g for 5 min, the cells were washed once with 10 ml of Wall digestion solution without enzymes, re-centrifuged at 100xg for 5 min and finally resuspended in 7 ml of Wall digestion solution. Cells were dispensed into a small Petri dish (3 cm) and incubate at 26 °C in the dark for 6 h while gently shaking at 50 rpm. Resulting protoplasts were collected by centrifugation at 100x g for 5 min in a Sorvall Legend RT centrifuge with a swing-out rotor and with the brake and acceleration set to the slowest level. Protoplasts were washed once with 10 ml of Wall digestion solution without enzymes and pelleted by centrifugation as above. The SN was removed and the protoplast pellet very gently resuspended in the remaining solution by slowly tilting the tube back and forth so that the liquid moved against the pellet gently. In a similar fashion, 10 ml of W5 solution were added in small portions and mixed in. After subsequent centrifugation as above, the protoplast pellet was resuspended in the same gentle manner as described in 10 ml of W5 solution. An aliquot of this suspension was used to count the protoplast in a Fuchs-Rosenthal chamber under the microscope while the remainder was stored for 20 min in the dark at 4 °C. All W5 solution was removed after standard centrifugation and the pellet gently resuspended in MMM solution to a density of $2x10^6$ protoplasts/ ml. Aliquots of 250 µl were distributed into 1.5 ml Eppendorf cups and 30 µg of plasmid DNA (obtained from Quiagen Midiprep columns) was added per sample. For co-transformations 15 µg per plasmid was used. Very slowly 250 µl PEG solution was added per sample. Mixing was done very gently as described above. After an incubation period of 20 min at 26 °C in the dark, 10 ml of W5 solution were added and mixed in gradually and gently. The protoplast were pelleted by centrifugation as above and resuspended in 2 ml of K3 solution. Final incubation took place at 26 °C in the dark for 24 h before confocal imaging.

Tobacco leaf infiltration

A 5ml culture of the respective sequenced construct transformed into *Agrobacterium tumefaciens* GV3101 was grown o.n. at 28 °C from a glycerol stock with liquid YEB medium plus gentamycin (25 µg ml^{-1}) and the appropriate antibiotic resistance encoded on the construct (kanamycin 50 µg ml^{-1} for BiFC constructs and spectinomycin 100 µg ml^{-1} for KC1-YFP). The following morning, the OD_{600} was determined and a 50 ml sub-culture was inoculated with OD_{600} 0.2. This culture was harvested at the end of the exponential growth phase (OD_{600} of 0.8- 1) by centrifugation at 8000 rpm for 5 min at RT. The pellet was washed two times with 50 ml sterile 10 mM $MgCl_2$ before resuspension in 2 ml of the same solution. The OD_{600} of this *Agrobacterium* 'stock' was again determined and a working suspension for leaf injection was obtained by dilution to the desired

OD_{600} (usually no more than 0.4 in total). For co-transformations the two cultures were mixed at this stage in the desired ratios of the respective OD_{600}. Subsequently, 100 µm acetosyringone was added from a stock solution of 1 M in DMSO (stored in small aliquots at -20 °C). The cells were left then at RT for 1- 2 h.

For *Nicotiana tabacum* leaf infiltration, plants had been grown in a growth chamber (Sanyo FitoTron) for 4- 6 weeks in long day conditions (16 h light, light intensity ~200 µmol m^{-2} s^{-1}, 26 °C/22 °C day/night, 60 %/70 % day/night relative humidity). A plant with 3- 4 true leaves was chosen (leaf size of about 5 cm^2). With a sharp tool the epidermis on the underside of a leaf was grazed and the *Agrobacterium* suspension injected into the abaxial air space by pressing the opening of a 1 ml syringe firmly to the wound. The infiltrated area, visible by a darker colour, was marked with a soft pen. The plant was watered and returned to the growth chamber.

For confocal microscopy (24 h- 72 h post-infiltration), the infiltrated areas of the leaf were collected by excising a ~1 cm^2 piece with a new sharp razor blade. To reduce background fluorescence due to air pockets, excised leaf samples were vacuum infiltrated with distilled water in the chamber of a 50 ml syringe. With the tip blocked the plunger was drawn up to remove air bubbles from the leaf.

Transient *Arabidopsis* seedling root transformation

Arabidopsis seedlings for co-incubation with *Agrobacterium rhizogenes* were grown under sterile conditions. Seeds were mixed with 7 ml 0.1 % Tween-20 (in distilled water) in a 15 ml Falcon tube, vortexed until no more clumps were visible and then mixed by head-over-end rotation for 20 min at RT. The seeds were allowed to settle and the SN replaced by 7 ml of 0.1 % Tween-20 in 95 % EtOH. Seeds were again vortexed to dispel clumps and then incubated 5 min with head-over-end rotation. The SN was decanted and instead a solution of 1.6 % sodium hypochloride and 0.1 % Tween-20 (in distilled water) was added. Following vortexing and rotation for 10 min, the SN was removed under a lamillar flow hood and the seeds washed 5 times with 10 ml sterile distilled water. Finally, depending on the amount of seeds, enough sterile distilled water was added that after shaking seeds were able to move freely. Seeds were vernalized in the dark at 4 °C for 2- 3d and stored under the same conditions between experiments for up to 2 weeks.

To sow seeds for transient root transformation under sterile conditions, the Falcon tube was shaken briefly until an equal distribution of seeds was obtained. With a 1 ml pipette and sterile filter tips enough liquid was taken up to obtain ~30 seeds. The seeds were allowed to settle above the opening of the tip by holding the pipette vertical. Seeds were released with gentle pressure into one well of a 6-well plate filled with 4 ml sterile liquid 0.5x MS medium (2.2 g l^{-1} in distilled water, pH 7.2). Care was taken to release as less water as possible with the seeds to not dilute the growth medium. By shaking the seeds every time before removing the same fixed volume, roughly the same number of seeds was obtained per well. The plate was sealed with parafilm and incubated for 3d in long day conditions (16 h photoperiod, light intensity 180 µmoles m^{-2} s^{-1}, 21 °C). Seedlings should have cotyledons but no primordia for the first true leaves should be visible yet.

Agrobacterium rhizogenes cultures for co-incubation were obtained as described above for tobacco leaf infiltration. However, all experimental procedures were performed strictly under sterile conditions in a lamillar flow hood and with sterile solutions and filter tips. In addition, the pellet after the final wash with 10 mM $MgCl_2$ was resuspended in 1 ml 0.5xMS medium instead. From the OD_{600} of this *Agrobacterium* 'stock' the amount of bacteria needed to obtain the desired OD_{600} (generally 0.5) in a final volume of 4 ml was calculated for both BiFC partners. The calculated volumes (usually in the range of 10- 20 µl) were added to 1 ml of liquid 0.5xMS medium that contained in addition enough acetosyringone to obtain a concentration of 100 µm in a final volume of 4 ml. This 1 ml 'stock' of *Agrobacterium* and acetosyringone was used to replace 1 ml of the seedling growth medium. Removal and replacement of 1 ml growth medium from each well of the 6-well plate containing the 3- 5 d old *Arabidopsis* seedlings was done very slowly and carefully so that the seedlings were disturbed as less as possible in order to avoid damaging of root hairs. The plate was with parafilm, rotated very slowly and gently to distribute the bacteria and incubated as before. Confocal imaging for BiFC constructs was usually performed after 72 h.

Material and Methods for Chapter 4

GUS assay

buffer	**composition in g l^{-1}**
assay buffer	50 mM NaH_2PO_4/ Na_2HPO_4 pH 7.2, 0.5 mM K ferrocyanide, 0.5 mM K ferricyanide, 1 mM X-Gluc (XglucDirect, www.x-gluc.com)

Seeds for promoter-*GUS* expressing plants and *Arabidopsis* Col0 wt control were sown in 6-well plates and grown as described for BiFC assays (p. 107). All procedures until the GUS assay itself were performed under strictly sterile conditions. For the promoter-*GUS* lines only, the growth medium (0.5x MS, pH 5.8) was supplemented with 50 µg ml^{-1} hygromycin (Invitrogen). After 3 d the surviving seedlings were transferred to a 6-well plate with fresh growth medium lacking hygromycin (1-3 plants per well). The transfer was done with a feather-light forceps that was used to gently lift the seedling by hooking under the cotyledons without actually gripping it. Seedlings were used for GUS assays after 7 d, 14 d and 21 d of total growth time (including pre-selection).

GUS staining was carried out essentially as described by Jefferson *et al.* (1987). In short, the growth medium was removed very gently from the wells to disturb the plants as little as possible and equally gently replaced with 8 ml of assay buffer. The plates were placed under vacuum three times for five minutes at RT. Following vacuum infiltration, the plants were incubated o.n. at 37 ºC in the dark. De-staining was done by replacing the assay buffer carefully with 20 %, 40 %, 60 %, and finally 80 % ethanol with incubation at RT for 20 min periods. Plants were stored in 100 % ethanol until imaging. Images were taken with a Nikon D1x camera or a Zeiss AxioVert S100TV light microscope with a Zeiss AxioVision camera attached (Zeiss, Jena, Germany).

Growth assay for K^+ uptake

Seedlings for this assay were sown under sterile conditions and grown as described for the BiFC assay (p. 107). The growth medium was composed as published by Spalding *et al.* (1999) with the following modifications: 0.3 % instead of 0.5 % sucrose was used and the medium was filter-sterilized to avoid the precipitations that Spalding *et al.* (1999) had reported to occur during normal autoclaving. These authors had avoided precipitation by shortening the autoclaving time to 10 min (Spalding *et al.*, 1999). After 7 d or 10 d of growth, the seedlings were placed gently (with feather-light forceps) on a black plastic surface in a small drop of water to avoid dehydration before imaging with a Nikon D1x camera. Images were used for root growth analysis with the EZ Rhizo software (Armengaud *et al.*, 2009) according to the instructions given on the web site (www.psrg.org.uk). Only the main root lengths were compared between mutants and wt seedlings as indicated.

AKT1-GFP localisation in root hairs

Seedlings of the syp121 mutant and *Arabidopsis* Col0 wt were sown under sterile conditions and grown as described for the BiFC assay (p. 107). Transient root transformation with *Agrobacterium rhizogenes* carrying AKT1-GFP (see p. 104) was performed as detailed earlier (p. 85).

Verification of anti-KC1 and anti-AKT1

LPC solubilised membrane material from *Sf9 i*nsect cells (Fig. 53 A, p. 213) was obtained as described previously (p. 99). Western Blot was performed with the standard procedure and membranes were probed with anti-KC1 antibody and pre-immune serum in a dilution of 1:700. For Fig. A 3 (p. 243), anti-AKT1 antibody and pre-immune serum were used in a dilution of 1:50. In both cases, the secondary anti-Rabbit-HRP dilution was 1:8000 and detection was performed with ECL Advance.

For Fig. 53B-D (p. 213), *Arabidopsis* Col0 wt root and shoot tissue was used. Plants had been grown in a Magenta-box (Fisher Scientific, Southampton, UK) that was fitted with a support for the seeds hand-made from 100 µm stainless steel net (John Staniar & Co., www.johnstaniar.co.uk). Such assemblies were autoclaved already containing the liquid growth medium (0.5x MS pH 5.7, 1 % sucrose). Seed were sterilised and distributed onto the steel need as was described previously for sawing seeds into 6-well plates (p. 107). All procedures took place under sterile conditions. The boxed were sealed with parafilm and incubated in long day conditions (16 h photoperiod, light intensity 180 µmoles m^{-2} s^{-1}, 21 °C). After 3 weeks of growth, root and shoot tissues were separated, blotted dry very gently, weighted into portions (5 g) and frozen in liquid nitrogen as fast as possible. Microsomal membrane fractions were obtained from these tissues with the following protocol:

buffer	composition
Homogenisation ($g\ l^{-1}$)	6.05 TRIZMA base, 167 sucrose, 125.7 glycerol, 20 mM EDTA-Na_2, 20 mM EGTA, 50 mM NaF, 6 PVP: average molecular weight from 30,000 to 40,000 (ICN, reference 102786), 1.76 ascorbic acid, 75 mM ß-mercaptoethanol, pH 8
Microsomal	330 mM sucrose, 5 mM KH_2PO_4/ K_2HPO_4 pH 7.8, 2 mM DTT, 10 mM NaF, Pi, 1 mM PMSF
Solubilisation	40 mM HEPES pH7.4, 600 mM NaCl, Pi, 1 mM PMSF, 2mM DTT

All procedures were performed on ice and in a cold room (4 °C). The frozen tissue (5 g fresh weight for root and shoot respectively) was immediately homogenised in a pre-cooled blender (Waring commercial, Eberbach Corporation) with 50 ml ice-cold Homogenisation buffer Homogenisation was performed for 5 times 5 sec at low speed and 5 times 5 sec at maximum speed with short breaks to avoid overheating. Directly after homogenisation, 2 mM DTT, Pi, 1 mM PMSF and 1 mM Na-orthovanadate were added. The homogenate was filtrated through 2 crosswise layers of MiraCloth (Calbiochem) placed in a funnel to remove coarse plant bits. Centrifugation at 10,000x g for 25 min at 4 °C pelleted the remaining plant bits. For this and all following centrifugation steps 75 ml polycarbonate centrifugation tubes (Sorvall, # 76002810) and an ultracentrifuge (Sorvall, A-641, Discovery) with a pre-cooled T865 rotor (Sorvall) were used. The SN after centrifugation was carefully decanted through a nylon membrane (50 µm), placed in funnel, into fresh centrifugation tubes to avoid disturbing the pellet. Microsomal (total) membranes were obtained from this supernatant by centrifugation at 100,000x g for 30 min at 4 °C. The SN was discarded and the pellet carefully dried with kimwipes bound around a long forceps. The microsomal membrane pellet was then resuspendend by homogenisation in a potter with 1 ml solubilisation buffer supplemented with a final concentration of either 2 % LPC or 4 % TritonX-114 (Sigma, # X-114). Solubilisation was performed o.n. at 4 °C with head-over-end rotation.

TritonX-114 samples were placed into a 30 °C water bath for 3min and then centrifuged for 3 min at 2300x g and RT in a microcentrifuge. The aqueous upper phase was removed with a pipette and the oily pellet of the detergent-enriched phase mixed with 100 µl of ice-cold solubilisation buffer without TritonX-114. Proteins were precipitated from this buffer by the addition of 10 volumes of ice-cold acetone and incubation at -20 °C o.n. After centrifugation in a microcentrifuge at max. speed for 15 min at 4 °C, the pellet was resuspended in 15 µl of 5 % SDS, 7.5 µl of 2x SDS Sample loading buffer (p. 87) were added and the mix incubated at 37 °C for 15 min before the whole sample was used for SDS-PAGE and Western Blot. LPC-solubilised samples were directly precipitated with acetone and used in total for Western Blot as described for the Triton samples. The Western Blot was performed essentially as described earlier with the exception of blotting was done here at 30 V o.n. at 4 °C. Anti-KC1 was used in a dilution of 1:100, secondary anti-Rabbit-HRP in a dilution of 1:5000 and the detection kit was Super Signal West Dura (Thermo Fisher Scientific, # 37071).

buffer	composition
Buffer A	5 mM TRIZMA base, 5 mM EDTA-Na_2, 5 mM EGTA, 4 mM Urea, 20 mM DTT, Pi, 1 mM PMSF, pH 9.5 with NaOH
Buffer B	5 mM TRIZMA base, 2 mM EDTA-Na_2, 2 mM EGTA, 20 mM DTT, Pi, 1 mM PMSF
Buffer C	2 % LPC, 7 M Urea, 2 M Thiourea, 0.5 % TritonX-100, 20 mM DTT, Pi, 1 mM PMSF

The microsomal fractions analyzed in Fig. C-D were derived from 5 g root tissue (fresh weight) per sample of 3 weeks old plants that had been grown in Magenta-boxes as described above. Microsomal membrane vesicles had been obtained as described above, with the exception that the final pellet was resuspended in 15 ml Buffer A. The samples were incubated 5 min on ice before being centrifuged at 170,000x g for 30 min. The SN was discarded, the pellet resuspended in 20 mM NaOH and re-centrifuged as before. The resulting pellet was resuspendend in 15 ml of Buffer B and centrifugated as above. The final pellet was resuspended in 1 ml Buffer C and solubilised o.n. at 4 °C. Proteins were precipitated from this solution with 1 volume of ice-cold 50 % TCA exactly as described for yeast protein extraction (p. 96). The final pellet was resuspended in 15 µl of 5 % SDS and 7.5 µl of 2x SDS Sample loading buffer were added. After incubation at 37 °C for 15 min, 5 µl of each sample was removed for protein quantification with an Amidoblack assay (p. 86) and the rest was stored at -20 °C. 50 µg microsomal proteins were loaded for each lane of the SDS gel. Blotting to PVDF membrane was performed at 30 V o.n. at 4 °C.

Anti-KC1 and anti-AKT1 were used in a 1:50 dilution. Un-conjugated secondary anti-rabbit (Sigma, # R2004) was marked with radioactive iodine ($Na^{125}I$, Perkin Elmer, # A-85380) in a chemical reaction that linked the isotope to exposed residues of the protein. This procedure was performed with Pierce Pre-Coated Iodination Tubes (Thermo Fisher Scientific, # 28601) and Pierce D-Salt Polyacrylamide columns (Thermo Fisher Scientific, # 43243) according to the manufacturer's instructions. The resulting ^{125}I-labeled secondary antibody was used in a 1:4000 dilution. All steps involving ^{125}I, including Western Blot washes and exposure to phosphorimager plates for 14 d were performed under lead protection in an isotope lab. The plates were developed with a Fujifilm FLA5000 phosphorimager.

Aqueous Two-phase partitioning

For this experiment, root tissue of 7 week old hydroponically grown *Arabidopsis* plants (see pictures below) was used. These plants were raised in a growth chamber (Sanyo FitoTron) under short day

conditions to obtain more root material (9 hours light, 15 hours darkness; light intensity ~150 µmol m^{-2} s^{-1}; 22 °C/18 °C day/night, 60 %/70 % day/night relative humidity). The protocol for hydroponics was kindly provided by Dr. Schaaf (ZMBP, University of Teubingen, Germany).

The hydroponic culture system was based on modified 1.5 ml Eppendorf tubes: the lids were removed and tube was cut off 0.8 - 1.3 mm below the opening. The open bottoms were sealed by heating it shortly in an open flame and quickly pressing it on a nylon mesh (400 µm). The sealed tubes were filled with quartz sand (0.6- 1.2 mm grain size, washed 3 times in distilled water and dry-sterilized at 180 °C for 6 h). About 30 to 40 of these sand-cups were placed in holes of appropriate size made in a circular piece of dark insulation mat. The insulation mat covered completely the surface of 2.5 l plant pots where it was floating (to disencourage algae growth). Seeds were surface sterilized and vernalized as described above (p. 107). Depending on the germination rate, 4- 6 seeds were sown per sand-cup with the method described for 6-well plates (p. 107). For the first week after sowing, the growth medium was 20 mg l^{-1} $CaSO_4$. This was sufficient for germination and repressed the growth of algae. Additionally the pots were covered with a perforated transparent plastic pane to increase the relative humidity. After one week, the $CaSO_4$ solution was replaced by 0.5x MS pH 5.8 and the plastic pane was partially removed to adapt the seedlings to a lower relative humidity. If more than 3 or 4 seeds had germinated in one cup, the excess plants were removed at this stage. In the middle of the second week, the plastic pane was removed completely. At the beginning of the third the growth medium was refreshed and aeration was started. The air pressure to aerate the solutions was built up by an aquarium pump and distributed over a system of silicon tubes connected by injection needles and ending up in 1 ml plastic pipettes (Greiner) submerged in each pot. The pressure was of moderate strength to avoid water splattering on the surface of the insulation mat (increased danger of algae growth). Growth medium was replaced every four days. At the end of the fourth week, the roots had usually reached a length of ~5 cm. At this stage the sand cups with the plants were transferred into the holes of a solid black plastic square that was sufficiently large to cover the pot (space for about 8 plants). The transfer was very fast to avoid the thin roots from drying out. The growth solution in the pots was kept just below the bottom of the sand cups. The advantage of this 'non-floating' system was that the roots were submerged in the nutrient solution while the sand was allowed to dry out. Thereby, any algae growth was prevented and the germination of fungal spores on lower rosette leaves touching the solution was avoided. The aeration system remained the same as described for the 'floating system'.

The method for aqueous Two-Phase (2P) partitioning was based on previous publications with some modifications (Larsson *et al.*, 1987). Five days before the actual experiment, the 2P-Phase systems were set up as follows:

	starter tube	phase extraction	final concentration
2P-system	2 g (2 ml tube)	40 g (50 ml tube)	
40 % w/w PEG 3550 stock	0.64 g	12.8 g	6.4 %
20 % w/w Dextran-T 500 stock	0.32 g	6.4 g	6.4 %
2 M sucrose	247.5 µl	6.6 ml	330 mM
200 mM KH_2PO_4/ K_2HPO_4 pH 7.8	37.5 µl	1 ml	5 mM
2 M KCl	3 µl	60 µl	3 mM
H_2O to	1.5 g	40 g	

The PEG (Sigma, # P3640) stock, the Dextran-T-500 (Pharmacosmos A/S, Holbaek, Denmark, # 40030) stock and the 2 M sucrose were set up and placed on a magnetic stirrer in the cold room o.n. to obtain complete dissolution. The K-phosphate buffer, KCl and water were placed in the cold room as well. All solutions were prepared with sterile distilled water. The following morning, the 2P-systems were assembled as indicated in the table above. All solutions were kept on ice and PEG, Dextran and sucrose were briefly stirred before removing an aliquot. The 2 ml Eppendorf for the 'starter tube' and the 50 ml Falcon tube for the '40g-system' were placed on the balance in ice for weighing in the components in the order as indicated in the table above. Tubes were vortexed briefly until an even suspension was obtained and stored upright in the cold room for 3- 4 d to allow the phases to separate. The two phases of the '40g-system' were separated into upper (PEG) and lower (Dextran) phase while taking care to discard the thin interphase between them.

All subsequent procedures were performed on ice and in a cold room (4 °C). Root tissue (~10 g) was harvested, gently blotted dry, weighted, placed on ice and as fast as possible homogenised for microsomal membrane extraction exactly as described above (p. 109). The final microsomal pellet was resuspended in a potter (at least 20 strokes) with 250 µl Microsomal buffer / g fresh weight of tissues used. 500 µl of this suspension were deposited into one starter tube ('2g-system'). The phases were mixed by vigorously shaking the tube for about 2 min. Subsequent centrifugation in a microcentrifuge for 5 min at 2000x g and 4 °C separated the phases again.

The upper phase from the centrifuged tube was transferred into a fresh 2 ml Eppendorf tube and 900 µl of fresh lower phase (from the separated phases of the '40-g system') were added, followed by vigorous shaking as described. To the remaining lower phase in the original starter tube, 900 µl of fresh upper phase (from the separated phases of the '40-g system') were added, shaken and centrifuged as before. After each separation a new round of extraction was done as described to further purify the upper and lower phases from cross-contaminations. A total of three extractions for each phase were performed. Finally, the upper phase that was used to purify the original lower phase was combined with the original upper phase and vice versa. The combined upper and lower phases were diluted 15 times with microsomal buffer and centrifuged for 1 h at 170,000x g and 4 ºC in the ultracentrifuge (centrifuge, rotor and tubes as for microsomal membrane extraction described above). The resulting PM and EM pellets were resuspended and further treated with Buffers A-C as described above (p. 111). After resuspension of the final pellet in 20 µl 5 % SDS, 2 µl were removed for protein quantification of protein concentration with a Micro-BCA assay (Thermo Fisher Scientific, # 23235). The remaining sample was mixed with 10 µl of 2x SDS Sample loading buffer incubated at 37 °C for 15 min and frozen at -20 ºC. 1.3 µg PM/EM proteins

per lane were separated by SDS-PAGE and transferred to PVDF membrane by 30 V o.n. at 4 °C.

Anti-KC1 and anti-AKT1 were used in a 1:50 dilution of the pH 2 elution after affinity purification (Agrisera). The anti-Sec61 marker-antibody for EM (Yuasa *et al.*, 2005) and the marker- antibody for PM (anti-AHA3, R. Serrano) were diluted 1:100. Secondary ^{125}I-labeled anti-Rabbit antibody was used 1:4000 and detected with Fujifilm FLA5000 phosphorimager after 2 weeks of exposure to the phosphorimager plate (Fujifilm FLA5000).

Methods for oocyte expression

The *AKT1*, *CIPK23* and *CBL1* constructs that provided the template for *in vitro* transcription were kindly supplied by the authors of a previous publication (Xu *et al.*, 2006). A former post-doc of Prof. Blatt's group, Dr. Johansson had cloned *KC1*, *SYP111* and *SYP122* in the oocyte expression vector pGEMHE and *SYP121* in the oocyte GT-vector. In preparation for *in vitro* transcription, all constructs were prepared from Quiagen Miniprep columns to achieve clean, RNAseA treated DNA. Subsequently, constructs (5 -10 µg DNA) were linearized at a unique restriction enzyme site behind the CDS and its following 3'UTR of *Xenopus laevis* β-globin. The β-globin sequences have been shown to greatly enhance translation efficiency of heterologous mRNA transcripts in oocytes (Krieg & Melton, 1984). For *AKT1*, *CIPK23*, *CBL1*, *SYP111* and *SYP122* the restriction enzyme PstI was used and for *SYP121* and *KC1* the enzymes HindIII and NheI respectively.

buffer	**composition in mM**
DEPC-H_2O	1ml DEPC (Sigma, # 32490) per 1 l distilled water, stirred for several hours, autoclaved twice
10x MOPS	200 MOPS, 50 sodium acetate, 10 EDTA pH7 with NaOH (stored at 4 °C in the dark)
denaturation mix	for 10 samples: 10 ul DEPC-H_2O, 10 ul 10xMOPS, 35 ul Formaldehyd, 100 ul Formamide, 20 ul RNAse free loading buffer*, 1 ul EtBr
ND96 w/o Ca^{2+}	96 NaCl, 2 KCl, 1 $MgCl_2$, 10 HEPES-NaOH pH 7.4, gentamycin (5 µg ml^{-1})
ND96	1 $CaCl_2$, 96 NaCl, 2 KCl, 1 $MgCl_2$, 10 HEPES-NaOH pH 7.4, gentamycin (5 µg ml^{-1})
bath	96 KCl, 1.8 $MgCl_2$, 1.8 $CaCl_2$, and 10 HEPES-NaOH, pH 7.2
extraction	20 Tris-HCl pH 7.4, 5 $MgCl_2$, 5 NaH_2PO_4, 1 EDTA, 80 sucrose, 1 PMSF, Pi

* supplied with the *in vitro* transcription kit (see above)

Digests were controlled for complete linearization by agarose gel and subsequently treated with 1 µl of Proteinase K (1 mg ml^{-1} stock) per 200 µl digest supplemented with 5 µl 5 % SDS to remove contaminating proteins, e.g. restriction enzyme or RNAses. After incubation in a 50 °C water bath for 1 h, the reactions were purified directly via gel extraction columns and eluted with 20 µl DEPC-H_2O. The DNA was quantified and diluted to a concentration of 1 µg $µl^{-1}$ with DEPC-H_2O. All following steps were performed with filter tips and RNAse free material as far as possible.

For expression in oocytes, here cRNA was injected into the cytoplasm. Thus, even though the CDS in pGEMHE provided a spliced template that made nuclear mRNA processing before translation in the cytoplasm unnecessary, polyadenylation and 7-methyl guanosine cap structure

had to be supplied as well to allow efficient translation of the exogenous cRNA. The polyadenylation sequence is located at the 3′ end of the MCS in oocyte vectors, so that it will be transcribed with the CDS together. The in vitro transcription kit, the mMESSAGEmMACHINE T7 KIT (Ambion, Applied Biosystems, # AM1344) contained an analogue to the 7-methyl guanosine cap structure that was incorporated as the first G of a newly synthesized cRNA molecule.

The reactions were set up according to the manufacturer's manual. T7 stands for the T7 RNA polymerase promoter site present in all the chosen vectors. In modification of the standard protocol recommended by Ambion, the transcription reaction was incubated at 37 °C o.n. to increase yields (~ 30 µg per 1 µl DNA). The cRNA purification steps were performed exactly as instructed by the manufacturer and the final pellet dissolved in DEPC-H_2O. The cRNA was quantified as described for DNA and the concentrations were adjusted to 1 µg μl^{-1}.

All cRNAs were quality controlled for the absence of degradation by means of a denaturating agarose gel as follows: Gel-running equipment was cleaned of RNAses by incubation in 1M NaOH/ 0.1 % SDS for 2- 3 h and rinsed thoroughly with DEPC-H_2O. Agarose (1.5 g) was melted with DEPC-H_2O in a microwave, cooled down in a pre-heated 60 °C water bath and mixed under the fume hood with pre-warmed 10x MOPS (11.2 ml) and Formaldehyde (20 ml) before pouring the gel. The gel running buffer was 1x MOPS in DEPC-H_2O. A denaturating mastermix (see table above) was prepared and 11.7 µl were mixed with 1 µg cRNA in a final volume of 3 µl, mixed and incubated in a preheated water bath at 65 °C for 15 min before snap- cooling on ice. Samples were loaded in total together with 2 µl of a RNA ladder (Millennium Size Marker, Ambion, Applied Biosystems, # 7150) and the gel handled as described for DNA agarose gels afterwards.

Xenopus oocytes and stage V and VI oocytes were isolated and the follicular cell layer digested for 1 h and gentle shaking with 2 mg ml^{-1} collagenase (Sigma, # C9891) dissolved in ND96 without calcium. The oocyte PM is surrounded by a vitelline membrane, which is a glycoprotein matrix that gives the oocyte some structural rigidity and helps to maintain a spherical shape. The vitelline membrane does not affect electrophysiological recordings since it is devoid of channels and transporters and has a large-enough mesh to allow permeation of ions and small molecules. Around the vitelline membrane is a layer of follicular cells. By contrast to the vitelline membrane, the follicular cells express ion channels and transporters that are electrically coupled to each other and to the oocyte by gap junctions and can create serious interference during electrophysiological recordings (Browne & Werner, 1984). Therefore, this layer of cells is eliminated prior to injection by a collagenase treatment. Following digest the oocytes were washed in a 50 ml Falcon tube several times with large volumes of ND96 for the calcium ions to inactivate the collagenase.

Suitable oocytes were selected under a binocular (10x objective) and incubated in ND96 at 18 °C o.n. Injection of cRNA was performed with a 3-D micromanipulator (Drummond, ‘Nanoject’). A vertical automatic pipette puller was used to pull the thin glass tubes used for injection into fine tips. Standard volumes of ~30 µl are released by the injector. The different cRNAs were prepared in the ratios as described in the results (p. 224). The final (equal) volumes

contained 1 ng μl^{-1} cRNA. Water injected oocytes served as control for endogenous hyperpolarisation-activated Cl^- currents that may appear in some batches of occytes.

Injected oocytes were incubated in ND96 at 18 °C for 3 d with daily buffer changes before electrophysiological recordings. Whole-cell currents were recorded using an Axoclamp 2B (Axon Instruments) and a clamping protocol as described in the results (p. 221). Data were analyzed with the HENRYIII software (Adrian Hills, University of Glasgow). Measurements were performed under continuous perfusion with bath buffer. Oocytes that yielded currents were harvested separately immediately after the measurements, stored briefly on ice and frozen separately at -20 °C. Following data analysis, the respective oocytes were pooled for membrane protein extraction. For each oocyte, 20 µl of extraction buffer (see table above) were added before thawing. Homogenisation of oocytes in this buffer was achieved by pipetting with a 100 µl tip and vortexing, Centrifugation for two times 10 min at 3000x g at 4 °C removed yolk proteins. Membranes were harvested from the SN by centrifugation at 16,000x g for 30 min and 4 °C. The membrane pellet was resuspended in a 1:1 mix of 5 % SDS: 2x Sample Loading Buffer, with 3 µl per originally used oocyte of the respective pool and used for standard Western Blot analysis. Antibodies against the three SYP1 SNAREs were used at dilutions of 1:5000 with a secondary anti-rabbit HRP in a dilution of 1:20,000. The detection kit was ECL Advance.

Chapter 1: Analysis of KC1 and SYP121 interaction in mbSUS assay

Introduction

An mbSUS library screen performed by Dr. Pratelli at the ZMBP (Tuebingen, Germany) had detected a putative interaction between KC1 and SYP121. This had been the first attempt to show an interaction between a SNARE and ion channel with this technique. All previous work on mammalian SNARE and ion channel interactions had involved the classical yeast-two-hybrid system (see p. 73), i.e. soluble domains of both interaction partners instead of full-length membrane proteins (Leung *et al.*, 2007). The experiments described in this chapter were aimed to confirm the interaction between KC1 and SYP121 with more extensive mbSUS assays that included the analysis of additional reporter genes compared to the high-throughput library screen. The reporter genes under the control of the lexA promoter are *ADE2*, *HIS3 and lacZ*. A high-throughput library screen would typically only detect the ability to grow on medium without Ade and His increasing the risk for a false positive. It generally also does not address the question of over-expression artefacts that can be addressed with mbSUS by reducing the expression level of bait fusion. Furthermore, the specificity of the interaction between KC1 and SYP121 was addressed by including closely related proteins for both partners, i.e. the Shaker channel subunits AKT1 and KAT1 as well as the SYP1 SNAREs SYP122 and SYP111.

As detailed in the General Introduction (p. 55), SYP122 is the plasma membrane SNARE that stands nearest to SYP121 on a phylogenetic tree (Sanderfoot *et al.*, 2000). These two SNAREs share 63.2 % sequence identity and 72.0 % sequence similarity on the aa level, while SYP121 and SYP111 in turn showed 39.9 % sequence identity and 60.9 % sequence similarity. Protein alignments of the Shaker channel subunits KC1 and AKT1 revealed 31.3 % sequence identity and 45.5 % sequence similarity on the aa level while KC1 and KAT1 share 39.8 % sequence identity and 52.9 % sequence similarity. These values are derived from pair wise global alignments using the Needleman-Wunsch algorithm with a Blosum62 scoring matrix, open gap penalty of 10, and gap extension penalty of 0.5. (Emboss- needle method available on www.ebi.ac.uk).

Furthermore, the fact that Shaker channel subunits form homo- and heterotetramers made them an ideal internal positive control for the assay technique itself. Indeed, interaction e.g. between AKT1 and KC1 has been observed previously in mbSUS assays (Obrdlik *et al.*, 2004).

In addition to these controls, another important question had to be considered prior to mbSUS experiments. As mentioned earlier, the detection of protein interaction in the mbSUS assay depends on the action of ubiquitin-specific proteases (UBS) that set the artificial transcription factor free from the Cub moiety to diffuse to diffuse to the nucleus and activate the reporter genes (Johnsson & Varshavsky, 1994c). These enzymes are located only in the cytoplasm. Hence, suitable bait and prey fusions must be of a membrane orientation that places the Cub and Nub

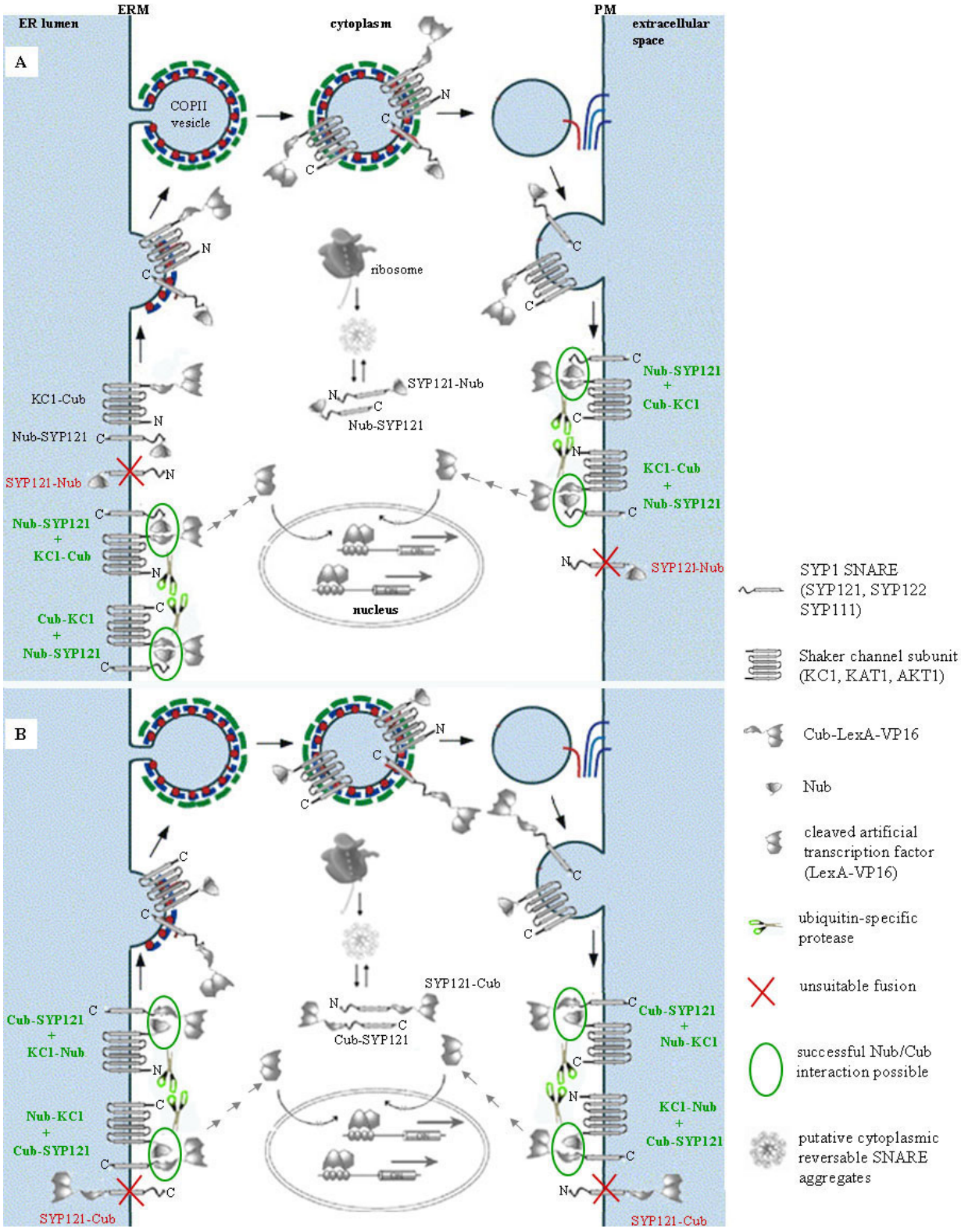

Fig. 21 Overview of expected successful Nub/Cub-tagged SNARE-channel pairs

In (A), KC1, representative for all three Shaker channel subunits used here, is the bait, either as Cub-X or X-Cub fusion. SYP121, representative for all three SYP1 SNAREs used here, is the prey, either as Nub-X or as X-Nub fusion. The reverse situation is pictured in (B), with SYP121 as bait (Cub) and KC1 as prey (Nub). Interaction might take place already in the ER (left hand side of A, B), or after COPII-dependent anterograde trafficking, in the PM (right hand side of A, B). For all fusions of Nub or Cub to the C-terminus of SYP121, the ubiquitin half should be inside the ER lumen/extracellular space, according to TA protein topology predictions. As ubiquitin-specific proteases are only present in the cytoplasm (Johnsson & Varshavsky, 1994c), these fusions were expected not do give rise to positive interactions in mbSUS assays (red cross). Alternatively, over-expressed SNAREs might form reversible aggregates in the cytoplasm. ERM =ER membrane

moiety in the cytoplasm.

As detailed in the General Introduction (see p. 27), the predicted membrane topology for KAT1 was experimentally verified (Sato *et al.*, 2002; Sato *et al.*, 2003; Mura *et al.*, 2004). In analogy, also KC1 and AKT1 would be expected to have both the hydrophilic N- and C-terminus in the cytoplasm. In contrast, the three SYP1 SNAREs, as tail-anchored (TA) proteins, would be expected to have only the N-terminus in the cytoplasm (pp. 59). Their C-terminus should be in the ER lumen after post-translational insertion and in the extracellular space after arrival at the PM.

Fig. 21 summarizes the prey and bait fusion combinations that were expected, on base of topology predictions, to yield a reconstituted ubiquitin via their interaction that faces the cytoplasm (green circles versus red crosses for unsuitable partner). Accordingly, fusion of the Cub or Nub moiety to the C-terminus of SYP1 SNAREs would not be expected to yield functional bait or prey fusions. In contrast, all fusions to the N-terminus of the SYP1 SNAREs or both N- and C-terminus of the three Shaker channel subunits should be suitable.

The aim of the work presented in this chapter was the verification of an interaction between KC1 and SYP121 in the mbSUS assay by adding additional layers of control with further reporter gene read-outs and from the use of closely related membrane proteins. SYP1 SNAREs with the highest structural and functional homology to SYP121 were intended to show specificity of KC1 for SYP121. Similarly, two closely related Shaker channel subunits were chosen to show converse specificity of SYP121 for KC1. Additionally, experiments will be discussed that were intended to address the question which domains of the two proteins might mediate an interaction.

Results

Construct preparation and vector design for mbSUS

The original mbSUS set of vectors for prey proteins allows cloning of a CDS (X) of interest as dual tagged Nub-X-HA fusion, with the Nub moiety at the N-terminus and a triple HA-tag at the C-terminus (pNXgate33-3HA) or the converse X-Nub-HA fusion, with both tags at the C-terminus (pXNgate21-3HA). Bait proteins are expressed as X-Cub fusions, with the Cub moiety at the C-terminus (pMetYCgate) (Obrdlik *et al.*, 2004). Constructs were prepared with these and additional vectors designed for this work by *in vivo* cloning as indicated in Table 1.

CDS (X) of:	***AKT1***	***KC1***	***KAT1***	***SYP121***	***SYP111***	***SYP122***
Nub-X	√	√	√	√	√	√
Nub-X-HA	√	√	√	√	–	–
*X-Nub	√	√	√	√	√	√
X-Nub-HA	√	√	√	√	–	–
X-Cub	√	√	√	√	√	√
*Cub-X	–	√	–	√	√	–

Table 1 Vectors and constructs prepared for mbSUS

CDS (X) = coding sequence (from TAIR; www.arabidopsis.org); HA = hemagglutinin epitope tag;
√ = fully sequenced; √ = partially sequenced; – = not available;
* = vectors newly created (see below)

In order to reproduce the initial screen of a Nub-X-3HA-library, the first one-on-one mbSUS assay was performed with KC1-Cub as bait and Nub-SYP121-3HA as prey. Consistent with the result of the original screen, interaction was detected (data not shown). No interaction with KC1-Cub was detected when SYP121-Nub-3HA, the converse HA-tagged X-Nub fusion, was tested (data not shown). To exclude possible interference of the HA-tag with the interaction, new prey constructs lacking this tag were designed and used subsequently for all experiments shown here (Table 1). To omit the triple HA-tag from the X-Nub fusion proteins the vector pXNgate21-3HA was modified via site directed mutagenesis. A point mutation introduced a stop codon directly after the Nub coding sequence (Appendix, Fig. A 2). Nub-X fusions without HA-tag were obtained by including a stop codon into the CDS during the *in vivo* cloning procedure. Furthermore, to allow for SYP1 family proteins to function as bait fusion, the existing vector pMetYCgate for X-Cub fusions (Obrdlik *et al.*, 2004) was modified. The modification in the new pMetCYgate allows for Cub-X fusions, i.e. attachment of the Cub-tag to the N- terminus of the protein of interest (see Fig. 19 with cloning details in M&M, p. 89ff.).

KC1-Cub interacts with Nub-SYP121 in mbSUS assay

Omitting the HA-tag from Nub-SYP121 did not interfere with the interaction of this prey with KC1-Cub (Fig. 22). The inclusion of control SNARE proteins in the mbSUS assay revealed the specificity of this interaction. The first step of an mbSUS assay is the transformation of bait and prey constructs into two different haploid *Saccharomyces cerevisiae* strains, THY.AP4 and THY.AP5, respectively. Both strains are loss-of-function mutants for their natural ability to synthesize the amino acids (aa) leucine (Leu; l), tryptophane (Trp; t), His and Ade. In addition, the THY.AP4 yeast strain has no ability to produce uracil (Ura; u) (Obrdlik *et al.*, 2004). The Leu synthase gene is restored to the THY.AP4 strain only via successful transformation with a bait vector, e.g. pMetYCgate, either empty or containing a CDS of interest. Likewise, the Trp synthase gene is encoded on the prey construct and serves as selection maker for positive haploid yeast transformants. By contrast, the ability to grow without Ade and His in the medium can only be restored to diploid yeast. These two genes serve together with the *lac*Z gene as reporter genes. They are encoded in the THY.AP4 chromosome under the control of the artificial lexA promoter and activated by an interacting bait-prey protein pair (Obrdlik *et al.*, 2004).

Therefore, the second step in any assay is the mating of two successfully transformed haploid strains. Resulting diploid yeast cells (each dot in Fig. 22) co-expressed bait (here KC1-Cub) and prey (Nub-X as indicated above the top panel). Expression was verified by the ability to grow on Synthetic Complete medium (SC) medium lacking the aa Trp, Leu and Ura (SC_{tlu}, Fig. 22, panel 1). The ability to synthesize Ura was contributed from the genome of the THY.AP5 strain, Leu and Trp synthesis were restored by the presence of bait and prey vector backbone, respectively. No selection pressure was initially exerted towards the expression of the reporter genes Ade- and His- synthesis on this medium. Nevertheless, the coloration of diploid yeasts after prolonged growth (6 d) gave a first indication, whether an interacting protein pair was expressed (white, see positive control: WtNub) or not (red, see negative control: NubG). The Ade present in this medium will be depleted over time and forces the diploids to rely on an activated *ade*2 reporter gene. As mentioned above, in both haploid yeast strains the *ade*2 gene was deleted or removed from its natural promoter. Hence in diploids without an interacting protein pair, the *ade*2 encoded phospho-ribosylaminoimidazole carboxylase, a key enzyme in the adenine biosynthetic pathway, was missing and an oxidized adenine precursor accumulates in the vacuole (Ugolini & Bruschi, 1996) that gave the cells their red appearence in the saturation phase of growth. In contrast, an interacting protein pair would have activated the *ade*2 reporter gene and thus remove the blockade in the adenine biosynthesis pathway. No pigment accumulated and the yeast was white or slightly pink depending on the strength of the interaction. Accordingly, KC1-Cub interacted strongly with Nub-SYP121 and Nub-AKT1 as well as weakly with Nub-KAT1. The interaction of KC1 with itself produced a mixture of mostly pink but also white colonies. Diploids expressing KC1-Cub with either Nub-SYP111 or Nub-SYP122 were stained almost as deeply red as the negative control indicating no or very weak interaction.

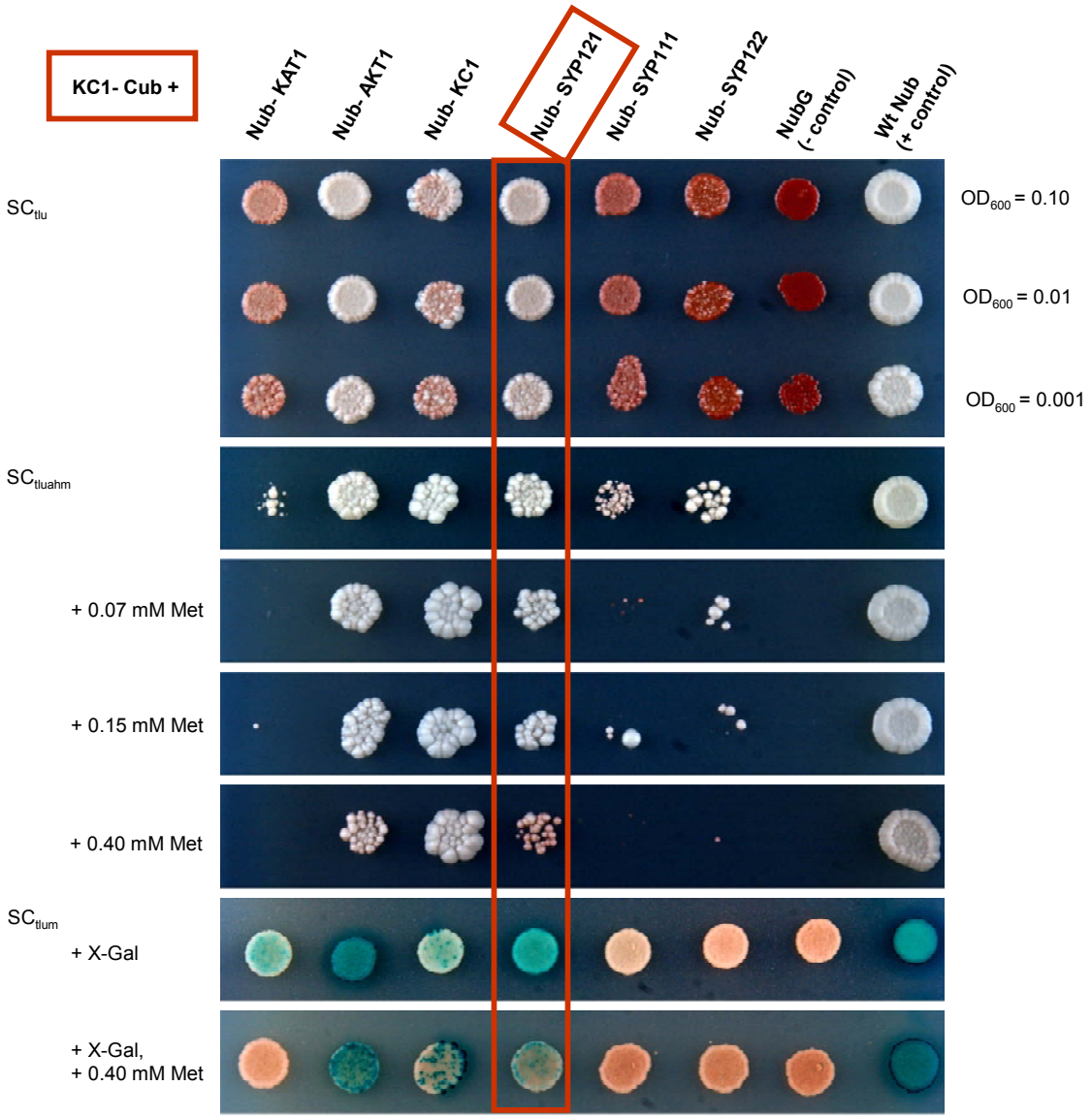

Fig. 22 mbSUS assay for interaction with KC1-Cub

Diploid yeasts resulting from crosses of haploids expressing KC1-Cub with haploids harbouring Nub-X fusions of either KAT1, AKT1, KC1, SYP121, SYP111, SYP122 or controls (negative: NubG; positive: WtNub) were spotted as indicated above the top panel (left to right) onto different media as indicated to the left of each panel. Synthetic Complete (SC) medium without tryptophan (t), leucine (l) and uracil (u) was used to verify the presence of both vectors and observe coloration that indicates an active adenine synthesis reporter (white colonies; top panel). SC_{tluahm}, SC medium that lacks adenine (a; Ade), histidine (h; His) and methionine (m; Met) in addition assessed reporter gene expression via Ade- and His-independent growth (second panel). The re-introduction of 0.07, 0.15 and 0.40 mM Met (next three panels) was used to verify interaction at lower KC1-Cub expression levels as this construct was under the control of a Met-repressed promoter. SC_{tlum} medium (last two panels) alone and with the re-addition of 0.4 mM Met was used with an overlay of X-Gal-containing agarose to assay the activity of the reporter gene β-gal. Serial dilutions (OD_{600} nm 0.1, 0.01 and 0.001) of diploid cultures were brought out as indicated for spots on SC_{tlu}, otherwise only 0.1 dilutions are shown. Yeast growth at higher Met concentrations and the X-Gal overlay showed KC1- Cub interaction with Nub-SYP121 but not Nub-SYP111 or Nub-SYP122. Furthermore, as published before (Obrdlik *et al.*, 2004), KC1-Cub interacted with Nub-AKT1 and weakly with Nub-KAT1. Incubation time was 6 d (3 d for SC_{tlum} +/- Met) at 28 °C.

Monitoring interaction-dependent ADE2 activity by visual analysis of the yeast colour is not very accurate because only one reporter gene is considered and only indirect by depleting existing adenine. The overall growth abilities of different diploids, for example, could influence the outcome through differences in the rates of growth. When a protein or protein pair is expressed that harms its host, the yeast would grow slower. When compared to diploids unharmed by their expressed proteins at a fixed time point, the deeper red colour would falsely indicate 'less interaction'. To an extent this can be analyzed by using three different dilutions of individual diploids on SC_{tlu}, here OD_{600} 0.1, 0.01 and 0.001 (Fig. 22, top panel) that must grow in the analyzed time frame at a comparable rate as seen here.

A more sensitive interaction screening was achieved by omitting three additional aa from the medium: Ade, His and Met (SC_{tluahm}) (Fig. 22, panel 2). Only diploids with reporter genes activated by an interacting protein pair were able to grow on this source, which accounts for the absence of yeast from the negative control. The negative control protein constitutes the unfused soluble N-terminal part of ubiquitin (NubG) expressed from the empty prey vector. The Nub moiety carries a point mutation that reduces its natural affinity for the Cub moiety, here as KC1-Cub fusion. Hence without the help of interacting proteins, the reporter genes should not be activated. In contrast, the unmodified Wt-Nub (NubI), similarly expressed from an empty prey vector, associates with Cub independent of additional protein-protein contacts. The reporter genes are strongly activated and yeast growth is expected on SC_{tluahm}.

The yeast growth phenotypes on this medium confirmed the trend indicated by the yeast colour in the top panel of Fig. 22. While interaction of KC1 with KAT1, SYP111 and SYP122 produced only a few colonies, interaction appeared strong with SYP121. Furthermore, strong interaction between KC1 and AKT1 was observed, as published previously for mbSUS assays (Obrdlik *et al.*, 2004).

Methionine (Met; M) was omitted from this medium because bait fusions, here KC1-Cub, are expressed under the control of the yeast *Met25* promoter that is repressed when cells are grown in the presence of Met. Increasing concentrations of Met in the growth medium (0.07 mM, 0.15 mM and 0.4 mM, Fig. 22, panel 3-5) had the purpose of down-regulating the amount KC1-Cub protein. This control was designed to distinguish a true interaction from a possible over-expression artefact (Obrdlik *et al.*, 2004). As mentioned in the General Introduction (see p. 73ff.), the mbSUS technique detects a close spatial proximity of proteins as well as their direct interaction. Therefore, an interaction detected on SC_{tluahm}, could potentially be the result of co-localising high amounts of over-expressed protein partners within the same membrane. As seen here for the slight yeast growth displayed by KC1 with SYP111 or SYP122 on SC_{tluahm}, such background interaction should quickly disappear with the addition of Met (Fig. 22, panel 5) (Obrdlik *et al.*, 2004). In contrast, a true interaction will be sustained, as it was the case for KC1 with SYP121 or AKT1. While considerably down-regulated on high Met concentrations (0.4 mM), as expected, these interactions were still strong enough to support yeast growth (Fig. 22, panel 5). The interaction of KC1 with itself did not appear to loose in strength (Fig. 22, panel 3-5), while no interaction of KC1 with KAT1 was observed even on low Met medium (Fig. 22, panel 3).

The third reporter, the β-gal enzyme activity of the *lacZ* gene was monitored on medium that did not simultaneously assessed for His- and Ade independent growth (SC_{tlum} with and without the addition of 0.4 mM Met; Fig. 22, panel 6 and 7). The plates were overlaid with agarose containing the enzymes substrate X-Gal (5-bromo-4-chloro-3-indolyl-β-D-galactopyranoside). The β-galactosidase (β-gal), the gene product of *lacZ*, is an *E.coli* enzyme, which catalyzes the hydrolysis of β-D-galactosides such as lactose or the artificial chromogenic substrate X-GAL in this case. Apart from galactose, the result is 5-bromo-4-chloro-3-hydroxyindole that oxidizes in the medium into an insoluble blue product responsible for the observed positive staining.

The β-gal activity-derived blue coloration of the diploids confirmed the results obtained from the two other reporter genes: the strongest interaction appeared to take place between KC1 and the positive control, followed by KC1 interaction with AKT1 and SYP121. Both these interactions were weakened by the addition of Met to the medium (see Fig. 22, panel 7). No enzyme activity, i.e. no blue coloration, confirmed the absence of KC1 interaction with the control SNAREs SYP122 and SYP111 (Fig. 22, panel 6, 7).

The faint blue colour resulting from the interaction of KC1 with itself contradicted the observation of a strong growth phenotype on medium selecting for the other two reporter genes. KC1 interaction with KAT1 showed a similar contraction. Here, a definitive blue staining indicated activation of the *lacZ* reporter gene, while there was practically no yeast growth on selective medium. Orbdlik *et al.* (2004), for example, had observed no yeast growth on selective medium for either interaction. *LacZ* reporter gene activity was not assessed in their experiments. Other techniques, such as yeast-two-hybrid and electrophysiological analysis after heterologous expression in *Xenopus leavis* oocytes similarly found no indication that KC1 Shaker subunits could form dimers. In contrast, the formation of functional heterotetramers between KAT1 and KC1 has been observed by different authors (Dreyer *et al.*, 1997; Pilot *et al.*, 2003a).

The reason for the discrepancy between the read-outs of the different reporter genes for KC1-KC1 and KC1-KAT1 interaction remain unknown. One could speculate that the interaction of KC1 with KAT1 had a growth suppressing effect. This effect would be enhanced with rising selection pressure towards expressed proteins on SC_{tluahm}. In contrast, SC_{tlum} medium for β-gal assays exerted no selection pressure towards Ade and His synthesis. Possibly, KC1 and KAT1 were expressed less on SC_{tlum} which in turn might have allowed the yeast to sustain growth, while the β-gal assay was sensitive enough to detect the existing amount of interacting proteins.

The possibility of such a scenario is one of the reasons why an X-GAL overlay on SC_{tlum} instead of SC_{tluahm} was used. It is also the reason why the β-gal assay was performed after only 3 d of growth, before the medium is depleted of Ade and His. Furthermore, SC_{tlum} allows the diploids of the negative control to grow. X-Gal will start to auto-hydrolyze after prolonged incubation time. Thus, the absence or extent of blue staining in the negative control provides a context to judge the interaction strength of positive appearing interactions.

In summary, all three reporter genes confirmed the interaction between KC1 and SYP121 observed in the initial mbSUS library screen. Furthermore, the absence of KC1 interaction with the

highly similar control SNAREs SYP122 and SYP111 under stringent conditions proved the specificity of this interaction in the mbSUS assay.

Experiments in support of the mbSUS assay with KC1-Cub

Western Blot analysis of total protein extracts from the same diploids as used in Fig. 22, verified the actual expression of the three Nub-SNARE prey fusions (Fig. 23). Polyclonal antibodies directed against the respective SNARE proteins (Tyrrell *et al.*, 2007) specifically detected a band of approximately the expected molecular weight (~ 44 kDa) for undegraded fusion protein in each case (Fig. 23; upper panels). The confirmation of protein expression for Nub-fusions designed to be negative controls for the interaction, here SYP122 and SYP111, is important information. The mbSUS reporter genes do not allow distinguishing a situation with no Nub-prey protein expression from a 'no-interaction' read-out on selective medium. Growth on SC_{tlu} medium only indicates that the prey-vector backbone is present.

The Western Blot also indicated that the expression levels of the three different prey SNAREs were comparable. Expression levels are to be considered as in a given time-frame higher amounts of expressed prey protein will likely influence the apparent strength of interaction detected by the reporter genes. When the UBS proteases can release more artificial transcription factor, reporter genes are increasingly activated to support e.g. a stronger growth phenotype. Numerous reasons might potentially influence levels of protein expression e.g. the copy number of the prey plasmid per diploid might differ for different SNAREs. A protein of higher molecular weight or with more transmembrane domains might need more of the cells resources to produce the protein or longer time to mature. For this reason, proteins closely related to SYP121 in primary and tertiary protein structure were selected as controls. In order to compare protein expression levels one should ideally make use of an antibody directed against an antigen that is part of all three proteins, such as the Nub moiety, for example, or the HA-tag that the original vector pNXgate33-3HA adds to each prey fusion.

As mentioned earlier, the triple HA-tag had been omitted from the prey fusions used in this thesis to exclude possible interference with protein interaction. No commercial antibody against Nub is available. Therefore, the individual anti-SNARE antibodies used here (Fig. 23) only allowed an approximation of relative protein amounts expressed. In order to create as comparable data as possible, primary and secondary antibodies were used in the same dilution in each Western Blot. Furthermore, the amount of total protein extract analysed for each of the three SNAREs was very comparable as indicated by the strength of the band pattern on the PonceauS stains (Fig. 23, lower panels). Other technical criteria such as incubation time with the detection solution and exposure time to film were kept identical. This approach does not take into account potentially different affinities each individual antibody might have towards its respective antigen sequence, which would affect the strength of the detected signal for a given identical amount of SNARE protein. Disregarding this factor, however, SYP121, SYP111 and SYP122 were seen to be represented in comparable amounts in their respective total protein extract as judged by the strength of each

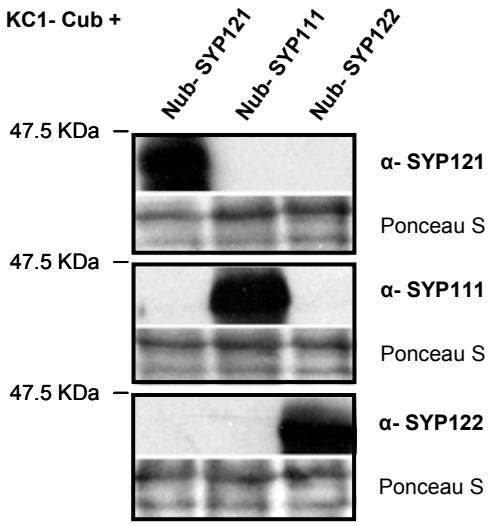

Fig. 23 Verification of prey protein expression

Western Blot analysis of total protein extracted from the yeast diploids co-expressing KC1-Cub with either Nub-SYP121, Nub-SYP111 or Nub-SYP122 as indicated above the top panel. Three independent membranes of the same extracts were probed individually using antibodies specific for SYP121, SYP111 or SYP122 (upper panels). PonceauS stains serve as loading control for the amount of total protein per lane (lower panels). Protein extracts different from the one targeted by the respective antibody were controls for the specificity of the detection. Each Nub-SNARE was expressed and specifically recognized by the corresponding antibody at the expected molecular size of approx. 44 kDa.

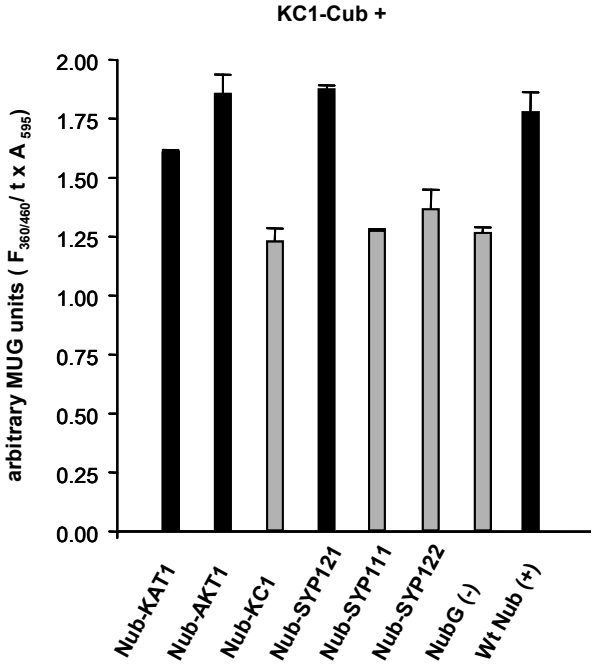

Fig. 24 Quantitative liquid β-galactosidase assay for diploid yeasts

Arbitrary units of β-gal activity (MUG units) were calculated as F360/460/ t × A600 where $F_{360/460}$, t, and A_{600} are sample fluorescence at the end of the reaction, time of reaction in minutes, and absorbance of the cell suspension, respectively. Error bars are standard deviation, n=3. Grey bars indicate samples (Nub-KC1, Nub-SYP111 and Nub-SYP122) with mean arbitrary MUG units not significantly different from the negative control (NubG) at P< 0.05 (see text). Black bars indicate samples with mean arbitrary MUG units significantly different from the negative control (NubG) at P< 0.05 (see text).

detected band (Fig. 23, upper panels). Therefore, it was concluded that the observed specificity of the interaction between KC1 and SYP121 over SYP122 and SYP111 was not a result of unexpressed or significantly weaker expressed control SNARE proteins.

With regard to the relative strength of KC1 interaction with the individual prey SNAREs as detected by the third reporter gene *(lacZ)*, a quantitative liquid β-gal assay was performed to support the semi-quantitative plate assay described above (Fig. 22, panel 6, 7). The semi-quantitative nature of the plate assay is considered to be primarily due to the overlay technique. An overlay with substrate (X-GAL) containing agar renders it unlikely that each individual yeast diploid contributes an equal number of cells from the same growth phase stadium to the colorimetric result. As the growing upper cell layers of a yeast colony are likely to prevent the SDS in the overlay agar from breaking open cells in lower layers, the substrate X-GAL is denied access to the enclosed β-gal enzyme. Possible variations due to differing colony sizes were reduced by spotting the same amount of a standard OD_{600} of each diploid on the assay plates.

Therefore, overlays with X-Gal containing agarose on plates are generally more suitable to assess the presence/absence of enzyme activity. In contrast, liquid assays can be used to compare the relative strength of the protein-protein interactions observed in selected diploids. They are of a quantitative nature as the use of liquid diploid cultures allows for stringent control of the yeast cell number used (OD_{600}) and ensures an equal growth phase, as well as uniform access. Common protocols involve multiple step manipulations such as harvesting cells at the exact same mid-log phase, several wash steps and lyses e.g. by subjecting yeast to freeze/thaw cycles to allow the substrate efficient access to the enzyme. This procedure is time-consuming and each step increases the risk of variations in between samples. The search for improved protocols on this technique yielded a publication in BioTechniques (Vidal-Aroca *et al.*, 2006). These authors reported the development of a one-step liquid β-gal assay, where enzyme activity is determined through the simple addition of the fluorogenic substrate 4-methylumbelliferyl β-d-galactopyranoside (MUG) to intact cells. This technique was adapted here.

A representative one-step liquid β-gal assay is shown in Fig. 24. Again the same diploids as in Fig. 22 and Fig. 23 were used. Diploids co-expressing KC1-Cub with the Nub-X fusions represented by grey bars yielded mean arbitrary MUG unit values not significantly different from the negative control (NubG) at $P< 0.05$ (Nub-KC1: $P= 0.6$, Nub-SYP111: $P= 0.731$ and Nub-SYP122: $P= 0.348$; t-test). Hence, it could be concluded that KC1 did not interact significantly with itself, SYP122 or SYP111. In contrast, diploids co-expressing KC1-Cub with the Nub-X fusions represented by black bars yielded mean arbitrary MUG unit values that were significantly different from the negative control at $P< 0.05$ (NubWT positive control: $P= 0.026$, Nub-SYP121: $P= 0.002$, Nub-AKT1: $P= 0.019$ and Nub-KAT1: $P= 0.005$; t-test), indicating a significant interaction between KC1 and SYP121 as well as the expected interaction with the closely related Shaker channel subunits AKT1 and KAT1. With regard to the positive control (NubWT), the obtained mean arbitrary MUG unit values were not significantly different for diploids with Nub-KAT1 ($P=0.169$), Nub-AKT1 ($P=0.569$) or Nub-SYP121 ($P= 0.357$) at $P< 0.05$ (t-test), indicating almost identical levels for the strength of these interactions in this assay.

Controls ruled out that the detected β-gal was released from dying cells during either growth or exposure to DMSO, in which MUG was dissolved: Fluorescence values of a MUG assay on culture medium (SC_{tlum}) from which cells had been removed after growth, were undistinguishable from a blank reference of assay buffer with MUG/ DMSO but no yeast. Similarly, DMSO containing assay buffer that had been used first to treat cells according to the standard protocol procedure and from which yeast was subsequently removed, yielded no fluorescence values different from the mentioned blank reference (data not shown).

For the negative control in the liquid β-gal assay pictured in Fig. 24 no interaction and therefore no activation of the *lacZ* reporter gene was expected from the absence of yeast growth and negative X-Gal overlay in the mbSUS assay (Fig. 22). However arbitrary MUG units of about 1.25 were detected. These values were almost identical to controls and therefore most likely resulted from auto-hydrolysis of MUG over the time of the assay and the overall much higher sensitivity achieved with fluorogenic substrates. This assay revealed in addition a clear interaction of KC1 with KAT1, supporting the interpretation of the mbSUS assay results as discussed above. Similarly, it is thought here that the liquid β-gal assay represented the true nature of KC1 self-interaction, i.e. its absence. The yeast growth phenotype that had indicated interaction (Fig. 22) was most likely an artefact. Diploids showed a mixture of pink and white colonies on SC_{tlu} (panel 1) and yeast growth on SC_{tluahm} did not decline with increasing amounts of Met (panel 2- 5).

Insensitivity of yeast growth to rising Met concentrations can be the result of a self-activating event. Self-activation can occur when the artificial transcription factor LexA-VP16 (that is part of the Cub moiety) is set free by degradation rather than by specific action of UBS. If the resulting fragment is smaller than 60 kDa, it is able to pass the pores of the nuclear membrane and activate the reporter genes independent of a true interaction. In this special case, it is possible that the co-expression of Nub-KC1 with KC1-Cub triggered degradation, as KC1-Cub on its own did not show self-activation: If the bait fusion in itself is unstable, diploids of the negative control should appear white on SC_{tlu}, display growth on SC_{tluahm} and blue staining with an X-GAL overlay. Thus, the mixture of pink and white colonies on SC_{tlu} could indicate that in the majority of cells no or only background levels of interaction took place between KC1-Cub and Nub-KC1 (pink colonies) but in some cases, maybe in cells with higher protein expression levels, interaction somehow triggered degradation and with it self-activation. These few cells would be selected for on SC_{tluahm} and sustain the observed growth, the insensitivity to Met and the weakly positive β-gal overlay assay. In summary, the results of the quantitative β-gal assay confirmed the specific interaction of KC1 with SYP121 over the closely related SNAREs SYP122 and SYP111.

Specificity of SYP121 for KC1

Further mbSUS experiments were performed to explore the reverse situation, the specificity of SYP121 for KC1 over AKT1 and KAT1. As explained in the introduction to this chapter (see Fig. 21, p. 118), fusion of the Cub moiety to the C-terminus of SYP1 SNAREs, in analogy to KC1-Cub, were not be expected to yield functional bait fusions. As this assumption rested only on predictions

of membrane orientation for TA proteins in general, all three SNAREs were tested anyway as X-Cub bait fusions (in vector pMetYCgate, see Table 1) on the same Nub-X fusions used in Fig. 22. For these mbSUS assays as well as all the following ones pictured in this chapter, unless stated otherwise, the exact same experimental conditions were used as in Fig. 22 to facilitate comparisons (M&M, p. 95ff.). Surprisingly, only SYP111-Cub behaved as expected. Diploids grew on SC_{tlu}, indicating the presence of both bait and prey vector after successful crosses. On selective medium SC_{tluahm} no yeast growth of diploids was observed, not even for the positive wt NubI control (data not shown).

In contrast, SYP121-Cub showed interaction with the positive control on selective medium that was sensitive to increasing Met concentrations and yielded an active *lacZ* reporter gene. No yeast growth or β-gal activity was detected in the negative control, confirming the apparent suitability of this bait fusion (Fig. 25). On the same medium the apparent strength of interaction for SYP121-Cub with the respective Nub-X fusions, as judged by yeast growth, was: SYP121> SYP122> KC1> (SYP111, AKT1, KAT1). Apart from the SYP121 self-interaction and to a lesser extend with SYP122 all of these interactions were abolished by the lowest amount of Met (0.07 mM, panel 3-5). This level of interaction, especially as seen with KAT1 and AKT1, was interpreted previously as background due to over-expression (compare Fig. 22, KC1 interaction with SYP122 and SYP111). However, for these background interactions no *lacZ* reporter gene activity had been detected. In contrast, SYP121-Cub interaction with all three Shaker channel subunits did show blue staining in the X-Gal overlay assay (Fig. 25, red box, panel 1, 6 and 7).

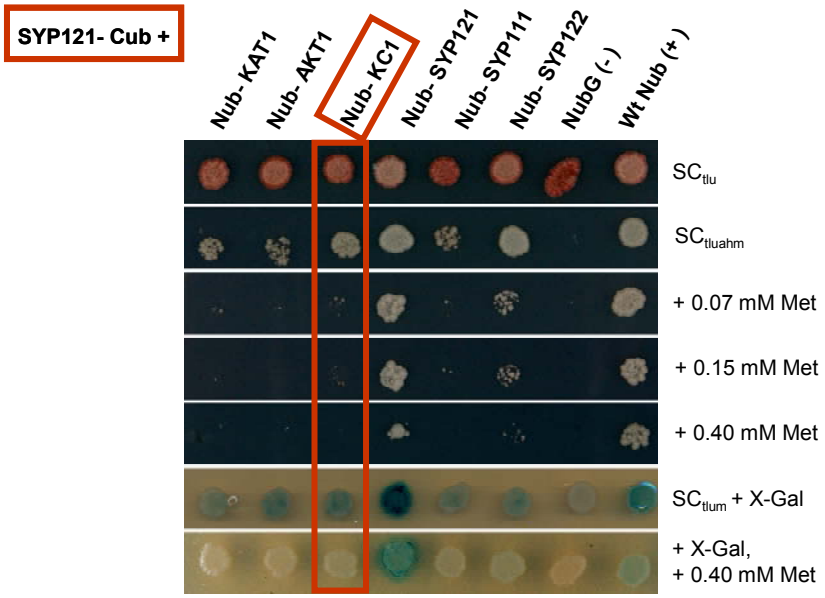

Fig. 25 mbSUS assay for interaction with SYP121-Cub

Spotted yeast diploids co-expressed the bait SYP121-Cub and a respective prey Nub-X fusion as indicated above the top panel. All experimental parameters including the succession of different media used (indicated to the right of each panel) were as indicated for Fig. 22. Yeast growth indicated that SYP121-Cub interacted with Nub-KC1 (compare red box, panel 2) and to a lesser extent with Nub-AKT1 and Nub-KAT1 (panel 2). All of these interactions were completely suppressed by the addition of 0.07 mM Met, compared to the interaction of SYP121 with itself and Syp122 (panel 3-5). The degree of β-gal activity observed in panel 6 and 7 confirmed these results.

With regard to positive and negative control, SYP122-Cub appeared to be a suitable bait-fusion as well. After the standard time of 6 d of incubation, it did not show interaction with any of the Shaker channel subunits, but self-interaction and interaction with the other two SNAREs (see Fig. 26).

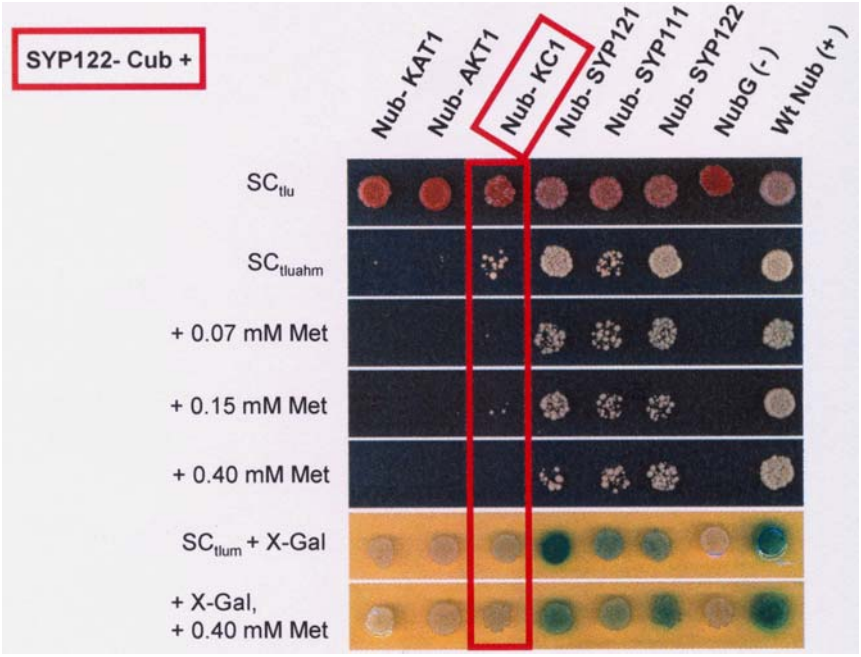

Fig. 26 mbSUS assay for interaction with SYP122-Cub

Pictured are diploids of SYP122-Cub with the indicated Nub-X constructs. No interaction was observed between Cub-SYP122 and Nub-KC1 as indicated by the absence of both blue staining in the X-Gal overlay assay and yeast growth apart from a few single colonies that disappeared with the addition of 0.07 mM Met to the growth medium and were negligible (compare red box). Interaction did occur between Cub-Syp122 and the Nub-X fusions of SYP121, SYP122 itself and to a lesser extent SYP111.

In contrast, the converse Cub-X fusion of SYP121 (Cub-SYP121) that was expected to have the Cub moiety in the cytoplasm, was an unsuitable bait-fusion (see Fig. 27, next page). Yeast growth in the negative control was observed that could be suppressed only by the addition of highest concentration of Met (0.4 mM, first column, panel 1-5). This background activation of the reporter genes in the negative control (compare also β-gal activity, panel 6) added to the read-out for each expressed protein pair and made it impossible to distinguish interaction from background activation. Hence, Cub-SYP121 appeared to interact almost equally strong with all tested preys, including Nub-KC1 and KC1-Nub (red boxes). Cub-SYP111 demonstrated the same interaction with the negative control as Cub-SYP121 (data not shown).

For these reasons, the question of SYP121 specificity for KC1 over AKT1 and KAT1 was approached differently by using KAT1 and AKT1 as bait (X-Cub) instead. Diploid yeast growth on SC_{tluahm} as well as an active *lacZ* reporter gene confirmed an interaction between KAT1-Cub and Nub-SYP121 (Fig. 28, red box, panel 2-7). When comparing the amount of sustained yeast growth on medium with increasing concentrations of Met, the interaction between KAT1 and SYP121 appeared almost as strong as between KC1-Cub and Nub-SYP121 in Fig. 22. Similarly, a measure of interaction appeared between KAT1 and the control SNAREs SYP122 and SYP111, but was not

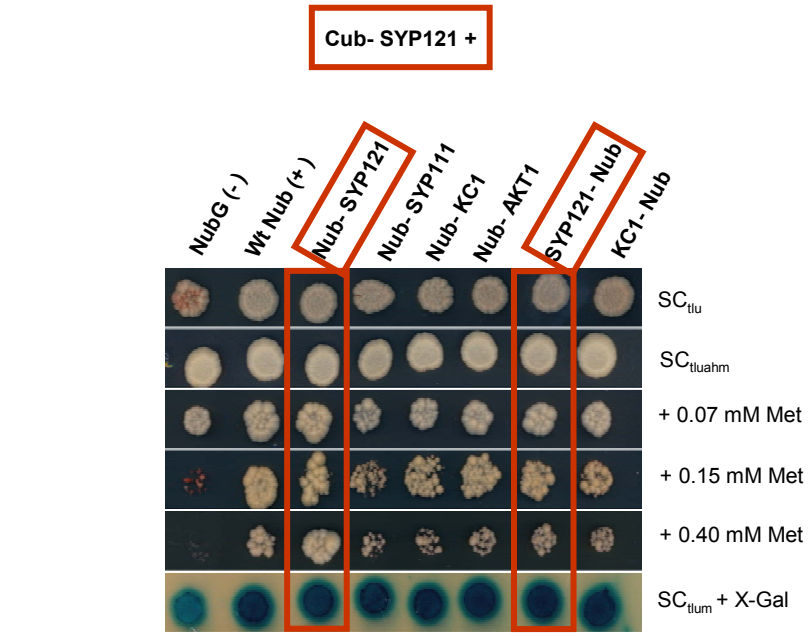

Fig. 27 mbSUS assays for interaction with Cub-SYP121

This figure shows diploids of Cub-SYP121 with Nub-X and X-Nub fusions as indicated above the top panel. Here, reporter gene activity was observed in the negative control (diploids of Cub-SYP121 with NubG). The corresponding yeast growth was only suppressed with the highest concentration of Met (0.4 mM). Therefore, the yeast growth (and *lacZ* gene activity) resulting from this background made the analysis of other diploids impossible, as all interactions appeared equally strong.

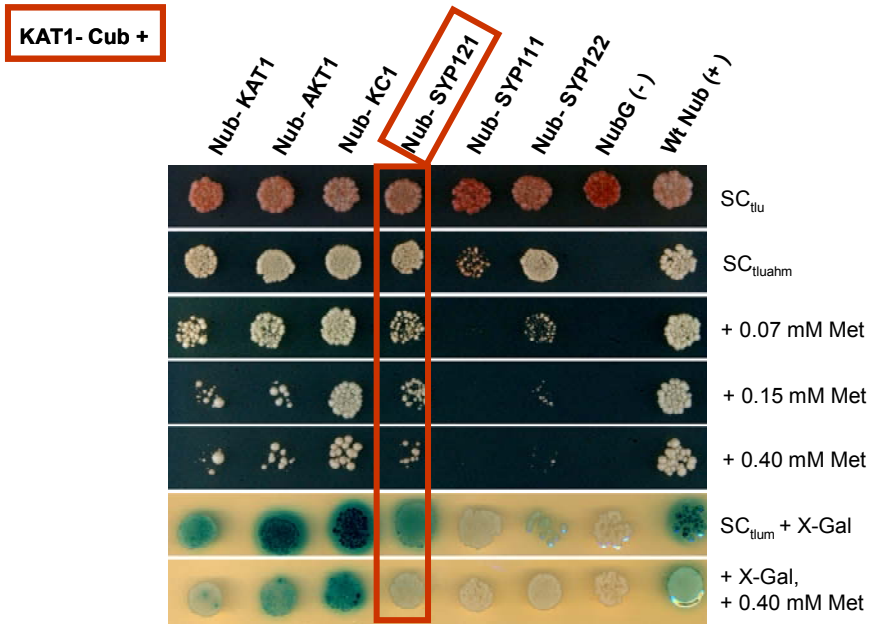

Fig. 28 mbSUS assay for interaction with KAT1-Cub

Diploids represent crosses of KAT1-Cub with the respective Nub-X constructs as indicated above the top panel. All experimental conditions were again as described previously (see Fig. 22). Yeast growth on SC_{tluahm} and with increasing concentrations of Met (panel 2-5) as well as blue staining after X-GAL overlay assay (panel 6-7) revealed an interaction between KAT1-Cub and Nub-SYP121 (red box), that appeared stronger than the interaction between KAT1 and SYP122 but clearly weaker than the interaction of KAT1 with KC1.

sustained with the lowest amounts of expressed bait fusion (0.4 mM Met, Fig. 28, panel 5). Furthermore, the results of this assay indicated, as supported by previously published data (Obrdlik *et al.*, 2004), the interaction of KAT1 with itself and the two other Shaker channel subunits AKT1 and KC1.

Similar results for the interaction between Shaker channel subunits were obtained with AKT1-Cub as bait, especially after a prolonged incubation time of 14 d instead of the standard 6 d (Fig. 29A and Fig. 29B). The extended growth phase revealed an interaction between AKT1-Cub and Nub-SYP121 that was negligible after 6 d (compare red boxes). After 14 d, some yeast growth was sustained in 0.4 mM Met and strong blue staining as a result of an active *lacZ* reporter gene supported this observation (Fig. 29B, red box, panel 4-6). Even after this extended incubation period, diploids co-expressing AKT1 with the control SNAREs SYP122 and SYP111 did not display interaction (Fig. 29B). The appearance of a few scattered colonies is interpreted here, as discussed above, as adaptive mutations that are even more likely to occur during long incubation times.

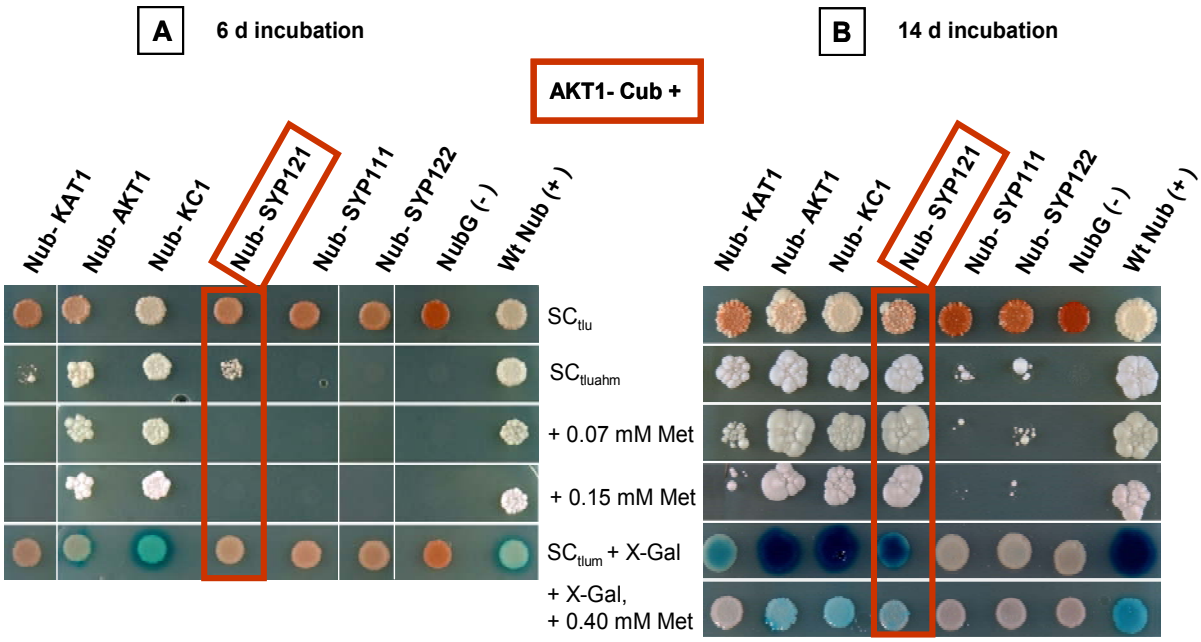

Fig. 29 mbSUS assay for interaction with AKT1-Cub

Both (A) and (B) show diploids of AKT1-Cub with the respective Nub-X construct as indicated above the top panels in two independent experiments with the standard conditions apart from the incubation time, which was 6 d for (A) and 14 d for (B). The prolonged incubation time was able to show an interaction between AKT1-Cub and Nub-SYP121 that appeared almost negligible after 6 d of growth (compare yeast growth in panel 2-4 of the two red boxes). The X-GAL overlay assay confirmed this observation as only after 14 d blue staining of diploids indicating an active *lacZ* reporter gene occurred (compare panel 5, of both red boxes). Even after prolonged incubation time no interaction was detected between AKT1 and the control SNAREs SYP122 and SYP111. As with KAT1-Cub (Fig. 28), interaction occurred between all three Nub-X prey Shaker channel subunits and the bait, here AKT1-Cub (B). (All yeast pictured in (B) was grown on the same plate but in a different order; the white bars indicate were the picture was assembled.)

Additional mbSUS assays for the KC1-SYP121 interaction

Additional mbSUS assays were performed to investigate which protein domains were involved in the observed interaction between KC1 and SYP121. Even though it was suspected on the base of the topology predictions for TA proteins that X-Nub fusions of SNARE proteins might not be suitable prey fusions, the observations for SYP121-Cub prompted a closer investigation. Attaching a tag such as Nub or Cub to parts of proteins that mediate interaction might result in the blocking of this interaction due to steric interference and thus point towards interacting domains. As mentioned above, initial experiments had failed to detect an interaction between KC1-Cub and SYP121-Nub-3HA (data not shown). This had prompted removal of the Ha-tag from all fusions of Nub to the C-termini of the three Shaker channels and SYP1 SNAREs (X-Nub, see Table 1). However, KC1-Cub did not interact with SYP121-Nub either even after 14 d of growth (Fig. 30A). Western Blot analysis confirmed the expression of the X-Nub SNARE proteins for this experiment to exclude that the absence of interaction was a result of unexpressed proteins (Fig. 30B).

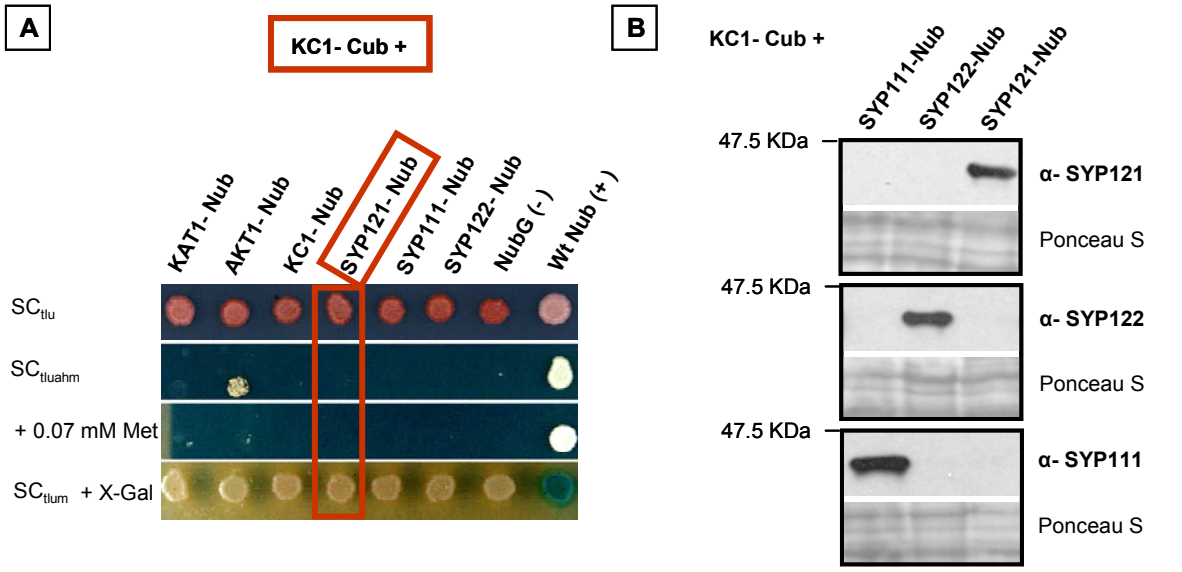

Fig. 30 mBSUS assay for interaction of KC1-Cub with X-nub prey proteins

Diploids of KC1-Cub with the X-Nub fusions as indicated above the top panel, revealed no interaction between this bait and SYP121-Nub. Apart from the positive control only very faint yeast growth was observed for KC1-Cub interaction with AKT1-Nub. Incubation time was 14 d in contrast to the standard condition (6 d). The Western Blot analysis performed on the diploids of this experiment (B) proved with individual polyclonal antibodies (Tyrrell *et al.*, 2007) directed against them that all three SNARE X-Nub fusions were expressed.

Diploids of SYP121-Cub with the same X-Nub fusions showed interaction only with the positive control (see Fig. 31, next page).

As mentioned above, diploids of the Cub-SYP121 fusion with KC1-Nub were unusable due to the background activity in the negative control. In contrast, a bait fusion of KC1 in the same vector (pMetCYgate: Cub-KC1) showed only very little yeast growth in the negative control and no *lacZ* reporter gene activity. The addition of 0.07 mM Met to the medium was able to suppress this background. Thus, it was possible to detect an interaction of Cub-KC1 with Nub-SYP121 and

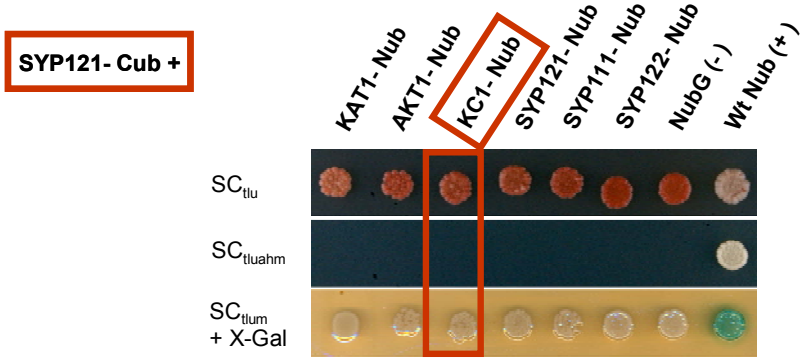

Fig. 31 mbSUS assay for interaction of SYP121-Cub with X-Nub prey proteins

Pictured are diploid yeasts of SYP121-Cub with the indicated X-Nub fusions. While the positive control confirmed the expression of this bait, no interaction with any other prey than wt NubI was detectable, even after 14 d of incubation.

to a lesser extent with SYP121-Nub (compare red boxes, yeast growth and β-gal derived blue staining).

Additional experiments were performed to explore the reason for background activity of reporter genes in the negative control of mbSUS assays that involved Cub-X fusions (Fig. 27, Fig. 32). One cause of background activity of reporter genes can be degradation of the bait fusion that results in self-activation (see above). Such a degradation event may be detected with an antibody directed against the VP16 part of the artificial transcription factor that is fused to the Cub moiety. Western Blot analysis of total protein extract from haploid yeast expressing Cub-SYP121 or Cub-KC1 was employed to investigate if such degradation was responsible for the observed reporter gene background activity in diploids with these bait-fusions. The anti-VP16 antibody detected a band of approx. the height expected for an un-degraded Cub-SYP121 (77 kDa) (Fig. 32B, lane 2, red arrow). In contrast, no signal was detected that would correspond to full-length Cub-KC1 (113 kDa) (Fig. 32B, lane 1). In addition, three prominent additional peptides of a molecular weight around 48 kDa were recognized by anti-VP16.

Replacing anti-VP16 with anti-SYP121 could confirm the presence of a band of a height expected for intact Cub-SYP121 in the same protein extracts (Fig. 32C, lane 2, red arrow). In addition, here too, one more prominent band at about 48 kDa was detected. This second band was much more prominent in a total protein extract from independent haploid yeast that was confirmed to contain the Cub-SYP121 construct by colony PCR (Fig. 32C, lane 3, Cub-SYP121-2). However, in this yeast the anti-SYP121 detected no protein of higher molecular weight that might correspond to an intact Cub-fusion. For this Western Blot, a total protein extract of haploid yeast expressing Cub-SYP111 was used as control against unspecific recognition of yeasts own protein by the anti-SYP121 (Fig. 32C, lane 1 for Cub-SYP111-1). The detection of a band corresponding in height to full-length Cub-SYP111 (and the additional band of approx. 48 kDa) was in turn verified with anti-SYP111 for this particular extract (Fig. 32D, lane 2, Cub-SYP111-1).

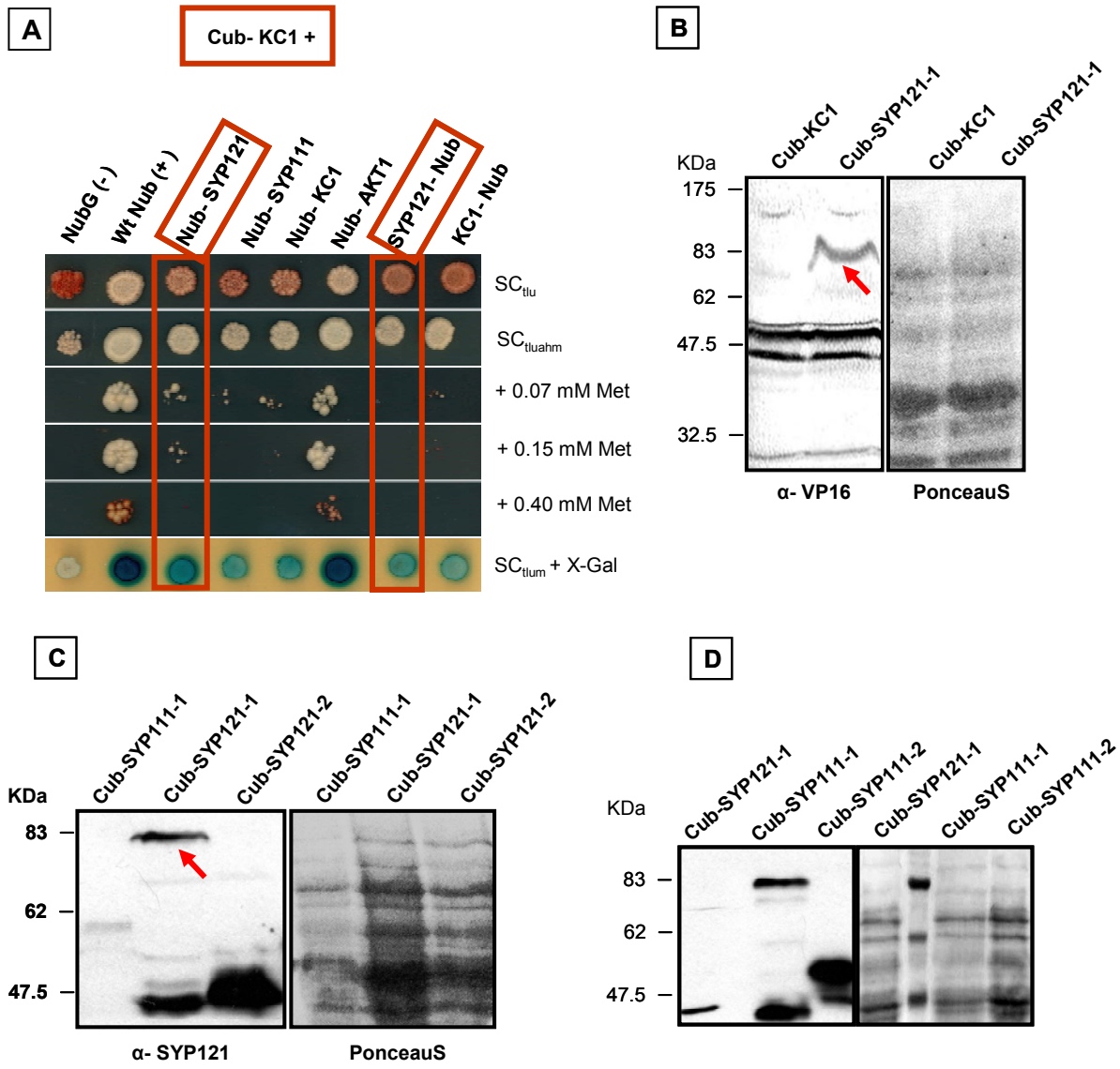

Fig. 32 mbSUS assay for interaction with Cub-KC1 and analysis of Cub-X constructs

(A) Diploids of Cub-KC1 with Nub-X and X-Nub fusions as indicated above the top panel. Similar to the background reporter gene activity with the negative control for Cub-SYP121 (Fig. 27), also KC1 as bait fusion in this vector, displayed interaction with the negative control (NubG). However, in contrast to Cub-SYP121, diploids of Cub-KC1 and NubG displayed no *lac*Z gene activity (no blue stain, panel 6) and the yeast growth was already suppressed by the addition of 0.07 mM Met to the medium (panel 3). Under these conditions, Cub-KC1 appeared to interact slightly stronger with Nub-SYP121 than with SYP121-Nub, mainly indicated by the darker blue staining after the X-Gal overlay assay (compare red boxes, panel 2-6). Western Blot analysis of total protein extracts from haploid yeast carrying the Cub-Syp121 construct revealed a band of approximately the height expected for full-length Cub-SYP121 when both a anti-VP16 directed against the Cub-part and a anti-SYP121 were used (~ 77 kDa; Cub- SYP121-1, red arrows, (B), lane 2 and Fig. 32C, lane 2). No signal that would correspond to full-length Cub-KC1 (113 kDa) was detected with the anti-VP16 on protein extracts from haploids expressing this construct (B, lane 1). Both antibodies yielded additional signals of a molecular weight of around 48 kDa in total protein extracted from yeast harbouring the Cub-KC1 and Cub-Syp121-1 constructs (B, lane 1 and 2; Fig. 32C, lane 2). PonceauS stains (left hand part of B and C) served as loading control for the amount of total protein per lane. Total protein extract of yeast expressing a Cub-SYP111 fusion represented a control for the specificity of detection with the anti-SYP121. Expression of full-length Cub-SYP111 in the same extract was verified in turn with an anti-SYP111 antibody (Tyrrell *et al.*, 2007) (~ 77 kDa; Cub-SYP111-1, lane 2). As for Cub-SYP121 expression, additional bands were detected by anti-SYP111, here of ~45 kDa (lane 2) and ~55 kDa (lane 3). The specific detection of SYP111 was confirmed by the absence of a signal of comparable high molecular weight in the total protein extract of yeast shown to express the Cub-Syp121-1 protein (B, lane 1). The lower molecular weight signal detected in the same lane, as well as the lower band for Cup-SYP111-2 (lane 3) are most likely result of unspecific detection of yeast proteins as they correspond closely to identical bands in the PonceauS stain that served as loading control for the amount of total protein per lane.

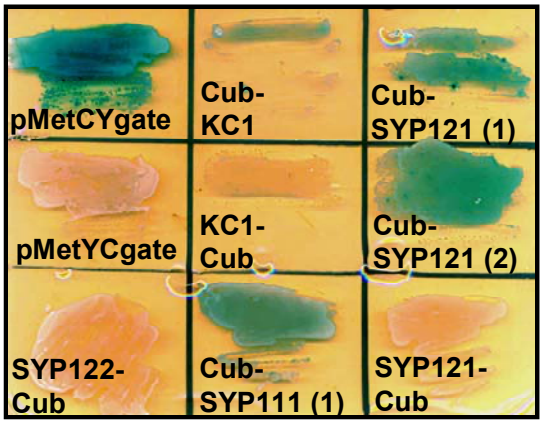

Fig. 33 Self-activation of Cub-X constructs

This X-gal overlay assay demonstrated self-activation of the *lac*Z reporter gene in haploids containing the empty vector pMetCYgate or the constructs Cub-Syp121-1, Cub-Syp121-2, Cub-Syp111-1 and Cub-KC1 (blue staining). No self-activation was observed for haploids transformed with pMetYCgate, Syp121-Cub, SYP122-Cub or KC1-Cub.

Fig. 33 shows an X-Gal overlay assay on haploid yeast transformed with the constructs used in the Western Blot analysis described above, and with several controls. On medium that selected only for the presence of these plasmids (Sc without Leu) haploid yeast transformed with the empty pMetCYgate (for Cub-X fusions), Cub-Syp121-1, Cub-Syp121-2 and Cub-Syp111-1 showed strong blue staining that indicated an activated *lac*Z reporter gene without the presence of an interacting protein fused to Nub. A haploid yeast strain expressing Cub-KC1 exhibited a faint blue colouring. In contrast, haploids harbouring the empty pMetYCgate (for X-Cub fusions), Syp121-Cub, SYP122-Cub or KC1-Cub did not exhibit blue staining due to a self-activated β-gal enzyme.

Discussion

Here, an interaction between KC1 and SYP121 that was first identified in an *Arabidopsis* membrane protein mbSUS library screen was confirmed. Three additional controls above the level of the library screen increased confidence in the specificity of this interaction. Firstly, the addition of Met to down-regulate KC1-Cub expression levels, showed that the interaction with SYP121 was supported even at the highest Met concentration at which an unspecific interaction caused by over-expression is generally not sustained (Obrdlik *et al.*, 2004). Such unspecific background interaction that disappeared with the addition of Met was observed for the interaction of KC1 with the close relatives of SYP121, the SNAREs SYP122 and SYP111. These two SNAREs represented the second control and allowed to verify the specificity of KC1 interaction with SYP121. The third control was derived from the analysis of the third reporter gene (lacZ). Both the X-Gal overlay on plates and the more accurate quantitative ß-gal assay confirmed that only in diploids of KC1 with SYP121, not SYP122 or SYP111 was this reporter gene switched on. The conclusion of specific interaction between KC1 and SYP121 rested on the assumption that all three SNAREs were

expressed and expression yielded comparable levels, which could be confirmed by Western Blot.

Regarding the reverse situation, the specificity of SYP121 for KC1 over the closely related Shaker channel subunits AKT1 and KAT1, no definitive conclusion could be drawn from the results of the mbSUS assays performed here. The analysis of this question was hindered by several problems. One impediment was present in the background reporter gene activity observed for all proteins expressed in the newly constructed vector pMetCYgate. It was assumed on the basis of the general topology prediction for TA proteins ($N_{cytoplasm}$-$C_{ERluminal}$) that only N-terminal tagged (Nub or Cub) SNARE proteins would be suitable for this technique. Only N-terminal fusions should allow the respective ubiquitin half to extend into the cytoplasm, where the ubiquitin-specific-proteases are active that are needed to cleave off the artificial transcription factor (Knecht *et al.*, 2009).

The pMetCYgate vector for fusion of the Cub moiety to the N-terminus of a protein of interest (Cub-X) was designed so that it would be possible to use SYP121 as bait when investigating its specificity for KC1. Surprisingly, diploid yeast expressing Cub-KC1, Cub-SYP121 or Cub-SYP111 failed to pass the negative control experiment that is required for this technique to confirm the suitability of a bait fusion: co-expression with soluble NubG showed unexpected reporter gene activity. The most common cause for such background activity of the reporter genes in the absence of reconstituted ubiquitin, i.e. an interaction partner, is self-activation due to protein degradation. If a degradation product of the bait fusion that contains the artificial transcription factor is smaller than 60 kDa, it is able to diffuse through the pores of the nuclear envelope and activate the reporter genes independent of an interaction partner. Indeed, as expected for self-activation of bait fusions, also haploid yeast expressing Cub-SYP121, Cub-SYP111 and Cub-KC1 showed lacZ reporter gene activity in an X-Gal overlay assay. In contrast, the converse X-Cub fusions, KC1-Cub and SYP121-Cub, that had proved to be suitable bait fusions, did not display blue colouring indicating self-activation.

The X-Gal overlay assay revealed another surprising result: haploid yeast expressing only the empty Cub-X vector (pMetCYgate) showed self-activation as well. An explanation for this phenomenon was discovered after sequencing of the Cub-X vector. It appears that the empty vector expresses the Cub moiety on its own as part of a protein that is derived from an unplanned stop codon in the vector sequences a very short distance downstream of the Cub coding sequence. The predicted size of this Cub-protein is ~ 40 kDa (Edit sequence program of DNASTAR software packet). Thus, it is small enough to diffuse into the nucleus and lead to the observed self-activation in yeast expressing the empty Cub-X vector. This unplanned stop codon will be lost once a CDS of interest is inserted by *in vivo* cloning into this vector, as it is located in the DNA sequence between the two recombination sites (B1, B2) that is replaced with the target gene. It follows that this Cub protein can not be responsible for self-activation in haploid yeast expressing e.g. Cub-SYP121. It was further ensured here, that the constructs containing Cub-KC1, Cub-SYP111-1 and Cub-SYP121-1 were fully sequenced after extracting them from a yeast glycerol stock derived from a single colony that was used for all experiments here. Thus, it was unlikely that either yeast expressed proteins with e.g. premature stop codons or frame shifts. In addition, picking a single

colony made it unlikely that a mix of yeast with empty vector and construct respectively was present. In such a situation, the yeast carrying the empty vector is likely to outgrow the protein-expressing one during the incubation time.

Therefore, the most likely explanation for self-activation of the Cub-KC1, Cub-SYP121 and Cub-SYP111 bait fusions remained protein degradation. The occurrence of protein degradation was investigated by Western Blot analysis. Antibodies directed against both the SNAREs and the Cub part, strongly suggested the expression of full-length Cub-SYP121 and Cub-SYP111 in haploid yeast. No full-length protein could be detected for Cub-KC1 which was not unexpected considering that very low expression levels for Shaker channel subunits were previously observed, not only for the native situation in plants, but also in mbSUS assays by Obrdlik *et al.* (2004). Additional distinctive bands of lower molecular weight, between ~46 to ~55 kDa, were detected in protein extracts of haploid yeast expressing Cub-KC1, Cub-SYP121-1 or Cub-SYP111-1 by the anti-VP16 and/ or the anti-SYP121/ anti-SYP111 antibodies. These bands might represent degradation products of the respective full-length protein that are derived from N-terminal fragments that contain both the VP16 and SYP121 antigen sequences (Tyrrell *et al.*, 2007).

Nevertheless, considering what is known about protein degradation, the occurrence of peptides with such defined and quite large size is surprising. In general, it is assumed that protein degradation during the heterologous over-expression of proteins that belong to the secretory pathway, such as e.g. the Shaker channels and SNAREs, originates in the ER (Wagner *et al.*, 2006). In the ER, protein folding and assembly underlies tight quality control mechanisms. Saturating the overall ER folding capacity by (membrane) protein over-expression can induce the unfolded protein response (UPR) (Wagner *et al.*, 2006). This response orchestrates the over-expression of a large set of proteins that are involved in protein folding and up-regulates the ER-associated protein degradation (ERAD) system (Nakatsukasa & Brodsky, 2008). ERAD substrates are tagged by poly-ubiquitination that leads, after re-translocated back to the cytoplasm by an unknown mechanism, to degradation by the cytoplasmic 26S proteasome (Nakatsukasa & Brodsky, 2008). It was demonstrated by size exclusion chromatography that proteolysis by the 26S proteasome yields only small oligopeptides from 500 Da to maximal 3.5 kDa (Kisselev *et al.*, 1999). Such degradation products would be detected as a smear rather than a defined band during Western Blot. In contrast, the putative degradation fragments for Cub-X fusion proteins were more than ten times larger than the biggest observed proteasome peptide product and detected as defined band.

Although this observation casts some doubt on the observed additional bands being the product of UPR induced degradation of Cub-KC1, Cub-SYP121 and Cub-SYP111 by the ERAD pathway, it is also true that most of the data concerning UPR response and the ERAD pathway were obtained for soluble proteins. Much less is known about how integral membrane proteins are folded in the ER, quality controlled and, if misfolded, sorted to the ERAD pathway, i.e. solubilised from lipid bilayer of the ER membrane to be translocated to the 26S proteasome in the cytoplasm (Nakatsukasa & Brodsky, 2008; Maattanen *et al.*, 2010).

It is tempting to speculate that down-regulation of the Cub-X-fusion expression levels by the addition of Met to the medium let the level of misfolded protein sink below the threshold for

UPR induction and degradation could be avoided to an extend that did not support detectable self-activation. Indeed, 0.07 mM Met was sufficient to suppress yeast growth in the negative control for diploids expressing Cub-KC1, while 0.4 mM was necessary to achieve the same in diploids with Cub-SYP121. The strength of the individual background reporter gene activity was in agreement with overall higher expression levels of the Cub-SYP121 fusion that made detection of full-length protein with the anti-VP16 antibody possible (see above).

An alternative source for the large observed degradation products might have been proteolysis in the yeast vacuole that has its own set of proteases, e.g. endopeptidases. These enzymes are capable of creating large protein fragments by breaking peptide bonds in the middle of a molecule. Retrograde trafficking or delivery by autophagosome could have brought Shakers/ SNAREs to the vacuole (Graciet & Wellmer, 2010). Autophagosomes are known to specifically target cytosolic protein aggregates (Finley, 2009). Entirely based on speculation, one could maybe imagine, that specifically in case of the TA proteins SYP121 and SYP111, such cytosolic aggregates could represent a side of the over-expression problem that manifests itself earlier than after posttranslational insertion into the ER membrane. All TA proteins are likely to depend *in vivo* on chaperones, even if only for targeting purposes for those who can insert into membranes unassisted (Borgese & Fasana, 2011). In yeast, the number of copies of Get4 and Get5 TA protein chaperones per cell are estimated at 5400 and 6500, respectively, in the face of ~300 000 ribosomes/cell. Therefore, maybe upon Cub-SYP121 over-expression, not enough chaperones were available to prevent Cub-SYP121 aggregation in the cytoplasm. Such aggregates might have been targeted by the autophagosome for degradation already before insertion into the ER. Finally, it is also possible that degradation only occurred during the protein extraction procedure. However, neither of these alternative degradation scenarios that would explain larger fragments allows for the artificial transcription factor to be free to enter the nucleus and cause the observed self-activation.

In conclusion, the cause for self-activation of the tested Cub-X bait fusions remains hidden. The observation that all three constructs were affected, suggests a general problem of the vector backbone, rather than the expressed individual protein or membrane protein type (e.g. TA protein). Clearly, more optimisation is necessary to make this vector a useful tool to explore interactions of TA proteins in mbSUS assays in general and to allow SNARE proteins to be bait fusions in this particular case. Although it is likely that after suppression of the background reporter gene activity with methionine, the observed yeast growth and *lacZ* gene activity should result only from genuine Cub-Nub-fusion protein interaction, it must be concluded that the Cub-SYP121 fusion was unable to reveal specificity of this SNARE for any of the three Shaker channel subunits.

In contrast to Cub-SYP121, the converse SYP121-Cub fusion showed interaction with the positive control but no yeast growth or *lacZ* gene activity in the negative control. This result suggested that despite contradicting topology predictions, SYP121-Cub was a functional bait fusion. Two possible scenarios might explain this result. Firstly, the SYP121-Cub protein may have never inserted into the ER (or any other membrane) in the first place. As detailed in the General Introduction, TA proteins with very hydrophobic TMDs were shown to depend on chaperones for both the prevention of irreversible aggregates in the cytoplasm and targeting to the proper

membrane (p. 61ff.). TA proteins with only moderately hydrophobic TMDs are capable of translocating their C-terminus across membranes unassisted and may depend on chaperones only for targeting to the correct membrane (Brambillasca *et al.*, 2005; Kalbfleisch *et al.*, 2007). Moderately hydrophobic TMDs confer a certain degree of water solubility, which led Borgese *et al.* (2007) to suggest that those TA proteins might form reversible cytoplasmic aggregates that help stabilize them before spontaneous membrane insertion. In support of this, it has been observed that the rabbit TA protein cytochrome b5, although usually found integrated into phospholipid bilayers, was soluble in aqueous solution after removal of detergents (Spatz & Strittma, 1971).

Assuming that SYP121 was of moderate hydrophobicity, it might have formed self-interactions at this stage of reversible aggregation (Sieber *et al.*, 2007). Perhaps in this way SYP121-Cub might 'catch' some of the simultaneously expressed Nub-SYP121 fusions before they insert into the ER membrane. Thus, the strong yeast growth and *lacZ* gene activity observed between SYP121-Cub and Nub-SYP121 (at least, if not stronger than the positive control) could be explained. In a similar manner, the observed interactions with the related TA proteins Nub-SYP122 and Nub-SYP111 might have occurred. Interaction with Nub-SYP122 appeared weaker than with Nub-SYP121, possibly because SYP121-Cub on the base of greater sequence homology interacted stronger with itself. Even weaker interaction with the more distantly related Nub-SYP111 might have a similar explanation and/ or other unknown reasons. Alternatively, cytoplasmic monomers of SYP121-Cub might be able to interact with Nub-fusions of the three SNAREs as well as the three Shaker channels subunits that are already inserted into a membrane. Those interactions might take place on the ER, the PM or in fact any membrane involved in anterograde trafficking, e.g. a secretory vesicle.

Weak interaction of SYP121-Cub was observed with all three Shaker channel subunits, when compared to the reporter gene read-outs for self-association. No apparent differences in blue staining after X-gal overlay assay and only slightly stronger yeast growth on selective medium without Met occurred for interaction with KC1 compared to interaction with KAT1 or AKT1. If indeed cytoplasmic SYP121-Cub interacted with membrane inserted Nub-fusions of the Shaker channels, perhaps less frequent interaction events based on the higher degrees of freedom for orientation of the SNARE could be expected. Also, the putatively interacting hydrophilic domains of SYP121 might be folded slightly differently in this 'new' protein version, so that steric distortions might hinder or allow only transient interactions. It is likely that N- and C-terminal hydrophilic domains of the SNARE would be folded, as otherwise proteins are not stable. Their unfolded state would quickly be detected by intracellular control mechanisms and targeted for degradation by ubiquitin-tagging (Stagljar *et al.*, 1998; Knecht *et al.*, 2009). In addition, one might also speculate that the folding state of the extended C-terminus contributed to this hypothetical cytoplasmic state for SYP121-Cub. As mentioned in the General Introduction, tight folding is not conductive to translocation (Dowhan & Bogdanov, 2009). However, it would be impossible to predict if the achieved tertiary protein structure would resemble the native protein situation.

Although one or more of these explanations might underlie the observed results, another scenario that involves a change in membrane topology seems more likely as explanation for the

unexpected suitability of the SYP121-Cub fusion in this mbSUS assay. In other words, it was questionable that the SYP121-Cub fusion behaved like a TA protein at all. Both SYP121 and SYP122 already have rather long tails after the C-terminal TMD, that are predicted to reside in the ER/extracellular space (41 and 36 aa, respectively, based on topology predictions at http://aramemnon.botanik.uni-koeln.de/). In contrast, SYP111 is a more conservative TA protein with an 8 aa long C-terminus. As mentioned above, the entire Cub-moiety that includes the artificial transcription factor is roughly 40 kDa which is about the size of SYP121 itself (~ 38 kDa; Edit sequence program of DNA-Star software packet). Thus, by attaching Cub-LexA-VP16 to the C-terminus, over 300 aa are added and the protein roughly doubles its size. It has been observed that polar C-terminal domains of even 100 aa were able to translocate unassisted *in vitro* across pure phospholipid bilayers (Brambillasca *et al.*, 2006). Also, a yeast syntaxin (Tlg2) has 59 predicted C-terminal aa (http://www.uniprot.org/) and clearly functions as a TA SNARE (Jahn & Scheller, 2006). However, as previously stated (Borgese *et al.*, 2007), extending the C-terminal domain of TA proteins beyond a certain length will most likely result in a protein that can potentially use the co-translational translocon-based pathway. In such cases, the defining feature of a TA protein is no longer given: the TMD would not still be contained in the ribosome tunnel while translation (from N- to C-terminus) finishes and thus it can be recognized by the SRP chaperone (see General Introduction, pp. 27) (Borgese & Fasana, 2011). The topology of this new 'non-TA' protein would then depend on several topogenic features, as detailed in the General Introduction for KAT1 ER insertion (p. 27ff.). With regard to the 'positive-inside rule', i.e. the TMD flanking segment with the more positive charge will be retained on the cytoplasmic side of the ER membrane, it was demonstrated that moving even a single positively charged residue from the cytoplasmic side to the opposite side of a TMD can result in inversion of topology (Nilsson & Vonheijne, 1990). Thus, it might be entirely possible that SYP121-Cub was present here in an inverse topology, i.e. with the C-terminus in the cytoplasm and the N-terminus in the ER lumen, and thus, in effect, representing a Type III instead of Type IV membrane protein. As the Cub is attached to the C-terminus, it would then be accessible to cytoplasmic ubiquitin-specific proteases upon interaction with a Nub-fusion of either another SNARE or a Shaker. In fact, such cases where the ubiquitin half supposedly disrupts the topology of a membrane protein, have been observed previously (Miller *et al.*, 2005). During their large-scale mbSUS assays in search of interactions between yeast integral membrane proteins, they found a small number of proteins with characterized extracytosolic C-termini that unexpectedly proved functional with a fusion of Nub or Cub to this particular end of the protein.

Whatever the reasons that allowed the observed SYP121-Cub interaction with other SNAREs or the three Shaker channel subunits (solubility in the cytoplasm or membrane reorientation) it is questionable if this situation can accurately represent how the proteins would interact *in planta*. Therefore, the results regarding SYP121-Cub interaction with the Shaker channel subunits must be regarded with extreme caution here and are not sufficient to determine specificity for a particular channel.

Due to the described problems when using SYP121 as bait, the only information regarding

the specificity of this SNARE for KC1 over the related Shaker channel subunits AKT1 and KAT1 could be derived from mbSUS assays, where those latter two Shakers were the bait, here as X-Cub fusions with Nub-X prey proteins. Results obtained from assays performed under the standard set of experimental conditions indicated that KAT1-Cub did interact with Nub-SYP121. In contrast, AKT1-Cub co-expression with Nub-SYP121 yielded only negligible yeast growth on selective medium and no *lacZ* reporter gene activity after the standard incubation time of 6 d. Prolonging the incubation time to 14 d revealed an interaction between AKT1 and SYP121. In contrast, results for interactions observed with KAT1-Cub did not change after prolonged incubation (data not shown).

The interpretation of these experiments was hindered by a limitation of the mbSUS technique already mentioned in the results. It would be tempting to compare the three X-Cub Shaker fusions with regard to their interaction with Nub-SYP121 on the basis that all experimental conditions that might influence the yeast growth phenotype were kept identical (e.g. growth phase, amount of cells spotted onto plates, incubation time etc.). However, as mentioned before, a conclusion about relative interaction strength is only meaningful in combination with protein expression levels. The mbSUS technique measures the local concentration, integrated over time, between Cub- and Nub-labelled protein partners. Provided that both fusion proteins localize to the same subcellular compartment, a higher overall expression level will be reflected in a higher local concentration of complementary Nub- and Cub-fusions. Hence, interactions between two partners of a protein pair fused to NubG and Cub, respectively, are more likely to occur in a given time frame, when the expression levels are high.

The mutated Nub moiety of ubiquitin (NubG) is presumably partially unfolded (alone or fused to a protein of interest) and therefore unable to recognize and bind to the Cub moiety (Johnsson & Varshavsky, 1994a). As the UBPs do not recognize Cub alone, no cleavage of the attached reporter takes place. Only upon interaction of the two partners of a protein pair fused to NubG and Cub, respectively, are the NubG and Cub moieties forced into very close proximity. This proximity induces a partial refolding of NubG, followed by re-association of NubG and Cub into quasi-native ubiquitin. This folded structure is then recognized and cleaved off by UBPs within minutes (Johnsson & Varshavsky, 1994a). In general, the extent of cleavage at the C-terminus of reassembled ubiquitin translates into the growth rate of yeast cells. Thus, when comparing relative interaction strength between a Cub-fusion with two or more different Nub-fusions (in a given time frame), the level of expression for the individual Nub-fusion will influence the apparent strength of interaction as perceived in yeast growth and/or *lacZ* gene activity.

Here, similar to Cub-KC1, neither of the X-Cub Shaker channel fusions could be detected with anti-VP16, most likely due to low expression levels of these proteins. As indicated by the interaction of AKT1-Cub with Nub-SYP121 that only revealed itself after prolonged incubation, also the chosen time frame for an experiment might alter the observed results. It is unknown here, why the interactions with the AKT1-Cub fusion displayed this delayed growth phenotype. Possibly, expression of this fusion protein harms its host cells.

Finally, it has to be mentioned that not necessarily stronger interactions result e.g. in more yeast growth (Estojak *et al.*, 1995; Miller *et al.*, 2005). The observed case of KC1-Cub interaction

Nub-KAT1 shows that reporter gene read-out may not necessarily correlate with the affinity of the underlying protein interaction. For this protein pair the mbSUS assay had indicated an active *lacZ* reporter gene in both X-Gal overlay and quantitative liquid β-gal assay but negligible growth on selective medium that is dependent on an active *HIS*3 and *ADE*2 reporter gene.

Similar findings were published previously (Estojak *et al.*, 1995). These authors found that there was no single reporter gene for which strength of interaction as predicted in Yeast-Two-Hybrid assays correlated linearly to differences in dissociation constants measured between the same protein pair *in vitro*. Some proteins appeared to interact strongly on the basis of the *LEU*2 phenotype but activated the *lacZ* reporter only weakly (Estojak *et al.*, 1995). The underlying reasons are unknown but in some instances may be correlated to another observation made by Estojak *et al.* (1995). These authors found that individual reporter genes demonstrated thresholds of activation. Apparently in those cases there was a certain amount of reporter gene transcription necessary (corresponding to a minimum affinity of interaction) before a cell could grow to form a colony, i.e. score as positive interaction. Therefore, some reporters only recognized moderate-to-strong interactions, while others were also responsive to weak interactions. In summary, it was only possible to conclude here, that in addition to interaction with KC1 there appeared to be a measure of interaction also between SYP121 and AKT1 or KAT1. In contrast, none of the three Shaker channel subunits, not even after prolonged incubation time (14 d), appeared to interact with SYP122 or SYP111 under stringent conditions.

Few conclusions could be drawn from the mbSUS assays that were intended to explore the identity of the domains mediating interaction between KC1 and SYP121. As discussed above, all results involving SYP121-Cub or SYP121-Nub fusions can be interpreted with caution. Comparing differences in yeast growth/ β-gal activity between KC1-Cub versus Cub-KC1 interaction with Nub-SYP121 was subject to all considerations discussed above for the interaction of different Shaker channel subunits with Nub-SYP121. These considerations aside, it appeared that KC1-Cub interaction with Nub-SYP121 supported more yeast growth under the most stringent condition than the interaction of Cub-KC1 with Nub-SYP121. Therefore, even if highly speculative, one might assume that steric obstruction of the N-terminus of KC1 with the Cub fusion might reduce interaction to Nub-SYP121. The ideal combination would have been the investigation of the Cub-SYP121 fusion in co-expression with Nub-KC1 and KC1-Nub, respectively, if it were not for the problem of background reporter gene activation (see above). Western Blot detection of this Cub-fusion is possible and its topology agreed with predictions for TA proteins. In addition, both KC1 fusions would present the Nub-fusion in the cytoplasm.

In conclusion, interaction between KC1 and SYP121 in mbSUS assays could be verified here with a high level of confidence derived from the additional controls compared to the library screen that had originally suggested this interaction. Furthermore, specificity of this interaction could be shown in the absence of significant reporter gene activity in diploids co-expressing the closest homologs of SYP121 together with KC1, namely SYP122 and SYP111. Experimental conditions for this assay were highly controlled by the verification of equal expression levels for all three SYP1 SNARE proteins. In contrast, specificity of SYP121 for KC1 over the closely related

Shaker channel subunits AKT1 and KAT1 could not be proven with such a high level of confidence. Although neither AKT1 not KAT1 showed significant interaction with prey fusions of SYP122 or SYP111, a minor level of interaction with SYP121 was observed. Direct comparisons of the interaction strength between the three Shaker channel subunits AKT1, KAT1 and KC1 with SYP121 was hindered by the absence of suitable antibodies to assess their expression levels and by the discussed problems in using SYP121 as bait Cub-fusion. Similar considerations made it impossible to draw firm conclusions from the mbSUS assays that were intended to explore the identity of the domains mediating interaction between KC1 and SYP121. Nevertheless, the most important aim of this chapter was achieved by verifying a specific interaction between KC1 and SYP121, the first ever observed interaction between a plant SNARE protein and ion channel.

Chapter 2: Co-immunoprecipitation between KC1 and SYP121

Introduction

Chapter 1 describes the specific interaction of KC1 with SYP121 in the mbSUS system. Despite the different levels of controls employed for this technique, there is always a possibility that an interaction found in a particular heterologous expression system is an artefact, e.g. due to involvement of yeast specific factors in this case. Therefore, a co-immunoprecipitation (Co-IP) assay of full-length tagged proteins expressed in insect cells was chosen to verify the interaction between KC1 and SYP121 (see p. 73). Since so far interactions between ion channels and SNAREs in plants have not been observed, no previous literature on this subject was available. For most of the characterised interactions between mammalian SNAREs and ion channels, Co-IP experiments were performed with soluble domains to avoid the often difficult solubilisation of full-length membrane proteins (reviewed in Leung *et al.* 2007).

The *Sf9* insect cell expression

Established insect cell lines such as the *Sf9* one used for this experiment are originally derived from ovary cells of the moth *Spodoptera frugiperda* (Kidd & Emery, 1993). Expression of heterologous protein is achieved by infection with a recombinant virus encoding the gene of interest. This recombinant virus must be created in two steps as the genome of the most commonly used *Autographa californica* nuclear polyhedrosis virus (AcMNPV) is to large for direct manipulation (over 100 Kbps). AcMNPV is a Baculovirus from a family of double stranded DNA viruses (Baculoviridae) that infects many different species of insects as their natural hosts (Luckow *et al.*, 1993). Firstly, the CDS of interest is cloned into a small transfer vector. This plasmid is then co-transfected with the AcMNPV virus DNA into *Sf9* cells, where homologous recombination creates the desired recombinant virus (see Fig. 34). Viral DNA replication in the host cell nucleus starts about 6 hours post-infection (hpi).

The replication cycle is biphasic, with gene expression occurring as a cascade of sequentially and temporally regulated events that create two different forms of the virus (Kidd & Emery, 1993). The first type buds from the PM between 10- 48 hpi and spreads the infection from cell to cell. Starting at about 18 hpi and then continuing to accumulate for 4 to 5 days until the infected cell lyses, a second type of virus, the so-called occluded virus, is assembled inside the nucleus. As these virus particles are designed to spread to a new host insect rather than the neighbouring tissues, their DNA is protected against environmental influences by a surrounding nucleocapsid, a rod-like crystalline matrix made predominantly of two viral-encoded structural proteins, polyhedrin and p10. In laboratory cell culture, the production of this second type is not necessary for propagation of the virus, which can rely instead on the budded virus particles. Hence, the coding sequence for the now non-essential nucleocapsid proteins can be replaced with the

sequence for a target protein of interest. The corresponding polyhedrin and p10 promoters drive very high-level transcription, e.g. naturally produced polyhedrin makes up about 30 % of the total cellular protein synthesized after infection (Kost *et al.*, 2005).

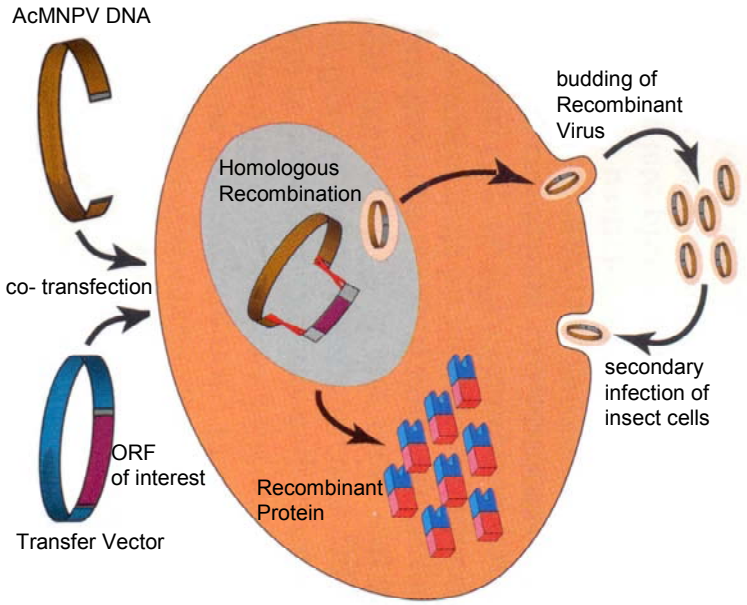

Fig. 34 Baculovirus mediated protein expression in insect cell culture

The large size of the Baculovirus (AcMNV) DNA prevents direct insertion of a CDS of interest. Instead, the CDS of interest is first cloned into a transfer vector that imparts it with flanking sequences homologous to the AcMNV DNA. After co-transfection into *Sf9* insect cells (orange), recombination takes place within the nucleus (grey). Thereby a recombinant virus is created that now harbours the CDS of interest. From the DNA of this new recombinant virus the host cell is forced to produce the desired recombinant protein. In addition, newly replicated recombinant virus DNA leaves the cell via budding and spreads the infection to the remaining unaffected cells. Not pictured is the creation of occluded virus particles that would occur during an infection of an insect in nature. Picture adapted from www.pharmingen.com.

Another reason in favour of the insect cell expression system were previous publications that reported the expression of functional *Arabidopsis thaliana* AKT1 and KAT1 in *Sf9* insect cells as well as their successful extraction (solubilisation) from these cells (Marten *et al.*, 1996; Gaymard *et al.*, 1996; Urbach *et al.*, 2000).

A brief introduction into membrane protein solubilisation

Solubilisation describes the complex process that removes hydrophobic membrane proteins such as the Shaker channel subunits AKT1, KAT1 and KC1 and the three SYP1 SNAREs from their native lipid bilayer environment and lends them enough hydrophilicity to disperse into aqueous solution. This process is mediated by detergents. Detergent monomers are amphipathic molecules just like the phospholipids that form biological membranes. However, while both possess a hydrophilic polar head group, their hydrophobic parts differ in that most detergents only contain one long alkyl chain compared to the two that are part of the majority of lipids that constitute biological membranes. This difference confers detergents a higher degree of hydrophilicity that allows their monomers to be soluble in aqueous solution at low concentrations. However, when the

concentration increases to a certain value specific for each detergent (C_{sat}), the monomers start to associate via hydrophobic interactions between their alkyl chains balanced by electrostatic repulsions between their head groups and partition into a phase, a monolayer at the air-water interface. Further increase in the detergent concentration above a critical value, referred to as the critical micelle concentration (CMC), leads to a point, where the hydrophobic interactions in the system predominate over electrostatic repulsions and thermodynamically stable aggregates called micelles start to form (Tanford, 1978; Misra *et al.*, 2010). In these micelles detergent monomers are arranged in an approximately spherical way, so that their interacting hydrophobic alkyl chains are sequestered from the water into the micelle centre and the hydrophilic head regions face outward, covering the surface of the micelle and engaging in hydrogen bonds with surrounding water molecules that keep the complex in solution (see Fig. 35). Therefore, the formation of micelles underlies the same general principle that supports the association between membrane lipids, only that those assemble into the extended structures typical of lipid bilayers instead.

Precisely this membrane-mimetic feature allows detergents to functionally replace the membrane lipids during membrane protein solubilisation. Integral membrane proteins are embedded into the bilayer by hydrophobic interactions between their hydrophobic domains and the alkyl chains of the lipids. In a detergent-protein mixed micelle after successful solubilisation, the hydrophobic regions of the membrane proteins are surrounded by the alkyl chains of detergent monomers instead of the ones from phospholipids. The hydrophilic portions of the membrane proteins are aligned with the hydrophilic headgroups of the detergent monomers and thus exposed to the aqueous medium (see Fig. 35).

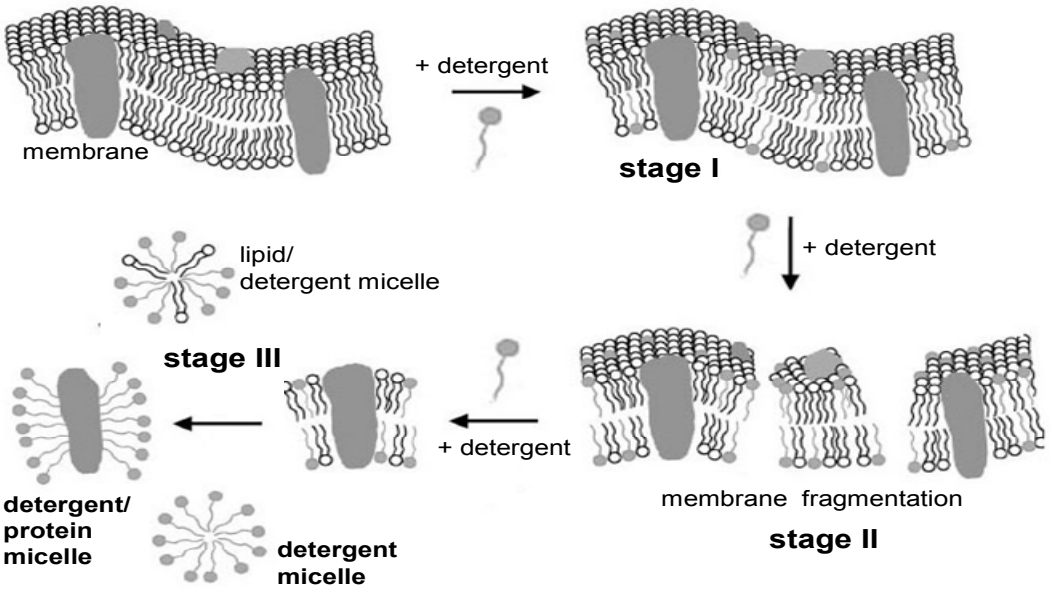

Fig. 35 Model for membrane protein solubilisation

The image was adapted from a previous publication (Kalipatnapu & Chattopadhyay, 2005).
Shown is the so-called three stage model that describes the solubilisation of artificial membranes made from pure phospholipids (and additional membrane proteins) by an increasing concentration of a detergent until all lipids (or proteins) are part of detergent micelles at stage III.

Solubilisation of artificial membranes with pure phospholipids follows a three stage model (Lichtenberg *et al.*, 1983; le Maire *et al.*, 2000) (see Fig. 35). In stage I, at low detergent concentrations, single detergent molecules partition into to the membrane by means of their hydrophobic portions and in a non-micellar form, meaning they interact only with surrounding lipids. With increasing amounts of detergent, membranes undergo various degrees of solubilisation (stage II). Stage II begins when the increasing numbers of detergent monomers within the membrane start to interact with each other (at the C_{sat}). This causes destabilisation and finally fragmentation of the membrane bilayer. At still higher detergent concentrations, more and more detergent monomers replace lipids in the membrane fragments, leading to lipid-detergent mixed micelles instead until Stage III is reached (at the CMC). At this point the membrane is fully disintegrated, i.e. solubilised and all lipids are present as part of lipid–detergent mixed micelles. In practice, transitions between these three different states are smooth and are found in co-existence (Reisinger & Eichacker, 2008). The solubilisation of membrane proteins from these artificial membranes progresses from lipid-protein-detergent mixed micelles during stage II to proteins being part of pure detergent micelles at stage III as the increasing detergent concentration forces the lipids to distribute among an increasing number of detergent micelles (see Fig. 35).

The aims of the work detailed in this chapter were therefore to establish a *Sf9* insect culture, create recombinant viruses and verify recombinant protein expression by finding suitable solubilisation conditions for the SNARE and Shaker channel membrane proteins. These steps were preparation to ultimately perform Co-IP experiments with co-solubilised KC1 and Syp121 in order to verify a direct physical interaction between these two proteins.

Results

Baculovirus transfer constructs and recombinant viruses

A monolayer culture of *Sf9* insect cells was set up with the help of Dr. J. Christie and Mrs. P. Ennis (Bower Building, University of Glasgow). Dr. G. Sibbet (Beatson Institute for Cancer Research, Glasgow) provided instructions to create the first recombinant virus. Constructs for heterologous protein expression in *Sf9* insect cells were designed with the Baculovirus Transfer Vector pVL1393 as backbone (Table 2; for details see M&M). KC1, SYP121, SYP111 and SYP122 constructs were cloned by two former members of Prof. Blatt's group in Glasgow: Dr. Johansson and Dr. Sokolovski.

CDS	C-terminal tag	external loop tag	N-terminal tag
KC1	Myc-HIS		
AKT1	VSVG		
KAT1	HA-HA		
KAT1		HA	
SYP121			FLAG-HIS
SYP122			FLAG-HIS
SYP111			FLAG-HIS

Table 2 Constructs designed for expression in *Sf9* insect cells

Second generation recombinant viruses for all these constructs were created. In short, the Baculovirus DNA was provided in a linearised state crated by restriction enzyme digest at dual sites. The resulting large deletion functionally inactivated an essential gene thus precluding replication of parental virus. This lethal deletion was rescued only by recombination with a Baculovirus Transfer Vector (here pVL1393 containing the respective CDS) when both were used for co-transfection of *Sf9* insect cells. Recombinant virus was created thereby at frequencies higher than 99 %.

Verification and optimization of recombinant protein expression in *Sf9* cells

As a prerequisite for the Co-IP experiments, protein expression after infection of *Sf9* cells with the respective recombinant virus (see Table 2) needed to be verified. The required membrane protein isolation and solubilisation procedure was optimised here with regard to several parameters such as, for example, the method of mechanical cell disruption, purity of used membrane fraction, buffer composition and solubilisation temperature and length (data not shown). The final version, used for all experiments shown here, involved re-suspension of infected *Sf9* cells in solubilisation buffer with incubation at 4 °C overnight. This step was followed by centrifugation to pellet out un-solubilised membrane fragments and resulted in the so-called solubilisation supernatant (sSN). However, the most important factor to optimize for the solubilisation procedure was the detergent. The six predicted TMDs of the Shaker channels were likely to confer KC1 a much higher degree of

hydrophobicity and in turn an increased resistance to solubilisation, compared to the single TMD of the SNAREs. Overall membrane hydrophobicity relies on the proportion between hydrophilic (not membrane integral) and hydrophobic transmembrane domains, although in some cases, post-translational protein modification with oligosaccharides might increase hydrophilicity (Marmagne *et al.*, 2006). As the aim was co-expression and, in consequence, co-solubilisation of both partners the search for a suitable detergent began with the more challenging KC1.

Urbach *et al.* (2000) tested eight detergents from three different classes (anionic, zwitterionic and nonionic, see below) in order to solubilise AtAKT1 and AtKAT1 from *Sf9* insect cells. They named the zwitterionic L-α-lysophosphatidylcholine (LPC) as the only efficient detergent for the solubilisation of both Shaker channels. Furthermore, out of a number of different LPC concentrations ranging from 0.01- 3 %, the value for optimal solubilisation was determined at 1 % for KAT1 and 1.5 % for AKT1 (Urbach *et al.*, 2000). Based on these results for closely related proteins, LPC was the first detergent tried in six different concentrations between 0.1- 1.5 % for the solubilisation of KC1. However, initial Western Blot analysis of solubilisation supernatants (sSN) employing an antibody against the C-terminal Myc-tag of KC1, yielded no bands of either the expected molecular weight (~ 78 kDa) or smaller size that might point to protein degradation (data not shown). PCR analysis of DNA extracted from infected *Sf9* cells confirmed the presence of the *KC1-Myc* CDS in the recombinant virus (data not shown). In addition, subjected insect cells showed signs of successful infection with virus such as increased size, enlarged nuclei and free floating (data not shown). Both observations supported the presence of recombinant protein and pointed towards an unsuitable protein extraction procedure. As it turned out, KC1 shared the tendency of polytopic membrane proteins to form aggregates when boiled in SDS containing Sample Loading Buffer (SLB) before separation on SDS gels (Sagne *et al.*, 1996; Kerkhoff *et al.*, 2000; Medina *et al.*, 2004). Large protein aggregates will be retained from migration during SDS-PAGE in both the sample well and the interface between the stacking and separation gel depending on the actual aggregate size. The standard procedure discards the stacking gel prior to blotting and with it the retained protein sample if aggregated. Fig. 36A shows Western Blots, where the stacking gel was retained for the blotting procedure. Analyzed here was the total protein extract of one batch of *Sf9* cells infected with recombinant virus for KC1-Myc. This batch was divided into three equal parts to ensure that the only difference between the three samples was the amount of LPC used for solubilisation (0.5 %, 1 %, 1.5 %, Fig. 36A, lane 1-3). Equal amounts of the total sSN were loaded per lane, which was visualised by the PonceauS stain in the right hand panel (Fig. 36A). No signal corresponding to the molecular weight of KC1-Myc could be detected after samples had been incubated at 98 °C for 4 min regardless of the LPC concentration used for solubilisation (Fig. 36A, panel 1, red arrow). Instead, a signal appeared well above the highest molecular weight marker band (175 kDa) at a position corresponding to the wells of the stacking gel. Thus, the occurrence of large KC1 aggregates was confirmed (Fig. 36A, panel 1). The signal was probably weaker for 1.5 % LPC despite equal amounts of protein loading due to loss during gel handling and blotting rather than reduced aggregate formation (Fig. 36A, panel 1, lane 1). In contrast, when samples were

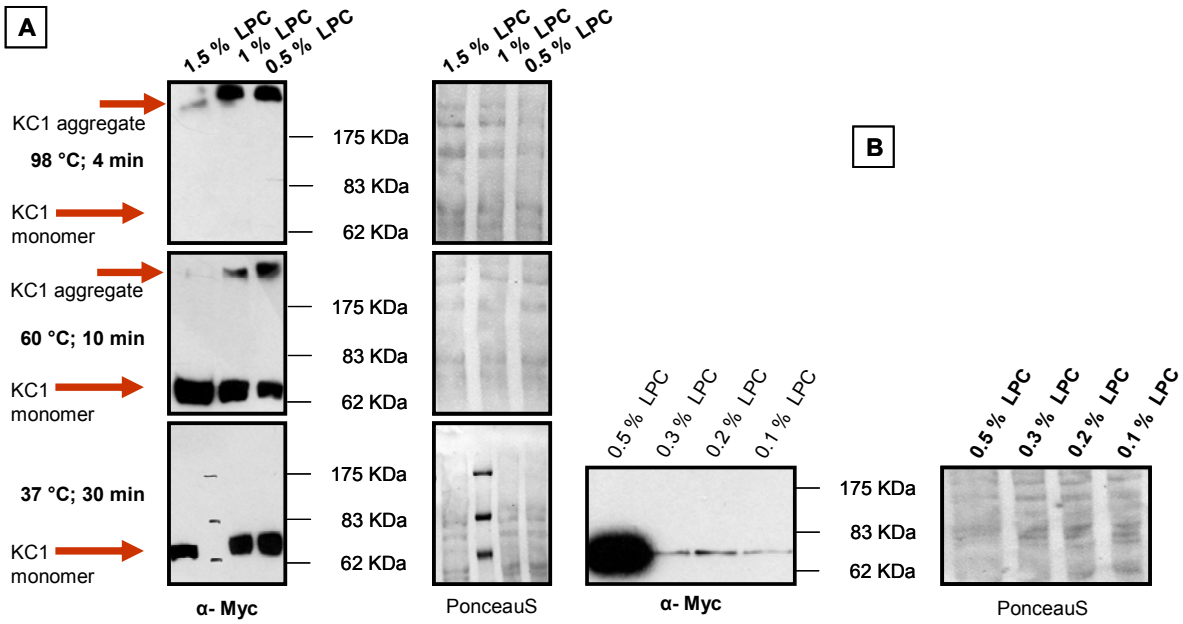

Fig. 36 KC1 solubilisation and aggregate formation

For (A) and (B) respectively, one batch of *Sf9* insect cells was infected with KC1 recombinant virus. Total protein extract from those cells was divided into three (A) or four (B) equal parts and solubilised with the LPC concentrations indicated. PonceauS stains are shown as loading control for 10 µg total protein of solubilised SN per lane in the right hand panels. Protein concentration was determined by Amidoblack assay and 7 µg were loaded per lane (data not shown). Each of the three different sSN (derived from 1.5 %, 1 % and 0.5 % LPC) used in (A) was further divided into again three samples that were mixed with identical amounts of SDS Sample Loading Buffer prior to SDS-PAGE and incubated at three different temperatures for different time periods as indicated on the very left side. The four different sSN (derived from 0.5 %, 0.3 %, 0.2 % and 0.1 % LPC) used in (B) were incubated only at 37 °C for 30 min. Western Blot analysis with an anti-Myc against the C-terminal Myc-tag of KC1 demonstrated with the appearance of only a very high molecular weight signal on the height of the stacking gel part that incubation at 98 °C for 4 min caused all KC1 to aggregate independent of the LPC concentration used for its solubilisation (A, first panel, left). When incubated at 60 °C for 10 min, increasing LPC concentrations reduced the formation of aggregates in favour of KC1 monomers (~ 78 kDa). Incubation at 37 °C for 30 min entirely prevented the formation of aggregates independent of the LPC concentration used for solubilisation (A, third panel, left). According to the signal strength in this Western Blot, the yield of solubilised KC1 did not appear to increase with LPC concentrations higher than 0.5%. However, as seen in (B), when LPC concentrations fell below 0.5 %, there was a sharp decline in solubilisation efficiency.

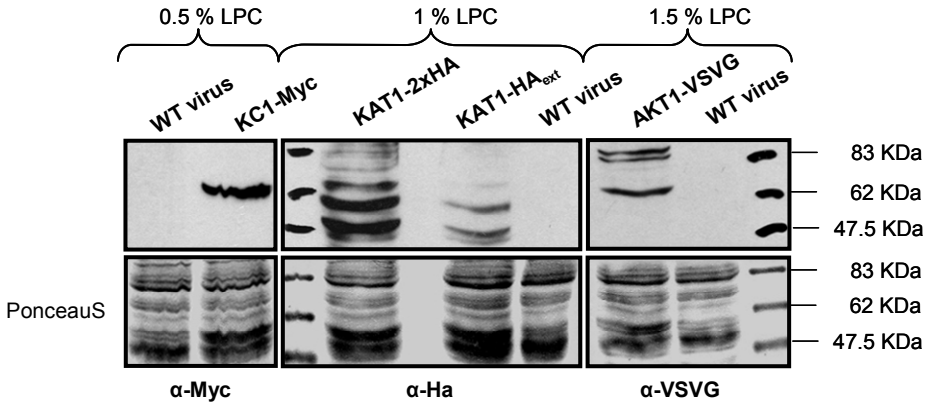

Fig. 37 Analysis of AKT1 and KAT1 expression in *Sf9* cells after solubilisation with LPC

Western Blot analysis of *Sf9* cells infected with the recombinant viruses and solubilised with the LPC concentrations as indicated above the top panels yielded specific signals confirming the expression of all four Shaker channel proteins when compared to cells infected with only wt (WT) virus, when approx. equal amounts of total protein were loaded (compare PonceauS stains in lower panels). However, apart from KC1, antibodies against the respective tags on the Shaker channels (KC1-Myc, KAT1-2xHA, KAT1-HA_{ext}, AKT1-VSVG) detected only (for KAT1-HA_{ext}) or additional lower molecular weight signals to a single band on the height of the expected molecular weight (KC1 ~78 kDa, KAT1 ~ 82 kDa, AKT1 ~ 98 kDa) most likely indicating protein degradation.

incubated at 60 °C for 10 min prior to SDS-PAGE, a band of the expected molecular weight for the KC1-Myc monomer was detected in addition to the band for aggregates in the stacking gel (Fig. 36A, panel 2, red arrow). Here, higher LPC concentrations in the solubilisation buffer led to progressively lower amounts of KC1 aggregates and in turn a stronger signal for the monomer until almost complete absence of aggregates at 1.5 % LPC. Incubating the samples at 37 °C for 30 min entirely prevented the formation of aggregates independent of the LPC concentration used for solubilisation (Fig. 36A, panel 3, red arrow). Based on this experiment all subsequent preparations of sSN from any of the recombinant membrane proteins used here were treated solely for 30 min at 37 °C prior to SDS-PAGE. In summary, LPC proved to be as suitable for the solubilisation of KC1 as Urbach *et al.* (2000) had observed for AKT1 and KAT1. In addition, it appeared from the quite comparable signal strength of the bands obtained in Fig. 36A (panel 3) that LPC concentrations higher than 0.5 % did not significantly increase the yield of solubilised KC1. In contrast, LPC concentrations below 0.5 % drastically reduced solubilisation efficiency (Fig. 36B). To obtain the results in Fig. 36B, the experimental set-up was as described for Fig. 36A, apart from the different LCP concentrations used for solubilisation (0.1 %, 0.2 %, 0.3 %, 0.5 %) and incubation of sSN only at 37 °C for 30 min. In conclusion, 0.5 % LPC seemed to be the most suitable detergent concentration for KC1 solubilisation from *Sf9* cell membranes.

Again following the data published by Urbach *et al.* (2000), *Sf9* cells infected with the KAT1 and AKT1 recombinant viruses created here (Table 2), were solubilised with 1 % LPC for the two different KAT1-HA proteins and 1.5 % for AKT1-VSVG. Western Blot analysis, pictured in Fig. 37, yielded specific signals for all three recombinant proteins when compared to solubilised proteins from cells infected with only wt Baculovirus. Similarly, the signal obtained for KC1 was not present in wt virus infected cells (Fig. 37, upper first panel from the left, lane 1 and 2). However, in contrast to KC1, no single band indicating only full-length protein could be obtained for either of the KAT1 or AKT1 recombinant proteins. Instead, detection of AKT1 with anti-VSVG resulted, in addition to a signal of the expected molecular weight (~98 kDa), in two lower bands most likely indicating protein degradation (Fig. 37, upper first panel from the right, lane 1). Similarly, even more pronounced degradation was likely the cause for several strong signals detected below the expected molecular weight (~ 82 kDa) by an anti-HA for both of the KAT1 recombinant proteins. For KAT1 with the tag in an external loop (KAT1-HA_{ext}) no band of a molecular weight corresponding to full length protein could be observed at all (Fig. 37, upper middle panel, lane 2). Solubilisation of KAT1 with a double C-terminal HA-tag (KAT1-2xHA) yielded only a very faint signal of the expected molecular weight (Fig. 37, upper middle panel, lane 1). A range of different LPC concentrations or other detergents (TritonX 100, Tween20, OGP, NP-40, CHAPSO, Digitonin) proved no more efficient for solubilisation or yielded more full- length protein in all three cases (data not shown).

Similarly, using a first generation virus stock, instead of the second generation normally employed for this work, was not successful (data not shown). In general, the second generation virus stock represents a good compromise between a high titre of infectious virus particles and the risk of an increasing number of mutant viruses in serially passaged stocks (Kumar & Miller, 1987).

The growth medium of the *Sf9* cells that were co-transfected in the initial production of recombinant virus (see above) constituted the 'generation zero' stock. It contained polyclonal virus at a low titre in form of the budded virus particles produced by the infected cells (see Fig. 34). Infecting fresh insect cells with this virus stock led to the more infectious 'generation one' stock and so forth. In later generations, several types of genomic alterations such as deletions and random insertions of host-derived retro-transposons were reported frequently (Kumar & Miller, 1987). Such mutations are a consequence of the absence of selection pressure on the virus to keep the foreign gene information in this expression system. Mutations that confer some growth advantage in cell culture will became predominant (Kumar & Miller, 1987). If such an event had already taken place in the second generation virus, for example in case of the recombinant KAT1- HA_{ext}, the presence of only bands of a lower molecular weight than expected could also be explained by the expression of stable truncated proteins. However, as no improvement was observed for all three Shakers with this strategy, the more likely explanation for the observed band patterns remained protein degradation. Therefore, the amount of virus stock used for infection (7.5 µl or 15 µl instead of 25 µl) and the time of harvest (36 h or 72 h instead of 48 h) were modified as well, because those two factors can have an influence on protein degradation.

The nature of the intracellular interactions between virus and host cell ensures that in general and within a certain time frame, there is a positive logarithmic relationship between the amount of heterologous protein produced and amount of virus titre used for infection that becomes only saturated when all cellular translation machinery is engaged (Licari & Bailey, 1991). However, forcing insect cells to a high expression rate by infecting with higher virus titres might overwhelm their ability to perform the proper post-translational modifications on the recombinant protein before the harvest. Such has been observed, for example, for the over-expression of the mammalian polytopic membrane G protein-coupled receptor, where a large portion of the recombinant protein was not properly glycosylated (Massotte, 2003). Protein modifications, including glycosylation, are thought to influence protein folding and stability and hence the amount of degradation (see Chapter 1, p. 153) (Benya *et al.*, 2000). The harvest of infected insect cells is in general only possible in a certain time frame which is limited ultimately by the host cell lysis that sets in 4-5 d post-infection (pi) (see Introduction, p. 145). From this point on, degradation of proteins due to proteolytic activity of environmental proteases becomes much more likely. An interesting experiment was performed on the synthesis and degradation rates of the soluble protein ß-galactosidase (ß-gal) in baculovirus mediated insect cell expression (Licari & Bailey, 1991). A pulse-chase technique with radiolabeled methionine revealed that until 24 h pi the degradation rate was of the same order of magnitude as the synthesis rate. However, at 96 h pi the synthesis rate was dramatically increased while the degradation rate was negligible. The authors proposed that the intracellular degradation witnessed at early times pi is primarily a defence mechanism of a healthy cell in response to the intracellular viral activities and increasing presence of heterologous protein (Licari & Bailey, 1991). Examples in both bacterial and mammalian cell systems have demonstrated the ability of a cell to identify a protein as foreign and target it for degradation (Goldberg & Dice, 1974). However, from about 24 h pi onwards host cellular processes have been

shown to be compromised for the viral activities and this was suggested to be the explanation for the negligible degradation rate of ß-gal during this time (Licari & Bailey, 1991). At still later time points, about 4 d pi, Licari *et al.* (1991) observed an increasing release of ß-gal into the medium. They interpreted this 'secretion' as the cell membranes losing integrity and becoming leaky until the ultimate lyses happens. Apart from these more general considerations about intracellular protein synthesis during virus infection, the time frame for harvest is also determined by the type of virus promoter that drives expression of the protein of interest. In the above described study (Licari & Bailey, 1991), the same polyhedrin promoter was used as for all the recombinant proteins created for this work (see Table 2). Baculovirus encoded promoters can be divided into four classes according to the time they are active during the viral infection cycle. The polyhedrin promoter (see Introduction, p.77) is of the 'very late' class, because it is only switched on when transcription of nearly all other genes, host cell and viral ones, has ceased. Hence, this promoter drives protein expression that generally starts at about 24 hpi and peaks 48–72 hpi, influenced also by the type and complexity of the recombinant protein (Kidd & Emery, 1993). Thus, a virus promoter of a different class might have been a further step in optimisation, as the above mentioned modifications in time of harvest and amount virus particles for infection were not successful in significantly reducing protein degradation for any of the three recombinant Shaker channel proteins (AKT1, KAT1). Gaymard *et al*. (1996), who had used the polyhedrin promoter to express AKT1 and KAT1 in *Sf9* insect cells as well had observed by immunogold labelling and electron microscopy that most of these proteins were present in internal membranes and only a very small fraction reached the PM. Although their protein signals showed no degradation during Western Blot, these data are perhaps an indication that the insect cells were already struggling with a too high amount of heterologous protein to achieve correct targeting. It is possible that very few changes in this situation might trigger ERAD response as discussed earlier in Chapter 1.

Finally, it has to be mentioned that protein degradation might have occurred despite optimized conditions, for example as a result of viral-encoded proteases responsible for the turnover of normal viral proteins that act inadvertently on the recombinant protein (Licari & Bailey, 1991). In addition, degradation as a result of the protein extraction procedure could not entirely be excluded here, although proteinase inhibitors were part of the standard protocol.

The intention had been to employ AKT1 and KAT1 as controls for the specific interaction between KC1 and SYP121 similar to the attempt in mbSUS assays. Although, despite the inability to resolve the degradation issue, attempts were made to use the least affected AKT1 for Co-IP with SYP121 or KC1, results were not promising (data not shown). Similarly, replacing AKT1 with an unrelated polytopic membrane protein (e.g. MDR, kindly provided by Dr. J. Christie, Glasgow) came with its own set of complications related to solubilisation and suitable expression levels, so that in the end, this set of potential control experiments was abandoned here.

Similar efforts to optimize virus amount and harvesting time were made for the expression of SYP121. For this purpose, nine independent *Sf9* monolayer cultures of the same age and started with the same amount of parent culture were infected with three different amounts of second generation virus (7.5 µl, 15 µl and 25 µl, three each) and harvested at three different time points

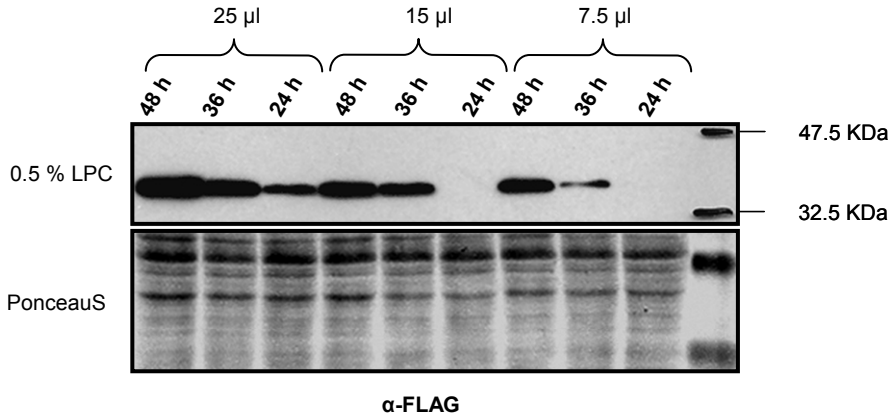

Fig. 38 Influence of harvest time and virus amounts on SYP121 expression in *Sf9* cells

Nine insect cell cultures of identical age and started from the same volume of parental culture were infected with three different volumes of second generation virus stock for SYP121 (7.5 µl, 15 µl, 25 µl, three each) and harvested at three time points pi (24 h, 36 h, 48 h). When equal amounts of total protein solubilised with 0.5 % LPC were loaded (compare PonceauS stain in lower panel), Western Blot employing an anti-FLAG against the N-terminal FLAG tag of SYP121 showed for all three amounts of virus increasing SNARE levels over time. However, only when infected with the highest amount of virus, SYP121 was detectable already 24 h pi. For all subsequent co-expressions with KC1, 15 µl and 48 h were chosen as standard for infection with SYP121 recombinant virus.

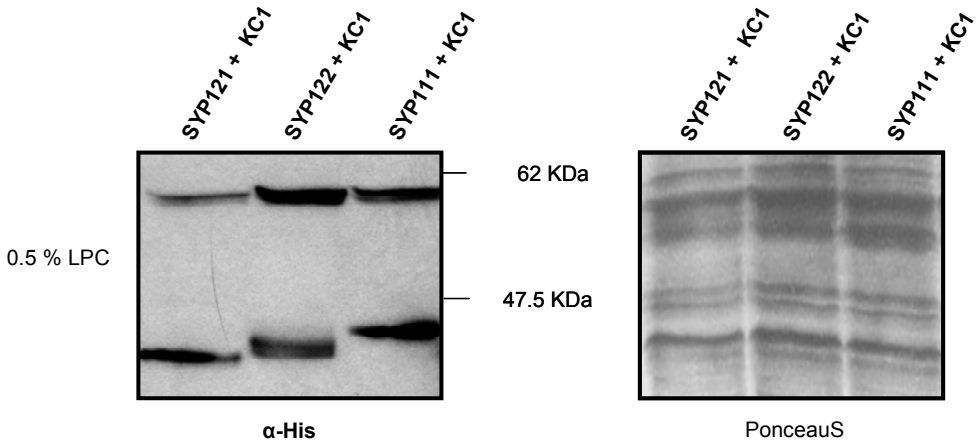

Fig. 39 Adjustment of KC1 and SNARE co-expression levels

Three *Sf9* cultures of the same age and grown from the same volume of parent culture were co-infected with 25 µl KC1 recombinant virus and 15 µl SNARE virus (SYP121, SYP122, SYP111, as indicated above the left hand panel). Cells were harvested 48 h pi and solubilised with 0.5 % LPC. Western Blot analysis with an anti-His against the His-tag present in all four proteins (compare Table 2) allowed simultaneous detection. Thus, expression of comparable amounts of each SNARE compared to KC1 and between the different SYP1 proteins could be confirmed. The PonceauS stain served as control for the presence of equal amounts of total solubilised protein to base the comparison on (right hand panel). The predicted molecular weight for the three SNAREs (including tags) was slightly different (SYP121 ~ 41 kDa, SYP122 ~ 40 kDa, SYP111 ~38 kDa). This was reflected in the detected bands albeit in reverse to what might be expected, with SYP111 appearing to have the highest molecular weight according to the height of the band.

post-infection (24 h, 36 h, 48 h) (Fig. 38 , top panel). Total protein fractions were prepared exactly as described for KC1 (see above), with 0.5 % LPC as the solubilisation agent and incubation at 37 °C for 30 min prior to SDS-PAGE. As it was the case for KC1, recombinant SYP121 could then be detected as a single band of approximately the expected molecular weight (~41 kDa) employing an anti-FLAG against the N-terminal FLAG-tag (Fig. 38, top panel).When equal amounts of total solubilised SN were loaded per lane (compare PonceauS, Fig. 38, lower panel), the strongest signal for SYP121 was obtained from *Sf9* cells infected with 25 µl virus stock and harvested at 48 hpi. Virus amounts of less than 25 µl (15 µl or 7.5 µl) did not yield detectable amounts of recombinant protein within 24 h pi (Fig. 38, top panel, lane 6 and 9 from the left). However, the generally observed positive correlation between higher amount of virus particles for infection and greater yield of recombinant protein was found here as well (Licari & Bailey, 1991). When compared at individual time points, for example 36 h pi, infection with 7.5 µl, 15 µl or 25 µl resulted in progressively higher amounts of SYP121 (Fig. 38, top panel, lane 2,5 and 8 from the left). Similarly, increasing yield for SYP121 could be obtained with later time points of harvest after infection with any of those three virus titres. These results indicated that the point of saturating the host cell translation machinery is reached either at or beyond values of 25 µl virus stock and harvest at 48 h pi for an insect culture of similar age and cell density. As this point is to be avoided due to the potential absence of proper post- translational modifications (see above), *Sf9* cells were infected with 15 µl SYP121 virus stock and harvested 48 h pi for all future experiments. In summary, it was possible to confirm the absence of detectable protein degradation for both KC1 and SYP121. Furthermore, successful co-expression, co-extraction and co-solubilisation of both proteins with the same protocol and the same concentration of LPC could be achieved; an essential prerequisite to allow complex formation for Co-IP (see discussion below).

Similar to SYP121, optimal harvest time and amount of infectious virus were determined for expression of KC1, SYP122 and SYP111 (data not shown, but compare Fig. 39). As a result, the chosen time of harvest was 48 h after co-infection with 15 µl of SNARE virus stock (SYP121, SYP122 or SYP111) and 25 µl of KC1 virus stock for all further co-expression experiments detailed below. As shown by Western Blot in Fig. 39, these values were chosen to yield comparable protein amounts for all SNAREs (left panel, lower bands) and for each SNARE in relation to KC1 (left panel, upper bands) which was also an important point for Co-IP (see discussion below). Higher amounts of KC1 virus were probably needed to achieve protein amounts similar to the SNAREs in the same time frame, because the channel has almost double the molecular weight and is with six transmembrane domains a more complex protein. In Fig. 39, equal amounts of co-expression SN solubilised with 0.5 % LPC (compare PonceauS, right panel) were analyzed as a prerequisite for comparisons. Furthermore, the anti-His directed against the additional His-tags present in all four proteins (see Table 2) allowed direct comparison of protein expression levels that would not have been possible with the individual antibodies.

Sf9 cell disruption	detergent for solubilisation	solubilisation condition	detergent (c) for solubilisation (%)	detergent (c) for Co-IP (%)	Co-IP condition	Co-IP support	detergent (c) for wash buffer (%)	NaCl (c) of wash buffer (mM)	elution
sonicate, membrane fraction, 4°C	LPC	head over end rotation, 4°C, o.n.	LPC: 1, 0.5, 0.4, 0.3, 0.2, 0.1	LPC: 0.03; 0.05; 0.1; 0.2; 0.3; 0.5; 0.6; 0.8; 1	head over end rotation, 4°C, o.n.	anti-FLAG/ anti- Myc agarose conjugate (covalently bound)	LPC: 0.03; 0.05; 0.1; 0.2; 0.3; 0.5; 0.6; 0.8; 1	120	Pierce kit
27g needle, membrane fraction, 4°C	TritonX-100	head over end rotation, 4°C, 1 h	TritonX-100/ Tween20/ OGP/ Digitonin: 1	TritonX-100/ Tween20/ OGP/ Digitonin: 0.1	head over end rotation at RT for 1 h	Pierce Kit resin + anti-FLAG / anti-Myc (covalently bound)	TritonX-100/ Tween20/ OGP/ Digitonin: 0.1	130	Glycine-Hcl
	Tween20								
	OGP								
sonicate, whole cell lysate, 4°C	Digitonin		Digitonin/ NP-40: 1 + 1 mM NDSB	Digitonin/ NP-40: 0.1 + 0.1 mM NDSB		Sepharose G + anti-FLAG (affinity bound)	Digitonin/ NP-40: 0.1 + 0.1 mM NDSB	140	FLAG-peptide
pipetting, whole cell lysate, 4°C	NP-40		NP-40: 1	NP-40: 0.1		Sepharose A + anti-FLAG / anti-Myc (affinity bound)	NP-40: 0.1	150	2x SDS Sample Loading Buffer
	Digitonin +NDSB							180	
	NP-40 + NDSB							200	

Table 3 Overview of tested conditions to optimize Co-IP of KC1 and SYP121

This table indicates which and how individual steps were varied to find optimal conditions for the Co-IP between KC1 and SYP121. The cells shaded in light grey indicate the combination of parameters that proved most successful for this experiment (see M&M, p. 99). (c = concentration).

Optimization of Co-IP between KC1 and SYP121

The principle of a Co-IP is simple: If protein X is immunoprecipitated out of a cell homogenate with an antibody against X that is in turn captured on a solid support, e.g. agarose, then any protein Y that forms a stable complex with X in the lysate, may be co-immunoprecipitated via this interaction. Following a wash step that should eliminate unbound or non-specifically bound proteins, the components of the captured immune complex are eluted from the support. Subsequent SDS-PAGE and Western Blot allow detection of successfully co-immunoprecipitated protein Y by anti-Y. A total of about 50 experiments were required to find optimal conditions for the Co-IP between KC1 and SYP121. Table 3 provides an overview of which and how individual steps of the protocol were varied but not in what combination per experiment. However, a final set of successful experimental conditions was shaded in light grey and a detailed description of the protocol is given in M&M (p. 100).

Initial Co-IP experiments were performed with solubilisation SN (sSN) obtained as described for Fig. 39, i.e. after co-expression of SNARE and Shaker channel and co-solubilisation with 0.5 % LPC as detergent. The results pictured in Fig. 40 indicated successful and reciprocal co-precipitation between SYP121 and KC1. Here, the sSN from one batch of *Sf9* cells was divided into two parts and incubated with either anti-Myc-agarose (Fig. 40A) or anti-FLAG-agarose (Fig. 40B). The SN of this incubation was then removed ('flow-through', FT) before washing the agarose six times. Antibody-bound protein was eluted with acidic conditions (Glycine-HCl, pH 3.5) in two fractions that were loaded in total for SDS-PAGE. In contrast, protein of the FT and three wash fractions (wash 1, 3, 6) had to be concentrated via StrataClean^{TM} resin because the volumes exceeded the available capacity of the stacking gel wells. Subsequent Western Blot analysis with an anti-FLAG detected FLAG-SYP121 (~41 kDa) co-immunoprecipitated by KC1-Myc (that in turn had been captured on the anti-Myc-agarose) in both elution fractions (Fig. 40A, bigger red arrow). Compared to the signal from a sample of the sSN before incubation with agarose (Fig. 40A, lane 1), the resulting bands were of identical height, supporting that the protein in the elution fraction was the same as in the input. Additional signals for SYP121 appeared in FT and wash fractions (Fig. 40A, lane 4-6). This could have indicated either suboptimal conditions for the Co-IP itself (4 °C, over night) or an overload of protein compared to available anti-Myc that might have caused SYP121 or complexes between SYP121 and KC1 to bind unspecifically to either the agarose itself or the antibody. In principle, SYP121 in the wash fractions could also have been the result of too harsh wash conditions that might destroy true protein-protein interactions, but those were very mild here (120 mM NaCl, 0.1 % LPC, see below). Therefore, an unknown but small part of eluted SYP121 was considered the result of unspecific co-precipitation. The second band of higher molecular weight in both FT and elution fractions (Fig. 40A, smaller red arrow), represented most likely the heavy chains of co-eluted disassociated anti-Myc. In both the commercially available anti-Myc and anti-FLAG conjugates, used here as solid support, the antibodies are immobilized on cyanogen bromide activated agarose to actually avoid this effect. However, the manufacturer (SIGMA) states that the conjugation procedure never captures all antibody, so that

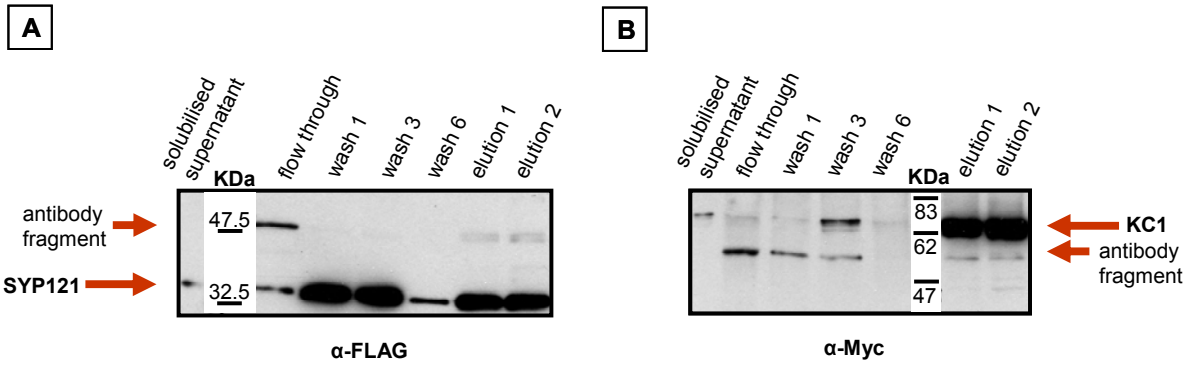

Fig. 40 KC1 and SYP121 co-immunoprecipitate reciprocally

Sf9 cells co-expressing KC1 and SYP121 were solubilised with 0.5 % LPC. Equal amounts of sSN were incubated with either anti-Myc-agarose (A) or anti-FLAG-agarose (B). The concentrated protein of the SN after Co-IP ('flow through') and three washes (wash 1, 3 and 6) as well as the total volume of two acid elution steps and a sample of the sSN before Co-IP were analyzed by Western Blot with an antibody against the respective putatively co-precipitated protein (anti-FLAG for SYP121 in (A); anti-Myc for KC1 in (B)). Although, as demonstrated by the detected signal in the elution fractions (bigger red arrows in A and B), in both cases specific co-precipitation occurred, the presence of some SYP121 protein in the last wash (wash 6) in (A) indicated that a fraction of the eluted protein was likely not bound by KC1 at the time of elution. In contrast, the last wash was free of KC1 in (B) supporting the assumption that all eluted protein had been bound specifically to SYP121. The second band detected by the antibodies in both Western Blots (smaller red arrows, A and B) represented most likely the heavy chain of co-eluted antibody fragments that occurred despite the covalent binding to the agarose.

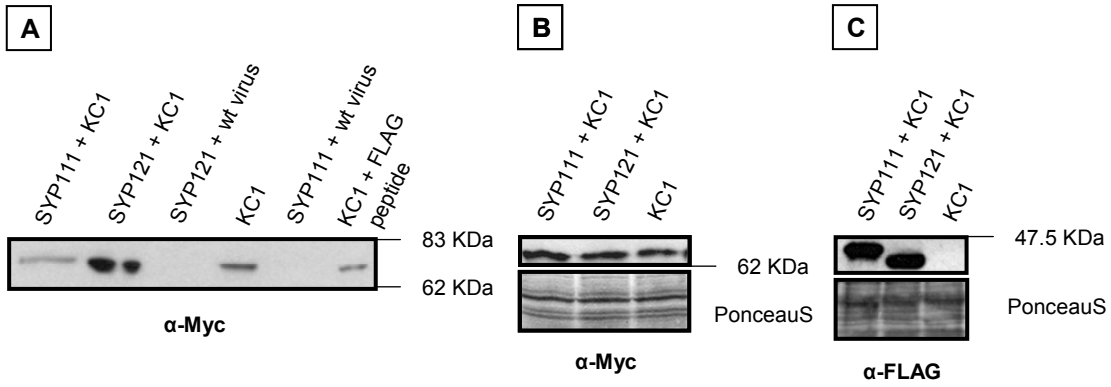

Fig. 41 Specificity of Co-IP between KC1 and SYP121

Co-IP was performed exactly as described for Fig. 40B. However, additional samples were analyzed as indicated above the panel in (A). Shown here is only the concentrated protein derived from five combined elution steps for each sample. Last washes were free of KC1 in all cases (data not shown). As seen in (A), a small quantity of KC1 was apparently precipitated by the control SNARE SYP111 (lane 1). Co-precipitation by co-expressed SYP121 yielded higher amounts of detected KC1 in the elution (A, lane 2). To allow comparisons between these two samples, it was determined before Co-IP that the sSN contained comparable amounts of SYP111 with regard to SYP121 by detection with anti-FLAG (C). Similarly, it was ensured that comparable amounts of KC1 were present in these samples by detection with anti-Myc (B). The absence of a signal after Co-IP with sSN co-expressing either SNARE with wt Baculovirus instead of KC1 confirmed that the protein detected by the anti-Myc was not an insect cell or virus derived protein (A, lane 3 and 5). Two further controls were included, where each had been incubated with identical amounts of anti-FLAG-agarose as for the previously described samples. The signal detected by the anti-Myc in (A, lane 4) was derived from Co-IP with a sSN of insect cells expressing only KC1 but in comparable amounts to the samples co-expressing a SNARE (B, lane 3). The signal detected in (A, lane 6) was derived from an identical sSN expressing only KC1 but mixed with a FLAG-peptide before Co-IP. The detection of a KC1 signal in these two controls revealed a problem of unspecific KC1 binding to the solid support, i.e. the agarose itself, that was most likely the reason for the KC1 apparently co-precipitated specifically by SYP111. Therefore, it was concluded that a similar fraction of the KC1 precipitated by SYP121 originated from the same event.

some is only associated with the agarose and might be co-eluted. In addition, the batch format of this assay made it impossible to always completely avoid the carry over of some agarose. When confronted with the harsh conditions of the SDS Sample Loading Buffer, some antibody molecules might have broken free despite the immobilization procedure. Furthermore, the reducing conditions of the SDS buffer are likely to destroy the disulfide bonds that connect the two identical heavy (50 kDa) and two identical light (25 kDa) polypeptide chains in the 'Y'-shaped antibody molecules. As both the anti-Myc coupled to the agarose and the anti-FLAG used for detection were raised in the same species (mouse), the secondary antibody (rabbit anti-mouse) reacts with those antibody fragments during Western Blot analysis. Such can account for the observed signals (~ 50 kDa) in this experiment (Fig. 40A) and the converse approach of co-precipitating KC1 with SYP121 on anti-FLAG-agarose (Fig. 40B, smaller arrow). For this approach, the experimental procedure was identical to the previously described Co-IP including the volume of used agarose (Fig. 40A). However, the same wash conditions were more successful here, as the precipitated sixth wash was free of unbound KC1 (Fig. 40B, lane 3-5). The absence of KC1 in the last wash supported the interpretation that all KC1-Myc, detected in the elution fractions by an anti-Myc, was specifically co-precipitated by SYP121 (Fig. 40B, bigger red arrow). According to the manufacturer, anti-Myc is immobilized to the agarose at a concentration of 1- 1.5 mg/ ml agarose, whereas the anti-FLAG-agarose contains 3.7 mg/ ml. The improved ratio of antibody to antigen input, the antigen being equal amounts of sSN in both Co-IP's, may have improved the efficiency of specific co-precipitation in case of the anti-FLAG-agarose (Fig. 40B). Another possibility could have been more effective antigen binding rather than higher antibody amounts. Apart from natural differences in the affinity of different antibodies for their epitope, less efficient KC1-Myc binding to the anti-Myc-agarose might occur because the position of the Myc-epitope at the C-terminus of KC1 was close to a site of interaction with SYP121 and the resulting steric interference impeded antibody binding. For these reasons, further optimization efforts focused on Co-IP's with anti-FLAG-agarose. Still, the ability to detect an interaction between KC1 and SYP121 by immunoprecipitating either protein in the complex, as demonstrated in Fig. 40, increased the level of confidence in the specificity and reciprocity of this interaction.

Further experiments, shown in Fig. 41, were carried out to include SYP111 as control for the specificity of the observed Co-IP between SYP121 and KC1. An identical experimental procedure was used as described for Fig. 40B. Again, Co-IP between KC1 and SYP121 was observed (Fig. 41A, lane 2). For this Western Blot (Fig. 41A), each lane was loaded with the concentrated protein (via StrataClean^{TM} resin) of five combined elution fractions from Co-IP samples as indicated above the panel. In contrast to previous experiments, more elution fractions were used to better assess the total amount of co-precipitated protein. Here, the anti-Myc revealed KC1 interaction also with the SYP111 control, albeit to a lesser extent than with SYP121 as evident from the signal strength (Fig. 41A, lane 1 and lane 2). Similar results were obtained in more than three repetitions (data not shown). A control experiment was able to exclude that the protein presumed to be KC1 co-precipitated by either SNARE, was actually un-specifically bound and detected insect cell or virus derived protein. When the Co-IP was performed on samples where

SYP111 or SYP121 had been co-expressed with wt Baculovirus instead of KC1, the anti-Myc yielded no signal in the eluates (Fig. 41, lane 3 and 5). Several other scenarios were considered here, that might have given rise to the unexpected co-precipitation between SYP111 and KC1. Under non-stringent conditions, the mbSUS too had shown a low level of interaction between KC1 and SYP111 (see Fig. 22, p. 122). This interaction disappeared with the reduction of bait protein expression, and was thus interpreted as over-expression artefact. Since proteins under the control of the polyhedrin promoter are similarly over-expressed in *Sf9* cells, Co-IP between KC1 and SYP111 might have been driven by the resulting non-physiological interactions as well. In this context, mammalian SNARE proteins frequently were found to be promiscuous in Co-IP experiments (Fasshauer *et al.*, 1999; Bethani *et al.*, 2007). Another issue related to protein expression that could lead to misinterpretation of co-precipitated protein in terms of true interaction might be the effect of differences in protein input. For example, more KC1 co-expressed with SYP121 than with SYP111 might falsely indicate stronger interaction after Co-IP even though in both cases the same amount of interaction with KC1 took place. Conversely, more co-expressed SYP121 than SYP111 might form more complexes with KC1 to same misleading effect. Therefore, it was ensured before the actual Co-IP that equal amounts of SYP111 to SYP121 as well as the same amount of KC1 co-expressed with both SNARE's were present in the sSN. This was achieved by using *Sf9* cells of identical age and raised with identical volumes of parent culture that were infected with the optimized ratios of the respective virus stocks as described above (compare Fig. 39). Subsequently, sSNs were analyzed by Western Blot prior to the Co-IP. When equal amounts of solubilised SNs for SYP111 + KC1, SYP121 + KC1 and KC1 alone were used (compare PonceauS stains in Fig. 41B and Fig. 41C), the anti-Myc detected comparable amounts of KC1 in all three samples (Fig. 41B) and the anti-FLAG showed the same for SYP111 in relation to SYP121 (Fig. 41C). In addition, it was ensured that the KC1 detected as co-precipitated by SYP111 was not a result of insufficient wash conditions as observed for Fig. 40A. The concentrated last wash was free of KC1 for all samples shown in Fig. 41 (data not shown). Having thereby excluded these two possibilities as explanation for a possible interaction artefact between KC1 and SYP111, the additional controls in this experiment revealed the reason most likely to be responsible. When solubilised SN containing KC1 expressed on its own was incubated with the same volume of anti-Flag-agarose as the co-expressed samples, unspecific binding of KC1-Myc to this support was observed with a signal strength comparable to that of the apparent SYP111- KC1 interaction (Fig. 41A, lane 3). This would suggest that either the agarose itself or its immobilized anti-FLAG had an unspecific affinity for KC1-Myc that was strong enough to resist the washing conditions. In fact, even monoclonal antibodies, such as the ones used here, frequently interact with proteins that are distinct from the antigen. Furthermore, in Western Blot analysis, it has been observed, that a primary antibody, for which no specific target is blotted on the membrane, will bind to the most abundant protein present in a kind of forced cross-reactivity. Therefore, one could argue that incubating an excess of KC1-Myc with anti-FLAG-agarose might create such an artefact and was therefore not a good control for the SYP111 + KC1 situation. However, blocking the specific antigen binding sites of the anti-FLAG with an excess of FLAG peptide before adding the KC1 containing solubilised

SN in the same volume as before, did not significantly reduce the amount of non-specifically precipitated KC1 (Fig. 41A, lane 6). From this observation it followed that most likely the agarose itself was the component that bound KC1-Myc non-specifically. In conclusion, this artefact of the experimental conditions was in all probability also responsible for the KC1 that first appeared to be specifically co-precipitated by SYP111. Furthermore, it will have constituted a part of the KC1 that was co-precipitated in the SYP121 + KC1 co-expression sample. However, based on the strategy of equal protein input and sample handling during Co-IP, the greater part of this precipitated KC1 must be considered as a result of specific KC1-SYP121 interaction. Nevertheless, removal of this unspecific background was needed to entirely confirm the specificity of KC1 interaction with SYP121 over the closely related control SNARE protein SYP111.

As the nature of the non-specific association between KC1-Myc and the agarose was unknown, e.g. whether hydrophilic or hydrophobic interactions were involved, more stringent wash and/ or Co-IP buffer conditions were tried in the first place. In general, both higher salt concentrations and higher concentrations of an ionic (or zwitterionic) detergent are more disruptive to interactions that rely on charged residues, e.g. ionic interactions between proteins. They are usually employed with the expectation, that a non-specific protein association is of weaker nature than a specific one and therefore more easily disrupted. However, such a compromise of conditions that left the KC1-SYP121 interaction intact but at the same time disrupted non-specific KC1 binding to the solid support could not be achieved here (for explored changes in NaCl and LPC concentrations compare Table 3). In all cases, where more than 140 mM salt and/ or LPC concentrations above 0.3 % were used in either Co-IP or wash buffer, both the interaction between KC1 and SYP121 and non-specific binding to the agarose were abolished (data not shown).

To approach the problem from another direction, i.e. the prevention of non-specific binding of KC1-Myc rather then its reduction, three different strategies were tested (separately or in different combinations with the changed salt and LPC conditions mentioned above). Firstly, the anti-FLAG-agarose was incubated with 4 % BSA prior to Co-IP. This small protein might in theory bind non-specifically to the sites that would otherwise interact with KC1 and thus block KC1 attachment to the agarose during Co-IP. The Co-IP itself was performed with the reduced amount of 1 % BSA to support this effect but avoid interference with specific binding. However, this strategy was not successful (data not shown). In addition, an attempt to ‘pre-clear’ the sSN of non-specific KC1-Myc binding to the solid support failed. For this purpose, the sSN was incubated before the Co-IP with an analogue of the agarose unconjugated to antibody (data not shown). Finally, different solid supports were tested. However, an amine-reactive gel to which one can covalently cross-link an antibody of choice (ProFound^{TM} Co-IP Kit, Pierce) displayed some non-specific KC1-Myc binding as well that could not be improved by either of the above described methods (data not shown). In contrast, sepharose immobilized to Protein G (SepharoseG) proved free of non-specific KC1-Myc binding. When incubated with solubilised KC1-Myc under the same Co-IP conditions as in Fig. 41, Western Blot analysis employing anti-Myc detected no bands in the concentrated last wash or elution fraction (Fig. 42, lane 3 and 4). Furthermore, after the addition of

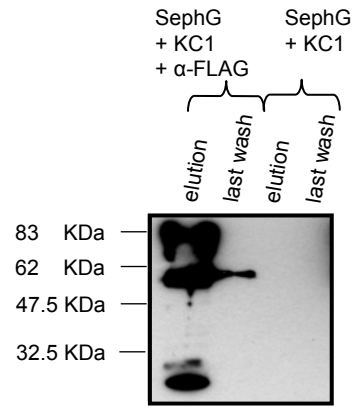

Fig. 42 Suitable solid support for Co-IP

After a mock Co-IP experiment where solubilised KC1-Myc was incubated with either SepharoseG (SephG) or SepharoseG together with affinity bound anti-FLAG, the anti-Myc detected no non-specifically bound KC1 in the concentrated elution or last wash fraction of either sample. The bands that appeared in the elution and last wash fraction of the containing experiment were a result of co-eluted anti-FLAG that was either in its intact form (75 kDa) or dissociated in heavy (50 kDa) and light chains (25 kDa).

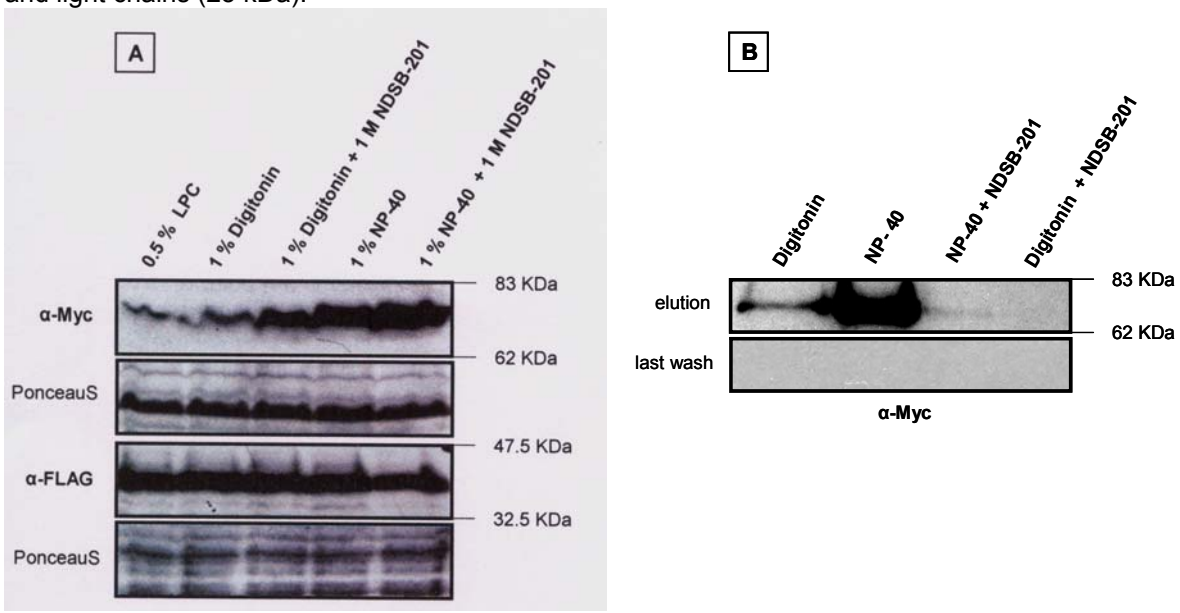

Fig. 43 Different non-ionic detergents for co-solubilisation and Co-IP of KC1 and SYP121

The non-ionic detergents Digitonin and NP-40 were used, either alone and in a concentration of 1 % or with the addition of 1 M NDSB to solubilise KC1 co-expressed with SYP121 in five individual batches of *Sf9* cells; as indicated above the top panel in (A). When compared to the solubilisation efficiency of 0.5 % LPC, none of these nonionic detergent conditions improved the amount of solubilised SYP121 detected by anti-FLAG after Western Blot analysis (A, panel 3). As indicated by the PonceauS corresponding to this Western Blot, equal amounts of total sSN for each sample had been loaded to allow comparison of solubilisation efficiency (A, panel 4). In contrast, all four conditions that employed a nonionic detergent proved more efficient for the solubilisation of KC1 than 0.5 % LPC as shown by Western Blot analysis with anti-Myc (A, panel 1 and corresponding PonceauS stain in panel 2). The addition of 1 M NDSB improved the yield of solubilised KC1 for both Digitonin and NP-40 when compared to the use of these two detergents alone. Both 1 % NP-40 and 1% NP-40 plus 1 M NDSB was more efficient than the respective Digitonin treatment. However, Co-IP experiments with equal volumes of the different sSN obtained for (A) revealed that the addition of 1 M NDSB completely or almost entirely prevented Co-IP between KC1 and SYP121 when combined with either nonionic detergent (B, panel 1, lane 3 and 4). Co-IP appeared more efficient with 1 % NP-40 compared to 1 % Digitonin (B, panel 1, lane 1 and 2). However, as equal volumes of the different sSN (A) were used, this might in part reflect the overall higher solubilisation efficiency of NP-40 for KC1. The precipitated proteins of the last wash were analyzed by anti-Myc for all these Co-IPs as well (B, panel 2). No KC1 was detected, confirming the specificity of KC1 precipitation by SYP121.

anti-FLAG to this mock Co-IP, still no signal of a molecular weight expected for KC1-Myc was observed (Fig. 42, lane 1 and 2). This confirmed the absence of unspecific interaction with the anti-FLAG itself. The detected bands in the elution and wash fraction corresponded to co-eluted anti-FLAG in its intact form (75 kDa) and dissociated into heavy chains (50 kDa) and light chains (25 kDa). This phenomenon was encountered earlier for anti-FLAG-agarose (see Fig. 40, p. 159). However, it was much more prominent compared to the previously tried solid supports. This was a consequence of the being attached to the sepharose only by affinity not covalently. ProteinG of SepharoseG binds to the Fc (Fragment, crystallisable) region of antibodies, i.e. to the base of their 'Y'-shaped molecules. Here, the acidic conditions of the elution buffer broke this affinity bonds easily and the entire amount of used antibody was co-eluted.

In parallel to the search for a suitable solid support, it was attempted to prevent non-specific KC1-Myc binding by using a different kind of detergent for solubilisation and Co-IP. Nonionic detergents for example, due to their chemical nature, may reduce non-specific binding that relies on the affinity of hydrophobic regions to each other (see discussion). As they do not interfere with charged residues as both salt and zwitterionic detergents such as LPC do, non-ionic detergents potentially allow more stringent wash conditions as well. Three common non-ionic detergents, i.e. TritonX-100, Tween-20 and n-octyl-ß-D-glucopyranoside, proved ineffective for the solubilisation of KC1 if not the SNAREs (data not shown). However, NP-40 and Digitonin, especially in combination with the component NDSB (Non-Detergent Sulfobetaine) were suitable for solubilisation of both KC1 and SNARE proteins. For the experiment shown in Fig. 43A, five *Sf9* insect cell cultures of the same age and started with identical amounts of parents cells, were infected to co-express KC1 and SYP121. Protein extraction and solubilisation procedure for these five cultures varied from previous experiments only in the types and concentration of detergents used, as indicated above the top panel. When identical amounts of sSN (compare PonceauS, Fig. 43A, panel 2 and 4) were used in Western Blot analysis with both anti-Myc to detect KC1 (Fig. 43A, panel 1) and anti-FLAG to detect SYP121 (Fig. 43A, panel 3), all five solubilisation methods proved equally efficient for SYP121 as indicated by the very similar signal strength obtained with the anti-FLAG. In contrast, all four conditions that employed a nonionic detergent proved more efficient for the solubilisation of KC1 than 0.5 % of the zwitterionic LPC (Fig. 43A, panel 1). Furthermore, the addition of 1 M NDSB improved the yield of solubilised KC1 in combination with both Digitonin and NP-40 when compared to the use of these two detergents alone. In addition, both 1 % NP-40 and 1% NP-40 plus 1 M NDSB was more efficient for the solubilisation of KC1 than the respective Digitonin treatment. NDSBs are zwitterionic compounds but unlike detergents they are not able to form micelles even at concentrations as high as 1 M.

Despite the ability to solubilise KC1 even more effectively than 0.5 % LPC, not all these detergent conditions were at the same time suitable for a successful Co-IP between the Shaker channel and SYP121. The different sSN analyzed in Fig. 43A, were used in equal volumes for Co-IP with identical amounts of SepharoseG/ anti- FLAG and with the experimental conditions shaded in grey in Table 3. Western Blot with an anti-Myc confirmed the absence of all KC1 in the concentrated last wash fraction (Fig. 43B, panel 2). The Western Blot analysis of the concentrated

total elution fractions indicated that under the same Co-IP and wash conditions NP-40 and Digitonin without NDSB supported Co-IP between KC1 and SYP121 (Fig. 43B, panel 1, lane 1-2). In contrast, the presence of the zwitterionic NDSB abolished this interaction when combined with Digitonin and NP-40, probably due to their ability to disrupt protein-protein interactions (Fig. 43B, panel 1, lane 3-4). Co-IP appeared more efficient with 1 % NP-40 compared to 1 % Digitonin (Fig. 43B, panel 1, lane 1 and 2). However, as equal volumes of the different sSN (A) were used, this might in part reflect the overall higher solubilisation efficiency of NP-40 for KC1.

Subsequent Co-IP's were performed with 1 % NP-40 and the above described SepharoseG. Further details of the final optimized protocol can be found Table 3 (shaded in grey) and in M&M (p. 100). The experiment pictured in confirmed that these optimized experimental parameters were suitable both not to harm the interaction between SYP121 and KC1 prove its specificity. The concentrated total elution fractions of Co-IP with samples co-expressing KC1 with either SYP121 or SYP111 showed after Western Blot analysis with anti-Myc that only SYP121 precipitated KC1, not SYP111 (Fig. 44, lane 1-2). At the same time, the concentrated last wash fractions for both samples were free of unbound KC1 supporting the conclusion that all eluted protein had been precipitated specifically (Fig. 44, lane 3-4). The presence of comparable amounts of SYP121 to SYP111 as well as comparable amounts of KC1 in both samples was confirmed in each solubilised SN before Co-IP (Fig. 44B and C). The absence of Co-IP between co-expressed KC1 and SYP111 taken together with this important control could thus verify, that the apparent interaction between SYP111 and KC1 detected in Fig. 41, relied solely on the problem of unspecific KC1 binding to the solid support. Therefore, this Co-IP experiment could confirm the specific interaction between full-length SYP121 and KC1 co-expressed in *Sf9* insect cells.

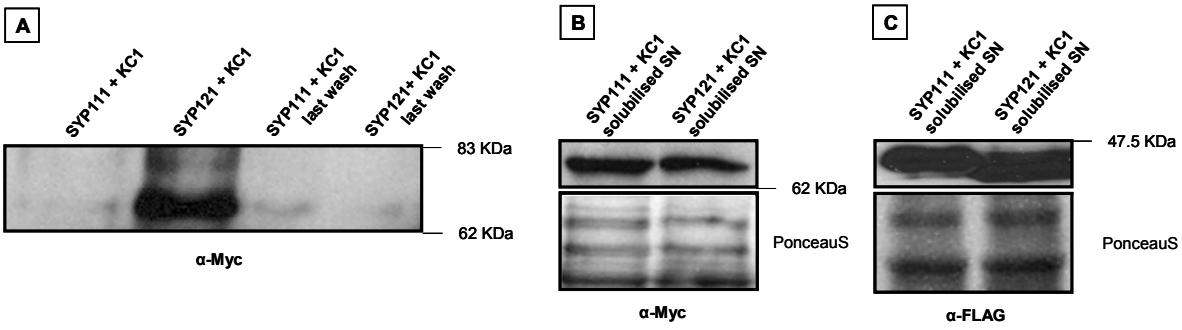

Fig. 44 Specific Co-IP between KC1 and SYP121

Sf9 cell cultures co-expressing KC1 with either SYP121 or SYP111 were solubilised with 1 % NP-40. Solubilisation SNs were analyzed by Western Blot before Co-IP to ensure equal amounts KC1 in both samples (B) and equal amounts of both SNAREs (C). Solubilisation and Co-IP conditions were as indicated in light grey in Table 3 and SepharoseG with affinity bound anti- FLAG was used as solid support. The precipitated last wash fraction was free of KC1 for both samples (A, lane 3 and 4). Under these conditions, KC1 was specifically co-immunoprecipitated by SYP121 but not SYP111 (A, lane 1 and 2).

Solubilisation of KC1 with LPC

Optimal, i.e. total solubilisation of a membrane protein is achieved at the so-called saturation point, where the protein is part of a pure detergent micelle without lipids. Following the above described three stage model (p. 147) for solubilisation of artificial membranes, this point, i.e. stage III, should be reached when a detergent is used in an amount that corresponds to its CMC (critical micelle concentration). However, the chemical nature of the more than hundred different lipid species that biological membranes can be composed of, as well as ionic strength, pH and temperature of the solubilisation buffer change the amount of detergent that is needed to reach its CMC in a way that is too complex to be predictable (Kalipatnapu & Chattopadhyay, 2005; van Meer *et al.*, 2008). Therefore, in practice, no more precise approach to determine the amount of detergent needed for solubilisation of a specific membrane protein exists than monitoring the process over a range of detergent concentrations (Banerjee *et al.*, 1995; Kalipatnapu & Chattopadhyay, 2005) as it was done here for solubilisation of KC1 from *Sf9* cell membranes with LPC (Fig. 36).

Western Blot had suggested that 0.5 % LPC was the detergent concentration that solublilised KC1 most efficiently, as higher LPC concentrations (1 %, 1.5 %) did not yield a stronger signal from the same amount of insect cell membranes (Fig. 36A, bottom panel). However, this observation was not the reason, why 0.5 % LPC was chosen as detergent concentration for the initial Co-IP experiments. As discussed in more detail below, total solubilisation, while preferable in terms of yield, may prove fatal for the purpose of Co-IP where the membrane proteins need to be preserved in as native a confirmation as possible. Total solubilisation at the saturation point (see above) is achieved in practice, when for a given amount of membrane material, increasing detergent concentrations no longer yield higher amounts of total solubilised protein (Banerjee *et al.*, 1995).

The Western Blot technique used here was only able to indicate that at 0.5 % LPC maximal amounts of KC1, not total membrane proteins, appeared solubilised (not considering the limited sensitivity in detection that might have masked small improvements between different detergent concentrations). In contrast, a true solubilisation rate, as published by Urbach *et al.* (2000) for the LPC-dependent solubilisation of KAT1 from *Sf9* cell membranes, takes into account the total amount of protein before and after solubilisation in comparison to the amount of solubilised target protein determined e.g. by ELISA. Therefore, a solubilisation rate shows very accurately the most effective detergent concentration to solubilise a target protein, which is not necessarily identical to the detergent concentration that solubilises the most membrane proteins. Meaning, individual detergent concentrations might be more effective for the solubilisation of a specific target protein such as KC1 compared to solubilisation of all the other insect cell and virus membrane proteins that occurs at the same time or vice versa. For example, Urbach *et al.* (2000) concluded that the concentration of 1 % LPC was most effective for KAT1 solubilisation, even though 1.5 % LPC slightly (~5 %), increased the solubilisation rate, i.e. the total amount of membrane proteins

solubilised from a fixed amount starting membrane material. Western Blot can reflect a changing ratio of total solubilised protein to solubilised target protein as long as equal amounts of total solubilised protein are analyzed (instead of identical total volumes of sSN). Such was assured here by amidoblack assay and PonceauS stain (Fig. 36A).

However, as the total amount of protein material before solubilisation compared to after solubilisation was not taken in account for Western Blot, this technique could not indicate the saturation point, where all membrane proteins are stripped of lipids and present in pure detergent micelles. Many publications reported cases, in which replacing the specific lipid microenvironment of a membrane protein with detergent molecules during solubilisation negatively affected the native protein structure (Johansson *et al.*, 2009). With respect to lipid–protein interactions in membranes, three different classes of lipids can be distinguished (Levy *et al.*, 1990). Class 1 comprises so called 'annular' lipids which surround membrane proteins or protein complexes on the outside and mediate the contact between lipid bilayer and protein. Lipids of class 2 ('non-annular surface lipids') are bound at specific positions on the surface of the protein and are typically situated between proteins e.g. at contact faces between different protein subunits of a holo-complex. In contrast, class 3 lipids are integral components of proteins. They bind in the interior of a protein, often in unexpected positions and orientations relative to the membrane plane but in close contact with the proteins. Tightly bound class 3 lipids were found in several high-resolution membrane protein crystal structures confirming their role as important modulators of membrane protein confirmation (Prive, 2007). In addition, the involvement of membrane lipids in maintaining membrane protein function that depends on native confirmation could be observed. Displacement of lipids from the receptor was the cause for detergent-induced inactivation in case of the mammalian nicotinic acetylcholine receptor (Jones *et al.*, 1988) and the hippocampal 5-HT1A receptor, where it was linked to loss of membrane cholesterol (Chattopadhyay *et al.*, 2005).

It is not possible to predict whether it makes a difference for the successful solubilisation of a specific membrane protein or protein complex in its native state, if any of the three classes of lipids is compromised by replacement through a specific detergent. However, in general, it is suggested that co-solubilisation of specific protein–lipid complexes at lower detergent concentrations might be more desirable than trying to remove lipids as completely as possible from the membrane proteins and obtain pure detergent–protein micelles (Kalipatnapu & Chattopadhyay, 2005). In addition, lower detergent concentrations might prove beneficial not only for the maintenance of important lipid-protein but also protein-protein interactions. Although in part influenced by the type of detergent (ionic, non-ionic, zwitterionic, see below), in general, higher detergent concentrations lead more easily to denaturation, i.e. loss of native confirmation by affecting also intra-or-inter-protein interactions. Membrane proteins solubilised by the zwitterionic LPC are generally found to be in their biologically active, non-denatured form (Egelandsdal *et al.*, 1991; Wang *et al.*, 1993). For example, size-exclusion chromatography has provided evidence that the tetrameric structure of *At*KAT1 and *At*AKT1 remained intact after solubilisation with 1- 1.5 % LPC. This result strongly suggested that the native conformation of the subunits and the holo-complex was not affected by this detergent and in the applied concentration (Urbach *et al.*, 2000).

This success rate is considered in part due to the fact that LPC is not an artificial detergent. Lysophospholipids are natural, if minor, constituents of all biological membranes where they serve to stabilize membrane structure (Maneri & Low, 1988). The stabilizing effect is derived from both the saturated fatty acids moiety and the zwitterionic head group (Maneri & Low, 1988).

In summary, the Western Blot in Fig. 36A, p. 151 (bottom panel) had indicated that 0.5 % LPC was most effective for KC1 solubilisation over solubilisation of general insect cell membrane proteins. However, as this technique did not allow determining the saturation point, the LPC concentration which is potentially harmful to native KC1 confirmation as all lipids are removed could not be determined, i.e. avoided. Similarly to the unknown extent to which the lipid microenvironment around KC1 was replaced by detergent monomers at 0.5 % LPC, it remained unclear, whether this detergent concentration might already affect negatively important intra-protein interactions.

A direct way of assessing the preservation of native confirmation in 0.5 % LPC would be an *in vitro* functional assay with the solubilised KC1. However, as KC1 is an electrically silent Shaker channel subunit this can not be accomplished easily (see General Introduction, p. 13). In theory, it might have been possible to reconstitute co-expressed and co-solubilised AKT1 and KC1 in artificial membranes such as liposomes and perform electrophysiological measurements. In practice no such attempt has ever been published for *Arabidopsis* Shaker channels so far and for this work would already have encountered the additional complication of partial AKT-VSVG degradation during solubilisation (compare Fig. 37, p. 151).

The reason that 0.5 % LPC was nevertheless chosen as the initial standard condition for solubilisation prior to Co-IP was connected to the aggregation phenomenon described in Fig. 36A. In general, membrane protein aggregation during solubilisation can be caused by a number of factors, e.g. an unsuitable type or amount of detergent. Although not mentioned so far, KC1 aggregation and the subsequent formation of white precipitates was also observed during changes in Co-IP and wash buffer conditions designed to avoid the problem of non-specific KC1-Myc binding to the solid support (data not shown). Whenever the final LPC concentration dropped below 0.05 %, KC1 aggregation occurred. Urbach *et al.* (2000) had reported the same effect of LPC dilution below 0.05 % on both AKT1 and KAT1. In this context, other authors suggested that to extensive removal of detergent promotes membrane protein aggregation as the mutual affinity of now exposed hydrophobic regions towards each other causes them to cluster (Chabre & le Maire, 2005). Other contributing factors are the loss of membrane mimicking effects such as lateral pressure, exclusion from water, topological constraints and alkyl chain packing, that detergent molecules should provide for a protein in its solubilised state (White & Wimley, 1999; Booth, 2005; Bowie, 2005).

Especially the lateral pressure generated within lipid bilayers is thought to stabilize integral membrane proteins in their native environment (Marsh, 1996; deKruijff, 1997). The so-called lateral pressure profile in membranes is created by the chemical properties of the phospholipids. Owing to surface tension, their hydrophilic headgroups and hydrophobic core acyl chains strive to minimise their contact area, thus generating strong negative pressure, i.e. pulling forces acting

laterally along the interfacial regions on both sides of a lipid bilayer. This tension is balanced by positive lateral pressure, i.e. pushing forces arising in the both headgroup and acyl chain regions in part from steric clash. Furthermore, electrostatic repulsion between charged headgroups and stiffening of lipid acyl chains, which incurs an entropic penalty, contributes to positive lateral pressure. It was proposed that the loss of lateral pressure would allow insufficiently solubilised membrane proteins to assume a wider range of conformational states (Engel *et al.*, 2002). Intermolecular collisions between membrane proteins with partially unfolded structure would then lead to kinetically trapped aggregates. In a similar way, the aggregation of soluble proteins was shown to occur from folding or unfolding intermediates rather than from native or fully unfolded proteins (Mitraki & King, 1989).

KC1 aggregation was observed not only after dilution of LPC, but also after boiling the solubilisation SN with SDS Sample Loading Buffer (SLB) prior to SDS-PAGE (Fig. 36A, p. 151). Aggregation in this situation is a rather common phenomenon for highly hydrophobic membrane proteins (Kerkhoff *et al.*, 2000; Ramsay *et al.*, 2002; Medina *et al.*, 2004). Heat induced aggregation has been reported, for example, for a bovine vesicular monoamine transporter with 12 predicted TMDs after solubilisation in the nonionic detergent NP-40 (Sagne *et al.*, 1996). The formed aggregates were remarkably stable and resistant to dissolution by even higher SDS concentrations. The authors (Sagne *et al.*, 1996) suggested that this aggregation was a consequence of secondary and tertiary structures which the protein retained in the presence of SDS (as ingredient of SLB).

In principle, SDS denatures membrane and soluble proteins alike (Otzen, 2002). For soluble proteins, e.g. serum albumin, interaction with SDS comprises different phases. Starting at concentrations below the CMC, detergent monomers bind to the protein at discrete sites in a reaction that is cooperative (Jones, 1992). The binding of one molecule of SDS increases the probability that another one will bind until, at higher detergent concentrations, a saturation value is reached that is relatively constant in the region of 1.2- 1.5 g/g protein (Takagi *et al.*, 1975). Thus, in theory, at the saturation point, proteins have a similar negative charge independent of their molecular weight and are completely denatured and unfolded so that their length is proportional to their molecular weight and separation on a SDS-PAGE can occur according to it. (There are two models for the complexes formed thereby between SDS and protein- the older view of rigid rods and the more recent so-called necklace model, where spherical SDS micelle-like structures are distributed like pearls along the extended polypeptide backbone (Samso *et al.*, 1995).

In contrast to soluble proteins, many membrane proteins demonstrably retained a significant amount of their native structure in SDS suggesting that this detergent is less effective at denaturing integral membrane proteins (Prive, 2007). For example, in case of lactose permease, the secondary structure or more precisely the α-helical content of transmembrane domains, was found mostly preserved in SDS micelles (Reynolds & Tanford, 1970; Mattice *et al.*, 1976; Viitanen *et al.*, 1986). Unfolding studies with bacteriorhodopsin indicated the preservation of even tertiary structure at high SDS concentrations with only a small change in the distance between the helices B and F (Huang *et al.*, 1981; Valluru *et al.*, 2006). Stable dimers of GPCRs (delta-receptors) were

observed in even 10% SDS buffer (Jordan & Devi, 1999).

These results are potentially linked to the fact that for membrane proteins, denaturation and unfolding by SDS is connected to either direct solubilisation from membranes or the presence of lipid-mimicking detergents before addition of SDS. While in the latter case, it has been shown that the result is the formation of mixed detergent micelles and subsequent denaturation of higher ordered membrane protein structure, the exact nature of these denaturation events is still enigmatic (Anbazhagan *et al.*, 2010). For the application of SDS to solubilise a protein from membranes directly, Kragh-Hansen *et al.* (1998) demonstrated that the mechanism is different to the one described above (p. 166). These authors were able to show on *in vitro* reconstituted Ca^{2+}-ATPase containing membranes that SDS monomers start out by specific binding to the protein rather then surrounding lipids. This led to cooperative unfolding and release of Ca^{2+}-ATPase before solubilisation of the lipid components. Kragh-Hansen *et al.* (1998) further suggested that this aggressive behaviour is due to the ability of SDS to bind to polar and non-polar residues in proteins. It was also observed that this SDS-binding occurs in the same concentration range and is very similar to its described attack on soluble proteins (Reynolds & Tanford, 1970; Hawkins *et al.*, 2005).

As mentioned above, in case of the monoamine transporter that been solubilised with NP-40 and boiled in SDS containing SLB buffer, Sagne *et al*. (1996) had suggested that such remaining secondary and/ or tertiary protein structures after SDS addition could ultimately be the reason for the observed aggregation. More precisely, the subsequent exposure of these remaining structures to conditions also known to disrupt protein structure, such as heating, would create a situation as described above for general aggregation of proteins. Meaning, partially unfolded intermediates would be more populated as the intra-protein interactions supporting those residual structures are further destroyed by heat. Intermolecular interactions of complementary proteins parts would take place instead, which would then result again in the formation of aggregates (Sagne *et al.*, 1996).

It was speculated here, that a similar situation as was observed for the monoamine transporter could explain KC1 aggregation. If that was the case, it would mean that in all three LPC concentrations tested (Fig. 36, panel 1, p. 151), SDS did not completely unfold the channel when the SLB was mixed with the solubilised SN. Thus, when subsequently incubated at 98 °C, the heat would have induced aggregation as described above. At 37 °C, the same residual structures after addition of SDS should have been present. However, at this temperature, KC1 did not form aggregates independent of the LPC concentration (Fig. 36, panel 3). Low temperature is a condition that favours compact, low energy states of detergent-solubilised membrane proteins and therefore enhanced protein stability (Reisinger & Eichacker, 2008). Hence, as opposed to boiling, no further unfolding of residual structures would have taken place and no aggregation was observed.

It remained the question about the situation at 60 °C, where higher LPC concentrations for initial solubilisation resulted in reduced KC1 aggregation. Again, it can only be speculated about the contributing factors of which one, however, was most likely the LPC concentration, as it was the only difference between the samples. As discussed above, solubilisation with higher detergent

concentrations is in general more denaturating towards membrane proteins because it is more likely that specific protein-bound lipids are removed that are needed to support the native structure and /or important protein-protein interactions are destroyed.

Differential scanning calorimetry, a technique very sensitive to conformation perturbation, was used to investigate the effect of LPC on myosin filaments (Egelandsdal *et al.*, 1991). Myosin itself is a soluble protein, but was used in this study as a membrane protein model, because hydrophobic interactions maintain the associated state (filaments). These authors indeed detected an increased degree of protein denaturation in higher concentrations of LPC (> 21 mM= ~1%). Furthermore, as observed here for KC1, they reported a steady decrease in aggregation with increasing amounts of LPC at higher temperatures (80 °C). Egelandsdal *et al*. (1991) attributed this result to LPC being a sufficiently strong solubilizer of the denatured state to prevent extensive aggregation.

One could speculate that the situation for KC1 was similar. Accordingly, with increasing LPC concentrations between 0.5 and 1.5 %, KC1 would progressively denaturate. However, as for myosin, aggregation did not take place because the hydrophobic domains were protected by LPC. After mixing with SDS, less residual structure remained, as it was 'pre-denatured' by LPC, and therefore, less aggregation due to fewer partial unfolding intermediates could occur at 60 °C.

As discussed before, without the possibility of a functional assay or other specialised methods such as the one used by Egelandsdal *et al*. (1991), it is not possible to determine, how affected the native structure of KC1 solubilised with different initial LPC concentrations really was in each case. However, if the previous assumptions were correct, one could have concluded from this experiment that LPC concentrations where no or less aggregation was observed at 60 °C, i.e. 1 % and 1.5 %, were not desirable for Co-IP as KC1 was initially denatured by LPC to a greater extent. In fact, testing for irreversible protein aggregation to assess the structural integrity of a solubilised membrane protein is recommended by some authors even if a direct functional assay is possible. They argued that even in cases where some activity can be measured, lower levels of aggregation indicating disrupted native structure for a certain fraction of the target protein may be masked (Prive, 2007). In conclusion, 0.5 % LPC appeared to be a promising compromise between the most efficient KC1 solubilisation and a detergent concentration at which the channel was least likely to be denaturated.

Co-expression and co-solubilisation of KC1 and SYP121

Co-IP of membrane proteins, in contrast to soluble ones, requires for the putative interaction partners to be co-expressed in order to allow complex formation. Hence, co-solubilisation of KC1 and SNAREs was necessary and had to be optimized (Fig. 38, p. 155; Fig. 39, p. 155). Separate expression and independent solubilisation would more likely lead to situations, where each protein would be present in its own detergent (or detergent-lipid) mixed micelle instead.

Within those micelles, detergent molecules are distributed as a uniform band about the protein surface, with their alkyl chains binding to the hydrophobic transmembrane domains in a

belt-like manner (see Fig. 35, p. 147) (Lemaire *et al.*, 1983). Single crystal neutron diffraction studies were able to visualise these detergent 'rings' in membrane protein crystals of the *Rps. viridis* photosynthetic reaction centre (Roth *et al.*, 1989) and the *E. coli* OmpF porin (Pebaypeyroula *et al.*, 1995). These studies showed that the hydrophilic parts of a solubilised membrane protein 'stick out' above and below its detergent belt. They face the aqueous environment, where they contribute to the formation of hydrogen bonds and electrostatic interactions with water molecules that keep the detergent-protein complex in solution (Lemaire *et al.*, 1983; Pebaypeyroula *et al.*, 1995). Picturing this, one could perhaps still imagine interactions between the hydrophilic parts of two such separated membrane proteins to be possible, while any contribution specific hydrophobic bonds between the two partners might add would definitely be prohibited by this detergent ring. In fact, the contacts between hydrophilic surfaces of two such solubilised proteins establish the crystal lattice during membrane protein crystallisation (Ostermeier & Michel, 1997).

However, the choice of detergent determines if those polar contacts can be realised during crystallisation, as the size and shape of the detergent 'belts' influence the close approach between the hydrophilic surfaces of their incorporated proteins. The size and shape of the detergent rings in turn, as for a pure detergent micelle, depends on the type, size, concentration and stereochemistry of the detergent monomer as well as the solvent environment (pH, ionic strength, etc.), and the protein itself (Dolder *et al.*, 1996). A detergent ring of large physical size for example, as formed by detergent molecules with long alkyl chains, can disturb the establishment of polar protein-protein contacts during crystallisation by acting as a steric physical barrier. Also, large polar head groups of detergent monomers are more likely to interact with the membrane protein polar surface and thereby block protein- protein interactions. In addition, the repulsion between similarly charged head groups of detergent molecules in a micelle will be equally present between the detergent surfaces of adjacent micelles.

Even if the chosen detergent would allow polar contacts between two solubilised proteins, the situation during crystallisation is very different from a normal solubilisation such as performed here. An appropriate precipitant is needed that drives the protein-detergent complex/ solvent system into a state of reduced solubility, where a certain degree of supersaturation will be attained and polar contacts between neighbouring molecules can be established or in other words the hydration shells get disrupted around the detergent micelles, enabling them to merge into extensive lattices (Wang & Kuhlbrandt, 1991). In the absence of such a precipitant, it is assumed that the hydration shells that keep two micelles apart can not be overcome to allow stable complex formation of interacting proteins. Those forces are also the reason why two detergent micelles do not easily merge with each other; another scenario that one might imagine to allow protein interaction after independent solubilisation of two putative protein complex partners. Only under certain conditions, for example the high local detergent concentration (20- 30 %) that can occur during the crystallisation process, micelles can deform and fuse together to form more complex macromolecular structures (Pebaypeyroula *et al.*, 1995). Micelle fusion was observed in the crystals of the *Rhb. spheroides* photosynthetic reaction center (Roth *et al.*, 1989) and presented

evidence that a bilayer-like detergent continuum is formed in the trigonal crystal of a *Rps. capsulatus* porin-detergent complex.

Hence, independent of the question whether LPC was a detergent that would physically (e.g. alky chain length) allow the formation of polar protein-protein contacts between individually solubilised membrane proteins, such as in this case the putatively interacting hydrophilic parts of KC1 (N- and C- terminus) and SYP121 (N- terminus), it was assumed that no interaction could take place under the conditions employed here for Co-IP. For this reason, individual expression and solubilisation is often used as negative control for the co-expression of putative protein complex partners in Co-IP experiments. Homo- and hetero-oligomerization between different members of the superfamily of mammalian GPCRs for instance, was observed only in solubilised lysates from co-transfected cells and not in mixed solubilised lysates from singly transfected cells (Jordan & Devi, 1999; Salim *et al.*, 2002). Both groups concluded that co-expression of these membrane proteins (seven predicted TMDs) in the same *Sf9* insect cell, was a major prerequisite for the physiological assembly of dimeric GPCRs. Similar results were obtained here for KC1 and SYP121 co-expression versus individual expression (data not shown).

For these reasons, it was necessary to assure that 0.5 % LPC would be as effective for SYP121 (or SYP111) as for KC1 during co-solubilisation (see Fig. 38, p. 155). As discussed for KC1, connected to this issue was the question if this detergent concentration might have had a negative effect on the native confirmation of the SNAREs. Similar to the situation for KC1, there was no easily accessible functional assay for solubilised SNAREs to answer this question. One possibility might have been *in vitro* SNARE complex formation. This has been investigated to a great extend for mammalian SNAREs, but is experimentally complex. In contrast to KC1, no aggregation of SYP121 or SYP111 was ever observed. Neither boiling in SDS containing SLB after solubilisation, nor diluting the LPC concentration to less than 0.05 % caused aggregation (data not shown). In addition, as seen also in Fig. 43 (p. 163) for different detergent types, detergent concentrations that were sub-optimal for KC1 solubilisation, proved maximal efficient for solubilisation of SYP121 (data not shown). Both features, easy solubilisation and lack of aggregation, were likely due to the considerable lower ratio of hydrophobic to hydrophilic domains that SNARE proteins with one TMD have when compared to Shaker channels with six TMDs. In support, Spatz *et al.* (1971) had observed that rabbit cytochrome b5, although firmly integrated into phospholipid bilayers, was soluble in aqueous solution after removal of detergents. They had speculated that this is probably also the case for other tail-anchored proteins, such as syntaxins. Due to this lack of aggregation, speculations about the native protein structure of SNAREs in 0.5 % LPC in analogy to KC1 were not possible. Nevertheless, the fact that Co-IP between KC1 and SYP121 could be achieved supported the assumption that this detergent concentration had not affected the native confirmation of either protein to an extent that would disrupt complexes during co-solubilisation (Fig. 40, p. 159).

However, as discussed for interaction in the mbSUS assay (p. 123), the observed Co-IP between KC1 and SYP121 could potentially have been an artefact caused by over-expression that might have forced crowded proteins in the insect cell membranes to interact. Over-expression was

high in the *Sf*9- Baculovirus system for proteins under the control of the polyhedrin promoter (see p. 145). As discussed earlier, co-expression levels for KC1 and the two SNAREs were adjusted to be equal and reproducible between experiments to control this effect as much as possible (see p. 161, Fig. 39, p. 155; Fig. 41, p. 159; Fig. 44, p. 165).

Specific Co-IP between KC1 and SYP121

After co-expression and co-solubilisation, Co-IP protocols in general recommend reducing the detergent concentration to allow efficient binding of the antibody coupled to the solid support to its antigen carried on one protein partner. The extent to which this dilution takes place must be a balance between allowing capture on the solid support and possible negative effects of too strong dilution such as membrane protein aggregation (e.g. for KC1 in LPC concentrations below 0.05 %, see above) and unspecific binding to the solid support and/ or its antibody. As discussed above, reducing the detergent concentration below a certain threshold might expose hydrophobic parts of the membrane proteins that could cause unspecific binding such as the observed KC1-Myc binding to the solid support (see Fig. 41, p. 159). For the experiment in Fig. 41, controls had indicated that after co-expression of KC1 and SYP111, KC1 binding to the solid support occurred independent of the control SNARE, i.e. that no interaction between these two proteins took place prior to co-solubilisation. Nevertheless, although less likely, the formation of unspecific complexes between KC1 and SYP111, perhaps due to the strong over-expression (see above), could not entirely be excluded by these controls. Similarly, it could not be excluded that during this experiment a smaller part of the KC1 that had appeared specifically co-precipitated by SYP121, represented in fact unspecifically bound KC1 to the solid support. Such unspecific KC1 might have been in complex with SYP121, in which case the purpose of Co-IP would not have been defeated. In contrast, not all co-expressed KC1 and SYP121 might have formed complexes during co-expression or co-solubilisation at 0.5 % might have disrupted a smaller part of KC1-SYP121 interactions, separating the proteins into different micelles. In both cases, unspecific KC1 binding would have mimicked specific Co-IP between KC1 and SYP121. As indicated in the results (p. 162), suitable detergent and/ or other buffer component concentrations (e.g. NaCl) that would have allowed completely specific capture on the solid support could not be found for experiments with LPC and the used solid support. Lower LPC concentrations (0.3 - 0.05 %) did either not entirely prevent unspecific KC1 binding or caused protein precipitation (data not shown). Higher LPC (0.3- 1 %) and/or higher NaCl concentrations prevented Co-IP possibly by preventing antigen binding to the antibody on the solid support or disrupting KC1-SYP121 interactions with putative redistribution into separate micelles (data not shown).

These results had prompted the change to a solid support that for unknown reasons did not bind KC1-Myc unspecifically under the same experimental conditions as in Fig. 41, p. 159). Furthermore, in parallel, a different type of detergent for solubilisation was tried (see Fig. 43, p. 163). While LPC is a zwitterionic detergent, NP-40 and Digitonin are of the nonionic class of detergents.

Based on the nature of their hydrophilic head group, detergents can be broadly classified as ionic, nonionic, or zwitterionic. Ionic detergents contain a head group with a net charge that can be either negative (anionic detergent, e.g. SDS) or positive (cationic detergent). In contrast, nonionic detergents possess uncharged, hydrophilic head groups that consist of either polyoxyethylene moieties as in TritonX-100 and NP-40 or glycosidic groups as in e.g. octyl glucoside. Zwitterionic detergents such as LPC contain both a cationic and an anionic group in the same molecule resulting in the absence of a net charge. In general, throughout the different classes of detergents, there is a correlation between the size and chemical properties of the head group with the ability of a detergent to solubilise a membrane protein or protein complex without affecting important structural features (Lund *et al.*, 1989). The larger the head group the milder the detergent (Cacace *et al.*, 1997). A similar correlation exists for the alkyl side chain volume. Detergents from one homologous series with longer alkyl chains (C12–C14) are milder than the ones with short alkyl chains (C7–C10) (Cacace *et al.*, 1997). Also, detergents with nonionic headgroups are usually better suited for breaking lipid-lipid and lipid-protein interactions than protein-protein interactions as they mainly interfere with hydrophobic interactions (Speers & Wu, 2007). In contrast, in the presence of ionic detergents, such as SDS, most proteins and protein complexes are found denatured/ separated after solubilisation, as the detergent disrupts mainly hydrophilic protein–protein interactions. Their advantage lies in a much more efficient solubilisation as a result of these properties (Kragh-Hansen *et al.*, 1998; Speers & Wu, 2007). Zwitterionic detergents are unique because they offer the combined properties of ionic and nonionic detergents yet both in a moderated form. They are in general more efficient solubilisers than nonionic detergents. However, increased solubilisation is mostly based on an increase in the release of protein–protein interactions (as their charged headgroups interfere with the interaction of charged protein residues) which renders them more denaturating (Seddon *et al.*, 2004; Speers & Wu, 2007).

It was speculated that successful co-solubilisation of the KC1-SYP121 interaction with a nonionic detergent might later allow for detergent dilution conditions during Co-IP and washes that would be more supportive to antigen-antibody dependent capture to the solid support while preventing unspecific interactions with the solid support. As antigen-antibody binding relies on hydrophilic protein-protein interactions rather than hydrophobic lipid-protein interactions, higher concentrations of a nonionic rather than zwitterionic detergent might have been tolerated better for this purpose. In addition, the ability of a nonionic detergent to interfere with hydrophobic interactions might have reduced unspecific KC1 binding that relied on the affinity of exposed hydrophobic regions. Similarly, as nonionic detergents are less likely to denature proteins, the overall risk of exposing hydrophobic domains and disrupting the KC1-SYP121 interaction at higher detergent concentrations was considered reduced compared by solubilisation with the zwitterionic LPC. This was most likely the reason why Co-IP after co-solubilisation with 1 % NP-40 was successful (Fig. 43, p. 163; Fig. 44, p. 165) while co-solubilisation with 1 % of LPC prevented Co-IP (data not shown). Similarly, the inclusion of the zwitterionic component NDSB during solubilisation with 1 % NP-40 (or 1 % Digitonin) prevented subsequent Co-IP (see Fig. 43). NDSB do not form micelles, because their hydrophobic part is too small. Nevertheless, their

zwitterionic nature allows the attack of ionic protein-protein interactions similar to LPC. Thus, again, this feature was most likely responsible for both improved solubilisation efficiency and prevention of Co-IP observed in Fig. 43.

A combination of the improved conditions for solid support, co-solubilisation, Co-IP and washes allowed the detection of a specific interaction of KC1 with SYP121 over the control SNARE Syp111 (see Fig. 44, p. 165; Table 3, grey fields). It was further attempted to employ the control SNARE SYP122 under these conditions. However, initial experiments revealed a certain amount of Co-IP between KC1 and SYP122. This result was perhaps not surprising considering the higher degree of similarity between SYP121 and SYP122 (see Fig. 14A, p. 52) in combination with the strong over-expression in this system. For this work, no further optimization of this situation was attempted (e.g. by choosing to express at lower levels as discussed previously, see p. 152ff.).

In conclusion, the results presented in this chapter verify a direct interaction between KC1 and SYP121. The various experimental controls discussed above, were necessary to avoid the detection of artefacts that the Co-IP system is prone to, as can be seen in some of the initial results. In addition, the ability to achieve Co-IP between KC1 and SYP121 after solubilisation with different detergents, contributed to the high level of confidence in these results. Interaction of KC1 with SYP121 was further specific over the control SNARE SYP111, which was in agreement with the results obtained in the mbSUS system. As for the mbSUS assay, it was not possible to verify the converse specificity of SYP121 for KC1 over the related Shaker channel subunits AKT1 and KAT1. Both control Shaker subunits could not be expressed in a satisfactory quality, i.e. a high level of degradation appeared to take place and initial Co-IP experiments failed. In addition, the expressed proteins could only be solubilised with high concentrations of LPC, a condition that was most likely disruptive to protein interaction with SYP121, as discussed for KC1 above.

Chapter 3: BiFC analysis of KC1-SYP121 interaction

Introduction

Although viable information was gained from investigating the interaction of KC1 and SYP121 *in vitro* (Co-IP) and *in vivo* (mbSUS), both techniques rely on heterologous over-expression, a situation that might not accurately represent the native cellular environment of the two *Arabidopsis thaliana* proteins. Therefore, an important step to further verify and investigate the significance of the interaction of these two proteins for *Arabidopsis* was the study of their complex formation *in planta*. As detailed in the introduction (p. 12ff.), this technique is widely used for soluble proteins in both plants and animals. Although interaction between some membrane proteins was shown (p. 12ff.), BiFC is generally not used in the publications that concern interactions of mammalian SNAREs and ion channels. Therefore, at the time, this was the first attempt at using BiFC to prove such an interaction for *Arabidopsis* proteins *in planta*.

Results

Vector design and construct preparation for BiFC assay

At the time, the available vectors for plant BiFC allowed fusions of the YFP halves only to the C-terminus of a protein of interest (Walter *et al.*, 2004). Therefore, their vectors, i.e. pSPYCE-35S (containing the C-terminal half of YFP) and pSPYNE-35S (containing the N-terminal half of YFP) had to be modified. The modification steps that resulted in two vectors allowing N-terminal split-YFP fusions to tail-anchored SYP1 syntaxins instead are pictured and described in detail in M&M (see p. 101ff.). The new vectors were named pN-SPYCE-35S and pN-SPYNE-35s. Subsequently, a number of constructs with C- and N-terminal fusions of SNAREs and KC1 were cloned into the four vectors as described in detail in Material and Methods (see p. 101ff.). Shown Fig. 45 are the constructs that were selected from among those for the BiFC experiments shown in this chapter and the combinations in which they were used for co-transformation. Repeated attempts to clone KAT1 or AKT1 with C-terminal or N-terminal FP halves were unsuccessful.

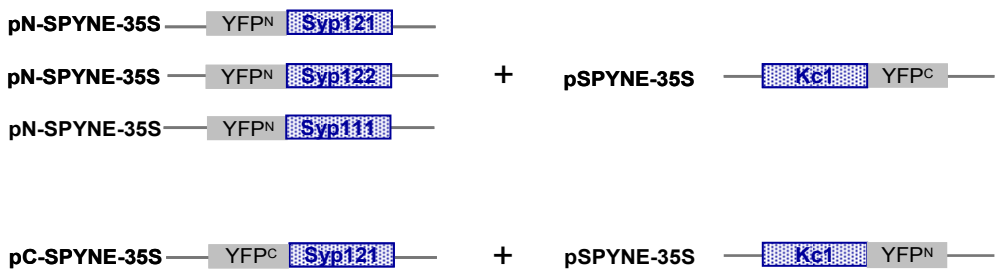

Fig. 45 Constructs for BiFC experiments

The above shown fusions of YFP-halves to the N-terminus of the three syntaxins, SYP121, SYP122, SYP111 and the C-terminus of KC1, respectively, were used in co-transformation experiments as indicated to obtain BiFC.

BiFC assay for the interaction of KC1 and SYP121

For initial BiFC experiments, onion epidermis bombardment was chosen as an easily transformable transient plant expression system with very low auto-fluorescent background. Two plasmids visualizing the homodimerisation of the basic leucine zipper (bZIP) transcription factor bZIP63 fused to YFP fragments served as positive control for the co-transformation technique (Walter *et al.*, 2004). Fig. 46d shows the detection of the resulting BiFC-YFP signal in the nucleus as expected from the previous publication (red arrow, compare bright field) (Walter *et al.*, 2004). An additional signal appeared in the cell periphery, which is most likely an artefact due to the extreme over-expression characteristic for this technique (Sambrook & Russell, 2006). Co-transformation of YFP^N-SYP121 (N-terminal half of YFP fused to N-terminus of SYP121) and KC1-YFP^C (C-terminal half of YFP fused to C-terminus of KC1) yielded an YFP signal in highly mobile punctuate structures located along the cell periphery (data not shown, but compare Fig. 46a). Onion bombardment with an AKT1-GFP fusion resulted in a signal of similar mobility and location (data not shown, but compare Fig. 46b, c). After simultaneous co-transformation with all three constructs highly mobile small dots labelled with both GFP and YFP indicated co-localisation of KC1, SYP121 and AKT1 (Fig. 46c, red arrows). However, these structures moved too fast to be captured in two-channel confocal scan images, since fluorescence in the second channel always appeared shifted. Therefore, although co-localisation of KC1, SYP121 and AKT1 seemed only partial in Fig. 46c, there was very likely a higher degree of uniformity in co-localisation present in the cell (compare pattern of both signals). The expected subcellular localisation of *Arabidopsis* AKT1 was the PM (see p. 13). Therefore, it appeared that this Shaker channel was miss-localised in onion cells, possibly as a consequence of over-expression under the strong constitutive promoter of the 35S RNA of the Cauliflower mosaic virus (35S) and the bombardment technique. The above described experiment that is pictured in Fig. 46a-d was repeated three times to show the reproducibility of the obtained results. Additional experiments were performed. These included observation at an earlier time point (24 h instead 36 h), where heterologous proteins presumably are less expressed and the use of less total plasmid DNA (2.5 µg instead of 5 µg). However, the results remained unchanged (data not shown). Nevertheless, BiFC was achieved for KC1 and SYP121, which also confirmed the functionality of the newly designed vector pN-SPYNE-35S.

To avoid the potential over-expression artefacts of the onion bombardment technique, transient *Agrobacterium*-mediated transformation of tobacco via leaf infiltration was attempted. No BiFC was observed for co-infiltration of YFP^N-SYP121 and KC1-YFP^C (data not shown). Similarly, the combination of YFP^C-SYP121 and KC1-YFP^N was unsuccessful (data not shown). Co-infiltration with the 35S-driven p19 protein of tomato bushy stunt virus, that enhances transient expression via suppression of gene silencing, did not improve these results (Voinnet *et al.*, 2003). Detection at different times after infiltration (24 h, 36 h, 48 h, 72 h) or co-infiltration with various ratios (OD_{600} nm) of *Agrobacterium tumefaciens* carrying KC1 and SYP121 constructs did not result in the detection of a BiFC signal either (data not shown). A total of 20 experiments were performed to include all the conditions described above. The positive control (bZIP63) yielded

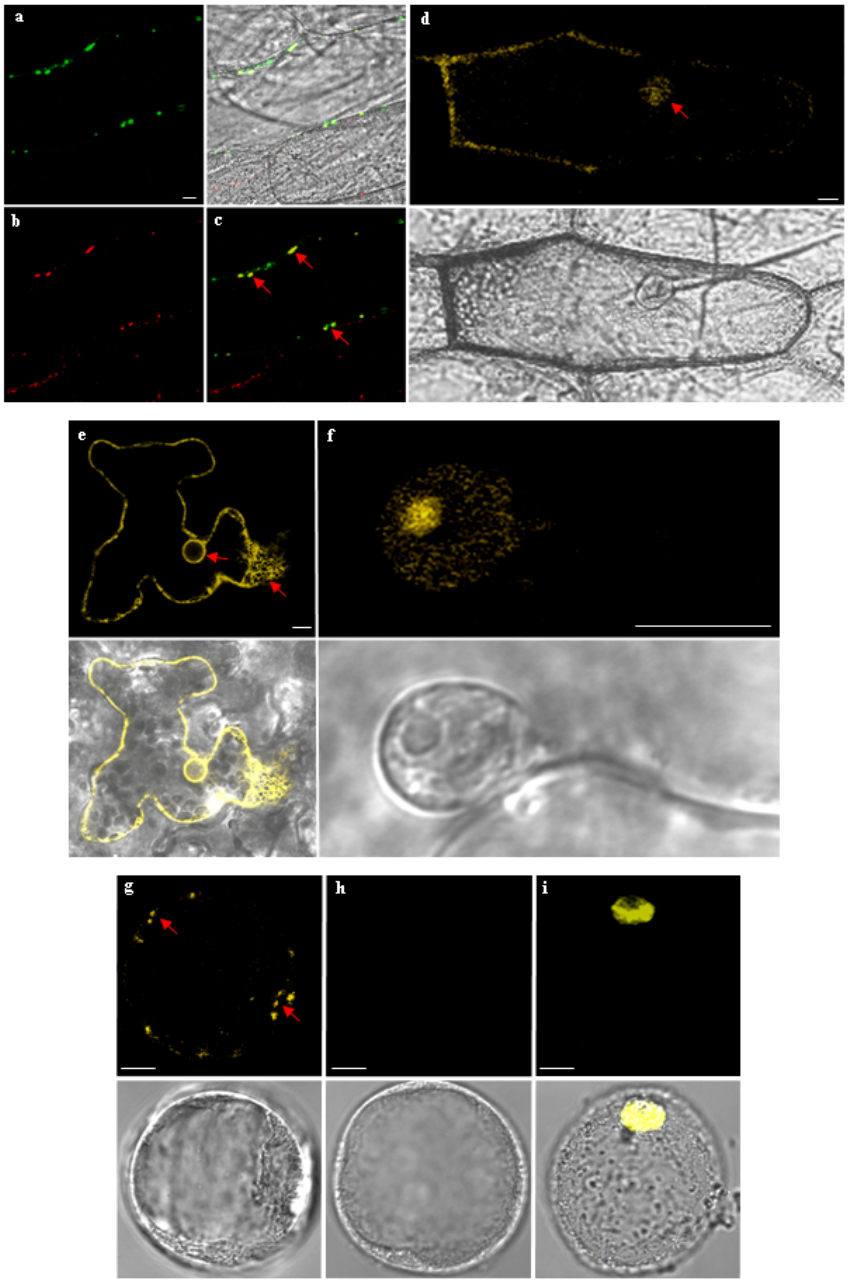

Fig. 46 BiFC experiments in different plant expression systems

Images show transient co-expression of YFP^N-SYP121 and KC1-YFP^C constructs in onion epidermis cells after particle bombardment (a) and in *Arabidopsis* protoplasts derived from a dark adapted cell culture and transformed with the PEG method (g). In both cases, BiFC signal indicating KC1-SYP121 interaction, appeared in a punctuate pattern. Punctuate structures were highly mobile in onion cells (imaged after 36 h) but immobile in protoplasts (imaged after 24 h). In onion cells, an AKT1-GFP fusion was found in similar mobile punctuate structures (b) that co-localised with the KC1-SYP121 BiFC signal (c); very likely to a higher degree than indicated here (see text). As positive control for the co-transformation event needed for BiFC in each of the employed techniques, BiFC constructs for homodimerization of the basic leucine zipper (bZIP) transcription factor bZIP63 fused to YFP fragments were used (Walter *et al.*, 2004). The bZIP63 BiFC signal was detected in nuclei after onion epidermis bombardment (d), transient *Agrobacterium* mediated transformation of tobacco leaves (f) and in transformed protoplasts (i) respectively. Water transformed protoplast (h) were imaged with identical confocal settings as (g) to demonstrate the absence of autofluorescence under these conditions. Miss-localisation, most likely driven by over-expression, led to an additional signal for the bZIP63 control in the onion cell periphery. Miss-localisation of KC1 to the ER in tobacco leaf cells (e) was the suspected cause for the inability to detect BiFC with SYP121 in this expression system. Brightfield images are provided for each data set (right hand side or below). White scale bar: 10 µm

again the expected nuclear YFP signal, confirming the suitability of the experimental procedure (Fig. 46f). Expression of KC1 as a fusion to full-length YFP (KC1-YFP) yielded fluorescence within the nuclear envelope and a dynamic reticulate network both indicative of typical plant ER structures (Staehelin, 1997) (Fig. 46e, red arrows). This result was reproduced three times. Previously published work and predictions of subcellular localisation indicated that KC1 should be a PM protein as the other members of the Shaker family in *Arabidopsis* (Reintanz *et al.*, 2002; Very & Sentenac, 2003). Here, it appeared to miss-localise to the tobacco ER after over-expression under the 35S promoter. A later publication confirmed this observation (Duby *et al.*, 2008).

As mis-localisation might also be due to heterologous expression, *Arabidopsis* transient expression systems were tested as alternative approach to tobacco leaf infiltration. *Arabidopsis* leaf infiltration and leaf bombardment did not yield promising or reproducible data (data not shown).

Subsequently, an *Arabidopsis* mesophyll cell suspension culture was established and dark adapted to reduce background fluorescence derived from chlorophyll autofluorescence. Protoplasts derived from these cells were transformed with the PEG method. Again, the bZIP63 control yielded fluorescence in the expected nuclear localisation (Fig. 46i). In contrast, after co-transformation with plasmid DNA for YFP^N-SYP121 and KC1-YFP^C, protoplasts only occasionally displayed a punctuate peripheral pattern of YFP fluorescence (Fig. 46g). BiFC signals obtained for KC1-SYP121 interaction were weak but still above background fluorescence as seen in comparison to pictures taken with identical confocal settings of protoplasts transformed with water (Fig. 46h). Even though immobile, the punctuate structures were reminiscent of the observations in onion cells. After a total of 15 experiments, *Arabidopsis* protoplast transformation was abandoned because of low co-transformation rates.

Instead, a new technique for transient *Arabidopsis* root transformation was employed that a former member of Prof. Blatt's laboratory, Dr. Campanoni, had just developed (Campanoni *et al.*, 2007). This technique is characterised by a simple co-cultivation of 3- 5 d old *Arabidopsis* seedlings with the *Agrobacterium rhizogenes* strain MSU440 in liquid medium. With this technique, BiFC was obtained after co-transformation with YFP^N-SYP121 and KC1-YFP^C (Fig. 47a). It was observed that co-cultivation with mid-log phase (OD_{600} of 0.8- 1.0) *Agrobacterium* cultures generally yielded optimum results. To give an impression of the obtained signal strength, it is estimated here on the base of experience that the expression of soluble YFP under the same conditions would need half the laser transmission output (9 % instead of 18 %, see M&M, p. 89) to produce an image with similar apparent YFP signal strength. Co-transformation with the alternative combination of YFP^C-SYP121 and KC1-YFP^N also yielded an YFP signal (Fig. 47c). However, signal strength for this latter combination was generally just above the fluorescence background obtained from the control of *Arabidopsis* roots co-cultivated with only the untransformed *Agrobacterium* (Fig. 47b). The pictures presented Fig. 47a-c (and Fig. 47e-g) are representative three-dimensional projections from confocal fluorescence image stacks. To allow quantification of BiFC-YFP fluorescence signals, such images were taken with identical confocal microscope settings, including laser strength, zoom and depth of z-stacks (for more details see M&M, p.89). Furthermore, all seedlings originated from the same experiment and a standard region of the root

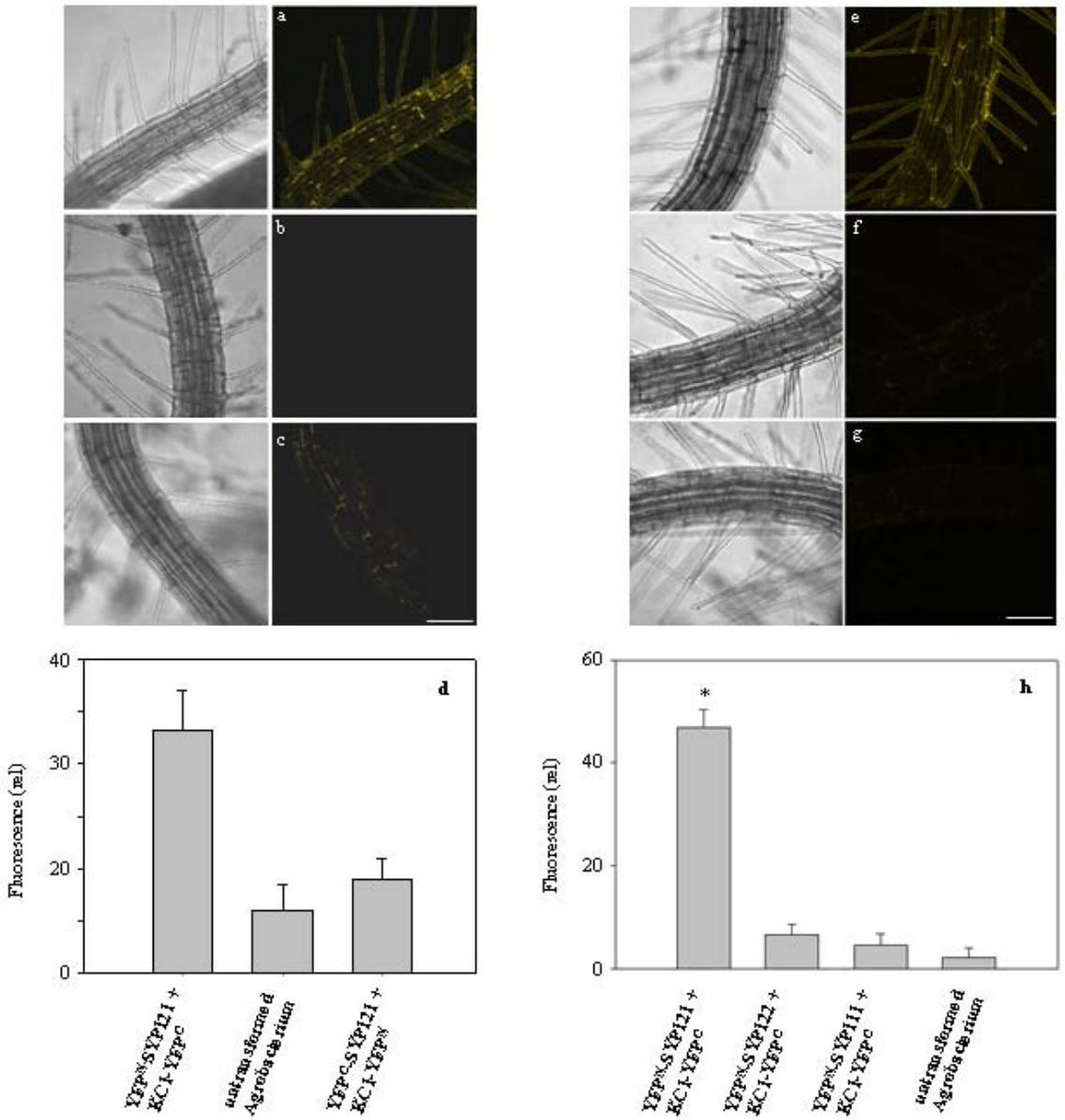

Fig. 47 BiFC experiments after transient *Arabidopsis* root transformation

Arabidopsis thaliana Col0 seedlings (3-5 d old) were imaged after 72 h of co-cultivation with *Agrobacterium rhizogenes* MSU440 that were transformed with the constructs indicated below. Pictures are three-dimensional projections from confocal fluorescence image stacks of seedlings that co-expressed (brightfield left, fluorescence right): YFP^N-SYP121 + KC1-YFP^C (a, e), YFP^C-SYP121 + KC1-YFP^N (c), YFP^N-SYP122 + KC1-YFP^C (f) or YFP^N-SYP121 and KC1-YFP^C (g). Untransformed *Agrobacterium* was used as control in the co-cultivation procedure (b). Fig. 47a-d and Fig. 47 e-h represent separate experiments. To allow quantification of BiFC fluorescence, images for each experiment were taken with identical confocal microscope settings, including zoom and depth of z-stacks and, as a standard, from the root hair maturation zone, where both root hair cells and non-hair cells were transformed. The quantification was summarised in (d) and (h), respectively, as relative mean fluorescence intensities (arbitrary units, ± Standard Error, n= 6 independent plants) after correction for background of plants not incubated with *Agrobacterium*. The results confirmed the specific interaction of KC1 with SYP121 over the control SNAREs SYP122 and SYP111 as indicated by BiFC YFP fluorescence (h). The YFP halves were positioned in all employed fusion constructs at the N-terminus of SYP121 and the C-terminus of KC1, respectively. However, the BiFC signal was reduced approx. by half when the C-terminal half of YFP was used in the N-terminal fusion to SYP121 (YFP^C-SYP121) instead of the corresponding N-terminal FP half (YFP^N-SYP121) (d). * indicates significant difference from the empty control at $P < 0.01$; white scale bar: 50 µm

was imaged (mature root hair zone). The quantification was summarised Fig. 47d (and similar Fig. 47h) as relative mean fluorescence intensities after correction for background fluorescence derived from seedlings that were incubated without *Agrobacterium*. Highly similar results were obtained in a total of 10 experiments. In summary, BiFC between KC1 and SYP121 could be observed with this technique. The fluorescent signal appeared in a subcellular localisation that indicated equal distribution along the cell periphery rather than the punctuate pattern observed in onion cells and Arabidopsis protoplasts (see below). Furthermore, the results pictured in Fig. 47a-d showed that attaching the N-terminal half of YFP to SYP121 (YFP^N-SYP121) and its C-terminal half to KC1 (KC1-YFP^C) rather than vice versa yielded a much more pronounced BiFC signal. Therefore, the same arrangement of N-and C-termini of YFP was used in further experiments that included the control SNAREs SYP122 and SYP111. YFP fluorescence obtained after co-transformation of KC1-YFP^C with either YFP^N-SYP122 (Fig. 47f, h) or YFP^N-SYP111 (Fig. 47g, h) was significantly reduced compared to the BiFC signal after co-transformation with YFPN-SYP121 (Fig. 47e, h) and not much stronger than fluorescence obtained from the control with untransformed *Agrobacterium* (Fig. 47h).

Subcellular localisation of BiFC signals for KC1-SYP121 interaction

Campanoni *et al.* (2007) demonstrated that their transient transformation technique targets specifically the root epidermis. Within the root epidermis, BiFC fluorescence for KC1-SYP121 was observed mainly in the root hair zone in both trichoblasts (root hair cells) and atrichoblasts (non-hair cells) alike (Galway *et al.*, 1994). Furthermore, the majority of root hairs displaying YFP fluorescence were mature root hairs as opposed to growing ones. In mature root hairs, a specific BiFC signal appeared in an uniform distribution at the cell periphery (Fig. 48a2) when compared to mature root hairs of control plants co-cultivated with the untransformed *Agrobacterium* (Fig. 48a1) under the same cofocal settings. The corresponding brightfield images in Fig. 48a1 and Fig. 48a2 show *Agrobacterium* surrounding the root hair (red arrow, Fig. 48a2). When young growing root hairs displayed a BiFC signal, it was located in addition to the cell periphery in the very tip in a cap-like structure (red arrow, Fig. 48a3). As Fig. 48b illustrates, the region of the very tip in root hairs consists of cytoplasm and at this point clearly separates the PM from the tonoplast (TP). Therefore, the peripheral located BiFC signal in mature root hairs was interpreted as most likely to represent the PM, whereas in young hairs an additional subcellular localisation was labelled.

The absence of YFP fluorescence in the cytoplasmic region of mature root hairs, co-expressing KC1 and SYP121 BiFC constructs, was further demonstrated in Fig. 48c. Shown are single plain images from the very tip of a transformed root hair, taken at the indicated intervals and over a time period of 60 seconds (s). In this series of pictures the cytoplasmic streaming of a living root hair can be observed in the brightfield (right hand). The cytoplasm is discernable as a more dense grey matter in the very tip at 31 s (red arrow). The corresponding confocal image (left hand) confirmed the lack of BiFC signal in this subcellular localisation.

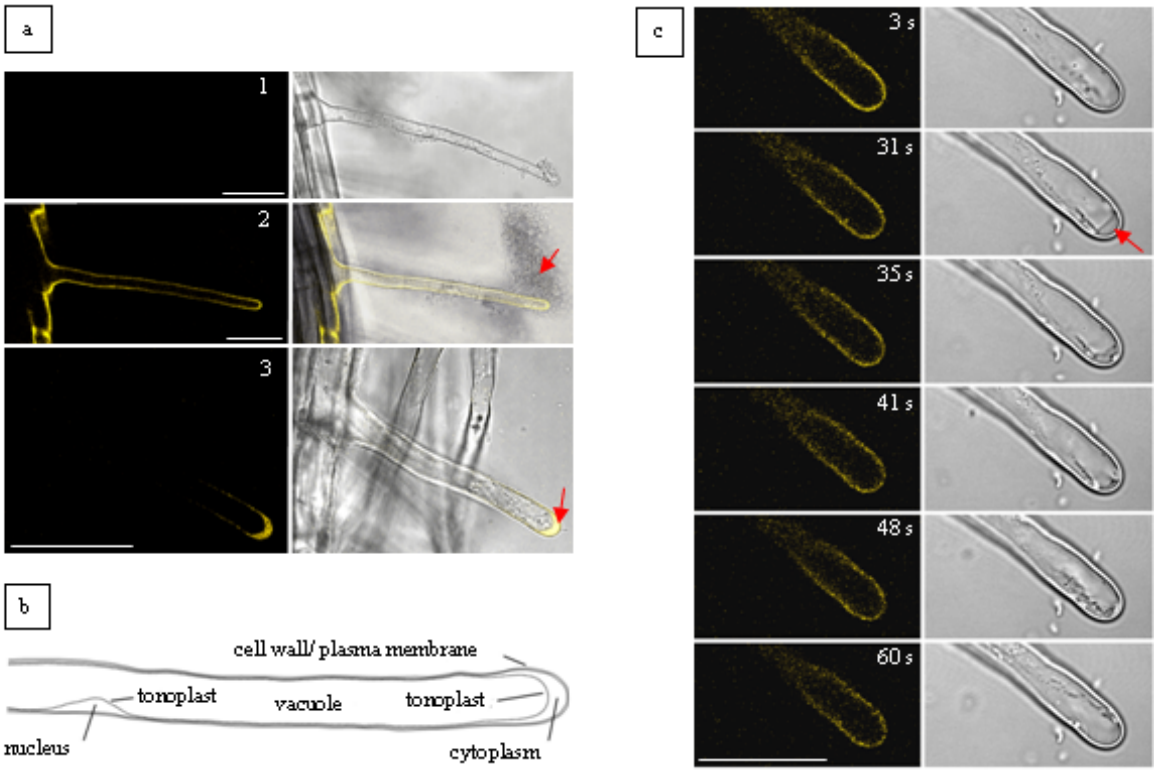

Fig. 48 Subcellular localisation of BiFC signals for KC1-SYP121 interaction

KC1-SYP121 interaction as indicated by BiFC-YFP fluorescence was observed primarily in mature root hairs as opposed to growing ones. In those mature root hairs, fluorescence was uniformly distributed at the cell periphery (a2). The absence of autofluorescence detection from e.g. cell walls with the confocal settings used in (a2) was indicated by the image of a mature root hair of the control plant co-cultivated with the untransformed *Agrobacterium* (a1). The BiFC signal in growing root hairs (a3) was located to the cell periphery as well, but in addition in a cap-like structure in the very tip (compare with d). The absence of YFP fluorescence from such additional structures in mature root hairs was shown more clearly in a time series of images taken from a tip region, where cytoplasmic streaming could be observed in the brightfield images (c). In contrast, the corresponding fluorescence images (c) displayed YFP signal only in the cell periphery in what was assumed to be the PM (compare with (b) for TP versus PM). All images are single plane (brightfield right, fluorescence left). White scale bar: 10 µm, except for (c): 20 µm

Discussion

Specificity of the interaction between KC1 and SYP121 in BiFC assays

BiFC experiments in transiently transformed *Arabidopsis* seedling roots showed that co-expression of YFP^N-SYP121 + KC1-YFP^C yielded approx. twice the amount of fluorescence than YFP^C-SYP121 + KC1-YFP^N under identical experimental and imaging conditions (Fig. 47a-d). As mentioned in the introduction, BiFC does not require the putative interaction partners to position the FP halves within a distance of less than 100 Å and in the correct relative orientation towards each other. In theory, as long as the linker sequences allow sufficient freedom of motion for FP fragments to collide with each other, the respective mature FP will be reformed, independent of their position on the interacting proteins (Hu *et al.*, 2002). Thus, each of the two FP fragments could be attached to the N- and C-terminal end of each interaction partner, so that a total of eight different combinations are possible. In practice, however, the rate of fragment association, i.e. the amount detectable fluorescence, is affected by steric constraints, which are only partially alleviated by flexible linker peptides and the dynamic motion of the fusion proteins (Kerppola, 2009). Hence, it has frequently been observed that not all combinations produce complexes that are sterically equivalent, i.e. allow fragments to associate equally efficient with each other (Kerppola, 2009), as it was the case for the two combinations of KC1 and SYP121 BiFC constructs mentioned above.

There are various factors that potentially could influence steric arrangement of the fragments in the complex made up of the interacting proteins and the two FP halves, e.g. a potential influence of the fluorescent protein fragments on the topology of the fusion protein themselves. Hence, the reason why the C-terminal half of YFP is less efficient than the N-terminal half in BiFC with KC1, when attached to the N-terminus of SYP121, remained unknown here. Similarly, it is generally not possible to predict the arrangement of the fluorescent protein fragments that will produce maximal signal (Kerppola, 2009) and empirical testing is necessary, as it was done here. Exceptions are cases where fusions are known to be non-functional from other experiments or known topological constraints exist that are likely to preclude the association between the fragments. As detailed in the General Introduction (see p. 59), SNAREs are tail-anchored proteins and as such their C-terminus is either luminal (regardless of which subcellular organelle they reside in) or extracellular in case of PM proteins. Therefore, the N-terminal position for tags on the three SYP1 SNAREs was preferred here, as with those fusions the FP half should reside in the cytoplasm. So should the complementary FP half fused to the C-terminus of KC1. As detailed in the General Introduction (p. 27) both N-and C-termini of Shaker channels are predicted to reside in the cytoplasm and for *At*KAT1 experimental proof was obtained. However, 35S driven FP fusions to the C-terminus are traditionally preferred and localisation to the PM was observed in most cases (Duby *et al.*, 2008). This preference possibly originates from the observation that N-terminal fusions have the potential to mask ER signal anchor sequences, or cause them to become stop transfer sequences and thereby generate localization artefacts (Tian *et al.*, 2004). Some experiments involving the converse fusions of YFP halves to the N-terminus of KC1 (e.g. YFP^C-KC1) were also

conducted in the transient *Arabidopsis* root transformation system and peripheral localisation of the resulting signal was observed (data not shown). However, as differences between combinations were not analyzed in great depth and with proper quantifications, no conclusions about those are drawn here. The key aim, a suitable combination that allowed confirming and proving specificity of the KC1-SYP121 interaction in *Arabidopsis* cells, was achieved with the observed BiFC between YFP^N-SYP121 and KC1-YFP^C. Nevertheless, as attempted in the mbSUS assays, more detailed analysis might prove valuable when determining the interacting domains in the future. As the association of YFP fragments depends on their steric arrangement in the complex, BiFC analysis could, in principle, be used to investigate the architecture of the KC1-SYP121 interaction, not considering factors such as the above mentioned potential influence of the FP fragments on the topology of the fusion protein. Both SYP121 and KC1 were previously shown to localize to the PM (Reintanz *et al.*, 2002; Collins *et al.*, 2003; Duby *et al.*, 2008). Therefore, the appearance of the BiFC-YFP signal for the successful combination of YFP^N-SYP121 and KC1-YFP^C in mobile and immobile punctuate structures in both onion cells and *Arabidopsis* protoplasts was unexpected (Fig. 46a, 2i, p. 179). Although later other alternatives were considered (discussed further below), initially, this phenomenon was interpreted as mis-localisation, most likely due to the high over-expression rate for heterologous proteins that is characteristic for both techniques. Despite the potential risk of mis-localisation, over-expression of the BiFC fusions under the 35S promoter was necessary for two reasons. Firstly, the expression level of plant ion channels under their native promoters is generally too low for detection by fluorescence (Wagner *et al.*, 2006). Secondly, the fluorescence intensity produced by BiFC complexes in living cells is usually less than 10% of that produced by the corresponding intact FP (Kerppola, 2009). Hu *et al.* (2002), who developed the BiFC technique, stated that *in vitro* both absorbance spectra and quantum yield, i.e. fluorescence intensity, of BiFC complexes were comparable to those of the corresponding intact FP when identical concentrations were used, indicating that the structure of the complex formed from re-associated fragment is likely to be similar to that of the intact protein. It was suggested that the difference in fluorescence intensity is due, at least in part, to competition for complex formation by endogenous proteins (Kerppola, 2006b). Furthermore, although none of the structures of FP fragments are known either alone or upon association with each other, it was assumed that the individual FP fragments do not fold into a structure resembling the intact protein in the absence of the complementary fragment (Robida & Kerppola, 2009). Instead they are likely to be unfolded, adopting an ensemble of rapidly inter-converting conformations, many of which are probably not permissive for complex formation. Indeed, *in vitro* studies of BiFC complex formation demonstrated that many fusions of fluorescent fragments to proteins of interest undergo irreversible miss-folding (and degradation) in the absence of the complementary fragment (Kerppola, 2009). Thus, even for specific interaction partners, typically only a minority of the fluorescent protein fragments will form BiFC complexes. Hence, over-expression was needed to raise the amount of fluorescent BiFC complexes to a detectable level, especially for interaction with the Shaker channel KC1. As a consequence, even though fluorescence might still appear weak, the ‘invisible’, i.e. non-interacting, over-expressed SNARE and /or KC1 proteins could overcrowd the ER and lead to

miss-localisation as was suspected for e.g. expression in *Arabidopsis* protoplasts.

Another problematic issue that relates to over-expression is promiscuous interaction (see also Chapter 1, p.123, p. 142). This feature is even more pronounced for a split FP, because re-association of e.g. split YFP, in contrast to split ubiquitin, is irreversible. As detailed in the introduction, BiFC complex formation is thought to occur stepwise. Initial reversible contacts between protein partners are thought to facilitate the subsequent association of their complementary FP fragments by increasing their local concentrations (Hu *et al.*, 2002). This second step was found to be irreversible and has therefore a stabilising effect on the BiFC complex (Kerppola, 2006b). The stabilization of BiFC complexes was explained with the extensive interaction interface that forms upon association of the two fragments (Robida & Kerppola, 2009). The three-dimensional structure of full-length FP such as GFP and YFP has been shown to contain 11 ß-strands forming a hollow cylinder through which is threaded an α-helix bearing the chromophore (Tsien, 1998). As mentioned above it is likely that the FP fragments are at least partially unfolded prior to their association, since neither of the fragments forms a contiguous ß-sheet in the intact FP. Therefore, during fragment association, four new ß-strand interfaces are formed. Each interface enables between six and nine hydrogen bonds between the peptide backbones of the two fragments. Thus, dissociation of BiFC complexes would require breaking a very stable network of more than 30 hydrogen bonds and solvating the hydrophobic interior of the ß-barrel. This energetically favourable association of FP fragments lends the BiFC technique the ability to investigate weak protein interactions (see introduction, p. 177). However, as in mbSUS, in principle, it also enables co-localisation within a small spatial domain to facilitate protein fragment association, meaning that the proteins, to which the FP fragments are fused, must not necessarily interact with each other directly (Kerppola, 2006b). This feature has been employed to show e.g. the assembly of BiFC fusion proteins in a macromolecular complex, where they are not in direct contact but the fragments are confined in a limited space (Kerppola, 2009). However, conversely, it also bears the possibility of stabilising complexes formed by proteins that do not normally interact with each other. This is more likely, when over-expression increases the local concentration of available FP fragment partners.

Finally, it has to be mentioned that even without the effect of over-expression and resulting elevated local concentrations of complementary FP fragments, those fragments have a finite ability to associate with each other independent of an interaction between the proteins fused to them. Again, this affinity can be explained by how energetically favourable the formation of a large interaction interface coupled to folding into the native protein structure is, for the association of the FP fragments. This low rate of autonomous FP fragment association generally produces very low levels of fluorescent complexes, which are the major source of background signal in BiFC assays (Kerppola, 2009). The resulting fluorescence intensity varies depending on the identities of the fusion proteins and again their levels of expression. This affinity of complementary FP fragments for each other is even more pronounced when they are expressed without a protein partner, because of the increased flexibility and possible steric interference introduced by attached proteins of interest. Therefore, cells that express FP fragments fused to proteins that do not interact with each

other often have lower fluorescence intensities than cells that express the FP fragments alone. Thus, the empty BiFC vectors do not represent a suitable negative control. To determine if BiFC complex formation reflects a specific interaction between the putative partners rather than an over-expression artefact, ideally, it is recommended, to make use of mutations in either protein partner that eliminate the interaction and thus the formation of detectable BiFC signals (Kerppola, 2006b). An important requirement would be that those mutations do not affect the levels of fusion protein expression or their localisation, as it is most likely to be the case for point mutations rather than deletions. As the interacting domains, not to mention the important aa within those domains were still unknown at the time, again the SYP1 SNAREs SYP122 and SYP111 were chosen as controls (Fig. 47, p. 181). Both effects, over-expression or autonomous FP fragment association are likely explanations for the BiFC-YFP signal observed for co-expression of KC1 with the control SNAREs SYP111 and SYP122. In contrast, co-expression of KC1 with SYP121 yielded a significantly higher amount of relative BiFC-YFP fluorescence after quantification (Fig. 47h).

An additional control revealed that a small amount of the fluorescence obtained for the co-expression of KC1 with all three SNAREs must be considered plant derived autofluorescence. After co-cultivated with untransformed *Agrobacterium rhizogenes,* seedlings showed on average more background fluorescence than plants that were incubated under the same experimental conditions but never in contact with *Agrobacterium*. Although autofluorescence is markedly reduced in seedling root tissues compared with leaves, depending on the laser intensity and other confocal settings, cell walls still showed a certain amount of background fluorescence, especially when seedlings had not been treated carefully and root hairs were bent or broken off. This cell wall autofluorescence is caused by phenolic components such as lignin and other aromatic molecules. Plant responses to attack by *Agrobacterium* are still not well understood (Pruss *et al.*, 2008). However, it is known that *A. tumefaciens* fails to elicit a hypersensitive response, interferes with SA-dependent defence and inhibits induction of pathogenesis-related genes (Pruss *et al.*, 2008). In general, attack by phytopathogens such as *A. rhizogenes* induces the production of plant extracellular matrix components such as aromatic hydroxyproline-rich glycoproteins to strengthen the cell wall (Meyer *et al.*, 2009). Also, certain types of phenolics are produced and accumulated in plant tissues exposed to stress and pathogen attack, e.g. catechins and acetosyringone in response to *Agrobacterium* (Bhattacharya *et al.*, 2010). An *Agrobacterium* transformed tobacco cell suspension culture showed a five-fold increase in cell wall thickness, higher expression of mRNAs coding for enzymes of lignin biosynthesis and increased amounts of xylan. Hence, the observed enhanced amount of autofluorescence in seedling roots incubated with untransformed *Agrobacterium* was not an expected phenomenon. Therefore, data given for quantifications of confocal images were corrected for the autofluorescence of bacteria-free seedlings and the amount of autofluorescence from plants co-cultivated with untransformed *Agrobacterium* is shown (Fig. 47d, h). In summary, it could be concluded from these results that most likely the BiFC signal obtained for co-expression of KC1 and SYP121 represented a specific interaction.

This conclusion still rested on two assumptions. Firstly, that all three SNARE proteins reached the same target membrane in which complex formation between the specific pair was

observed and secondly, that all three SNARE proteins were expressed to comparable levels in combination with comparable KC1 levels. In this aspect the BiFC assay has all the same features as discussed for the mbSUS assay, and that were a consideration for the Co-IP. As detailed in the General Introduction (p. 55), SYP121 and its closest neighbour on a phylogenetic tree, SYP122 were previously characterised as PM SNAREs of *Arabidopsis* (Leyman *et al.*, 1999; Collins *et al.*, 2003; Nuhse *et al.*, 2003; Assaad *et al.*, 2004; Alexandersson *et al.*, 2004). Even under the control of the strong 35S promoter, both syntaxins were faithfully targeted to the PM of *Arabidopsis* protoplasts derived from suspension culture cells when expressed as N-terminal fusion to GFP (Uemura *et al.*, 2004). Furthermore, PM localisation of 35S driven GFP-*At*SYP121 and CFP-*At*SYP122 was also detected in leave cells of stably transformed *Arabidopsis* lines (Assaad *et al.*, 2004; Pajonk *et al.*, 2008). SYP111 (KNOLLE), is expressed in *Arabidopsis* only in dividing cells, where it localises to the plane of division and mediates cell-plate formation (Lauber *et al.*, 1997). However, when Uemura *et al*. (2004) transiently expressed a *35S-GFP-Syp111* construct in *Arabidopsis* protoplasts they detected the fluorescent signal in the PM. This observation was confirmed by different authors (Dhonukshe *et al.*, 2006), who found that ectopic expression of SYP111 by the 35S promoter led to PM localisation in non-proliferating cells of stable transformed *Arabidopsis* plants. These authors detected miss-localised SYP111 in PM protein fractions from mature leaves and stems, both of which consist of differentiated cells that normally do not contain SYP111 protein (Dhonukshe *et al.*, 2006). Furthermore, in roots of *35S::Syp111* transgenic seedlings, immunohistochemistry employing an anti-SYP111 showed strong and stable SYP111 accumulation in expanding cells of the central cylinder as well as growing and mature root hairs, in contrast to the wt. In mature root hairs, SYP111 was found strictly at the surface of the cell, where it co-localised with an immunostain for a PM-ATPase and resembled PM staining with a lipophilic fluorescent dye, FM1-43 (Dhonukshe *et al.*, 2006). In young tip-growing root hairs, SYP111 and the PM-ATPase additionally co-localised to the apical tip region, not only at the surface but also internally.

Root hairs are a local outgrowth of non-proliferating epidermal cells that undergo tip growth by targeting membrane vesicles from the trans-Golgi to the apical PM. By immunogold labelling electron microscopy, SYP111 was detected in Golgi stacks, the trans-Golgi network and these apical vesicles. Dhonukshe *et al*. (2006) concluded that SYP111 was targeted like an integral membrane protein destined to the apical PM of the growing and mature root hairs. However, this miss-targeting of SYP111 to the PM did not interfere with essential cellular processes, involving SNARE complex partners and membrane fusion which are required for normal plant development. Tip-growing root hairs and in fact the entire *35S::Syp111* transgenic plant developed morphologically indistinguishable from wt plants, similar to the observations made for SYP121 and SYP122 over-expressing *Arabidopsis* (Pajonk *et al.*, 2008). This agreed with the finding that in the root tip meristem of *35S::Syp111* transgenic seedlings SYP111 protein was correctly localised to the cell plate (Dhonukshe *et al.*, 2006). Expression levels driven by the 35S promoter apparently provided no interference, as comparative *in situ* hybridisation showed that relative to the endogenous *Syp111* promoter, the 35S promoter yielded low levels of *Syp111* mRNA accumulation

in these proliferating cells. Thus, Dhonukshe *et al*. (2006) suggested that SYP111 in non-proliferating cells might be a biologically inactive passenger protein on vesicles destined to the PM. As mentioned in the General Introduction (p. 54), it had been suggested that even in proliferating cells the PM might be a natural target membrane for SYP111 before cell plate initiation (Volker *et al.*, 2001).

In conclusion, the observed targeting of 35S over-expressed SYP111 in both growing and mature root hairs (Dhonukshe *et al.*, 2006) was highly similar to the localisation of the BiFC fluorescent signal for SYP121-KC1 interaction detected after transient *Arabidopsis* seedling root transformation. Thus, a PM localisation for the interaction between KC1 and SYP121 in mature root hairs was strongly supported by these data (Fig. 48c, p. 183). In addition, the mentioned previously published results for 35S over-expression of N-terminal FP-tagged SYP121 and SYP122 strongly supported the assumption, that all three syntaxins shared the PM as target membrane also in this assay and over-expression did not harm the cell or causes artefacts of localisation. Therefore, with regard to localisation, both SYP122 and SYP111 could be considered suitable controls for the specificity of SYP121-KC1 interaction *in planta*.

Apart from an identical target membrane, protein expression levels of SYP122 and SYP111 should be comparable to SYP121 to allow them to be suitable BiFC control proteins for interaction with KC1. As discussed above, this need arises from the frequently observed influence of expression levels on the fluorescence intensity of an individual protein pair. All three SNAREs were expressed under the control of the strong constitutive cauliflower mosaic virus 35S promoter. For example, the *35S::Syp111* transgene yielded approximately hundred-fold accumulation of SYP111 protein in seedlings, when compared with the wild-type control (Dhonukshe *et al.*, 2006). This result is consistent with the common use of the 35S promoter for transgene over-expression in plants (Benfey & Chua, 1990; Holtorf *et al.*, 1995). However, the use of an identical promoter for different transgenes does not guarantee similar expression levels after *Agrobacterium* mediated plant transformation. Each successfully (co)-transformed cell must be considered an independent transformation event with potentially different expression levels for both BiFC partners. Variation in expression levels may have several different sources.

To start with, the bacterium–plant interaction in itself does not limit the transformation frequency of each plant cell (DeNeve *et al.*, 1997). For *A. tumefaciens*, the transformation process begins with recognition of plant signals such as acetosyringone that is usually synthesized by wounded plant cells. Acetosyringone detection by the bacterial VirA/VirG sensory system is followed by activation of the bacterial *vir* loci and attachment of the bacterium to the host cell (Dafny-Yelin & Tzfira, 2007). The T-DNA is then spliced from the bacterial Ti plasmid as single-strand T-DNA (ss-T-DNA) and thought to exist as a protein–DNA complex, with a single VirD2 molecule covalently attached to its 5′ sequence. VirD2 functions as a pilot protein that guides the T-DNA out of the bacterium and into the plant cell through a so called T-pilus, a VirB2/D4 type IV secretion system (Dafny-Yelin & Tzfira, 2007). In principal, a single plant cell might receive the same T-DNA from several different *Agrobacterium* cells and/ or multiple T-DNA copies from a single bacterium. Although binary vectors are usually not high copy plasmids, 7- 8 copies per

Agrobacterium are common and each of these copies might mobilize a T-DNA upon exposure to acetosyringone (Jacob & Veluthambi, 2002). Similarly, during co-transformation, *Agrobacteria* carrying either BiFC construct may transfer T-DNAs in varying ratios. Hence, variations in BiFC partner protein expression levels in different plant cells might result from variations in the number of T-DNA templates per cell.

The subsequent steps during *Agrobacterium* transformation of plant cells can potentially contribute to variations in protein expression levels as well. In order to function as template for protein production, it is absolutely necessary for the T-DNA to enter the plant cell nucleus. As *Agrobacterium* does not simultaneously transfer a protein with DNA polymerase activity into the plant cell (Citovsky *et al.*, 2007), plant polymerases are needed to convert the ss-T-DNA to double-stranded T-DNA (ds-T-DNA). Ds-DNA is the only possible template for transcription by RNA polymerases. So far, no RNA polymerase has been observed that uses ss-DNA as template, not even among viral proteins (Cortese *et al.*, 1980). RNA polymerases in turn and in fact the entire host transcription machinery that synthesizes mRNA templates for translation in the cytoplasm is found only in the plant cell nucleus.

The nuclear import of T-DNA occurs in a polar fashion with the VirD2 molecule attached to the 5′ end of the T-strand initiating the import process through the nuclear pores by means of its C-terminal nuclear localisation signal (Citovsky *et al.*, 1992). Nuclear uptake is thought to be very efficient and the T-DNA is protected from degradation by cytoplasmic nucleases by forming a so-called T-complex with bacterial VirE2 proteins that are transferred separately through the T-pilus. Therefore, these steps are not likely to infer great differences in the number of T-DNA templates competent for protein expression, i.e. potential differences in expression levels of BiFC partners.

In contrast, once inside the nucleus, the ss-T-DNA is uncoated in order to be converted to ds-DNA, which renders it vulnerable to nuclear nucleases. Although in some instances circularization of extra-chromosomal T-DNA was observed, it does not appear to be a general mechanism during *Agrobacterium* transformation (Bakkeren *et al.*, 1989). As cells efficiently recognize free DNA ends that indicate DNA damage to them, degradation of extra-chromosomal ss-or ds-T-DNA is essentially the reason that during transformation of somatic tissues, such as the *Arabidopsis* seedlings used here, the vast majority of transformation events will remain transient. Most of the transferred T-DNA molecules will be lost after 7- 10 days due to nuclease dependent degradation (Jones *et al.*, 2009). Only very few stable T-DNA integration events into the plant cell chromosome are likely to occur in somatic cells as this step appears to be limited by the occurrence of ds-DNA breaks.

Although the T-DNA integration mechanism is still not entirely understood, recent evidence indicated that for stable transformation, ds-DNA breaks in the host genome and ds-T-DNA intermediates play an important role (Citovsky *et al.*, 2007). In plants, ds-DNA breaks are mainly repaired by the non-homologous end-joining (NHEJ) pathway (Chilton & Que, 2003). Research so far has indicated that *Agrobacterium* in general, if maybe not exclusively, is hijacking its hosts NHEJ DNA repair machinery during the integration step (Citovsky *et al.*, 2007). Ds-DNA breaks are an intentionally frequent and highly regulated event during meiosis for the purpose of

genetic recombination in the so-called Holliday model (Sanchez-Moran *et al.*, 2008). This fact was associated with the usually high number of successful stable transformation events during *Arabidopsis* germ-line transformation via floral dip (Zhang *et al.*, 2006). In contrast, in somatic cells, ds-DNA breaks are a much rarer event that the cell tries to avoid, as they pose serious risks of large-scale fatal genome alterations. Ds-DNA breaks in somatic cells only arise e.g. through off-target action by nuclear enzymes or from the mechanisms of transposon insertion (Chilton & Que, 2003; Shrivastav *et al.*, 2008). They might also occur as a transient step during other DNA repair mechanism, e.g. single strand nicks that can occur during exposure in transcription. Furthermore, ds-DNA breaks are produced when cells are exposed to DNA damaging agents including ionizing radiation, chemical agents and UV light (Shrivastav *et al.*, 2008).

Thus, during transient transformation of somatic plant cells, not all T-DNAs that are finally taken up into the nucleus might undergo second strand synthesis. Both ss-T-DNA and ds-T-DNA might persevere in the nucleus for different length of time before degradation. All of these factors can potentially influence the overall efficiency of mRNA production and in consequence the level of target protein expression for transformation with a specific T-DNA. As a consequence, it is a general observation for the BiFC technique that the differences in the levels of fusion protein expression cause the absolute fluorescence intensities of individual cells to vary over a wide range (Robida & Kerppola, 2009).

To be able to properly compare the relative efficiencies of fluorescence complementation between different partners, as it was done here to determine specificity of KC1 interaction with SYP121 over SYP122 or SYP111, it would be necessary to correct for these differences in the levels of protein expression in individual cells. For this purpose, a Western Blot establishing the levels of protein expression is frequently published with BiFC results (Walter *et al.*, 2004; Waadt *et al.*, 2008). However, although Western Blot will confirm that proteins of the negative control are indeed expressed, this technique can only show an average expression level over a specific amount of e.g. tobacco leaf tissue. In contrast, the observed fluorescence intensities are in general only averaged over a limited number of cells from the analyzed tissue sample. Thus, a Western Blot does not really provide the required relation of expression levels of BiFC constructs in individual cells to measured fluorescence intensity but rather gives an impression of the overall expressed protein amounts. Cells expressing only one partner will contribute to the Western Blot just as much as cells expressing a detectable BiFC pair. Therefore, newer adaptations of the BiFC technique in mammalian cell systems now co-transform with the plasmids encoding the two fusion proteins a third plasmid as an internal reference marker (Kerppola, 2008; Kerppola, 2009; Robida & Kerppola, 2009). This plasmid encodes an unfused full-length FP with distinct spectral characteristics (e.g. CFP). The ratio of BiFC fluorescence to CFP fluorescence represents a more accurate measure of the efficiency of bimolecular fluorescence complementation in individual cells, although, as discussed above, differences in expression levels might still occur between the BiFC constructs and the full-length FP (Kerppola, 2008). Recently, an adaptation for plants was published (Citovsky *et al.*, 2006; Lee *et al.*, 2008). The authors reported the development of a multi-gene expression binary vector for *Agrobacterium* mediated transformation that allows co-

expression of interacting BiFC partners and an additional mCherry FP that may serve as an internal transformation reference and/ or marker of subcellular compartments. The system is based upon the pSAT series of expression vectors, where different rare-cutting restriction sites surround the expression cassette of different vectors. This feature allows the transfer of multiple cassettes in a modular fashion onto a single *Agrobacterium* binary vector backbone (pPZP-RCS2). This may result in a huge vector, but all genes will be on a single T-DNA, albeit with their own tandem 35S-promoter/ terminator each. This system might even be more suitable for the control of expression levels than direct DNA transfer of three independent plasmids as currently performed in mammalian systems. However, at the time, these vectors were not yet available. To compensate as much as possible for the resulting lack of knowledge about the expression levels for the different SNARE proteins and KC1, low magnification images (20x) encompassing the mature root hair zone were analysed instead of single cells. It was expected that this would yield a more accurate measure of the average fluorescence.

This approach was supported by the observation that, in general, when seedlings were transformed, the transformation efficiency was very high within the root epidermis. Especially in the mature root hair zone, almost uniform transformation of both trichoblasts and atrichoblasts was observed (Fig. 47a, e, p. 181). In contrast to high transformation efficiency in the root epidermis, no inner root cell layers (e.g. cortex) and no shoot tissues were ever detectably transformed. As similar observations were made by Campanoni *et al*. (2007) during the development of this transient *Arabidopsis* root transformation technique, it is unlikely that this pattern of transformed cells is linked to the use of any particular construct. The following speculations are made here in an attempt to explain this phenomenon.

Difficulty in transforming *Arabidopsis* shoot tissue was observed frequently (Dekathen & Jacobsen, 1995; Marion *et al.*, 2008; Li *et al.*, 2009). According to Dekathen *et al*. (1995), *Agrobacterium* attachment was never observed on the well-developed cuticle of epicotyl segments, unless treated with chloroform. The inability to adhere to plant cells was linked previously with resistance to both transient and stable transformation by *Agrobacterium* (Nam *et al.*, 1999). Hence, it was suggested that the waxy surface represents a physical barrier to *Agrobacterium* attachment and thus transformation (Dekathen & Jacobsen, 1995). Root epidermis cells naturally have a less well-developed cuticle. Li *et al*. (2009), who later published an *Arabidopsis* transient transformation technique that specifically targets shoot tissue, were able to overcome this problem for cotyledon transformation of young seedlings by the addition of the surfactant Silwet L-77 during co-cultivation. Still, even this group stated that older seedlings (more than 7 days) with emerging true leaves had a sharp decline in the transient expression efficiency. Li *et al*. (2009) further published that even with Silwet L-77 no root tissue was ever transformed. These authors used *Agrobacterium tumefaciens* exclusively. Here, *Agrobacterium rhizogenes* adhered in large numbers to the surface of the root (e.g. Fig. 48a1, a2, p. 183). Thus, the use of *A. rhizogenes* (without Silwet L-77) instead of *A. tumefaciens* might have supported the targeting of root versus shoot tissue.

A. rhizogenes is a close relative of *A. tumefaciens*. However, in contrast to the crown gall

tumours found on *A. tumefaciens* infected plants in nature, *A. rhizogenes* induces neoplastic growth of plant cells that differentiate to form "hairy roots" (also known as root-mat disease) (Gelvin, 2009). Also, the physiological basis of tumour genesis is fundamentally different (Gelvin, 1990). Crown gall tumours result from the overproduction of the phytohormones auxin and cytokinin specified by *A. tumefaciens* T-DNA genes. In contrast, hairy root tumours stem from the increased sensitivity of transformed cells to endogenous auxin levels (Gelvin, 1990). Just as virulent strains of *A. tumefaciens* contain the tumour-inducing (Ti) plasmid, from which a segment of DNA is transferred (T-DNA) into the host cell, *A. rhizogenes* harbours a root-inducing (Ri) plasmid.

In contrast to the 'disarmed' *A. tumefaciens* laboratory strains, the *A. rhizogenes* MSU440 strain that was employed for the BiFC experiments is in principal still virulent (Sonti *et al.*, 1995). It contains a special Ri plasmid, pRiA4, that harbours two T-DNAs, T_L (T-DNA left) and T_R (T-DNA right), which can be transferred independently or simultaneously (Gelvin, 1990; Veena & Taylor, 2007). The T_R does contain auxin biosynthetic genes. However, if transferred alone, it did not induce root formation on carrot disks. Hairy roots were only efficiently induced by the T_L that in an unknown way sensitizes the plant cells to auxin (Gelvin, 1990). In the BiFC assays performed here with the help of *A. rhizogenes* MSU440, the *vir* genes on the pRiA4 Ri plasmid would act in *trans* to activate the T-DNA of interest on the BiFC binary vectors, but could also mobilise the two Ri T-DNAs. Transformed cells may have obtained between one and four different T-DNAs (T_L, T_R, two BiFC partners). Therefore, in addition to unknown factors that might enable *A. rhizogenes* but not *A. tumefaciens* to preferably target root tissue, root cells, in principle, could have been induced to neoplastic growth of root hairs. This could have contributed to the apparently uniform transformation of root hairs.

However, seedlings successfully transformed with *A. rhizogenes* MSU440 for BiFC assays were morphologically identical to control seedlings from the same experimental conditions that were never in contact with the bacterium. It is possible that the standard 3 days of co-cultivation might not have been sufficient to develop any symptoms in cases of T_L transfer. Indeed, carrot disks transformed with pRiA4 harbouring *A. rhizogenes* showed the first adventitious hairy roots only 14 d after inoculation (Baranski *et al.*, 2006). In addition, it has been observed previously that Ri T-DNA-transformed roots displayed growth and morphology comparable to normal roots (Collier *et al.*, 2005). Given the fact, that even less detail is know about the transformation process by *A. rhizogenes* than by *A. tumefaciens*, it can only be speculated about the nature of the transformation events that led to BiFC expression here.

It was further speculated that the uniform transformation of cells, especially in the mature root hair zone, might be linked to the observation that the rate of both stable and transient transformation events is significantly increased in somatic cells that undergo cell cycle divisions (Iida *et al.*, 1991; Wilke *et al.*, 1996; Villemont *et al.*, 1997; Yi *et al.*, 2002). These authors suggested that the enhanced activity of DNA polymerases for DNA replication during S-phase could enhance the efficiency of both transient and stable transformation in dividing cells by increasing the amount of transcription/integration-competent ds-T-DNA molecules present in the nucleus. In agreement with these observations, other authors were able to show that specific

regions of *Arabidopsis* seedling roots were hyper-susceptible to transformation (Yi *et al.*, 2002). These regions included the meristematic zone of the main root tip with part of the elongation zone and lateral root primordia; both places contain the dividing somatic cells of roots.

For the BiFC assays, the standard co-cultivation time was 72 h. It was previously published that root hairs of *Arabidopsis* Col0 wt seedlings initiated within ~ 1 mm of the root tip and grew to a mean final length of ~ 634 µm by the time they were ~ 2.5 mm from the root tip (Yi *et al.*, 2010). Though growing no further, these hairs remained alive until they were ~ 10 mm from the root tip. The average root hair growth rate was 1.5 µm/ min. The average root elongation rate for Col0 was measured to be ~ 182 µm/ h (Beemster *et al.*, 2002). Both groups agree that the size of the growth zone (meristem + elongation zone) typically ranges between 1 and 2.5 mm (Beemster *et al.*, 2002; Yi *et al.*, 2010). Using these data, it was calculated here that a root hair would need about 7 h to reach its mature length. For the meristem cells that give rise to root hair forming epidermis cells, it should take about 14 h to reach the end of the elongation zone and about 55 h until the 10 mm mark is reached. In conclusion, one might imagine that for the BiFC assays the transient transformation rate was so high, because also here *A. rhizogenes* specifically targeted the meristematic zone of the root apex of seedlings. Even allowing for the influence of different growth conditions and other factors, such as e.g. seed quality, on the root and root hair elongation rates, these transformed dividing meristematic cells would probably have had time enough to form the highly transformed mature root hair zone by the time confocal analysis took place (72 h). That is when one assumes that most transformation events took place soon after the initiation of co-cultivation.

It remained unknown here, why *A. rhizogenes* transformed only root epidermis cells, no inner root cell layers. *Agrobacterium* is known to multiply in the intercellular spaces of infected tissues and can spread out this way (Gelvin, 2009). Maybe, the young seedling roots do not offer as much intercellular spaces as mesophyll cell tissue of leaves for example. In addition, maybe the suberin layer of cortex cells could help protect against infection.

In conclusion, although the details of the transient transformation process via *A. rhizogenes* are unclear, the high efficiency of root epidermis transformation supported the approach of averaging BiFC signals by taking standardized images of the mature root zone rather than single cells in order to counteract the above discussed limitations of the BiFC technique. The thus obtained data strongly supported the specificity of KC1 for SYP121 over SYP122 and SYP111. Furthermore, these results allowed the conclusion that the interaction between KC and SYP121 is sustained *in planta,* and therefore not likely to be an artefact of heterologous expression.

Subcellular localisation of BiFC signals for KC1-SYP121 interaction

In contrast to the peripheral localisation of the BiFC signal in mature root hairs that indicated the PM as the most likely subcellular compartment for the occurrence of interaction between KC1 and SYP121, the reconstituted YFP fluorescence was localized to punctuate structures in both onion cells and *Arabidopsis* protoplasts (Fig. 46a, I, p. 179). These punctuate subcellular compartments carrying the KC1-SYP121 interacting complex were highly mobile and co-localised with AKT1-

GFP in onion cells (Fig. 46c), but immobile in *Arabidopsis* protoplasts (Fig. 46i). Interpretation is hindered here and must remain highly speculative, because the nature of the punctuate structures was not explored by e.g. co-localisation with organelle markers. Organelle dynamics, in terms of shape, size, number and mobility, are known to vary dramatically depending on cell type, developmental stage and environmental stimuli (Mano *et al.*, 2009). Therefore, in general, a mobile/immobile punctuate structure of the type observed in onion cells or *Arabidopsis* protoplasts could represent clusters of mitochondria, recycling or other endosomal entities, peroxisomes, PVC, Golgi stacks, or simply bodies of unidentified origin which are frequently observed and partly as overexpression artefacts (the plant organellome database: http://podb.nibb.ac.jp/Organellome/) (Mano *et al.*, 2008).

What can be concluded with some confidence is that neither in onion cells, *Arabidopsis* protoplasts, mature *Arabidopsis* root hairs, nor tobacco leaves, the BiFC signal for interaction KC1-SYP121 interaction was observed in a structure resembling the ER. It is suggested here that no BiFC fluorescence could be obtained after tobacco leaf infiltration with the same constructs that were successfully used in *Arabidopsis* root transformation because KC1 was unable to leave the ER (Fig. 46e, p. 179). When expressed on its own as a fusion to full-length YFP, KC1 was detected in tobacco leaf epidermal cells solely in the typical lattice-like network of membrane tubules and cisternae of the ER that is distributed throughout the cytoplasm and is continuous with the nuclear envelope (nuclear ring, red arrow, Fig. 46e). Also, in these cells the ER constantly remodeled with some strands being in fast motion and other reticulate and tubular areas moving over a slower relatively longer time course, indicating that they were still alive (data not shown). While the reason that no BiFC could be obtained in tobacco could still originate in a failure to achieve the co-transformation events needed for this technique, a large number of experiments were conducted with varying conditions. Not a single co-transformed cell was ever observed. In contrast, the positive control for the BiFC technique, the homodimerization of bZIP63 (Walter *et al.*, 2004), could be detected in its expected nuclear localisation, indicating that the experimental conditions were in principle suitable for co-transformation (Fig. 46f).

As mentioned in the General Introduction (p. 36), a later publication by Duby *et al.* (2008) confirmed the observation that in tobacco, KC1 expressed on its own, is retained in the ER. Duby *et al.* (2008) were able to show KC1 re-localisation to the PM by co-expression with AKT1 or KAT1. It was suggested that formation of heterotetramers between subunits with ER export signals (e.g. AKT1, KAT1) overrides a putative ER retention signal in KC1. Duby *et al.* (2008) further proposed that KC1 subunits are entirely unable to associate with each other, based on the absence of KC1 self-interaction in yeast-two-hybrid studies. Therefore, following the concept of a dimerisation of dimers for tetrameric channel assembly (see General Introduction, p. 31ff.), homomeric channels of KC1 would not exist. Although KC1-YFP accumulated in the ER in tobacco, BiFC fluorescence was detected at the cell periphery in mature *Arabidopsis* root hairs, indicating that the SYP121-KC1 complex was localisation most likely at the PM.

Therefore, a way for KC1 must have existed to reach the PM without simultaneous co-expression of an inward rectifying subunit such as AKT1. Very *et al.* (2003) specifically stated that

the concept KC1 inability to form homomers does not agree with the finding that there are cell types such as trichomes, where only KC1 expression was detected. In addition, so far the molecular nature of the ER retention signal could not be identified (Jeanguenin *et al.*, 2008). It appears different from the ER retention signals identified in mammalian voltage gated K^+ channels (Kv) so far. The overall steady-state cell surface expression levels and subunit composition of mammalian Kv channels appears to be regulated by a hierarchical system of regulatory steps, many of which operate at the level of the ER (Vacher *et al.*, 2008). Just as plant Shakers, different mammalian brain Kv1 subfamily α-subunits exhibit high amino acid sequence identity but show striking differences in trafficking and functioning (compare GORK, AKT1, and KC1). For Kv1 α-subunits the primary determinant for the regulation of cell surface trafficking appears to be a potent ER retention (ERR) signal consisting of residues in the so-called turret region at the external face of the channel pore domain. Cell surface expression of Kv1 subunits can also be influenced by a cytoplasmic C-terminal VXXSL motif that acts as a forward trafficking signal and by auxiliary ß-subunits. In heterologous cells, these motifs dictate the steady-state distribution of Kv1 channels, such that homotetrameric Kv1.1 channels are essentially localized to the ER, Kv1.4 channels mainly to the cell surface and Kv1.2 channels to both the ER and the cell surface. The generation of chimeras between Kv1.1 and Kv1.4 revealed that any Kv1.4 α-subunit containing the Kv1.1 pore region, including the turret domain, was ER retained. Conversely, any Kv1.1 α-subunit containing the Kv1.4 P-loop was efficiently exported from the ER. Interestingly, Kv1.1 homomeric channels, retained in the ER, appeared to be properly folded and assembled as tetramers with no evidence of aggregation or gross miss-folding (Vacher *et al.*, 2008). Thus, it is possible that similar ER retention mechanism exists in *Arabidopsis*, i.e. KC1 homomers would exist in the ER only but never reach the PM. Thus, they would be electrically silent and will only be exported with an AKT subunit just as observed by Duby *et al.* (2008).

It is worth noting that the heterologous expression system of tobacco leaf epidermal protoplasts was chosen because those cells specifically did not show the typical inward rectifying currents attributed to Shaker channels (see p. 13) in order to facilitate electrical recordings of expressed *Arabidopsis* proteins (Hosy *et al.*, 2005; Duby *et al.*, 2008). This led to the suggestion that tobacco leaf epidermal cells do not express Shaker inward rectifying subunits (Bregante *et al.*, 2008). Quite possibly this might be an explanation why only in tobacco, KC1 appeared retained in the ER. *Arabidopsis* root hairs, in contrast, do show Shaker typical inward rectifying currents and represent moreover the cell type that naturally expresses KC1 and AKT1 transcripts at high levels. Therefore, it is possible that native AKT1 subunits 'helped' the KC1-BiFC fusion to the PM. Alternatively, other root hair specific ER export support systems such as *Arabidopsis* auxiliary ß-subunit or 14-3-3 proteins (p. 64) might exist specifically in root hairs to promote native KC1 or KC1-AKT1 heteromeric cell surface expression that are missing in the tobacco cells. This could also explain, why in protoplasts from dedifferentiated *Arabidopsis* leaf mesophyll suspension cells, no PM localisation of the BiFC fluorescence was observed. Also, in onion cells, not even co-expression with AKT1 seemed to help achieve PM localisation for either Shaker subunit. Nevertheless, even though it is tempting to speculate that SYP121 might function as auxiliary

subunit, the absence of BiFC signal in the tobacco ER supports the assumption that SP121 was properly localised to the PM. In conclusion, interaction of KC1 and SYP121 is more likely to occur at the PM in mature root hairs. The formation of KC1 homomers would also agree much better with the results from mbSUS assays and Co-IP. As summarized in the General Introduction (p. 31ff.), the ER can be regarded as a highly versatile protein factory that is equipped with chaperones and folding enzymes essential not only for protein folding and exit but also for retention and degradation of misfolded or aberrantly assembled protein complexes. If KC1 would only exist as monomers, it is very unlikely to be properly folded. Therefore, its halftime in the ER would be quite short. It is hard to imagine, how this scenario would agree with a stable Co-IP and moreover the expression of undegraded KC1 in *Sf9* insect cells. It is imagined here, that in case of Co-IP and mbSUS at least, possibly also BiFC, KC1 homomers interacted with SYP121.

In contrast, in young root hairs, the situation is less clear. The ER marker used by Campanoni *et al.* (2007) showed an enhanced density within the first 3–5 µm from the tip of growing root hairs, not unlike the BiFC signal obtained for KC1-SYP121 interaction. As mentioned earlier, in these cells, the ER containing cytoplasm is concentrated in the subapical region. Therefore, without co-localisation of the BiFC signal with either an ER marker, localisation in the ER/cytoplasm or other trafficking compartments can not entirely be excluded in this case. Co-localisation was attempted, however, the co-transformation with three different constructs could not be achieved (data not shown). Also for this purpose, the above mentioned new modular binary vector system could be employed for future experiments. It was mentioned above that over-expressed SYP111 could be detected by immunogold labelling electron microscopy on exocytotic vesicles that were located in the very tip region of growing young hairs (Dhonukshe *et al.*, 2006). As the BiFC-YFP signal after co-transformation with KC1 and SYP121 appeared in the same general tip localised region in addition to a peripheral uniform signal, one might speculate, that these two proteins too, were localised and interacted on such exocytotic vesicles. However, the resolution of confocal imaging as opposed to electron microscopy does not allow drawing this conclusion here. Thus, it was concluded here, that the subcellular localisation for the interaction between KC1 and SYP121 as detected in BiFC assays was the PM.

Furthermore, one could speculate that the punctuate structures observed in onion epidermis cells and *Arabidopsis* protoplasts to be of endosomal nature when reviewing the literature for SYP121. Uemura *et al.* (2004) reported the occasional cytoplasmatic dot in addition to strong PM label after 35S-driven GFP-*At*SYP121 over-expression in protoplast derived from *Arabidopsis* suspension culture cells. When expressing cells were labelled with the lipophilic styryl dye, FM4-64, which is known to follow an endocytic pathway from the PM via endosomes to the vacuole, they showed co-localisation of dye and GFP-SYP121 in these dots (Uemura *et al.*, 2004). Therefore, the dots were interpreted as endosomal entities. Similar observations were made by different authors for the tobacco homologue GFP-*Nt*SYP121 in tobacco protoplasts (Di Sansebastiano *et al.*, 2006). These authors also investigated a converse *Nt*SYP121-GFP fusion and were able to follow this construct through the secretory pathway. In the early stages of expression (less than 18 h) the *Nt*SYP121-GFP fusion was detected in ER-like structures and many small

compartments. With time, the protein reached the cell surface, labelling the PM more or less homogeneously. Later, in a restricted percentage of protoplasts, the fluorescence was concentrated in patches on the cell surface and internal punctuate compartments. Also in these experiments, punctuate structures that appeared after, but not before, PM arrival could be labelled with FM4-64 and were interpreted as endosomes (Di Sansebastiano *et al.*, 2006). Very recently, a stable *Arabidopsis* line (Col0) expressing a N-terminal GFP fusion of *At*SYP121 with its 5'and 3'UTR regions and under its own promoter was analysed (Kato *et al.*, 2010) that had been created earlier by a different group (Enami *et al.*, 2009). It could be shown that in primary roots of seedlings from this line that had been grown for 4 d in the dark, GFP–SYP121 did not localise to the PM. Instead, another compartment that filled a big cell volume was labelled and suggested by Kato *et al.* (2010) to be the vacuole. In contrast, light-grown seedlings showed fluorescence at the PM and formed brefeldin-A compartments, a marker for recycling endosomes. The control, GFP–SYP132 (stable line) was localised to the PM in both dark- and light-grown seedlings and did not form brefeldin-A labelled compartments. Kato *et al.* (2010) suggested that the PM localisation of SYP121, but not SYP132, may be regulated both by light and the protein recycling mechanism, i.e. in the dark SYP121 became first endocytosed and then degraded in the vacuole. Interestingly, for both the PEG-mediated transformation of protoplasts and the onion cell bombardment, the transformed cells were incubated in the dark before confocal analysis. For protoplasts, incubation at 16 °C in the dark is a common procedure to slow down the cell wall reassembly (Hosy *et al.*, 2005). In contrast, co-cultivation with *A. rhizogenes* was performed under long day conditions (16 h light). Thus, to speculate upon a speculation, one might imagine that the complex of SYP121 and KC1, after interaction in the PM, was endocytosed due to dark induced regulation of SYP121, yielding only punctuate endosomal structures in onion and *Arabidopsis* protoplasts at the time of analysis.

In conclusion, the aim of detecting KC1-SYP121 interaction with the BiFC technique could be achieved here. Detection of this interaction in plant cells was an important step in excluding the possibility of an artefact of heterologous expression. Furthermore, the use of an *Arabidopsis* tissue where AtKC1 is suggested to have a function in potassium nutrition (Reintanz *et al.*, 2002), supported proper localisation of the overexpressed KC1 protein, which in turn supports that an observed interaction might have an actual function in plants. In addition, the specificity of KC1 interaction with SYP121 over the control SNAREs SYP122 and SYP111 was again supported by this data set, even when considering the discussed limitations of the BiFC technique. The obtained results pointed most strongly to the PM of transiently transformed mature root hairs as the subcellular localisation of this interaction. As with mbSUS and Co-IP, the converse specificity of SYP121 for KC1 over AKT1 and KAT1 could not be addressed here, because the two latter Shaker channel subunits could not be cloned into the available vectors.

Chapter 4: A function for the interaction between SYP121 and KC1

Introduction

The combined results of the mbSUS, Co-IP and BiFC assays provided strong support for a specific interaction between KC1 and SYP121 despite the individual weaknesses of each technique. The work detailed in this chapter was aimed to discovering a function for this interaction *in planta*. As mentioned earlier (p. 36), KC1 is thought to be a silent regulatory Shaker channel subunit. Expressed on its own, it does not yield measurable K^+ currents (Reintanz *et al.*, 2002; Duby *et al.*, 2008). It was, however, shown that KC1 interacts with other inward-rectifying K^+ channel subunits, including AKT1 and KAT1. The resulting heteromeric channels demonstrated unique K^+ uptake properties in response to membrane voltage different from e.g. AKT1 homomeric channels (Obrdlik *et al.*, 2004; Duby *et al.*, 2008) . Here, the focus was on KC1 interaction with AKT1 and its function in root K^+ uptake.

Results

Expression patterns of *KC1*, *SYP121* and *AKT1* from transcript analysis

As a prerequisite for an interaction between proteins partners that has significance *in planta*, one would expect a temporal and spatial overlapping expression pattern for the respective genes, i.e. the resulting proteins. Therefore, in a first step, the gene expression data available from the online source of the electronic Fluorescent Pictograph (eFP) browser were analyzed (www.bar.utoronto.ca/efp) (Winter *et al.*, 2007). Pictured in Fig. 49A are the cell-type and tissue-specific gene expression profiles of *AKT1*, *KC1*, *SYP121*, and *SYP122* in roots of 6 d old *Arabidopsis thaliana* Col0 seedlings as published in 2003 (Birnbaum *et al.*, 2003). These authors made use of five separate marker lines that expressed GFP in specific cell types of the root: stele, endodermis, endodermis plus cortex, epidermal atrichoblasts, and lateral root cap (see Fig. 49A, grey). All the different root cell types arise from a quiescent centre, where initial cells divide that surround a mitotically less active stem cell niche. Cell types are constrained within cell files, so that each new cell division successively displaces an older cell distal to the quiescent centre. Cells undergo division, elongation, and differentiation when they enter the meristematic, elongation, and maturation zones, respectively, along the longitudinal axis (see Fig. 49A, grey). Because cells are constrained within these files and new cells are born at the root apex, a cell's developmental time line can be tracked along the root's longitudinal axis. For this purpose, Birnbaum *et al.* (2003) dissected roots into independently analyzed pieces according to three developmental-stage-specific cellular landmarks along the longitudinal axis: the meristematic zone until the point where the root tip reached its full diameter (about 0.15 mm from the root tip), the elongation zone (from 0.15 mm to about 0.3 mm from the root tip) and the maturation zone, where root hairs were fully elongated

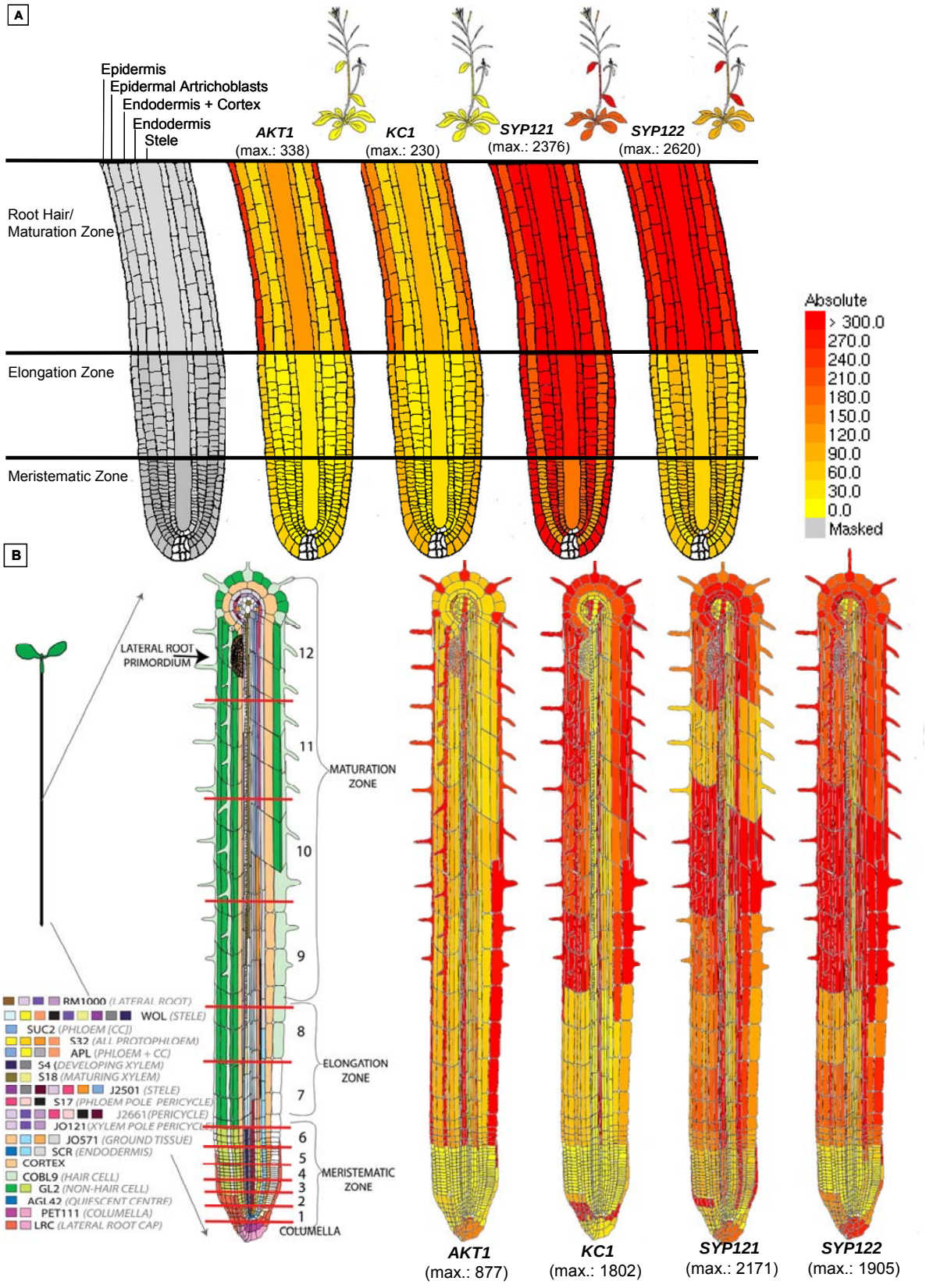

Fig. 49 Root expression patterns of *SYP121*, *KC1* and *AKT1* from transcript analysis

Pictographs were obtained from the online database Fluorescent Pictograph (eFP) browser (Birnbaum *et al.*, 2003; Winter *et al.*, 2007; Brady *et al.*, 2007). The settings of the database output were chosen to reflect absolute absolute transcript levels with a threshold of 300 for (A) and (B) (see colour scale). The maximum expression levels in the investigated tissue (roots of 6 d old *Arabidopsis* plants and adult shoots) are indicated in breaks for (A) and (B). Data for expression levels in individual cell types and tissues were obtained from fluorescently sorted protoplast of 5 (A) or 19 (B) GFP-marked lines. For (B, scheme on left) the colours associated with each marker line reflected the developmental stages of the examined cell type.

(about 0.45 to 2 mm from the root tip) (Fig. 49A, grey) (Birnbaum *et al.*, 2003). The chosen tissues were turned into protoplasts and their GFP-expressing cells isolated with a fluorescence-activated cell sorter. The mRNA of these cells was analyzed by hybridization to Affymetrix ATH1 GeneChips (Birnbaum *et al.*, 2003). The resulting data sets were made available as pictographic representations in the eFP browser (Winter *et al.*, 2007). The images in Fig. 49A for *AKT1*, *KC1*, *SYP121* and *SYP122* were obtained from this database. The settings were chosen to show the 'absolute' mode of interpretation, where the expression level for a gene in the investigated tissue is directly compared to the highest signal recorded for this particular gene. Thus, low levels of expression are coloured yellow and high levels are coloured red. Winter *et al.* (2007) stated that the appropriate colour of a tissue was determined by evaluating the ratio of the averaged replicates to the positive or negative maximum and converting it to the equivalent place on the colour scale (Fig. 49). To facilitate comparisons, the signal threshold for the shown colour-scale was set here to 300 for each gene, meaning that anything coloured red in the respective images was expressed at absolute values of 300 or higher. The maximum absolute expression level for each gene is given in brackets under the respective gene name.

According to the presented data, *AKT1*, *KC1*, *SYP121* and also *SYP122* showed high and overlapping expression in the epidermis of the root hair/ maturation zone, with the exception of atrichoblasts (epidermal cells that do not give rise to root hairs). While the specific localisation of the trichoblasts was represented here as the place of highest expression for *AKT1* and *KC1* with maximum values of 338 and 230 respectively, both *SYP121* and *SYP122* were expressed not only in the trichoblasts but in all investigated cell types of the root hair/ maturation zone and in uniformly high overall values (2376 and 2620 respectively). *SYP121* was additionally expressed throughout all investigated cell types of the elongation and meristematic zone to equally high and uniform levels almost everywhere. In contrast, *SYP122* was not or only slightly expressed (0-90) in these regions. No GFP-marker cell lines are available for shoot tissue yet. However, the eFP browser provides data for overall expression in rosette leaves versus cauline leaves and stem (Fig. 49A, small insets). Both Shaker channel subunits, *AKT1* and *KC1* showed no expression in shoot tissues, while *SYP121* was highly expressed in all tested shoot tissues.

More recently, the eFP browser published an additional data set for gene expression in *Arabidopsis* seedling roots based on the data published in 2007 (Brady *et al.*, 2007). These authors used the same technique and plant tissue (6-7 d old Col 0) as described for Birnbaum *et al.* (2003). However, they created microarray expression profiles of higher resolution by taking in account nearly all the different *Arabidopsis* root cell types and thirteen transverse sections along the root's longitudinal axis (Fig. 49B, left side, red lines). In total, 19 fluorescently sorted GFP-marked lines were analyzed as indicated in Fig. 49B (left side). The colours associated with each marker line reflect the developmental stages of the examined cell type. Again, the settings of the database output were chosen to reflect absolute expression values with a threshold of 300 (see colour scale, Fig. 49).

The resulting pictographs (Fig. 49B) confirmed the overlapping high gene expression of *AKT1*, *KC1*, *SYP121* and *SYP122* in root epidermal trichoblasts of the maturation zone only. Both

data sets agreed on the very low expression of *AKT1* in atrichoblasts. In contrast to the previous data set, *KC1* appeared to be expressed equally high in these two cell types (trichoblast and atrichoblasts). Furthermore, in contrast to the previous data set, the maximum absolute expression value for *KC1* (1802) was about two times higher than for *AKT1* (877), where it had been lower than *AKT1* before. This result also brought the expression level of *KC1* closer to the maximum absolute values obtained for *SYP121* and *SYP122* expression in this experiment (2171 and 1905, respectively). Previously, the expression of both SNAREs had appeared almost seven times stronger than that of the two Shaker channels. Furthermore, the newer data set indicated slightly lower *SYP121* expression in trichoblasts than in atrichoblast, while the opposite appeared to be the case for *SYP122*. A noticeable difference was also the expression of *AKT1* in trichoblasts of both the maturation and elongation zone, while previously only the maturation zone had shown expression. In contrast, expression of *SYP121* in the elongation zone and in a part of the maturation zone appeared reduced in the dataset from Brady *et al.* (2007). In summary, both datasets confirmed an overlapping expression pattern for *KC1*, *SYP121* and *AKT1* in root epidermal trichoblasts of the maturation zone.

Analysis of *Syp121* Promoter-GUS plants

To investigate the overlapping expression of *KC1*, *SYP121* and *AKT1* indicated by the eFP browser, on the level of promoter activity, promoter fusions to the CDS of the GUS enzyme (Jefferson *et al.*, 1987; de Ruijter *et al.*, 2003) were analyzed. At the time, promoter GUS studies for *KC1* and *AKT1* had already been published by Reintanz *et al.* (2002) and Largarde *et al.* (1996), respectively (Fig. 50-I). The images, taken from the respective publications, showed X-GLUC (5-bromo-4-chloro-3-indolyl ß-D-glucuronide; chromogenic substrate of GUS enzyme) stained seedlings at the cotyledone-stage of development. Both the *AKT1* and *KC1* promoter appeared to drive GUS expression exclusively in the root and root hairs at this developmental stage.

The promoter-*SYP121*-GUS expressing plants investigated here, were created but not investigated by a former post-doc of Prof. Blatt's group, Dr. M. Paneque (University of Chile, Chile). Dr. Paneque fused both a 2 kb and 3 kb region immediately 5' of the start codon of the Syp121 gene to the GUS reporter CDS present in the vector pCAMBIA 1301 (www.cambia.org). He selected stable lines with hygromycin and further propagated those to the second generation (T2). Here, three independent T2 lines for each construct (2 kb and 3 kb) were pre-selected on hygromycin to ensure that each individual T2 plant had at least one copy of the transgenic allele and subsequently grown in liquid MS medium. These plants were analyzed at three different developmental stages: 7 d (which corresponded here to fully developed cotyledons), 14 d (with a fully developed first pair of true rosette leaves) and 21 d (6 rosette leaves).

A representative sample for a 2 kb and 3 kb promoter *SYP121* expressing line at each time point is pictured in Fig. 50-II together with a wt *A. thaliana* Col0 plant. The wt served as control and indicated the absence of plant intrinsic GUS activity under the chosen experimental conditions (Jefferson *et al.*, 1987). Both lines (2 kb and 3 kb) showed *SYP121* promoter activity in roots

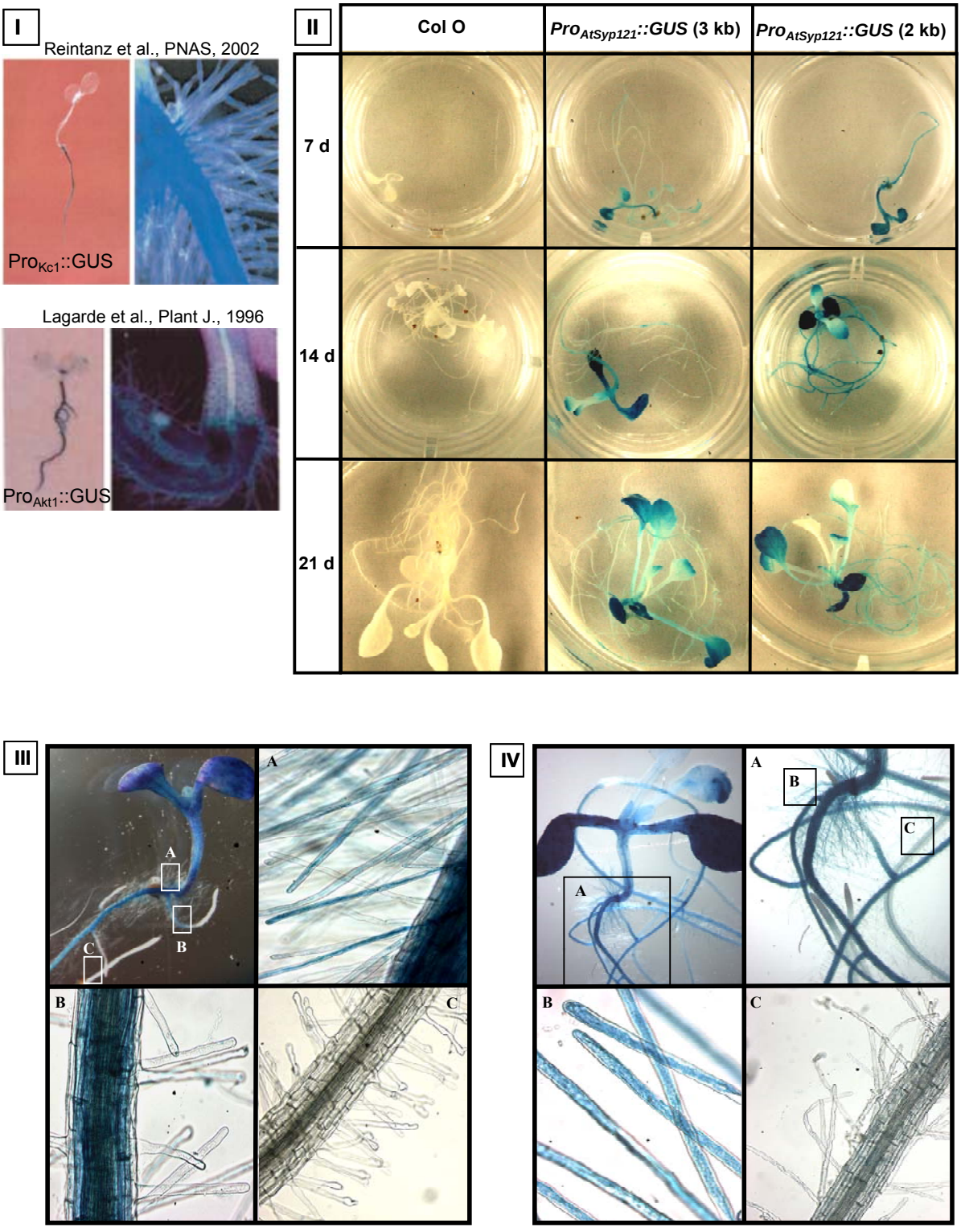

Fig. 50 Analysis of *Syp121* Promoter-*GUS* plants

Seedlings (cotyledon-stage) of promoter-*GUS* plants for *AKT1* (Lagarde *et al.*, 1996), *KC1* (Lagarde *et al.*, 1996) (I) and *SYP121* (2 kb and 3 kb line, Dr. Paneque) exhibited GUS activity in root tissues. Root tissues of older plants (14 d and 21 d), especially for the 2 kb *Pro$_{SYP121}$::GUS* line, also showed GUS staining as was reported previously for *Pro$_{Akt1}$::GUS* lines (Lagarde *et al.*, 1996). In contrast to the promoter of *AKT1* and *KC1*, the promoter of *SYP121* was strongly active in cotyledons and true leaves (stronger in apex). Magnified views of the 7 d (III) and 14 d (IV) old plants from the 2 kb *Pro$_{SYP121}$::GUS* revealed strong GUS staining of mature root hairs and root epidermis at the end of the maturation zone. In contrast, young root hairs and atrichoblast cells in the beginning of the maturation zone, as well as the elongation and meristematic zone in general exhibited no or only very faint *SYP121* promoter activity.

throughout all three developmental stages, although GUS staining was more pronounced for expression of the reporter gene under the control of the 2 kb SYP121 promoter (Fig. 50-II). In addition, in all pictured plants, GUS activity appeared strong in hypocotyl and cotyledons as well as the apex of young true leaves (14 d). Older leaves (21 d) appeared more uniformly stained but stronger towards the apex.

Magnified views of the 7 d and 14 old plants from the 2 kb ProSYP121::GUS line are shown in Fig. 50-III and Fig. 50-IV, respectively. In both plants mature root hairs and root epidermis of the maturation zone showed strong SYP121 promoter expression (Fig. 50-III-A and Fig. 50-IV-B). No cross-sections were performed here to obtain information about the inner layers of root cell tissue (e.g. cortex, endodermis). However, GUS staining was absent from the root epidermis and younger growing root hairs in the middle of the maturation zone (Fig. 50-III-B). The youngest root hairs in the beginning of the maturation zone, as well as the elongation and meristematic zone in general exhibited no or only very faint SYP121 promoter activity (Fig. 50-III-C and Fig. 50-IV-A/IV-C).

A phenotype for *kc1* and *syp121* mutants in K^+ uptake

The authors of the two papers that initially described the *Arabidopsis akt1* loss-of-function mutant, had already suggested that AKT1 mediates growth-sustaining K^+ uptake into roots over a wide range of external K^+ concentrations and significantly contributes to high-affinity K^+ uptake within low external K^+ concentration ranges (Hirsch *et al.*, 1998; Spalding *et al.*, 1999). Hirsch *et al.* (1998) and Spalding *et al.* (1999) had based their early conclusions in part on growth experiments of *akt1* mutant seedlings in comparison to wt plants. For this purpose, two sets of growth media were employed that each contained three different K^+ concentrations (1 mM, 0.1 mM and 0.01 mM). One set of media was made up with 2 mM ammonium ions (NH_4^+) in addition to the different K^+ concentrations and one set was without addition of NH_4^+.

The first three panels of Fig. 51A (panel numbers in upper right corner) show a reproduction of the growth experiment performed by Hirsch *et al.* (1998) with highly similar results. Ten days after sowing, seedlings of the *akt1* mutant were indistinguishable from the wt in all three K^+ concentrations as long as the medium was NH_4^+-free (upper rows of seedlings). In addition, the different K^+ concentration themselves did not led to apparent growth differences for either wt or *akt1* mutant plants (upper rows of seedlings). On medium with NH_4^+, again no growth difference was observed between wt and *akt1* mutant in the highest K^+ concentration (1 mM; lower rows of seedlings, right side). However, with intermediate and low K^+ concentrations plus NH_4^+, differences between wt and *akt1* mutant became apparent. In these two conditions, the *akt1* mutant showed noticeably reduced root growth already at 0.1 mM K^+ and to an extreme in 0.01 mM K^+ (lower rows of seedlings, middle and left side respectively). Also cotyledon development was affected to some extent.

Spalding *et al.* (1999) had measured a similar NH_4^+-dependent inhibition of Rb^+ uptake into *akt1* mutant seedlings under low external Rb^+ concentrations. The isotope $^{86}Rb^+$ is used widely

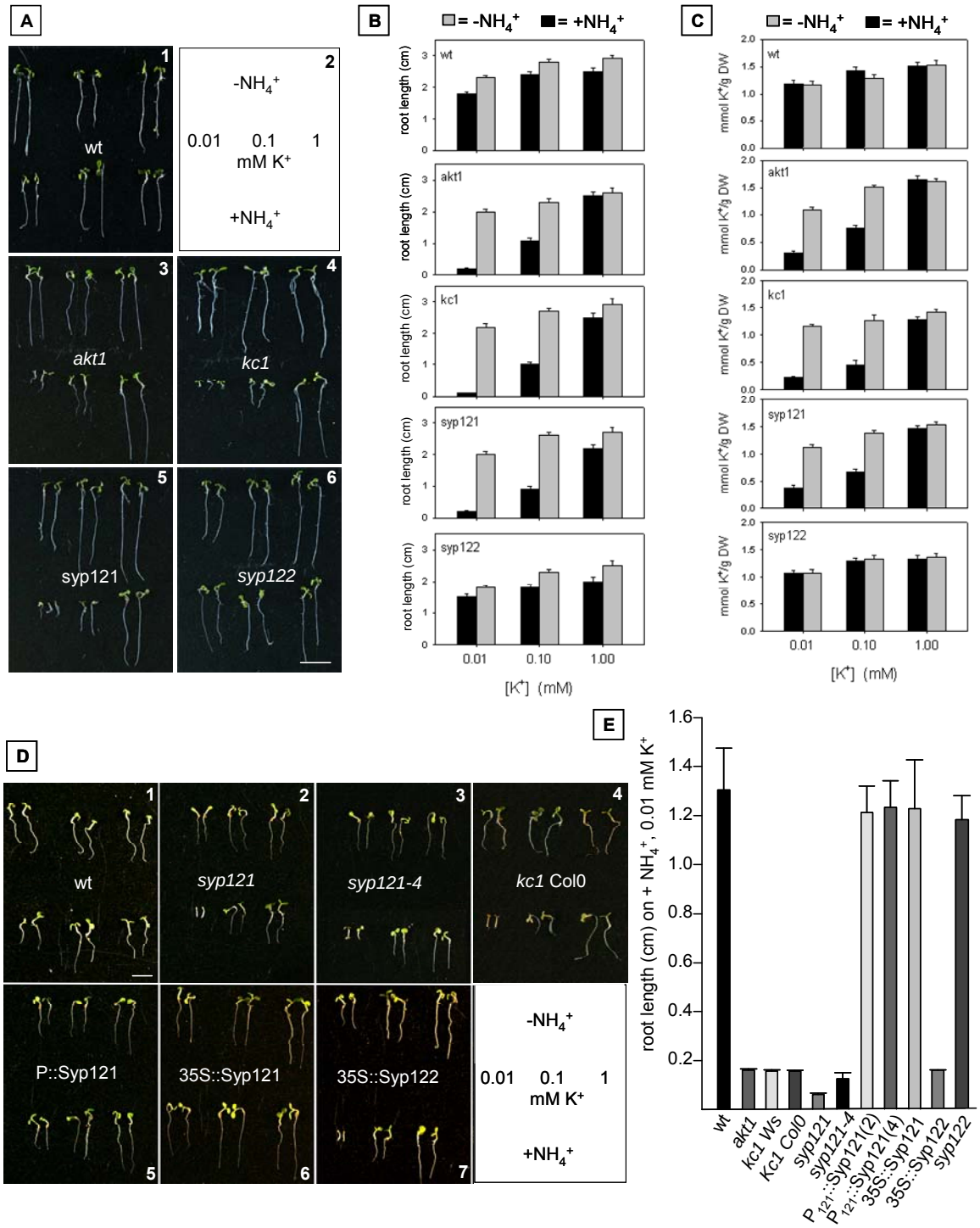

Fig. 51 A growth phenotype for *kc1* and *syp121* in K^+ uptake

Plants in (A-E) were grown in sterile liquid growth medium containing 0.01, 0.1, and 1.0 mM K^+ with and without 2 mM NH_4^+ for 10 d (A-C) and 7 d (D-E) in long day conditions. Both a *kc1* and a *syp121* mutant mirrored the previously reported phenotype of the *akt1* mutant (Hirsch *et al.*, 1998; Spalding *et al.*, 1999): under conditions of low external K^+ (0.01 mM) and the presence of NH_4^+, root (and cotyledon) growth of the *akt1* mutant was severely inhibited compared to the wt (A). The absence of NH_4^+ restored *akt1* growth under the same low external K^+ concentrations. In contrast, plants with a loss-of-function mutation in the control SNARE SYP122 behaved in all conditions as the wt. These observations were reflected in the statistical analysis of root length (B for A and E for D) and whole seedling K^+ contents normalized to dry weight (C) as measured by ICPOES (n= 20 seedlings per one of three replicas for each line and each growth condition, bars are means ±SE for B, C, E). NH_4^+-sensitivity in K^+-dependent growth was not allele specific as demonstrated by independent mutant lines for Kc1 (*kc1* Col0) and Syp121 (*syp121-4*) (D, panel 3 and 4) and (E). Furthermore, NH_4^+ independence for growth in low external K^+ was restored in *syp121* mutant *Arabidopsis* complemented with a fluorescently tagged construct of SYP121 but not SYP122 when driven by the SYP121 or 35S promoters (D, panel 5-6) and (E). white scale bar = 1 cm.

as a K^+ tracer in transport kinetic studies because of its similar ion radius (Marschner, 1995). From these results, Hirsch *et al.* (1998) and Spalding *et al.* (1999) concluded that wt roots employ at least two genetically distinct K^+ uptake mechanisms. One component of the 'high affinity' K^+ uptake mechanism operating under low K^+ conditions is the AKT1 channel and the other is represented by K^+ transporters that are specifically inhibited by NH_4^+ (mostly HAK5) (Pyo *et al.*, 2010). NH_4^+ specifically inhibits the non-AKT1 component by competing for substrate (K^+) binding sites on these transporter(s).As mentioned in the General Introduction, more recent experiments with *akt1/hak5* double and single mutant confirmed that these two K^+ uptake systems operate in parallel and contribute each significantly as high-affinity uptake mechanism under external K^+ concentrations between 0.01 and 0.1 mM K^+ (see Fig. 4, p. 24) (Pyo *et al.*, 2010; Rubio *et al.*, 2010). The inclusion of NH_4^+ in the medium made K^+ uptake dependent on AKT1, which led to the observed growth reduction of *akt1* mutant seedlings under very low external K^+ (0.01 mM). A 'true' double mutant of *akt1/hak5* is unable to grow on 0.01 mM K+ after the radicle has emerged from the seed (Pyo *et al.*, 2010). Higher external K^+ concentration (see 0.1 mM, 1 mM), increasingly protected the *akt1* mutant from K^+ deficiency despite the presence of NH_4^+. This effect was again a consequence of competition. Rising K^+ in turn 'out-competed' NH_4^+ and thus liberated the K^+ transporter component increasingly from its blockage.

The regulatory Shaker channel α-subunit KC1 is thought to preferably form heterotetramers with the α-subunit AKT1 (see General Introduction, p. 22) (Dreyer *et al.*, 1997; Reintanz *et al.*, 2002; Pilot *et al.*, 2003a; Obrdlik *et al.*, 2004; Duby *et al.*, 2008; Geiger *et al.*, 2009). At the time, electrophysiological measurements on root hairs of wt, *kc1* and *akt1* plants had already suggested that KC1 contributes to the inward K^+ conductance in wt plants, probably in association with AKT (Reintanz *et al.*, 2002). Thus, it was speculated that a *kc1* loss-of-function mutant should exhibit a similar phenotype as the *akt1* mutant, when AKT1 and KC1 were to function as heterotetramers in root K^+ uptake. The homozygous *kc1* mutant used here was kindly provided by H. Sentenac (INRA, France, unpublished result). As the fourth panel in Fig. 51A shows, indeed *kc1* mutant seedlings grown under the same experimental conditions as described above, exhibited identical NH_4^+ dependent (root) growth retardation in low external K^+ concentrations as the *akt1* mutant (0.1 mM and 0.01 mM, lower row). Again, in the absence of NH_4^+ or with NH_4^+ but high K^+, *kc1* mutant and wt grew similarly well.

The observed interaction between KC1 and SYP121 in mbSUS, Co-IP and BiFC studies, raised the question whether this SNARE might be implicated in root K^+ uptake as well. As can be seen in Fig. 51A (panel 5), a *syp121* loss-of-function mutation (Collins *et al.*, 2003) specifically suppressed seedling (root) growth in low K^+ concentrations in the presence of NH_4^+, mimicking both the *akt1* and *kc1* mutant (0.1 mM and 0.01 mM, lower row).

By contrast, plants with a loss-of function mutation in the control SNARE SYP122 (Assaad *et al.*, 2004) behaved as the wt with regard to the relative root growth behaviour in the six different growth conditions (Fig. 51A, panel 6). A difference to the wt was observed in an overall reduction of root length in the *syp122* mutant (about 20%, Fig. 51B). However, this effect was independent of NH_4^+ and evident at all K^+ concentrations (compare first and last graph). Null

mutants for *syp111* are seedling lethal (Lukowitz *et al.*, 1996). Therefore, this control SNARE was not used for the growth assays.

The five graphs of Fig. 51B summarise the root length measurements for the experiment of which representative seedlings were photographed for Fig. 51A. This statistical analysis closely reflected the above detailed description of the growth behaviour of the different loss-of-function mutants in the respective media. Wt plants showed only slight reductions in root length with decreasing external K^+ and irrespective of the presence or absence of NH_4^+.

It has to be mentioned here that wt, *akt1* and *kc1* were of the ecotype Wassilewskija *(*Ws), while *syp121* and *syp122* had Col0 background. Wt plants of both ecotypes were analyzed but then pooled (data not shown) as no significant differences were found under these particular growth conditions. In general, genetic variation among *Arabidopsis* ecotypes has been shown to result in quantitative traits of physiological importance (Koornneef *et al.*, 2004). However, similar observations as reported here, had previously been made by other authors (Gierth *et al.*, 2005; Pyo *et al.*, 2010). Pyo *et al.* (2010) could show that all progeny of *akt1* (Ws) crosses with *hak5* (col0) showed essentially the same low K^+-dependent phenotype, indicating that an impact on phenotype occurrence due to *Arabidopsis* ecotype differences was unlikely.

As would be expected for a functional involvement of SYP121 and KC1 in AKT1-dependent root K^+ uptake, the total K^+ content of *syp121*, *kc1* and *akt1* seedlings mirrored their root growth phenotype. The five graphs in Fig. 51C show an ICPOES analysis of the K^+ content of whole seedlings (normalized to dry weight) for an identical experiment as described in Fig. 51A/B. The ICPOES measurements and data analysis pictured in Fig. 51C were performed by Prof. Blatt with the kind help of Dr. Armengaud and Dr. Littlejohn (University of Glasgow). Seedlings of the *akt1*, *kc1* and *syp121* knock-out lines alike showed strongly reduced K^+ content indicating reduced K^+ uptake when grown in low K^+ medium with NH_4^+ (0.1 mM and 0.01 mM). In contrast, the *syp122* mutant and the wt were only slightly affected by K^+ content reduction under the same conditions.

To confirm that the NH_4^+ sensitivity in K^+ -dependent growth was not allele specific, an independent *kc1* loss-of function mutant of the Col0 ecotype (Reintanz *et al.*, 2002) as well as the an additional *syp121-4* mutant (Col0) (Collins *et al.*, 2003; Zhang *et al.*, 2007) were analyzed. As the photographs in Fig. 51D (panel 3 and 4) and the corresponding statistical analysis of root length measurements in Fig. 51E show, both independent mutants demonstrated an identical phenotype as their corresponding allele (*kc1* Ws and *syp121*) in Fig. 51A/B. Fig. 51E summarises only root length data from seedling growth (7 d) on NH_4^+/ 0.01 mM K^+ medium. Not all of the data sets represented in Fig. 51E have a corresponding picture in Fig. 51D for reasons of space. Omitted data sets showed high similarity to their counterparts pictured in Fig. 51A.

Three different types of complementation lines were investigated to relate the observed K^+ uptake phenotype of the *syp121* mutant to the genetic lesion in this SNARE. These plants were kindly supplied by Pajonk *et al.* (2008). The first type was represented by stable transformants of *syp121* (Col0) mutant plants expressing an YFP-SYP121 fusion under the control of the Syp121 promoter (two lines: P_{121}::Syp121 (2) and (4)). For the second type of complementation lines

syp121 had been transformed stably with a CFP-SYP121 fusion expressed from the 35S promoter (35S::Syp121). NH_4^+ independent growth in low K^+ conditions was restored to all these plants (Fig. 51D, panel 5 and 6, E). In contrast, the third type of stable complemented *syp121* mutant plants, where the 35S promoter controlled a CFP-SYP122 fusion instead (35S::Syp122) behaved exactly as the (untransformed) *syp121* mutant, i.e. showed reduced root and overall growth in medium with NH_4^+ and decreasing external K^+ concentrations (Fig. 51D, panel 7, Fig. 51E).

Subcellular localisation of AKT1-GFP in the *syp121* mutant

At least two scenarios could possibly explain the observed NH_4^+-dependent phenotype of the *syp121* mutant on low K^+ medium in its resemblance to the *akt1* and *kc1* mutants under these conditions (Fig. 51). Based on the direct interaction between KC1 and SYP121, the favoured explanation was a complex of all three proteins. Optimal K^+ uptake via AKT1-KC1 heteromeric channels would thus require every component of such a complex. It was speculated that SYP121 might influence the heteromeric AKT1-KC1 channel in a regulatory manner via its direct interaction with KC1, reminiscent of the observations made for channel regulation by the mammalian Syntaxin1A (see p. 64). As alternative explanation, the more classical vesicle trafficking related function of SYP121 needed to be considered. In principle, a SNARE complex involving the PM Qa-SNARE SYP121 might be responsible for the fusion of secretory vesicles that carry the ER-derived pre-assembled AKT1-KC1 heteromeric channels to the PM (see General Introduction, p. 38). Assuming that there would be no redundancy with other PM Qa-SNAREs of the SYP1 subfamily (see General Introduction, p. 52), the AKT1-KC1 channel should fail to reach the PM in *syp121* loss-of-function mutants. This failure to deliver the heteromeric channel to the sites of K^+ uptake in the *syp121* mutant, e.g. the root hair PM, should thus in effect mimic the *akt1* and *kc1* mutants with regard to the above described K^+ uptake and root growth phenotype. In a first attempt to discriminate between these two scenarios, an AKT1-GFP fusion under the control of the 35S promoter was expressed in *syp121* mutant and wt plants. After transient root transformation as described for Chapter 3 (p. 180 and 107), GFP-fluorescence was detected at the cell periphery in mature root hairs of the *syp121* mutant. A representative root hair is pictured in Fig. 52A. The white dashed lines in the third panel of Fig. 52A indicate positions at which digital transects of this root hair were taken. These transects were obtained from a three-dimensional projection of the confocal image stack corresponding to the pictured root hair.

The resulting images of the respective transects (shown in the fourth panel) supported a peripheral localisation of the AKT1-GFP fluorescence that was distinct from the cytoplasm and tonoplast (TP). Transects taken at a distance between 0.4- 1 µm from the root hair apex, for example, were in the region of the cytoplasm. As mentioned in Chapter 3, the apical root hair cytoplasm is densely packed with ER, Golgi apparatus and mitochondria and thus visible as 'cap' in the brightfield (see panel 1, 2 and root hair scheme). The corresponding transect images showed a hollow ring of fluorescence indicating the absence of AKT1-GFP from the cytoplasm and its enclosed organelles.

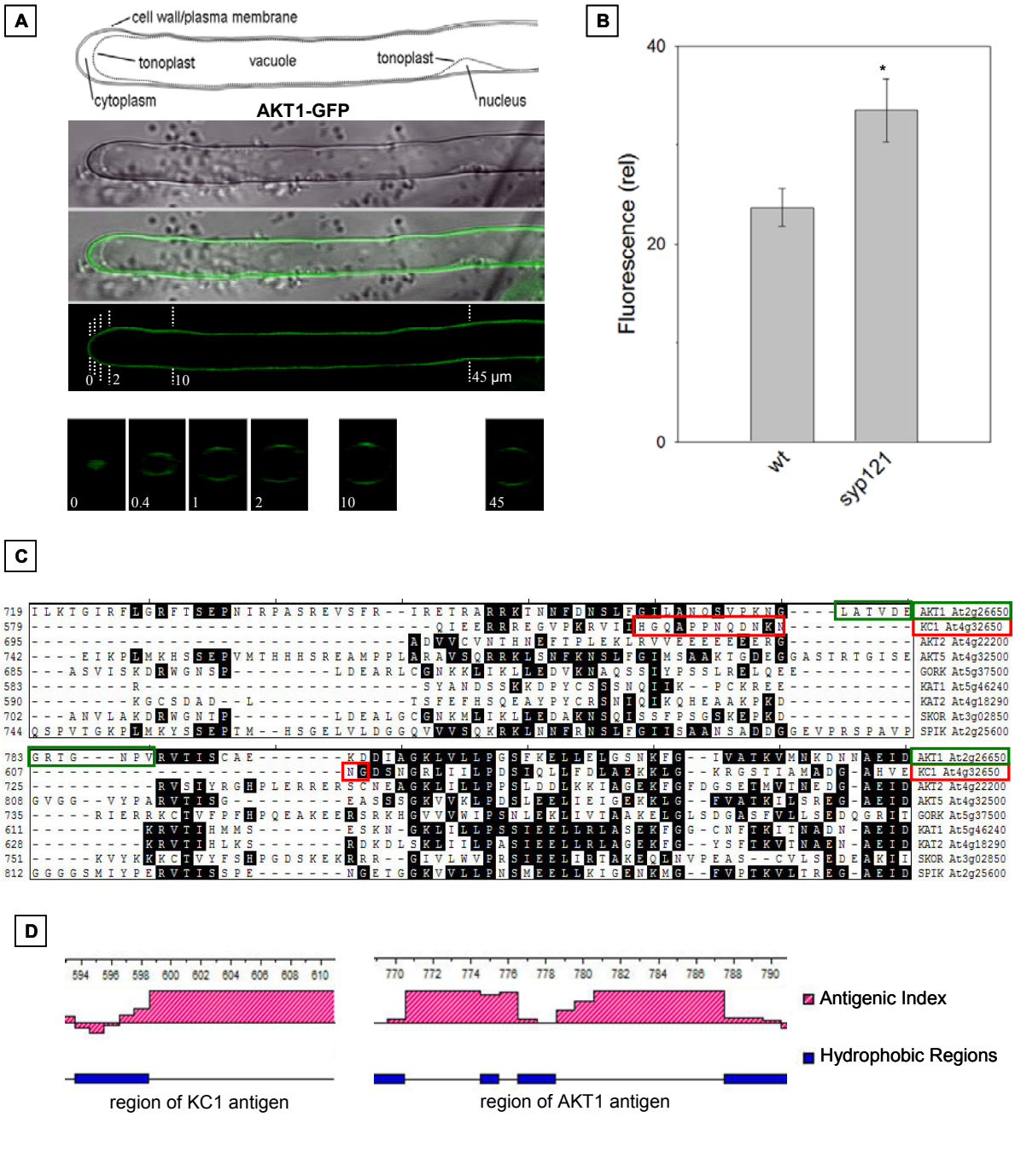

Fig. 52 AKT1-GFP localises to the cell periphery in *syp121* root hairs

After transient root transformation with an AKT1-GFP fusion, mature root hairs of the *syp121* mutant (and wt, data not shown), displayed a defined peripheral distribution of the GFP fluorescence (A). Digital three-dimensional transect analysis of the AKT1-GFP distribution indicated absence from the dense cytoplasm and tonoplast boundary behind the tip and around the nucleus (A, panel 3 and 4). Transects were taken at positions (in µm) from the apex as indicated by the white dashed lines. The shown images are single plane views of confocal stacks with the transects being the exception. Quantification of AKT1-GFP fluorescence in mature root hairs after transient transformation of *syp121* and wt plants (B) revealed significantly higher values in the *syp121* mutant after correction for background fluorescence from control measurements of plants incubated with untransformed *Agrobacterium* (bars are means ±SE of fluorescence in arbitrary units, n= 20, means differ significantly at $P < 0.05$). white scale bar: 5 µm
Shown in (C) is the c-terminal end of an alignment of the nine *Arabidopsis* Shaker channel proteins (ClustalW, MegAlign software of DNASTAR package). Boxes indicate the chosen regions for synthesis of peptide antibodies against AKT1 (green) and KC1 (red). For the chosen regions, antigenic properties were confirmed with the indicated tools of the Protean (DNASTAR package) software (E).

Transects at a distance of 2 µm and 45 µm from the root hair apex were taken to distinguish between TP and PM. The section at 45 µm represented the place where the root hair nucleus separated the PM from the TP (see panel 1, 2 and root hair scheme). The corresponding image below would be expected to show TP labelling as indentation in the circular periphery. In contrast, the fluorescence was detected again as full circle, supporting the conclusion that AKT1-GFP was absent from the TP. Similar results for the localisation of AKT1-GFP fluorescence were obtained for transient expression in mature root hairs of wt plants (data not shown). Together these results implicated that the loss-of-function mutation in the Qa-SNARE SYP121 did not lead to an appreciable retention of the Shaker channel subunit AKT1 within the secretory pathway (ER, Golgi) or to miss-localisation (TP).

To further confirm that the peripheral localisation of AKT1-GFP indicated PM localisation, an HA-HA tag was inserted into the extracellular loop between the first and second TMD of the Shaker channel. Double labelling with cytosolic GFP and an external tag recognized by an antibody-coupled flourisher had been a very efficient tool to confirm the PM localisation of KAT1 in tobacco leaf protoplasts (Sutter *et al.*, 2006b). Here a protocol was developed for the successful isolation of root hair protoplasts from *Arabidopsis* seedlings. However, transformation with AKT1-HA-HA_{ext}-GFP could not be achieved. Protein extraction of seedlings co-incubated with *Agrobacterium* tissue and Western Blot analysis with anti-GFP revealed a band of roughly the size of the fluorophore indicating protein degradation (data not shown).

The observations that AKT1-GFP appeared to reach the PM in the *syp121* mutant could not exclude entirely that a lack of the vesicle trafficking function of SYP121 caused the observed K^+ uptake phenotype in the *syp121* mutant. For example, a partial redundancy in PM Qa-SNAREs responsible for Shaker channel delivery to the PM would result only in a reduced number of available channels in the *syp121* mutant. The overall localisation (PM) would stay the same and lead to a result as described in Fig. 52A and B despite a lack in SYP121-dependent vesicle delivery. In theory, such a reduced amount of K^+ uptake competent channels might already be sufficient to cause the observed phenotype in the *syp121* mutant. Quantification of AKT1-GFP fluorescence was indented to reveal differences in the extent to which this Shaker channel reached the PM after transient root transformation of *syp121* mutant and wt plants (Fig. 52C).

Single plane images were taken with identical confocal settings, zoom and depth of focus from mature root hairs of approx. the same location in the maturation zone (see Fig. 49) to ensure similar developmental stage, i.e. age. The bar chart in Fig. 52C shows the mean fluorescence intensities (arbitrary units) of a representative experiment. For both sets of data the background fluorescence derived from a control with untransformed *Agrobacterium rhizogenes* was subtracted. Several repetitions of this experiment confirmed that the mean fluorescence obtained for AKT1-GFP expression in the *syp121* mutant was significantly higher (at $P < 0.05$) than for expression in the wt. An explanation for this unexpected result was not found. Thus, reservations were placed on the conclusions drawn from this fluorescence quantification experiment. It appeared that the loss of SYP121 protein did not cause a reduced number of AKT1-GFP channels to be delivered to the PM.

In summary, transient over-expression of AKT1-GFP suggested that loss of the SYP121

function in SNARE complex formation for vesicle fusion, did not contribute to the observed K^+ uptake phenotype in *syp121* mutant plants (Fig. 52A-C).

Design and testing of antibodies against *Arabidopsis* AKT1 and KC1

Distinction between a vesicle trafficking or a putative channel regulation mode for SYP121 in AKT1-dependent K^+ uptake was of vital interest for this work. Therefore, it was necessary to investigate, whether also native AKT1 (and KC1) is delivered to the root epidermal PM in the *syp121* mutant. Localisation of native proteins required antibodies against the two Shaker channel subunits. Gaymard *et al.* (1996) had already created an anti-*At*AKT1 to verify their solubilisation of heterologously expressed *At*AKT1 from *Sf9* insect cell membranes. Prof. Sentenac (INRA, France) kindly provided an aliquot of this antibody. However, in agreement with previous results published for this antibody by Urbach *et al.* (2000), all attempts to obtain a specific signal in Western Blot analysis of plant proteins failed (data not shown). Reintanz *et al.* (2000) had published the successful KC1 detection in total membrane fractions of *Arabidopsis* roots with a polyclonal peptide antibody. Unfortunately they were no longer able to provide aliquots of this antibody. Thus, new antibodies against AKT1 and KC1 were designed here.

For this purpose, the amino acid (aa) sequences of the nine *Arabidopsis* Shaker channel subunits (see p. 13) were aligned using the ClustalW algorithm for multiple alignments (MegAlign software of DNASTAR package, default parameters). A region with low sequence homology between the Shaker family members could only be identified in the very C-terminus of this aligment (see Fig. 52D, identical aa shaded in black). The pictured part of the alignment encompasses the aa 719- 857 of AKT1 (full-length: 858 aa) and the aa 579- 662 of KC1 (full-length: 663 aa). Out of these regions, the sequences boxed in green (AKT1, aa 776- 789) and red (KC1, aa 595- 608) were chosen as antigens for the production of peptide antibodies.

In addition to low homology with the respective other members of the Shaker family, the two chosen regions did not contain any known protein motifs. A number of different search engines (e.g. www.expasy.org; superfam, prints, pfam on www.geneinfinity.org/sp/sp_proteindom.html) had agreed on the absence of such motifs as are predicted to interact with other proteins or DNA (e.g. potential coiled-coil domains). The predicted motifs closest to the chosen AKT1 antigen were an anchoring domain involved in protein-protein interaction (Pilot *et al.*, 2003b) further upstream (aa 680- 709) and a KHA domain with a putative function in channel clustering (Ehrhardt *et al.*, 1997) directly downstream (aa 801- 857). For KC1, a KHA domain was predicted just downstream of the chosen antigen as well (aa 610- 662) together with an upstream potential coiled-coil domain (aa 528- 558).

The default parameters of the Protean software (DNASTAR package) were used to predict the antigen city of the chosen AKT1 and KC1 regions. This tool uses the Jameson-Wolf algorithm to predict antigenic determinants by combining existing methods for protein structural predictions (Jameson & Wolf, 1988). As can be seen in Fig. 52E, results appeared as multiple peaks (pink), each of which represents potential antigenic determinants. Since antigenic sites are typically

located in areas of greatest local hydrophilicity, the prediction of hydropath with the Hop-Woods method in the same software was added as complementary information (blue). From these results, the chosen regions for AKT1 and KC1 were expected to have good antigenic properties during immunization of the carrier animal. Finally, the chosen peptides were blasted against the set of *Arabidopsis* protein sequences available at NCBI (http://blast.ncbi.nlm.nih.gov). This search excluded that a highly similar peptide was present in an unrelated protein, which could potentially cross-react later with the antigen-specific antibody (data not shown).

Peptide synthesis, production of the corresponding polyclonal antibodies in rabbit and affinity purification against the antigen were performed by Agrisera (Sweden, www.agrisera.com). At the end of the purification procedure, the antibodies were eluted in two steps with neutral and low pH respectively. While neutral pH prevents irreversible denaturation during elution, this mild treatment usually reduces the total yield of antibody and in particular of the fraction that has the highest affinity for epitomes on the antigen. Polyclonal antibodies recognize a mixture of different epitomes from one antigen. An epitope is represented by 2-3 aa, either in a row (linear epitope) or brought together by the three-dimensional structure of the antigen. In initial tests, the pH 7 elution fractions of the anti-KC1 yielded either no signal or several weak bands (data not shown). Thus, for all experiments described below, the acid elution fraction was used which yielded much better results. In case of the anti-AKT1 only the Western Blot in Fig. 53F was performed solely with the acid elution fraction. As all of the initial experiments yielded no (specific) signals for the use of this antibody, membranes were in general probed with both elution fractions (see below).

Initially, the anti-AKT1 and anti-KC1 were tested in Western Blot analysis of LPC-solubilised membrane fractions from *Sf9* insect cells over-expressing AKT1-VSVG, KC1-Myc or KAT1-2xHA (compare Chapter 2, p. 151ff.). Infection with empty Baculovirus served as control. Equal amounts of the different solubilised membrane fractions were separated by SDS-PAGE on two identical gels (Fig. 53A, compare PonceauS stains in lower panel). After blotting, one membrane was probed with anti-KC1 antibody in a 1: 700 dilution and the other with an identical dilution of pre-immune serum (upper panel, left and right side, respectively). The red arrow in Fig. 53A (left panel) points to the single band detected by the anti-KC1. The molecular weight indicated by the height of this band corresponded to the signal obtained with anti-Myc for KC1-Myc (see Fig. 37, p. 151). No signal of a similar height was detected by the pre-immune serum in the corresponding KC1-expressing membrane fraction (upper panel, right side). This control excluded the possibility that an antibody that was already present before immunization recognised per chance a protein of a similar molecular weight than KC1.

The anti-KC1 detected no signal in membrane fractions of insect cells infected with empty Baculovirus indicating that the protein recognized as KC1 was not an incorrectly identified insect or virus protein (upper panel, left side, lane 1 versus lane 2). Finally, the anti-KC1 produced no signal on solubilised membrane fractions of *Sf9* cells expressing AKT1 or KAT1 (upper panel, left side, lane 2 and 3). This result indicated that the anti-KC1 did not cross-react with these two Shaker channel subunits. A possible criticism might be derived from earlier experiments with these Shaker channel constructs. Results described in Chapter 2 had shown signals obtained for AKT1-VSVG

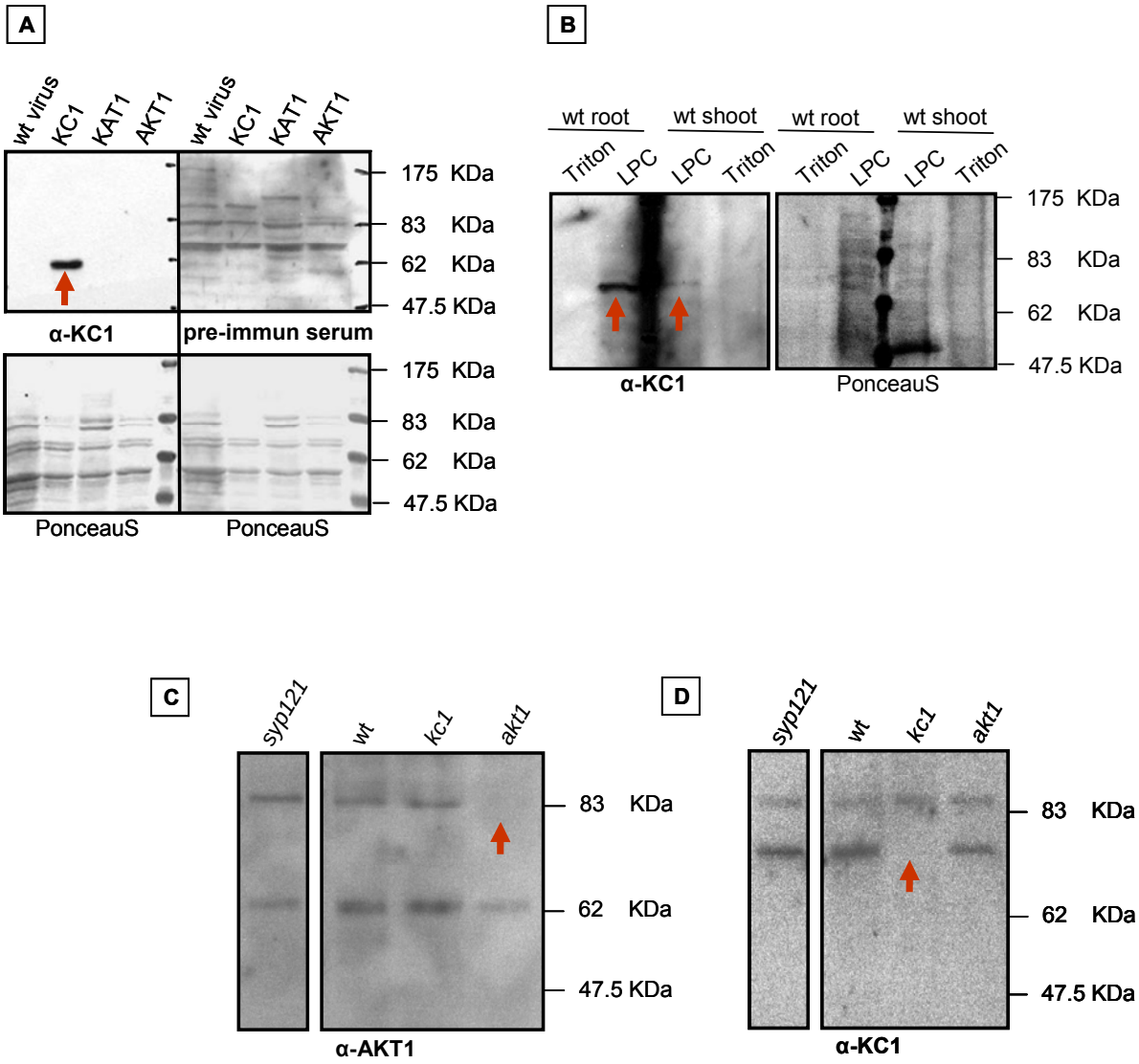

Fig. 53 Assessment of anti-KC1 and anti-AKT1

New rabbit polyclonal anti-KC1 (Agrisera) was tested on *Sf9* insect cells expressing either wt Baculovirus, KC1-Myc, KAT1-2xHA or AKT1-VSVG (A). A single band was detected in KC1-Myc containing LPC-solubilised membrane fractions that was absent from all other samples. The molecular weight corresponded to the detection of KC1-Myc by anti-Myc (see Fig. 37). No signal of similar height was derived from detection with pre-immune serum instead, indicating an antibody specific to the antigen (A, upper right panel). The absence of a signal in the wt Baculovirus control indicated the detected protein was not of insect cell or virus origin (A, upper left panel). The absence of a signal in AKT1 and KAT1 expressing insect cells supported specificity of the anti-KC1 for KC1 over heterologously expressed AKT1 and KAT1 (A). Anti-KC1 also detected native KC1 in root and shoot tissue of *Arabidopsis* wt but only when solubilised with LPC instead of TritonX-114 (B, left panel, lane 2 and 3). A single band appeared on a height that corresponded closely to the predicted molecular weight for native KC1 (75.6 kDa) and indicated stronger presence of native KC1 in roots than in shoots. Both anti-AKT1 and anti-KC1 detected specific signals that were absent in a knock-out mutant for their respective genes (red arrows, C-D). The signal for AKT1 ran lower (~83 kDa) than the predicted molecular weight (97 kDa). Both antibodies detected one additional signal (AKT1: ~62 kDa; KC1 ~85 kDa) (see text).

and KAT1-2xHA expression in insect cells were specific (by recognition of their respective tags) but a significant amount of protein degradation was detected as well (see Fig. 37, p. 151ff.) Still, it seems unlikely that here all degradation products would have been of a nature that either hid or lacked the epitope for which the anti-KC could show cross-reactivity, i.e. in case of cross-reactivity a signal of some sort would be expected. Thus, in conclusion, the anti-KC1 design and production had been successful, leading to the detection of a single KC1-specific band.

In contrast, when testing the anti-AKT1 and pre-immune serum on the same four solubilised membrane fractions as described above, no specific signal was derived from AKT1 expressing cells even when the antibody was used as concentrated as 1:50 (see Appendix, Fig. A 3). Furthermore, the anti-AKT1 proved similarly unable to detect a specific signal on solubilised membrane fractions of AKT1-expressing mbSUS yeast strains and *Xenopus leavis* oocytes (data not shown). In case of the oocyte expression system at least, it was absolutely certain that functional AKT1 protein had been expressed because of the measurable currents through this channel (see below, p. 221). In addition, Agrisera had performed an ELISA test on the affinity purified elution fractions of the anti-AKT1 antibody that indicated the presence of average titres of antibody molecules that had specifically recognized the antigen during purification. Thus, it was suspected that the failure to detect AKT1 in these experiments might not have been due to the absence of a suitable antibody in the rabbit serum. Instead, similar aggravating factors that are generally encountered for work with native (plant) ion channels were likely to have affected the detection of the heterologously expressed AKT1. As mentioned earlier, the expression level of (plant) ion channels under their native promoters is generally very low (Sussman & Harper, 1989; Wagner *et al.*, 2006). Sussman *et al.* (1989) stated that as few as 10 channel proteins as per cell may be sufficient to regulate cytoplasmic levels of an ion. Even the PM proton pumps such e.g. AHA3 (Pardo & Serrano, 1989) that are one of the most abundant polypeptides in the PM of higher plants, accounted only for 1 % of the membrane and 0.01 % of the total protein extracted from oat roots (Sussman & Harper, 1989). In practice, Lagarde *et al.* (1996) had to load 50 µg of a PM fraction obtained from *Brassica napus* whole seedlings to be able to detect the *Brassica* AKT1 homologue in Western Blot analysis. In comparison, here 10 g of *Arabidopsis* root tissue yielded 3-5 µg of a PM fraction (see below for Fig. 53A and B). On average 10 g of root tissue was obtained here from ca. 20 hydroponically grown 7 week old plants. These low yields are indicative of both the low abundance of ion channels in membrane and the difficulty in membrane protein purification, i.e. solubilisation (see Chapter 2 discussion, p. 166ff.). Even when (heterologously) over-expressed under a strong promoter, ion channels often fail to produce high protein levels. This might be related in part to their size and number of TMDs or some internal regulating mechanism that restricts the number of potentially harmful proteins (e.g. AKT1 might be functional in the heterologous system and disturb the vital cellular K balance). It has been observed during the cause of this work that both yeast cells and *Agrobacterium* transformed with *AKT1*-containing constructs for over-expression generally need about half a normal doubling time longer during the logarithmic growth phase (data not shown). That 35S promoter activity is not restricted to plant tissues is not a novel observation (Assaad & Signer, 1990). It was found, for example, that the 35S promoter was

leaky in *Agrobacterium* and the residual expression of SOS1 under its control was deleterious to *Agrobacterium* in the presence of sodium (Martinez-Atienza *et al.*, 2007). The 35S promoter is composed of a modular array of subdomains that all contribute to the constitutive expression in virtually all plant tissues. Experimental evidence had indicated that this combinatorial code of subdomains might be interpreted differently in different species (Benfey & Chua, 1990).

In summary, it was concluded that heterologous expression levels for AKT1 might still have been too low for detection from the amount of cellular material used and/ or the solubilisation procedure was not optimized. As discussed in the Co-IP section (p. 166), several aspects contribute to successful solubilisation. For one, membranes of different organisms, tissues or even organelles show vast differences in the types of lipids and proteins that compose them. Therefore, a detergent, or a particular concentration of a detergent that had been suitable for the solubilisation of KC1 or AKT1 from insect cell membranes might not work e.g. on oocyte membranes or plant membranes. As the aim was localisation of native AKT1 and KC1 in membranes of the *syp121* mutant, subsequent efforts were concentrated on achieving the solubilisation and detection from plant membranes. The Western Blot analysis shown in the left panel of Fig. 53B was performed on either LPC solubilised or TritonX-114 solubilised microsomal (i.e. total) membrane fraction of root and shoot material from *Arabidopsis* Col0 wt plants. The anti-KC1 detected a signal in LPC-solubilised root and shoot samples representing most likely native KC1 (Fig. 53B, red arrows in left panel, lane 2 and 3). The signal constituted a single band corresponding quite accurately to the predicted molecular weight for native KC1 (75.6 kDa). From this result it appeared that native KC1 was expressed much stronger in roots than in shoots (lane 2 versus lane 3). While this can not be concluded with absolute certainty without having related the signal to e.g. an appropriate 'house-keeping' protein, stronger expression in roots is in agreement with the Northern Blot analysis published by Reintanz *et al.* (2002). Higher KC1 protein levels in root and the predominant expression of *AKT1* promoter-GUS in root tissue (see above, p. 203ff.) supported the decision to concentrate on root material for the following experiments. The described experiment further verified the ability to detect native KC1 protein from plant membranes with the new anti-KC1. Thus, the process of solubilisation with the zwitterionic detergent LPC was as successful for native *At*KC1 from plant cell membranes as it had been for extracting heterologously over-expressed *At*KC1 from insect cells membranes.

In contrast, after solubilisation with the nonionic detergent TritonX-114 instead of LPC, the anti-KC1 detected no signal in either root or shoot sample (Fig. 53B, left panel, lane 1 and 4). Solubilisation with this particular detergent was attempted here for to achieve a higher concentration of membrane proteins as well as solubilisation in one step. Normally, microsomal membrane fractions still contain a high amount of 'contaminating' soluble and peripheral proteins. The procedure to separate them further from the membrane proteins involves long high speed centrifugation (see below). Higher purity, i.e. concentration of membrane proteins was desirable because of the bottleneck that is caused by standard Western Blot analysis: only a limited volume can fit an SDS gel well (~20- 30 µl) and only a limited amount of total protein can be loaded per well without getting obscure running patterns and horizontal protein diffusion during the run (about

40–60 µg for crude samples and 0.5- 4 µg for purified samples, also depending on other factors such as contaminating lipids, pH etc.). Thus, higher amounts of target protein per total protein sample, i.e. membrane as opposed to contaminating soluble proteins, in as small a volume as possible would significantly improve the chances to detect e.g. the apparently very low expressed native AKT1 channel from a given amount of starting material.

Concentration of solubilised membrane proteins by TritonX-114 can be achieved by a simple step of temperature-induced phase separation (Bordier, 1981). When this detergent is present above its critical micelle concentration (CMC, see p. 166), it increases its micelle weight when warmed from 0 °C to 30 °C. This induces inter-micellar interactions, which eventually lead to separation of the detergent into a phase at 30 °C. Solubilised membrane proteins should then have partitioned with the detergent-enriched phase, and most peripheral and cytosolic proteins should have been present in the overlaying aqueous buffer phase that was discarded. The detergent phase separation procedure was most likely successful in itself. This was suggested by the absence of the prominent protein band that had appeared in the PonceauS stain of the LPC shoot sample but was missing in the Triton shoot sample (Fig. 53B, right panel, bottom of lane 3 versus lane 4). This band most likely represented the disassociated large subunits (55 kDa) of the enzyme Rubisco (Ribulose-1.5-bisphosphate carboxylase/oxygenase) (Parry *et al.*, 1987), i.e. indicated the 'contamination' of soluble proteins in the LPC sample that was removed by the Triton procedure. Furthermore, removal of soluble proteins could be one explanation for the reduced overall total amount of proteins from the same amount of starting material in the root and shoot Triton samples (compare intensity of PonceauS stain with LPC samples). The absence of a signal for KC1 detection in the Triton fractions was therefore most likely a consequence of the nonionic detergent TritonX-114 being unable to sufficiently solubilise KC1. Similarly, related nonionic detergents (e.g. Tween20, TritonX-100) had proven unsuccessful for the solubilisation of KC1 expressed in *Sf9* insect cells (data not shown). A repetition of the entire experiment described above for detection with the anti-AKT1 showed that neither LPC nor TritonX-114 solubilisation yielded a specific signal indicating the presence of successfully extracted native AKT1 (data not shown).

Failing the TritonX-114 strategy, a method developed for integral membrane protein enrichment prior to 2D-electrophoresis was adapted here. The membranes vesicles obtained after preparation of microsomal membrane fractions, are present mostly (~ 95 %) in a right-side-out orientation. Therefore, they contain some of the soluble and loosely attached membrane proteins from their original organelle/cytoplasm (Larsson *et al.*, 1994). Loosely attached membrane proteins might be embedded only in one leaflet of the membrane bilayer. For example, lipidation with fatty acids (palmitoylation, myristoylation or prenylation) anchors proteins to the inner face of the PM. Additionally, the so-called peripheral membrane proteins are linked to membranes through ionic or hydrophobic interactions with other (integral) membrane proteins (Marmagne *et al.*, 2006). In fact, 60- 80 % of proteins in a membrane enriched fraction are such 'contaminating', i.e. non-integral proteins (Santoni *et al.*, 1998) .

Solubilisation at this stage, as was done above, means the recovery of all these proteins alongside of the integral membrane proteins that are represented only in very low concentration. As

explained above, this was undesirable here because of the Western Blot 'bottleneck'. A previously published method uses a urea-NaOH treatment to enrich integral membrane proteins (Véronique, 2007). It is thought, that the high pH interferes with the electrostatic interactions between the polar head groups of lipids. Thus, closed membrane vesicles are converted into open membrane sheets and content soluble proteins are released (Fujiki *et al.*, 1982). Urea is a chaotrope (Hatefi & Hanstein, 1969) that interferes with non-covalent interactions and is thought to help disrupt protein-protein and protein-lipid interactions to release integral and pheripheral membrane proteins. Subsequent solubilisation with LPC and precipitation of the solubilised proteins will therefore yield a much more concentrated integral membrane protein fraction.

In addition to enrichment of integral membrane proteins, a more sensitive Western Blot detection method was employed. So far the most sensitive chemiluminescence detection kits available for Western Blot had been used in combination with very low antibody dilutions (up to 1:10 for anti-AKT1). For all the experiment described below, the secondary antibody had been radiolabeled with ^{125}I and detected by phosphoimager. These changes finally allowed obtaining a specific signal with the anti-AKT1 (Fig. 53C). For Fig. 53C and D, root material from *Arabidopsis* wt (Ws) and *kc1*, *akt1* and *syp121* mutant plants had been treated with the urea-NaOH method followed by solubilisation with LPC.

After detection with anti-AKT1, a signal on the height of the 83 kDa molecular weight marker band appeared in the *syp121* and *kc1* mutant as well as the wt (Fig. 53C, lane 1-3). This signal was missing in the *akt1* mutant (red arrow). Although the predicted molecular weight for AKT1 is 97 kDa, it is a common observation that membrane proteins appear on SDS gels in lower positions than expected. In other words they move faster through the gel pores than would be expected for their fully stretched out form that is achieved by attachment of SDS molecules. As discussed earlier (see Chapter 2, p. 169), membrane proteins often retain some secondary structure in SDS and therefore would present a more compact form that moves through the gel pores faster. Thus, the 83 kDa signal most likely represented AKT1.

Detection of native KC1 with anti-KC1 confirmed the previously obtained signal (Fig. 53B). While this ~75 kDa band was detected in *syp121*, *akt1* and wt plants it did not show in *kc1* mutant plants. Thus, the experiments in Fig. 53C and D were able to confirm that both the anti-KC1 and the anti-AKT1 specifically recognized their target antigen, i.e. KC1 and AKT1. Both antibodies detected an additional band in all investigated mutants and the wt: a ~62 kDa band for anti-AKT1 (Fig. 53C) and a ~85 kDa band for anti-KC1 (Fig. 53D). These bands were convenient for the purpose of showing that indeed comparable amounts of total protein had been loaded for each sample and thus the lack of signal in the respective knock-out mutant was not the result of sample loss before or during the run (e.g. precipitation or retention in sample well as described for Fig. 36).

However, these additional bands meant also that cross-reactivity to other Shaker channels could not entirely be dismissed. In case of the anti-KC1, the additional band (~ 85 kDa) was well in the range of the predicted molecular weight for all other *Arabidopsis* Shaker channel subunits including AKT1, i.e. between 78- 99 kDa (KAT1: 78.3, KAT2: 80.2, AKT2: 91, SKOR: 93.9,

GORK: 94.5, AKT5: 98.5, SPIK: 99.2, by Edit sequence software of DNASTAR package). In contrast, the additional signal obtained with the anti-AKT1 was with ~62 kDa lower than the band detected for KC1. Therefore, while it might still be possible that other Shaker subunits might run at ~62 kDa and thus could represent the additional band, it was possible to conclude that the anti-AKT1 had no cross-reactivity for KC1.

The converse situation could not entirely be excluded as the ~85 kDa band was only slightly different from the height detected for AKT1. Without a molecular weight marker that is recognized by the secondary antibody directly (not used here), inaccuracy in determining the molecular weight could account for such slight size differences as appeared between the unknown protein and AKT1 in Fig. 53C and D, respectively. Against cross-reactivity of the anti-KC1 for AKT1, however, spoke the absence of any signal detected by anti-KC1 on insect cells infected with virus for AKT1-expression (see above, Fig. 53A).

Additional bands detected by polyclonal antibodies might have alternative explanations to cross-reactivity with close family members as well. For example, the serum of immunized rabbits will contain only 0.5- 10 % of antigen-specific antibodies. The remaining antibodies are active against other antigens and might persist even after affinity purification. In addition, the presence of anti-KLH antibodies that cross-react in turn with plant proteins, might be responsible for non-specific background signals (Tavares *et al.*, 2002). KLH (keyhole limpet haemocyanin), is a large carrier protein that was added to the synthetic peptides before immunization to increase their antigenicity (increase in protein mass prevents degradation of the antigen by the host animal). Thus, polyclonal antibody production against peptides conjugated to KLH will result in antibody production against both KLH (up to 10 % of total antibodies) and the target antigen (Tavares *et al.*, 2002). The nature of the additionally detected bands, i.e. the question of cross-reactivity with other Shaker channel subunits is certainly an important consideration for different future applications.

However, the results presented below made its answer irrelevant for the purpose of identifying in which membrane native AKT1 and KC1 are present in the *syp121* mutant compared to the wt. To differentiate between PM and other subcellular membranes (endomembranes, EM) derived e.g. from Golgi, ER, mitochondria and chloroplasts, an experimental procedure called aqueous two-phase (2P) partitioning was used here (Larsson *et al.*, 1987; Larsson *et al.*, 1994). This technique relies on differences in surface properties between membrane vesicles of different origins, i.e. PM and EM. For example, vesicles derived from the PM frequently contain glycosylated proteins. The preparation of microsomal membrane fractions (without urea-NaOH treatment), represents the first step of this method. Homogentisation with a blender creates membrane vesicles from the sheared membranes with predominantly right-side-out orientation, i.e. the same membrane side faces outward as did in the native state. Right-side-out is important to expose the above mentioned surface properties that help separating the various vesicles when the mixture is subsequently loaded onto a two-phase system of polyethylene glycol (PEG) 3350 and Dextran T500. These two water soluble, high-molecular weight polymers do not mix above a certain concentration, but will form separate phases, each composed of more than 85 % water. According to their surface properties, the PM vesicles of the microsomal membrane fraction

partition preferably into the PEG (upper) phase and the EM vesicles in the dextran (lower) phase.

Aliquots of PM and EM fractions derived from root tissue of either the *syp121* mutant or wt (Col0) during the same 2P experiment were separated on two independent SDS gels. The resulting membranes were first probed with anti-KC1 and anti-AKT1 respectively (Fig. 54A and B, upper panels). Subsequently, both membranes were stripped of these antibodies and re-probed with anti-Sec61 and anti-AHA3 respectively (Fig. 54A and B, lower panels). The second set of antibodies (anti-Sec61, anti-AHA3) represented markers indicating the extent to which PM and EM could be separated in this particular experiment. As the PM constitutes only 5-20 % of the total membranes of a plant cell, it is much more difficult to obtain suitable amounts of highly enriched PM fractions than it is for EM fractions (Larsson & Widell, 2000). Complete separation is impossible, at best a purity of up to 95 % can be achieved for PM fractions (Larsson *et al.*, 1994; Alexandersson *et al.*, 2004).

Therefore, the marker antibody anti-Sec61 (Yuasa *et al.*, 2005) (kindly provided by Prof. Matsuoka, Riken, Japan) was used to show the degree of EM contamination in the PM phase. Yusada *et al.* (2005) stated that the antigenic peptide they used corresponds to the N-terminal region of the Sec61 α-subunit homologs of several plant species. In *Arabidopsis* a ca. 45 kDa polypeptide is recognized. As mentioned in the General Introduction, the Sec61 α-subunit (10 TMDs) is part of the translocon, a protein complex that forms a channel across the ER membrane through which co-translational ER integration of newly synthesised proteins takes place (p. 27). As PM marker, i.e. to show PM contamination in the EM fraction, anti-AHA3 (Pardo & Serrano, 1989) was chosen (kindly provided by Prof. Serrano, University of Valencia, Spain). The PM H^+-ATPase AHA3 (104.5 kDa) is expressed in phloem companion cells and pollen (Dewitt & Sussman, 1995; Dewitt *et al.*, 1996; Robertson *et al.*, 2004). As indicated by these two marker antibodies, both EM and PM fraction were so well separated as to show no cross-contamination under the applied experimental conditions, i.e. the anti-Sec61 detected not EM in the PM fraction and the anti-AHA3 registered no PM contamination in the EM fraction (see Fig. 54A and B, lower panels). Anti-KC1 and anti-AKT1 detected bands for native KC1 and AKT1 only in the PM fractions of wt and *syp121* mutant. As the marker- antibodies had confirmed the virtual absence of EM in the PM fraction, these results taken together allowed to conclude that native KC1 and AKT1 had been present in the PM but not EM of root cells from both wt and *syp121* mutant. (see Fig. 54A and B, upper panels).

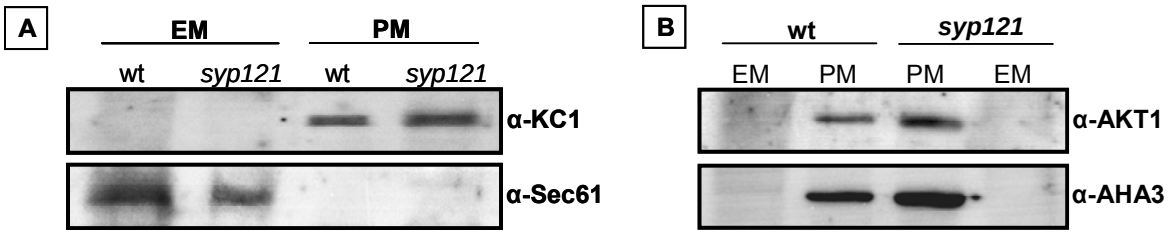

Fig. 54 Native AKT1 and KC1 partition only into PM fractions in *syp121* roots

Two-phase partitioning (see text) was performed on root tissue from hydroponically grown *Arabidopsis* Col0 and *syp121* mutant. PM and EM fractions had been enriched in integral membrane proteins by a urea-NaOH treatment before solubilisation with 2 % LPC. 1.3 µg protein/ lane were separated on two identical (except sample order) SDS gels for Western Blot (A, B).
Under the applied experimental conditions, the EM marker-antibody anti-Sec61 recognized no protein in the PM fractions of wt and *syp121*, indicating that no EM derived proteins contaminated the PM fractions (A, lower panel). Conversely, the PM marker-antibody anti-AHA3 yielded no signal in EM fractions of wt and *syp121* mutant, suggesting that no PM derived proteins contaminated the EM fractions (B, lower panel). Anti-KC1 and anti-AKT1 detected native KC1 and AKT1 only in PM fractions of both wt and *syp121* mutant (A and B, upper panels). Together, these observations strongly suggested that native KC1 and AKT1 had been purified only from the PM of both wt and *syp121* mutant and had not been present in EM.

As explained above, separation is never a 100 % complete although it was sufficiently good here to appear that way in the Western Blots. It is likely that small but undetectable amounts of AKT1 and KC1 are present in the EM as well, as would be expected for PM proteins in membranes of the secretory pathway. The results can however confirm that the vast majority of the two Shaker channels were not present in EM as would be expected for proteins stuck in the ER or on their way to degradation. Furthermore, it could be concluded, as much as the sensitivity of Western Blot allows, that there were no great differences in the amounts of AKT1 and KC1 in the PM of *syp121* compared to wt. This was indicated by the signal strength of the three band pairs for PM detection. Although, both anti-KC1 and anti-AKT1 seemed to yield slightly stronger signals in the *syp121* PM fraction compared to wt, this difference was reflected in the detection by anti-AHA3, indicating that the difference was most likely due to slightly uneven loading of the SDS gel (Fig. 54A and B, upper panels versus Fig. 54B, lower panel). Therefore, in the frame of this experiment, it could be concluded that the number of KC1 and AKT1 proteins reaching the PM is not negatively influenced by the loss of the Qa-SNARE vesicle trafficking function in the *syp121* mutant. Although the *syp121* mutant was previously characterized (Collins *et al.*, 2003; Zhang *et al.*, 2007), the absence of SYP121 protein in the PM and EM fraction of root tissue was confirmed in an additional 2P (see Appendix, Fig. A 4, p. 244).

K^+ currents of AKT1/KC1 heteromeric channels are affected by SYP121

The function in ion cannel regulation that was observed for the mammalian Syntaxin1A (p. 64) raised the question, whether the NH_4^+ and low K^+-dependent growth phenotype in the *syp121* mutant might have been caused by the loss of a regulatory function that the SNARE SYP121 imparts onto heteromeric AKT1/KC1 K^+ channels via its direct interaction with KC1. For this purpose it was decided to co-express AKT1, KC1 and SYP121 in oocytes and analyse the Shaker channel-dependent K^+ currents.

As mentioned in the General Introduction (p. 24), only in recent years has the discovery of the CIPK/CBL-dependent activation of AKT1 by phosphorylation made it possible to obtain electrophysiological recordings of this Shaker channel subunit expressed in oocytes (Li *et al.*, 2006; Xu *et al.*, 2006; Lee *et al.*, 2007). Therefore, all the experiments described in Fig. 55 were obtained by co-expression of AKT1 (and/ or KC1 and SYP121) with the kinase CIPK23 and its upstream regulator the calcineurin-B-like (CBL) CBL1.

Protein expression was achieved by manually microinjecting *in vitro* transcribed complementary RNA (cRNA) into the cytoplasm of oocytes. Oocytes are large (diameter of ~1.2 mm) immature egg cells of the South-African clawed frog *Xenopus laevis*, arrested in the first meiotic division in the G2-phase. To record the influx of K^+ ions into oocytes mediated by expressed Shaker channels in response to changes in membrane voltage, electrical measurements were carried out under voltage clamp using a classic Two-Electrode Voltage-Clamp (TEVC) system. TEVC measures current that results from the movement of ions across the membrane directly through an electronic feedback circuit. The oocyte is impaled with two separate microelectrodes, one of which is serves to monitor the transmembrane voltage (membrane potential) and the other serves as a pathway for current injection. The membrane potential recorded by the first microelectrode is compared against a command voltage input to the circuit (normally by a computer and digital-to-analogue converter). Any difference between these two signals is fed into the feedback circuit through a current injection amplifier and, from there, into the oocyte via the second microelectrode. The net effect of this circuit is to ensure that the membrane voltage of the oocyte is corrected for any deviation from the command voltage over a time period orders of magnitude shorter than the response time of any transporter in the oocyte membrane; the circuit also ensures that any current that flows across the oocyte membrane is balanced by an equal (but opposite) current injection from the second microelectrode into the oocyte. Thus, the injection current provides a measure of the current passing across the membrane. By measuring this current as a function of the (clamped) membrane potential it is possible to identify the voltage-dependence of ion channels such as AKT1, and from the relaxation of the current following steps in clamp voltage it is possible to derive the time-dependent kinetics of the channels. For the purposes of this study, the entire process of clamping the membrane voltage at desired values for specific periods of time, and the recording of the resulting data was computer-controlled via the HENRYIII software package developed by Adrian Hills (University of Glasgow).

The current traces pictured in Fig. 55A were recorded by injecting oocytes with cRNA for

CIPK23, *CBL1* and the genes indicated above each trace. After 3 d of incubation to allow time for cRNA translation and protein insertion into the PM, the oocytes were measured under continuous perfusion with a bath solution of 96 mM KCl. Such high (unphysiological) external K^+ concentrations were used to ensure that, following the electrochemical gradient for K^+, K ions would carry a strong current across the oocyte PM once the Shaker channels were activated by the membrane voltage. An increase in current response (activation) to imposed (clamped) changes in membrane voltage means for Shaker channels the opening of their gates for K ions, i.e. a change in the conformation of the channel protein, notably around the pore domain and the K^+ selectivity filter (see p. 13). Inward rectifying (K^+ uptake) Shaker channels such as AKT1 open their gates in response to more negative membrane potential values than the prevailing equilibrium potential for K^+. The equilibrium potential for K^+ describes the state where efflux of K^+ from the oocyte along the K^+ concentration gradient (K^+ concentration is higher inside the cell) is balanced by the charge (voltage) difference between the inside of the PM and the outside of the PM (inside more negative). Similarly, the equilibrium potentials of all ions to which the membrane is permeable (e.g. Cl^-, Na^+) are determined by the respective concentrations inside and outside of the cell. In oocytes, the electrochemical potential across the membrane, i.e. the membrane potential, is determined largely by their combined effects.

During the TEVC measurements performed here, the K^+ channels were activated and their current recorded while clamping the membrane at hyperpolarising voltages. Hyperpolarisation renders the inside of the PM more negative, i.e. the inward electrical force on K^+ increases until it is stronger than the outward diffusion and the driving force on K^+ aids its entry to the oocyte.

As published previously, AKT1 expressed in oocytes together with CIPK23 and CBL1 formed functional channels enabling time- and voltage-dependent currents of large amplitudes to flow through the ooctye membrane (Li *et al.*, 2006; Xu *et al.*, 2006; Lee *et al.*, 2007; Duby *et al.*, 2008; Geiger *et al.*, 2009).

The current traces pictured Fig. 55A were evoked by hyperpolarizing the oocyte from a holding membrane potential of –50 mV in 10 mV steps to -160 mV. Each voltage was clamped for 8 sec followed by a voltage step back to the holding potential for 7 sec before stepping to the next voltage. Each trace shows the current carried by K^+ influx through all AKT1 channels opening their gates in response to the respective clamped membrane voltage. Current at the end of each pulse was plotted against the clamp voltage to obtain the current-voltage curve pictured in Fig. 55B (yellow curve). The amplitude of the current at -160 mV (last of the traces in A) is charted Fig. 55C. Fig. 55A shows a representative current trace for AKT1 expressing oocytes, Fig. 55B and C show means from several measured oocytes (n= 10 ± SE).

The yellow arrow in Fig. 55A indicates the clamped membrane voltage threshold at which the AKT1 channels started to open (around -50 mV). This activation threshold indicates a feature intrinsic to the Shaker channel, i.e. which membrane voltage is detected by positive aa charges in the voltage sensor of the 4th TMD (see p. 13). The total current amplitude is determined by the number of active AKT1 channels in the entire oocyte PM.

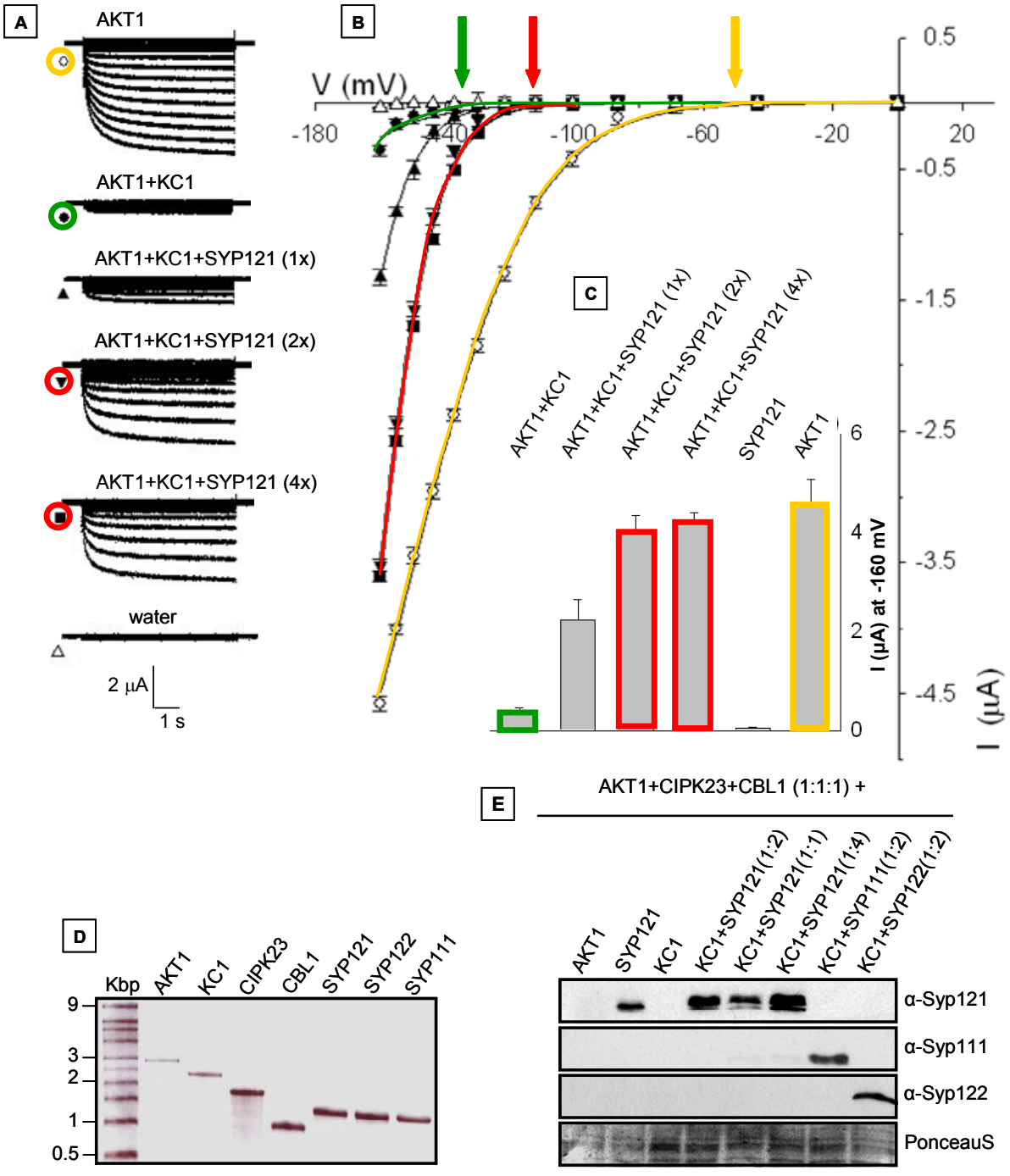

Fig. 55 SYP121 influences AKT1-KC1 dependent K^+ influx in oocytes

(A) Typical current traces recorded from oocytes expressing the combinations of heterologous cRNA indicated above each trace together with *CIPK23* and *CBL1* cRNA in a molar ratio of 1:1 (for all traces). *AKT1* cRNA (first trace) was added to this mix 1:1:1 and *KC1* (second trace) 1:1:1:1. Further addition to this combination of *SYP121* cRNA was performed in molar ratios of 1:1:1:1:1, 1:1:1:1:2 or 1:1:1:1:4 (traces 3- 5). The last current trace shows typical recordings for water-injected oocytes. Recordings were obtained under two-electron-voltage-clamp in a bath solution of 96 mM KCl. Membrane voltage was clamped to hyperpolarising values by stepping from a holding potential of –50 mV to -160 mV. (B) Current voltage curves were obtained from n= 10 oocytes (means ± SE) expressing cRNA as indicated in (A) (compare symbols and colours of A and B). (C) Amplitude (means ± SE) of the current response at -160 mV for oocytes injected as shown above the chart (derived from B). (D) Confirmation of degradation-free cRNA analyzed by denaturating agarose gel analysis. (E) Western Blot of total membrane protein extracted from oocytes collected after the electrical recordings summarized in (B). Detection with anti-SYP111 and anti-SYP122 confirmed expression of the control SNAREs (cRNA injected in molar ratios of 1:1:1:1:2). Detection with anti-SYP121 showed that the protein levels roughly reflected the amount of injected cRNA.

As was published previously (Duby *et al.*, 2008; Geiger *et al.*, 2009), when KC1 was co-expressed with AKT1, the oocyte responded differently to the same applied hyperpolarisation protocol (Fig. 55A, green in B and C). The current traces still showed time-and voltage dependent currents but the amplitude was strongly reduced (compare Fig. 55C at -160 mV). In addition, the formation of heteromeric AKT1-KC1 channels changed the way how membrane voltage was sensed. As indicated by the arrow above the current–voltage curve in Fig. 55B (green), the activation threshold of the heteromeric channel gates was now much more negative than the activation threshold for the homomeric AKT1 channel (around –140 mV).

Co-expression of SYP121 with AKT1 and KC1 modified the current responses to the hyperpolarisation protocol yet again (Fig. 55A, red in B and C). Injecting *SYP121* cRNA in a molar ratio (see below) of 1:1 with the AKT1-KC1 heteromeric channel increase only the amplitude of the characteristic current traces (compare response to -160 mV in Fig. 55C). Adding *SYP121* cRNA in molar ratios of 1:2 or 1:4 further increased the amplitude in response to membrane voltages clamped at the same values as before (Fig. 55A, red in B and C). Furthermore, at these ratios, SYP121 reversed the effect that KC1 co-expression had on the activation threshold of AKT1 to a certain extent; the activation threshold now around –100 mV.

To control the amount of heterologous protein expressed per oocyte as much as possible, i.e. reduce the variation it might contribute to overall current amplitude, the following steps were taken. After in vitro transcription, the cRNA was analyzed on a denaturating RNA gel to confirm that no degradation products were present (Fig. 55D). The quantified RNA of different constructs was then mixed in molar ratios of 1:1:1 for *CIPK23*:*CBL1*:*AKT1*. *KC1* cRNA was added in the same molar ratio (1:1:1:1). SYP121 cRNA was mixed with the two Shaker channels in molar ratios of 1:1:1:1:1, 1:1:1:1:2 or 1:1:1:1:4. All different cRNA combinations were brought with water to the same final volume and the injection delivered equal volumes to each oocytes. All oocytes which contributed to the measurements summarized in (Fig. 55B, C) had been harvested immediately after the measurement. Membrane proteins were extracted from these oocytes with a fixed volume of buffer per oocyte and equal volumes of each sample were used for Western Blot analysis (Fig. 55E). The total protein amount derived from the equal volume strategy was quite comparable for these three samples (compare PonceauS for co-expression of AKT1-KC1-SYP121 in the three ratios, Fig. 55D, last panel). Detection with anti-SYP121 showed that the molar ratios of cRNA injected were reflected in the amounts of SNARE protein expressed in the measured oocytes (1: 2.04: 3.4). The detection of expressed AKT1 or KC1 was not possible, as at the time the antibodies described above, were not available yet. For AKT1 at least, expression in itself is demonstrated by the appearance of a measurable current in response to hyperpolarisation. However, the relative expression levels would have been of interest here.

The co-expression of *SYP122* or *SYP111* (1:1:1:1:2) produced current traces undistinguishable from those of AKT-KC1 expressing oocytes (data not shown). Western Blot analysis with the corresponding antibodies as described above could confirm that in the measured oocytes these SNAREs had been expressed (Fig. 55E). Oocytes expressing *SYP121* (or *KC1*) alone with *CIPK23* and *CBL1* (1:1:1) exhibited no time-and voltage-dependent currents similar to the

control of oocytes injected only with water (Fig. 55A). Western Blot analysis showed SYP121 expression in these oocytes as well (Fig. 55D).

Discussion

The previously published interaction of KC1 with AKT1 and the interaction of KC1 with SYP121 in turn that was observed here in mbSUS, Co-IP and BiFC experiments raised interest in a possible common function for these three proteins in AKT1-mediated K^+ uptake.

When seedlings in the cotyledon stage were forced to rely only on AKT1-mediated K^+ uptake by inhibiting K^+ transporters (HAK5) with high concentrations of NH_4^+ ions competing for K^+-binding sites, *kc1* and *syp121* mutants showed a highly similar phenotype to the previously published *akt1* mutant (Hirsch *et al.*, 1998; Spalding *et al.*, 1999) (Fig. 51, p. 205). All three mutants showed strongly reduced root and also overall growth when the K^+ concentration in the external medium was low (0.01 mM). This was reflected in low plant K^+ contents indicating a failure to take up K^+ in sufficiently high amounts to support normal growth after the K^+ storage of the seed was depleted.

Seed germination, noticeable as radicle emergence, depends on cell expansion, which is driven by passive water uptake during seed imbibition. Dehydrated seeds contain storage reserves of mineral nutrients like K^+ that contribute to the osmotic potential in germinating seeds and hence to water uptake. These storage reserves can be used during the initial phase of embryo axis elongation, culminating in seed coat rupture and radicle emergence. Subsequently, the seedling needs to absorb K^+ and other mineral nutrients from the external medium in order to sustain growth, since storage reserves are limited.

AKT1-GFP localised to the periphery but not TP or cytoplasm of *syp121* mutant mature root hairs. The amount AKT1-GFP fluorescence that reached the PM was not reduced in comparison to AKT1-GFP transformed wt plants (Fig. 52A, B, p. 209). The implication that AKT1 was able to reach the PM despite a null mutation in the SYP121 PM SNARE was supported by 2P partitioning experiments with root tissue from adult plants. After membrane fractionation, anti-AKT1 detected the presence of native AKT1 only in the PM not EM fraction of *syp121* and wt plants alike. Similarly, anti-KC1 detected the presence of native KC1 only in PM fractions of both *syp121* and wt root tissue. It was concluded that SYP121 either did not contribute to AKT1 or KC1 delivery to the PM or was sufficiently replaced in this function by another syntaxin from the SYP1 subfamily (see p. 52). These observations supported the conclusion that the loss of vesicle trafficking ability by genetic deletion of *SYP121* did not cause K^+ uptake deficiency in the corresponding mutant through a reduced number or lack of Shaker channels at the PM. An alternative function for SYP121, the direct regulation of AKT1-KC1 heteromeric channel through interaction with KC1, was indicated from electrophysiological measurements after of all three proteins in oocytes (Fig. 55, p. 223).

The cells that represented the most likely localisation for a function of such a tripartite complex between AKT1, KC1 and SYP121 in K^+ uptake were root hairs. This was supported by

the gene expression patterns derived from public database search (eFP browser) that placed the highest expression of *AKT1* in root epidermis trichoblasts. *AKT1* expression overlapped with *KC1* and *SYP121* expression in root hairs (Fig. 49, p. 200). The eFP browser data agreed with already published promoter-*GUS* experiments indicating strong expression of *AKT1* and *KC1* in roots of seedlings in the cotyledon stage (Lagarde *et al.*, 1996; Reintanz *et al.*, 2002). *SYP121* promoter-*GUS* plants that were investigated here confirmed strong expression of this SNARE in roots and mature root hairs as well (Fig. 50, p. 203).

In contrast, the youngest root hairs in the beginning of the maturation zone, as well as the elongation and meristematic zone in general exhibited no or only very faint *Syp121* promoter activity. The eFP browser data confirmed lower expression levels of *SYP121* in elongation and meristematic zone. In addition, also the promoter-*SYP121-GFP* plants that were analyzed by Enami *et al.* (2009) (see Fig. 14, p. 52) had indicated that GFP fluorescence was weaker in developing root hairs. Lagarde *et al.* (1996) had observed that in older roots (6 weeks) *AKT1* gene promoter-*GUS* activity was strong along the mature root, preferentially in root hairs and epidermis, cortex and endodermis but relatively weak at the root tip in the elongation and meristematic zone. These authors commented that expression in mature but not growing parts of the root correlates with the distribution of the K^+ net flux along maize roots determined with K^+ selective surface micro-electrodes. The K^+ net flux at the root surface was directed inwards to the root cells in the mature regions, and outwards at the apex. Thus, also the overlapping expression pattern for AKT1, KC1 and SYP121 in root cells known to important for K^+ uptake supported a common function for these three proteins.

Although the AKT1-GFP localisation in *syp121* root hairs and the 2P data for native AKT1 and KC1 at the PM of *syp121* root cells gave strong support, that indeed both Shaker channel proteins would reside in the PM of specifically root hairs, ultimate proof for this localisation still needs to be obtained. For example, *in situ* hybridisation with the now available anti-AKT1 and anti-KC1 antibodies or possibly a more sensitive immunogold labelling of electron micrographs could provide this evidence.

According to the eFP browser, the SYP1 SNARE that shows the highest sequence identity on the aa level to SYP121, namely SYP122 is almost as highly expressed in root hairs as *SYP121* (Fig. 49, p. 200). Despite this overlapping expression pattern, SYP122 was unable to rescue the observed growth and K^+ uptake phenotype of the *syp121* mutant under low external K^+ and NH_4^+, when over-expressed as a CFP-SYP122 fusion in this background. Conversely, the *syp122* mutant behaved as the wt under these conditions (Fig. 51, p. 205). Assaad *et al.* (2004) had previously proven the functionality of a CFP-SYP122 fusion as it was able to rescue the dwarfed and necrotic phenotype of the *syp121/syp122* double mutant (see p. 58). As detailed in the General Introduction, both overlapping and independent functions were discovered for SYP121 and SYP122 in leaf tissues (p. 58ff.). Syp121 is required for timely formation of papillae against powdery mildew attack, a role that it does not share with SYP122 (Collins *et al.*, 2003; Assaad *et al.*, 2004; Meyer *et al.*, 2009). In contrast, both SNAREs share a role as negative regulators of programmed cell death, SA, JA and ET pathways in post-invasive defence that causes the *syp121/syp122* double mutant to

develop the typical dwarfism and leaf necrosis (Assaad *et al.*, 2004; Zhang *et al.*, 2007).

Consistent with the results of the mbSUS and BiFC interaction studies where SYP122 did not interact with KC1, it did not share the function that causes the high NH_4^+/low K^+ phenotype in the *syp121* mutant. However, an overall reduction of root length was observed in *syp122* mutant plants in all growth conditions (Fig. 51B, p. 205). Possibly in this case, the missing Qa-SNARE at the PM negatively affected vesicle trafficking events that contribute to growth. As mentioned in the General Introduction (p. 58), Assaad *et al.* (2004) had suggested that SYP122 has a general function in delivering cell wall components to the apoplast by mediating exocytosis at the PM. Without the contribution of SYP122, overall cell growth might be slowed down and could thus explain the observed root growth reduction independent of K^+ or NH_4^+ content of the medium.

In summary, it was not surprising to learn that SYP122 was not redundant to its closest relative SYP121 for the observed root growth and K^+ uptake phenotype when considering that other functions exist that both proteins do not share even when their expression pattern overlaps as in leaf epidermis cells. As summarized in the General Introduction (p. 41ff.), SNARE proteins themselves represent only one layer of specificity for vesicle fusion events. A whole array of other intracellular factors apparently regulates spatio-temporal fine-tuning of vesicle fusion for different cargos, from the exocyst to the SM proteins. In addition, the PM of all cell types in all tissues must make do with only 9 SYP1 family members. Thus, involvement of individual SNAREs in many specialized functions does make sense when upstream regulating factors exist (see p. 52).

Although the *syp121/syp122* double mutant is severely dwarfed and necrotic and shows a complex change in cell wall composition, consistent with a function of SYP122 in cell wall biogenesis, no root hair defect has been reported for this mutant or the *syp121* mutant (Assaad *et al.*, 2004). These observations suggested that other SNAREs of the SYP1 subfamily than SYP121 or SYP122 are involved in vesicle trafficking housekeeping functions in root hairs. As mentioned in the General Introduction (p. 52), Sanderfoot *et al.* (2000) had proposed that in all tissues PM SNAREs of the SYP13 subgroup are involved in housekeeping roles such as constitutive secretion, while members of the SYP12 subgroup would have more specialized roles. These predictions fit well to the observations by Enami *et al.* (2009) who found that *SYP132* (as *SYP132*-promoter-*GFP* fusion) was the only SYP1 PM SNARE to be expressed throughout all *Arabidopsis* tissues and developmental stages (see Fig. 14, p. 52). With regard to the roots of seedlings in the cotyledon stage, gene expression of only three other members of the SYP1 family aside from *SYP121* and *SYP122* were detected in this study: *SYP111*, *SYP132* and *SYP123* (Enami *et al.*, 2009). *SYP132* was expressed ubiquitously in almost all root cells, including the root apical meristem, epidermis, cortex, endodermis, stele and root hair. As expected from previous studies, *SYP111* was localised only to the dividing cells of the root apical meristem (see p. 54). *SYP123* had a highly specific localisation as well, as it was detected only in root hairs. While expression was strong in young, growing hairs, it appeared weak in mature hairs. As would be expected for a function in polarized secretion during root hair tip growth, the PM subcellular localisation of *SYP123* expression included a focal accumulation pattern in the cytoplasmic tip region (Enami *et al.*, 2009). Thus, it seems likely that SYP132 (possibly even SYP123) was responsible for delivery of the Shaker

channels to the PM in mature root hairs of the *syp121* mutant.

Having excluded as best as possible that the root growth and K^+ uptake phenotype in the *syp121* mutant was derived from a lack of channel delivery to the PM, electrophysiological measurements in oocytes provided support for a direct interaction between SYP121 and heteromeric AKT1-KC1 channels. SYP121 appeared to influence gating of the heteromeric Shaker channel to facilitate K^+ influx, possibly in a stochiometric manner of interaction (Fig. 55, p. 223).

As published before (Reintanz *et al.*, 2002; Duby *et al.*, 2008; Geiger *et al.*, 2009), it was observed here that homomeric AKT1 channels displayed a different activation threshold than the heteromeric AKT1-KC1 channels. AKT1 channels sensed and responded with opening of the gate that allows K^+ influx to a much slighter hyperpolarisation, i.e. less negative membrane voltages. Apparently, the physical interaction between AKT1 and KC1 α-subunits modified the voltage sensing properties of the resulting heteromeric channel to respond only to more negative membrane voltages.

It is not yet understood precisely how membrane voltage is sensed in Shaker channels and how the perception of only one specific membrane voltage is achieved and translated into opening the gate to K ions. Most of the information available to date is derived from the crystal structure of animal Shaker channels and analysis of aa mutations in these channels. As indicated by the crystal structure in Fig. 3B (p. 20) that shows a top view of a voltage-gated K^+ channel, the voltage-sensing modules (S1–S4, i.e. TMD1-4) of each of the four α-subunits form an outer ring-like arrangement. The four pore-forming modules with the K^+ selectivity filter (S5–P–S6) in turn form an inner ring-like arrangement. Outer and inner ring are supposedly connected by critical aa interactions and of cause the S4–S5 linker within each subunit itself. It was suggested that during voltage sensing structural rearrangements within the voltage-sensing modules cause the outer ring to rotate clockwise (Dreyer & Blatt, 2009). This movement would in turn induce conformational changes in the pore forming modules of the inner ring via the connections of the S4–S5 linkers that ultimately could result e.g. in opening of the gate.

The mechanism by which the voltage sensing modules themselves move in response to membrane voltage is also a subject of active debate. As mentioned in the General Introduction (p. 13), the fourth TMD (S4) of the voltage sensing module incorporates a set of four highly conserved positively charged aa residues (arginine or lysine). These aa are regularly spaced at three residue intervals along the whole S4 α-helix residing within the lipid bilayer. Their positive charge is responding to the transmembrane voltage and gating (opening of the K^+ passage pathway) entails the movement of this charge through the membrane electrical field (Catterall & Yarov-Yarovoy, 2010). Or in other words, the S4 TMD that carries these charges is displaced from the cytoplasmic to the external side of the membrane.

In the ‘helical screw’ model, the S4 segments remain in a transmembrane position in the closed state, and move from a resting to an activated position by a helical motion through the protein structure. Outward movement of the S4 segment is catalyzed by stepwise exchange of ion pair partners (Catterall & Yarov-Yarovoy, 2010). In contrast, in the ‘paddle model’, the S3-S4 helical hairpin lies separate from the rest of the voltage sensor near the intracellular surface in the

resting state and moves like a paddle through the lipid bilayer during activation (Catterall & Yarov-Yarovoy, 2010).

All nine Shaker channel subunits are structurally highly similar. Even KC1 that does not appear to form a functional homomeric channel has a voltage sensor. In addition to the open questions about voltage sensing and subsequent opening of the gate, it is still not entirely certain, which domains contribute to interaction between the plant Shaker channels, i.e. how a particular interaction between two different α-subunits might affect the voltage sensing mechanism.

As detailed in the General Introduction (p. 33), it seems that a dimerisation of dimers in the ER is involved in the formation of tetrameric channels. Deletion mutants in the cytoplasmic C-terminus of the outward-rectifying Shaker SKOR revealed two separate domains that both needed to be present to form functional channels (Dreyer *et al.*, 2004). A 'proximal' interacting region, comprising a putative cyclic nucleotide-binding domain, was sufficient to mediate the interaction of cytoplasmic C-termini in yeast two-hybrid assays. In contrast, a region more 'distal' (at the very C-terminus) that has been named K_{HA}, because of its richness in hydrophobic and acidic residues (Ehrhardt *et al.*, 1997) required an intact 'proximal' region to show interaction in this assay. Dreyer *et al.* (2004) suggested that one possible explanation for these results could be a model according to Green *et al.* (2005) (see p. 33ff.). Thus, the 'proximal' domain would be essential in the initial dimerisation of two SKOR *α*-subunits. This dimerisation would cause conformational changes in both subunits, creating a new interaction site specific to the dimer that includes the 'distal' region and will mediate the assembly of functional tetramers (Dreyer *et al.*, 2004). The K_{HA} domain is conserved in all Shaker channels. In contrast, KAT1, KAT2 and KC1 are the only Shaker subunits that do not contain a so-called ankyrin domain upstream of the K_{HA} domain in the cytoplasmic C-terminus (Pilot *et al.*, 2003b). Ankyrin domains are found in several kinds of proteins (e.g., cytoskeleton binding proteins and transcription factors) and are likely to mediate protein–protein interactions. As mentioned earlier, the ankyrin domain in AKT1 appears to be responsible for CIPK23 binding and subsequent phosphorylation of AKT1 by this kinase (p.24).

Despite this lack of information about the mode of interaction between KC1 and AKT1, it can be concluded that actual physical interaction and resulting confirmation changes in the protein structure are the cause for the different voltage-dependent activation threshold when compared to homomeric AKT1 channels (~ -140 mV and ~ -50 mV respectively, Fig. 55, p. 223). By a similar reasoning, the unique voltage-dependent activation threshold (~ -100 mV) that was found with measured oocyte whole-cell currents after co-expression of SYP121 supported a direct interaction of the SNARE with the heteromeric AKT1-KC1 channel presumably via the association of KC1 and SYP121. Rearrangements in the KC1 protein structure through its association with SYP121 might affect its voltage sensing module (e.g. by affecting the electric field around the KC1 voltage sensor itself), which would in turn act on the protein dynamics coupling voltage sensing and gating of the pore for the entire heteromeric channel. The differences in the displayed activation thresholds after co-expressing *SYP121* cRNA in molar ratios of 1:1, 1:2 or 1:4 might support speculations about a certain stochiometry of this interaction e.g. each of the two KC1 subunits in a tetrameric channel with AKT1 would bind two SYP121 protein for full effect.

The conclusion that a change in activation threshold results from underlying conformational changes of protein structure due to protein-protein interaction also makes an alternative scenario for the observations in oocytes much less likely. One might perhaps imagine that SYP121 interaction with KC1 would make this subunit unavailable for interaction with AKT1, i.e. 'titrate it out'. If that were case, however, one should expect a voltage-dependent activation threshold during co-expression of AKT1-KC1-SYP121 that is equal to the one derived from AKT1 expressed on its own.

The similarity in the observed root growth and K^+ uptake phenotype of *akt1*, *kc1*, or *syp121* null mutants indicated that all three proteins were essential for AKT1 to function under growth conditions of low external K^+ and high NH_4^+ (Fig. 51, p. 205). Additional data, obtained by past and present members of Prof. Blatt's group, supported this hypothesis. Fitting to a Boltzmann function allowed Prof. Blatt to determine from the steepness of the current-voltage curves shown in Fig. 55B (p. 223) that the gating charge displayed by currents from oocytes expressing AKT1-KC1-SYP121 compared favourably with values recorded from plants cells (2.18 versus 1.97 respectively). The gating charge describes the sensitivity of a voltage-gated ion channel to a change in membrane potential (Dreyer & Blatt, 2009). Currents from oocytes expressing either AKT1 alone or AKT1-KC1 together exhibited a much lower gating charge (1.21), as had been observed previously (Duby *et al.*, 2008). Similar to the threshold of activation, the gating charge is a feature intrinsic to protein structure and not affected by expression levels. Thus, as discussed above for the activation threshold, the difference in gating charge indicated a change in protein confirmation that supports a direct interaction between SYP121 and the AKT1-KC1 channel. Furthermore, the similarity to the gating charge of inward currents measured in plant cell protoplasts supported a function of this interaction *in planta*.

A function for a tripartite complex of AKT1-KC1-SYP121 *in planta* was also supported by data obtained by Dr. Sokolovski, a former member of Prof. Blatt's group. He performed whole-cell patch clamp measurements on protoplasts derived from the root epidermis of *Arabidopsis* wt, *syp121*, *akt1*, *kc1* and *syp122* mutants. Under similar conditions as in the oocytes (100 mM external K^+ and hyperpolarising membrane voltage clamp of values up to – 180 mV), *syp121* and *kc1* mutants showed almost no inward rectifying (influx) currents (Honsbein *et al.*, 2009). The absence of inward rectifying currents in root epidermis protoplasts of the *akt1* mutant had been published previously (Hirsch *et al.*, 1998; Spalding *et al.*, 1999) and could be confirmed in these measurements. In contrast, protoplasts from the *syp122* mutant showed inward rectifying currents similar to the wt. Dr. Chen, a current member of Prof. Blatt's group, further demonstrated that the inward-rectifying current was restored in protoplasts of the *syp121* mutant rescued with YFP-SYP121 either under the control of its own or the 35S promoter (compare growth assay in Fig. 51, p. 205) (Honsbein *et al.*, 2009).

Dr. Grefen, a current member of Prof. Blatt's group has developed a method based on mbSUS that allowed him to show a tripartite complex between AKT1, KC1 and SYP121 in yeast that depended on KC1 as bridge between the two other proteins (Honsbein *et al.*, 2009). These data complemented the observations in oocytes and supported the existence of a tripartite complex *in*

planta.

An alternative suggestion to explain the observed low K^+/ high NH_4^+ phenotype in the *kc1* mutant has been made (Geiger *et al.*, 2009). These authors recorded currents from oocytes expressing homomeric AKT1 channels in bath solution of low K^+ (0.1- 0.5 mM). Their results led them to propose that under such low external K^+ concentrations homomeric AKT1 channels would open at voltages positive of the equilibrium potential for K^+, a condition resulting in cellular K^+ leakage. When the AKT1 channel gates open in response to clamping the oocyte membrane potential at more positive values than the prevailing equilibrium potential for K^+, K^+ ions would follow the concentration gradient out of the cell. Geiger *et al.* (2009) suggested that such AKT1-mediated K^+ loss could result in the impaired growth and K^+ uptake phenotype in the *kc1* mutant. In contrast, a wt plant would express preferably AKT1-KC1 heteromeric channels. The activation threshold of these channels is shifted to more negative membrane voltages. This modulation would allow them to open at membrane voltages negative of the equilibrium potential for K^+ and thus allow K^+ influx. With such a scenario, the plant would be harmed by SYP121 as partner in the complex, as the measurements in oocytes here had revealed a shift of the activation potential to again more positive membrane voltages.

However, the situation in root (hair) cells can not be expected to resemble the oocyte expression system entirely. Oocytes as animal cells have a resting membrane potential of ~ -40 mV. As these *Xenopus* egg cells are designed to be virtually independent from exogenous nutrients after fertilisation, they express in their PM only a very low number of endogenous membrane transporters and channels. In addition, the primary ATPase in animal cells such as oocytes drives a largely electro-neutral exchange of Na^+ with K^+ and thus does not contribute significantly to the overall electrical properties of the membrane. Therefore, the equilibrium potential for K^+ would mostly depend on the activity of heterologously expressed K^+ channels and the actual K^+ gradients (inside versus outside of the cell).

In contrast, in plant cells, the highly active ATP-consuming H^+-ATPases generates and maintains the membrane potential at much more negative values (-100 mV to -200 mV). This provides the driving force for K^+ entry through K^+ transporting proteins in roots against the concentration gradient: typical cytoplasmic K^+ concentration of plant cells reaches more than 100 mM, while the free K^+ levels in most of soils are below 1 mM. Furthermore, in plant cells, the equilibrium potential for K^+ is influenced by the activity and concentration gradients of all other ions for which the plant PM is permeable. Thus, measurements of the resting membrane potential in root cells are needed to determine if under low external K^+ conditions the equilibrium potential for K^+ *in planta* would indeed be depolarised (more positive) enough to arrive at values that could cause K^+ loss through active homomeric AKT1 channels. In this context, it was observed that root membrane potential generally becomes more negative (hyperpolarisarion) as K^+ starvation increases (Walker *et al.*, 1996). This would work against efflux through open AKT1 channels.

A recent study provided the first evidence that heteromeric Shaker channels actually exist in plants and not just as a result of heterologous expression (Lebaudy *et al.*, 2008). These authors measured transpiration water loss of four different *Arabidopsis* lines: wt, a homozygous knock-out

for the *KAT2* gene (KO), a wt transformed with a dominant-negative *KAT2* gene under its own promoter (DN), and the *KAT2*-KO transformed with the same dominant-negative construct (DN-KO). The dominant-negative version of KAT2 carried two aa exchanges in the ion conducting pore that occluded the gate. Therefore, non-functional channels were formed in all cases, where at least one subunit of a tetrameric channel carried this mutation. The K^+ inward rectifier KAT2 is proposed to play a role in guard-cell movement, and thus in regulating the aperture of stomata that in turn determines water loss during transpiration (Pilot *et al.*, 2001). Lebaudy *et al.* (2008) observed that in terms of transpiration rates, the wt was indistinguishable from the KO and DN plants. In contrast, transpiration of the DN-KO plant was significantly lowered. They concluded that this result can only be explained if heteromeric channels between KAT2 and other inward rectifying Shaker channel subunits such as for example KAT1 exist *in planta* (Lebaudy *et al.*, 2008). As seen in Fig. 3D (p. 20), multiple inward rectifiers are co-expressed in *Arabidopsis* guard cells beside KAT2 including KAT1, AKT1 and AKT2/3 that may all play a role in stomatal opening (Latorre *et al.*, 2003). KAT1 was shown to form heteromeric channels with KAT2 after co-expression in oocytes and in yeast-two-hybrid studies of the hydrophilic C-terminus (Pilot *et al.*, 2001). Lebaudy *et al.* (2008) reasoned that if only homomers of KAT2 were present and in addition the transpiration phenotype would only be carried by the *KAT2* gene, one should expect a phenotype in the *KAT2*-KO that is identical to the DN-KO. However, if two different Shaker channel subunits contributed to the transpiration phenotype, i.e. homomers as well as heteromers existed the measured transpiration rates would be consistent with this situation. In the wt plants, KAT1 and KAT2 homomers as well KAT1-KAT2 heteromers would be active. In the *KAT2*-KO, KAT1 homomers might take over sufficiently to prevent a transpiration phenotype. In the DN plant, in addition to possible homomers of KAT1 and KAT2, different heteromeric combinations of the wt KAT1 or KAT2 with the mutated KAT2 subunit should be present. Therefore, in comparison to the wt, a reduced number of functional heteromeric channels would be expected, as the mutated subunit 'dilutes out' the functional ones by inactive tetramer formation. Lebaudy *et al.* (2008) suggested that the absence of a transpiration phenotype in the DN plant was due to a sufficiently high number of remaining active channels for the normal regulation of plant transpiration under the conditions tested (similar to the KO situation). In contrast, with the DN-KO strategy, where the number of active channels was further reduced, this additional reduction resulted in an altered regulation of transpiration and the observed phenotype. For the DN-KO, an even more reduced number of active channels than in the DN plant would be expected, because no functional KAT2 subunits are present, and all the mutated DN-KAT2 subunits are forced to form heteromers with KAT1 subunits, thus reducing the number of functional KAT1 homomers. In conclusion, this study suggested that heteromeric Shaker channels exist *in planta* and contribute alongside with homomeric channels to the functional diversity of K^+ channels.

It is therefore possible to imagine that the findings by Geiger *et al.* (2009) and the observations by this study are not mutually exclusive. Perhaps AKT1 homomeric, AKT1-KC1 heteromeric and AKT1-KC1-SYP121 tripartite complexes co-exist at the PM and endow root (hair) cells with a range of sensitivity to changes in membrane potential. Even interaction with SYP121 in

different stoichiometric combinations might contribute to this plasticity. Perhaps the ability to answer to a change in membrane potential quickly by an existing suitable subpopulation of these channels would allow the cells to specify and/or fine-tune responses not only to changes in external K^+ for the purpose of nutrition but also to other external stimuli that provoke fast changes in membrane potential (e.g. pathogen attack, wounding or pH). This would fit well to the observation that *AKT1* is generally not regulated on the transcriptional level in response to stresses such as K^+ and high salt (Lagarde *et al.*, 1996; Pilot *et al.*, 2003a). Transcriptional control implies that proteins need to be produced and properly localized first, a process that takes time to respond to a signal. Thus, the up-regulation of *HAK5* transcripts in response to K^+ deprivation are thought to represent the long-term adaption to low K^+, while the channel AKT1 mediates responses to short-term fluctuations (Amtmann *et al.*, 2006). From studies with null mutants for *hak5* or suppression of *hak5* by K^+ competing NH_4^+ as done here for different external K^+ concentrations, it is obvious that the AKT1 channel can adjust its apparent affinity for K^+ from the low to the high affinity range, depending on the presence of other membrane transporters and experimental conditions. It is not known, how this flexibility is achieved exactly. However, as described in the General introduction and above, both the AKT1 regulation through interaction with CBL/CIPK proteins (Li *et al.*, 2006; Xu *et al.*, 2006) and heterotetramer formation with KC1 (Geiger *et al.*, 2009) has been implicated into the molecular nature of this complex K^+ channel activity modulation. It is suggested here that SYP121 might represent another component involved in AKT1 activity modulation via a tripartite complex with KC1.

General Discussion and Outlook

In summary, the results of the mbSUS assays and Co-IP revealed an interaction between heterologously expressed KC1 and SYP121 that is specific when compared with the two closely related SNAREs SYP122 and SYP111. BiFC assays were able to confirm that this interaction also takes place and is specific *in planta*. The BiFC assays were purposely performed in *Arabidopsis* root hairs, a cellular environment where the native proteins are expressed. This was indicated by information about mRNA levels from the eFP browser database and GUS studies. Loss-of-function plants for all three genes showed a similar phenotype of seedling root and overall growth inhibition and reduced plant K^+ content, when K^+ uptake by channels was limiting. This phenotype was not observed in *syp122* knock-out plants, supporting the existence of an *in planta* function for SYP121 in K^+ nutrition that is specific for this PM SNARE. Electrophysiological measurements of oocytes co-expressing AKT1, KC1 and SYP121 revealed that the SNARE modifies the resulting channel currents in a way that can only be explained by changes in protein conformation as a result from direct interaction of SYP121 with the AKT1-KC1 heteromeric channel. It was concluded from these results that AKT1, KC1 and SYP121 form a tripartite complex and the absence of either component leads to a failure in K^+ uptake from the environment that causes the observed similar phenotype in plants mutated in either gene. This interpretation was supported by the observation that the root cell PM content of native AKT1 and KC1 channel subunits is unchanged between wt and *syp121* mutant plants. Thus, a reduced number of Shaker channel subunits in the PM due to a disruption of the vesicle trafficking function of the SNARE SYP121 could be disregarded as cause for a reduced K^+ uptake capacity in *syp121* mutant plants.

How does this new discovery of an interaction between KC1 and SYP121 fit into the current model of how plants adapt to a K^+-deficient environment? So far, the earliest detectable event induced by low external K^+ concentrations is hyperpolarisation of the root cell membrane potential to more negative values, which happens within a few minutes after subjecting plants to K^+ deprivation (Nieves-Cordones *et al.*, 2008) (see Fig. 56). As detailed in the introduction, the membrane potential of plant cells depends mainly on the activity of the PM H^+-ATPase and the external K^+ concentration (see p.13ff.). A roughly linear relationship of the membrane potential with the log of external K^+ concentration over several orders of magnitude was determined experimentally (Maathuis & Sanders, 1993). At the same time, as explained earlier, the pH gradient, i.e. the electrochemical potential generated by the H^+ pumps provides the motive force for K^+ transport into plant cells in the first place (Palmgren, 2001). An even more complex situation, where K^+ acts as an intrinsic negative regulator of the PM-located H^+-ATPases was suggested (Buch-Pedersen *et al.*, 2006). It is thought that K ions bind to the cytoplasmic part of H^+ pumps and prevent the conformational status change of the H^+-ATPase that allows transmembrane transport of H^+. Thus, under conditions of low external K^+, the reduced K^+ uptake into the cytoplasm and the subsequent decrease of local cytoplasmic K^+ concentration removes the negative regulation from the H^+-ATPases, which leads to an increase in the transmembrane pH gradient, i.e. membrane

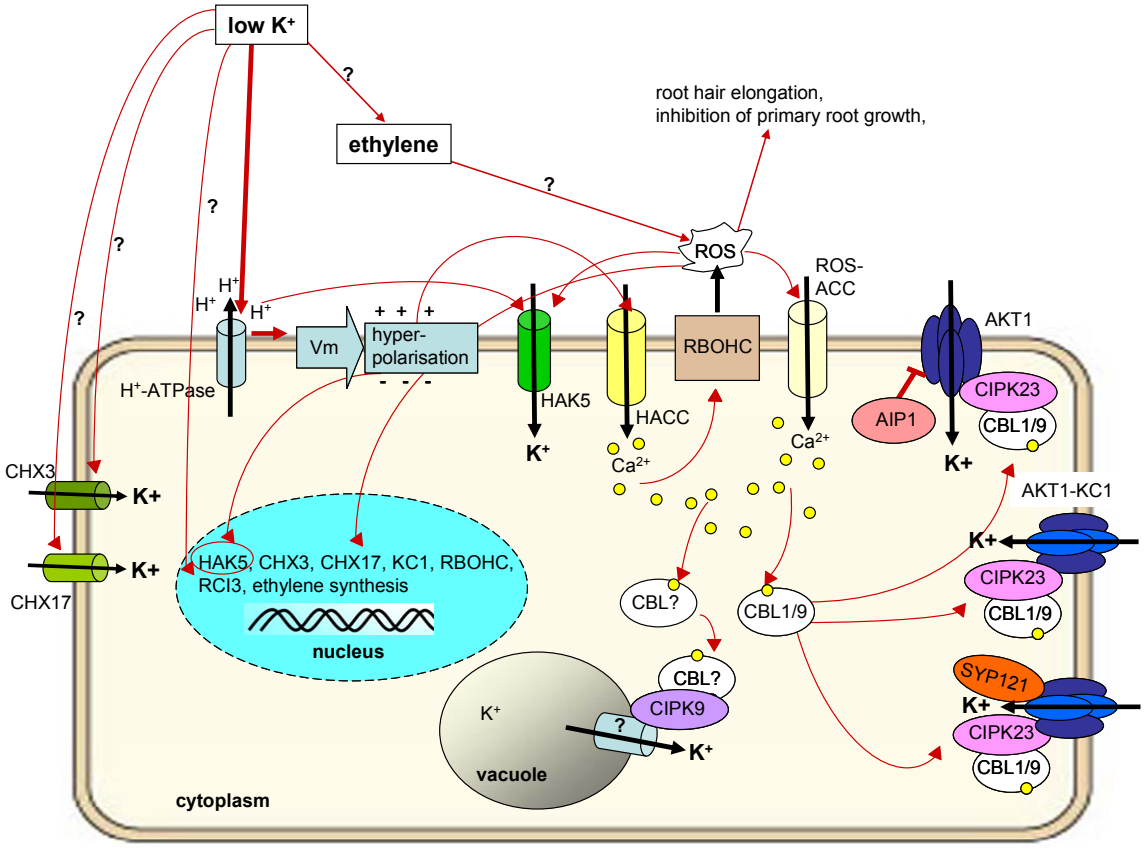

Fig. 56 A model for the low K^+ response in *Arabidopsis*

Shown is an integrative model for the components of the low K^+ sensing and signalling network in *Arabidopsis* root cells. For details see text. All steps, where the specific signalling events for a connection between two points of the signalling network are unknown, are marked with a question mark.

hyperpolarisation (Buch-Pedersen *et al.*, 2006) (see Fig. 56).

This hyperpolarisation is thought to have different effects on both short term and long term plant adaption to K^+ deprivation. With regard to the short term adaptations, the extracellular acidification that is the consequence of enhanced H^+ pump activity may enhance K^+ transporter activity, such as the K^+/H^+ symporter HAK5 in turn (see Fig. 56). As detailed in the introduction (see p. 22ff.), the AKT1 Shaker channel and carrier HAK5 mediate K^+ uptake under low external K^+ conditions (Rubio *et al.*, 2010).

Although AKT1 is a voltage dependent channel that is activated by membrane hyperpolarisation, it has been shown that, at least in heterologous expression systems, hyperpolarisation does not open the channel gates unless AKT1 was phosphorylated first (Li *et al.*, 2006; Xu *et al.*, 2006; Lee *et al.*, 2007). As detailed in the introduction (see Fig. 5, p. 25), AKT1 phosphorylation depends on Ca^{2+} signalling events.

It has been observed that in root cells of *Arabidopsis* plants a low external K^+ concentration induces cytoplasmic Ca^{2+} elevation and strong ROS production (Shin & Schachtman, 2004; Shin *et al.*, 2005) but it is not entirely understood, how these processes are mediated and connected with each other. It was suggested that initially hyperpolarisation-activated Ca^{2+} channels (HACC) in the root cell PM lead to Ca^{2+} influx (see Fig. 56). The resulting cytoplasmic Ca^{2+} elevation can stimulate the PM NADPH oxidase RBOHC to produce ROS (Pitzschke *et al.*, 2006)

(see Fig. 56). ROS in turn can affect ROS-activated Ca^{2+} channels (ROS-ACC) at the PM to achieve further Ca^{2+} influx (Demidchik *et al.*, 2007) (see Fig. 56). Recently, the RCI3 peroxidase has been described as another component of the low K^+ signal transduction pathway (Kim *et al.*, 2010). Plants that overexpressed RCI3 showed more ROS production under low external K^+ conditions.

As a result of these processes, the increase in cytoplasmic Ca^{2+} concentration is thought to exist as Ca^{2+} signals with distinct spatiotemporal variations that are recognized and transduced further downstream by specific Ca^{2+} sensors (White & Broadley, 2003). As detailed in the introduction, the Ca^{2+} sensor CBL1 (and/or CBL9) interacts with the cytoplasm-located Ser/Thr kinase CIPK23 and recruits it to the PM, where CIPK23 activates AKT1-mediated K^+ uptake via phosphorylation of AKT1 (Li *et al.*, 2006; Xu *et al.*, 2006; Lee *et al.*, 2007) (see Fig. 56).

A different CBL/CIPK interaction is thought to mobilize K^+ from the storage pool in the vacuole to maintain K^+ homeostasis in the cytoplasm during the early stage of K^+ deficiency (Walker *et al.*, 1996; Pandey *et al.*, 2007; Schachtman & Shin, 2007b). Pandey *et al.* (2007) observed that mutation of CIPK9 resulted in plants with a low K^+ phenotype of inhibited root growth, while K^+ uptake and whole plant K^+ content was not affected when compared with wt plants. It was suggested that CIPK9 may interact with an as yet unidentified CBL protein to activate through phosphorylation tonoplast K^+ transporters such as e.g. TPK1 (Amtmann & Armengaud, 2007; Pandey *et al.*, 2007) (see Fig. 56).

The generation of ROS by RBOHC and RCI3 was found to be responsible not only for the activation of Ca^{2+} influx channels at the PM (see above) but also necessary for the transcriptional upregulation of *HAK5* (Shin & Schachtman, 2004; Gierth *et al.*, 2005; Kim *et al.*, 2010) (see Fig. 56). An increase in *HAK5* mRNA levels was detected as soon as one day (Ahn *et al.*, 2004) or even six hours (Shin & Schachtman, 2004) after K^+ withdrawal. Apart form ROS, it could be shown that upregulation of *HAK5* at transcript level is directly correlated with the initial hyperpolarisation (Nieves-Cordones *et al.*, 2008). Interestingly, this response on the transcript level could also be triggered by hyperpolarising conditions when the external K^+ concentration was high. It was suggested that hyperpolarisation might trigger a Ca^{2+} signal independent of the external K^+ concentration that in turn affects HAK5 transcript via ROS production (Nieves-Cordones *et al.*, 2008).

K^+ deprivation also led to a rapid induction of the genes encoding the NADPH oxidase RBOHC, the peroxidase RCI3 and the two cation/ H antiporter CHX13, and CHX17 (Cellier *et al.*, 2004; Zhao *et al.*, 2008) and KC1 (Shin & Schachtman, 2004) via unknown signalling mechanisms (see Fig. 56). Thus, in addition to the very fast low K^+ response achieved by Ca^{2+} signalling and posttranslational modification of AKT1, the three K^+ transporters HAK5, CHX13, and CHX17 represent the proteins that enhance K^+ uptake and K^+ redistribution during the early stage of K^+-deprivation. CHXs proteins are thought to mediate K^+/H antiport but the mechanism by which they contribute to K^+ uptake is not clear yet.

Another important signal component involved in potassium deprivation is ethylene. K^+ deprivation up-regulates several genes encoding enzymes related to ethylene production and it also

leads to increases in ethylene in starved plants (Shin & Schachtman, 2004) (see Fig. 56). In addition, under low K^+ conditions, the promotion of root hair elongation, the inhibition of primary root growth, ROS production and the induction of *HAK5* expression were eliminated in plants treated with ethylene inhibitors, and partially eliminated in ethylene insensitive mutants (Jung *et al.*, 2009). Jung *et al.* (2009) concluded from these results that ethylene acts upstream of ROS in response to K^+ deprivation and thus expression of *HAK5* depends on ethylene signalling. Nevertheless, these authors also found indications that an ethylene independent signalling pathway must exist.

During periods of K^+ starvation that last for several days to weeks, plants start to initiate specific long-term responses when the cellular K^+ homeostasis collapses and the cytoplasmic K^+ concentration starts to decline. Metabolic changes are induced that are thought to result mainly from an activity decline in K^+ dependent metabolic enzymes (Amtmann *et al.*, 2008; Amtmann & Armengaud, 2009) (see p. 24ff.). In summary, although many immediate and longer term effects of lowering the external K^+ concentration are known, a lot of information about how they are connected in a network of signalling events is still missing. Most importantly, the signal receptor that perceives low external K^+ conditions in the first place is still missing as well.

In *E. coli*, the kinase KdpD functions as a specific sensor for K^+ (Walderhaug *et al.*, 1992). KdpD is a sensor kinase that undergoes autophosphorylation and transfers a phosphoryl group to the response regulator KdpE. This response regulator controls the expression of an operon that encodes a high-affinity potassium uptake system in *E. coli*. The sensor kinase transduces changes in turgor caused by low K^+. No such system has been observed in plants yet.

It was recently proposed that K^+ transporting proteins with a wide range of affinity to K^+ might be K^+ sensors in analogy to the suggestions made for the *Arabidopsis* nitrate transporter CHL1 (Wang & Wu, 2010). In response to low external concentrations of nitrate, CIPK23 phosphorylates CHL1 at a threonine residue (T101) which makes CHL1 a high-affinity nitrate transporter. When exposed to high external concentrations of nitrate, T101 phosphorylation is prohibited and dephosphorylated CHL1 acts as a low affinity nitrate transporter. Thus, CHL1 is a nitrate sensor and dual-affinity nitrate transporter at the same time and the phosphorylation status of CHL1 T101 switches the transport mode (Ho *et al.*, 2009).

Wang *et al.* (2010) proposed a hypothetical working model, where AKT1 is a K^+ sensor that functions in analogy to CHL1. As detailed in the introduction, AKT1 was found to mediate K^+ uptake over a wide range of external K^+ concentrations (0.01 and 0.05 mM K^+, see Fig. 4, p. 24) (Hirsch *et al.*, 1998; Spalding *et al.*, 1999; Rubio *et al.*, 2010). Wang *et al.* (2010) speculate that AKT1 switches its working mechanism between high affinity and low affinity in response to changes in the external K^+ concentration controlled by a CIPK23-mediated phosphorylation switch. The observed interaction of AKT1 with the phosphatase AIP1 (see Fig. 56) could deactivate AKT1 channel activities through dephosphorylation (Lee *et al.*, 2007) to cease the low K^+ induced signalling as was observed for dephosphorylation of CHL1 (Ho *et al.*, 2009). However, although AKT1 operates in the high-affinity range of external K^+ concentrations (0.01 mM), it does not display a true dual affinity kinetic of uptake such as CHL1. It is membrane hyperpolarisation that

still allows K^+ uptake under low external K^+ conditions. Another observation that might not agree with the hypothesis of AKT1 functioning as a K^+ sensor in analogy to CHL1 is the absence of measurable K^+ currents in oocytes independent of the external K^+ concentration when the CBL1/CIPK23 system was not co-expressed, i.e. AKT1 was not phosphorylated (Li *et al.*, 2006; Xu *et al.*, 2006; Lee *et al.*, 2007). According to the CHL1-like model, dephosphorylated AKT1 should display low affinity K^+ uptake. Still, oocytes are a heterologous expression system that very obviously is not able to represent the plant cell situation, as it can not phosphorylate AKT1 by itself.

Even if the exact mechanism that would allow AKT1 to function as K^+ sensor and transporter simultaneously is not understood, it is not unreasonable to think that AKT1 is involved in K^+ sensing. When considering the model in Fig. 56, it must be concluded that the membrane potential is involved in sensing the external K concentration. As explained above, it is thought that K^+ acts as an intrinsic negative regulator of the PM H^+-ATPases and thereby affects the membrane potential (Buch-Pedersen *et al.*, 2006). Hyperpolarisation under low K^+ in turn is the first step in creating the Ca^{2+} signal that leads to AKT1 phosphorylation. K ions taken up via AKT1 (or other K^+ transporters, e.g. HAK5) are therefore needed to relate the external K^+ status to the membrane potential. Interestingly, Hirsch *et al.* (1998) had already observed that in root cells of *akt1* mutant plants in the presence of NH_4^+ the dependence of the membrane potential on the external K^+ concentration disappeared. These observations suggest that AKT1 may function as a K^+ sensor in coupling with the PM H^+-ATPases.

It is then the question, how heteromeric AKT1-KC1 channels and tripartite complexes with SYP121 fit into this model. Possibly one could imagine a feedback situation between AKT1 and H^+-ATPase that would benefit from the simultaneous presence of AKT1 homomers, AKT1-KC1 heteromers and tripartite channel complexes of AKT1-KC1-SYP121 as discussed in Chapter 4 (see also Fig. 56). Assuming AKT1 is in its phosphorylated state, one would expect the membrane potential to be quite negative (hyperpolarised) according to the model suggested above, i.e. negative regulation of H^+-ATPase is removed as external K^+ is low. As discussed in Chapter 4, AKT1 homomeric channels, at least after heterologous expression in oocytes, have their activation threshold at quite positive membrane voltages (around -50 mV). In contrast, for AKT1-KC1 heteromeric channels and AKT1-KC1-SYP121 channel complexes, the activation threshold was shifted to values around -160 mV and -100 mV respectively. This would mean that the AKT1-KC1 heteromers are most likely the ones that respond, when phosphorylated under low K^+, to the prevailing hyperpolarised membrane voltage. The resulting K^+ influx via these heteromeric AKT1-KC1 channels would again shift the membrane potential to more positive values (depolarisation) according to the model described above, i.e. negative regulation of H^+-ATPase is increased. As also observed in oocytes, AKT1-KC1 heteromeric channels show, in addition the negative shift of the voltage activation threshold, a reduction of the inward current at any given potential, i.e. less K^+ is taken up when compared to AKT1 homomers (Duby *et al.*, 2008; Geiger *et al.*, 2009). One could perhaps imagine that this effect of reduced ability for K^+ uptake in heteromers and/ or other effects such as the spatiotemporal fluctuations of the K^+ concentration in the soil solution and the

contribution of other K^+ influx systems (e.g. HAK5, CHX3 and CHX7) allow the membrane potential to depolarises to a value that only fits the activation threshold AKT1-KC1-SYP121 complexes (-100 mV). These channels could then respond immediately and take up more K^+ without delay which in turn might depolarise the membrane potential to values that allow AKT1 homomers to respond (-50 mV). At this stage, the increasing local K^+ concentration might eventually hyperpolarize the membrane potential again below values that fit the activation threshold of AKT1 homomers and so on. In this way, the presence of AKT1-KC1 heteromers and AKT1-KC1-SYP121 tripartite channel complexes could add dynamic modulation and optimisation to the K^+ sensing and uptake process. Such a model that requires all three different combinations of AKT1, KC1 and SYP121 channel assemblies would also fit the observed low K^+ phenotype in mutants with loss-of-function in either gene, when the K^+ uptake via HAK5 is blocked by NH_4^+ (see Chapter 4).

At this stage there are many open questions about the specific interaction between KC1 and SYP121. A hypothetical model as discussed above would, for example, allow for the interaction between SYP121 and KC1 to be transient or stable. As mentioned in the introduction (see p.73), a transient interaction would require, for example, a phosphorylation event. It has been shown that CIPK23 does not phosphorylate KC1 (Li *et al.*, 2006; Xu *et al.*, 2006). However, the *Arabidopsis* genome encodes for 25 CIPK family members. Their functional characterisation and contribution to Ca^{2+} signalling networks has just begun (Luan, 2009). One might also imagine that SYP121 itself could be phosphorylated *in planta* in response to low external K^+, and thus recruited to AKT1-KC1 heteromeric channels already present in the PM. In contrast, stable interactions of AKT1-KC1-SYP121 tripartite complexes would be expected to assemble in the ER *in planta*, in analogy to the auxillary subunits forming complexes with mammalian Kv Shaker channels (see p. 64ff.). The data obtained from the mbSUS, Co-IP and BiFC assays in this work are inconclusive with regard to the question whether the interaction between KC1 and SYP121 is stable and takes place in the ER or is transiently formed at the PM. As discussed earlier (see p. 73ff.), the mbSUS technique can not discriminate between these two possibilities, as even a transient interaction event will activate the reporter genes as soon as the artificial transcription factor is cleaved off. Furthermore, interaction may take place in any membrane of the cell as long as both Nub and Cub are present in the cytoplasm. The Co-IP between KC1 and SYP121 would indicate a stable interaction or perhaps a strong transient interaction that might need e.g. a dephosphorylating event to be terminated. Weaker transient interactions would not allow for Co-IP as the complex disassociates too quickly. As discussed in Chapter 3 (p. 194ff.), the results of the BiFC assays indicate an interaction between KC1 and SYP121 that can be detected at the PM but not the ER.

With regard to the question of the protein domains that mediate this interaction, recently made progress showed that the N-terminus of the SYP121 SNARE is involved (Grefen *et al.*, 2010). Experiments for this work had narrowed the domain on the Shaker subunit KC1 down to the N-terminus as well with the help of truncated KC1-Cub constructs in mbSUS assays with Nub-SYP121 (data not shown). These protein domains are currently being prepared for NMR analysis.

The interaction with of KC1 with the N-terminus of SYP121 connects to the question, how

the whole array of vesicle trafficking regulating factors, from SM proteins to the exocyst components (p. 41ff.) behaves in relation to SYP121-KC1 interaction. As mentioned in the introduction, it is thought very unlikely that syntaxin proteins such as SYP121 are free molecules in the cell, as they are capable of spontaneous SNARE-complex formation with cognate SNARE partners. The described modes of SM binding to open/closed SNAREs involve the N-terminus of syntaxins. Possibly, a competition for this SYP121 domain might take place that in turn could have a regulatory effect on the SNARE with regard to vesicle fusion function or ion channel regulation. Preliminary data with a constitutive-open SYP121 mutation indicated less interaction with KC1 in mbSUS assays and no effect on AKT1-KC1 currents recorded form oocyte expression as described in Chapter 4 (data not shown). It will be interesting to link the known vesicle trafficking regulatory factors to the KC1-SYP121 interaction which might reveal such a fine-tuned function as in the model of Syntaxin1A regulation in insulin secretion that could integrate vesicle fusion with ion channel regulation (p. 64). For example, one could measure K^+ uptake rates in mutant plants where SYP121 has been replaced with its constitutive-open form or the *pen1-3* mutant, where SNARE complex formation with the SYP121 syntaxin is inhibited due to point mutation in the SNARE motif (Collins *et al.*, 2003).

Fine tuning of Shaker channels via interaction with SYP121 could be relevant not only to K^+ uptake but also to other signalling networks in *Arabidopsis*. Interestingly, the situation in guard cells is, if not quite the same, in many aspects not so different from the signalling events that link vesicle fusion and insulin exocytosis to a high-blood glucose signal. Ca^{2+} influx, changes in membrane potential driven by e.g. K^+ channels from the same Shaker superfamily and the event of vesicle fusion to the PM of guard cells to accommodate changes in cell volume have same similarities to pancreatic cells or presynaptic neurons. Even though speculative, SYP121 has been implicated in a form of ion channel regulation in the stomatal regulation cascade (see p. 68). In addition, the regulatory Shaker channel subunit KC1 is well known to associate with KAT1, for example, an important inward rectifier in guard cells (Hosy *et al.*, 2005; Duby *et al.*, 2008). Possibly, the fine-tuning effect that was suggested for KC1-SYP121 interaction on AKT1 might have an implication for functions of other Shaker inward subunits such as KAT1 as well.

In this context, it is interesting to note that important functions for SYP121 have been discovered for SYP121 in pathogen defence (see p. 55ff.). Work by Zhang *et al.* (2007) had suggested that SYP121 shares with SYP122 a function as regulators of a signalling node that controls SA, JA and ET and HR-like defence pathways. In addition, SYP121 has a function in pre-invasive defence against powdery mildew fungi that is not shared with SYP122. While for the pre-invasive defence vesicle fusion events have been implicated that involve the first SNARE complex discovered from plants, it is entirely unknown how SYP121 might control the defence signalling pathways (Zhang *et al.*, 2007). Nuhse *et al.* (2003) showed that Syp122 was phosphorylated in response to a microbial elicitor of defence (flagellin) and that this step was Ca^{2+} dependent *in vitro*. It has since then been shown that also the tobacco homologue of SYP121 is rapidly and transiently phosphorylated in response to a fungal pathogen elicitor (Avr9) in tobacco (Heese *et al.*, 2005). The tomato *R* gene *Cf-9* is required for resistance against races of the leaf fungus expressing *Avr9*.

The *Cf-9* gene encodes a highly glycosylated type I membrane protein with a domain structure characteristic of receptor-like proteins. Its extracellular Leu-rich repeat domain plays a major role in Avr9 specificity. In *Cf-9*-expressing plants, elicitation with the elicitor Avr9 triggers rapid changes in ion flux, the production of ROS, the activation of the mitogen-activated protein kinases and salicylic acid-inducible protein kinase and the activation of calcium-dependent protein kinases. It is interesting to note that these defence signalling events (Ca^{2+}, ROS) are not so different from the low K^+ stress signal that eventually targets AKT1 (p. 22ff.). Again, highly speculative, perhaps there is a defence signalling function for SYP121 that links the observed rapid changes in ion flux to a function of fine-tuning the response of Shaker K+ channels to changes in membrane potential that would occur with e.g. Ca^{2+} fluxes, possibly even fusion of vesicles for exocytosis of toxic components for pathogen defence.

Pajonk *et al.* (2008) had observed as well that SYP121 phosphorylation (in the N-terminus) was necessary for its function in pre-invasive defence. Possibly, SYP121 might associate with KC1, i.e. AKT1-KC1 heteromeric channels upon receiving a phosphorylation signal and could then modulate channel properties to transduce a defence signal that relies on rapid changes in ion flux.

Even more speculative is a possible function for the external C-terminus of SYP121 and SYP122. Comparison of all known yeast, mammalian and *Arabidopsis* SNAREs from databases revealed that only a few other SNAREs have such extended extracellular C-termini and nothing no report could be found in the literature about their possible function. For SYP121, the study mentioned in the discussion of Chapter 3 (p. 194ff.) by DiSansebastaino *et al.* (2006) could confirm with the help of a GFP fusion to the C-terminus of SYP121 the expected correct membrane orientation *in planta*. Interestingly, the DPP-like auxiliary subunits of mammalian Kv Shaker channels (see Fig. 16) have one TMD domain and a long external N- or C-terminus as well (Vacher *et al.*, 2008). They have been shown to affect Kv trafficking to the cell surface as well as modulation of Kv electrical properties but it is not known yet what purpose the external protein part might have (Vacher *et al.*, 2008). Possible might be some kind of signal perception. Lastly, it was noticed with interest that SYP121 presence at the PM appeared to be light-regulated with regard to a recent study of light-induced modification of plant PM ion transport (see discussion of Chapter 3, p. 194ff.) (Marten *et al.*, 2010).

Finally, the question of SYP121 specificity for KC1 over AKT1 and KAT1 (and the remaining three inward rectifying *Arabidopsis* Shaker channel subunits) had to remain unanswered here, mostly due to techniqual problems with the mbSUS, Co-IP and BiFC assays. Improved design of the Cub-X vector and the new antibodies against KC1 and AKT1 will help with future mbSUS assays to answer this question. Similarly, new BiFC vectors that allow Gateway cloning of multiple constructs into one T-DNA will help with future BiFC assays. It is unsure, whether the problems of AKT1 and KAT1 expression and solubilisation in insect cells are avoidable. A pull-down with soluble domains might be an alternative solution.

Appendix I

No.	primer sequence 5'-3'
1	cccagctttcttgtacaaagtggttggtggtggcggacatatgtagggggcgcgaccggacccgcatcccccgtctgggt
2	acccagacgggggatgcgggtccggtcccgcccccctacatatgtccgccaccaccaaccactttgtacaagaaagctgg
3	P-GATACAATTCTATTACCCCCATCCATACtta
4	P-GAGCCTGCTTTTTTGTACAAACTTGTTaat
5	atgaaagcgttaacggccagg
6	attgacgagtacggtgggtgcctcgag
7	ccgCTCGAGatgGGTATCCCTCCAGATCAACAAA
8	gtgctaaggctaagaggtggttctaga-gc
9	ccTTAATTAAatgaaagcgttaacggccagg
10	CCttaattaaaccacctcttagccttagcac
11	acaagtttgtacaaaaaagcaggctctccaaccaccATGTCTACGACGACTACTGAGG
12	acaagtttgtacaaaaaagcaggctctccaaccaccatgtcgatctcttggactcgaaa
13	acaagtttgtacaaaaaagcaggctctccaaccaccATGAGAGGAGGGGCTTTGTTAT
14	acaagtttgtacaaaaaagcaggctctccaaccaccATGAACGATTTGTTTTCCAGCTCA
15	acaagtttgtacaaaaaagcaggctctccaaccaccATGAACGACTTGATGACGAAATC
16	acaagtttgtacaaaaaagcaggctctccaaccaccATGAACGATCTTCTCTCCGGCT
17	tccgccaccaccaaccactttgtacaagaaagctgggtaGAAAATATATAAATGATCGTTTTCTC
18	tccgccaccaccaaccactttgtacaagaaagctgggtaatttgatgaaaaatacaaatgatcac
19	tccgccaccaccaaccactttgtacaagaaagctgggtaAGAATCAGTTGCAAAGATGAGATG
20	tccgccaccaccaaccactttgtacaagaaagctgggtaACGCAATAGACGCCTTGCCTG
21	tccgccaccaccaaccactttgtacaagaaagctgggtaAGAAGAGCTGAAACTGGTAATGA
22	tccgccaccaccaaccactttgtacaagaaagctgggtaGCGTAGTAGCCGCCGATTCA
23	tccgccaccaccaaccactttgtacaagaaagctgggtaTTAGAAAATATATAAATGATCGTTTTCTC
24	tccgccaccaccaaccactttgtacaagaaagctgggtatcaatttgatgaaaaatacaaatgatcac
25	tccgccaccaccaaccactttgtacaagaaagctgggtaTTAAGAATCAGTTGCAAAGATGAGATG
26	tccgccaccaccaaccactttgtacaagaaagctgggtaTCAACGCAATAGACGCCTTGCCTG
27	tccgccaccaccaaccactttgtacaagaaagctgggtaTCAAGAAGAGCTGAAACTGGTAATGA
28	tccgccaccaccaaccactttgtacaagaaagctgggtaTTAGCGTAGTAGCCGCCGATTC
29	acaagtttgtacaaaaaagcaggctctccaaccaccaatgtctacgacgactactgagg
30	acaagtttgtacaaaaaagcaggctctccaaccaccaatgaacgatttgttttccagctca
31	acaagtttgtacaaaaaagcaggctctccaaccaccaatgaacgacttgatgacgaaatc
32	cggaattcatgagaggaggggctttgttat
33	ccaatgcattggtcctgcagttacttacccaggcggttcatttcgatatcagtgtaagaatcagttgcaaagatgagatg
34	cgggatccATGTCGATCTCTTGGACTCGAAATTT
35	ttctgcagtcaagcgtagtctgggacgtcgtatgggtatctagcgtagtctgggacgtcgtatgggtaagatctatttgatgaaaaatacaaatgatcac
36	ccaatgcactgcagTCAATTTGATGAAAAATAC
37	GactagtATGGTGAGCAAGGGCGAGGA
38	GCtctagaAAGATCCTCCTCAGAAATCAACTTTTGCTCggcggtgatatagacgttgtgg
39	GactagtATGgacaagcagaagaacggca
40	GCtctagaAGCGTAATCTGGAACATCGTATGGGTAtagtggAGCGTAATCTGGAACATCGTATGGGTActtgtacagctcgtccatgcc
41	GactagtATGAACGATTTGTTTTCCAGCTC
42	GactagtTCAACGCAATAGACGCCTTGC
43	gactagtatgaacgacttgatgacgaaatc
44	gactagttcaagaagagctgaaactggtaa
45	gactagtatgaacgatcttctctccggc
46	gactagtttagcgtagtagccgccgattc
47	GCtctagaATGTCTACGACGACTACTGAGGC
48	GCtctagaTTAGAAAATATATAAATGATCGTTTTC
49	gctctagattagaaaatatataaatgatcgttttc
50	ccgctcgagttacttgtacagctcgtccatgcc
51	P-cgaaaattcaagacaaggaatgaatccctggttaccc

Table A 1 List of used primers (numbers are as given in M&M)

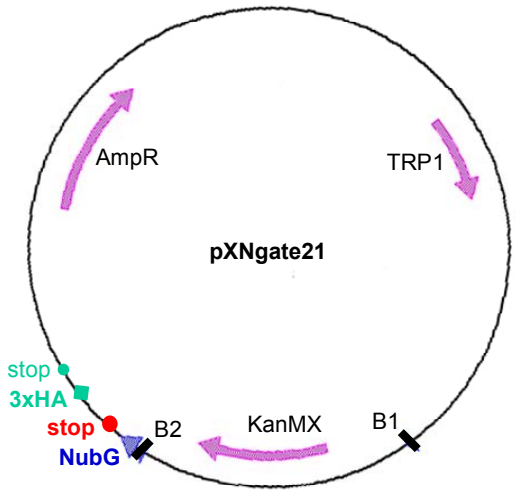

Fig. A 2 Modification of pXNgate21-3HA to pXNgate21

The original vector pXNgate21-3HA (Obrdlik *et al.*, 2004) allows fusions of a Nub-3xHA part to the C-terminus of a CDS of interest by exchanging it for the KanMX cassette between the B1 and B2 recombination sites. This vector was changed into pXNgate21 via site directed mutagenesis. A point mutation introduced a new stop codon (red dot) directly after the Nub coding sequence, thereby omitting the 3-HA tag from future X-Nub fusions. The primers No. 51 (for) and 52 (rev) were used.

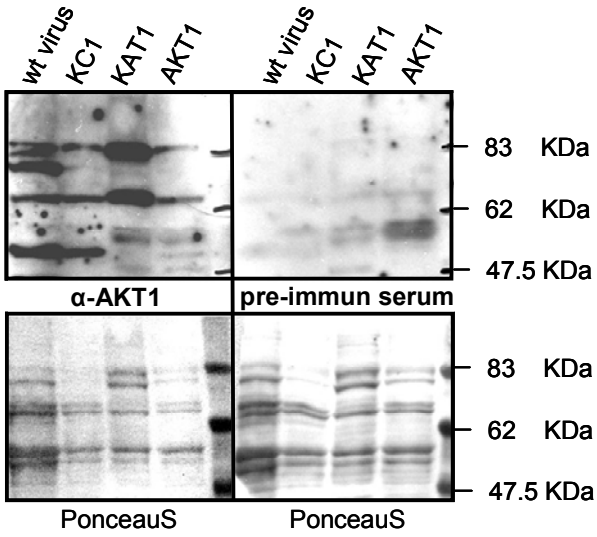

Fig. A 3 Anti-AKT1 antibody yielded no specific signal on insect cell proteins

New rabbit polyclonal anti-AKT1 (Agrisera) was tested (here 1:50, pH2 elution) on LPC-solubilised membrane fractions of *Sf9* insect cells expressing either wt Baculovirus, KC1-Myc, KAT1-2xHA or AKT1-VSVG (same as for Fig. 53A). No specific signal, unique to the AKT1-VSVG membrane fraction was obtained. The wt Baculovirus control indicated that most detected proteins were likely insect cell or virus derived. The weaker band pattern derived from the detection with pre-immune serum (1:50) was quite similar, at least in the upper ranges, to the one in the left upper panel, indicating that signals were likely derived from antibodies not specific for the antigen. However, it was considered that the problem of weak expression and partial degradation for AKT1-VSVG in insect cells that was determined with an anti-VSVG (see Fig. 37) might have contributed to this negative result. True but weak and/ or partial degraded signals might be masked by unspecific bands that are enhanced by the low dilution of the antibody. Using the corresponding pH7 elution or Ab dilutions ranging from 1:700 to 1:50 did not improve these results. For further experiments see p. 213ff.)

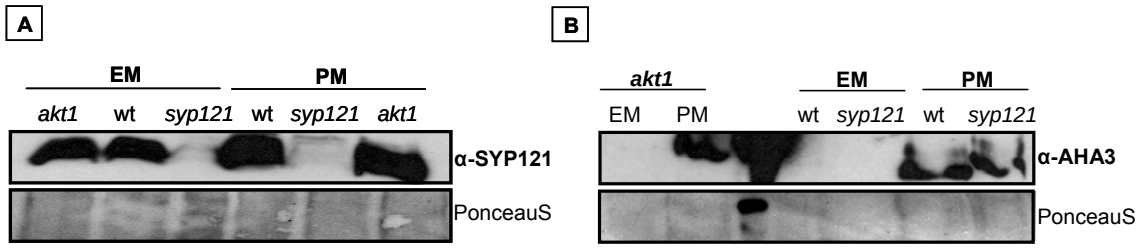

Fig. A 4 SYP121 is present in PM and EM fractions of wt but not *syp121* plants

Two-phase partitioning was performed as described earlier (see p. 218) but without the urea-NaOH treatment to concentrate integral membrane proteins and no solublilisation of PM or EM fractions. Root tissue (10 g fresh weight/ sample) of 3 week old hydroponically grown *Arabidopsis* Col0, *syp121* and *akt1* long day plants (16:8- light:dark) was used. Protein samples were quantified by amidoblack assay and 8 µg/ lane were separated on two identical (except sample order) SDS gels for Western Blot (A, B). Anti-SYP121 was used in a 1:40,000 dilution (A) and marker-antibody for PM, anti-AHA3 (R. Serrano), in a 1:1000 dilution (B). Secondary anti-Rabbit-HRP was used 1:10,000 and detected with ECL Advance (GE healthcare) (A, B).
Anti-SYP121 confirmed the previously published absence of SYP121 protein in the *syp121* mutant (Collins *et al.*, 2003; Zhang *et al.*, 2007) (EM and PM in A, upper panel). In contrast, both wt and *akt1* mutant showed SYP121 protein in both the PM and the EM fractions (A, upper panel). The marker-antibody anti-AHA3 recognized no protein in the EM fractions of wt, *syp121* and *akt1*, indicating that no PM derived proteins contaminated the EM fractions (B). Thus, these results suggested, that in wt (and *akt1*) plants native SYP121 is found not only in the PM but also in either internal membranes or as part of 'contaminating' soluble proteins, i.e. cytoplasm derived. As discussed earlier (p. 59ff.), SYP121 is a TA protein and as such expected to reside on ribosomes in the cytoplasm before post-translational insertion into the ER membrane. Both locations might provide SYP121 protein to PM/ EM vesicles forming during the homogenisation of tissues. The amount of SYP121 detected in PM (and EM) fractions of wt compared to *akt1* mutant appeared

List of References

Ahn, S. J., Shin, R., & Schachtman, D. P. (2004). Expression of KT/KUP genes in Arabidopsis and the role of root hairs in K+ uptake. *Plant Physiology* **134**, 1135-1145.

Alexandersson, E., Saalbach, G., Larsson, C., & Kjellbom, P. (2004). Arabidopsis plasma membrane proteomics identifies components of transport, signal transduction and membrane trafficking. *Plant and Cell Physiology* **45**, 1543-1556.

Amtmann, A. & Armengaud, P. (2007). The role of calcium sensor-interacting protein kinases in plant adaptation to potassium-deficiency: new answers to old questions. *Cell Research* **17**, 483-485.

Amtmann, A. & Armengaud, P. (2009). Effects of N, P, K and S on metabolism: new knowledge gained from multi-level analysis. *Current Opinion in Plant Biology* **12**, 275-283.

Amtmann, A., Hammond, J. P., Armengaud, P., & White, P. J. (2006). Nutrient sensing and signalling in plants: Potassium and phosphorus. *Advances in Botanical Research, Vol 43* **43**, 209-257.

Amtmann, A., Troufflard, S., & Armengaud, P. (2008). The effect of potassium nutrition on pest and disease resistance in plants. *Physiologia Plantarum* **133**, 682-691.

Anbazhagan, V., Cymer, F., & Schneider, D. (2010). Unfolding a transmembrane helix dimer: A FRET study in mixed micelles. *Archives of Biochemistry and Biophysics* **495**, 159-164.

Anderson, J. A., Huprikar, S. S., Kochian, L. V., Lucas, W. J., & Gaber, R. F. (1992). Functional Expression of A Probable Arabidopsis-Thaliana Potassium Channel in Saccharomyces-Cerevisiae. *Proceedings of the National Academy of Sciences of the United States of America* **89**, 3736-3740.

Armengaud, P., Zambaux, K., Hills, A., Sulpice, R., Pattison, R. J., Blatt, M. R., & Amtmann, A. (2009). EZ-Rhizo: integrated software for the fast and accurate measurement of root system architecture. *Plant Journal* **57**, 945-956.

Ashley, M. K., Grant, M., & Grabov, A. (2006). Plant responses to potassium deficiencies: a role for potassium transport proteins. *Journal of Experimental Botany* **57**, 425-436.

Assaad, F. F., Huet, Y., Mayer, U., & Jurgens, G. (2001). The cytokinesis gene KEULE encodes a Sec1 protein that binds the syntaxin KNOLLE. *Journal of Cell Biology* **152**, 531-543.

Assaad, F. F., Qiu, J. L., Youngs, H., Ehrhardt, D., Zimmerli, L., Kalde, M., Wanner, G., Peck, S. C., Edwards, H., Ramonell, K., Somerville, C. R., & Thordal-Christensen, H. (2004). The PEN1 syntaxin defines a novel cellular compartment upon fungal attack and is required for the timely assembly of papillae\. *Molecular Biology of the Cell* **15**, 5118-5129.

Assaad, F. F. & Signer, E. R. (1990). Cauliflower Mosaic-Virus P35S Promoter Activity in Escherichia-Coli. *Molecular & General Genetics* **223**, 517-520.

Atlas, D. (2001). Functional and physical coupling of voltage-sensitive calcium channels with exocytotic proteins: ramifications for the secretion mechanism. *Journal of Neurochemistry* **77**, 972-985.

Baizabal-Aguirre, V. M., Clemens, S., Uozumi, N., & Schroeder, J. I. (1999). Suppression of inward-rectifying K+ channels KAT1 and AKT2 by dominant negative point mutations in the KAT1 alpha-subunit. *Journal of Membrane Biology* **167**, 119-125.

Bakkeren, G., Koukolikovanicola, Z., Grimsley, N., & Hohn, B. (1989). Recovery of Agrobacterium Tumefaciens T-Dna Molecules from Whole Plants Early After Transfer. *Cell* **57**, 847-857.

Banerjee, P., Joo, J. B., Buse, J. T., & Dawson, G. (1995). Differential Solubilization of Lipids Along with Membrane-Proteins by Different Classes of Detergents. *Chemistry and Physics of Lipids* **77**, 65-78.

Baranski, R., Klocke, E., & Schumann, G. (2006). Green fluorescent protein as an efficient selection marker for Agrobacterium rhizogenes mediated carrot transformation. *Plant Cell Rep.* **25**, 190-197.

Bassham, D. C., Brandizzi, F., Otegui, M. S., & Sanderfoot, A. A. (2008). The Secretory System of Arabidopsis. In *The Arabidopsis Book* pp. 1-29. The American Society of Plant Biologists.

Beemster, G. T. S., De Vusser, K., De Tavernier, E., De Bock, K., & Inze, D. (2002). Variation in growth rate between Arabidopsis ecotypes is correlated with cell division and A-type cyclin-dependent kinase activity. *Plant Physiology* **129**, 854-864.

Benfey, P. N. & Chua, N. H. (1990). The Cauliflower Mosaic Virus-35S Promoter - Combinatorial Regulation of Transcription in Plants. *Science* **250**, 959-966.

Benya, R. V., Kusui, T., Katsuno, T., Tsuda, T., Mantey, S. A., Battey, J. F., & Jensen, R. T. (2000). Glycosylation of the gastrin-releasing peptide receptor and its effect on expression, G protein coupling, and receptor modulatory processes. *Molecular Pharmacology* **58**, 1490-1501.

Berggard, T., Linse, S., & James, P. (2007). Methods for the detection and analysis of protein-protein interactions. *Proteomics* **7**, 2833-2842.

Berkowitz, G., Zhang, X., Mercier, R., Leng, Q., & Lawton, M. (2000). Co-expression of calcium-dependent protein kinase with the inward rectified guard cell K+ channel KAT1 alters current parameters in Xenopus laevis oocytes. *Plant and Cell Physiology* **41**, 785-790.

Bethani, I., Lang, T., Geumann, U., Sieber, J. J., Jahn, R., & Rizzoli, S. O. (2007). The specificity of SNARE pairing in biological membranes is mediated by both proof-reading and spatial segregation. *EMBO J* **26**, 3981-3992.

Betz, W. J., Mao, F., & Smith, C. B. (1996). Imaging exocytosis and endocytosis. *Current Opinion in Neurobiology* **6**, 365-371.

Bezprozvanny, I., Zhong, P. Y., Scheller, R. H., & Tsien, R. W. (2000). Molecular determinants of the functional interaction between syntaxin and N-type Ca2+ channel gating. *Proceedings of the National Academy of Sciences of the United States of America* **97**, 13943-13948.

Bhat, R. A., Lahaye, T., & Panstruga, R. (2006). The visible touch: in planta visualization of protein-protein interactions by fluorophore-based methods. *Plant Methods* **2**, 12.

Bhattacharya, A., Sood, P., & Citovsky, V. (2010). The roles of plant phenolics in defence and communication during Agrobacterium and Rhizobium infection. *Molecular Plant Pathology* **11**, 705-719.

Bihler, H., Eing, C., Hebeisen, S., Roller, A., Czempinski, K., & Bertl, A. (2005). TPK1 is a vacuolar ion channel different from the slow-vacuolar cation channel. *Plant Physiology* **139**, 417-424.

Birnbaum, K., Shasha, D. E., Wang, J. Y., Jung, J. W., Lambert, G. M., Galbraith, D. W., & Benfey, P. N. (2003). A gene expression map of the Arabidopsis root. *Science* **302**, 1956-1960.

Booth, P. J. (2005). Same in the membrane: designing systems to modulate membrane proteins. *Current Opinion in Structural Biology* **15**, 435-440.

Bordier, C. (1981). Phase-Separation of Integral Membrane-Proteins in Triton X-114 Solution. *Journal of Biological Chemistry* **256**, 1604-1607.

Borgese, N., Brambillasca, S., & Colombo, S. (2007). How tails guide tail-anchored proteins to their destinations. *Current Opinion in Cell Biology* **19**, 368-375.

Borgese, N., Brambillasca, S., Soffientini, P., Yabal, M., & Makarow, M. (2003). Biogenesis of tail-anchored proteins. *Biochemical Society Transactions* **31**, 1238-1242.

Borgese, N. & Fasana, E. (2011). Targeting pathways of C-tail-anchored proteins. *Biochimica et Biophysica Acta-Biomembranes* **1808**, 937-946.

Boutte, Y., Frescatada-Rosa, M., Men, S. Z., Chow, C. M., Ebine, K., Gustavsson, A., Johansson, L., Ueda, T., Moore, I., Jurgens, G., & Grebe, M. (2010). Endocytosis restricts Arabidopsis KNOLLE syntaxin to the cell division plane during late cytokinesis. *Embo Journal* **29**, 546-558.

Bowie, J. U. (2005). Solving the membrane protein folding problem. *Nature* **438**, 581-589.

Bradford, M. M. (1976). Rapid and Sensitive Method for Quantitation of Microgram Quantities of Protein Utilizing Principle of Protein-Dye Binding. *Analytical Biochemistry* **72**, 248-254.

Brady, S. M., Orlando, D. A., Lee, J. Y., Wang, J. Y., Koch, J., Dinneny, J. R., Mace, D., Ohler, U., & Benfey, P. N. (2007). A High-Resolution Root Spatiotemporal Map Reveals Dominant Expression Patterns. *Science* **318**, 801-806.

Brambillasca, S., Yabal, M., Makarow, M., & Borgese, N. (2006). Unassisted translocation of large polypeptide domains across phospholipid bilayers. *Journal of Cell Biology* **175**, 767-777.

Brambillasca, S., Yabal, M., Soffientini, P., Stefanovic, S., Makarow, M., Hegde, R. S., & Borgese, N. (2005). Transmembrane topogenesis of a tail-anchored protein is modulated by membrane lipid composition. *Embo Journal* **24**, 2533-2542.

Bregante, M., Yang, Y., Formentin, E., Carpaneto, A., Schroeder, J. I., Gambale, F., Lo Schiavo, F., & Costa, A. (2008). KDC1, a carrot Shaker-like potassium channel, reveals its role as a silent regulatory subunit when expressed in plant cells. *Plant Molecular Biology* **66**, 61-72.

Browne, C. L. & Werner, W. (1984). Intercellular-Junctions Between the Follicle Cells and Oocytes of Xenopus-Laevis. *Journal of Experimental Zoology* **230**, 105-113.

Brunger, A. T. (2005). Structure and function of SNARE and SNARE-interacting proteins. *Quarterly Reviews of Biophysics* **38**, 1-47.

Bubeck, J., Scheuring, D., Hummel, E., Langhans, M., Viotti, C., Foresti, O., Denecke, J., Banfield, D. K., & Robinson, D. G. (2008). The syntaxins SYP31 and SYP81 control ER-Golgi trafficking in the plant secretory pathway. *Traffic* **9**, 1629-1652.

Buch-Pedersen, M. J., Rudashevskaya, E. L., Berner, T. S., Venema, K., & Palmgren, M. G. (2006). Potassium as an intrinsic uncoupler of the plasma membrane H+-ATPase. *Journal of Biological Chemistry* **281**, 38285-38292.

Cacace, M. G., Landau, E. M., & Ramsden, J. J. (1997). The Hofmeister series: salt and solvent effects on interfacial phenomena. *Quarterly Reviews of Biophysics* **30**, 241-277.

Campanoni, P., Sutter, J. U., Davis, C. S., Littlejohn, G. R., & Blatt, M. R. (2007). A generalized method for transfecting root epidermis uncovers endosomal dynamics in Arabidopsis root hairs. *Plant Journal* **51**, 322-330.

Catterall, W. A. (1999). Interactions of presynaptic Ca2+ channels and snare proteins in neurotransmitter release. *Molecular and Functional Diversity of Ion Channels and Receptors* **868**, 144-159.

Catterall, W. A. & Yarov-Yarovoy, V. (2010). Helical motion of an S4 voltage sensor revealed by gating pore currents. *Channels* **4**.

Cellier, F., Conejero, G., Ricaud, L., Luu, D. T., Lepetit, M., Gosti, F., & Casse, F. (2004). Characterization of AtCHX17, a member of the cation/H(+) exchangers, CHX family, from Arabidopsis thaliana suggests a role in K(+) homeostasis. *Plant Journal* **39**, 834-846.

Chabre, M. & le Maire, M. (2005). Monomeric G-protein-coupled receptor as a functional unit. *Biochemistry* **44**, 9395-9403.

Chatre, L., Brandizzi, F., Hocquellet, A., Hawes, C., & Moreau, P. (2005). Sec22 and Memb11 are v-SNAREs of the anterograde endoplasmic reticulum-Golgi pathway in tobacco leaf epidermal cells. *Plant Physiology* **139**, 1244-1254.

Chatre, L., Wattelet-Boyer, V., Melser, S., Brandizzi, F., & Moreau, P. (2008). Golgi targeting of SYP31: Requirement of a di-acidic motif. *Comparative Biochemistry and Physiology A-Molecular & Integrative Physiology* **150**, S201.

Chattopadhyay, A., Jafurulla, M., Kalipatnapu, S., Pucadyil, T. J., & Harikumar, K. G. (2005). Role of cholesterol in ligand binding and G-protein coupling of serotonin(1A) receptors solubilized from bovine hippocampus. *Biochemical and Biophysical Research Communications* **327**, 1036-1041.

Cheong, Y. H., Pandey, G. K., Grant, J. J., Batistic, O., Li, L., Kim, B. G., Lee, S. C., Kudla, J., & Luan, S. (2007). Two calcineurin B-like calcium sensors, interacting with protein kinase CIPK23, regulate leaf transpiration and root potassium uptake in Arabidopsis. *Plant Journal* **52**, 223-239.

Cherel, I. (2004). Regulation of K+ channel activities in plants: from physiological to molecular aspects. *Journal of Experimental Botany* **55**, 337-351.

Chilton, M. D. M. & Que, Q. D. (2003). Targeted integration of T-DNA into the tobacco genome at double-stranded breaks: New insights on the mechanism of T-DNA integration. *Plant Physiology* **133**, 956-965.

Chin, K., Moeder, W., & Yoshioka, K. (2009). Biological roles of cyclic-nucleotide-gated ion channels in plants: What we know and don't know about this 20 member ion channel family. *Botany-Botanique* **87**, 668-677.

Citovsky, V., Kozlovsky, S. V., Lacroix, B., Zaltsman, A., Dafny-Yelin, M., Vyas, S., Tovkach, A., & Tzfira, T. (2007). Biological systems of the host cell involved in Agrobacterium infection. *Cellular Microbiology* **9**, 9-20.

Citovsky, V., Lee, L. Y., Vyas, S., Glick, E., Chen, M. H., Vainstein, A., Gafni, Y., Gelvin, S. B., & Tzfira, T. (2006). Subcellular localization of interacting proteins by bimolecular fluorescence complementation in planta. *Journal of Molecular Biology* **362**, 1120-1131.

Citovsky, V., Zupan, J., Warnick, D., & Zambryski, P. (1992). Nuclear-Localization of Agrobacterium Vire2 Protein in Plant-Cells. *Science* **256**, 1802-1805.

Clary, D. O., Griff, I. C., & Rothman, J. E. (1990). Snaps, A Family of Nsf Attachment Proteins Involved in Intracellular Membrane-Fusion in Animals and Yeast. *Cell* **61**, 709-721.

Collier, R., Fuchs, B., Walter, N., Kevin Lutke, W., & Taylor, C. G. (2005). Ex vitro composite plants: an inexpensive, rapid method for root biology. *Plant Journal* **43**, 449-457.

Collins, M. O. & Choudhary, J. S. (2008). Mapping multiprotein complexes by affinity purification and mass spectrometry. *Current Opinion in Biotechnology* **19**, 324-330.

Collins, N. C., Thordal-Christensen, H., Lipka, V., Bau, S., Kombrink, E., Qiu, J. L., Huckelhoven, R., Stein, M., Freialdenhoven, A., Somerville, S. C., & Schulze-Lefert, P. (2003). SNARE-protein-mediated disease resistance at the plant cell wall. *Nature* **425**, 973-977.

Cross, B. C. S., Sinning, I., Luirink, J., & High, S. (2009). Delivering proteins for export from the cytosol. *Nature Reviews Molecular Cell Biology* **10**, 255-264.

Dafny-Yelin, M. & Tzfira, T. (2007). Delivery of multiple transgenes to plant cells. *Plant Physiology* **145**, 1118-1128.

Dancourt, J. & Barlowe, C. (2010). Protein Sorting Receptors in the Early Secretory Pathway. *Annual Review of Biochemistry* **79**, 777-802.

Daram, P., Urbach, S., Gaymard, F., Sentenac, H., & Cherel, I. (1997). Tetramerization of the AKT1 plant potassium channel involves its C-terminal cytoplasmic domain. *EMBO J.* **16**, 3455-3463.

de Ruijter, N. C. A., Verhees, J., van Leeuwen, W., & van der Krol, A. R. (2003). Evaluation and comparison of the GUS, LUC and GFP reporter system for gene expression studies in plants. *Plant Biology* **5**, 103-115.

de Virgilio, M., Kiosses, W. B., & Shattil, S. J. (2004). Proximal, selective, and dynamic interactions between integrin alphaIIbbeta3 and protein tyrosine kinases in living cells. *J.Cell Biol* **165**, 305-311.

Deal, K. K., Lovinger, D. M., & Tamkun, M. M. (1994). The Brain Kv1.1 Potassium Channel - In-Vitro and In-Vivo Studies on Subunit Assembly and Posttranslational Processing. *Journal of Neuroscience* **14**, 1666-1676.

Deeken, R., Sanders, C., Ache, P., & Hedrich, R. (2000). Developmental and light-dependent regulation of a phloem-localised K+ channel of Arabidopsis thaliana. *Plant Journal* **23**, 285-290.

Dekathen, A. & Jacobsen, H. J. (1995). Cell Competence for Agrobacterium-Mediated Dna Transfer in Pisum-Sativum l. *Transgenic Research* **4**, 184-191.

deKruijff, B. (1997). Biomembranes - Lipids beyond the bilayer. *Nature* **386**, 129-130.

Demidchik, V., Shabala, S. N., & Davies, J. M. (2007). Spatial variation in H2O2 response of Arabidopsis thaliana root epidermal Ca2+ flux and plasma membrane Ca2+ channels. *Plant Journal* **49**, 377-386.

DeNeve, M., DeBuck, S., Jacobs, A., VanMontagu, M., & Depicker, A. (1997). T-DNA integration patterns in co-transformed plant cells suggest that T-DNA repeats originate from co-integration of separate T-DNAs. *Plant Journal* **11**, 15-29.

Desbrosses, G., Josefsson, C., Rigas, S., Hatzopoulos, P., & Dolan, L. (2003). AKT1 and TRH1 are required during root hair elongation in Arabidopsis. *J.Exp.Bot.* **54**, 781-788.

Dewitt, N. D., Hong, B. M., Sussman, M. R., & Harper, J. F. (1996). Targeting of two Arabidopsis H+-ATPase isoforms to the plasma membrane. *Plant Physiology* **112**, 833-844.

Dewitt, N. D. & Sussman, M. R. (1995). Immunocytological localization of an epitope-tagged plasma membrane proton pump (H+-ATPase) in phloem companion cells. *Plant Cell* **7**, 2053-2067.

Dhanoa, P. K., Richardson, L. G. L., Smith, M. D., Gidda, S. K., Henderson, M. P. A., Andrews, D. W., & Mullen, R. T. (2010). Distinct Pathways Mediate the Sorting of Tail-Anchored Proteins to the Plastid Outer Envelope. *Plos One* **5**.

Dhonukshe, P., Baluska, F., Schlicht, M., Hlavacka, A., Samaj, J., Friml, J., & Gadella, T. W. J. (2006). Endocytosis of cell surface material mediates cell plate formation during plant cytokinesis. *Developmental Cell* **10**, 137-150.

Di Sansebastiano, G. P., Gigante, M., De Domenico, S., Piro, G., & Dalessandro, G. (2006). Sorting of GFP Tagged NtSyr1, an ABA Related Syntaxin. *Plant Signal Behav.* **1**, 77-85.

Dolder, M., Engel, A., & Zulauf, M. (1996). The micelle to vesicle transition of lipids and detergents in the presence of a membrane protein: towards a rationale for 2D crystallization. *Febs Letters* **382**, 203-208.

Dowhan, W. & Bogdanov, M. (2009). Lipid-Dependent Membrane Protein Topogenesis. *Annual Review of Biochemistry* **78**, 515-540.

Dreyer, I., Antunes, S., Hoshi, T., Muller-Rober, B., Palme, K., Pongs, O., Reintanz, B., & Hedrich, R. (1997). Plant K+ channel alpha-subunits assemble indiscriminately. *Biophys.J.* **72**, 2143-2150.

Dreyer, I. & Blatt, M. R. (2009). What makes a gate? The ins and outs of Kv-like K+ channels in plants. *Trends in Plant Science* **14**, 383-390.

Dreyer, I., Poree, F., Schneider, A., Mittelstadt, J., Bertl, A., Sentenac, H., Thibaud, J. B., & Mueller-Roeber, B. (2004). Assembly of plant Shaker-like K(out) channels requires two distinct sites of the channel alpha-subunit. *Biophys.J* **87**, 858-872.

Duby, G., Hosy, E., Fizames, C., Alcon, C., Costa, A., Sentenac, H., & Thibaud, J. B. (2008). AtKC1, a conditionally targeted Shaker-type subunit, regulates the activity of plant K+ channels. *Plant Journal* **53**, 115-123.

Dulubova, I., Khvotchev, M., Liu, S. Q., Huryeva, I., Sudhof, T. C., & Rizo, J. (2007). Munc18-1 binds directly to the neuronal SNARE complex. *Proceedings of the National Academy of Sciences of the United States of America* **104**, 2697-2702.

Dulubova, I., Yamaguchi, T., Gao, Y., Min, S. W., Huryeva, I., Sudhof, T. C., & Rizo, J. (2002). How Tlg2p/syntaxin 16 'snares' Vps45. *Embo Journal* **21**, 3620-3631.

Dulubova, I., Sugita, S., Hill, S., Hosaka, M., Fernandez, I., Sudhof, T. C., & Rizo, J. (1999). A conformational switch in syntaxin during exocytosis: role of munc18. *EMBO J* **18**, 4372-4382.

Egelandsdal, B., Fretheim, K., & Harbitz, O. (1991). The Denaturing Action of Lysophosphatidylcholine As Studied by Calorimetric and Rheological Techniques. *Chemistry and Physics of Lipids* **57**, 81-86.

Ehrhardt, T., Zimmermann, S., & MullerRober, B. (1997). Association of plant K-in(+) channels is mediated by conserved C-termini and does not affect subunit assembly. *Febs Letters* **409**, 166-170.

Elias, M., Drdova, E., Ziak, D., Bavlnka, B., Hala, M., Cvrckova, F., Soukupova, H., & Zarsky, V. (2003). The exocyst complex in plants. *Cell Biology International* **27**, 199-201.

Enami, K., Ichikawa, M., Uemura, T., Kutsuna, N., Hasezawa, S., Nakagawa, T., Nakano, A., & Sato, M. H. (2009). Differential Expression Control and Polarized Distribution of Plasma Membrane-Resident SYP1 SNAREs in Arabidopsis thaliana. *Plant and Cell Physiology* **50**, 280-289.

Engel, C. K., Chen, L., & Prive, G. G. (2002). Stability of the lactose permease in detergent solutions. *Biochimica et Biophysica Acta-Biomembranes* **1564**, 47-56.

Epstein, E., Elzam, O. E., & Rains, D. W. (1963). Resolution of Dual Mechanisms of Potassium Absorption by Barley Roots. *Proceedings of the National Academy of Sciences of the United States of America* **49**, 684-&.

Estojak, J., Brent, R., & Golemis, E. A. (1995). Correlation of 2-Hybrid Affinity Data with In-Vitro Measurements. *Molecular and Cellular Biology* **15**, 5820-5829.

Fang, D. Y. & Kerppola, T. K. (2004). Ubiquitin-mediated fluorescence complementation reveals that Jun ubiquitinated by Itch/AIP4 is localized to lysosomes. *Proceedings of the National Academy of Sciences of the United States of America* **101**, 14782-14787.

Faso, C., Boulaflous, A., & Brandizzi, F. (2009). The plant Golgi apparatus: Last 10 years of answered and open questions. *Febs Letters* **583**, 3752-3757.

Fasshauer, D., Antonin, W., Margittai, M., Pabst, S., & Jahn, R. (1999). Mixed and non-cognate SNARE complexes - Characterization of assembly and biophysical properties. *Journal of Biological Chemistry* **274**, 15440-15446.

Fasshauer, D., Sutton, R. B., Brunger, A. T., & Jahn, R. (1998). Conserved structural features of the synaptic fusion complex: SNARE proteins reclassified as Q- and R-SNAREs. *Proceedings of the National Academy of Sciences of the United States of America* **95**, 15781-15786.

Fernandez, I., Ubach, J., Dulubova, I., Zhang, X. Y., Sudhof, T. C., & Rizo, J. (1998). Three-dimensional structure of an evolutionarily conserved N-terminal domain of syntaxin 1A. *Cell* **94**, 841-849.

Fili, O., Michaelevski, I., Bledi, Y., Chikvashvili, D., Singer-Lahat, D., Boshwitz, H., Linial, M., & Lotan, I. (2001). Direct interaction of a brain voltage-gated K+ channel with syntaxin 1A: Functional impact on channel gating. *Journal of Neuroscience* **21**, 1964-1974.

Finley, D. (2009). Recognition and Processing of Ubiquitin-Protein Conjugates by the Proteasome. *Annual Review of Biochemistry* **78**, 477-513.

Foresti, O., daSilva, L. L. P., & Denecke, J. (2006). Overexpression of the Arabidopsis syntaxin PEP12/SYP21 inhibits transport from the prevacuolar compartment to the lytic vacuole in vivo. *Plant Cell* **18**, 2275-2293.

Fujiki, Y., Hubbard, A. L., Fowler, S., & Lazarow, P. B. (1982). Isolation of Intracellular Membranes by Means of Sodium-Carbonate Treatment - Application to Endoplasmic-Reticulum. *Journal of Cell Biology* **93**, 97-102.

Furgason, M. L. M., MacDonald, C., Shanks, S. G., Ryder, S. P., Bryant, N. J., & Munson, M. (2009). The N-terminal peptide of the syntaxin Tlg2p modulates binding of its closed conformation to Vps45p. *Proceedings of the National Academy of Sciences of the United States of America* **106**, 14303-14308.

Galway, M. E., Masucci, J. D., Lloyd, A. M., Walbot, V., Davis, R. W., & Schiefelbein, J. W. (1994). The Ttg Gene Is Required to Specify Epidermal-Cell Fate and Cell Patterning in the Arabidopsis Root. *Developmental Biology* **166**, 740-754.

Gaymard, F., Cerutti, M., Horeau, C., Lemaillet, G., Urbach, S., Ravallec, M., Devauchelle, G., Sentenac, H., & Thibaud, J. B. (1996). The baculovirus/insect cell system as an alternative to Xenopus oocytes. First characterization of the AKT1 K+ channel from Arabidopsis thaliana. *J.Biol.Chem.* **271**, 22863-22870.

Gaymard, F., Pilot, G., Lacombe, B., Bouchez, D., Bruneau, D., Boucherez, J., Michaux-Ferriere, N., Thibaud, J. B., & Sentenac, H. (1998). Identification and disruption of a plant shaker-like outward channel involved in K+ release into the xylem sap. *Cell* **94**, 647-655.

Geiger, D., Becker, D., Vosloh, D., Gambale, F., Palme, K., Rehers, M., Anschuetz, U., Dreyer, I., Kudla, J., & Hedrich, R. (2009). Heteromeric AtKC1.AKT1 Channels in Arabidopsis Roots Facilitate Growth under K+-limiting Conditions. *Journal of Biological Chemistry* **284**, 21288-21295.

Geldner, N., Anders, N., Wolters, H., Keicher, J., Kornberger, W., Muller, P., Delbarre, A., Ueda, T., Nakano, A., & Jurgens, G. (2003). The Arabidopsis GNOM ARF-GEF mediates endosomal recycling, auxin transport, and auxin-dependent plant growth. *Cell* **112**, 219-230.

Gelvin, S. B. (1990). Crown Gall Disease and Hairy Root Disease - A Sledgehammer and A Tackhammer. *Plant Physiology* **92**, 281-285.

Gelvin, S. B. (2009). Agrobacterium in the Genomics Age. *Plant Physiology* **150**, 1665-1676.

Gierth, M. & Maser, P. (2007). Potassium transporters in plants - Involvement in K+ acquisition, redistribution and homeostasis. *Febs Letters* **581**, 2348-2356.

Gierth, M., Maser, P., & Schroeder, J. I. (2005). The potassium transporter AtHAK5 functions in K+ deprivation-induced high-affinity K+ uptake and AKT1 K+ channel contribution to K+ uptake kinetics in Arabidopsis roots. *Plant Physiology* **137**, 1105-1114.

Giese, B., Roderburg, C., Sommerauer, M., Wortmann, S. B., Metz, S., Heinrich, P. C., & Muller-Newen, G. (2005). Dimerization of the cytokine receptors gp130 and LIFR analysed in single cells. *J.Cell Sci.* **118**, 5129-5140.

Glick, E., Zrachya, A., Levy, Y., Mett, A., Gidoni, D., Belausov, E., Citovsky, V., & Gafni, Y. (2008). Interaction with host SGS3 is required for suppression of RNA silencing by tomato yellow leaf curl virus V2 protein. *Proceedings of the National Academy of Sciences of the United States of America* **105**, 157-161.

Gobert, A., Isayenkov, S., Voelker, C., Czempinski, K., & Maathuis, F. J. M. (2007). The two-pore channel TPK1 gene encodes the vacuolar K+ conductance and plays a role in K+ homeostasis. *Proceedings of the National Academy of Sciences of the United States of America* **104**, 10726-10731.

Gobert, A., Park, G., Amtmann, A., Sanders, D., & Maathuis, F. J. M. (2006). Arabidopsis thaliana Cyclic Nucleotide Gated Channel 3 forms a non-selective ion transporter involved in germination and cation transport. *Journal of Experimental Botany* **57**, 791-800.

Goder, V. & Spiess, M. (2001). Topogenesis of membrane proteins: determinants and dynamics. *Febs Letters* **504**, 87-93.

Goldberg, A. L. & Dice, J. F. (1974). Intracellular Protein Degradation in Mammalian and Bacterial-Cells. *Annual Review of Biochemistry* **43**, 835-869.

Graciet, E. & Wellmer, F. (2010). The plant N-end rule pathway: structure and functions. *Trends in Plant Science* **15**, 447-453.

Green, W. N. & Millar, N. S. (1995). Ion-Channel Assembly. *Trends in Neurosciences* **18**, 280-287.

Grefen, C., Chen, Z. H., Honsbein, A., Donald, N., Hills, A., & Blatt, M. R. (2010). A Novel Motif Essential for SNARE Interaction with the K+ Channel KC1 and Channel Gating in Arabidopsis. *Plant Cell* **22**, 3076-3092.

Grefen, C., Lalonde, S., & Obrdlik, P. (2007). Split-ubiquitin system for identifying protein-protein interactions in membrane and full-length proteins. *Curr Protoc Neurosci.* **Chapter 5**, Unit.

Grefen, C., Obrdlik, P., & Harter, K. (2009). The determination of protein-protein interactions by the mating-based split-ubiquitin system (mbSUS). *Methods Mol Biol* **479**, 217-233.

Gu, C., Jan, Y. N., & Jan, L. Y. (2003). A conserved domain in axonal targeting of Kv1 (shaker) voltage-gated potassium channels. *Science* **301**, 646-649.

Hala, M., Cole, R., Synek, L., Drdova, E., Pecenkova, T., Nordheim, A., Lamkemeyer, T., Madlung, J., Hochholdinger, F., Fowler, J. E., & Zarsky, V. (2008). An exocyst complex functions in plant cell growth in Arabidopsis and tobacco. *Plant Cell* **20**, 1330-1345.

Hamilton, D. W. A., Hills, A., Kohler, B., & Blatt, M. R. (2000). Ca2+ channels at the plasma membrane of stomatal guard cells are activated by hyperpolarization and abscisic acid. *Proceedings of the National Academy of Sciences of the United States of America* **97**, 4967-4972.

Han, X., Wang, C. T., Bai, J., Chapman, E. R., & Jackson, M. B. (2004). Transmembrane Segments of Syntaxin Line the Fusion Pore of Ca2+-Triggered Exocytosis. *Science* **304**, 289-292.

Hanton, S. L., Renna, L., Bortolotti, L. E., Chatre, L., Stefano, G., & Brandizzi, F. (2005). Diacidic Motifs Influence the Export of Transmembrane Proteins from the Endoplasmic Reticulum in Plant Cells. *Plant Cell* **17**, 3081-3093.

Hartje, S., Zimmermann, S., Klonus, D., & Mueller-Roeber, B. (2000). Functional characterisation of LKT1, a K+ uptake channel from tomato root hairs, and comparison with the closely related potato inwardly rectifying K+ channel SKT1 after expression in Xenopus oocytes. *Planta* **210**, 723-731.

Hatefi, Y. & Hanstein, W. G. (1969). Solubilization of Particulate Proteins and Nonelectrolytes by Chaotropic Agents. *Proceedings of the National Academy of Sciences of the United States of America* **62**, 1129-&.

Hawkins, C. A., Alba, E. d., & Tjandra, N. (2005). Solution Structure of Human Saposin C in a Detergent Environment. *Journal of Molecular Biology* **346**, 1381-1392.

He, B. & Guo, W. (2009). The exocyst complex in polarized exocytosis. *Current Opinion in Cell Biology* **21**, 537-542.

Hebert, D. N., Bernasconi, R., & Molinari, M. (2010). ERAD substrates: Which way out? *Seminars in Cell & Developmental Biology* **21**, 526-532.

Heese, A., Ludwig, A. A., & Jones, J. D. G. (2005). Rapid phosphorylation of a syntaxin during the Avr9/Cf-9-race-specific signaling pathway. *Plant Physiology* **138**, 2406-2416.

Heese, M., Gansel, X., Sticher, L., Wick, P., Grebe, M., Granier, F., & Jurgens, G. (2001). Functional characterization of the KNOLLE-interacting t-SNARE AtSNAP33 and its role in plant cytokinesis. *Journal of Cell Biology* **155**, 239-249.

Hermans, C., Hammond, J. P., White, P. J., & Verbruggen, N. (2006). How do plants respond to nutrient shortage by biomass allocation? *Trends in Plant Science* **11**, 610-617.

High, S. & Dobberstein, B. (1992). Mechanisms that determine the transmembrane disposition of proteins. *Curr Opin.Cell Biol* **4**, 581-586.

Hirsch, R. E., Lewis, B. D., Spalding, E. P., & Sussman, M. R. (1998). A role for the AKT1 potassium channel in plant nutrition. *Science* **280**, 918-921.

Ho, C. H., Lin, S. H., Hu, H. C., & Tsay, Y. F. (2009). CHL1 Functions as a Nitrate Sensor in Plants. *Cell* **138**, 1184-1194.

Holtorf, S., Apel, K., & Bohlmann, H. (1995). Comparison of different constitutive and inducible promoters for the overexpression of transgenes in Arabidopsis thaliana. *Plant Molecular Biology* **29**, 637-646.

Homann, U., Meckel, T., Hewing, J., Hutt, M. T., & Hurst, A. C. (2007). Distinct fluorescent pattern of KAT1 :: GFP in the plasma membrane of Vicia faba guard cells. *European Journal of Cell Biology* **86**, 489-500.

Honsbein, A., Sokolovski, S., Grefen, C., Campanoni, P., Pratelli, R., Paneque, M., Chen, Z. H., Johansson, I., & Blatt, M. R. (2009). A Tripartite SNARE-K+ Channel Complex Mediates in Channel-Dependent K+ Nutrition in Arabidopsis. *Plant Cell* **21**, 2859-2877.

Hoshi, T. (1995). Regulation of Voltage-Dependence of the Kat1 Channel by Intracellular Factors. *Journal of General Physiology* **105**, 309-328.

Hosy, E., Duby, G., Very, A. A., Costa, A., Sentenac, H., & Thibaud, J. B. (2005). A procedure for localisation and electrophysiological characterisation of ion channels heterologously expressed in a plant context. *Plant Methods* **1**, 14.

Hosy, E., Vavasseur, A., Mouline, K., Dreyer, I., Gaymard, F., Poree, F., Boucherez, J., Lebaudy, A., Bouchez, D., Very, A. A., Simonneau, T., Thibaud, J. B., & Sentenac, H. (2003). The Arabidopsis outward K+ channel GORK is involved in regulation of stomatal movements and plant transpiration. *Proceedings of the National Academy of Sciences of the United States of America* **100**, 5549-5554.

Hu, C., Ahmed, M., Melia, T. J., Sollner, T. H., Mayer, T., & Rothman, J. E. (2003). Fusion of cells by flipped SNAREs. *Science* **300**, 1745-1749.

Hu, C. D., Chinenov, Y., & Kerppola, T. K. (2002). Visualization of interactions among bZip and Rel family proteins in living cells using bimolecular fluorescence complementation. *Molecular Cell* **9**, 789-798.

Hu, C. D. & Kerppola, T. K. (2003). Simultaneous visualization of multiple protein interactions in living cells using multicolor fluorescence complementation analysis. *Nature Biotechnology* **21**, 539-545.

Huang, K. S., Bayley, H., Liao, M. J., London, E., & Khorana, H. G. (1981). Refolding of An Integral Membrane-Protein - Denaturation, Renaturation, and Reconstitution of Intact Bacteriorhodopsin and 2 Proteolytic Fragments. *Journal of Biological Chemistry* **256**, 3802-3809.

Hurst, A. C., Meckel, T., Tayefeh, S., Thiel, G., & Homann, U. (2004). Trafficking of the plant potassium inward rectifier KAT1 in guard cell protoplasts of Vicia faba. *Plant Journal* **37**, 391-397.

Hwang, I. & Robinson, D. G. (2009). Transport vesicle formation in plant cells. *Current Opinion in Plant Biology* **12**, 660-669.

Hwang, J. U., Suh, S., Yi, H. J., Kim, J., & Lee, Y. (1997). Actin filaments modulate both stomatal opening and inward K+-channel activities in guard cells of Vicia faba L. *Plant Physiology* **115**, 335-342.

Iida, A., Yamashita, T., Yamada, Y., & Morikawa, H. (1991). Efficiency of Particle-Bombardment-Mediated Transformation Is Influenced by Cell-Cycle Stage in Synchronized Cultured-Cells of Tobacco. *Plant Physiology* **97**, 1585-1587.

Jabs, T., Tschope, M., Colling, C., Hahlbrock, K., & Scheel, D. (1997). Elicitor-stimulated ion fluxes and O-2(-) from the oxidative burst are essential components in triggering defense gene activation and phytoalexin synthesis in parsley. *Proceedings of the National Academy of Sciences of the United States of America* **94**, 4800-4805.

Jach, G., Pesch, M., Richter, K., Frings, S., & Uhrig, J. F. (2006). An improved mRFP1 adds red to bimolecular fluorescence complementation. *Nature Methods* **3**, 597-600.

Jacob, S. S. & Veluthambi, K. (2002). Generation of selection marker-free transgenic plants by cotransformation of a cointegrate vector T-DNA and a binary vector T-DNA in one Agrobacterium tumefaciens strain. *Plant Science* **163**, 801-806.

Jahn, R. & Scheller, R. H. (2006). SNAREs - engines for membrane fusion. *Nature Reviews Molecular Cell Biology* **7**, 631-643.

Jameson, B. A. & Wolf, H. (1988). The Antigenic Index - A Novel Algorithm for Predicting Antigenic Determinants. *Computer Applications in the Biosciences* **4**, 181-186.

Jarvis, P., Chen, L. J., Li, H. M., Pete, C. A., Fankhauser, C., & Chory, J. (1998). An Arabidopsis mutant defective in the plastid general protein import apparatus. *Science* **282**, 100-103.

Jeanguenin, L., Lebaudy, A., Xicluna, J., Alcon, C., Hosy, E., Duby, G., Michard, E., Lacombe, B., Dreyer, I., & Thibaud, J. B. (2008). Heteromerization of Arabidopsis Kv channel alpha-subunits: Data and prospects. *Plant Signal Behav* **3**, 622-625.

Jefferson, R. A., Kavanagh, T. A., & Bevan, M. W. (1987). Gus Fusions - Beta-Glucuronidase As A Sensitive and Versatile Gene Fusion Marker in Higher-Plants. *Embo Journal* **6**, 3901-3907.

Johansson, L. C., Wohri, A. B., Katona, G., Engstrom, S., & Neutze, R. (2009). Membrane protein crystallization from lipidic phases. *Current Opinion in Structural Biology* **19**, 372-378.

Johnsson, N. & Varshavsky, A. (1994a). Split Ubiquitin As A Sensor of Protein Interactions In-Vivo. *Proceedings of the National Academy of Sciences of the United States of America* **91**, 10340-10344.

Johnsson, N. & Varshavsky, A. (1994b). Split Ubiquitin As A Sensor of Protein Interactions In-Vivo. *Proceedings of the National Academy of Sciences of the United States of America* **91**, 10340-10344.

Johnsson, N. & Varshavsky, A. (1994c). Ubiquitin-Assisted Dissection of Protein-Transport Across Membranes. *Embo Journal* **13**, 2686-2698.

Jones, H. D., Doherty, A., & Sparks, C. A. (2009). Transient Transformation of Plants. In *Plant Genomics*, eds. Gustafson, J. P., Langridge, P., & Somers, D. J., pp. 131-152. Humana Press.

Jones, M. N. (1992). Surfactant Interactions with Biomembranes and Proteins. *Chemical Society Reviews* **21**, 127-136.

Jones, O. T., Eubanks, J. H., Earnest, J. P., & Mcnamee, M. G. (1988). A Minimum Number of Lipids Are Required to Support the Functional-Properties of the Nicotinic Acetylcholine-Receptor. *Biochemistry* **27**, 3733-3742.

Jordan, B. A. & Devi, L. A. (1999). G-protein-coupled receptor heterodimerization modulates receptor function. *Nature* **399**, 697-700.

Jung, J. Y., Shin, R., & Schachtman, D. P. (2009). Ethylene Mediates Response and Tolerance to Potassium Deprivation in Arabidopsis. *Plant Cell* **21**, 607-621.

Jurgens, G. (2005). Cytokinesis in higher plants. *Annual Review of Plant Biology* **56**, 281-299.

Kalbfleisch, T., Cambon, A., & Wattenberg, B. W. (2007). A bioinformatics approach to identifying tail-anchored proteins in the human genome. *Traffic* **8**, 1687-1694.

Kalipatnapu, S. & Chattopadhyay, A. (2005). Membrane protein solubilization: Recent advances and challenges in solubilization of serotonin(1A) receptors. *Iubmb Life* **57**, 505-512.

Kaplan, B., Sherman, T., & Fromm, H. (2007). Cyclic nucleotide-gated channels in plants. *Febs Letters* **581**, 2237-2246.

Kargul, J., Gansel, X., Tyrrell, M., Sticher, L., & Blatt, M. R. (2001). Protein-binding partners of the tobacco syntaxin NtSyr1. *Febs Letters* **508**, 253-258.

Karley, A. J. & White, P. J. (2009). Moving cationic minerals to edible tissues: potassium, magnesium, calcium. *Current Opinion in Plant Biology* **12**, 291-298.

Kato, N., Fujikawa, Y., Fuselier, T., Adamou-Dodo, R., Nishitani, A., & Sato, M. H. (2010). Luminescence detection of SNARE-SNARE interaction in Arabidopsis protoplasts. *Plant Molecular Biology* **72**, 433-444.

Kemper, C., Habib, S. J., Engl, G., Heckmeyer, P., Dimmer, K. S., & Rapaport, D. (2008). Integration of tail-anchored proteins into the mitochondrial outer membrane does not require any known import components. *Journal of Cell Science* **121**, 1990-1998.

Kerkhoff, C., Trumbach, B., Gehring, L., Habben, K., Schmitz, G., & Kaever, V. (2000). Solubilization, partial purification and photolabeling of the integral membrane protein

lysophospholipid : acyl-CoA acyltransferase (LAT). *European Journal of Biochemistry* **267**, 6339-6345.

Kerppola, T. K. (2006a). Design and implementation of bimolecular fluorescence complementation (BiFC) assays for the visualization of protein interactions in living cells. *Nature Protocols* **1**, 1278-1286.

Kerppola, T. K. (2006b). Visualization of molecular interactions by fluorescence complementation. *Nature Reviews Molecular Cell Biology* **7**, 449-456.

Kerppola, T. K. (2008). Bimolecular fluorescence complementatlon: Visualization of molecular interactions in living cells. *Fluorescent Proteins* **85**, 431-470.

Kerppola, T. K. (2009). Visualization of molecular interactions using bimolecular fluorescence complementation analysis: Characteristics of protein fragment complementation. *Chemical Society Reviews* **38**, 2876-2886.

Kerschensteiner, D., Soto, F., & Stocker, M. (2005). Fluorescence measurements reveal stoichiometry of K+ channels formed by modulatory and delayed rectifier alpha-subunits. *Proceedings of the National Academy of Sciences of the United States of America* **102**, 6160-6165.

Kida, Y., Mihara, K., & Sakaguchi, M. (2005). Translocation of a long amino-terminal domain through ER membrane by following signal-anchor sequence. *Embo Journal* **24**, 3202-3213.

Kida, Y., Morimoto, F., Mihara, K., & Sakaguchi, M. (2006). Function of positive charges following signal-anchor sequences during translocation of the N-terminal domain. *Journal of Biological Chemistry* **281**, 1152-1158.

Kida, Y., Morimoto, F., & Sakaguchi, M. (2009). Signal Anchor Sequence Provides Motive Force for Polypeptide Chain Translocation through the Endoplasmic Reticulum Membrane. *Journal of Biological Chemistry* **284**, 2861-2866.

Kida, Y., Sakaguchi, M., Fukuda, M., Mikoshiba, K., & Mihara, K. (2000). Membrane topogenesis of a type I signal-anchor protein, mouse synaptotagmin II, on the endoplasmic reticulum. *Journal of Cell Biology* **150**, 719-729.

Kidd, I. M. & Emery, V. C. (1993). The Use of Baculoviruses As Expression Vectors. *Applied Biochemistry and Biotechnology* **42**, 137-159.

Kim, M. J., Ciani, S., & Schachtman, D. P. (2010). A Peroxidase Contributes to ROS Production during Arabidopsis Root Response to Potassium Deficiency. *Molecular Plant* **3**, 420-427.

Kisselev, A. F., Akopian, T. N., Woo, K. M., & Goldberg, A. L. (1999). The sizes of peptides generated from protein by mammalian 26 and 20 S proteasomes - Implications for understanding the degradative mechanism and antigen presentation. *Journal of Biological Chemistry* **274**, 3363-3371.

Klaiber, K., Williams, N., Roberts, T. M., Papazian, D. M., Jan, L. Y., & Miller, C. (1990). Functional Expression of Shaker-K+ Channels in A Baculovirus-Infected Insect Cell-Line. *Neuron* **5**, 221-226.

Kloepper, T. H., Kienle, C. N., & Fasshauer, D. (2007). An elaborate classification of SNARE proteins sheds light on the conservation of the eukaryotic endomembrane system. *Molecular Biology of the Cell* **18**, 3463-3471.

Knecht, E., Aguado, C., Carcel, J., Esteban, I., Esteve, J. M., Ghislat, G., Moruno, J. F., Vidal, J. M., & Saez, R. (2009). Intracellular protein degradation in mammalian cells: recent developments. *Cellular and Molecular Life Sciences* **66**, 2427-2443.

Kohno, M., Fukushima, N., Yoshida, A., & Ueda, H. (2000). G(il) and G(oA) differentially determine kinetic efficacies of agonists for kappa-opioid receptor. *Febs Letters* **473**, 101-105.

Koornneef, M., Alonso-Blanco, C., & Vreugdenhil, D. (2004). Naturally occurring genetic variation in Arabidopsis thaliana. *Annual Review of Plant Biology* **55**, 141-172.

Kost, T. A., Condreay, J. P., & Jarvis, D. L. (2005). Baculovirus as versatile vectors for protein expression in insect and mammalian cells. *Nature Biotechnology* **23**, 567-575.

Kovermann, P., Meyer, S., Hortensteiner, S., Picco, C., Scholz-Starke, J., Ravera, S., Lee, Y., & Martinoia, E. (2007). The Arabidopsis vacuolar malate channel is a member of the ALMT family. *Plant Journal* **52**, 1169-1180.

Kragh-Hansen, U., le Maire, M., & Moller, J. V. (1998). The mechanism of detergent solubilization of liposomes and protein-containing membranes. *Biophysical Journal* **75**, 2932-2946.

Kriechbaumer, V., Shaw, R., Mukherjee, J., Bowsher, C. G., Harrison, A. M., & Abell, B. M. (2009). Subcellular Distribution of Tail-Anchored Proteins in Arabidopsis. *Traffic* **10**, 1753-1764.

Krieg, P. A. & Melton, D. A. (1984). Functional Messenger-Rnas Are Produced by Sp6 Invitro Transcription of Cloned Cdnas. *Nucleic Acids Research* **12**, 7057-7070.

Kumar, S. & Miller, L. K. (1987). Effects of Serial Passage of Autographa-Californica Nuclear Polyhedrosis-Virus in Cell-Culture. *Virus Research* **7**, 335-349.

Kutay, U., Hartmann, E., & Rapoport, T. A. (1993). A class of membrane proteins with a C-terminal anchor. *Trends Cell Biol* **3**, 72-75.

Kwon, C., Neu, C., Pajonk, S., Yun, H. S., Lipka, U., Humphry, M., Bau, S., Straus, M., Kwaaitaal, M., Rampelt, H., El Kasmi, F., Jurgens, G., Parker, J., Panstruga, R., Lipka, V., & Schulze-Lefert, P. (2008). Co-option of a default secretory pathway for plant immune responses. *Nature* **451**, 835-840.

Lacombe, B., Becker, D., Hedrich, R., DeSalle, R., Hollmann, M., Kwak, J. M., Schroeder, J. I., Le Novere, N., Nam, H. G., Spalding, E. P., Tester, M., Turano, F. J., Chiu, J., & Coruzzi, G. (2001). The identity of plant glutamate receptors. *Science* **292**, 1486-1487.

Lacombe, B., Pilot, G., Michard, E., Gaymard, F., Sentenac, H., & Thibaud, J. B. (2000). A shaker-like K+ channel with weak rectification is expressed in both source and sink phloem tissues of Arabidopsis. *Plant Cell* **12**, 837-851.

Lacroix, B., Vaidya, M., Tzfira, T., & Citovsky, V. (2005). The VirE3 protein of Agrobacterium mimics a host cell function required for plant genetic transformation. *Embo Journal* **24**, 428-437.

Laemmli, U. K. (1970). Cleavage of Structural Proteins During Assembly of Head of Bacteriophage-T4. *Nature* **227**, 680-685.

Lagarde, D., Basset, M., Lepetit, M., Conejero, G., Gaymard, F., Astruc, S., & Grignon, C. (1996). Tissue-specific expression of Arabidopsis AKT1 gene is consistent with a role in K+ nutrition. *Plant J.* **9**, 195-203.

Lang, T. & Jahn, R. (2008). Core proteins of the secretory machinery. *Handb Exp Pharmacol* **184**, 107-127.

Larsson, C., Sommarin, M., & Widell, S. (1994). Isolation of Highly Purified Plant Plasma-Membranes and Separation of Inside-Out and Right-Side-Out Vesicles. *Aqueous Two-Phase Systems* **228**, 451-469.

Larsson, C., Widell, S., & Kjellbom, P. (1987). Preparation of High-Purity Plasma-Membranes. *Methods in Enzymology* **148**, 558-568.

Larsson, C. & Widell, S. (2000). Isolation of Plant Plasma Membranes and Production of Inside-Out Vesicles. In *Aqueous Two-Phase Systems: Methods and Protocols* pp. 159-166.

Latorre, R., Olcese, R., Basso, C., Gonzalez, C., Munoz, F., Cosmellli, D., & Alvarez, O. (2003). Molecular coupling between voltage sensor and pore opening in the Arabidopsis inward rectifier K+ channel KAT1. *Journal of General Physiology* **122**, 459-469.

Lauber, M. H., Waizenegger, I., Steinmann, T., Schwarz, H., Mayer, U., Hwang, I., Lukowitz, W., & Jurgens, G. (1997). The Arabidopsis KNOLLE protein is a cytokinesis-specific syntaxin. *Journal of Cell Biology* **139**, 1485-1493.

le Maire, M., Champeil, P., & Moller, J. V. (2000). Interaction of membrane proteins and lipids with solubilizing detergents. *Biochimica et Biophysica Acta-Biomembranes* **1508**, 86-111.

Lebaudy, A., Hosy, E., Simonneau, T., Sentenac, H., Thibaud, J. B., & Dreyer, I. (2008). Heteromeric K+ channels in plants. *Plant Journal* **54**, 1076-1082.

Lebaudy, A., Very, A. A., & Sentenac, H. (2007). K+ channel activity in plants: Genes, regulations and functions. *Febs Letters* **581**, 2357-2366.

Lee, L. Y., Fang, M. J., Kuang, L. Y., & Gelvin, S. B. (2008). Vectors for multi-color bimolecular fluorescence complementation to investigate protein-protein interactions in living plant cells. *Plant Methods* **4**, 24-35.

Lee, S. C., Lan, W. Z., Kim, B. G., Li, L. G., Cheong, Y. H., Pandey, G. K., Lu, G. H., Buchanan, B. B., & Luan, S. (2007). A protein phosphorylation/dephosphorylation network regulates a plant potassium channel. *Proceedings of the National Academy of Sciences of the United States of America* **104**, 15959-15964.

Lemaire, M., Kwee, S., Andersen, J. P., & Moller, J. V. (1983). Mode of Interaction of Polyoxyethyleneglycol Detergents with Membrane-Proteins. *European Journal of Biochemistry* **129**, 525-532.

Leng, Q., Mercier, R. W., Yao, W. Z., & Berkowitz, G. A. (1999). Cloning and first functional characterization of a plant cyclic nucleotide-gated cation channel. *Plant Physiology* **121**, 753-761.

Lerman, J. C., Robblee, J., Fairman, R., & Hughson, F. M. (2000). Structural analysis of the neuronal SNARE protein syntaxin-1A. *Biochemistry* **39**, 8470-8479.

Leshem, Y., Golani, Y., Kaye, Y., & Levine, A. (2010). Reduced expression of the v-SNAREs AtVAMP71/AtVAMP7C gene family in Arabidopsis reduces drought tolerance by suppression of abscisic acid-dependent stomatal closure. *Journal of Experimental Botany* **61**, 2615-2622.

Leshem, Y., Melamed-Book, N., Cagnac, O., Ronen, G., Nishri, Y., Solomon, M., Cohen, G., & Levine, A. (2006). Suppression of Arabidopsis vesicle-SNARE expression inhibited fusion of H2O2 containing vesicles with tonoplast and increased salt tolerance. *Proceedings of the National Academy of Sciences of the United States of America* **103**, 18008-18013.

Leung, Y. M., Kang, Y. H., Gao, X. D., Xia, F. Z., Xie, H. L., Sheu, L., Tsuk, S., Lotan, I., Tsushima, R. G., & Gaisano, H. Y. (2003). Syntaxin 1A binds to the cytoplasmic C terminus of Kv2.1 to regulate channel gating and trafficking. *Journal of Biological Chemistry* **278**, 17532-17538.

Leung, Y. M., Kang, Y. H., Xia, F. Z., Sheu, L., Gao, X. D., Xie, H. L., Tsushima, R. G., & Gaisano, H. Y. (2005). Open form of syntaxin-1A is a more potent inhibitor than wild-type syntaxin-1A of Kv2.1 channels. *Biochemical Journal* **387**, 195-202.

Leung, Y. M., Kwan, E. P., Ng, B., Kang, Y., & Gaisano, H. Y. (2007). SNAREing voltage-gated K+ and ATP-Sensitive K+ channels: Tuning beta-Cell excitability with syntaxin-1A and other exocytotic proteins. *Endocrine Reviews* **28**, 653-663.

Levy, D., Gulik, A., Seigneuret, M., & Rigaud, J. L. (1990). Phospholipid Vesicle Solubilization and Reconstitution by Detergents - Symmetrical Analysis of the 2 Processes Using Octaethylene Glycol Mono-N-Dodecyl Ether. *Biochemistry* **29**, 9480-9488.

Leyman, B., Geelen, D., Quintero, F. J., & Blatt, M. R. (1999). A tobacco syntaxin with a role in hormonal control of guard cell ion channels. *Science* **283**, 537-540.

Li, J., Krichevsky, A., Vaidya, M., Tzfira, T., & Citovsky, V. (2005). Uncoupling of the functions of the Arabidopsis VIP1 protein in transient and stable plant genetic transformation by Agrobacterium. *Proc.Natl.Acad.Sci.U.S A* **102**, 5733-5738.

Li, J. F., Park, E., von Arnim, A. G., & Nebenfuhr, A. (2009). The FAST technique: a simplified Agrobacterium-based transformation method for transient gene expression analysis in seedlings of Arabidopsis and other plant species. *Plant Methods* **5**, 6-21.

Li, L. G., Kim, B. G., Cheong, Y. H., Pandey, G. K., & Luan, S. (2006). A Ca2+ signaling pathway regulates a K+ channel for low-K response in Arabidopsis. *Proceedings of the National Academy of Sciences of the United States of America* **103**, 12625-12630.

Li, M., Unwin, N., Stauffer, K. A., Jan, Y. N., & Jan, L. Y. (1994). Images of Purified Shaker Potassium Channels. *Current Biology* **4**, 110-115.

Li, W. W. & Assmann, S. M. (1993). Characterization of A G-Protein-Regulated Outward K+ Current in Mesophyll-Cells of Vicia-Faba l. *Proceedings of the National Academy of Sciences of the United States of America* **90**, 262-266.

Licari, P. & Bailey, J. E. (1991). Factors Influencing Recombinant Protein Yields in An Insect Cell Baculovirus Expression System - Multiplicity of Infection and Intracellular Protein-Degradation. *Biotechnology and Bioengineering* **37**, 238-246.

Lichtenberg, D., Robson, R. J., & Dennis, E. A. (1983). Solubilization of Phospholipids by Detergents - Structural and Kinetic Aspects. *Biochimica et Biophysica Acta* **737**, 285-304.

Lipka, V., Kwon, C., & Panstruga, R. (2007). SNARE-Ware: The role of SNARE-Domain proteins in plant biology. *Annual Review of Cell and Developmental Biology* **23**, 147-174.

Long, S. B., Campbell, E. B., & MacKinnon, R. (2005). Crystal structure of a mammalian voltage-dependent Shaker family K+ channel. *Science* **309**, 897-903.

Low, S. H., Vasanji, A., Nanduri, J., He, M., Sharma, N., Koo, M., Drazba, J., & Weimbs, T. (2006). Syntaxins 3 and 4 Are Concentrated in Separate Clusters on the Plasma Membrane before the Establishment of Cell Polarity. *Molecular Biology of the Cell* **17**, 977-989.

Luan, S. (2009). The CBL-CIPK network in plant calcium signaling. *Trends in Plant Science* **14**, 37-42.

Luckow, V. A., Lee, S. C., Barry, G. F., & Olins, P. O. (1993). Efficient Generation of Infectious Recombinant Baculoviruses by Site-Specific Transposon-Mediated Insertion of Foreign Genes Into A Baculovirus Genome Propagated in Escherichia-Coli. *Journal of Virology* **67**, 4566-4579.

Lukowitz, W., Mayer, U., & Jurgens, G. (1996). Cytokinesis in the Arabidopsis embryo involves the syntaxin-related KNOLLE gene product. *Cell* **84**, 61-71.

Lund, S., Orlowski, S., Deforesta, B., Champeil, P., Lemaire, M., & Moller, J. V. (1989). Detergent Structure and Associated Lipid As Determinants in the Stabilization of Solubilized Ca-2+-Atpase from Sarcoplasmic-Reticulum. *Journal of Biological Chemistry* **264**, 4907-4915.

Ma, D. & Jan, L. Y. (2002). ER transport signals and trafficking of potassium channels and receptors. *Current Opinion in Neurobiology* **12**, 287-292.

Maathuis, F. J. M. & Sanders, D. (1993). Energization of Potassium Uptake in Arabidopsis-Thaliana. *Planta* **191**, 302-307.

Maathuis, F. J. M. & Sanders, D. (1992). Plant membrane transport. *Current Opinion in Cell Biology* **4**, 661-669.

Maattanen, P., Gehring, K., Bergeron, J. J. M., & Thomas, D. Y. (2010). Protein quality control in the ER: The recognition of misfolded proteins. *Seminars in Cell & Developmental Biology* **21**, 500-511.

MacDonald, P. E., Ha, X. F., Wang, J., Smukler, S. R., Sun, A. M., Gaisano, H. Y., Salapatek, A. M. F., Backx, P. H., & Wheeler, M. B. (2001). Members of the Kv1 and Kv2 voltage-dependent K+ channel families regulate insulin secretion. *Molecular Endocrinology* **15**, 1423-1435.

Maneri, L. R. & Low, P. S. (1988). Structural Stability of the Erythrocyte Anion Transporter, Band-3, in Different Lipid Environments - A Differential Scanning Calorimetric Study. *Journal of Biological Chemistry* **263**, 16170-16178.

Mano, S., Miwa, T., Nishikawa, S., Mimura, T., & Nishimura, M. (2009). Seeing Is Believing: On the Use of Image Databases for Visually Exploring Plant Organelle Dynamics. *Plant and Cell Physiology* **50**, 2000-2014.

Mano, S., Miwa, T., Nishikawa, S. I., Mimura, T., & Nishimura, M. (2008). The plant organelles database (PODB): a collection of visualized plant organelles and protocols for plant organelle research. *Nucleic Acids Research* **36**, 929-937.

Margittai, M., Widengren, J., Schweinberger, E., Schroder, G. F., Felekyan, S., Haustein, E., Konig, M., Fasshauer, D., Grubmuller, H., Jahn, R., & Seidel, C. A. M. (2003). Single-molecule fluorescence resonance energy transfer reveals a dynamic equilibrium between closed and open conformations of syntaxin 1. *Proceedings of the National Academy of Sciences of the United States of America* **100**, 15516-15521.

Marion, J., Bach, L., Bellec, Y., Meyer, C., Gissot, L., & Faure, J. D. (2008). Systematic analysis of protein subcellular localization and interaction using high-throughput transient transformation of Arabidopsis seedlings. *Plant Journal* **56**, 169-179.

Marmagne, A., Rouet, M. A., Ferro, M., Rolland, N., Alcon, C., Joyard, J., Garin, J., Barbier-Brygoo, H., & Ephritikhine, G. (2004). Identification of new intrinsic proteins in Arabidopsis plasma membrane proteome. *Molecular & Cellular Proteomics* **3**, 675-691.

Marmagne, A., Salvi, D., Rolland, N., Ephritikhine, G., Joyard, J., & Barbier-Brygoo, H. (2006). Purification and Fractionation of Membranes for Proteomic Analyses. In *Arabidopsis Protocols* pp. 403-420.

Marschner, H. (1995). *Mineral Nutrition of Higher Plants* Academic Press, London.

Marsh, D. (1996). Components of the lateral pressure in lipid bilayers deduced from HII phase dimensions. *Biochimica et Biophysica Acta-Biomembranes* **1279**, 119-123.

Marten, I., Deeken, R., Hedrich, R., & Roelfsema, M. R. G. (2010). Light-induced modification of plant plasma membrane ion transport. *Plant Biology* **12**, 64-79.

Marten, I., Gaymard, F., Lemaillet, G., Thibaud, J. B., Sentenac, H., & Hedrich, R. (1996). Functional expression of the plant K+ channel KAT1 in insect cells. *Febs Letters* **380**, 229-232.

Martinez-Atienza, J., Jiang, X. Y., Garciadeblas, B., Mendoza, I., Zhu, J. K., Pardo, J. M., & Quintero, F. J. (2007). Conservation of the salt overly sensitive pathway in rice. *Plant Physiology* **143**, 1001-1012.

Massotte, D. (2003). G protein-coupled receptor overexpression with the baculovirus-insect cell system: a tool for structural and functional studies. *Biochimica et Biophysica Acta-Biomembranes* **1610**, 77-89.

Mattice, W. L., Riser, J. M., & Clark, D. S. (1976). Conformational properties of the complexes formed by proteins and sodium dodecyl sulfate. *Biochemistry* **15**, 4264-4272.

Mcnew, J. A., Parlati, F., Fukuda, R., & Rothman, J. E. (2000a). Compartmental specificity of cellular membrane fusion encoded in SNARE proteins. *Molecular Biology of the Cell* **11**, 153-159.

Mcnew, J. A., Weber, T., Parlati, F., Johnston, R. J., Melia, T. J., Sollner, T. H., & Rothman, J. E. (2000b). Close is not enough: SNARE-dependent membrane fusion requires an active mechanism that transduces force to membrane anchors. *Journal of Cell Biology* **150**, 105-117.

Meckel, T., Hurst, A. C., Thiel, G., & Homann, U. (2004). Endocytosis against high turgor: intact guard cells of Vicia faba constitutively endocytose fluorescently labelled plasma membrane and GFP-tagged K+-channel KAT1. *Plant Journal* **39**, 182-193.

Medina, R., Perdomo, D., & Bubis, J. (2004). The hydrodynamic properties of dark- and light-activated states of n-dodecyl beta-D-maltoside-solubilized bovine rhodopsin support the dimeric structure of both conformations. *Journal of Biological Chemistry* **279**, 39565-39573.

Meyer, D., Pajonk, S., Micali, C., O'Connell, R., & Schulze-Lefert, P. (2009). Extracellular transport and integration of plant secretory proteins into pathogen-induced cell wall compartments. *Plant Journal* **57**, 986-999.

Michaelevski, L., Chikvashvili, D., Tsuk, S., Fili, O., Lohse, M. J., Singer-Lahat, D., & Lotan, I. (2002). Modulation of a brain voltage-gated K+ channel by syntaxin 1A requires the physical interaction of G beta gamma with the channel. *Journal of Biological Chemistry* **277**, 34909-34917.

Miedema, H., Demidchik, V., Very, A. A., Bothwell, J. H. F., Brownlee, C., & Davies, J. M. (2008). Two voltage-dependent calcium channels co-exist in the apical plasma membrane of Arabidopsis thaliana root hairs. *New Phytologist* **179**, 378-385.

Mikosch, M., Hurst, A. C., Hertel, B., & Homann, U. (2006). Diacidic motif is required for efficient transport of the K+ channel KAT1 to the plasma membrane. *Plant Physiology* **142**, 923-930.

Mikosch, M., Kaberich, K., & Homann, U. (2009). ER Export of KAT1 is Correlated to the Number of Acidic Residues within a Triacidic Motif. *Traffic* **10**, 1481-1487.

Miller, J. P., Lo, R. S., Ben Hur, A., Desmarais, C., Stagljar, I., Noble, W. S., & Fields, S. (2005). Large-scale identification of yeast integral membrane protein interactions. *Proceedings of the National Academy of Sciences of the United States of America* **102**, 12123-12128.

Misra, P. K., Panigrahi, S., Dash, U., & Mandal, A. B. (2010). Organization of amphiphiles. Part XI: Physico-chemical aspects of mixed micellization involving normal conventional surfactant and a non-ionic gemini surfactant. *Journal of Colloid and Interface Science* **345**, 392-401.

Misura, K. M. S., Scheller, R. H., & Weis, W. I. (2000). Three-dimensional structure of the neuronal-Sec1-syntaxin 1a complex. *Nature* **404**, 355-362.

Mitraki, A. & King, J. (1989). Protein Folding Intermediates and Inclusion Body Formation. *Bio-Technology* **7**, 690-697.

Montecucco, C., Schiavo, G., & Pantano, S. (2005). SNARE complexes and neuroexocytosis: how many, how close? *Trends in Biochemical Sciences* **30**, 367-372.

Mori, I. C., Uozumi, N., & Muto, S. (2000). Phosphorylation of the inward-rectifying potassium channel KAT1 by ABR kinase in Vicia guard cells. *Plant and Cell Physiology* **41**, 850-856.

Mouline, K., Very, A. A., Gaymard, F., Boucherez, J., Pilot, G., Devic, M., Bouchez, D., Thibaud, J. B., & Sentenac, H. (2002). Pollen tube development and competitive ability are impaired by disruption of a Shaker K+ channel in Arabidopsis. *Genes & Development* **16**, 339-350.

Mukhopadhyay, R., Ho, Y. S., Swiatek, P. J., Rosen, B. P., & Bhattacharjee, H. (2006). Targeted disruption of the mouse Asna1 gene results in embryonic lethality. *Febs Letters* **580**, 3889-3894.

Muller, I., Wagner, W., Volker, A., Schellmann, S., Nacry, P., Kuttner, F., Schwarz-Sommer, Z., Mayer, U., & Jurgens, G. (2003). Syntaxin specificity of cytokinesis in Arabidopsis. *Nature Cell Biology* **5**, 531-534.

Munson, M., Chen, X., Cocina, A. E., Schultz, S. M., & Hughson, F. M. (2000). Interactions within the yeast t-SNARE Sso1p that control SNARE complex assembly. *Nature Structural Biology* **7**, 894-902.

Mura, C. V., Cosmelli, D., Munoz, F., & Delgado, R. (2004). Orientation of Arabidopsis thaliana KAT1 channel in the plasma membrane. *Journal of Membrane Biology* **201**, 157-165.

Murray, D. H. & Tamm, L. K. (2009). Clustering of Syntaxin-1A in Model Membranes Is Modulated by Phosphatidylinositol 4,5-Bisphosphate and Cholesterol. *Biochemistry* **48**, 4617-4625.

Nadal, M. S., Amarillo, Y., Vega-Saenz de Miera, E., & Rudy, B. (2006). Differential characterization of three alternative spliced isoforms of DPPX. *Brain Research* **1094**, 1-12.

Nagai, T., Sawano, A., Park, E. S., & Miyawaki, A. (2001). Circularly permuted green fluorescent proteins engineered to sense Ca2+. *Proceedings of the National Academy of Sciences of the United States of America* **98**, 3197-3202.

Nakagawa, Y., Katagiri, T., Shinozaki, K., Qi, Z., Tatsumi, H., Furuichi, T., Kishigami, A., Sokabe, M., Kojima, I., Sato, S., Kato, T., Tabata, S., Iida, K., Terashima, A., Nakano, M., Ikeda, M., Yamanaka, T., & Iida, H. (2007). Arabidopsis plasma membrane protein crucial for Ca2+ influx and touch sensing in roots. *Proceedings of the National Academy of Sciences of the United States of America* **104**, 3639-3644.

Nakahara, S., Hogan, V., Inohara, H., & Raz, A. (2006). Importin-mediated nuclear translocation of galectin-3. *Journal of Biological Chemistry* **281**, 39649-39659.

Nakatsukasa, K. & Brodsky, J. L. (2008). The recognition and retrotranslocation of misfolded proteins from the endoplasmic reticulum. *Traffic* **9**, 861-870.

Nam, J., Mysore, K. S., Zheng, C., Knue, M. K., Matthysse, A. G., & Gelvin, S. B. (1999). Identification of T-DNA tagged Arabidopsis mutants that are resistant to transformation by Agrobacterium. *Molecular and General Genetics* **261**, 429-438.

Negi, J., Matsuda, O., Nagasawa, T., Oba, Y., Takahashi, H., Kawai-Yamada, M., Uchimiya, H., Hashimoto, M., & Iba, K. (2008). CO2 regulator SLAC1 and its homologues are essential for anion homeostasis in plant cells. *Nature* **452**, 483-U13.

Nieves-Cordones, M., Aleman, F., Martinez, V., & Rubio, F. (2010). The Arabidopsis thaliana HAK5 K+ Transporter Is Required for Plant Growth and K+ Acquisition from Low K+ Solutions under Saline Conditions. *Molecular Plant* **3**, 326-333.

Nieves-Cordones, M., Martinez-Cordero, M. A., Martinez, V., & Rubio, F. (2007). An NH4+-sensitive component dominates high-affinity K+ uptake in tomato plants. *Plant Science* **172**, 273-280.

Nieves-Cordones, M., Miller, A. J., Aleman, F., Martinez, V., & Rubio, F. (2008). A putative role for the plasma membrane potential in the control of the expression of the gene encoding the tomato high-affinity potassium transporter HAK5. *Plant Molecular Biology* **68**, 521-532.

Nilsson, I. M. & Vonheijne, G. (1990). Fine-Tuning the Topology of A Polytopic Membrane-Protein - Role of Positively and Negatively Charged Amino-Acids. *Cell* **62**, 1135-1141.

Nuhse, T. S., Boller, T., & Peck, S. C. (2003). A plasma membrane syntaxin is phosphorylated in response to the bacterial elicitor flagellin. *Journal of Biological Chemistry* **278**, 45248-45254.

Obrdlik, P., El Bakkoury, M., Hamacher, T., Cappellaro, C., Vilarino, C., Fleischer, C., Ellerbrok, H., Kamuzinzi, R., Ledent, V., Blaudez, D., Sanders, D., Revuelta, J. L., Boles, E., Andre, B., & Frommer, W. B. (2004). K+ channel interactions detected by a genetic system optimized for systematic studies of membrane protein interactions. *Proceedings of the National Academy of Sciences of the United States of America* **101**, 12242-12247.

Ostermeier, C. & Michel, H. (1997). Crystallization of membrane proteins. *Current Opinion in Structural Biology* **7**, 697-701.

Otzen, D. E. (2002). Protein unfolding in detergents: Effect of micelle structure, ionic strength, pH, and temperature. *Biophysical Journal* **83**, 2219-2230.

Pajonk, S., Kwon, C., Clemens, N., Panstruga, R., & Schulze-Lefert, P. (2008). Activity determinants and functional specialization of Arabidopsis PEN1 syntaxin in innate immunity. *Journal of Biological Chemistry* **283**, 26974-26984.

Palmgren, M. G. (2001). Plant plasma membrane H(+)-ATPases: Powerhouses for nutrient uptake. *Annual Review of Plant Physiology and Plant Molecular Biology* **52**, 817-845.

Pandey, G. K., Cheong, Y. H., Kim, B. G., Grant, J. J., Li, L. G., & Luan, S. (2007). CIPK9: a calcium sensor-interacting protein kinase required for low-potassium tolerance in Arabidopsis. *Cell Research* **17**, 411-421.

Pardo, J. M. & Serrano, R. (1989). Structure of A Plasma-Membrane H+-Atpase Gene from the Plant Arabidopsis-Thaliana. *Journal of Biological Chemistry* **264**, 8557-8562.

Parry, M. A. J., Schmidt, C. N. G., Cornelius, M. J., Millard, B. N., Burton, S., Gutteridge, S., Dyer, T. A., & Keys, A. J. (1987). Variations in Properties of Ribulose-1,5-Bisphosphate Carboxylase from Various Species Related to Differences in Amino-Acid-Sequences. *Journal of Experimental Botany* **38**, 1260-1271.

Pebaypeyroula, E., Garavito, R. M., Rosenbusch, J. P., Zulauf, M., & Timmins, P. A. (1995). Detergent Structure in Tetragonal Crystals of Ompf Porin. *Structure* **3**, 1051-1059.

Peiter, E., Maathuis, F. J. M., Mills, L. N., Knight, H., Pelloux, M., Hetherington, A. M., & Sanders, D. (2005). The vacuolar Ca2+-activated channel TPC1 regulates germination and stomatal movement. *Nature* **434**, 404-408.

Perkins, J. R., Diboun, I., Dessailly, B. H., Lees, J. G., & Orengo, C. (2010). Transient Protein-Protein Interactions: Structural, Functional, and Network Properties. *Structure* **18**, 1233-1243.

Phizicky, E. M. & Fields, S. (1995). Protein-Protein Interactions - Methods for Detection and Analysis. *Microbiological Reviews* **59**, 94-123.

Pilot, G., Gaymard, F., Mouline, K., Cherel, I., & Sentenac, H. (2003a). Regulated expression of Arabidopsis shaker K+ channel genes involved in K+ uptake and distribution in the plant. *Plant Mol.Biol.* **51**, 773-787.

Pilot, G., Lacombe, B., Gaymard, F., Cherel, I., Boucherez, J., Thibaud, J. B., & Sentenac, H. (2001). Guard cell inward K+ channel activity in Arabidopsis involves expression of the twin channel subunits KAT1 and KAT2. *Journal of Biological Chemistry* **276**, 3215-3221.

Pilot, G., Pratelli, R., Gaymard, F., Meyer, Y., & Sentenac, H. (2003b). Five-group distribution of the shaker-like K+ channel family in higher plants. *Journal of Molecular Evolution* **56**, 418-434.

Pimpl, P., Taylor, J. P., Snowden, C., Hillmer, S., Robinson, D. G., & Denecke, J. (2006). Golgi-mediated vacuolar sorting of the endoplasmic reticulum chaperone BiP may play an active role in quality control within the secretory pathway. *Plant Cell* **18**, 198-211.

Pitzschke, A., Forzani, C., & Hirt, H. (2006). Reactive oxygen species signaling in plants. *Antioxidants & Redox Signaling* **8**, 1757-1764.

Pratelli, J., Sutter, J. U., & Blatt, M. R. (2004). A new catch in the SNARE. *Trends in Plant Science* **9**, 187-195.

Prive, G. G. (2007). Detergents for the stabilization and crystallization of membrane proteins. *Methods* **41**, 388-397.

Pruss, G. J., Nester, E. W., & Vance, V. (2008). Infiltration with Agrobacterium tumefaciens Induces Host Defense and Development-Dependent Responses in the Infiltrated Zone. *Molecular Plant-Microbe Interactions* **21**, 1528-1538.

Puig, O., Caspary, F., Rigaut, G., Rutz, B., Bouveret, E., Bragado-Nilsson, E., Wilm, M., & Seraphin, B. (2001). The tandem affinity purification (TAP) method: A general procedure of protein complex purification. *Methods* **24**, 218-229.

Pyo, Y. J., Gierth, M., Schroeder, J. I., & Cho, M. H. (2010). High-Affinity K+ Transport in Arabidopsis: AtHAK5 and AKT1 Are Vital for Seedling Establishment and Postgermination Growth under Low-Potassium Conditions. *Plant Physiology* **153**, 863-875.

Qi, Z., Hampton, C. R., Shin, R., Barkla, B. J., White, P. J., & Schachtman, D. P. (2008). The high affinity K+ transporter AtHAK5 plays a physiological role in planta at very low K+ concentrations and provides a caesium uptake pathway in Arabidopsis. *Journal of Experimental Botany* **59**, 595-607.

Rabu, C., Schmid, V., Schwappach, B., & High, S. (2009). Biogenesis of tail-anchored proteins: the beginning for the end? *Journal of Cell Science* **122**, 3605-3612.

Ramsay, D., Kellett, E., Mcvey, M., Rees, S., & Milligan, G. (2002). Homo- and hetero-oligomeric interactions between G-protein-coupled receptors in living cells monitored by two variants of bioluminescence resonance energy transfer (BRET): hetero-oligomers between receptor subtypes form more efficiently than between less closely related sequences. *Biochemical Journal* **365**, 429-440.

Rancour, D. M., Dickey, C. E., Park, S., & Bednarek, S. Y. (2002). Characterization of AtCDC48. Evidence for multiple membrane fusion mechanisms at the plane of cell division in plants. *Plant Physiology* **130**, 1241-1253.

Rehman, R. U., Stigliano, E., Lycett, G. W., Sticher, L., Sbano, F., Faraco, M., Dalessandro, G., & Di Sansebastiano, G. P. (2008). Tomato Rab11a characterization evidenced a difference between SYP121-dependent and SYP122-dependent exocytosis. *Plant and Cell Physiology* **49**, 751-766.

Reichardt, L., Stierhof, Y. D., Mayer, U., Richter, S., Schwarz, H., Schumacher, K., & Jurgens, G. (2007). Plant cytokinesis requires de novo secretory trafficking but not endocytosis. *Current Biology* **17**, 2047-2053.

Reintanz, B., Szyroki, A., Ivashikina, N., Ache, P., Godde, M., Becker, D., Palme, K., & Hedrich, R. (2002). AtKC1, a silent Arabidopsis potassium channel alpha-subunit modulates root hair K+ influx. *Proceedings of the National Academy of Sciences of the United States of America* **99**, 4079-4084.

Reisinger, V. & Eichacker, L. A. (2008). Solubilization of membrane protein complexes for blue native PAGE. *Journal of Proteomics* **71**, 277-283.

Rengel, Z. & Damon, P. M. (2008). Crops and genotypes differ in efficiency of potassium uptake and use. *Physiologia Plantarum* **133**, 624-636.

Reuff, M., Mikosch, M., & Homann, U. (2010). Trafficking, lateral mobility and segregation of the plant K plus channel KAT1. *Plant Biology* **12**, 99-104.

Reynolds, J. A. & Tanford, C. (1970). Gross Conformation of Protein-Sodium Dodecyl Sulfate Complexes. *Journal of Biological Chemistry* **245**, 5161-5165.

Richmond, J. E., Weimer, R. M., & Jorgensen, E. M. (2001). An open form of syntaxin bypasses the requirement for UNC-13 in vesicle priming. *Nature* **412**, 338-341.

Richter, S., Voss, U., & Jurgens, G. (2009). Post-Golgi Traffic in Plants. *Traffic* **10**, 819-828.

Rigas, S., Debrosses, G., Haralampidis, K., Vicente-Agullo, F., Feldmann, K. A., Grabov, A., Dolan, L., & Hatzopoulos, P. (2001). TRH1 encodes a potassium transporter required for tip growth in Arabidopsis root hairs. *Plant Cell* **13**, 139-151.

Rizo, J. & Rosenmund, C. (2008). Synaptic vesicle fusion. *Nature Structural & Molecular Biology* **15**, 665-674.

Rizo, J. & Sudhof, T. C. (2002). SNAREs and Munc18 in synaptic vesicle fusion. *Nature Reviews Neuroscience* **3**, 641-653.

Roberts, S. K. & Tester, M. (1995). Inward and outward K+-selective currents in the plasma membrane of protoplasts from maize root cortex and stele. *Plant Journal* **8**, 811-825.

Robertson, W. R., Clark, K., Young, J. C., & Sussman, M. R. (2004). An Arabidopsis thaliana plasma membrane proton pump is essential for pollen development. *Genetics* **168**, 1677-1687.

Robida, A. M. & Kerppola, T. K. (2009). Bimolecular Fluorescence Complementation Analysis of Inducible Protein Interactions: Effects of Factors Affecting Protein Folding on Fluorescent Protein Fragment Association. *Journal of Molecular Biology* **394**, 391-409.

Rodriguez-Navarro, A. & Rubio, F. (2006). High-affinity potassium and sodium transport systems in plants. *Journal of Experimental Botany* **57**, 1149-1160.

Roth, M., Lewitbentley, A., Michel, H., Deisenhofer, J., Huber, R., & Oesterhelt, D. (1989). Detergent Structure in Crystals of A Bacterial Photosynthetic Reaction Center. *Nature* **340**, 659-662.

Roy, P., Mikhailov, M., & Bishop, D. H. L. (1997). Baculovirus multigene expression vectors and their use for understanding the assembly process of architecturally complex virus particles. *Gene* **190**, 119-129.

Rubio, F., Aleman, F., Nieves-Cordones, M., & Martinez, V. (2010). Studies on Arabidopsis athak5, atakt1 double mutants disclose the range of concentrations at which AtHAK5, AtAKT1 and unknown systems mediate K plus uptake. *Physiologia Plantarum* **139**, 220-228.

Rubio, F., Nieves-Cordones, M., Aleman, F., & Martinez, V. (2008). Relative contribution of AtHAK5 and AtAKT1 to K+ uptake in the high-affinity range of concentrations. *Physiologia Plantarum* **134**, 598-608.

Sagne, C., Isambert, M. F., Henry, J. P., & Gasnier, B. (1996). SDS-resistant aggregation of membrane proteins: Application to the purification of the vesicular monoamine transporter. *Biochemical Journal* **316**, 825-831.

Salim, K., Fenton, T., Bacha, J., Urien-Rodriguez, H., Bonnert, T., Skynner, H. A., & Watts, E. (2002). Oligomerization of G-protein-coupled receptors shown by selective co-immunoprecipitation. *Journal of Biological Chemistry* **277**, 15482-15485.

Sambrook, J. & Russell, D. W. (2006). DNA Transfection by Biolistics. *Cold Spring Harbor Protocols* **2006**.

Samso, M., Daban, J. R., Hansen, S., & Jones, G. R. (1995). Evidence for Sodium Dodecyl Sulfate/Protein Complexes Adopting A Necklace Structure. *European Journal of Biochemistry* **232**, 818-824.

Sanchez-Moran, E., Osman, K., Higgins, J. D., Pradillo, M., Cunado, N., Jones, G. H., & Franklin, F. C. H. (2008). ASY1 coordinates early events in the plant meiotic recombination pathway. *Cytogenetic and Genome Research* **120**, 302-312.

Sanderfoot, A. (2007). Increases in the number of SNARE genes parallels the rise of multicellularity among the green plants. *Plant Physiology* **144**, 6-17.

Sanderfoot, A. A., Assaad, F. F., & Raikhel, N. V. (2000). The Arabidopsis genome. An abundance of soluble N-ethylmaleimide-sensitive factor adaptor protein receptors. *Plant Physiology* **124**, 1558-1569.

Sanderfoot, A. A., Kovaleva, V., Bassham, D. C., & Raikhel, N. V. (2001). Interactions between syntaxins identify at least five SNARE complexes within the golgi/prevacuolar system of the arabidopsis cell. *Molecular Biology of the Cell* **12**, 3733-3743.

Santoni, V., Rouquie, D., Doumas, P., Mansion, M., Boutry, M., Degand, H., Dupree, P., Packman, L., Sherrier, J., Prime, T., Bauw, G., Posada, E., Rouze, P., Dehais, P., Sahnoun, I., Barlier, I., & Rossignol, M. (1998). Use of a proteome strategy for tagging proteins present at the plasma membrane. *Plant Journal* **16**, 633-641.

Sato, Y., Sakaguchi, M., Goshima, S., Nakamura, T., & Uozumi, N. (2002). Integration of Shaker-type K+ channel, KAT1, into the endoplasmic reticulum membrane: Synergistic insertion of voltage-sensing segments, S3-S4, and independent insertion of pore-forming segments, S5-P-S6. *Proceedings of the National Academy of Sciences of the United States of America* **99**, 60-65.

Sato, Y., Sakaguchi, M., Goshima, S., Nakamura, T., & Uozumi, N. (2003). Molecular dissection of the contribution of negatively and positively charged residues in S2, S3, and S4 to the final membrane topology of the voltage sensor in the K+ channel, KAT1. *Journal of Biological Chemistry* **278**, 13227-13234.

Schachtman, D. P. & Shin, R. (2007b). Nutrient sensing and signaling: NPKS. *Annual Review of Plant Biology* **58**, 47-69.

Schachtman, D. P. & Shin, R. (2007a). Nutrient sensing and signaling: NPKS. *Annual Review of Plant Biology* **58**, 47-69.

Schaffner, W. & Weissman, C. (1973). Rapid, Sensitive, and Specific Method for Determination of Protein in Dilute-Solution. *Analytical Biochemistry* **56**, 502-514.

Schmidt, C. & Schroeder, J. I. (1994). Anion Selectivity of Slow Anion Channels in the Plasma-Membrane of Guard-Cells - Large Nitrate Permeability. *Plant Physiology* **106**, 383-391.

Schwappach, B. (2008). An overview of trafficking and assembly of neurotransmitter receptors and ion channels (Review). *Molecular Membrane Biology* **25**, 270-278.

Seddon, A. M., Curnow, P., & Booth, P. J. (2004). Membrane proteins, lipids and detergents: not just a soap opera. *Biochimica et Biophysica Acta-Biomembranes* **1666**, 105-117.

Sekar, R. B. & Periasamy, A. (2003). Fluorescence resonance energy transfer (FRET) microscopy imaging of live cell protein localizations. *Journal of Cell Biology* **160**, 629-633.

Shen, J. S., Tareste, D. C., Paumet, F., Rothman, J. E., & Melia, T. J. (2007). Selective activation of cognate SNAREpins by Sec1/Munc18 proteins. *Cell* **128**, 183-195.

Shih, T. M. & Goldin, A. L. (1997). Topology of the Shaker potassium channel probed with hydrophilic epitope insertions. *Journal of Cell Biology* **136**, 1037-1045.

Shin, R., Berg, R. H., & Schachtman, D. P. (2005). Reactive oxygen species and root hairs in Arabidopsis root response to nitrogen, phosphorus and potassium deficiency. *Plant and Cell Physiology* **46**, 1350-1357.

Shin, R. & Schachtman, D. P. (2004). Hydrogen peroxide mediates plant root cell response to nutrient deprivation. *Proceedings of the National Academy of Sciences of the United States of America* **101**, 8827-8832.

Shrivastav, M., De Haro, L. P., & Nickoloff, J. A. (2008). Regulation of DNA double-strand break repair pathway choice. *Cell Research* **18**, 134-147.

Sieben, C., Mikosch, M., Brandizzi, F., & Homann, U. (2008). Interaction of the K+-channel KAT1 with the coat protein complex II coat component Sec24 depends on a di-acidic endoplasmic reticulum export motif. *Plant Journal* **56**, 997-1006.

Sieber, J. J., Willig, K. I., Kutzner, C., Gerding-Reimers, C., Harke, B., Donnert, G., Rammner, B., Eggeling, C., Hell, S. W., Grubmuller, H., & Lang, T. (2007). Anatomy and Dynamics of a Supramolecular Membrane Protein Cluster. *Science* **317**, 1072-1076.

Skarp, K. P., Zhao, X., Weber, M., & Jantti, J. (2008). Use of Bimolecular Fluorescence Complementation in Yeast Saccharomyces cerevisiae. *Methods in Molecular Biology* 165-175.

Sokolovski, S., Hills, A., Gay, R. A., & Blatt, M. R. (2008). Functional interaction of the SNARE protein NtSyp121 in Ca2+ channel gating, Ca2+ transients and ABA signalling of stomatal guard cells. *Molecular Plant* **1**, 347-358.

Sollner, R., Glasser, G., Wanner, G., Somerville, C. R., Jurgens, G., & Assaad, F. F. (2002). Cytokinesis-defective mutants of Arabidopsis. *Plant Physiology* **129**, 678-690.

Sollner, T., Whitehart, S. W., Brunner, M., Erdjumentbromage, H., Geromanos, S., Tempst, P., & Rothman, J. E. (1993). Snap Receptors Implicated in Vesicle Targeting and Fusion. *Nature* **362**, 318-324.

Sonti, R. V., Chiurazzi, M., Wong, D., Davies, C. S., Harlow, G. R., Mount, D. W., & Signer, E. R. (1995). Arabidopsis Mutants Deficient in T-Dna Integration. *Proceedings of the National Academy of Sciences of the United States of America* **92**, 11786-11790.

Sottocornola, B., Gazzarrini, S., Olivari, C., Romani, G., Valbuzzi, P., Thiel, G., & Moroni, A. (2008). 14-3-3 proteins regulate the potassium channel KAT1 by dual modes. *Plant Biology* **10**, 231-236.

Sottocornola, B., Visconti, S., Orsi, S., Gazzarrini, S., Giacometti, S., Olivari, C., Camoni, L., Aducci, P., Marra, M., Abenavoli, A., Thiel, G., & Moroni, A. (2006). The potassium channel KAT1 is activated by plant and animal 14-3-3 proteins. *Journal of Biological Chemistry* **281**, 35735-35741.

Spalding, E. P., Hirsch, R. E., Lewis, D. R., Qi, Z., Sussman, M. R., & Lewis, B. D. (1999). Potassium uptake supporting plant growth in the absence of AKT1 channel activity: Inhibition by ammonium and stimulation by sodium. *J.Gen.Physiol* **113**, 909-918.

Sparkes, I. A., Ketelaar, T., de Ruijter, N. C. A., & Hawes, C. (2009). Grab a Golgi: Laser Trapping of Golgi Bodies Reveals in vivo Interactions with the Endoplasmic Reticulum. *Traffic* **10**, 567-571.

Spatz, L. & Strittma, P. (1971). Form of Cytochrome B5 That Contains An Additional Hydrophobic Sequence of 40 Amino Acid Residues. *Proceedings of the National Academy of Sciences of the United States of America* **68**, 1042-1046.

Speers, A. E. & Wu, C. C. (2007). Proteomics of integral membrane proteins-theory and application. *Chemical Reviews* **107**, 3687-3714.

Staehelin, L. A. (1997). The plant ER: A dynamic organelle composed of a large number of discrete functional domains. *Plant Journal* **11**, 1151-1165.

Stagljar, I. & Fields, S. (2002). Analysis of membrane protein interactions using yeast-based technologies. *Trends in Biochemical Sciences* **27**, 559-563.

Stagljar, I., Korostensky, C., Johnsson, N., & te Heesen, S. (1998). A genetic system based on split-ubiquitin for the analysis of interactions between membrane proteins in vivo. *Proceedings of the National Academy of Sciences of the United States of America* **95**, 5187-5192.

Stolpe, T., Susslin, C., Marrocco, K., Nick, P., Kretsch, T., & Kircher, S. (2005). In planta analysis of protein-protein interactions related to light signaling by bimolecular fluorescence complementation. *Protoplasma* **226**, 137-146.

Sudhof, T. C. & Rothman, J. E. (2009). Membrane Fusion: Grappling with SNARE and SM Proteins. *Science* **323**, 474-477.

Surpin, M. & Raikhel, N. (2004). Traffic jams affect plant development and signal transduction. *Nature Reviews Molecular Cell Biology* **5**, 100-109.

Sussman, M. R. & Harper, J. F. (1989). Molecular-Biology of the Plasma-Membrane of Higher-Plants. *Plant Cell* **1**, 953-960.

Sutter, J. U., Campanoni, P., Blatt, M. R., & Paneque, M. (2006a). Setting SNAREs in a different wood. *Traffic* **7**, 627-638.

Sutter, J. U., Campanoni, P., Tyrrell, M., & Blatt, M. R. (2006b). Selective mobility and sensitivity to SNAREs is exhibited by the Arabidopsis KAT1 K+ channel at the plasma membrane. *Plant Cell* **18**, 935-954.

Sutton, R. B., Fasshauer, D., Jahn, R., & Brunger, A. T. (1998). Crystal structure of a SNARE complex involved in synaptic exocytosis at 2.4 angstrom resolution. *Nature* **395**, 347-353.

Suwastika, I. N., Uemura, T., Shiina, T., Sato, M. H., & Takeyasu, K. (2008). SYP71, a Plant-specific Qc-SNARE Protein, Reveals Dual Localization to the Plasma Membrane and the Endoplasmic Reticulum in Arabidopsis. *Cell Structure and Function* **33**, 185-192.

Szyroki, A., Ivashikina, N., Dietrich, P., Roelfsema, M. R., Ache, P., Reintanz, B., Deeken, R., Godde, M., Felle, H., Steinmeyer, R., Palme, K., & Hedrich, R. (2001). KAT1 is not essential for stomatal opening. *Proc.Natl.Acad.Sci.U.S.A* **98**, 2917-2921.

Taiz, L. & Zeiger, E. (1998). Plant physiology, Second edition. *Sinauer*.

Takagi, T., Tsujii, K., & Shirahama, K. (1975). Binding Isotherms of Sodium Dodecyl-Sulfate to Protein Polypeptides with Special Reference to Sds-Polyacylamide Gel-Electrophoresis. *Journal of Biochemistry* **77**, 939-947.

Tanford, C. (1978). Hydrophobic Effect and Organization of Living Matter. *Science* **200**, 1012-1018.

Tang, H. X., Vasconcelos, A. C., & Berkowitz, G. A. (1996). Physical association of KAB1 with plant K+ channel alpha subunits. *Plant Cell* **8**, 1545-1553.

Tareste, D., Shen, J., Melia, T. J., & Rothman, J. E. (2008). SNAREpin/Munc18 promotes adhesion and fusion of large vesicles to giant membranes. *Proceedings of the National Academy of Sciences of the United States of America* **105**, 2380-2385.

Tavares, R., Vidal, J., van Lammeren, A., & Kreis, M. (2002). Non-purified anti-peptide sera generate tissue specific artefacts in immunohistochemical staining of Arabidopsis thaliana. *Plant Science* **162**, 309-314.

Thellmann, M., Rybak, K., Thiele, K., Wanner, G., & Assaad, F. F. (2010). Tethering Factors Required for Cytokinesis in Arabidopsis. *Plant Physiology* **154**, 720-732.

Thordal-Christensen, H. (2003). Fresh insights into processes of nonhost resistance. *Current Opinion in Plant Biology* **6**, 351-357.

Tian, G. W., Mohanty, A., Chary, S. N., Li, S. J., Paap, B., Drakakaki, G., Kopec, C. D., Li, J. X., Ehrhardt, D., Jackson, D., Rhee, S. Y., Raikhel, N. V., & Citovsky, V. (2004). High-throughput fluorescent tagging of full-length arabidopsis gene products in planta. *Plant Physiology* **135**, 25-38.

Tse, F. W., Iwata, A., & Almers, W. (1993). Membrane Flux Through the Pore Formed by A Fusogenic Viral Envelope Protein During Cell-Fusion. *Journal of Cell Biology* **121**, 543-552.

Tsien, R. Y. (1998). The green fluorescent protein. *Annual Review of Biochemistry* **67**, 509-544.

Tu, L. W. & Deutsch, C. (1999). Evidence for dimerization of dimers in K+ channel assembly. *Biophysical Journal* **76**, 2004-2017.

Tyrrell, M., Campanoni, P., Sutter, J. U., Pratelli, R., Paneque, M., Sokolovski, S., & Blatt, M. R. (2007). Selective targeting of plasma membrane and tonoplast traffic by inhibitory (dominant-negative) SNARE fragments. *Plant Journal* **51**, 1099-1115.

Uemura, T., Sato, M. H., & Takeyasu, K. (2005). The longin domain regulates subcellular targeting of VAMP7 in Arabidopsis thaliana. *Febs Letters* **579**, 2842-2846.

Uemura, T., Ueda, T., Ohniwa, R. L., Nakano, A., Takeyasu, K., & Sato, M. H. (2004). Systematic analysis of SNARE molecules in Arabidopsis: Dissection of the post-Golgi network in plant cells. *Cell Structure and Function* **29**, 49-65.

Ugolini, S. & Bruschi, C. V. (1996). The red/white colony color assay in the yeast Saccharomyces cerevisiae: Epistatic growth advantage of white ade8-18, ade2 cells over red ade2 cells. *Current Genetics* **30**, 485-492.

Uozumi, N. & Schroeder, J. (2010). *Ion Channels and Plant Stress: Past, Present, and Future*, pp. 1-22. Springer Press, Berlin.

Urbach, S., Cherel, I., Sentenac, H., & Gaymard, F. (2000). Biochemical characterization of the Arabidopsis K+ channels KAT1 and AKT1 expressed or co-expressed in insect cells. *Plant Journal* **23**, 527-538.

Vacher, H., Mohapatra, D. P., & Trimmer, J. S. (2008). Localization and targeting of voltage-dependent ion channels in mammalian central neurons. *Physiological Reviews* **88**, 1407-1447.

Vahisalu, T., Kollist, H., Wang, Y. F., Nishimura, N., Chan, W. Y., Valerio, G., Lamminmaki, A., Brosche, M., Moldau, H., Desikan, R., Schroeder, J. I., & Kangasjarvi, J. (2008). SLAC1 is required for plant guard cell S-type anion channel function in stomatal signalling. *Nature* **452**, 487-U15.

Valluru, N., Silva, F., Dhage, M., Rodriguez, G., Alloor, S. R., & Renthal, R. (2006). Transmembrane helix-helix association: Relative stabilities at low pH. *Biochemistry* **45**, 4371-4377.

van den Bogaart, G., Holt, M. G., Bunt, G., Riedel, D., Wouters, F. S., & Jahn, R. (2010). One SNARE complex is sufficient for membrane fusion. *Nature Structural & Molecular Biology* **17**, 358-364.

van Meer, G., Voelker, D. R., & Feigenson, G. W. (2008). Membrane lipids: where they are and how they behave. *Nature Reviews Molecular Cell Biology* **9**, 112-124.

Vanneste, S. & Friml, J. (2009). Auxin: A Trigger for Change in Plant Development. *Cell* **136**, 1005-1016.

Vaynberg, J. & Qin, J. (2006). Weak protein-protein interactions as probed by NMR spectroscopy. *Trends in Biotechnology* **24**, 22-27.

Veena, V. & Taylor, C. G. (2007). Agrobacterium rhizogenes: recent developments and promising applications. *In Vitro Cellular & Developmental Biology-Plant* **43**, 383-403.

Véronique, S. (2007). Plant Plasma Membrane Protein Extraction and Solubilization for Proteomic Analysis. In *Plant Proteomics-Methods and Protocols* pp. 93-109. Springer.

Very, A. A. & Sentenac, H. (2002). Cation channels in the Arabidopsis plasma membrane. *Trends in Plant Science* **7**, 168-175.

Very, A. A. & Sentenac, H. (2003). Molecular mechanisms and regulation of K+ transport in higher plants. *Annual Review of Plant Biology* **54**, 575-603.

Vidal-Aroca, F., Giannattasio, M., Brunelli, E., Vezzoli, A., Plevani, P., Muzi-Falconi, M., & Bertoni, G. (2006). One-step high-throughput assay for quantitative detection of beta-galactosidase activity in intact Gram-negative bacteria, yeast, and mammalian cells. *Biotechniques* **40**, 433-434.

Viitanen, P., Newman, M. J., Foster, D. L., Wilson, T. H., & Kaback, H. R. (1986). Purification, Reconstitution, and Characterization of the Lac Permease of Escherichia-Coli. *Methods in Enzymology* **125**, 429-452.

Villemont, E., Dubois, F., Sangwan, R. S., Vasseur, G., Bourgeois, Y., & SangwanNorreel, B. S. (1997). Role of the host cell cycle in the Agrobacterium-mediated genetic transformation of Petunia: Evidence of an S-phase control mechanism for T-DNA transfer. *Planta* **201**, 160-172.

Voelker, C., Schmidt, D., Mueller-Roeber, B., & Czempinski, K. (2006). Members of the Arabidopsis AtTPK/KCO family form homomeric vacuolar channels in planta. *Plant Journal* **48**, 296-306.

Voinnet, O., Rivas, S., Mestre, P., & Baulcombe, D. (2003). An enhanced transient expression system in plants based on suppression of gene silencing by the p19 protein of tomato bushy stunt virus. *Plant Journal* **33**, 949-956.

Volker, A., Stierhof, Y. D., & Jurgens, G. (2001). Cell cycle-independent expression of the Arabidopsis cytokinesis-specific syntaxin KNOLLE results in mistargeting to the plasma membrane and is not sufficient for cytokinesis. *Journal of Cell Science* **114**, 3001-3012.

Vranova, E., Tahtiharju, S., Sriprang, R., Willekens, H., Heino, P., Palva, E. T., Inze, D., & Van Camp, W. (2001). The AKT3 potassium channel protein interacts with the AtPP2CA protein phosphatase 2C. *Journal of Experimental Botany* **52**, 181-182.

Waadt, R., Schmidt, L. K., Lohse, M., Hashimoto, K., Bock, R., & Kudla, J. (2008). Multicolor bimolecular fluorescence complementation reveals simultaneous formation of alternative CBL/CIPK complexes in planta. *Plant Journal* **56**, 505-516.

Wagner, S., Bader, M. L., Drew, D., & de Gier, J. W. (2006). Rationalizing membrane protein overexpression. *Trends in Biotechnology* **24**, 364-371.

Waizenegger, I., Lukowitz, W., Assaad, F., Schwarz, H., Jurgens, G., & Mayer, U. (2000). The Arabidopsis KNOLLE and KEULE genes interact to promote vesicle fusion during cytokinesis. *Current Biology* **10**, 1371-1374.

Walderhaug, M. O., Polarek, J. W., Voelkner, P., Daniel, J. M., Hesse, J. E., Altendorf, K., & Epstein, W. (1992). Kdpd and Kdpe, Proteins That Control Expression of the Kdpabc Operon, Are Members of the 2-Component Sensor-Effector Class of Regulators. *Journal of Bacteriology* **174**, 2152-2159.

Walker, D. J., Leigh, R. A., & Miller, A. J. (1996). Potassium homeostasis in vacuolate plant cells. *Proceedings of the National Academy of Sciences of the United States of America* **93**, 10510-10514.

Walter, M., Chaban, C., Schutze, K., Batistic, O., Weckermann, K., Nake, C., Blazevic, D., Grefen, C., Schumacher, K., Oecking, C., Harter, K., & Kudla, J. (2004). Visualization of protein interactions in living plant cells using bimolecular fluorescence complementation. *Plant Journal* **40**, 428-438.

Wang, D. N. & Kuhlbrandt, W. (1991). High-Resolution Electron Crystallography of Light-Harvesting Chlorophyll-A/B-Protein Complex in 3 Different Media. *Journal of Molecular Biology* **217**, 691-699.

Wang, D. N., Kuhlbrandt, W., Sarabia, V. E., & Reithmeier, R. A. F. (1993). 2-Dimensional Structure of the Membrane Domain of Human Band-3, the Anion Transport Protein of the Erythrocyte-Membrane. *Embo Journal* **12**, 2233-2239.

Wang, Y. & Wu, W. H. (2010). Plant Sensing and Signaling in Response to K+-Deficiency. *Molecular Plant* **3**, 280-287.

Ward, J. M., Maser, P., & Schroeder, J. I. (2009). Plant Ion Channels: Gene Families, Physiology, and Functional Genomics Analyses. *Annual Review of Physiology* **71**, 59-82.

Weber, T., Zemelman, B. V., Mcnew, J. A., Westermann, B., Gmachl, M., Parlati, F., Sollner, T. H., & Rothman, J. E. (1998). SNAREpins: Minimal machinery for membrane fusion. *Cell* **92**, 759-772.

White, P. J. & Broadley, M. R. (2003). Calcium in plants. *Annals of Botany* **92**, 487-511.

White, S. H. (2007). Biochemistry - Crowds of syntaxins. *Science* **317**, 1045-1046.

White, S. H. & Wimley, W. C. (1999). Membrane protein folding and stability: Physical principles. *Annual Review of Biophysics and Biomolecular Structure* **28**, 319-365.

Wick, P., Gansel, X., Oulevey, C., Page, V., Studer, I., Durst, M., & Sticher, L. (2003). The expression of the t-SNARE AtSNAP33 is induced by pathogens and mechanical stimulation. *Plant Physiology* **132**, 343-351.

Wilke, M., Fortunati, E., vandenBroek, M., Hoogeveen, A. T., & Scholte, B. J. (1996). Efficacy of a peptide-based gene delivery system depends on mitotic activity. *Gene Therapy* **3**, 1133-1142.

Winter, D., Vinegar, B., Nahal, H., Ammar, R., Wilson, G. V., & Provart, N. J. (2007). An 'Electronic Fluorescent Pictograph' Browser for Exploring and Analyzing Large-Scale Biological Data Sets. *Plos One* **2**, 718-730.

Wittke, S., Lewke, N., Muller, S., & Johnsson, N. (1999). Probing the molecular environment of membrane proteins in vivo. *Molecular Biology of the Cell* **10**, 2519-2530.

Xia, F. Z., Gao, X. D., Kwan, E., Lam, P. P. L., Chan, L. L., Sy, K. Y., Sheu, L., Wheeler, M. B., Gaisano, H. Y., & Tsushima, R. G. (2004). Disruption of pancreatic beta-cell lipid rafts modifies K(v)2.1 channel gating and insulin exocytosis. *Journal of Biological Chemistry* **279**, 24685-24691.

Xicluna, J., Lacombe, B., Dreyer, I., Alcon, C., Jeanguenin, L., Sentenac, H., Thibaud, J. B., & Cherel, I. (2007). Increased functional diversity of plant K+ channels by preferential heteromerization of the shaker-like subunits AKT2 and KAT2. *J Biol Chem* **282**, 486-494.

Xie, Z., Zhang, Z. L., Zou, X. L., Yang, G. X., Komatsu, S., & Shen, Q. X. J. (2006). Interactions of two abscisic-acid induced WRKY genes in repressing gibberellin signaling in aleurone cells. *Plant Journal* **46**, 231-242.

Xu, J., Li, H. D., Chen, L. Q., Wang, Y., Liu, L. L., He, L., & Wu, W. H. (2006). A protein kinase, interacting with two calcineurin B-like proteins, regulates K+ transporter AKT1 in Arabidopsis. *Cell* **125**, 1347-1360.

Xu, J., Yu, W. F., Jan, Y. N., Jan, L. Y., & Li, M. (1995). Assembly of Voltage-Gated Potassium Channels - Conserved Hydrophilic Motifs Determine Subfamily-Specific Interactions Between the Alpha-Subunits. *Journal of Biological Chemistry* **270**, 24761-24768.

Yamaguchi, T., Dulubova, I., Min, S. W., Chen, X. H., Rizo, J., & Sudhof, T. C. (2002). Sly1 binds to Golgi and ER syntaxins via a conserved N-terminal peptide motif. *Developmental Cell* **2**, 295-305.

Yi, H. C., Mysore, K. S., & Gelvin, S. B. (2002). Expression of the Arabidopsis histone H2A-1 gene correlates with susceptibility to Agrobacterium transformation. *Plant Journal* **32**, 285-298.

Yi, K., Menand, B., Bell, E., & Dolan, L. (2010). A basic helix-loop-helix transcription factor controls cell growth and size in root hairs. *Nature Genetics* **42**, 264-267.

Yu, I. M. & Hughson, F. M. (2010). Tethering factors as organizers of intracellular vesicular traffic. *Annu Rev Cell Dev Biol* **26**, 137-156.

Yuasa, K., Toyooka, K., Fukuda, H., & Matsuoka, K. (2005). Membrane-anchored prolyl hydroxylase with an export signal from the endoplasmic reticulum. *Plant Journal* **41**, 81-94.

Zamyatnin, A. A., Solovyev, A. G., Bozhkov, P. V., Valkonen, J. P. T., Morozov, S. Y., & Savenkov, E. I. (2006). Assessment of the integral membrane protein topology in living cells. *Plant Journal* **46**, 145-154.

Zelazny, E., Borst, J. W., Muylaert, M., Batoko, H., Hemminga, M. A., & Chaumont, F. (2007). FRET imaging in living maize cells reveals that plasma membrane aquaporins interact to regulate their subcellular localization. *Proceedings of the National Academy of Sciences of the United States of America* **104**, 12359-12364.

Zhang, X. A., Ma, J. O., & Berkowitz, G. A. (1999). Evaluation of functional interaction between K+ channel alpha- and beta-subunits and putative inactivation gating by co-expression in Xenopus laevis oocytes. *Plant Physiology* **121**, 995-1002.

Zhang, X. R., Henriques, R., Lin, S. S., Niu, Q. W., & Chua, N. H. (2006). Agrobacterium-mediated transformation of Arabidopsis thaliana using the floral dip method. *Nature Protocols* **1**, 641-646.

Zhang, Y., Liu, C. M., Emons, A. M. C., & Ketelaar, T. (2010). The Plant Exocyst. *Journal of Integrative Plant Biology* **52**, 138-146.

Zhang, Z. G., Feechan, A., Pedersen, C., Newman, M. A., Qiu, J. L., Olesen, K. L., & Thordal-Christensen, H. (2007). A SNARE-protein has opposing functions in penetration resistance and defence signalling pathways. *Plant Journal* **49**, 302-312.

Zhao, J., Cheng, N. H., Motes, C. M., Blancaflor, E. B., Moore, M., Gonzales, N., Padmanaban, S., Sze, H., Ward, J. M., & Hirschi, K. D. (2008). AtCHX13 is a plasma membrane K+ transporter. *Plant Physiology* **148**, 796-807.

Zheng, H. Y., Bednarek, S. Y., Sanderfoot, A. A., Alonso, J., Ecker, J. R., & Raikhel, N. V. (2002). NPSN11 is a cell plate-associated SNARE protein that interacts with the syntaxin KNOLLE. *Plant Physiology* **129**, 530-539.

Zilly, F. E., Sorensen, J. B., Jahn, R., & Lang, T. (2006). Munc18-bound syntaxin readily forms SNARE complexes with synaptobrevin in native plasma membranes. *Plos Biology* **4**, 1789-1797.

Zimmermann, S., Talke, I., Ehrhardt, T., Nast, G., & Muller-Rober, B. (1998). Characterization of SKT1, an inwardly rectifying potassium channel from potato, by heterologous expression in insect cells. *Plant Physiology* **116**, 879-890.

Zuzarte, M., Rinne, S., Schlichthorl, G., Schubert, A., Daut, J., & Preisig-Muller, R. (2007). A di-acidic sequence motif enhances the surface expression of the potassium channel TASK-3. *Traffic* **8**, 1093-1100.

Appendix II

Honsbein, A., Sokolovski, S., Grefen, C., Campanoni, P., Pratelli, R., Paneque, M., Chen, Z. H., Johansson, I., & Blatt, M. R. (2009). A Tripartite SNARE-K+ Channel Complex Mediates in Channel-Dependent K+ Nutrition in Arabidopsis. *Plant Cell* 21, 2859-2877.

To this paper I contributed the mbSUS data (Fig. 1, Fig. S1), the Co-IP data (Fig. 1) the BiFC data (Fig. 2, Fig. S2), the electrophysiological measurements after heterologous expression in *Xenopus* oocytes (Fig. 3), the root growth phenotypical analysis (Fig. 5, Fig. S4), the characterization of the AKT1 and KC1 antibodies (Fig. S6) as well as their use on enriched root plasma membrane fractions (Fig. 6C), and the transient expression and localisation of AKT1-GFP to the plasma membrane of *Arabidopsis* root cells (Fig. 7, Fig. 8, Fig. S5).